CRANFIELD UNIVERSITY

SCHOOL OF APPLIED SCIENCES

PhD THESIS

Academic Year 2006-2007

Theocharis Liratzis

Tandem Gas Metal Arc Pipeline Welding

Supervisor David Yapp

April 2007

To my father Σωτήρη, my mother Μαρία and my nephew Χρήστο

Abstract

Energy consumption has grown by 2% per year worldwide over the past ten years. In 2005 worldwide 900,000 barrels of oil and 7.6 billion cubic metre of natural gas were produced daily. The exploitation of fields to meet the increased demands in energy requires the presence of adequate infrastructures.
High strength pipeline steels (X100) have been developed to operate at higher pressures allowing a greater volume of fuel to be transported. Additional advantages arising from the reduction in wall thickness contribute to reduction in construction costs and steel volume.
High welding speeds and deposition rates can also generate significant reductions in labour and equipment costs.
This thesis is focussed on several aspects of welding of high strength pipeline steels, as follows:

- high productivity dual tandem pipeline welding,
- single and dual tandem welding of X100 pipeline steels,
- high productivity low heat input dual tandem welding for double jointing,
- tie-in welds using basic flux-cored consumables to achieve the overmatching criterion for the weld metal strength,
- mathematical models to describe the effect of welding parameters on weld geometry,
- optimisation of shielding gas composition.

The present work confirmed that the single tandem PGMAW (one torch with two wires) process is capable of welding in all positions (5G girth welds) and that high quality welds in a narrow groove can be achieved at twice the welding speed (1270mm/min) and deposition rate compared to traditional single wire mechanised GMAW. The dual tandem (two separate torches each with two wires) PGMAW process operates at similar welding speeds to the single tandem welding and further enhances productivity with four welding arcs operating simultaneously. This reduces the total arc time for pipe welding and will result in considerable reductions in labour and welding equipment on a typical pipeline spread. The dual tandem process was developed for the first time during the present work

High quality tandem and dual tandem welds were obtained. Optimum weld metal yield strength level was established in the range 810-860MPa meeting the overmatching criterion required for strain-based design. Filler wires for X100 pipe steel were selected and mechanical properties were determined. Procedure welds were qualified to EN 288-9, API 1104 and BS 4515.
The single tandem procedure weld used the Oerlikon NiMo-1 (1%Ni0.3%Mo) filler wire and 36 in OD x 19.05mm X100 pipe. The weld metal yield strength of 910MPa met the overmatching criterion. The Cross weld tensile, Nick break and Side bend tests were all acceptable. Charpy tests were performed at -20°C, -40°C, -60°C and -80°C. Toughness values were very acceptable giving values over 80J at -60°C.
Several dual tandem procedure welds were performed on 36 in OD x 19.05mm and 52 in OD x 22.9mm pipes. Initially trials using the same consumable as single tandem gave a yield strength of 771MPa and did not meet the established criteria for the weld metal

strength, while a higher alloyed consumable(1.8%Ni0.5%Mo0.25Cr) Thyssen Union X85-IG gave 912MPa, exceeding the upper strength limit. The Cranfield tandem torch, where two wires work in the same pool, allowed the Thyssen X85-IG and the Oerlikon NiMo-1 to be fed in the same torch as lead and trail wire accordingly. Procedure welds using the "mixed" wire technique were developed and qualified. The weld metal yield strength of 840MPa now met the overmatching criterion. The Cross weld tensile, Nick break and Side bend tests were all acceptable. Toughness values were very acceptable giving values over 80J at -60°C.

Double jointing welding in pipeline spreads is carried out offline where usually welding speed is not critical. Submerged arc welding is the typical process applied with 2.5kJ/mm heat input. These SAW welds fail to achieve the overmatching criterion due to the high heat input and high dilution. The dual tandem process was developed for application to double jointing, with a corresponding low heat input (0.5kJ/mm and 0.4kJ/mm for the lead and trail torch). The procedure weld used the "mixed" wire technique described earlier. The weld metal yield strength resulted in 766MPa due to a wider joint configuration (6.0mm instead of the typical 4.6-5.0mm). The Cross weld tensile, Nick break and Side bend tests were all acceptable. Toughness values were acceptable giving values over 60J at -60°C. Very competitive deposition rates were achieved (20.5Kg/hr) confirming that the dual tandem process may be the viable alternative for double jointing in high strength pipeline steels.

Tie-in welds are typical parts of a pipeline spread and are required for the connection between pipe and a facility, for road or bridge crossings etc. Because they are made without internal clamping, the joint fit up is not as good as the mainline and misalignments may occur. A typical standard 30° API bevel preparation is used. In the beginning tie-in welds were made using cellulosic electrodes and as pipe strength increased, basic electrodes were employed. Joint completion rates were increased with rutile flux cored wires (mechanised) but did not meet the required strength level in X100 pipeline steels. In this project, basic flux cored wires were used in pulsed transfer mode in order to achieve smooth transfer and minimise spatter generation. In the present work bevel preparation was reduced to 15° and weld trials on X100 pipe using the Philarc PZ6149 filler wire were carried out. Weld metal strength (966MPa) exceeded the desired optimum range (810-860MPa). Toughness values were around 50J at -60°C. Considering that basic flux wires for X100 steels in pulsed welding were tested for the first time in the present work, these preliminary tests were very promising for further optimisation.

A detailed study of the effect of the welding parameters on weld geometry of single tandem narrow gap PGMAW was performed. The large number of the welding parameters involved in weld profile formation were limited to four (wire feed speed, travel speed, wire distance from sidewall and arc length) for the purposes of the present study. Statistically designed experiments and statistical analysis of the results were carried out. Statistics have been widely used in welding to provide comprehensive information on the effects of the main variables and their interactions, minimising number of experiments, leading to time and cost savings.
The central composite design of experiments was selected for its ability in optimising the response. Depth of penetration, groove sidewall penetration and corner angle were considered in the present analysis. Mathematical models describing the effect of

welding parameters on weld profile were developed and validated in 0°, 30°, 60°, 90°, 120°, 150° and 180° position. The significant effect of welding position was emphasised.

The effect of shielding gas composition on weld bead geometry in single tandem pulsed-GMAW was investigated using a statistical design (D-Optimal) intended for analysis of mixtures. Several gas mixtures of $Ar/CO_2/He/O_2$ were tested. Depth of penetration, sidewall penetration and concavity were considered in the analysis. Mathematical models were developed and emphasised the strong effect of carbon dioxide. Results have shown that argon-carbon dioxide mixtures provided equivalent weld geometry to the mixtures containing $Ar/CO_2/He$.

Some of the techniques developed during this project have already been applied in field trials and commercial pipelines.
In March 2003 the dual tandem system was field tested on 40 in OD x 19.1mm X80 linepipe in Canada. Good arc stability and acceptable quality welds were produced. Some minor teething problems were associated with the power sources operating at -40°C.
In February 2004 the single tandem PGMAW system was used on the construction of a 2km section of 36 in OD x 13.2mm X100 pipeline (TransCanada Peerless Project). During five days of welding 174 welds were completed and there were seven repairs for lack-of-fusion.
The TransCanada Stittsville/Deux Rivieres project implemented the single tandem process on a 5km X100 pipeline 40 in OD x 12.7mm and 40 in x 14.3mm thickness. The pipe section of 12.7mm thickness presented zero rejects while the 14.3mm thickness gave a 4.3% reject rate.

Acknowledgments

I would like to express my gratitude to my supervisor Mr D. Yapp for his support and guidance throughout the research work. I would also like to thank Mr S. Blackman for giving me the opportunity to pursue this course of study and Prof. S. Williams for the constructive discussion and advice.

Thanks are also due to the technical staff at Welding Engineering Research Centre-Cranfield. In particular to Mr J. Savill for his continuous help, support and encouragement, and to Mr B. Brooks who helped with the practical aspects of the work. Dr J. Spurrier contributed to many discussions on metallurgy and fracture mechanics, Prof. A. Scotti on process characteristics and Dr E. Tolle on metallurgy and welding processes.

My appreciation goes to Mrs M. Yapp who helped with English grammar.

I wish also acknowledge the financial support of BP Exploration and TransCanada in funding this research, and in particular the support of Mr J. Hammond and Dr M. Hudson of BP Exploration, and Dr D. Dorling of TransCanada.

Thanks are due to my colleagues at Cranfield G. Lopes, A. Varughese, N. Pepe, P. Marmelo.

I would also like to acknowledge the help of the Kings Norton Library staff and in particular of Mrs H. Woodfield.

Finally, I could not forget my family for their support and encouragement. This is highly appreciated.

Table of Contents

List of Figures

List of Tables

Nomenclature

α	Wetting Angle
β	Fusion Angle
γ_s	Surface Tension of Liquid Metal
γ_t	Surface Tension of Solid Metal
γ_{st}	Solid/Liquid Interfacial Tension
δm	Value of CTOD at the first attainment of a maximum force plateau for fully plastic behaviour
δu	Critical CTOD at the onset of brittle crack extension or pop-in when the event is preceded by Δa equal to or greater than 0.2mm
δc	Critical CTOD at the onset of brittle crack extension or pop-in when Δa is less than 0.2mm
Θ	Corner Angle
ζ	Concavity
Π	Position
A	Elongation
A_c	Arc Length Correction
Ar_1	Temperature at which the transformation of austenite to ferrite is completed during cooling
d_e	Filler Wire Diameter
D	Wire Distance from Sidewall
G_{Ar}	Argon
G_{CO2}	Carbon Dioxide
G_{He}	Helium
G_{O2}	Oxygen
I	Welding Current
I_m	Welding Mean Current
P_α	Average Sidewall Penetration
P_d	Depth of Penetration
P_s	Sidewall Penetration
P_{GS}	Groove Sidewall Penetration
$R_{p0.2}$	0.2% Proof Stress
$R_{t0.5}$	0.5% Tensile Elongation Stress
R_m	Ultimate tensile stress
T	Travel Speed
$t_{8/5}$	Cooling time from 800°C to 500°C
Y/T	Yield to Tensile ratio
U	Undercut
v	Welding speed
V_l	Lead Wire Voltage
V_t	Trail Wire Voltage
W	Wire Feed Speed

Abbreviations

AC	Alternating Current
ALC	Arc Length Correction
ANOVA	Analysis of Variance
API	American Petroleum Institute
ASCII	American Standard Code for Information Interchange
ASME	American Society of Mechanical Engineers
ASNT	American Society for Nondestructive Testing
ASTM	American Society for Testing and Materials
AWS	American Welding Society
BOC	British Oxygen Company
bpm	beats per minute
BS	British Standard
CAPS	Cranfield Automated Pipeline System
CCD	Central Composite Design
CE	Carbon Equivalent
CSA	Canadian Standards Association
CTOD	Crack Tip Opening Displacement
CTWD	Contact Tip to Workpiece Distance
Cv	Charpy V-Notch
DOE	Design of Experiments
DSP	Digital Signal Processor
EN	European Standard
FCAW	Flux Cored Arc Welding
GMAW	Gas Metal Arc Welding
GTAW	Gas Tungsten Arc Welding
HAZ	Heat Affected Zone
HSLA	High Strength Low Alloy Steel
HV	Vickers Hardness
ID	Internal Diameter
IIW	International Institute for Welding
MAG	Metal Active Gas
MCAW	Metal Cored Arc Welding
MIG	Metal Inert Gas
ND	Neutral Density
NDT	Non-Destructive Testing
NG	Narrow Gap
OD	Outside Diameter
Pcm	Parameter Crack Measurement
PGMAW	Pulsed Gas Metal Arc Welding
PI	Prediction Interval
PM	Parent Material
ppm	Parts per million by weight
fps	Frames per second
PQR	Procedure Qualification Record
PWHT	Post Weld Heat Treatment
RSM	Response Surface Methodology

RMS	Root Mean Square
SAW	Submerged Arc Welding
SMAW	Shielded Metal Arc Welding
STT	Surface Tension Transfer
TPS	Trans Pulse Synergic
TS	Travel Speed
UKAS	United Kingdom Accreditation Service
UTS	Ultimate Tensile Strength
WD	Wire Distance from the Sidewall
WERC	Welding Engineering Research Centre, Cranfield University
WFS	Wire Feed Speed
WPS	Welding Procedure Specification
WT	Wall Thickness
YS	Yield Strength

1. Introduction

There is a strong rate of oil and gas consumption worldwide resulting from increased energy demands. High growth of natural gas is reported as consequence of continuous industrial development. However, most of the oil and gas fields are located in remote areas and far from the demand centres, requiring significant investments in the construction of pipelines. The capital cost of a pipeline installation is governed among the other factors by material and welding costs. The use of high strength steels X70, X80 and recently X100 has contributed to savings resulting from the reduced material volume, welding material and time. In addition, the lean alloy compositions and the low carbon equivalent values associated with these steels promote the reduction of the preheating temperatures.

Recently, research work performed on X100 linepipe [1],[2] has established properties of girth, double jointing and tie-in welds in this material. Detailed study and extensive data relative to welding procedures is necessary before the technology can be transferred to pipeline contractors for field application. The metallurgical properties of the parent pipe (X100) and weld metal require careful selection of filler wire and shielding gas for successful welding procedure qualification. Mechanised gas metal arc welding (GMAW) has been the most popular process for mainline pipeline welding. With the introduction of higher productivity variants of mechanised narrow gap welding, such as tandem welding (two wires in the same torch) and dual tandem welding (two torches, two wires each torch) further economic savings can be expected.

Previous work at Cranfield [1] had established welding procedures and determined mechanical properties for single tandem welding on X100. The programme work described in this thesis included single tandem and dual tandem narrow gap PGMAW of X100 girth welds. The equipment and methods used were designed to be as close as possible to common practice for field pipeline installation. Two pipe diameters and thicknesses from different manufacturers were used for research purposes. Key objectives of the present work was to establish, for the first time, that the dual tandem process can be used to make high quality girth welds, and to determine the relationship between mechanical properties and welding parameters. Using four wires (two wires in each weld pool) the total arc time for pipe welding will further reduce resulting in substantial reduction in welding personnel and welding equipment while allowing high welding speeds compared to traditional GMA welding. A further objective was to demonstrate that the required mechanical properties (e.g. overmatching the weld metal proof stress) could be achieved using this new high productivity dual tandem process. The aim was to demonstrate that the required properties could be achieved on full procedure welds in conformity with European and International standards.

In addition to the major programme on development of the dual tandem welding process, it was also necessary to consider the issues associated with achieving adequate strength levels for double jointing and tie-in welds in X100 linepipe when overmatching is required. Submerged arc welding (SAW) is traditionally used for double jointing of lower strength materials. However, high heat input and dilution levels involved mean that it has not been possible so far to achieve overmatching in X100 steel with SAW. The intent in this project was to determine whether dual tandem welding could be used

for double jointing, to achieve the necessary strength levels while still providing productivity comparable to that of SAW.

Flux cored welding is frequently used for tie-in welds, with an open "V" preparation, and using rutile wires and vertical up welding. However, it has proved difficult to achieve overmatching for X100 with rutile wires [1],[3]. It is known that better properties can be obtained with basic flux cored wires, and the objective in this project was therefore to determine whether it is possible to develop workable procedures with basic wires welding vertically down.

The suitability of mechanised tandem narrow gap PGMAW has been widely researched in this and previous projects. However, there is very limited work on the relationship between process parameters and weld geometry and quality. An extensive and systematic study was planned which could contribute to a better understanding of the relationships that occur between tandem weld process parameters and weld bead geometry. Such information is of high importance in order to eliminate side-lack-of-fusion defects commonly presented in narrow gap gas metal welding. These defects can considerably reduce productivity due to significant time spent to repair the defective joints. The one-variable-at-the time technique has been widely used in welding applications in the past in order to analyse the influence of the welding parameters on weld bead profile, but provides very limited prediction capabilities, due to the interactions that occur between the welding variables and the high number of experiments required. Statistical modelling presents an alternative technique and has been successfully used in welding in the past [4]. The present work makes use of statistically designed and analysed experiments and aims at establishing models applicable to narrow groove pipeline welding. The response surface methodology technique was chosen for its advantage in optimising the responses (weld bead dimensions). Central composite designs were used to model the weld bead geometry in flat, vertical down and overhead positions.

Finally, the effect of gas composition on weld geometry and quality was selected as an area for study. The previous research development work carried out at Cranfield [5],[1] used 82.5%Ar12.5%$CO_2$5%He as gas mixture based on the conclusions of the research programme of Thompson [6]. For this study, the effect of the shielding gas composition (Ar, CO_2, He and O_2) on the weld bead profile of tandem narrow groove X100 pipe steels was to be evaluated again using systematic studies based on statistically designed and analysed experiments. It was considered that properly designed statistical experiments would be essential to determine the relative effects of the different gas mixtures.

In summary, this project had a series of major objectives, all associated with achieving very high productivity and high quality welds in X100 linepipe. This included:

- Development of the dual tandem PGAW process for narrow groove pipeline welding
- Determination of the relationship between weld metal composition, strength and toughness
- Establishing viability of tandem and dual tandem welding in X100 linepipe using full-scale procedure welds

- Development of the dual tandem PGMAW process for double jointing, and evaluation of productivity compared to conventional SAW
- Investigation of the feasibility of mechanised basic flux cored vertical down welding for tie-in applications
- Determination of the relationship between welding parameters and weld bead geometry, and optimisation of parameter selection to minimise chances of side-wall fusion defects
- Investigation of the relationship between shielding gas composition and weld quality, and selection of optimum shielding gas mixtures.

2 Literature Survey

2.1 Steels for Transmission Pipelines

Over the past 30 years there has been a continuous increased demand for energy, which has promoted the development of new materials in the pipeline industry. It has been estimated that in 2005 worldwide, 900,000 barrels of oil, and 7.6 billion cubic metres of natural gas were produced daily [7]. High strength steels contribute significantly to a reduction in transportation costs of fuel by allowing use of pipes with reduced wall thickness. A summary of pipeline steel development history is shown in Figure 2.1.

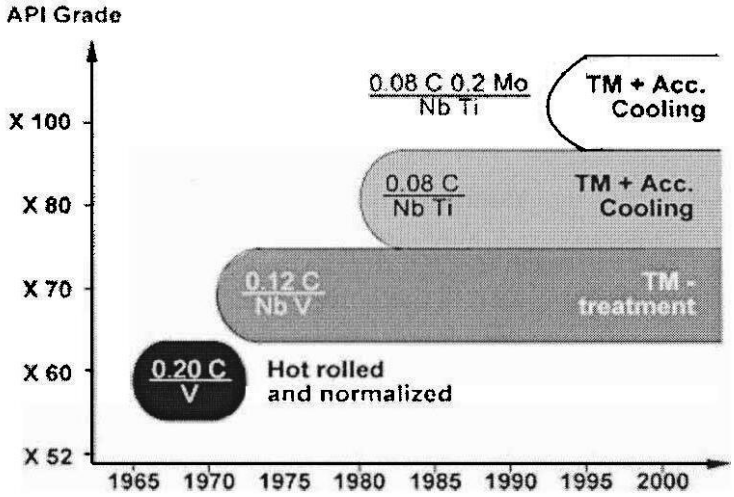

Fig. 2-1 History of pipeline steel development (large diameter pipe) [8]

As can be seen in Figure 2.1, the production of high strength and high toughness steels has been achieved by the addition of different alloying elements in the steel composition and by the different forming processes applied.

Typically, ferrite and pearlite grains are the characteristic microstructures of the X60 steels; the microstructure of the thermomechanically treated X70 steels has finer ferrite grains while very fine bainitic microstructure is obtained by thermomechanical rolling following by accelerated cooling in X80 steel. Bainitic microstructures are reported to be the predominant constituents of the X100 pipeline steels [9],[10],[11]. A bainitic microstructure generates high tensile strength while toughness remains at good levels.

The addition of alloying elements promotes the formation of bainite, and accompanying hardenability increases. Impact properties are controlled with additions of alloying elements such as Al, Ti, and V and grain refinement control.

A detailed description of the forming processes, properties, and the related microstructures of the high strength pipeline steels is outside the scope of this thesis. Details of reference sources on steel microstructures, composition, mechanical properties and fabrication process can be found in Hudson's work [1].

Traditionally, onshore pipelines are designed on a stress-based approach, where the applied hoop stress is at a lower level than the yield strength [12]. Where displacement-controlled loads occur on the pipeline, due to frost, ground movement, strain-based design becomes of importance [13],[14]. For example, the Trans-Alaska oil pipeline

was subjected to a 7.9 magnitude earthquake (November 3, 2002) that produced a 2.5m lateral displacement [15]. In these cases displacements due to ground movements can produce excessive local strains and potential failure of the pipeline. In a strain-based design, the pipeline must be able to successfully "absorb" the strain, providing adequate elongation levels.

2.2 Field Weldability of Transmission Pipelines

Hudson [1] has recently reviewed this topic in detail, and hence only brief summaries are provided here.
The welding of transmission pipelines is mainly composed of:
-mainline welding (5G girth welding and double jointing welding)
-tie-in welding for road/river/utilities crossings etc
-repair welding
Mainline welding consists of repetitive welds usually every 12m (length of the pipe spool). In order to increase productivity, double jointing techniques are sometimes applied. In this technique, two 12m pipe spools are welded in a different place and after completion the 24m welded pipe section is transferred to its final position. This reduces the number of welds performed on the mainline and significantly increases the rate at which the pipeline can progress.
Mechanised GMAW using a solid wire is the predominant process for mainline welds, and mechanised FCAW (flux cored arc welding) can be used for the tie-in welds. However, manual SMAW (shielded metal arc welding) is still used quite widely.

2.2.1 5G Girth Welding

2.2.1.1 Tandem PGMAW (one torch, two wires in the same weld pool)

Mechanised GMAW welding is used by industry due to its increased rates of productivity (high deposition rates and increased travel speeds) together with improvement in weld quality compared to SMAW [16].
The first narrow groove tandem GMAW welding (Figures 2.2 and 2.3) of high strength steels (HSLA-100 and HY-100) was reported by Lassaline [17]. Although it was not clearly described whether the system operated with one torch (two wires) or two torches (single wire each), the two arcs worked in very close proximity to each other and arc blow effects were minimised by synchronising the pulsed current waveforms provided by the two power sources.
Among the other control features this tandem system provided a synchronous / asynchronous control determining whether the two power units operate in phase with identical pulse frequencies for both units (master / slave) or independently. The weld produced provided good mechanical properties.

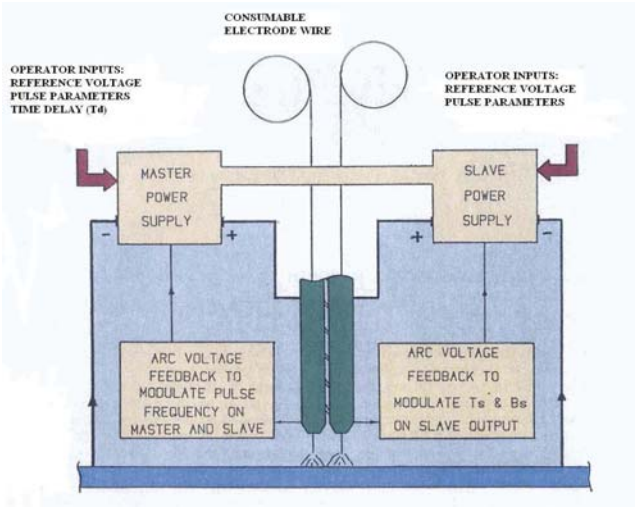

Fig. 2-2 View of the twin-wire system with the two synchronised power sources [17]

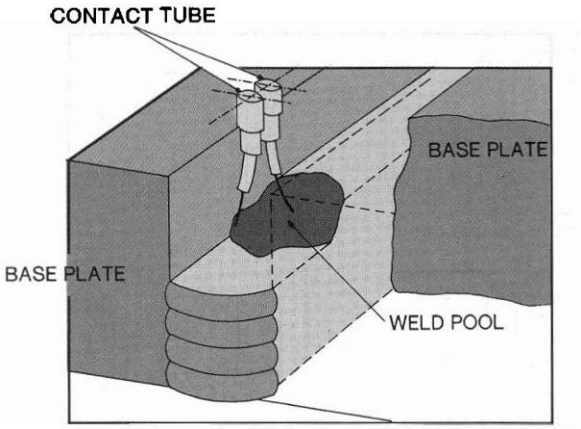

Fig. 2-3 Filler wires arrangements to ensure sidewall fusion [17]

The first tandem PGMAW system for orbital narrow gap pipeline welding with both welding arcs working in the same weld pool was tested by Michie [5] at Cranfield University. His work demonstrated the potential applicability of the process to pipeline girth welding, with almost doubled deposition rates compared to the single wire welding equipment.

Walker [18] confirmed the benefits to productivity of the tandem PGMAW process and reported excellent mechanical properties: hardness values below 250HV and Charpy impact toughness exceeding 80J (test temperature not quoted) in the root weld metal and 200J at the root fusion line for X80 pipeline steels.
The feasibility of the process was further tested on X100 pipeline steel by Hudson [1] where overmatching of the weld metal strength compared to the parent steel strength was required.

Overmatching requires a higher value of the weld metal yield strength than the actual yield strength of the parent pipe. This means ensure that the weld remains in the elastic zone during stress while the pipe commences the plastic deformation. This will reduce

the probabilities of a fracture of the structure in the presence of a defect in the weld metal.

Among the solid filler wires tested the 1.0%Ni0.3%Mo wire generated weld metal strength levels in excess of 900MPa, slightly higher than the required range of 810 to 860 MPa. Good toughness properties (above 50J at -60°C for both weld metal and fusion line) were also achieved.

2.2.1.2 Dual Tandem PGMAW (two separated torches, two wires in the same pool for each torch)

Blackman [19] reported that Serimer Dasa's Saturnax welding system was the first GMAW pipeline welding carriage to support two single wire torches separated from each other able to deposit two weld passes at the same time. Subsequently other pipeline contractors including CRC Evans Automatic Welding, RMS Welding Systems, Vermaat Technics and Saipem have developed their own dual-torch welding systems. A dual torch (two separated torches, single wire each torch) mechanised GMAW system tested on mild steel pipelines at Cranfield [20] emphasised the importance of the torch separation distance in arc blow elimination.

The concept of dual torch welding was combined with that of tandem weld to create a system capable of further substantial increases in productivity. This system named CAPS (Cranfield Automated Pipeline System) uses two tandem torches supported by the same welding carriage and combines the high speed of tandem GMAW with two welding passes deposited at the same time. It has been estimated that CAPS can provide savings of up to 26% in overall pipe alignment, welding and non destructive testing costs compared to the traditional mechanised welding systems [21].
The literature has not reported any previous development of the dual tandem torch technique for the pipeline industry, and this topic is the main subject of this thesis.

2.2.2 Double Jointing Narrow Gap Welding

Double jointing welding is carried out offline hence welding speed is not always critical [22]. Welding is performed using a fixed head and rotating pipe, effectively welding in the flat position, and allowing use of much larger weld pools than for 5G positional welding. For pipeline steel grades up to X70 the SAW process with an 8mm root face and 2.5kJ/mm heat input is typically used [23]. However, tests on X80 steels did not overmatch the weld metal strength [23]. This was attributed to the high dilution levels and to the high heat input levels produced by high current SAW. A typical SAW joint preparation is shown in Figure 2.4.

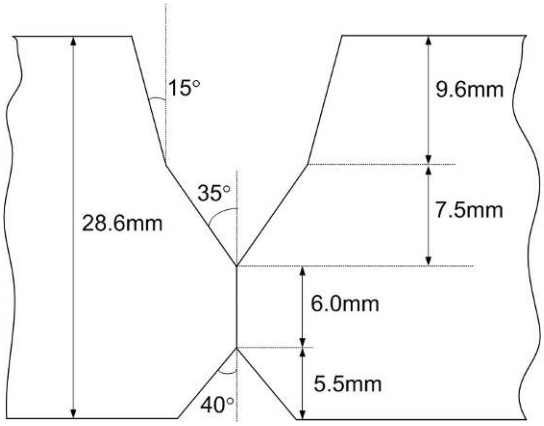

Fig. 2-4 Typical SAW joint configuration for pipelines [3]

A remedy to the above problem would be to reduce the root land to 3-4mm and at the same time reduce the heat input leading to dilution reduction and increased cooling rate, contributing to a weld metal strength increase. However, productivity of the SAW process then decreases and that may make gas metal arc welding in a compound bevel with the welding head fixed over a rotating pipe a faster solution [23].

SAW low heat input procedures (1.44kJ/mm) have recently been developed [24] but their applicability to high strength steels (X100) still needs to be validated. The joint preparation is shown in Figure 2.5.

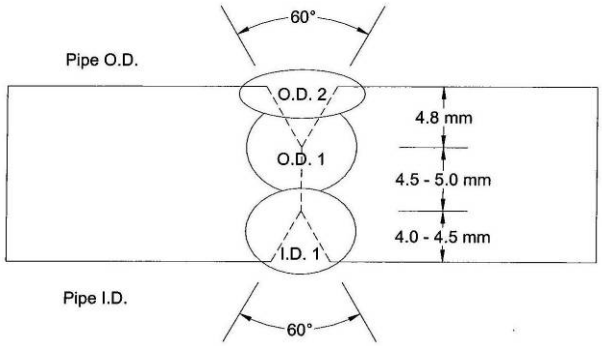

Fig. 2-5 Low heat input joint design for SAW pipeline procedures [24]

However, Saipem has developed a SAW twin arc system with enhanced productivity which was successfully applied on an X65 pipeline steel (Blue stream project), [25]. The system is shown in Figure 2.6

Fig. 2-6 Twin arc heads for pipeline SAW welding (photo courtesy ESAB UK)

A possible solution to the failure of the SAW process to meet the overmatching criterion for the weld metal strength in high strength steels is the use of dual tandem PGMAW process for double jointing welding. This was developed during the present work and for the first time applied to X100 pipeline steels, as will be discussed later.

2.2.3 Tie-In Welding

Typically, tie-in joints (crossing roads, bridges etc) for field welding are characterised by difficulties in the joint alignment. Consequently the typical API wide bevel preparations with almost 60° included angle is applied [26], leading to use of SMAW electrodes or flux-cored wire, both suitable for wide bevel preparations [22].

For many years tie-in welds were carried out using cellulosic electrodes, uphill for the root pass and downhill for the fill/cap passes but for higher strength steels basic electrodes were introduced. However, welding procedures for X80 pipe steels have been successfully developed [22] using different rutile flux-cored wires with close control of heat input and welding procedures.

The first tie-in rutile FCAW (vertical up) on X100 pipeline was reported by Hudson [1] but the weld metal yield strength (730-740MPa) failed to satisfy the overmatching criterion (810-860MPa). Attempts to improve the weld metal strength by reducing the angle of the joint configuration and selecting filler wires with higher alloy content were not successful. The above results demonstrate that rutile flux-cored wires are reaching their limits for application to X100 tie-in welds. This last was recently confirmed [3] by all weld round bar tensile results of Tie-In X100 rutile FCAW wire carried out by a pipeline contractor. The bevel angle was 25°, GMAW STT manual for the root pass and mechanised FCAW for hot to cap passes, and the ESAB Tubrod 15.09 filler wire were used. With heat input levels within the range 1.0 to 1.5 kJ/mm, weld metal strength values were reported between 745-769MPa.

Development of basic flux-cored welding methods for X100 pipelines is a subject of this thesis.

2.3 Shielding Gas Mixtures for GMAW and their Effects

2.3.1 Introduction

The technology of using shielding gases in welding has been developed for several years. Originally, it was thought that the use of shielding gas during a welding operation served only to protect the weld pool from being exposed to the air. It is now well known that the gases have a multifunctional effect on:

- stability of the arc and its ignition,
- metal transfer and droplets size,
- bead profile (appearance and geometry),
- welding speed,
- metallurgical and therefore mechanical properties through the loss of alloying elements,
- emission of fumes,
- weld pool surface tension.

The costs of a welding operation are generally composed of three main factors: labour, materials and shielding gas.

According to Cording [27] labour costs contribute as much as 85%, shielding gas usually between 2% to 6% and the rest materials such as welding wire. Very similar analyses were reported by Irving [28]. Based on an Airco Gases welding cost analysis (for mild steel) labour is estimated at 77% of the overall cost, shielding gas 3%, welding wire 18% and power 2%. Although a very detailed shielding gas cost analysis for pipeline welding has not been reported, the above cost analyses suggest that labour costs would be in the range 80%-85% of the overall onshore pipeline welding cost.

Any welding operation that requires cleaning and grinding after welding is a labour intensive operation. Therefore using the optimum shielding gas implies less postweld cleanup, fewer rejects, increased welding speeds and more product produced. Since the direct cost of shielding gas is a minor component of total costs, it can be concluded that attention should be focussed on the consequences of selecting optimum gas mixtures, rather than the direct cost of gas.

2.3.1.1 Shielding Gases and their Properties

Gas Density

When an effective shield in the welding zone is required it is important that the gas does not readily disperse. Since helium has a lower density than air (Figure 2.7) its tendency to disperse needs to be considered. Gas mixtures with high density gas components will provide a good shielding efficiency of the weld pool, in particular in the overhead position.

Ionisation Energy [29]

Figure 2.8 shows the ionisation potential of the traditional gases. Ionisation potential is reflected in the ease of striking an arc, and its stability. It is a measure of the voltage required to form an arc. If the ionisation potential is high (e.g. welding with helium), the initiation and maintenance of an arc becomes more difficult. A remedy for lowering the ionisation potential could be the use of gas mixtures.

Thermal Conductivity [29]

Thermal conductivity determines the radial transfer of heat from the centre to the periphery of the arc and therefore determines the size of the core of the arc. It has an influence on the thermal profile of the arc, and hence on the weld shape and depth of penetration. Thermal conductivity for different gases is shown in Figure 2.9. Gas mixtures with high thermal conductivity components are expected to improve weld bead geometry and to provide a more rounded penetration profile, which improves fusion characteristics especially when welding inside the groove.

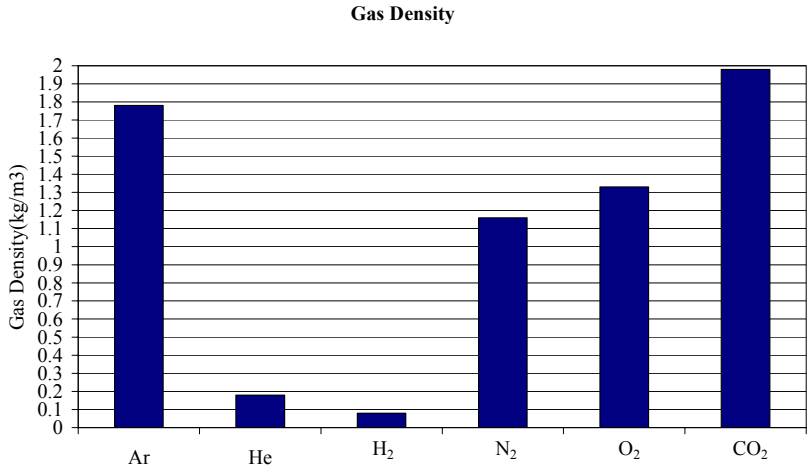

Fig. 2-7 **Gas density** [30]

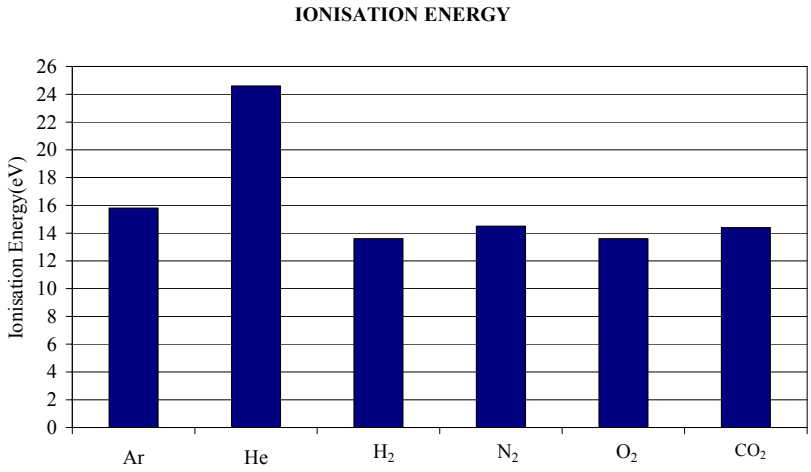

Fig. 2-8 **Gas ionisation energy** [31]

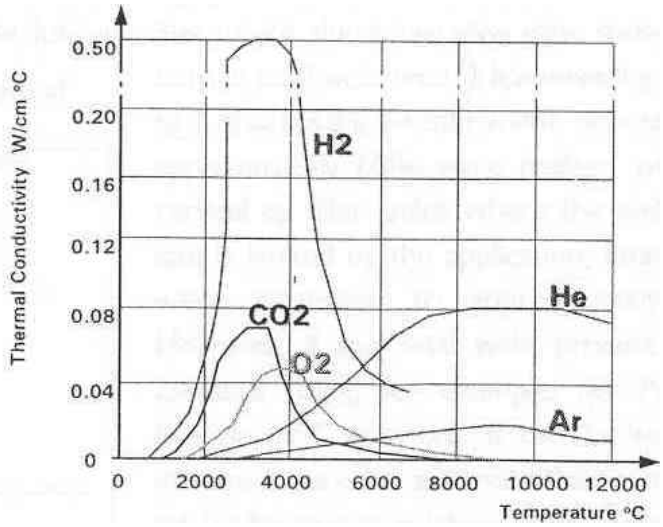

Fig. 2-9 Gas thermal conductivity [29]

Specific Heat [29]

Figure 2.10 shows the specific heat capacities of gases at 21.1ºC and 1 atmosphere pressure. The specific heat capacity provides an indication of the ability of the gas to absorb and store the heat. The thermal profile of the arc, weld bead profile and fusion characteristics are affected by gas specific heat. Gas mixtures with high specific heat capacity are expected to be beneficial in improving fusion characteristics and bead geometry

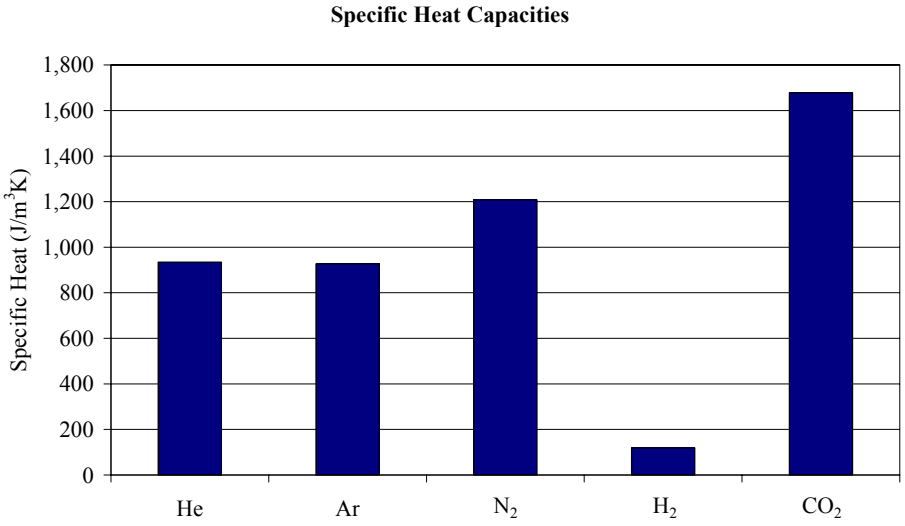

Fig. 2-10 Gas specific heat capacity [29]

Argon [32],[33],[34]

Argon is an inert gas. It is denser than the air and that makes it very efficient for welding operations in the flat position. It constitutes 0.94% of the atmosphere and that makes it widely available. Figure 2.9 shows that Argon has a low thermal conductivity.

This leads to a narrow arc core. This type of arc produces bead profiles that have a narrow finger at the root and wider top as shown in Figure 2.11

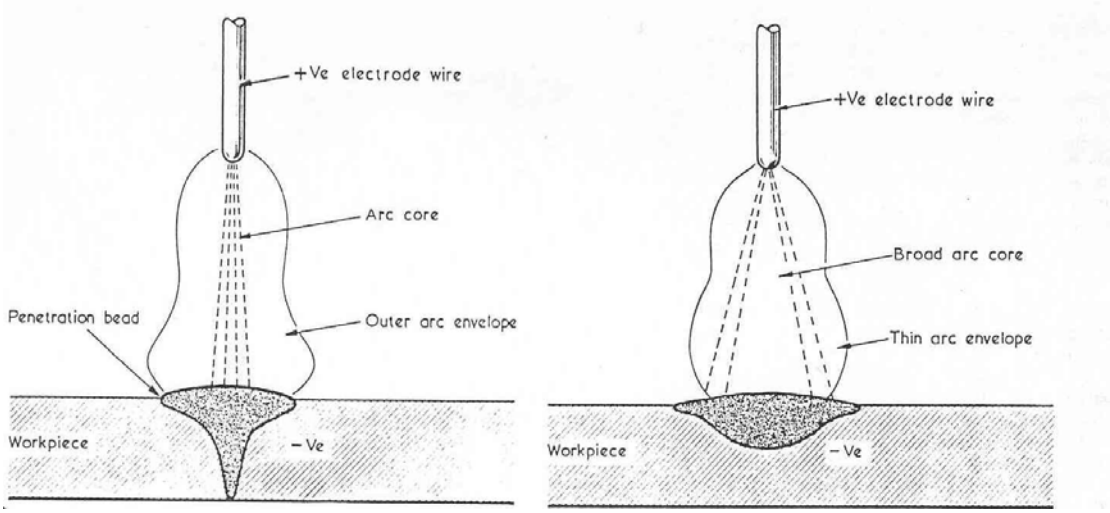

Fig. 2-11 Penetration profile and schematic diagram of the arc in an (a) argon or (b) carbon dioxide and helium atmosphere [35]

Helium [33],[34]

Helium has the second lowest density of the common shielding gases as Figure 2.7 shows. It is present in the air at a very low concentration (0.0004%) and that makes it uneconomic to produce helium from air. The main sources of helium are the natural gas fields. Originally, helium industrial use was located in the USA. That made helium widely used and at competitive prices. Europe imports helium and that has made it quite expensive in the past. The recent availability of the Russian fields [29] and the Algerian fields, has now made helium a "mainstream" shielding gas.

Carbon Dioxide [33],[34]

Carbon dioxide is an active gas (Active or reactive gas is a non inert gas). Carbon dioxide dissociates (or reacts with other elements in the weld pool) in the arc into oxygen and carbon monoxide. Oxygen reacts with the alloying elements such as Mn, Si, Al and forms oxides. This results in a reduction of the alloying elements in the weld metal. Spray transfer transition current increases and unbalanced arc forces are generated. Large globules formed at the end of the wire tip can be affected by strong plasma jets, causing them to be repelled from the weld pool. Since carbon dioxide is a triatomic gas, it can dissociate in the upper part of the arc and re-combine on the weld pool surface, improving the transfer of heat into the weld metal

Oxygen [33]

Oxygen is usually used as a constituent of argon based shielding gas mixtures. It is more easily ionised than carbon dioxide and consequently the arc is more effectively stabilised and metal transfer is improved. It reduces surface tension by forming oxides on the surface. When surface tension is reduced, droplet size is reduced, and transfer is

improved with a reduction in spatter. However, oxygen reduces the content of the alloying elements by forming oxides.

2.3.2 Shielding Gas Mixtures for Conventional GMAW

2.3.2.1 Effect of Shielding Gas Composition on Fusion Characteristics, Mechanical Properties and Weld Metal Microstructure

Gas metal arc welding (GMAW) was first used around 1925 [36]. It was not until the early fifties that the process was successfully applied to the welding of mild steel.
Since then, the major changes in terms of shielding gases as reported by Salesse [36] are:
1950: Carbon Dioxide
1960: Argon mixtures with 70 to 80% Argon (balance CO_2)
1970: Argon mixtures with 85 to 90% Argon (balance CO_2+O_2)
1985: Argon mixtures with 95% Argon and up
The above changes are also related to the power source improvement. The new generation of power sources provide better control of short circuit transfer mode when welding is carried out e.g. in a carbon dioxide environment. Furthermore, a wide range of welding conditions for different shielding gases and filler wires are also offered by modern power supplies.

Gouda [37] studied the influence of heat input and shielding gas composition on microstructure and properties of GMA weld metal of HSLA-100 steel grade. Single pass deposits were performed with different gas mixtures: pure Ar; 90%Ar10%CO_2; 85%Ar15%CO_2; 80%Ar20%CO_2 and 75%Ar25%CO_2.
They concluded that:
1. Weld heat input slightly increased with the carbon dioxide content in the shielding gas.
2. The oxygen content in the weld metal increased with the carbon dioxide in the shielding gas, while Mn, Si, Al and Ti contents decreased due to oxidation.
3. The microstructure of the weld metal consisted mainly of martenistic and bainitic areas. Bainitic areas increased with the CO_2 content in the shielding gas.
4. Microstructure changes to the weld metal caused by increased carbon dioxide can be attributed to the losses of alloying elements such as Mn, Si, Ti and Al.

A different study was carried out by Ramanathan [38]. They studied the effect of five different shielding gas mixtures on fusion characteristics and weld metal properties of flux cored arc welding. The mixtures tested were: 100%CO_2 ; 20%Ar 80%CO_2 ; 40%Ar60%CO_2 ; 80%Ar20%CO_2. Their investigation has shown that as CO_2 content increased penetration and dilution were improved, while in the case of bead width and bead wetting angle no clear trend is observed. At high CO_2 levels, the levels of oxygen and elemental loss (Mn, Si) both increased. Toughness properties of the weld metal decreased at high CO_2 levels. Optimum toughness was obtained using a shielding mixture of 60%Ar40%CO_2. Beyond this CO_2 content excessive spatter and irregular transfer was reported.
Canto and Machado [39] discussed the influence of shielding gas mixtures on toughness, ultimate tensile strength and elongation of low dilution weld metal deposits

on 15mm thick carbon steel using an open V groove. GMAW was used throughout this work.
Ten different gas mixtures were used: 97%Ar3%O_2 ; 92%Ar8%O_2 ; 73%Ar27%CO_2 ; 60%Ar40%CO_2; 83%Ar2%$O_2$15%CO_2 ; 73%Ar2%$O_2$25%CO_2 ; 100%CO_2 ; 96%$CO_2$4%O_2 ; 85%$CO_2$15%O_2 ; 75%$CO_2$25%O_2.
They arrived at the following conclusions:

1. Shielding gas mixtures affect weld metal microstructure and toughness
2. Mixtures with low oxygen content produced welds with higher toughness due to the presence of acicular ferrite.
3. Tensile properties of the welds produced with the different gas mixtures were almost the same.
4. Deposition rates were not affected by the different gases used.
5. Gas mixtures such as 96%$CO_2$4%O_2 and 85%$CO_2$15%O_2 developed higher penetration than conventional mixtures. This is claimed to be because of strong exothermic reactions.

Grubic and Panic [40] investigated the effects of type of shielding gases upon the weld geometry. Welding trials were carried out on 10mm thick plates of St 52-3 steel grade and 1.2mm diameter as filler wire and using a conventional MAG power source. For statistical data analysis the Design Expert software program package was used. Sixteen different gas mixtures were tested during the welding trials:
100%Ar; 94%Ar6%CO_2 ; 91%Ar9%CO_2 ; 88%Ar12%CO_2 ; 82%Ar18%CO_2 ; 94%Ar6%O_2 ; 91%Ar9%O_2; 88%Ar12%O_2 ; 82%Ar18%O_2 ; 82%Ar6%$CO_2$12%O_2 ; 82%Ar9%$CO_2$9%O_2; 82%Ar12%$CO_2$6%O_2 ; 88%Ar6%$CO_2$6%O_2 ; 94%Ar3%$CO_2$3%O_2 ; 85%Ar12%$CO_2$3%O_2 ; 85Ar3%$CO_2$12%O_2.

The research that they conducted has led to the following conclusions:

1. The greatest depth of penetration is reported for the 82%Ar18%CO_2 gas mixture and the lowest for the 94%Ar6%CO_2.
2. The largest fused area is obtained with the 82%Ar18%CO_2 gas mixture and the smallest fused area with 94%Ar6%CO_2 and 94%Ar6%O_2.
3. When carbon dioxide and oxygen contents increase in the gas mixture, depth of penetration and cross-section of fused area are increased accordingly. The carbon dioxide effect is stronger.
4. A finger shape profile is produced when pure argon or argon mixtures containing 1 to 2% of carbon dioxide are used. Increasing carbon dioxide content produces a wider pattern. These effects are less evident with oxygen additions.

Generally, the mechanical properties reported above (and those in later stages of the present work) are referred to the particular filler wire used with the gas mixture.

2.3.2.2 Effect of Shielding Gas Oxidising Components (Oxygen and Carbon Dioxide) on Mechanical Properties and Arc Characteristics

The effect of the oxidising gas components on the mechanical properties has shown a strong influence on the weld metal [41]. Reducing the CO_2 or O_2 content of the shielding gas, results in reduced formation of oxide inclusions. The microstructure

becomes more fine-grained, with improved impact strength. A lower content of CO_2 or O_2 gives a smaller loss of alloying elements (Si, Mn) which results in higher yield and ultimate tensile stress.

Meyendorf [42] states that the proportion of oxygen partial pressure (in the sum of the partial pressures of the shielding gas components) is suitable for describing the alloy element (e.g. Mn, Si) losses between filler wire and weld metal.

Uygur and Gulenc [43] carried out studies on the effect of shielding gas composition on mechanical properties. Their studies have included the following compositions: 95%Ar5%CO_2; 85%Ar15%CO_2; 70%Ar30%CO_2 ; 91%Ar5%$CO_2$4%O_2 and 83%Ar13%$CO_2$4%O_2.

They concluded that:
1. Fatigue strength is decreased as CO_2 content is increased in the shielding gas.
2. Increasing the CO_2 content increases the tensile strength and decreases the ductility.
3. The composition 70%Ar30%CO_2 had the lowest impact energy. This can be explained because of the high level of the oxygen potential.

Norrish [44] reported that the toughness properties of ferritic steels are improved by increasing the oxidising potential through addition of up to 2% O_2 and 15%CO_2 to the argon shielding gas. However, Francis [45] found that a range between 2 to 4% O_2 and the composition of the wire are critical in achieving high fracture toughness.

The effect of oxygen additions in the argon shielding gas on the arc characteristics has been studied by Jonsson [46]. They concluded that small oxygen additions 2 to 5% have insignificant effects on the arc characteristics corresponding to minor changes in the thermophysical transport and thermodynamic properties caused by the additions of oxygen.
Further experimental observations have shown that additions of oxygen increase weld pool length, width and cross-section as reported by Walsh and Savage [47]. Stenbacka and Persson [48] found that additions of oxygen to 8% or more lead to a firmer attachment of the slag on the surface.

Another important effect of oxygen, as a component in an argon gas composition, is that oxygen can react with alloying elements of the base material leading to oxides in the form of non metallic inclusions. The importance of the presence of these metallic inclusions in striking the arc has been reported by Doan and Myer [49].

The influence of oxygen on the toughness properties and microstructure of the weld metal was studied by Ito [50]on single pass MIG welds deposited in HT50 steel plates 25mm with 50° V grooves. Three different filler wires of 4mm diameter were tested: Si-Mn, Si-Mn-Ti and Si-Mn-Ti-B. They concluded that impact properties are low at both low and high oxygen levels but high at the intermediate oxygen level (Figures 2.12 and 2.13). At intermediate oxygen levels (270ppm) fine accicular ferrite was formed, while at low oxygen levels (60ppm) bainitic microstructures were formed, and at high oxygen levels grain boundary ferrite and ferrite side plates were reported.

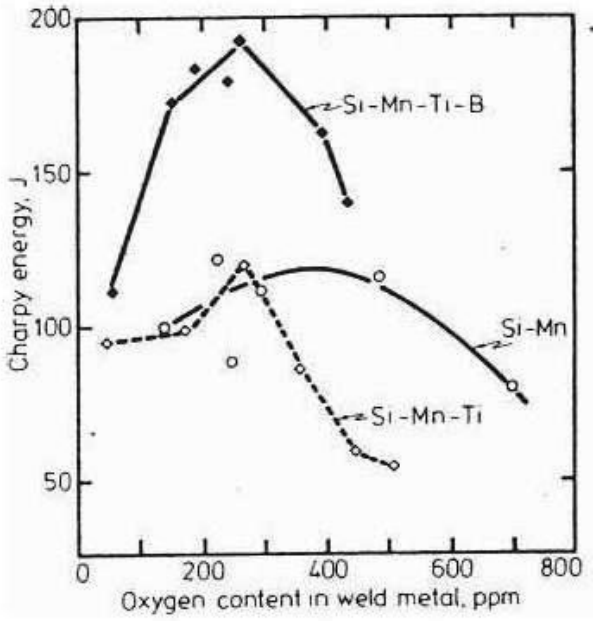

Fig. 2-12 Effect of oxygen content on Charpy absorbed energy [50]

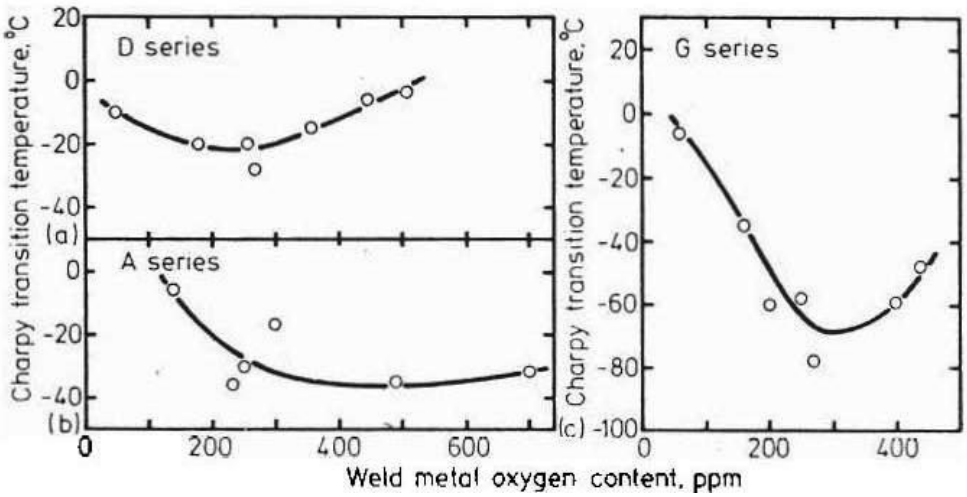

Fig. 2-13 Effect of oxygen on weld metal notch toughness: a) Si-Mn; b) Si-Mn-Ti; c)Si-Mn-Ti-B [50]

The strong relationship between weld metal oxygen content, acicular ferrite content, and toughness properties was confirmed by Onsoien [51]. Welds were deposited in a 60° V-groove in ASTM A737 Grade B steel plate using three different filler wires: ER 70S-3, ER70S-6 and ER70S-7. The weld metal acicular ferrite content in relation to the shielding gas oxygen content is shown in both Figures 2.14 and 2.15. Both plots lead to almost identical conclusions that a shielding gas oxygen equivalent of two to three volume percent gives the highest content of acicular ferrite in the weld metal.

Figure 2.16 also confirms the strong interrelation between weld metal microstructures and toughness properties. The Charpy 35J transition temperature reached a minimum level when the shielding gas oxygen equivalent was around two to three volume percent corresponding to welds with the highest amount of acicular ferrite. The oxygen equivalent was defined as follows:

$[\text{Oxygen Equivalent}]_{\text{Shielding gas}}=[\text{Effective Oxygen Content}]_{\text{Shielding gas}}=$
$-0.088+0.148[CO_2]^{1.524}{}_{\text{Shielding gas}}$

Similarly Potapov [52] reported 200ppm to 300ppm O_2 content in the weld metal as the optimum level for good toughness properties. However, results showed that weld hardness is decreased when shielding gas oxygen content is increased. This is due to the loss of hardenabillity elements such as Mn and Si.

Schumann [53] reviewed the literature regarding the relationship between acicular ferrite and toughness and reported that the optimum level of cleavage resistance is at about 90% acicular ferrite.

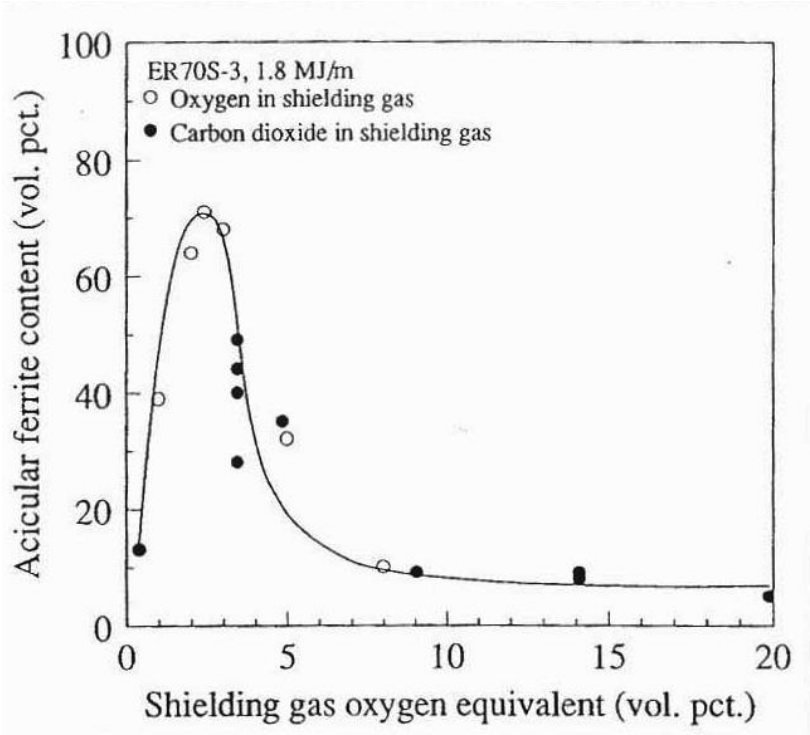

Fig. 2-14 Weld metal acicular ferrite (AF) content as a function of shielding gas oxygen equivalent (ER70S-3, 1.8kJ/mm) [51]

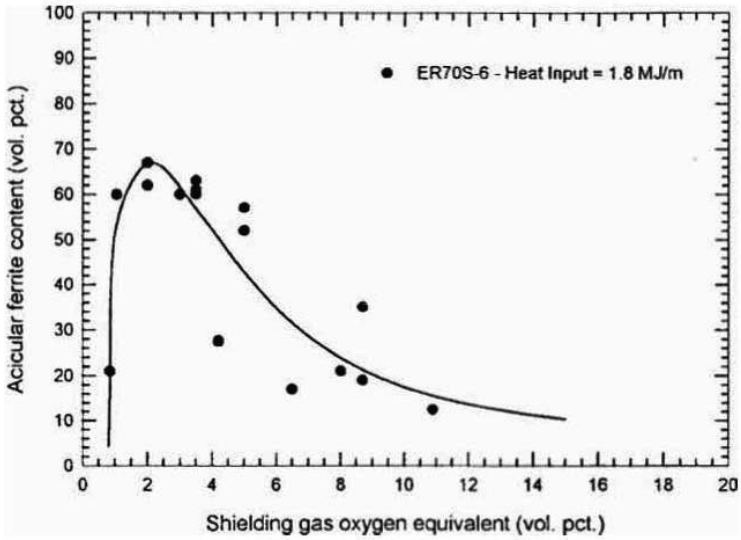

Fig. 2-15 Weld metal acicular ferrite (AF) content as a function of shielding gas oxygen equivalent (ER70S-6, 1.8kJ/mm) [51]

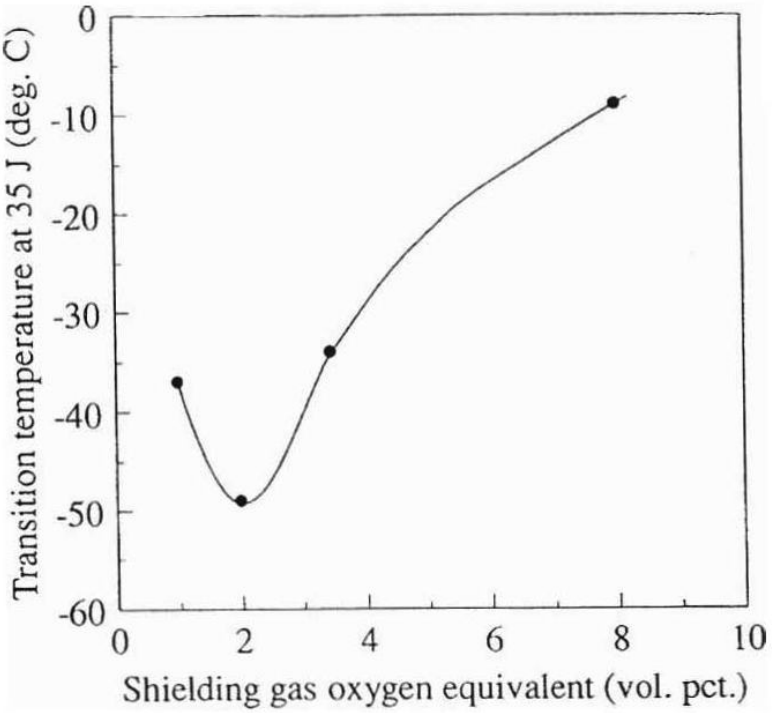

Fig. 2-16 Weld metal Charpy V-notch toughness expressed as transition temperature at 35J as a function of shielding gas oxygen equivalent [51]

However, Gianetto [2] reported good toughness properties on X100 girth welds (120J at -80°C) associated with fine martensitic/bainitic structures formed within the grain interiors. Contrarily, the weld metal toughness properties of X70 girth welds were attributed to the presence of high proportions of acicular ferrite presented in the weld metal.

Studies on the effect of oxygen content in the shielding gas on the microstructure of GMAW microalloyed HSLA steels have been carried out by Francis [45].The gas/metal reactions were studied to determine the effect of shielding gas composition on the weld metal composition. They concluded that oxygen activity, as determined by the oxygen or carbon dioxide content of the cover gas, has an influence on the weld metal oxygen content. Increasing the oxygen activity of the shielding gas resulted in weld metal oxygen increase.
Finally Lucas [54] has found that oxygen promotes low contact angle of the workpiece by the weld pool.
A low contact angle (θ, Figure 2.17) is desirable in order to achieve good wetting conditions.

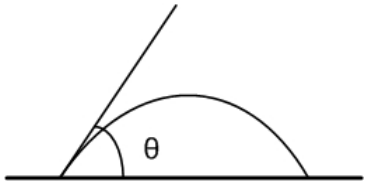

Fig. 2-17 Definition of θ, the contact angle

2.3.3 Shielding Gas Mixtures for PGMAW

2.3.3.1 Effect of Gas Composition on Fusion Characteristics, Mechanical Properties and Microstructure

For the case of mild steel welding Melmoth-Bennett [55] suggested gas mixtures of Ar/CO_2 with small quantities of oxygen. These provide higher welding speeds, less spatter, improved surface appearance and improved metal transfer over conventional dip transfer. The proposed gas mixture is 93%Ar5%$CO_2$2%O_2.

Foote [56] compared 95%Ar5%CO_2, 80%Ar20%CO_2, 46%Ar52%$CO_2$2%O_2, 99%Ar1%O_2 in pulsed welding. He found that 95%Ar5%CO_2 gives a smoother arc than 93%Ar5%$CO_2$2%O_2. Fusion characteristics were reported as almost identical.

Allum and Quintino [57] investigated the effect of shielding gas composition on fusion characteristics. The gases tested were: 99%Ar1%O_2, 98%Ar2%O_2, 95%Ar5%CO_2, 80%Ar20%CO_2, 100%CO_2 and 75%He23%Ar2%CO_2. They reported that bead profile in terms of contact angle depends on arc voltage. By increasing the oxygen levels in the shielding gas the contact angle is decreased. The greatest penetration is obtained by the 95%Ar5%CO_2 and 99%Ar1%O_2 mixtures. Increasing the CO_2 and O_2 levels to 20% and 2% respectively has an adverse effect on penetration. They concluded that the best result is obtained with the mixture 95%Ar5%CO_2.
Urmston [58] tested the following gas mixtures: 95%Ar5%CO_2;93.2%-93%Ar5%$CO_2$1.8%-2%O_2;77.8%-78%Ar20%$CO_2$1.8%-2%O_2;70%Ar30%He; 50%Ar50%He;30%Ar70%He;81.5%He15%Ar1.5%$CO_2$2%O_2;38%He60%Ar2%O_2. He reported that bead width increases and reinforcement height decreases with increasing helium content. This is due to the high ionisation potential of helium which leads to a hotter arc than argon. As a consequence of the higher heat input, weld pool fluidity

increases and therefore bead width increases and reinforcement height decreases. A similar trend is found with 93.2%-92.8%Ar5%$CO_2$1.8%-2.2%O_2, 78.2%-77.8%Ar20%$CO_2$1.8%-2.2%O_2 and 95%Ar5%CO_2 although a greater spread of reinforcement height with 95%Ar5%CO_2 was reported. Welding tests have shown that fusion area increases with an increase in the ratio of helium to argon in the shielding gas. Again, this is due to the high ionisation potential of helium. The same tests also have confirmed that there is an increased heat input corresponding to higher active content. This can be attributed to the dissociation of the CO_2 increasing the heat input.
Weld profile analysis has shown that the tendency to finger penetration decreases with increasing helium and active gas additions. This is explained on the basis that when a gas has a high thermal conductivity, the heat is conducted outwards from the centre to the edge of the arc.

2.3.4 Shielding Gas Mixtures for Pipeline Welding

Dorling [59] examined the fusion characteristics of shielding gas mixtures on thick-section steels (CSA Z245.1 Grade 483) with typical application in offshore structures and pipelines; using mechanised PGMAW. Bead on plate and bead in groove welds were carried out. The mixtures tested were: 95%Ar5%CO_2, 80%Ar20%CO_2, 88%Ar10%He2%CO_2 and 87.5%Ar10%He2%$CO_2$0.5%H_2 with eight welding wires with varying alloying and microalloying additions.(C-Mn-Si ; LowC-Mn-Si ; C-Mn-Si-Ti ; C-Mn-Ti-B ; C-Mn-Ni ; C-Mn-Ni-Ti ; C-Mn-Mo ; C-Mn-Mo-Ti) The selection of H_2 as a constituent of the shielding gas mixture was based on previous findings by Bicknell and Pickett [60]. They found that, when this hydrogen gas mixture is used in PGMAW mode, lateral stability of the arc is improved and uneven or preferential penetration to one side is reduced.
The above experiments showed that depth of penetration and dilution are increased when welding with 95%Ar5%CO_2, 88%Ar10%He2%CO_2 and 87.5%Ar10%He2%$CO_2$0.5%H_2, relative to 80%Ar20%CO_2. The hydrogen-containing shielding gas appeared to eliminate lateral “wandering” of the central finger penetration. Another interesting conclusion in terms of mechanical properties (e.g. Charpy, CTOD) was the need to establish a balance between wire consumable and shielding gas composition.

Thompson [6] carried out a further study on the influence of shielding gas composition on mechanised PGMAW of arctic and offshore structures and pipelines. Bead in groove welds were carried out and metallurgical properties fusion characteristics and process parameters were evaluated. Shielding gas mixtures were selected (for 0.9mm C-Mn-Si-Ti wire) based on the following sequence criteria:

a. Investigate the preferred Ar-He ratio through an analysis of the effect of variations of He in Ar-He-CO_2 mixtures on fusion characteristics while maintaining an acceptable metal transfer and arc stability. The optimum gas oxygen potential was established by investigating the effect of carbon dioxide variations of Ar-CO_2 mixtures on weld metal properties.
b. Using the preferred Ar-He ratio as the base mixture, to investigate the effect of O_2 and H_2 additions on fusion characteristics while maintaining desirable metal transfer and arc stability.

Weldment analysis confirmed the following conclusions:

1. Toughness properties of the weld metal are affected by the oxidation potential of the shielding gas.
2. Fusion characteristics are affected by the addition of Helium (Figure 2.18). As an example lateral fusion (Figure 2.19) is improved by 60% when a mixture of 82.5%Ar12.5%$CO_2$5%He is used compared to 0% helium content when welding in vertical down.
3. Addition of 0.5% hydrogen does not affect fusion characteristics and arc stability.
4. Oxygen additions of more than 1% to the 82.5%Ar12.5%$CO_2$5%He base composition, result in sidewall undercutting in the narrow gap preparation. No benefit to fusion characteristics and arc stability is noticed.
5. The combination of C-Mn-Ti-B/82.5%Ar12.5%$CO_2$5%He wire/shielding gas is appropriate for the qualification of 1067mm O.D 19mm W.T., Grade 483 pipe.

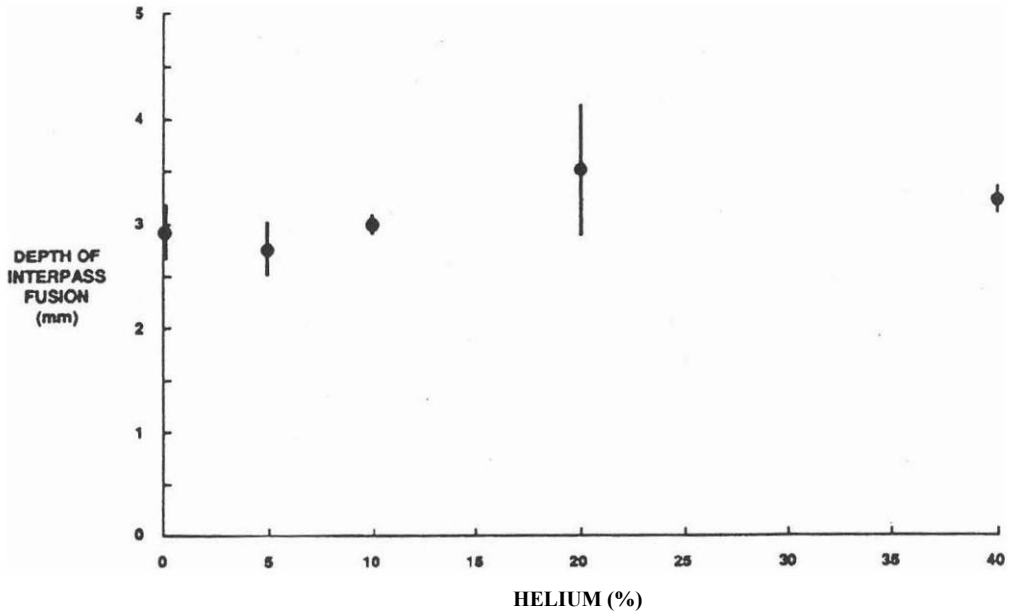

Fig. 2-18 Effect of helium on narrow gap interpass fusion [6]

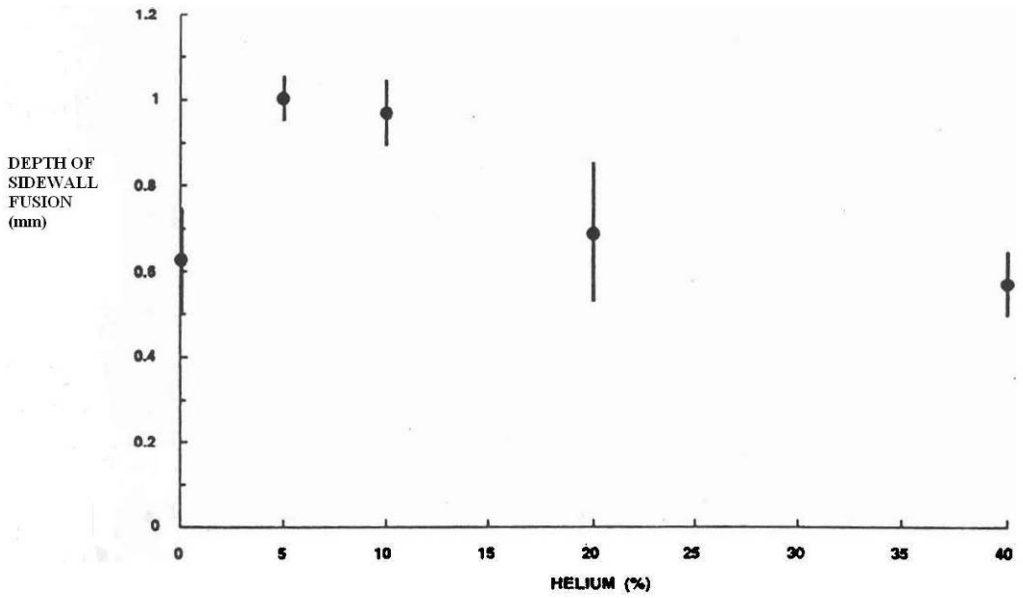

Fig. 2-19 Effect of helium on narrow gap sidewall fusion [6]

The benefits of trimix shielding gas mixture (82.5%Ar12.5%$CO_2$5%He) for mechanised field welding of large diameter X80 pipelines with narrow gap preparation is confirmed by Laing [61].

Brun [62] investigated the weldability of consumables available for X80 and X100 pipeline, the difference between GMAW and PGMAW and the difference between shielding gases for PGMAW.
Three shielding gas compositions were tested for these purposes:

a. Argoshield 5 (93.2%Ar5%$CO_2$1.8%O_2),
b. Argoshield 20 (78.2%Ar20%$CO_2$1.8%O_2) and
c. Trimix (82.5%Ar12.5%$CO_2$5%He).

Groove welds (30 V-bevel) in 40mm of 50D steel grade plate (BS 4360) and bead on X100 pipe welds were carried out. It was observed that the trimix mixture improves arc stability as compared to the other two mixtures (Argoshield 5 and Argoshield 20). The different gas mixtures used for pulsed conditions seemed not to affect the hardness values as the difference between them was less than 10HV10 points. Hardenability in the pulsed conditions showed values almost 15HV10 higher than in the non-pulsed conditions.
Some other important conclusions are:
-Pulsed GMAW produces a noticeable reduction in spatter.
-Toughness values in pulsed condition are significantly increased compared to non-pulsed.

Norrish [63] investigated the optimum shielding gas mixtures for pulsed MAG welding of line pipe. The range of shielding gases selected was as follows:

95%Ar5%CO_2 ; 92%Ar8%CO_2 ; 85%Ar15%CO_2 ; 80%Ar20%CO_2. These mixtures were tested with four different filler wires. Bead on plate and bead in grooves of 15mm X65 plate were carried out.
Results showed the following:

a. The 85%Ar15%CO_2 mixture gives the best arc stability, fusion characteristics and weld metal toughness.
b. Modified power sources allow increasing carbon dioxide to higher levels.

Green and Stares [64] conducted investigations on the effect of shielding gas mixtures in pulsed GMAW of carbon and low alloy steels. In their research programme carbon dioxide varied between 0% and 20%, oxygen between 0% and 8% and the balance was made up by argon.
They evaluated the performance of the different gas mixtures based on the following:

a. Arc stability characteristics
b Fusion characteristics
c Industrial joint evaluation (automatic H/V fillets and manual vertical butt welds).

For the fusion characteristics an image analysis system was used. Penetration area, bead or reinforcement area, bead width, weld depth, penetration depth, minimum depth and wetting angle were measured.
Penetration profile was evaluated using the parameter called Profile Index. This is the ratio between the minimum depth to the penetration depth (Figure 2.20).

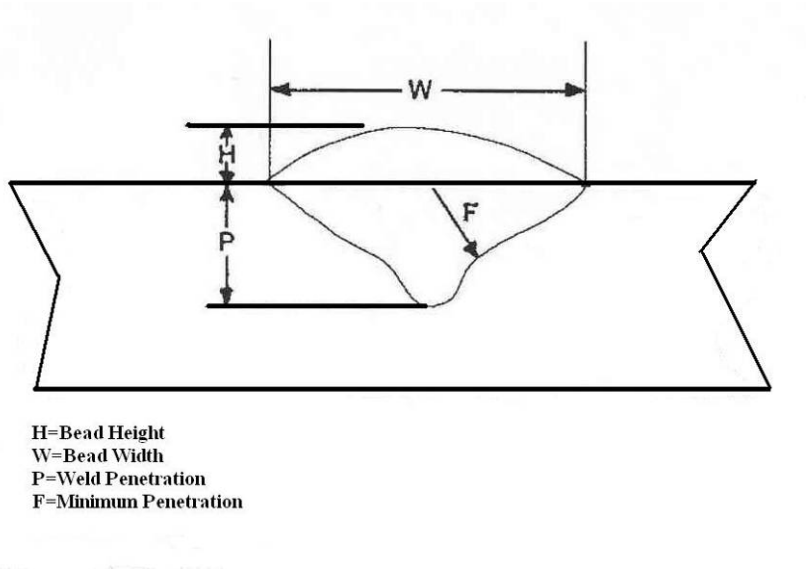

Fig. 2-20 Definition of profile index [64]

This provides a measure of the finger-shaped penetration that occurs in the weld metal with a given shielding gas. The minimum penetration is the shortest distance to the weld fusion zone boundary. If the above ratio exceeds or equals 1, then the profile tends to be semicircular; if the ratio is less than 1, then the weld cross-section tends to be finger shaped.
Their main conclusions were:

a. The power source characteristic has a major effect on the performance of the shielding gas.

b. For good process stability a certain level of oxidising components is required.
c. By increasing the oxidising components of the shielding gas, process stability, penetration characteristics, and bead appearance are improved. This occurs up to a certain level of oxidising components. Bead profile deteriorates if oxidising components are increased further.
d. Mixtures of Ar / O_2 did not produce acceptable welds.
e. Ternary mixtures Ar/CO_2/O_2 give better welding performance (stability, penetration characteristics etc) than Ar/CO_2 or Ar/O_2.
f. The gas mixtures that perform best overall were 90%Ar8%$CO_2$2%O_2 to 12%$CO_2$2%O_2.

Modenesi [4] studied the effect of helium content in Ar-He-2%O_2 mixtures on weld bead characteristics. He welded bead-on-plate and narrow gap specimens (mild steel) in flat and horizontal vertical position using pulsed current. He found that axial penetration area in both narrow gap and bead-on-plate trials increase with %He in the shielding gas. Additionally, in the analysis of the effect of the welding parameters on the weld bead geometry, he concluded that helium based shielding gas mixtures tend to increase lateral penetration (Figure 2.21) while no significant improvement is associated with carbon dioxide contents for argon based shielding mixtures.

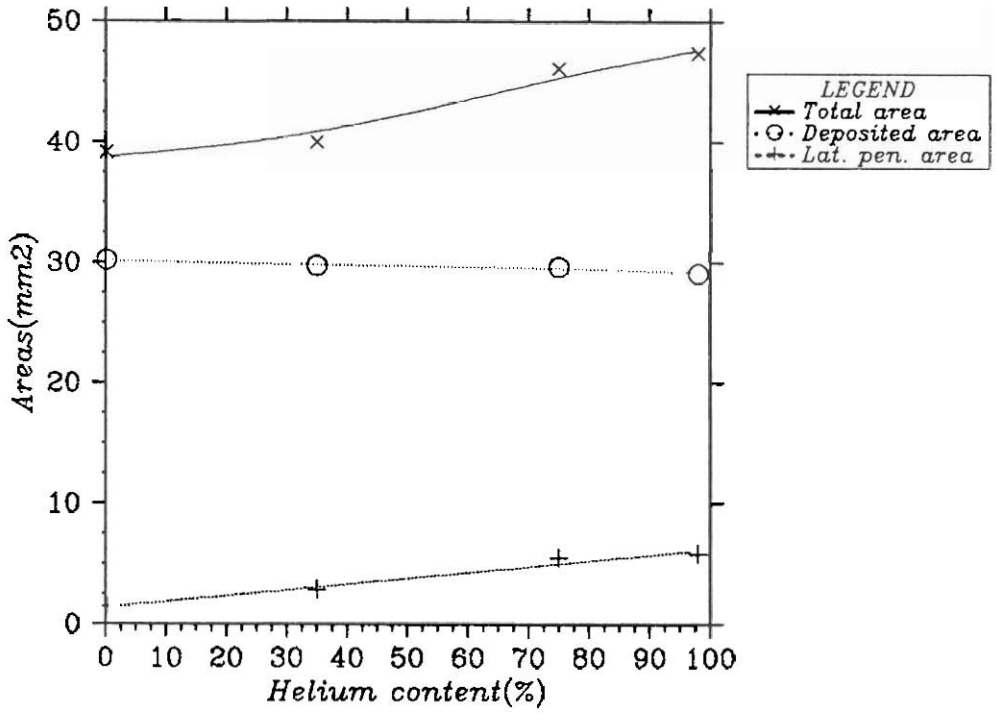

Fig. 2-21 Effect of Helium content in the shielding gas on bead characteristics of narrow gap welds [4]

However, pipeline contractors have developed and qualified welding procedures for pipeline steels using two gas components (Ar/CO_2) as shielding gas in dip transfer [65]:
1. Welds were carried out on X70 and X80 pipeline steels. For the root pass a gas mixture of 75%Ar25%CO_2 was used while for all fill passes 100% CO_2 was

used. All completed welds were tested and showed very good mechanical properties: e.g. weld metal Charpy V-notch (at -5°C) greater than 100J, heat affected zone Charpy V-notch greater than 200J; hardness levels in the heat affected zone between 219-238HV10 and in the weld metal between 220-245HV10

2. Similarly, welds were qualified on X70 pipeline steels using 50%Ar50%CO_2 as shielding gas and again showed very good mechanical properties (e.g. hardness in the heat affected zone 187-212HV10, and in the weld metal 205-221HV10).

Recently (Feb. 2004) field implementation of tandem pulsed GMAW on a 2km length of X100 pipeline steels was carried out [66]. The shielding gas mixture used was 85%Ar15%CO_2 and welding procedures were qualified and showed very good mechanical properties (e.g. CTOD results were between 0.2mm to 0.26mm at -10°C testing temperature).

Despite the relatively low effect of the shielding gas cost (section 2.1.1) on the overall welding cost, it is important to emphasise that a two gas composition (e.g. Ar/CO_2) will further contribute to the cost reduction compared to three (e.g. Ar/CO_2/He) or four gas mixtures (e.g. Ar/CO_2/He/O_2), subject to acceptable transfer mode and mechanical properties being achieved. It should also be noted that it may be difficult to source complex mixtures in remote locations.

2.3.5 Summary

A review of the properties of the main constituents of the shielding gas mixtures used in welding and in particular in pipeline steels is presented.
The literature [44],[32] confirms that shielding gas mixtures rich in argon present a "finger" weld bead profile in contrast to the bowl profile associated with carbon dioxide rich gas mixtures.
The present review is mainly concerned with the effect of the shielding gases on the weld bead geometry (i.e. depth of penetration, sidewall penetration etc) and with their effect on process stability.

Most of the authors [37],[38],[39],[41],[43]reported that an increase in the oxygen and carbon dioxide contents of the shielding gas composition produces a decrease in both the alloying elements (Mn, Si, Al, Ti) and the toughness properties of the weld metal. However, Norrish [44] reported that toughness properties of the ferritic steels are improved by adding up to 2%O_2 and 15%CO_2 in the shielding gas.

The effect of the oxygen in the GMAW process is mainly associated with the benefits arising from promoting the wetting contact angle [54] and in reducing the surface tension [67],[46],[44] found that the addition of 1% to 2% oxygen improves arc stability although Jonsson [46] concluded that oxygen additions of 2% to 5% have an insignificant effect on the arc characteristics.
The significant influence of the oxygen content (in the shielding gas composition and also in the weld metal content) on the mechanical properties such as toughness and hardness and on the weld metal microstructure has been clearly established [51],[50].

Regarding the weld bead geometry, Ramanathan [38] found that penetration improves with an increase in the carbon dioxide content. Grubic [40] obtained similar results although depth of penetration and cross section of the fused area increase when both carbon dioxide and oxygen increase, but the effect of carbon dioxide is more apparent. However, Quintino and Allum [57] reported an adverse effect on penetration by increasing the levels of carbon dioxide.

Urmston [58] in his experimental work concluded that fusion area increases with an increase in the ratio of helium to argon in the shielding gas.
Finally, the effect of shielding gas composition on GMAW of onshore pipeline is reviewed.

The main reference is the work reported by Thompson [6]. Among the conclusions, the most important is the considerable (60%) increase of the lateral fusion with the addition of He in the 82.5%Ar12.5%$CO_2$5%He mixture. Furthermore, oxygen at more than 1% produces sidewall undercutting in the narrow gap preparation.

In an earlier stage of his research, Dorling [59] tested different compositions of Ar/CO_2, Ar/He/CO_2, Ar/He/CO_2/H_2 and concluded that mixtures with lower carbon dioxide content produce better penetration than the mixture 80%Ar/20%CO_2. Norrish [63] tested different percentages of Ar/CO_2 and concluded that the 85%Ar15%CO_2 mixture gives the best results.

Recent welding procedures [65] have been developed for X70 and X80 linepipe steel grade and successfully qualified using Ar/CO_2 mixtures in dip transfer. Furthermore, for the first time tandem pulsed GMAW using as shielding gas the 85%Ar15%CO_2 composition was carried out on a X100 steel grade pipeline installation [66]. All the mechanical properties of the weld metal were considered very good and acceptable in accordance with the applicable standards.
Brun [62] confirmed that weld metal toughness was dramatically higher for pulsed GMAW compared (for the same filler wire) to conventional GMAW using the trimix (82.5%Ar12.5%$CO_2$5%He) gas mixture. He attributed this result to the lower oxygen potential of the shielding gas.
A review of the results from the work of other authors shows some disagreements in their conclusions. There can be a number of reasons for these discrepancies including:
-no systematic approach in the study of the process,
-the results covered a limited range of gas compositions,
-no optimisation of the welding parameters for the specific shielding gas composition tested,
-different power supplies used with different characteristics,
-the changes in the arc length were not considered for the different shielding gases.
It was concluded therefore, that for the purpose of the present study all these factors would have to be carefully controlled.

The conclusion from the work performed by Thompson that 82.5%Ar12.5%$CO_2$5%He is the optimum shielding gas mixture, has dominated the subsequent work carried out at Cranfield [1],[18],[68]. Most of the work presented here on tandem and dual tandem procedure development was performed using the same shielding gas mixture. The

reasons for this selection were attributed to the reported fusion characteristics, the arc characteristics and the mechanical properties.
Summarising the effect of the gas mixtures in the weld bead geometry reported in the literature can be concluded that:

- increasing the carbon dioxide content causes an increase in depth of penetration
- increasing the helium content causes an increase in sidewall penetration
- increasing the oxygen content reduces surface tension and increases wetting contact angle.

Nevertheless, a systematic approach to the study of the gas composition effects on the weld bead geometry of high strength steel (X100) narrow gap welds in tandem welding has not been undertaken so far. Furthermore, the use of the new generation of power sources (TPS Fronius 4000 thermo) was expected to improve transfer mode and arc characteristics.
It was decided, therefore, to study the performance of the different gas mixtures on the weld profile and to confirm the use of the 82.5%Ar12.5%$CO_2$5%He composition or to propose an alternative able to produce better results.

2.4 Welding Parameter Effects on Weld Bead Geometry

2.4.1 Introduction

There have been numerous attempts to successfully describe and predict the weld bead geometry and size since welding processes were originally carried out. Studies concentrated on correlating the experimental data with the resulting weld profile.
Despite the initial lack of success arising from difficulties in dealing with the significant number of variables (welding parameters) and their interrelations, the improvement in computing power has allowed the analysis of this complex data to be achieved.

2.4.2 Modelling

A model is a representation of a system, Cross and Moscardini [69] proposed five main steps in building a mathematical model:

1. system understanding,
2. design,
3. optimisation,
4. control,
5. training.

Several studies on the interrelation between input parameters (welding current, welding voltage, welding speed, shielding gas composition etc) and output parameters (weld profile, weld size, weld mechanical properties etc) have concentrated on the mathematical modelling of the weld bead geometry.
McGlone [70] reported three main categories of mathematical models:

a. Theoretical approach,
b. Qualitative approach,
c. Empirical approach

Modenesi [4] who carried out research on GMAW narrow groove welding referred to the theoretical and empirical approaches.
Other approaches at modelling the weld bead shape will be included in the present review.

2.4.2.1 Theoretical Approach

Theoretical models have been developed to predict the weld bead profile mainly based on the work carried out by Rosenthal [71] who studied the heat dissipation (by conduction) of a moving heat source on an infinite plate. However, the following simplifying assumptions were made:
-the heat source was considered as a point source,
-heat losses through the surface of the parent material to the surrounding atmosphere were neglected compared to the heat flow in the parent material,
-heat generated by the joule effect was ignored due to the heat of the arc,
-the physical characteristics of the parent material remain constant.

Christensen [72] adopted Rosenthal's theory of travelling point source but modified the results in a non-dimensional form in order to extend the studies over a wide range of materials and heat inputs.

Eagar and Tsai [73] expanded the theory of the heat travel source from a point to a distributed heat source but with simplifying assumptions of absence of convective and radiant flow, constant thermal properties and a quasi-steady state semi-infinite medium. They claimed that the model proposed can be used to assess how modifications in the process can influence the weld bead geometry.
Although Rosenthal did not directly relate heat dissipation theory to the weld bead geometry, his work has been used as the basis for future investigations.

The Rosenthal model did not consider fluid flow in the weld pool or phase changes, both of which may have an important role in the final shape of the weld pool. Studies [74] in the mechanism of minor elements effects on the GTAW fusion geometry have shown:
-radial outward surface fluid in welds rich in aluminum and radial inward surface fluid in sulphur presence,
-significant changes in fusion zone shape with the addition of small amount of elements such as aluminum or selenium.

Oreper [75] confirmed the work of Heiple and Roper [74] and emphasised that significant convection (convective heat flow) exists in the weld pool due to the combination of surface tension, electromagnetic and buoyancy forces, with the surface tension forces being the dominant in many instances. The model developed predicts the shape and the penetration of the weld pool in a qualitative way.

Nunes [76] attempted to incorporate the effects of the liquid metal flow and phase changes by introducing higher order poles in the moving heat source described by Rosenthal [71]. While the monopole (Rosenthal) heat source model represents the power flow in the workpiece, the higher order poles represent flow from one point to

another within the weld. As described above, in the non consumable process (i.e. GTAW) the penetration is affected by the flow of the weld pool caused by the action of the surface tension, buoyancy and electromagnetic forces. In GMAW where a consumable electrode is used, penetration is affected by the momentum that the droplets carry into the weld pool [77],[34] and the heat content transferred by the molten metal droplets influences the total cross-section area of weld penetration [77].
A mathematical model developed by Tsao and Wu [78] attempted to estimate the effect of the field caused by the electromagnetic forces, the velocity field and the temperature field in gas metal arc welding pool configuration. They found that the distinct finger penetration associated with the GMAW process (particularly for spray transfer) is due to the heat transferred into the weld pool through the high frequency molten droplets. As the frequency increases deeper weld pools are obtained.

Kim and Na [79] studied the three-dimensional heat transfer and fluid flow in gas metal arc welding for analysing the effect of the contact tip-to-workpiece distance on the weld pool shape by considering the electromagnetic, buoyancy and the surface tension forces together with the effect of the molten electrode droplets. However, the effect of the droplet impact on the surface deformation was ignored. They concluded that the convective motion in the weld pool plays an important role (more heat transfer from the heat source to the weld pool root) in the finger shape penetration in gas metal arc welds instead of a round profile obtained if the only conductive flow is considered, and they verified the importance of the molten electrode droplets on the motion of the weld pool and the effect on depth of penetration. They reported that by increasing the contact tip-to-workpiece distance arc length increases, the weld bead becomes wider and bead reinforcement is reduced.

Cao, Yang and Chen [80] developed a 3-D thermo fluid weld pool model considering the heat transfer and fluid flow determined by surface tension, electromagnetic, buoyancy and arc pressure forces. Among their conclusions they found that the metal droplet impact is the primary force promoting penetration, and in combination with the tension gradient force causes the finger penetration, while the tension gradient force only controls weld bead width.
The combined effect of droplet heat input and impact force contribute to finger type penetration in gas metal arc welds was reported by Cao and Dong [81]. A three dimensional weld pool model was proposed to study the fluid flow and heat transfer process.

2.4.2.2 Empirical Approach

Empirical models rely on mathematical expressions that adequately fit the data of a systematic experimental approach and study the relationships that occur between the welding process parameters and the weld bead profile.
This approach is widely used in the studies of submerged arc welding and this can be explained by the fact that the range of operation of the welding variables is wide enough to generate clear relationships between variables and responses (e.g. weld profile) [82].
In the 70's Lutsenko [83] determined the weld bead geometry (weld width, penetration etc.) in CO_2 gas metal arc welding using a parameter which characterised the arc pressure: $P=(I^2 / de)*v10^{-4}$ A^2/s (I is the current, d_e is the wire diameter and v is the

welding speed). He obtained graphs of the variation of the specific seam width (B_0), depth of penetration (H_0) and height of seam reinforcement (h_0) in relation to arc pressure parameter variations.
Quintino [84] proposed a model of the dilution in PGMAW in mild steel based only on the conduction heat effect while convection and radiation were neglected. It was concluded that for given material factors (plate, filler wire and shielding gas) the dilution is expressed as a function of the quantity I_m* v, where I_m is the mean current and v is the welding speed. A chart of the fusion characteristics of pulsed arc welding (Figure 2.22) was proposed.
Generally, regression models have been very popular in order to study the relationships between the welding parameters and the weld bead shape. However, their use is limited to the specific case for which they were built (e.g. specific range of welding parameters, process etc.).

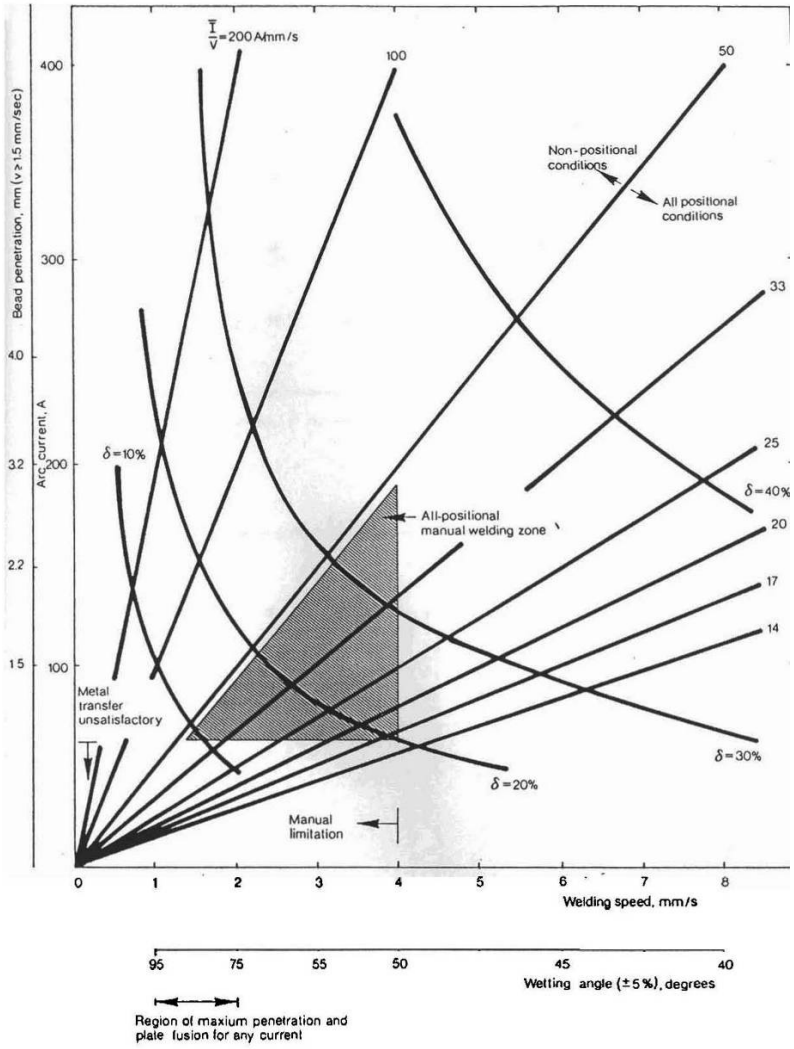

Fig. 2-22 Representation of fusion characteristics in pulsed welding [84]

Raveendra and Parmar [85] developed mathematical equations to predict penetration, weld width, reinforcement height, width to penetration ratio and percentage dilution in CO_2 shielded flux cored arc welding.
Harris and Smith [86] obtained equations to predict weld bead width, height, hardness and dilution while Modenesi [4] obtained regression equations to describe bead geometry, dilution, undercut and lack of fusion in narrow gap gas metal arc welding in flat and horizontal-vertical positions.
Absi Alfaro [87] and Paranhos [88] determined regression equations to describe the weld bead profile in narrow gap SAW.

2.4.3 Experiment Approaches

Different approaches have been developed in order to generate relationships between process parameters and weld profile:

2.4.3.1 One Variable at a Time Approach

In this approach the value of the response is determined for a particular combination of factors and after that the factors are altered one-at-a-time while all the others are kept constant at their initial values [89].
Two serious drawbacks can be attributed to the above approach:
-no estimation of the experimental error,
-no estimation of the factor interaction effects.

2.4.3.2 Tolerance Box Approach

This is a graphical based approach. It starts with a relatively high number of experiments and determines an area where the welding parameters produce acceptable welds. Its main limitations are in representing the results when more than two variables are used as input, and the high number of experiments required to build the acceptable welds area.
Figure 2.23 [90] graphically shows an example of this technique. Briefly, the experimental technique can be described as follows:
Butt weld roots were carried out in flat plates in different positions to simulate the pipe girth welds (Figure 2.23a) and welding parameters were determined for the different positions. Three electrode diameters and five root faces were used in this investigation to assess the minimum and maximum root gaps tolerable in each position. This was achieved by making welds with small increments in the root opening. The optimum data (Figure 2.23b) for the 0.9 diameter electrode was obtained. In addition, the misalignment effect was superimposed (Figure 2.23c).

2.4.3.3 The “Arcwise” Approach

The “Arcwise” approach was developed by Edison Welding Institute and has been used since 1996 [91]. It is a systematic approach which provides a data set that relates welding parameters with productivity and weld quality [91].

The typical characteristic of the method is that all welds are carried out at constant ratio of deposition rate to weld speed and therefore the deposited area is kept constant and consequently the effect of arc length or shielding gas composition can be evaluated.
The method is composed of five components [91]:
-weld size and acceptance criteria,
-constant deposit area,
-constant arc length tests,
-weld bead shape measurements,
-voltage-current and voltage-wire feed speed (process characteristics), current-wire feed speed and heat input-deposition rate graphs (productivity windows). Each graph is plotted as a function of the arc length.
A typical example of the technique (parametric graphs) in the case of a 6.35mm fillet weld using a GMAW process is shown in Figure 2.24

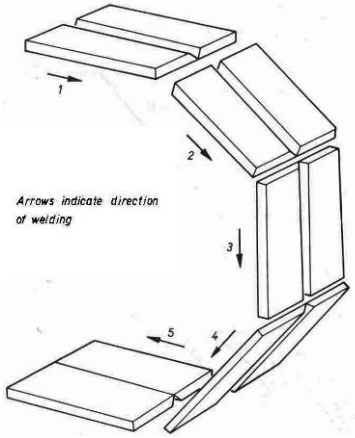

a

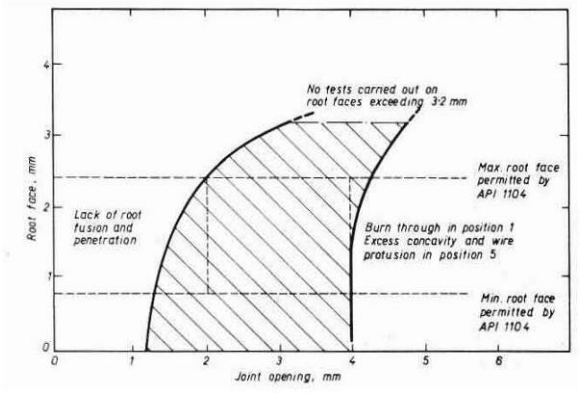

b

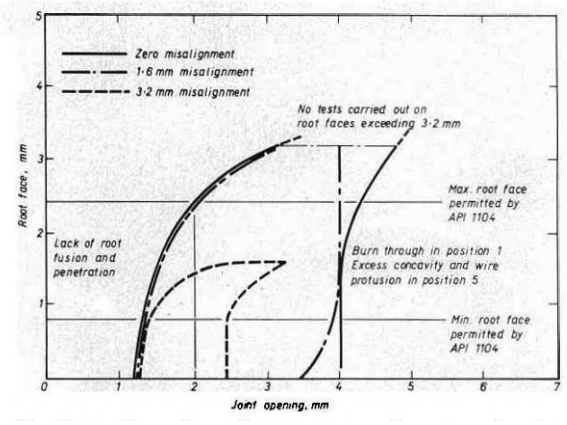

c

Fig. 2-23 Positions (a) for plate butt welds to simulate the pipe girth weld, (b) the limiting values of root opening and (c) limiting values of root opening with different levels of root misalignment [90]

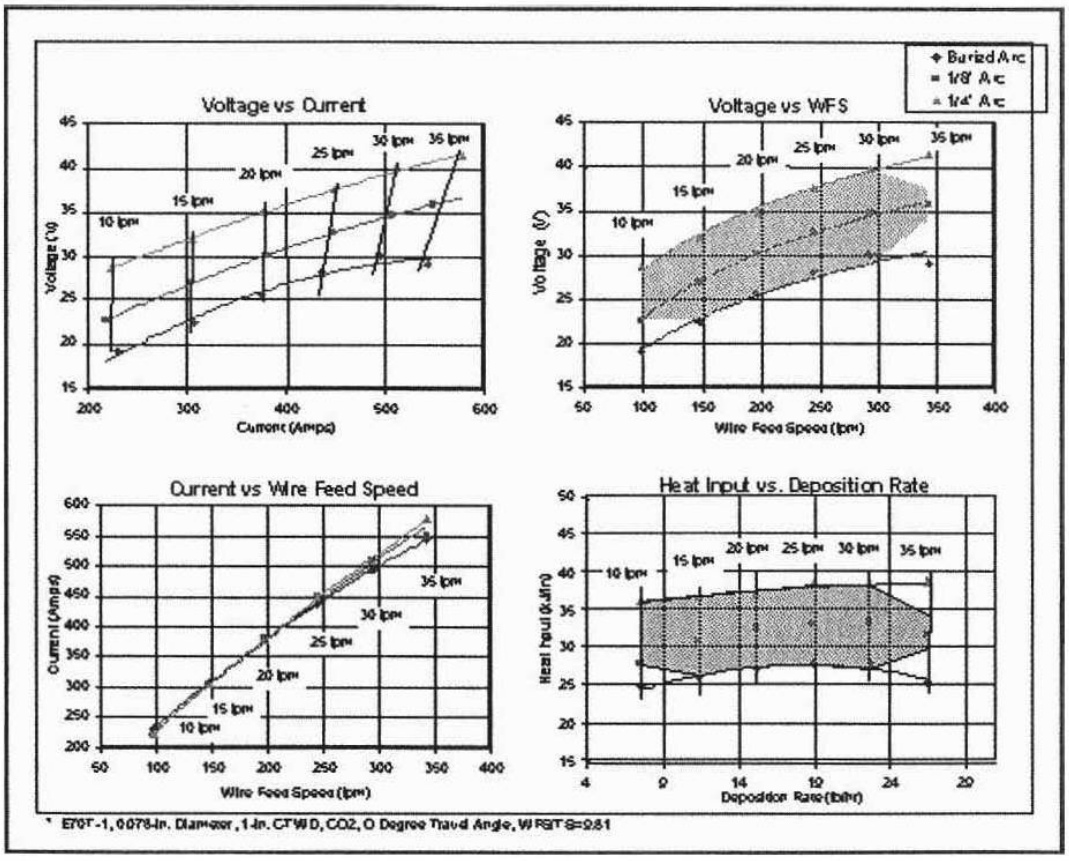

Fig. 2-24 Parametric graphs for 1/4 in fillet welds using GMAW process in fillet welds [91]

2.4.3.4 Statistical Approach

The statistical techniques and the statistically designed experiments can successfully be applied when the effects (responses) investigated can significantly be influenced by experimental error (variability not explained by known influences). Statistical analysis can also provide measures of precision [92]. Factor interaction effects are also considered. A brief description of the statistical design and analysis of experiments and of applications in welding will be given below.

2.4.4 Statistical Design of Experiments

Statistical design of experiments is the process of planning a series of experiments, so that appropriate data can be collected and analysed by statistical methods. There are two aspects associated with an experimental problem:

- the design of the experiment and the statistical analysis of the data obtained after the experimental analysis,
- the application of techniques in order to minimise the experimental error and maximise the precision of the results [93],[94] as follows:

- **replication**

Replication is the repetition of one or more experiments of the experimental group. Two important properties are associated with replication:

a estimation of the experimental error,

b consideration of the mean value of a factor in the evaluation of the factor effect on the process. Replication allows more precise estimations of this effect.

- **randomisation**

Randomisation is a random determination of the order of the experimental trials. By randomising the experiment the effect of any noise present in the system is averaged.

- **blocking**

Blocking is a method to eliminate the effects of factors that are not directly dependent on the experimental process.

Montgomery [94] recommended the following procedures for successfully designing and analysing experiments:

-recognition and statement of the problem,
-choice of factors, levels and range,
-selection of the response variable,
-choice of experimental design,
-performing the experiments,
-statistical analysis of the data,
-conclusions and recommendations.

Factorial design and response surface methodology are the most popular techniques in welding experimentation. A brief description of the main points of both designs will be given below. Both subjects are standard parts of any textbook on experimental design and statistical analysis [92],[94].

2.4.4.1 Factorial Design

In factorial design a fixed number of levels for the factors is selected and the experiments are carried out in all possible combinations. The effect of an individual factor on the response is obtained by changing the level of the factor (main effect).

When the difference in responses between the levels of a factor depends on the levels of the other factors involved in the experiment an interaction occurs.

Generally each factor is attributed two values (levels).The low level is indicated with the symbol (-) and the high with the symbol (+) and consequently the factors are transformed in a normalised form (-1 for the low level and +1 for the high).

This design consists of 2^k experimental runs (where k is the number of factors or variables in the experimental design) and is called 2^k factorial design.

An alternative way to the above full factorial design is the use of fractional factorial design. This is usually used when the number of factors is high and provides information for the main factor effects and the low order interactions in a relatively small number of experiments.

The results of a factorial design are expressed in terms of a regression model. The regression analysis is a statistical technique applied to investigate and determine the relationships between the experimental variables. The regression model is used

afterwards to obtain the predicted value of a response within the design space. Consequently the residuals (difference between actual and predicted values) or error can be estimated. The analysis of the residuals is very important in evaluating the model adequacy and graphically several plots (e.g. normal probability plot, plot of residuals versus predicted) are used to determine the presence of any outliers.
Analysis of variance, model adequacy checking, lack-of-fit tests etc and the relative statistical terminology are included in all text books on statistical analysis [92],[94].
Current commercial software for design and statistical analysis of experiments [95] provides very powerful tools and includes in detail all statistical approaches.

2.4.4.2 Response Surface Methodology [94]

This is a technique applied for modelling and analysis of experiments where the response is influenced by several factors (variables) and the main task is to optimise the response [94]. If the response is a linear function of the independent variables the model is a first-order model, while if there is curvature in the system the model is second order.
The most popular class of designs in order to fit a second order model is the central composite design or CCD. This consists of 2k factorial points, 2k axial or star points (α) and a number of centre points n_c (Figure 2.25). The 2^k term fits the first order model while the axial points (runs) fit the quadratic.

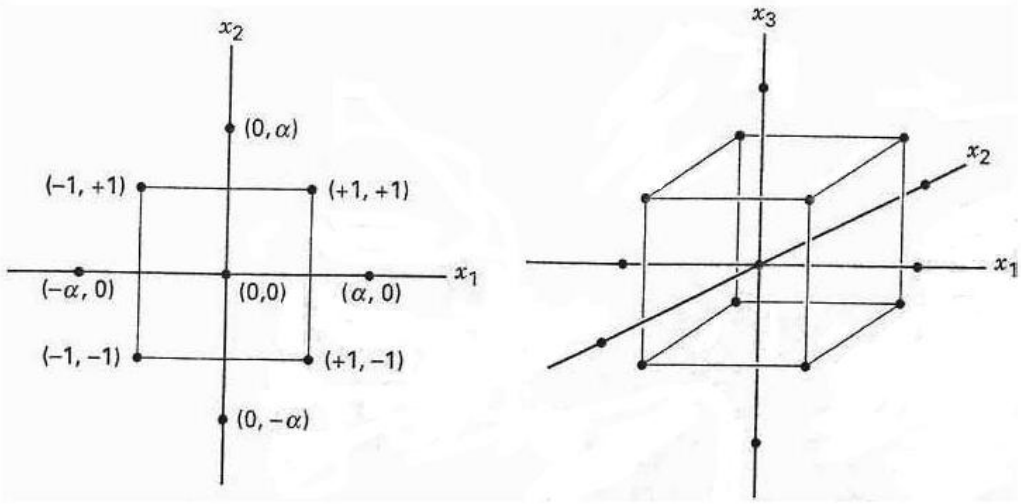

Fig. 2-25 Central composite design for k=2 and k=3

2.4.4.3 D-Optimal Design [94]

An optimal design is intended to be the "best" design for given criteria. These designs are generated with the use of computer programmes (computer algorithm).

2.4.5 Prediction of Weld Bead Geometry using Statistical Analysis

2.4.5.1 Introduction

In 1975 Tsygan and Lebedev [96] reported, by using rational experiment planning and statistical analysis in submerged arc welding of low carbon steel butt joints, an empirical formula relating the depth of penetration, the welding speed and the gap between the edges. With the introduction of this technology they estimated savings of 25,000 roubles.

Konkol and Koons [98] conducted statistically designed experiments (32 point central composite) in two wire AC-AC submerged welding (bead on plates) of X-60 linepipe steel. Five independently controllable process variables were selected (current, voltage, travel speed, electrode extension and electrode angle). Among other conclusions they found that:
-depth of penetration increases with current and this is more significant at low travel speeds and at low values of electrode extension; increasing electrode angle results in an increase of depth of penetration,
-bead height decreases as current decreases and travel speed increases,
-bead width increases with increasing current only at high voltage levels.

Absi Alfaro [87] investigated the effect of the welding parameters in narrow gap submerged welding. He performed statistically designed experiments (fractional factorial 2^{6-1}_{IV}). He investigated the effect of six variables (current, voltage, welding speed, standoff, filler wire diameter and joint gap) on fifteen responses (e.g. depth of penetration, maximum lateral penetration, dilution, bead concavity and convexity etc.) representing the weld bead geometry. Prediction equations were developed.
Among the other conclusions, he found that depth of penetration increases with increasing joint gap and current, and decreases with increasing standoff, filler wire diameter and voltage. The maximum lateral penetration depended on joint gap, welding speed and voltage. In particular maximum lateral penetration increased with increasing voltage and decreased with increasing joint gap and welding speed.

Paranhos [88] applied experimental blocks of 2^k factorial designed experiments to produce data from welds performed in SAW square-edged gapped joints. For the first weld bead, five input parameters (current, voltage, travel speed, gap, and metal powder) and 12 responses (e.g. penetration length, dilution, lack of fusion length etc.) were considered**.** He reported that length of penetration increases with increasing current and decreases with increasing welding speed and joint gap. Lack of fusion length was determined as voltage and joint gap dependent. In particular he found that lack of fusion increases with increasing both voltage and joint gap.

Statistically designed and analysed experiments have also been used in FCAW welding. Raveendra and Parmar [85] used a fractional factorial design (2^{5-1}) to predict the effect of welding parameters on weld bead geometry while Palani and Murugan [98] used a three factor five level CCD design with six central points.

2.4.5.2 Statistical Analysis in GMAW for Weld Bead Profile Prediction

With increasing use of automatic GMAW there have been an increasing number of studies in mathematical modelling of the weld bead geometry. Empirical models and mathematical equations have been developed using statistically designed experiments. Murugan and Parmar [99] used a four factor five level factorial design to predict weld bead geometry for depositing 316L stainless steel onto structural steel. This was a 31 point central composite design. The input variables considered were arc voltage, wire feed speed, welding speed and stand off, while the responses measured were depth of penetration, height of reinforcement, weld width and dilution. Four regression equations were developed and the main factor effects and interactions were determined. Among the other conclusions they found that:

- Depth of penetration increases with increasing wire feed speed and this is attributed to the higher level of current with the increased wire feed speed enhancing heat input.
- Bead width increases with increase in wire feed speed due to the larger pool created from the combined effect of current and heat input.
- Dilution increases with increases in wire feed speed attributed to the increased area of molten metal which is greater than the area of metal deposited.
- Penetration, reinforcement and bead width decrease with increase in welding speed. This is likely to be due to reduced heat input per unit length. However, dilution decreases initially with the travel speed, then increases. The increase in dilution may be due to the fact that the rate of decrease in penetration is less than the reinforcement.
- Increases in arc voltage increase penetration (due to increase in current and therefore in heat input) weld width (due to larger spread of arc cone) and dilution (due to increase in arc energy, V*I, causing more base metal to melt) but decrease reinforcement.
- Reinforcement and bead width were not significantly affected by stand-off.
- Both dilution and penetration decrease as stand-off increases. This is because an increase in stand-off increases the circuit resistance and therefore current level and voltage drop. Less energy is available and this reduces penetration and dilution.

Pandey and Parmar [100] conducted bead on aluminium alloy 5083 plate welds and used a fractional factorial design in order to predict the weld bead geometry relationship and wire feed rate, arc voltage, nozzle to plate distance, welding speed, torch angle and gas flow rate. Sixteen experiments were carried out and regression equations were developed. Main factor and interaction effects were determined. It was found that depth of penetration, bead width, reinforcement height and % dilution increase with increase in wire feed rate.

Feldthusen [101] studied the effect of the welding parameters on weld bead geometry of GMAW fillet welds of thin metal sheet in horizontal-vertical position using factorial design. The experimental design consisted of four blocks of 2^k factorial experiments. Modelling equations for bead throat thickness, reinforcement height and centre penetration were developed.

Modenesi [4] carried out a similar study to that reported in this thesis. He studied the effect of welding parameters on the fusion characteristics of NG-GMAW in downhand and horizontal vertical positions, simulating the welding positions used during the

application of the J-laying technique for the construction of offshore pipelines. Factorial design and a 'customised' factorial scheme were used. Mathematical equations were developed using multiple linear regression. Some conclusions are reported below:

Downhand position

$y^{1/2}=23.03-0.980w+1.926g$ (y=response production time (s/m), w=wire feed rate(m/min), g=gap width(mm)). Higher wire feed rates result in shorter joint completion time, and for wider gap widths more runs are required to fill the joint volume and hence completion time is increased accordingly. Figure 2.26 shows the response surface plots of production time in relation to wire feed rate and gap width.

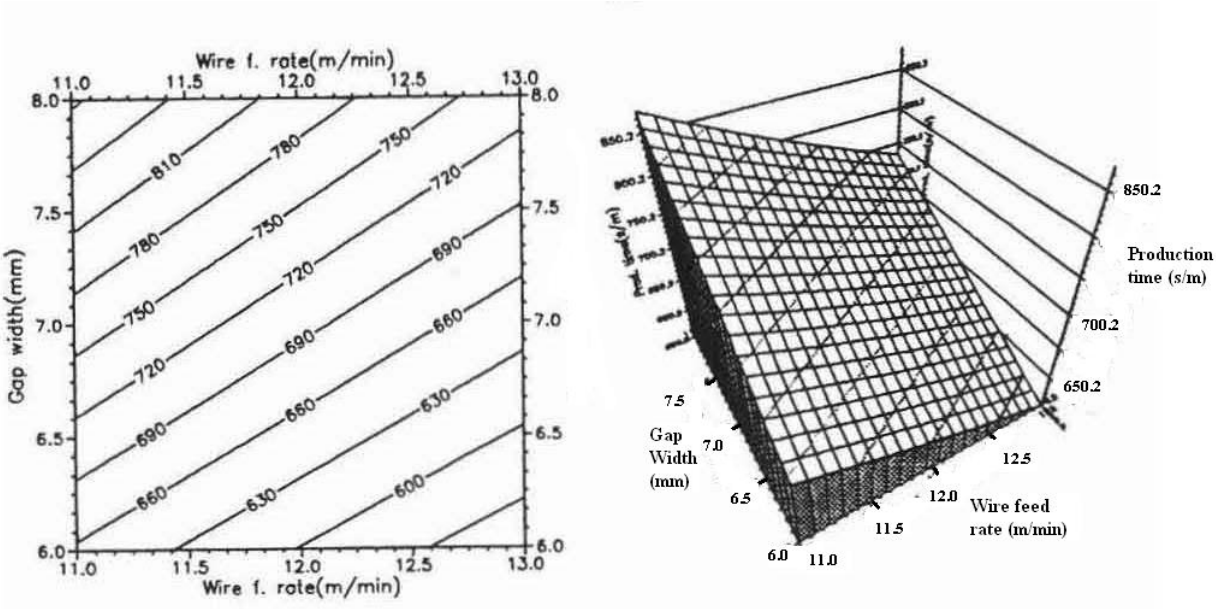

Fig. 2-26 Response surface plots for production time [4]

$\ln(y)=5.889+0.0137I-0.208w-0.316v-0.446g$ (y=response lateral penetration area(mm^2); I=welding current(A); w=wire feed rate(m/min); v=welding speed(mm/s); g=gap width(mm)) meaning that lateral penetration increases with current and decreases with wire feed rate, welding speed and gap width (Figure 2.27). Relationships between current, wire feed rate, voltage, and arc length were generated (Figure 2.28) meaning that both voltage and arc length can be expected to influence lateral penetration.

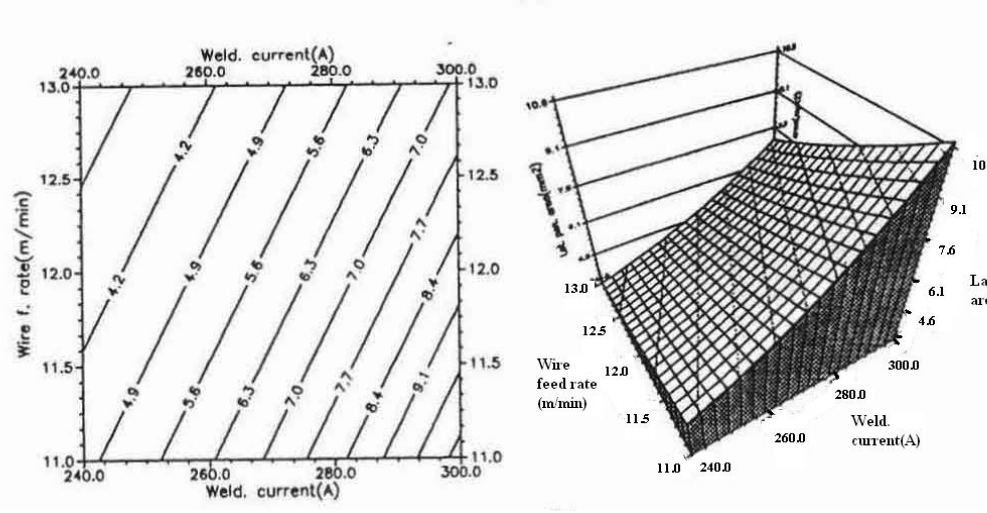

Fig. 2-27 Response surface plots for lateral penetration area [4]

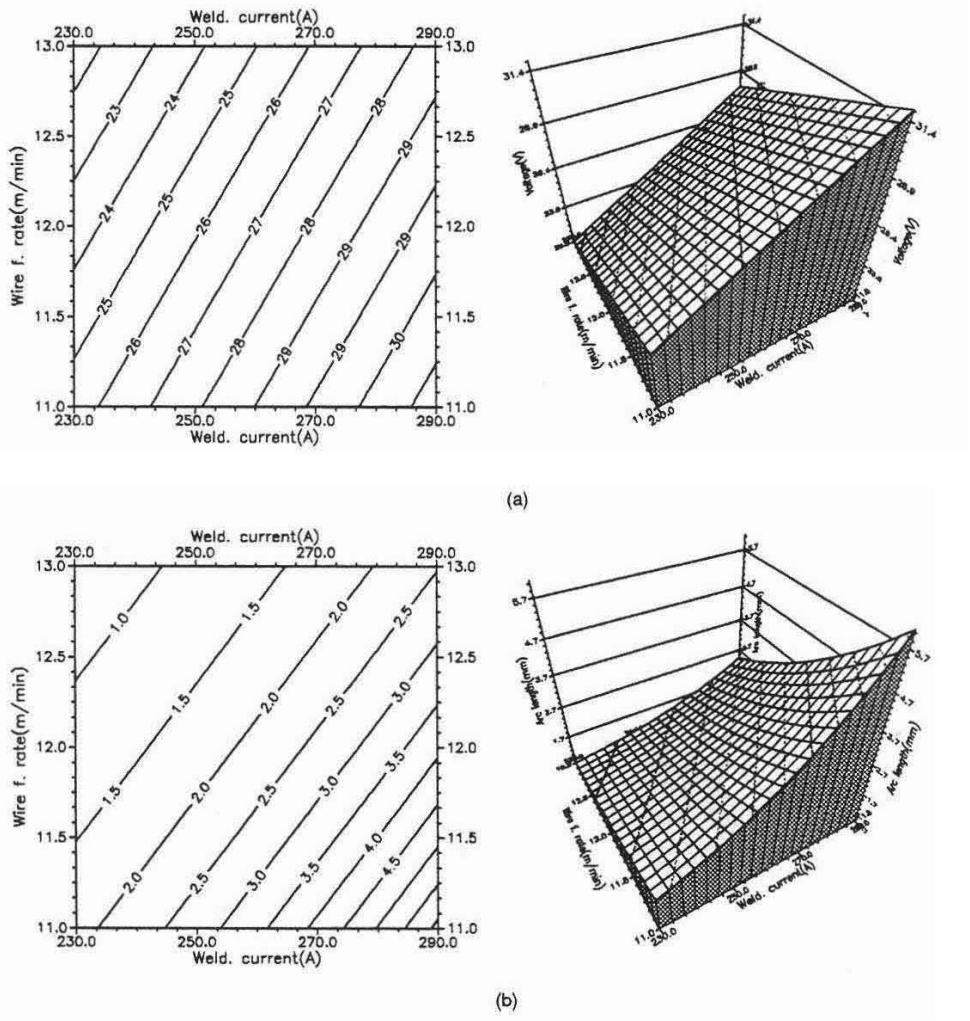

Fig. 2-28 Response surface plots for predicted voltage and arc length [4]

y=-33.4+0.0825I+3.091g (y= axial penetration area (mm^2). The strong effect of the gap width is attributed to the fact that increasing the gap reduces the confining effect of the sidewalls.

2.4.5.3 Model Validation

Montgomery [102] proposed three useful procedures for the validation of a regression model:

1. Analysis of model coefficients and predicted values with prior experience.
2. Collection of new data with which to investigate the model's predictive performance.
3. Data splitting that is, setting aside some of the original data and using these observations to investigate the model's predictive performance.

The intended use of the model usually indicates the validation procedure that should be employed.

Paranhos [88] set a criterion in order to evaluate the performance of a model: the results obtained from "fresh" data should lie in the range of the predicted value plus or minus 1.645 or 1.96 times the standard deviation of the regression equation.

2.4.6 Conclusions

Statistically designed and analysed experiments have been widely and successfully used in welding. The other approaches used in the analysis of weld bead profile (i.e. tolerance box, theoretical etc.) are often based on simplifying assumptions or require an extensive number of experiments. It has been found that properly designed and performed experiments can provide detailed information of the effects of the welding parameters on weld bead geometry together with their interactions with a limited number of experiments.

The present work aims:

-to determine the significant welding parameters and their effect on weld bead geometry,

-to determine mathematical equations capable of describing and predicting the weld profile in all welding positions,

-to determine appropriate welding conditions in order to optimise the weld bead geometry.

3 Aims and Objectives

Mechanised welding for the construction of onshore pipelines requires a fast welding process that can produce sound (defect free) welds and improve productivity.
At the start of this work limited data were available on tandem pulsed gas metal arc welding for X100 linepipes. Procedure test data had been previously generated at Cranfield [5],[18],[1] but there had been no parameter study on the effect of welding conditions on weld quality.
Although the process has been developed and welding procedures have been qualified and implemented for X100 5G pipeline girth welds, an extensive study that could provide a better understanding of the relationship between process variables and the physical process involved in the formation of the weld bead has not been carried out. One aim of this research work is therefore to develop a greater understanding of process characteristics through a systematic approach of studying the effect of the welding parameters on weld bead profile. Again, no previous work on the effect of the welding parameters on weld bead profile for 5G pipe welds has been reported in the literature.
This study is expected to provide the necessary information to improve welding conditions and establish mathematical expressions for easier interpretation of the relationship between shielding gas composition, welding parameters and weld bead profile.
No previous work has been reported in the dual tandem PGMAW for 5G pipe welds.

The objectives of this work can be therefore summarised as follows:

a. Development of the tandem welding process for X100 girth welds.
Development of welding parameters, procedures and investigation of the weld metal and HAZ (heat affected zone) microstructure and mechanical properties, with the aim of achieving a minimum yield strength 810MPa (and preferably within 810-860MPa), combined with good toughness properties.

b. Development of dual tandem procedures for X100 girth welds.
Feasibility and development of the process, investigation of weld metal and HAZ properties for a strain-based X100 pipeline design with adequate overmatching (810-860MPa) of the pipe specified minimum yield stress.

c. Development of a double jointing dual tandem procedure for X100 girth welds.
Analysis of weld metal and HAZ mechanical properties, and assessment of process productivity compared to traditional SAW procedures.

d. Development of welding procedures for Tie-In X100 girth welds.
Development of suitable waveforms and procedures for single wire PGMAW, to meet the overmatching strength requirements.

e. Study of welding parameters effect on weld bead geometry.
Determination of the relationship between welding parameters and weld bead profile including an analysis of the effect of shielding gas composition on weld bead geometry.

The experimental flowchart graph is shown in Figure 3.1.

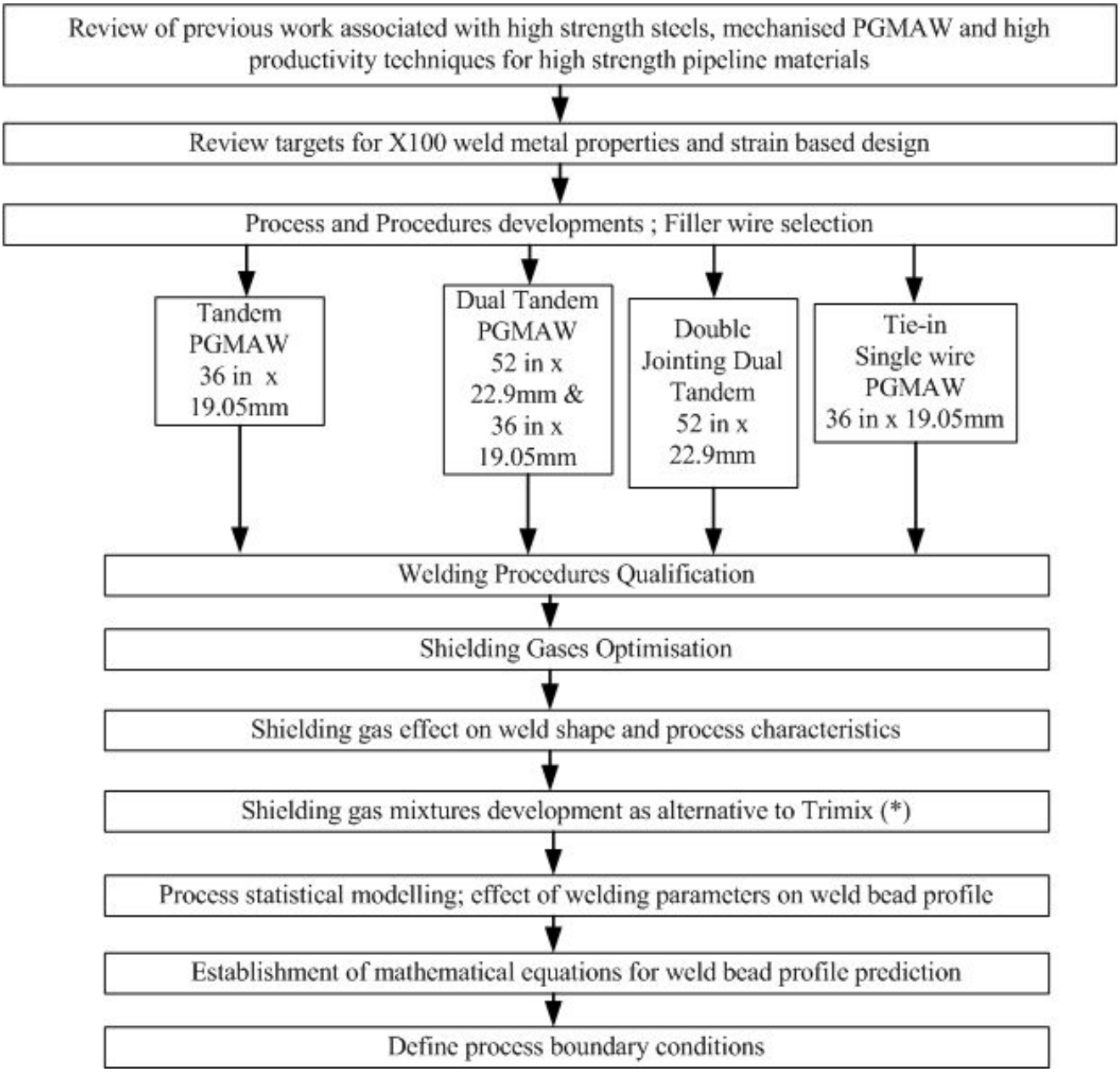

*Trimix : 82.5%Ar12.5%$CO_2$5%He

Fig. 3-1 Experimental flowchart graph

The Figure 3.2 shows the modelling process related to the present work.

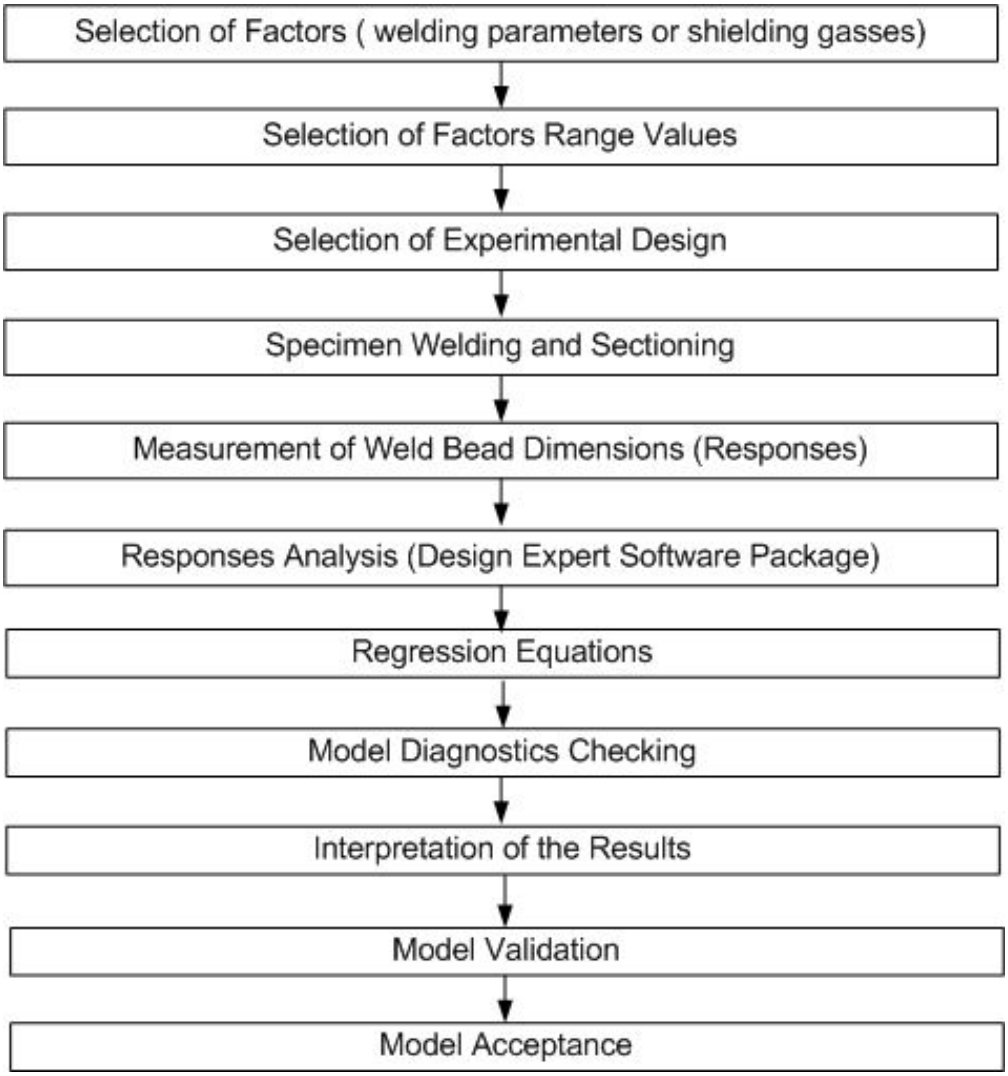

Fig. 3-2 Modelling process flowchart

4 Equipment and Materials

4.1 Pipe Material

The pipeline material used in this programme was X100 (API 5L) with a specified minimum yield strength of 690MPa. Plates of the same composition as the 19.05mm thickness pipe were also supplied. The dimensions are shown in Table 4.1.
The pipe dimensions were: 914mm OD (36 in) x 19.05mm WT and 1321mm OD x 22.9mm WT. Two different chemical compositions of the 1321 mm OD (52 in) pipe diameter were supplied and were classified as medium carbon (C=0.057%) and low carbon (C=0.043%). Several pipe "nipples" were extracted from the full pipe length by oxyacetylene flame cutting. Both "nipple" ends were bevelled. Two "nipples" were assembled to form a pipe spool (approx. 1m length). The pipe heat number was transferred to the spools for traceability purposes.
The chemical composition and mechanical properties of the pipes used are shown in Tables 4.2, 4.3 and 4.4.
The tests were carried out by a commercial company (Bodycote) accredited to UKAS.

4.2 Filler Wires

The solid wires used were all of nominal 1.0mm diameter (except for the K-Nova used for the root pass which was 0.9mm diameter) ; the wire types and the analysis results are shown in Tables 4.5 and 4.6.
Filler wire selection was based on previous work at Cranfield [1] and on chemical composition. The main elements considered in the filler wires composition were Ni, Mo and Cr.
Two basic FCAW wires of nominal 1.2mm diameter were also selected for the tie-in experimental trials.
For the shielding gas and welding parameters trials the Oerlikon Carbofil NiMo-1 filler wire was used throughout the experimental work

4.3 Shielding Gases

The weld procedures development work utilised a three component shielding gas mixture (Trimix) supplied by BOC. This gas composition consists of:
82.5%Ar12.5%$CO_2$5%He.
This gas was chosen because it had provided good results (mechanical properties, transfer characteristics and bead profile) in work carried out on 19.00mm thick CSA Z245.1 Grade 483 steel line pipe [6] and the earlier work at Cranfield [5],[18],[1].

For the tie-in root run and the narrow gap internal root weld procedures a standard BOC gas (Argoshield Heavy) was used. Its chemical composition consists of:
78%Ar20%$CO_2$2%O_2.
This was used successfully in previous work carried out at Cranfield [103].

Pipe Supplier Identification	Nominal Wall Thickness (mm)	Nominal Pipe Outside Diameter (mm)
B19	19.05	914 (36 in)
D1(Medium Carbon)	22.9	1321 (52 in)
D2(Low Carbon)	22.9	1321 (52 in)
Plate A	19.05	1000 x 2000
Plate B	19.05	1400 x 2000

Table 4-1 Typical X100 pipes.

Pipe B19	Tensile Dimen (mm)	Bodycote Yield $Rp_{0.2}$ (MPa)	Supplier Yield $Rp_{0.2}$ (MPa)	Bodycote Yield $Rt_{0.5}$ (MPa)	Supplier Yield $Rt_{0.5}$ (MPa)	Bodycote Ultimate Rm (MPa)	Supplier Ultimate Rm (MPa)	Bodycote Elong A (%)	Supplier Elong A (%)	Bodycote Y/T Yield = $Rp_{0.2}$	Supplier Y/T Yield = $Rt_{0.5}$
X100 Pipe – round bar transverse 1 o'clock	ϕ8.00	671	792*			838	833	19.5	22.2	0.80	0.95
X100 Pipe – round bar longitudinal 1 o'clock (room temp.)	ϕ8.00	701				847		20.8		0.83	
X100 Pipe – round bar longitudinal 1 o'clock 200°C	ϕ8.00	667				799		14		0.83	
X100 Pipe – strip transverse 1 o'clock	38x19	759		758	766	856	860	32.7	33.9	0.89	0.89
X100 Pipe – strip longitudinal 1 o'clock	38x19	733		723	774	837	849	34.4	33.2	0.88	0.91
X100 Pipe – round bar transverse 3 o'clock	ϕ7.90	772				869		18.5		0.89	
X100 Pipe – round bar longitudinal 3 o'clock	ϕ8.00	655				820		19.5		0.80	
X100 Pipe – strip transverse 3 o'clock	38x19	696		679		855		33.3		0.81	
X100 Pipe – strip longitudinal 3 o'clock	38x19	710		705		833		34.8		0.85	
X100 SAW Seam ID all weld tensile	ϕ6.25		829				891			0.93	
X100 SAW Seam centre all weld tensile	ϕ6.25		883				938			0.94	
X100 SAW Seam OD all weld tensile	ϕ6.25		824				894				
X100 Pipe – strip transverse weld seam	38x19						838				
	* Supplier transverse round bar gauge diameter = 8.9mm										
	NB. All Bodycote tensile specimens were considered proportional i.e. elongation calculated using gauge length = $5.65x\sqrt{S_0}$; S_0 is the original cross-sectional area (BS EN 10 002-1)										

A=Percentage elongation after fracture
Rm=Stress corresponding to the max. force (or ultimate tensile strength)
$Rp_{0.2}$=0.2% proof stress
$Rt_{0.5}$=0.5% tensile elongation stress (total extension)

Table 4-2 Pipe B19 (X100, 36 in OD, 19.05mm WT) mechanical properties (after Hudson [1])

Pipe No.		Round Bar Specimen d=12.7mm , GL=50.8mm				All Weld Tensile d=6mm , GL=24mm					Flattened Strip Specimen GL=50.8mm			
		Rt0.5 (MPa)	Rm (MPa)	A (%)	Y/T		Rt0.5 (MPa)	Rm (MPa)	A (%)	Y/T	Rt0.5 (MPa)	Rm (MPa)	A (%)	Y/T
4251-01-0001-**D1**	L	621	766	24	81	O/W	681	856	23	80	561	770	38	73
	T	685	778	25	88	I/W	750	943	23	79	640	771	39	83
4251-01-0002-**D1**	L	632	772	23	82	O/W	647	840	23	77	651	774	37	84
	T	719	803	24	90	I/W	783	952	27	82	577	793	37	73
4251-01-0003-**D1**	L	612	769	23	80	O/W	667	857	22	78	568	769	39	74
	T	705	805	24	88	I/W	785	941	22	83	553	795	37	70
4251-01-0006-**D2**	L	683	774	22	88	O/W	727	863	20	84	604	785	38	77
	T	777	810	20	96	I/W	775	963	23	80	637	806	36	79
4251-01-0007-**D2**	L	689	793	22	87	O/W	703	850	22	83	710	805	37	88
	T	744	815	24	91	I/W	759	962	24	79	631	807	36	78
4251-01-0008-**D2**	L	705	827	21	85	O/W	680	846	22	80	672	816	35	82
	T	814	862	22	94	I/W	781	970	20	81	690	849	36	81
4251-01-0009-**D2**	L	684	820	22	83	O/W	707	849	23	83	703	798	34	88
	T	777	841	22	92	I/W	760	967	19	79	650	832	35	78
4251-01-0010-**D2**	L	687	821	20	84	O/W	700	841	22	83	720	819	37	88
	T	826	860	21	96	I/W	811	966	20	84	613	848	35	72
4251-01-0011-**D2**	L	685	819	22	84	O/W	656	834	26	79	686	818	37	84
	T	781	861	22	91	I/W	787	943	20	83	606	854	34	71

Three batches of pipe marked as D1 and six of pipe D2 were supplied by the manufacturer. Test specimen extraction locations were not provided by the manufacturer.

O/W= SAW seam outside diameter all weld tensile; I/W= SAW seam inside diameter all weld tensile, L=Longitudinal, T=Transverse

Table 4-3 Pipes D1 (medium carbon) & D2 (low carbon) mechanical properties (supplier data)

	C	Mn	P	S	Si	Cr	Ni	Mo	Cu	Al	V	Nb	Ti	O_2	N_2	B	P_{CM}	CET	CE_{IIW}
	wt%	wt%	wt%	wt%	wt%	wt%	wt%	wt%	wt%	wt%	wt%	wt%	wt%	ppm	ppm	ppm			
Pipe B19 – Nominal 0.5Ni-0.25Mo-0.3Cu-Al-Nb-Ti																			
X100 Pipe (Bodycote Analysis)	0.066	1.88	0.008	<0.005	0.18	0.022	0.49	0.26	0.30	0.04	0.005	0.05	0.018	10	46	<5	0.209	0.308	0.489
X100 Pipe (Bodycote Analysis)	0.059	1.89	0.007	<0.005	0.18	0.022	0.50	0.26	0.30	0.04	0.005	0.06	0.018			<5	0.203	0.303	0.485
Base Metal Ladle (Supplier Analysis)	0.06	1.84	0.008	0.0011	0.18	0.03	0.50	0.25	0.31	0.036	-	0.05	0.018		55	1	0.201	0.299	0.477
X100 Pipe Seam Weld Metal ID(Bodycote Analysis)	0.059	1.99	0.008	<0.005	0.21	0.36	1.00	0.78	0.26	0.026	0.007	0.04	0.02	328	56	6	0.269	0.392	0.704
X100 Pipe Seam Weld Metal ID (Supplier Analysis)	0.06	1.88	0.008	0.003	0.22	0.37	1.03	0.76	0.26	0.015	-	0.033	0.02	279	61	11	0.266	0.381	0.685
X100 Pipe Seam Weld Metal OD(Bodycote Analysis)	0.053	1.91	0.007	<0.005	0.2	0.33	2.03	0.63	0.26	0.023	0.007	0.03	0.018	289	56	6	0.264	0.387	0.717
X100 Pipe Seam Weld Metal OD(Supplier Analysis)	0.06	1.78	0.008	0.003	0.21	0.34	2.04	0.6	0.24	0.012	-	0.027	0.018	335	60	9	0.264	0.378	0.697
Pipe D1 – Nominal 0.4Ni-0.25Mo-0.4Cu-Nb-Ti (medium C)																			
X100 Pipe (Supplier Analysis)	0.057	1.90	0.008	0.0012	0.28	0.02	0.41	0.26	0.40	0.004	0.002	0.049	0.015	20	31	<5	0.208	0.301	0.484
Pipe D2 – Nominal 0.45Ni-0.4Mo-0.5Cu-0.4Cr-Nb-Ti -V (low C)																			
X100 Pipe (Supplier Analysis)	0.043	1.92	0.008	0.0008	0.24	0.42	0.46	0.41	0.49	0.004	0.061	0.047	0.012	16	31	<5	0.235	0.332	0.605

$Pcm = C + Mn/20 + Mo/15 + Ni/60 + Cr/20 + V/10 + Cu/20 + Si/30 + 5B$
$CET = C + (Mn+Mo)/10 + (Cr+Cu)/20 + Ni/40$ (BS EN 1011-2)
$CE_{IIW} = C + Mn/6 + (Cr +Mo+V)/5 + (Cu+Ni)/15$

Balance F_e
N.B. where B level stated as <5ppm, 4ppm used in CE calculations

Table 4-4 Pipe chemical composition (pipe B19 after Hudson [1]; pipes D1 and D2 supplier data)

Solid GMAW Wires for Tandem & Dual Tandem Procedure Welds

Manufacturer	Wire Name	Diameter	Classification	Heat No.	Batch No.	Coil Size
Thyssen	K-Nova/ TS-6	0.9mm	AWS 5.18 ER70S-6	186096		2.8Kg
Oerlikon	Carbofil NiMo-1	1.0mm	AWS 5.28 ER100S-G		14233	15Kg
Oerlikon	Carbofil 120	1.0mm	AWS 5.28 ER120S-G		227737	15Kg
Bohler	X70-IG	1.0mm	AWS 5.28 ER110S-G	529472	402945L	18Kg
Bohler	X90-IG	1.0mm	AWS 5.28 ER120S-G	317186		18Kg
Thyssen	X85-IG	1.0mm	AWS 5.28 ER110S-G	496086		18Kg

FCAW / MCAW Wire for Tie-In Procedure Welds

Manufacturer	Wire Name	Diameter	Classification	Heat No.	Batch No.	Coil Size
Oerlikon	Fluxofil M10S	1.2mm	AWS 5.18 E70C-6C + 6M		1D6343	16Kg
Filarc	PZ 6148	1.2mm	AWS 5.29 E111T5-K4		2151039	16Kg
Filarc	PZ 6149	1.2mm	AWS 5.29 E121T5-G		3142019	16Kg

Table 4-5 Types of filler wires tested throughout the experimental programme

Solid Wires	Dia (mm)	Batch No	C %	Mn %	P %	S %	Si %	Cr %	Ni %	Mo %	Cu %	Al %	V %	Nb %	Ti %	O_2 ppm	N_2 ppm	B ppm	P_{CM}	CET	CE_{IIW}
Thyssen K-Nova/TS6	0.9	186096	0.06	1.47	0.01	0.01	0.8	0.03	0.02	<0.005	0.12	<0.005	<0.005	0.006	0.06	30	46	5	0.17	0.22	0.32
Oerlikon Carbofil NiMo-1	1.0	14233	0.09	1.62	0.009	0.008	0.63	0.03	0.91	0.31	0.1	<0.005	<0.005	0.006	0.07	79	68	5	0.23	0.31	0.5
Oerikon Carbofil 120	1.0	227737	0.11	1.66	0.006	<0.005	0.9	0.32	2.24	0.56	0.16	0.014	0.007	0.006	0.1	41	83	8	0.33	0.41	0.72
Bohler X70-IG	1.0	58974	0.08	1.45	0.008	0.016	0.59	0.26	1.32	0.25	0.08	0.005	0.1	0.005	0.05	37	56		0.24	0.30	0.54
Bohler X-90-IG	1.0	317186	0.08	1.79	0.006	0.015	0.8	0.37	2.22	0.58	0.06	0.01	0.009	0.007	0.05	26	61		0.29	0.39	0.72
Thyssen X-85(*)	1.0	496086	0.08	1.68	0.012	0.012	0.68	0.32	1.77	0.54	-	-	-	-		-	-		0.27	0.36	0.65
Flux / Metal Cored Wires																					
Filarc PZ6148(*)	1.2	2151039	0.08	1.56	0.009	0.007	0.45	0.45	2.03	0.46	-	-	-	-		-	-		0.26	0.35	0.66
Filarc PZ6149(*)	1.2	321029	0.079	1.73	0.011	0.017	0.44	0.9	2.25	0.51	-	-	-	-		-	-		0.30	0.40	0.80
Oerlikon Fluxofil M10S(*)	1.2	1D6343	0.06	1.6		-	0.5	-	-	-	-	-	-	-		-	-		-	-	-

PCM= C+Mn/20+Mo/15+Ni/60+Cr/20+V/10+Cu/20+Si/30+5B ; CEIIW=C+Mn/6+(Cr+Mo+V)/5 +(Cu+Ni)/15 ;
CET=C+(Mn+Mo)/10+(Cu+Cr)/20+Ni/40

N.B. where B level stated as <0.0005, 0.0004 used in CE calculation, and when V <0.005, 0.004 used in CE calculation
Balance F_e
Wire analyses prior work by Hudson [1]
* = Wire analyses as per manufacturer's batch test certificates

Table 4-6 Filler wire chemical composition

For tie-in fill runs a standard BOC gas (Argoshield Light) was used. This mixture consists of:
93%Ar5%$CO_2$2%O_2
This selection was based on welding trials which indicated good metal transfer (low spatter) and arc characteristics.

For the shielding gas study, four different shielding gases were mixed in a mixer panel in order to obtain the required gas percentages at the welding torch. The gases selected and their percentages are:
Ar: 70%-95% ; CO_2: 5%-30% ; He: 0%-20% ; O_2 : 0%-3%. Percentages are referred to 30L/min gas flow.
The selected ranges were chosen based on an evaluation of the literature concerning shielding gas mixtures for pipeline welding.

For the welding parameters trials the three component shielding gas mixture supplied by BOC was used. Its composition was 82.5%Ar12.5%$CO_2$5%He and is referred to as "Trimix" in this thesis.

4.3.1 Gas Mixer Panel

The Witt Gas Mixer KM30-5 DI SO is designed to mix up to 5 different gases in the required proportions. The mixing is achieved by means of a pressure equalizing system and high accuracy metering valves linked to a digital counter to enable pre-setting of the individual flows required.
The gas inlet connections and metering valves are labelled with different gas types. However each valve can be used with other gases to achieve varying proportions and the gas label is used primarily to identify the correct inlet connections relating to a particular valve. Each valve has a digital counter with a 0-900 scale.

Valve Nos. 14 & 15 provide a flow capacity of 30 L/min maximum using carbon dioxide.
Valve No. 16 has a flow capacity of 12 L/min maximum using carbon dioxide.
Valve No. 17 has a flow capacity of 9.5 L/min maximum using helium.
Valve No. 18 has a flow capacity of 2.0 L/min maximum using helium.

The gases were supplied from high pressure cylinders to the mixer, and after flow control went to a mixing chamber before being fed into the welding torch.
The manufacturer provided flow graphs in order to determine the required valve setting for a specific flow rate. For gases other than those used for the calibration, conversion factors have to be applied to obtain the required settings.
However, this equipment was independently calibrated using several Platon Gapmeter type GTLK gas flow meters, and this calibration was used for valve settings. Each valve was calibrated for the specific gas with the equivalent gas flow meter. For that purpose Ar, CO_2, He, O_2 flow meters were used. The WITT KM30-5 Mixer and the Platon Gapmeter type GTLK flow meters are shown in Figure 4.1
The Platon flow meters used for calibration were always used with gas exit to atmosphere since they are only accurate at normal temperature and pressure. The stated accuracy of the Platon flow meters is $\pm$1.25%, this combined with an approximate $\pm$2%

accuracy due to reading flow meter scale discrepancies provided an overall accuracy of $^{+}_{-}$3%.
The derived valve calibration charts are shown in Figures 4.2 to 4.5.

Fig. 4-1 The Witt KM-S gas mixer and Platon Gapmeter type GTLK gas flow meter

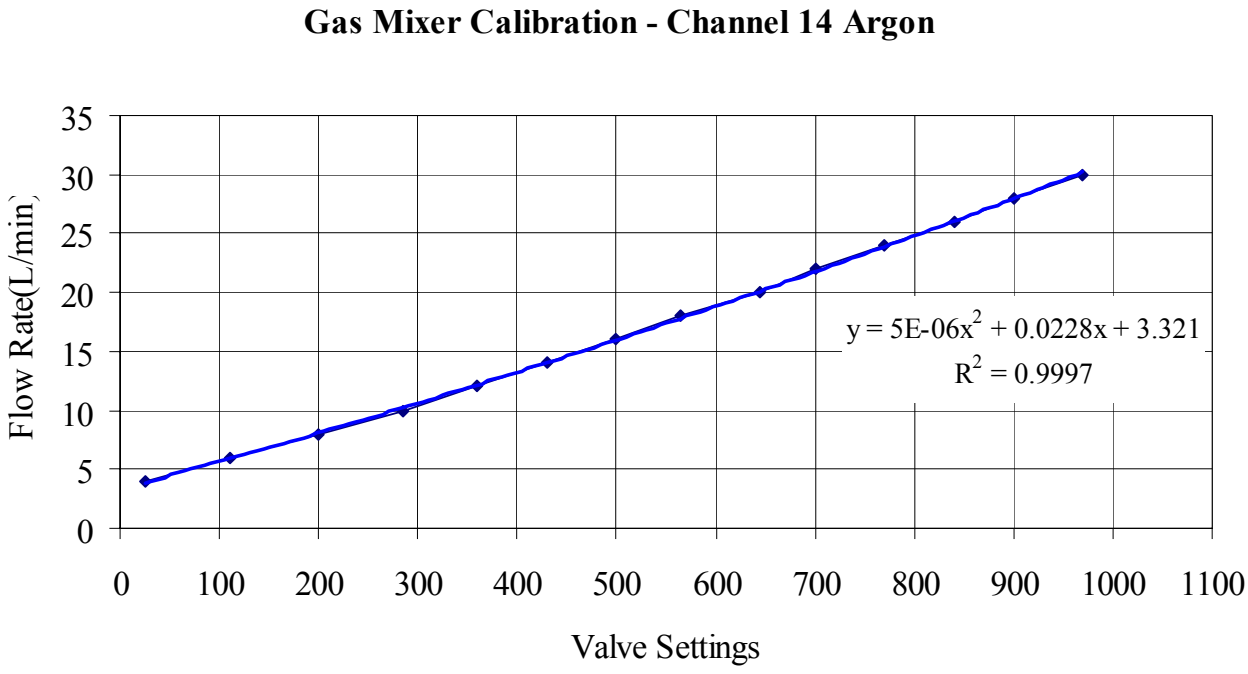

Fig. 4-2 Argon valve calibration flow rate chart

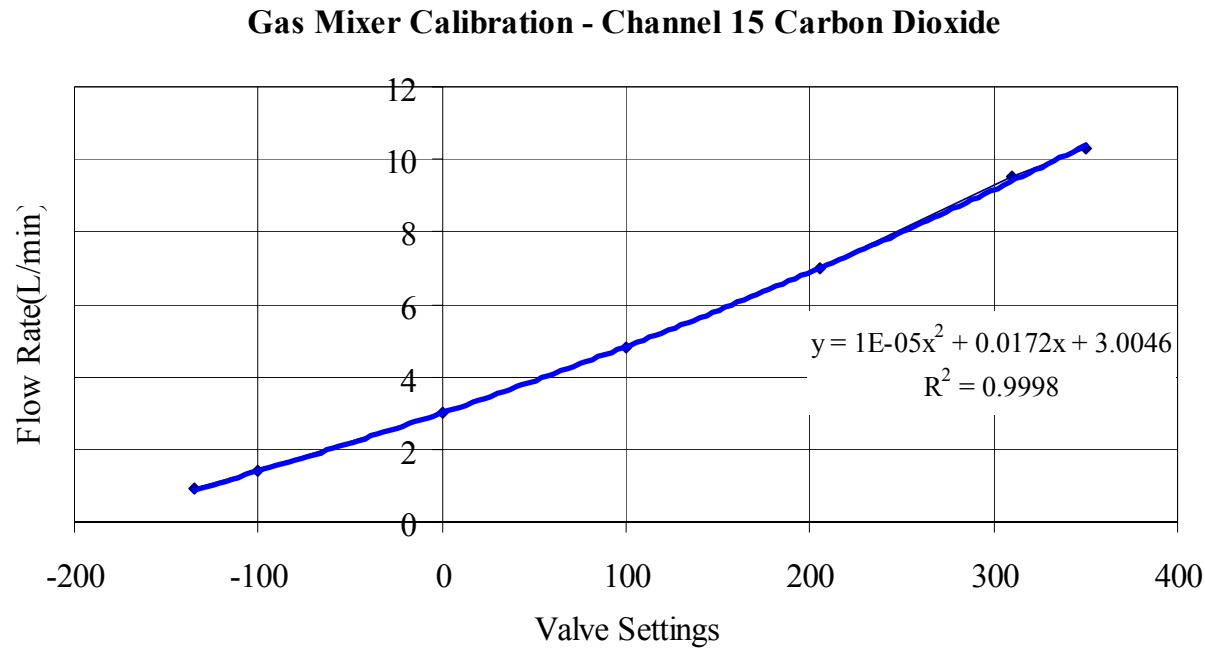

Fig. 4-3 **Carbon dioxide valve calibration flow rate chart**

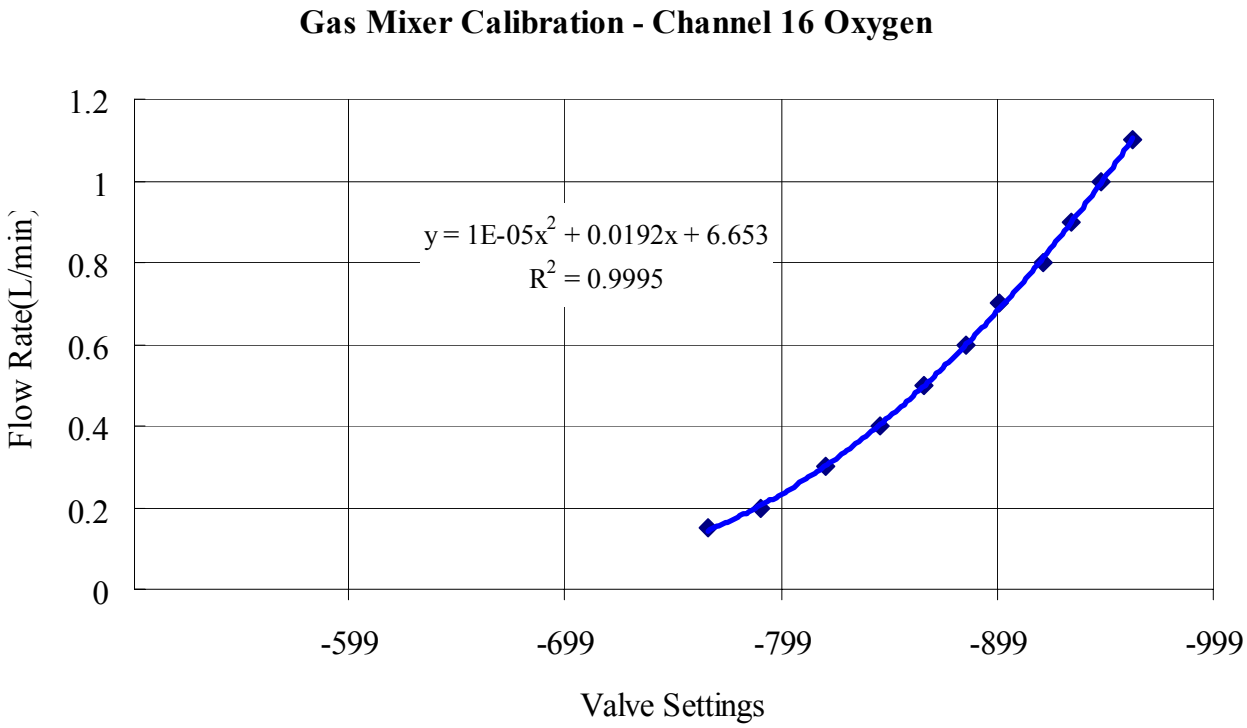

Fig. 4-4 **Oxygen valve calibration flow rate chart**

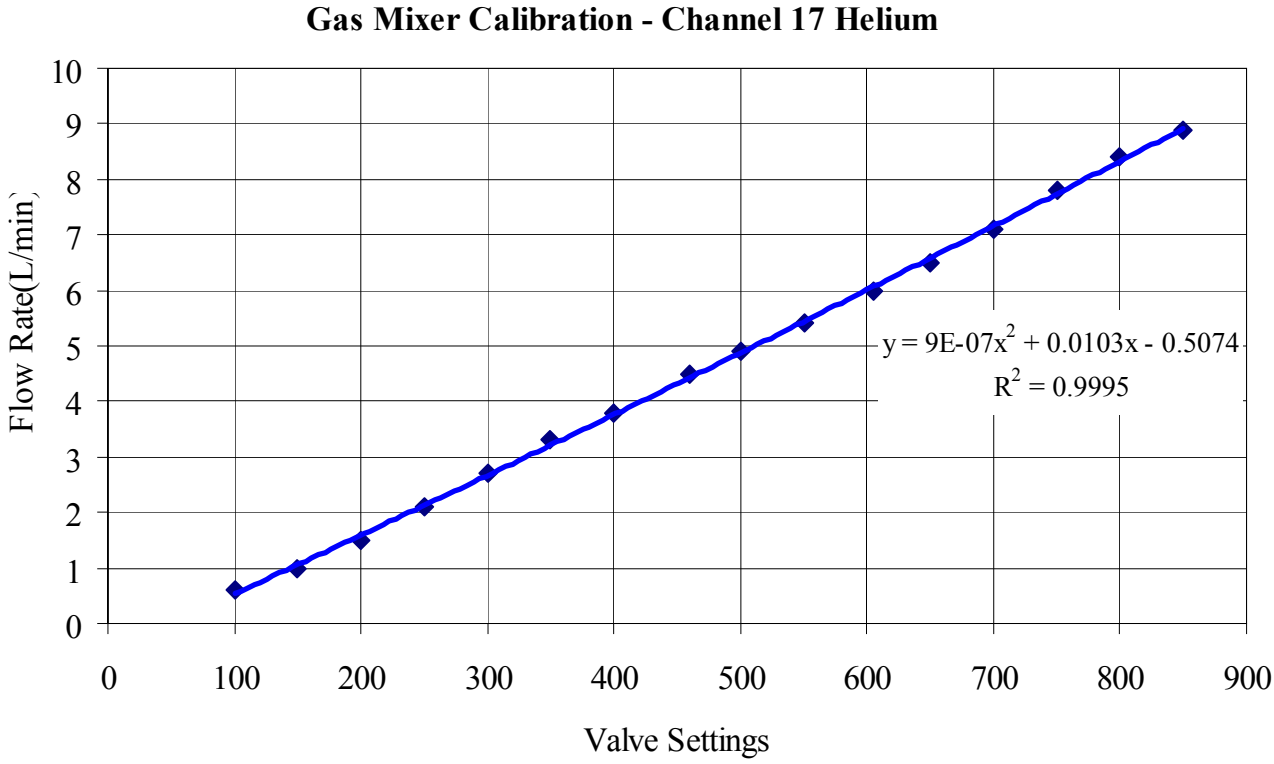

Fig. 4-5 Helium valve calibration flow rate chart

Gas mixtures of this type can be affected by the gas pressure at the flow control valves. They do not provide true mass gas flow control. The long umbilicals used in pipe welding can generate significant back pressures of up to 1 bar and this can vary with the total flow rate. Hence the pressure at the outlet of the gas mixture was measured and a pressure at the flow control valve was set to be always equal to 0.8 bar. Additional experiments showed that the mixer control was not strongly affected by pressure variations of +/- 0.5 bar.

4.4 Linear Welding Rig

The linear welding rig consisted of a table that could be moved while the welding torch was kept fixed. A simple support was built and attached to the table. The table could be inclined at 0°, 30°, 60°, 90°, 120°, 150° and 180° to the horizontal simulating different positions on the pipe circumference.
The welding torch was controlled by the RMS control pendant which will be explained later. The welding rig is shown in Figure 4.6

a) 60° welding position

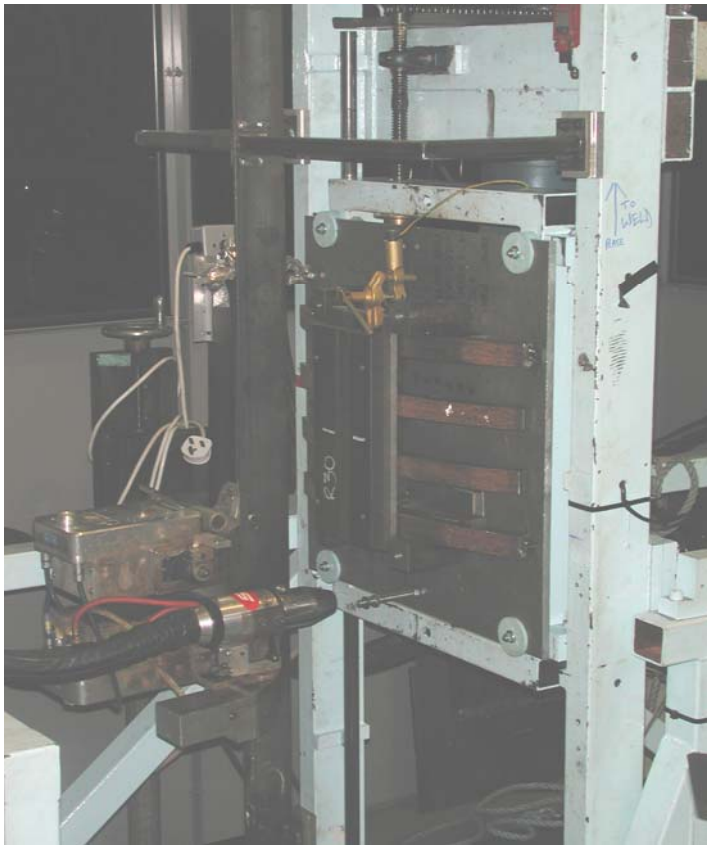

b) 90° welding position

Fig. 4-6 Linear Welding rig

Prior to welding, the table speed was calibrated and the calibration chart is shown in Figure 4.7.

In order to calibrate the welding rig speed a setting was selected on the rig's pendant. The corresponding travel distance was then measured over a set time period of 30s.
To develop the calibration chart thirteen (13) different pendant settings were tested. The estimated accuracy was $\pm$ 2%.

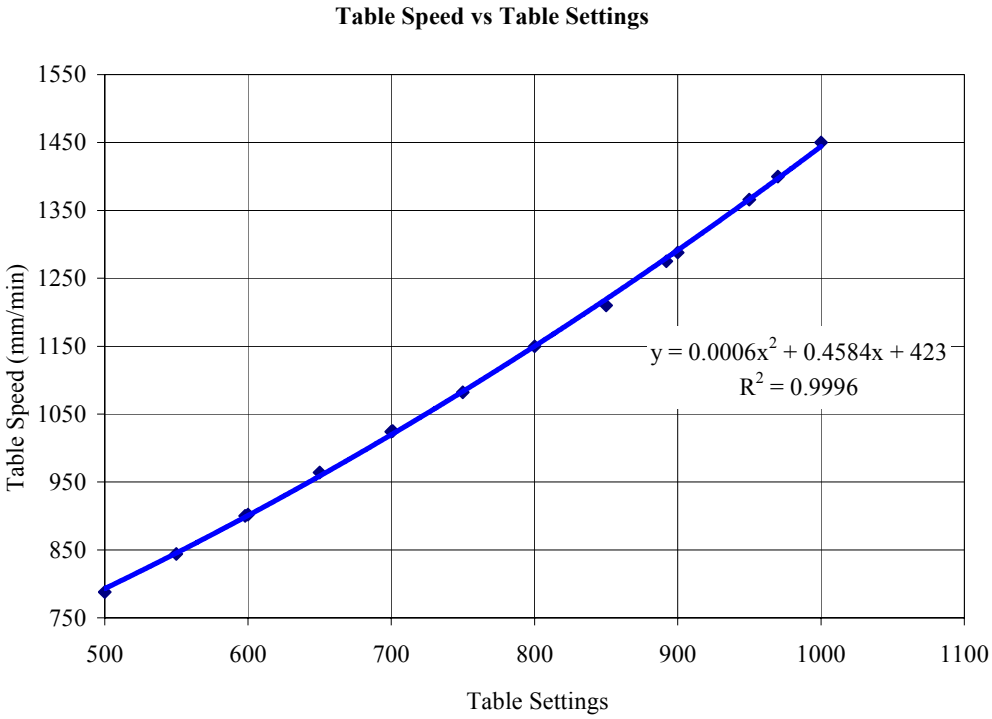

Fig. 4-7 Welding table speed calibration chart

4.5 Power Supplies

Three types of welding power equipment were used during this work:
•ESAB Aristo LUD 450W
•Lincoln Powerwave 455 STT
•TPS (Trans pulse synergic) Fronius 4000 Thermo

4.5.1 Tie-In Root and Narrow Gap Root Power Supplies

Tie-in root runs and root runs for narrow gap welds utilised the Esab Aristo LUD 450W (Figure 4.8).
This power source is capable of 360A at 100% duty cycle, 425A at 60% duty cycle and 450A at 45% duty cycle. For the purposes of this work this power source was operated in dip transfer mode. Prior to welding, wire feed speed, voltage and inductance values were selected. Wire feed speed and voltage can be adjusted during welding.

Fig. 4-8 The ESAB Aristo LUD 450W and the associated wire feeder

4.5.2 Tie-In Power Supplies

Fill runs for the tie-in trial welds utilised the Lincoln Powerwave 455 STT (Figure 4.9). This power source is designed to give 400A at 100% duty cycle (500A at 60% duty cycle) and was linked to the Wave Designer Pro software for online waveform control. This feature gives the opportunity to fully control the pulsed waveform parameters.

The Power Wave 455STT is a digitally controlled inverter welding power source capable of supporting the GMAW, PGMAW, FCAW, SMAW, GTAW processes and the Surface Tension Transfer (STT) mode.

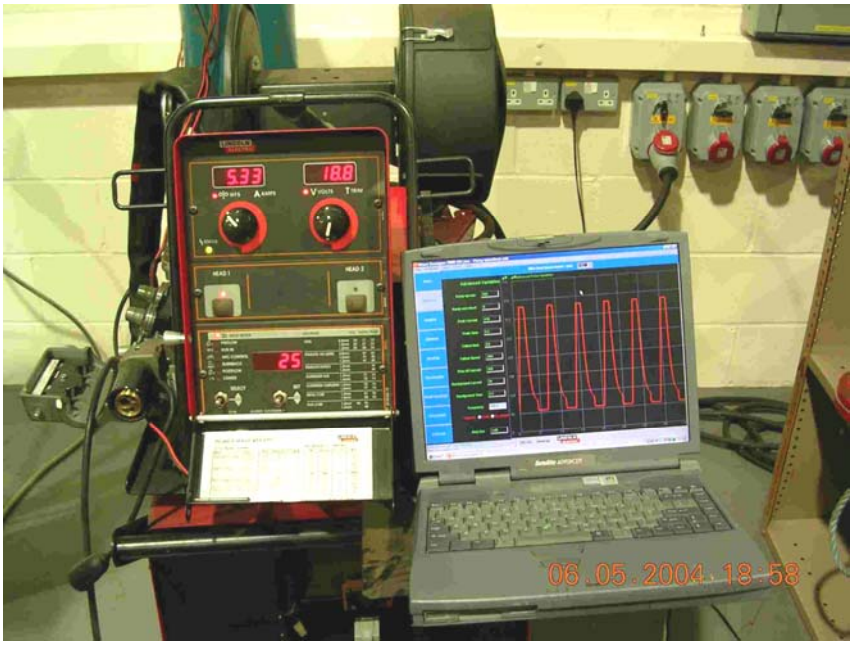

Fig. 4-9 The Lincoln powerwave 455 STT, illustrating the use of the Wave Designer Pro on a lap top computer

4.5.3 Tandem PGMAW Power Supplies

The tandem welding trials and experimental procedure work utilised a set (master and slave) of synchronised and totally digitised microprocessor TPS (TransPuls Synergic) 4000 Thermo Fronius power sources. An interactive power-source manager is coupled with the digital signal processor (DSP) which together control and regulate the entire welding process. The actual output is measured continuously, and the machine responds very quickly to any changes. These machines offer a duty cycle of 300A for a period of 10 minutes at 40°C, 365A at 60% duty cycle and 400A at 40% duty cycle all at 40°C.
Control panels are installed in the front part of the machine but accessibility to the synergic curve is only possible via the RCU 5000i remote panels. These power sources were operated exclusively in pulsed transfer mode and the one drop per pulse technique was adopted. This was thought to provide the most stable and efficient transfer mode for positional welding. This power supply enabled the waveforms of the lead and trail wires to be synchronised. It was considered important to operate the waveforms out of phase, in order to minimise the magnetic interaction effects of adjacent arcs.
Suitable waveforms for narrow gap PGMAW were originally developed at WERC (Welding Engineering Research Centre, Cranfield University) by Michie [5] and Walker [18] and further optimised by Hudson [1].
Shielding gas and welding parameter trials were carried out using a set (master/slave) of Fronius TPS 4000 Thermo power sources.
A set of Fronius TPS 4000 Thermo power sources is shown in Figure 4.10

Fig. 4-10 Fronius TPS 4000 thermo power supplies

4.6 Pipe Bevel Preparation Equipment

Two pipe bevel machines (Figure 4.11) for 36 in and 52 in outside diameter pipe were used for machining weld preparations.

a) 52 in BROOKS pipe bevel preparation machine

b) 36 in CRC pipe bevel preparation machine

Fig. 4-11 Pipe facing machines

4.7 Internal and External Welding Equipment

4.7.1 Welding Carriage

A CRC Evans P100 (Figure 4.12) welding bug was used for the tie-in welds (single wire) with a CRC torch, lead, and gas nozzles. The "slow travel" gear motor box was installed for the "low" welding (travel) speeds involved. CTWD was controlled manually during welding. Oscillation width and frequency were selected before welding; the equipment does not allow adjustments to the preset parameters values during welding which can limit to its potential use. Indeed, it was noticed that modifications to the oscillation width during welding were sometimes desirable.

Travel speed was regulated by adjusting a screw on the PC board. To calibrate this speed, a particular setting on the PC board was selected and measured, the corresponding carriage travel over the period of 30s was then subsequently converted to travel speed in mm/min.

The estimated accuracy was $\pm$ 2%.

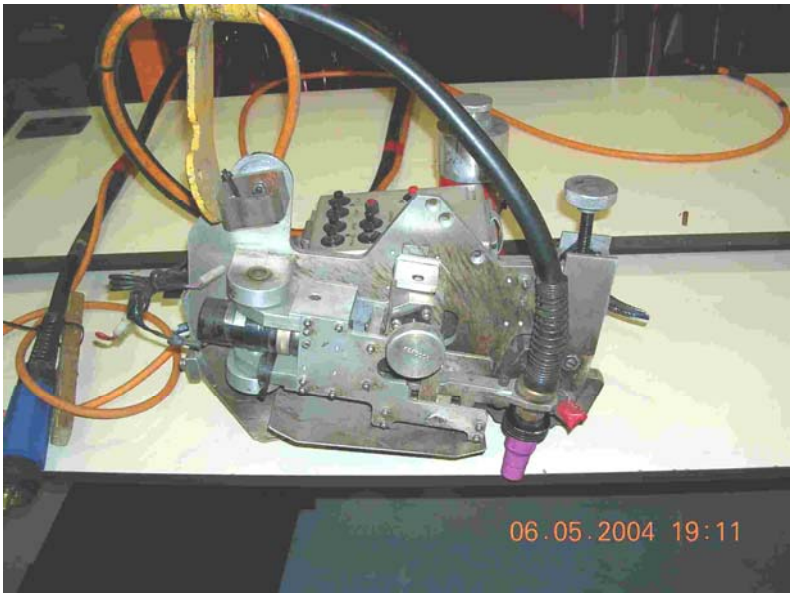

Fig. 4-12 CRC-Evans P100 welding carriage and single wire air cooled torch

The internal run (root pass) for the narrow gap procedure welds was deposited by rotating the pipe and using a conventional GMAW torch (Figure 4.13)

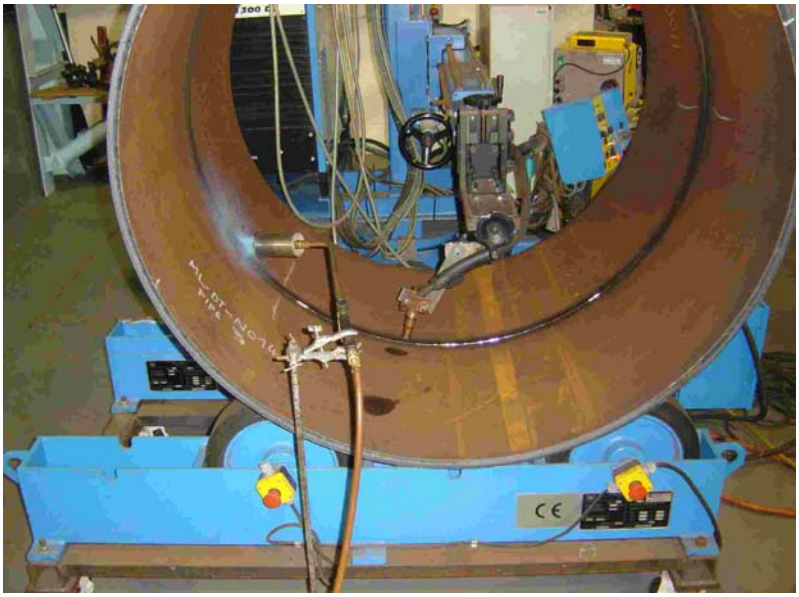

Fig. 4-13 Air Liquide column and boom system, with preheating for internal welding

Tandem and dual tandem narrow gap PGMAW was carried out externally using an RMS welding systems welding carriage, MOW II, which is capable of holding two tandem torches and allows independent control of the position of each torch head. Control of the bug utilises a pendant coupled with switching units for the power supplies. The MOW II welding bug and pendant are shown in Figures 4.14 and 4.15.

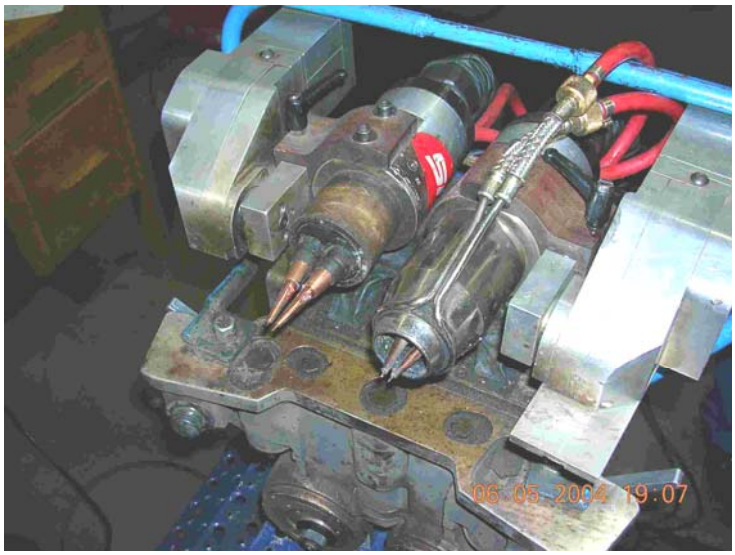

Fig. 4-14 MOW II RMS welding carriage and Fronius tandem torch

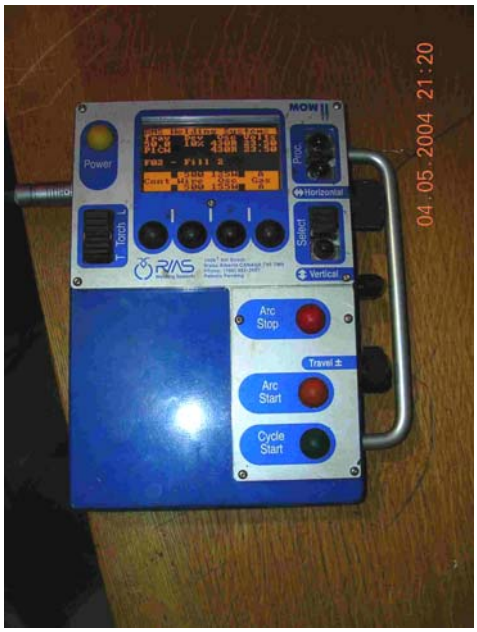

Fig. 4-15 RMS control pendant

4.7.2 Welding Torches and Contact Tips

Initially, for the single tandem and dual tandem trial welds the Cranfield designed air-cooled torch was used but overheating problems were reported. A new water cooled torch was developed, based on the experience gained with the air cooled torch. Torch performance was improved at the expense of a heavy hose pack.
Fronius subsequently, designed a commercial water cooled tandem torch based on the Cranfield designs and with a significant reduction in hose-pack weight (Figure 4.14).

4.8 Current and Voltage Measurements

Current and voltage values were monitored using a Yokogawa DL750 Scopecorder oscilloscope (Figure 4.16). Four channels for voltage and four channels for current were available. 10kS/s (10 kHz) acquisition rate was used during the experimental work.
This oscilloscope allows a detail study of the waveform and measurements of the pulse structure (pulsed current and voltage). Waveforms can be stored and transferred to a personal computer for further analysis via the waveform viewer program supplied by Yokogawa.

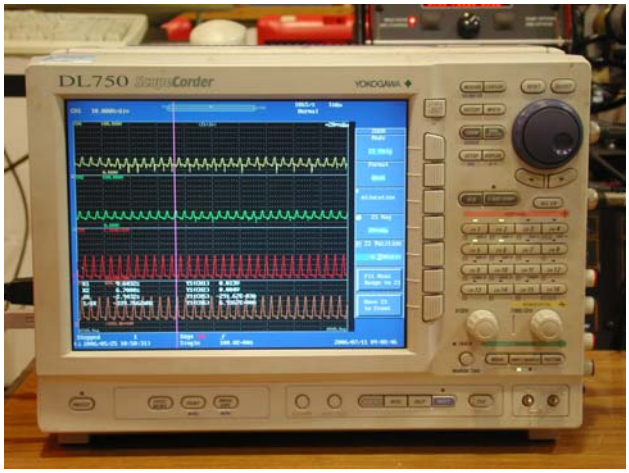

Fig. 4-16 The Yokogawa DL750 scopecorder oscilloscope

4.9 Metallographic Examination

Welded specimens were sectioned on a vertical band saw and polished on 120, 240, 1200 mesh silicon carbide papers. For finishing 6μm and 1μm diamond polishing was used. 2% Nital (2% nitric acid in ethanol) was used as etchant.
Macro photographs of the welded specimens were taken using a Nikon Coolpix 990 camera for the shielding gas trials. For the welding parameters trials a JVC (model KYF 55B 3-CCD) colour camera and image acquisition software (supplied by ACQUIS syncroscopy) were used.

4.10 Weld Bead Measurement

For analysis the effects of different shielding gas mixtures on weld profile, a scale was used to measure the linear dimensions on magnified tracings of the weld bead (estimated of accuracy $\pm$ 10%).
For the effect of welding parameters on weld profile the Microsoft Office Visio (2003) software was used to measure the linear weld dimensions in magnified tracings (estimated of accuracy $\pm$ 2%).

4.11 Arc Shape and Metal Transfer Images

Arc characteristics, metal transfer droplet size and arc length were detected using high speed photographic imaging. The Phantom V4 series high speed black/white camera was used at frame capture rates of 3500 per second.

4.12 Thermocouple Materials and Temperature Measurement Equipment

The materials selected to provide the thermoelectric voltage were platinum (-ve limb) and platinum/13% rhodium (+ve limb) R-type thermocouples. The wires were manufactured in accordance to BS 60584 [104]. Operating temperature for the R-type thermocouples is of prime importance since limbs can face temperatures above 1500°C when placed in the weld pool. For that reason R-type thermocouples were preferred over the K-type (NiCr/Ni) thermocouples usually used in the HAZ, which are limited to a maximum temperature of 1370°C. Typical limb diameter selected was 0.5mm. The material chosen to insulate each individual limb was sintered alumina in the form of 3.0mm round tubes and twin bores of 0.8mm.
The thermoelectric voltage from the thermocouples was transferred via National Instruments modules, (which allowed up to16 channels) to a data acquisition system on an industrial PC.
Thermocouples and the temperature measurement equipment are shown in Figure 4.17.

4.13 Chemical Analysis

Weld metal chemical analysis (dual tandem and tie-in welds) was performed by Bodycote. The optical emission technique was used on a 10mm diameter section of the specimen. Root weld metal was avoided. The O_2 and N_2 contents were analysed via infra-red detection and thermal conductivity systems respectively.

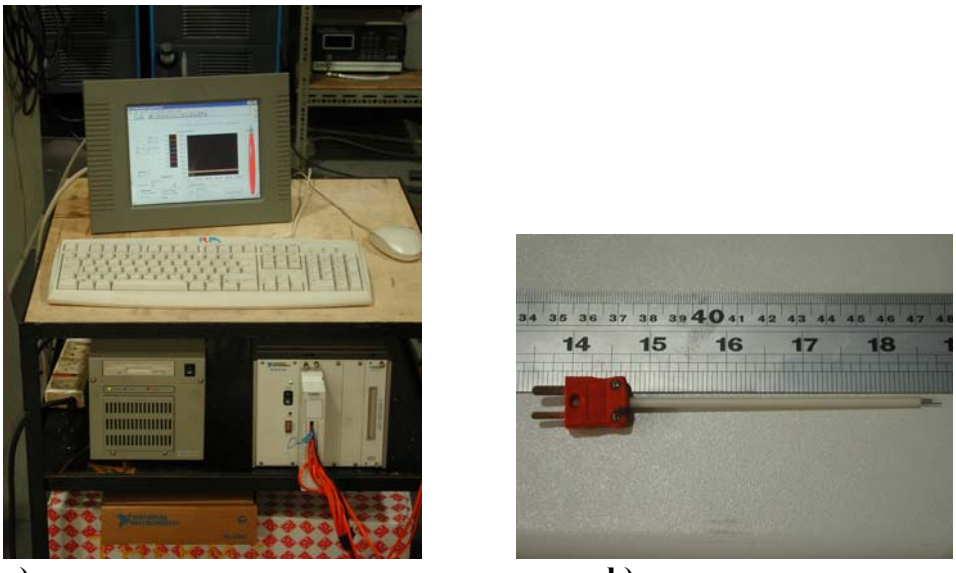

a) **b)**

Fig. 4-17 (a) Thermocouple data acquisition system (b)R-type thermocouple

5 Experimental Procedure

5.1 Welding Procedure Development for Narrow Gap Girth Pipeline Welds

This section includes single and dual tandem welds carried out in the ASME IX 5G position of mainline, and in the 1G position for double jointing girth welds. Details of the bevel preparation are shown in Figure 5.1.

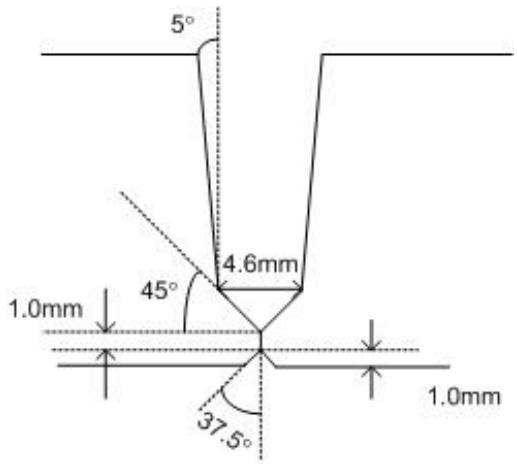

Fig. 5-1 Typical narrow gap weld preparation used throughout the procedure development

The root run was deposited internally with a 0.9mm diameter AWS 70S-6 Thyssen K-Nova filler wire.
The waveform implemented in previous work [1] performed well during initial trials and was adopted for all procedure qualification work. The main criteria for acceptance or rejection of welds were the fusion characteristics and the bead profile. Minor modifications to process parameters were made, including Arc Length Correction and adjustment of the power supply droplet detachment force parameter. Arc length correction and droplet detachment force parameters can be modified manually within a range. Arc length correction occurs through small modifications to the pulse parameters of the waveform. Negative values of the arc length correction setting provide a shorter arc length and positive values a longer arc length. Negative values of the droplet detachment force setting provide low droplet detachment force and positive values increase detachment force.
A typical "bevel offset" length of 2.3 mm provides a gap width of 4.6mm at the base of the groove as shown in Figure 5.1. By adopting low values of the bevel offset, the total volume to be welded is considerably reduced, improving productivity. Low values of bevel offset also help with control of the weld bead profile during positional welding. Alternative bevel offsets tested during this research work were 2.5mm and 3.0mm, used for double jointing.
Efforts in the trial welds concentrated on identifying the correct balance between welding (travel) speed and wire feed speed and obtaining the appropriate torch

oscillation width and arc length. This was particularly critical when welding between 4 to 6 o'clock positions and at the 3 o'clock position. Wire oscillation width was also found to be of high importance. Wide oscillation led to the wires touching the pipe sidewalls, which produced instabilities and undercut. On the other hand, lack of adequate oscillation width can lead to lack-of-sidewall-fusion defects. In principle welding speed was kept constant around the pipe for the first two or three runs but for the remaining fill runs, speed was reduced and sometimes oscillation width was increased in order to reduce lack-of-sidewall fusion defects(no rotation of the contact tip was provided). The arc length is important to the process stability and trials were targeted to generate a smooth (spatter free) transfer process. Weld sections of excessive spatter and slag were removed by grinding; otherwise grinding was used only at the weld start/stop points.
Mechanised pipe welding requires a high degree of operator interaction in the welding process. Control of the contact-tip-to-work-distance is essential for a smooth metal transfer and process stability. It is also essential during welding, that the welding carriage (welding bug) remains in the centre of the pipe weld preparation to guarantee an acceptable bead profile. Unless a seam-tracking sensing system is provided, high operator skills are required.
To minimise any interference of the torch hose pack weight on the torch position within the groove, brackets were installed to support the end of the hose-pack.

Wire separation in the lead and trail torch was between 3 and 4mm and torch separation was 60 to 70mm.

For the double jointing welding procedures, the pipe is rotated at the same speed but in the opposite direction to the welding carriage. By this method, the welding was carried out at a fixed position, (between11:00 to 11:30 o'clock). Details are shown in Figure 5.2.

The torch oscillation frequency varied within a wide range. Oscillation frequency was defined as beats/minute (torch sequence: groove centre to one sidewall, across to the other side and back to the centre). Initially for single tandem welding (36 in OD x19.05mm) pipe, 320bpm (5.33Hz) were applied. This was increased to 350bpm (5.83Hz) for the dual tandem welding process. For the 52 in OD x 22.9mm dual tandem procedures the oscillation frequency was set between 430 to 470 bpm (7.17 to 7.83Hz).

Preheat and interpass temperatures were maintained between 100°C and 130°C for all the tests. This preheat level had been used in earlier work by Hudson [1] to minimise the possibility of hydrogen cracking, and was used in this project to enable comparison with the earlier work
Preheating/interpass temperatures were checked at several points of the pipe circumference before welding. A calibrated Rytek model ST20 infrared thermometer was used.
Welding parameter details, preheating measurements etc. are included in the relevant Appendix B (Welding Procedures)

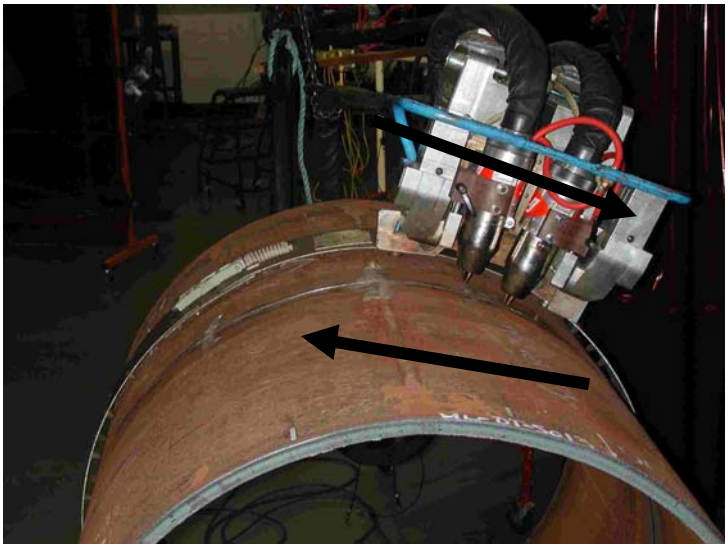

Fig. 5-2 Double joint weld procedure

5.1.1 Filler Wire Selection for Narrow Gap Tandem, Dual Tandem and Double Jointing Procedures

For single tandem welds, all fill (external) runs were deposited using 1.0mm Oerlikon Carbofil NiMo-1 for both lead and trail filler wires, based on the results of previous research work [1].
Efforts in the selection of filler wires for this project were concentrated on dual tandem procedure development. Several short length (200-300mm) dual tandem weld trials were carried out on pipe and all weld metal tensile specimens were tested. Initially both torches used the same wires, either Oerlikon NiMo-1 or Bohler X70-IG but yield strength failed to meet the minimum yield strength of 810MPa and comply with the overmatching criterion (Table 6.1, page 112).
At that point the tests were repeated as full procedure welds and in addition, welds were carried out using filler wires with higher levels of alloying elements (e.g. Thyssen X85-IG, Oerlikon Carbofil 120, Bohler X90-IG). The higher alloy filler wires resulted in weld metal yield strengths of 900MPa and 1000MPa. A list of filler wires tested is reported in Table 6.2 (page 112). The overmatching criterion requires weld metal yield strength between 810MPa and 860MPa but preferably closer to 860MPa.
The two wires in the Cranfield tandem torch design operate within the same weld pool, therefore it was possible to use different consumables for lead and trail wire. It was therefore decided to use the Oerlikon NiMo-1 as lead wire and the Thyssen X85-IG as trail, to provide a weld metal composition which would generate yield strength between 810MPa and 860MPa. This was adopted for both torches.

Following this selection full procedure welds were made and all weld-metal-strip tensile and hardness tests were carried out. Typical all weld metal yield strength was now 842MPa (Table 6.2, page 112), meeting the desired target.

The “combined” technique (Oerlikon NiMo-1/ Thyssen X-85) was adopted for the remaining part of the experimental work on 52 in OD x 22.9mm pipe.

Details of the welding procedures are reported in Appendix B.

5.1.2 Welding Procedure and Filler Wire Selection for Tie-In Welds

The Tie-in weld procedure was carried out according to ASME IX 5G (12 o'clock to 6 o'clock.) position. Details of the bevel preparation are shown in Figure 5.3. The 15° bevel angle will considerably reduce the joint volume compared to the standard 30° of the API 5L, but with an additional cost for bevel machining.

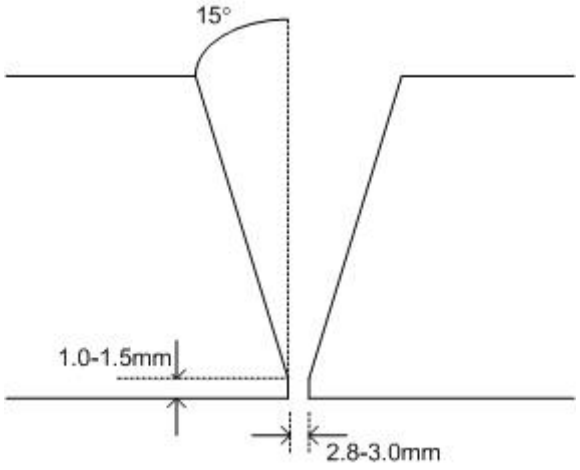

Fig. 5-3 Bevel preparation for Tie-In procedure welds

The root run was deposited in a vertical up direction externally (semi-automatic GMAW) with the Oerlikon Fluxofil M10S(AWS A5.20 E71T1MJH4) metal cored wire 1.2mm diameter (Tables 4.5, page 50 and 4.6, page 51).
In previous work by Hudson [1], it had been found that fill and cap passes with high strength rutile wires using mechanised FCAW and a conventional API 30° bevel did not attain the $Rp_{0.2}$ minimum of 810MPa.
Downhill mechanised pulsed GMAW was used. The pipe bevel was reduced to 15° and basic flux cored wires (Philarc PZ6148 and PZ6149) were used in an attempt to increase minimum yield stress and satisfy the overmatching criterion. Pulsed welding was selected for its low spatter characteristics, and the ability to use low-medium average currents. Upwards pulsed GMA welding with basic flux wires generated significant arc instabilities and when downwards welding direction was adopted the process characteristics were improved. Considerable time was spent in obtaining a pulsed waveform for the basic flux cored wire. Given the time limitations only one working point was developed and all fill runs were deposited at the same operating point. Details of the operating point are included in Appendix A.
Hot pass and the first fill were deposited as "single" passes. The remaining fill and cap runs were split (side by side).
A wire brush was used to remove the slag inclusions, although a grinding wheel was also used over the completed surface and in the overlapping section of split passes.
All procedure details are reported in Appendix B.

5.1.3 Electrical Parameter Measurement

The calculation of heat input or arc energy is a very important parameter and it is reported in the WPSs and PQRs. Heat input is directly proportional to the process average voltage and current and for almost all the international standards is treated as an essential variable, directly affecting the mechanical properties. However, Joseph [145] reported that the most representative method to calculate the heat input for pulsed welding is the average instantaneous power ($P_{INST}=\sum_{i=1}^{n} I_i * V_i / n$) rather than power calculated from the RMS (root mean square; $P_{RMS}=I_{RMS}*V_{RMS}$ where: $I_{RMS}=\sqrt{\sum_{i=1}^{n} I_i^2 / n}$ and $V_{RMS}=\sqrt{\sum_{i=1}^{n} V_i^2 / n}$) or the power calculated from average voltage and current.
The Yokogawa DL750 Scopecorder oscilloscope was used to store the current and voltage waveforms. For current measurements calibrated LEM Hall probes and voltage leads were used. Current probes were placed at the power cables at the wire feeders, and the voltage was measured between the wire feeders and the workpiece.
A typical sampling rate of 10kHz/s and a bandwidth of 4kHz allowed adequate recording time for full procedure pipe welds.

5.1.4 NDT and Mechanical Testing

A normal radiographic examination technique (panoramic) was adopted for the NDT inspection of all the welded pipe joints. Examination was carried out by an independent NDT company (Bodycote /NDIS).
Gamma Ray sources (Iridium 192) were used and radiography was conducted in accordance to BS EN 1435 1997, using 6Fe EN Penetrameter and 5 wire sensitivity for the 52 in x 22.9 mm WT pipe; and 10 Fe EN Penetrameter 1 wire sensitivity for the 36 in x19.05mm pipe), with D7 film quality. In an attempt to improve the quality of the images and increase the capability of detecting all the potential weld defects, X-Ray and D4 film quality replaced Gamma-Ray and D7 for all procedure qualification welds. The I.Q.I Type used was in accordance with EN 462-1. All defects were reported and evaluation criteria were established in accordance with BS 4515-1 2000. Radiographic reports were issued and signed by an ASNT/PCN Level III or Level II qualified inspector. All films were reviewed by WERC personnel and all defective areas or single defects were marked on the pipe, to enable only defect-free sections to be taken for further destructive testing.

The standards applied for the destructive tests are listed below:

- BS EN 288-9:1999 [105]. Specification and approval of welding procedures for metallic materials-Part 9: Welding procedure test for pipeline welding on land and offshore site butt welding of transmission pipelines,

- BS 4515-1:2000 [106]. Specification for welding of steel pipeline on land and offshore- Part 1: Carbon and carbon manganese steel pipelines.

The above standards were used in order to specify the requirements for qualification, and testing of pipeline welding procedures and description of the essential parameters.

- API 1104:1999 [107]. Welding of pipelines and related facilities. Used for the location, sample preparation and testing requirements for cross weld tensile, fracture and side bend testing.

Additional destructive tests involved macro sections in three positions (12, 3 and 6 o'clock), hardness of seam/girth weld interaction, all weld metal tensile tests and CTOD testing of weld metal and HAZ [108],[109],[110],[111].
The specimen extraction locations and the related positions around the pipe are shown in Figure 5.4 and were in accordance to API 1104 followed prior work by Hudson [1].

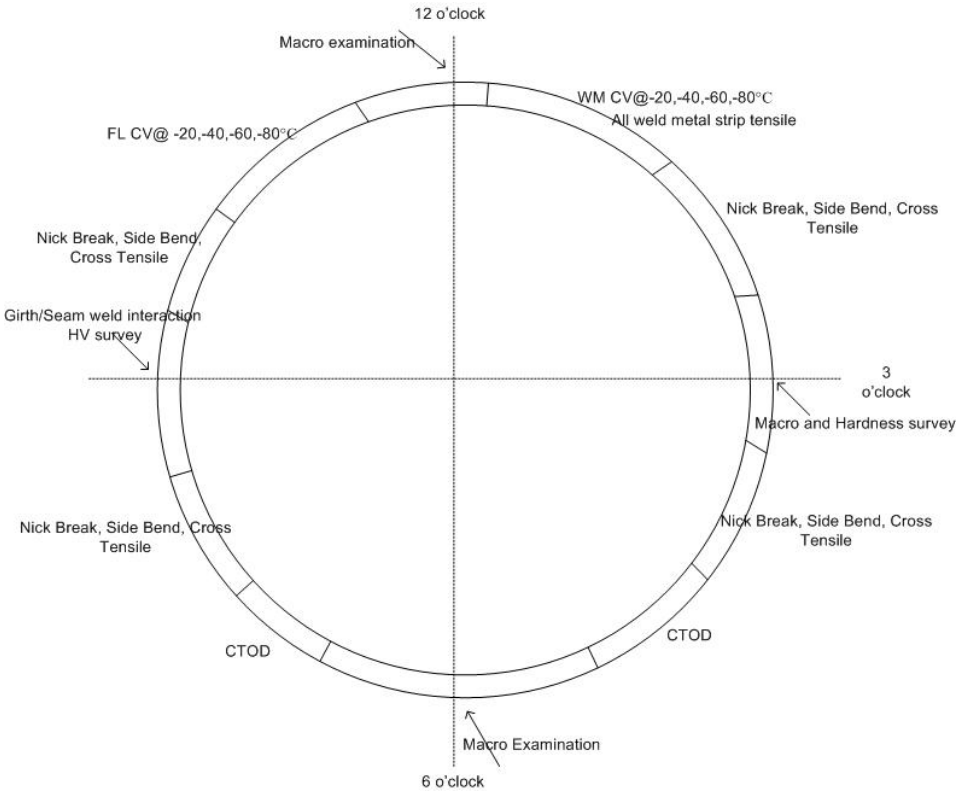

Fig. 5-4 5G pipe test specimen extraction locations

5.1.5 Weld Metal Tensile Testing

Rectangular (strip) tensile specimens (Figure 5.5) were selected in an attempt to incorporate as much as possible of the fill passes weld metal in the test specimen.
Due to the wider joint preparation used for the tie-in welds (15°), a 7mm diameter all weld tensile round bar specimen was extracted allowing more thermal cycles of the fill passes to be incorporated in the testing section.
The standard gauge length (l_0) / original gauge length cross sectional areas (S_0) relationship ($l_0=5.65(S_0)^{1/2}$) was adopted. The $Rp_{0.2}$ proof strength, UTS (ultimate tensile strength) and elongation (A, %) were recorded.

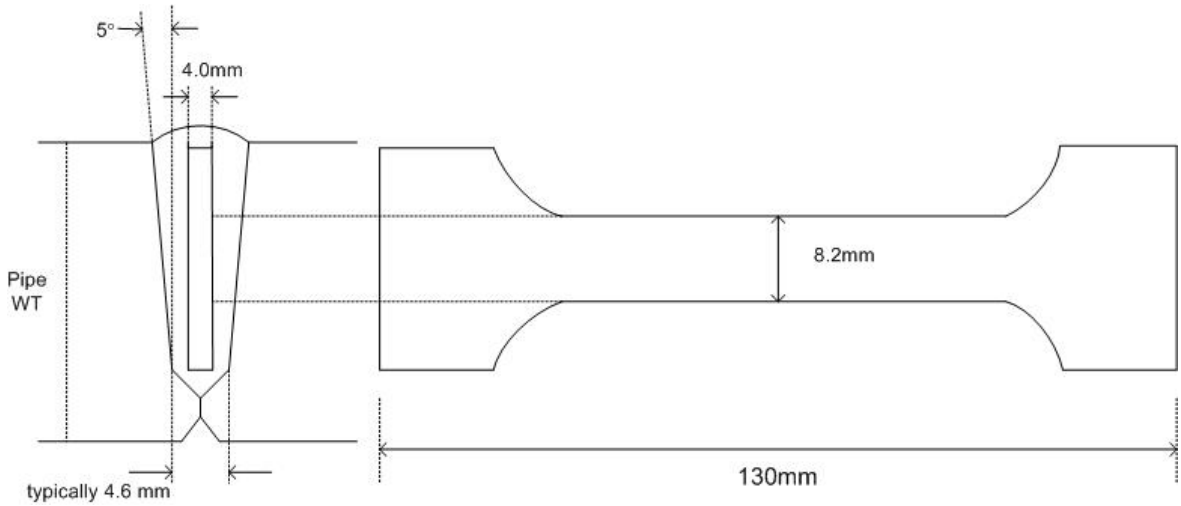

Fig. 5-5 All weld metal strip tensile dimensions and location

5.1.6 Hardness Testing

For the hardness survey, one specimen of the girth weld was extracted from the 3 o'clock pipe position and one from the girth/seam weld interaction. The girth/seam specimen hardness test included the girth narrow gap weld, with the seam weld on one side and the parent metal on the other or the seam weld on both sides. The hardness survey was carried out in accordance with BS 4515-1. Details of the locations of the macrohardness indentations (10 kg load) are shown in Figure 5.6.

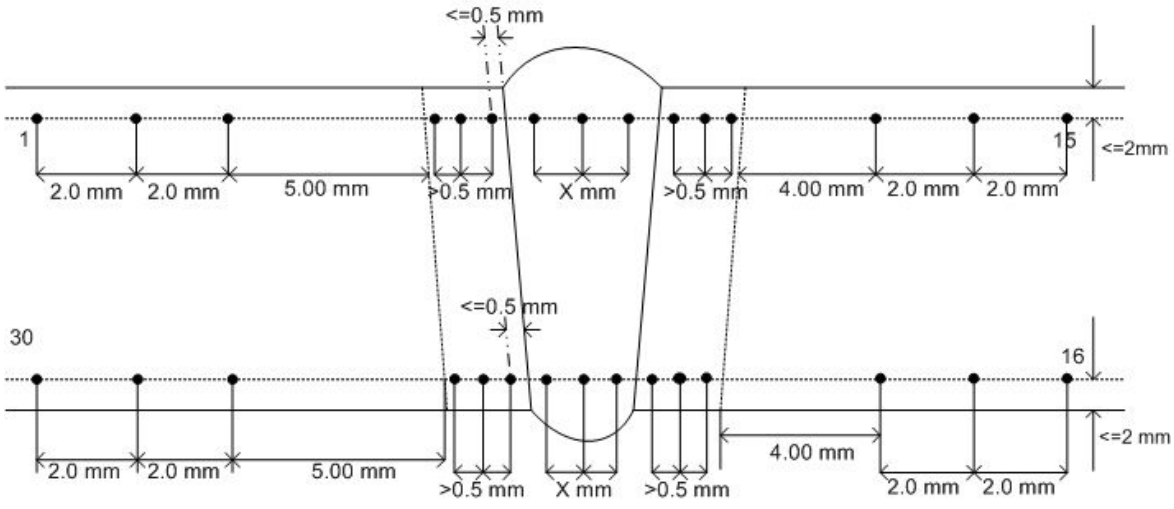

Fig. 5-6 Macro Hardness (HV10) indent locations

Microhardness (0.5kg load) survey indents were located as shown in Figure 5.7.

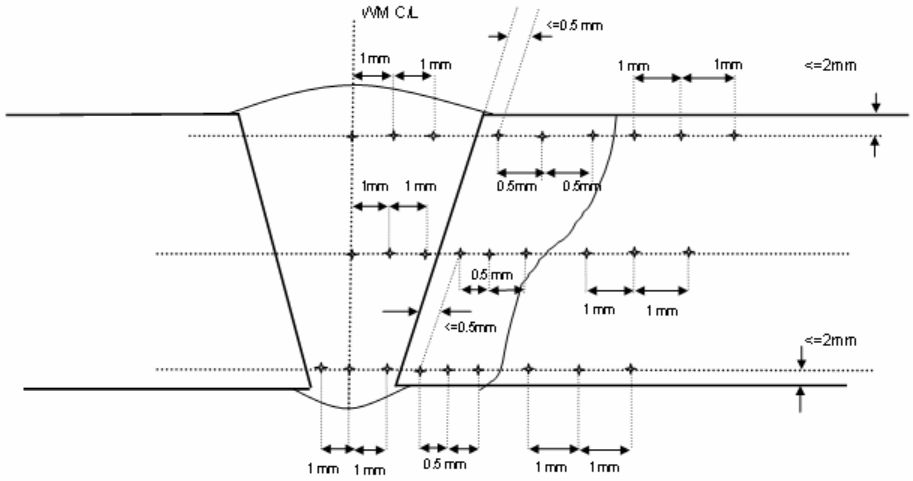

Fig. 5-7 Microhardness (HV0.5) indent locations

In addition to the weld microhardness, the parent material microhardness was measured. The location of the indents is shown in Figure 5.8.

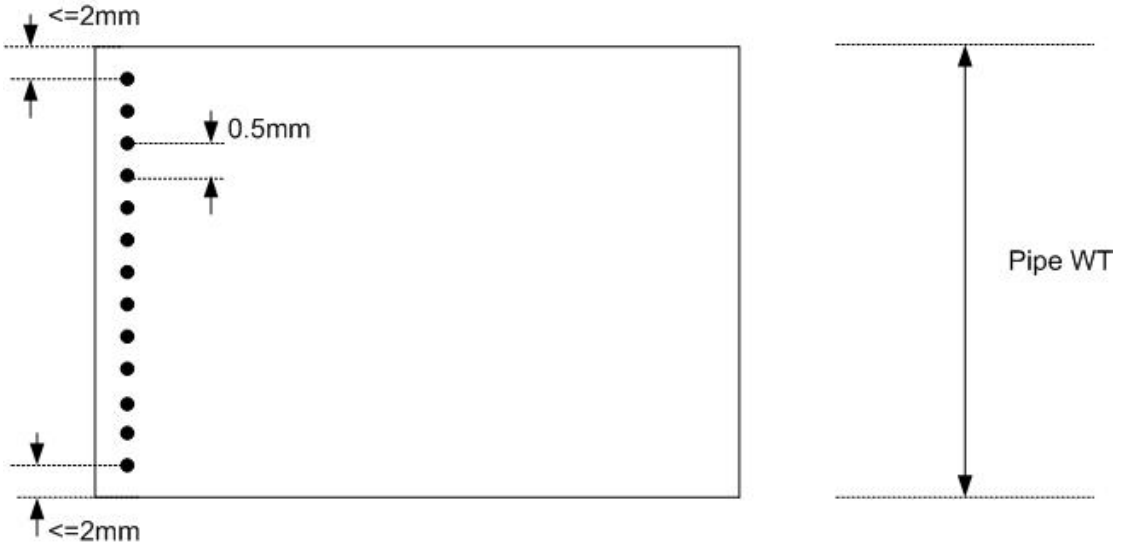

Fig. 5-8 Parent material microhardness (HV0.5) indent locations

5.1.7 Impact Toughness Tests

The impact toughness specimens were extracted from a location 2mm from of the internal diameter of the pipe. Additional specimens were extracted from 2mm the external diameter of the pipe. Tests included both weld centre-line and fusion-line and were conducted in accordance to BS 4515-1. Charpy tests were performed at -20°C, -40°C,-60°C, -80°C and transition curves were plotted.

5.1.8 CTOD Toughness Tests

Tests were carried out in accordance with BS 7448-1/2 [108]: Fracture mechanics toughness tests; with the crack tip located either on the weld centreline or the fusion line. Three specimens at each crack location were prepared and tests were conducted at -10°C.

5.1.9 Nick Break, Side Bend and Cross Weld Tensile Tests

Tests were conducted in accordance with API 1104:1999 [107] and specimens were extracted from 45° , 135° , 225° and 315° positions around the pipe.

5.1.10 Mechanical Test Equipment and its Calibration

The majority of the mechanical tests described above were carried out by Bodycote (Daventry branch) an independent UKAS accredited company. For all mechanical tests, the relevant certificates were issued and for the all metal strip tensile tests additional electronic information was provided as ASCII files.
The hardness survey performed at Cranfield University premises utilised a Vickers-Armstrong pyramid diamond indenter and a Matsuzawa Seiki Co microhardness tester.

5.2 Welding Parameter and Shielding Gas Trials

5.2.1 Introduction

As described earlier in the review of literature (section 2.4, page 28) several approaches have been developed to determine the effect of the welding parameters on the weld bead geometry. It is important to emphasize that much of the work was performed on bead-on-plate weld trials and quite limited studies have been carried out in narrow groove preparations.
The theoretical approach relies on a series of simplifications. Only axial spray transfer is considered; the effect of the droplets, the convection in the weld pool and the radiation from the plate surface are ignored, and the physical properties are assumed to be constant at all temperatures.
The tolerance box and the Arcwise techniques represent a systematic approach. They are orientated towards industrial applications although they can be expensive and time consuming. They do not provide prediction equations on the main factors and their interaction effects.
The Design of Experiments techniques use quantitative approaches in order to determine the borders of a given group of experimental parameters, and employ statistical techniques to investigate variations within these boundaries. Mathematical equations describing the bead geometry can be derived and the interaction of welding parameters is determined. The number of experiments required is relatively limited leading to significant economy in experimental requirements.

5.2.2 Plate Preparation

X100 plate specimens were prepared on a band saw and typical dimensions were 350 x 350 mm for the shielding gas trials and 150 x 350 mm for the welding parameter trials work. Grooves were machined either at 11mm (shielding gases trials) or at 8mm (welding parameter trials) depth of the plate thickness. Details are shown in Figure 5.9.
This preparation was selected for the following reasons:

- to reconstruct the original preparation in order to measure the bead profile as shown in Figure 5.10,
- to simulate the heat flow in a real weld reasonably accurately.

It is clear that the bevel preparation at the bottom of the groove is not typical of a real weld, however it allows precise measurements of the groove sidewall penetration.

Ten grooves per plate were machined for the shielding gas trials and two grooves per plate for the welding parameter trials. The number of grooves was reduced in order to minimise the distortions that might affect process performance e.g. difficulties in torch positioning in groove centreline, variations in CTWD etc.
Two single weld beads per groove, of approximately 160mm each in length, were deposited.
Specimens were clamped in a jig, avoiding restricting movement during welding and preventing significant distortion.
Acetone was used to degrease all grooves before welding. After welding the plates were allowed to cool down before they were removed from the jig.

5.2.3 Welding Positions

The experiments for the shielding gas trials were carried out in flat (0°) position,
while experiments for the welding parameters trials were carried out in flat (0°) , vertical down (90°) and overhead (180°) positions. Supplementary trials were performed at 30°, 60°, 120° and 150° angular positions.

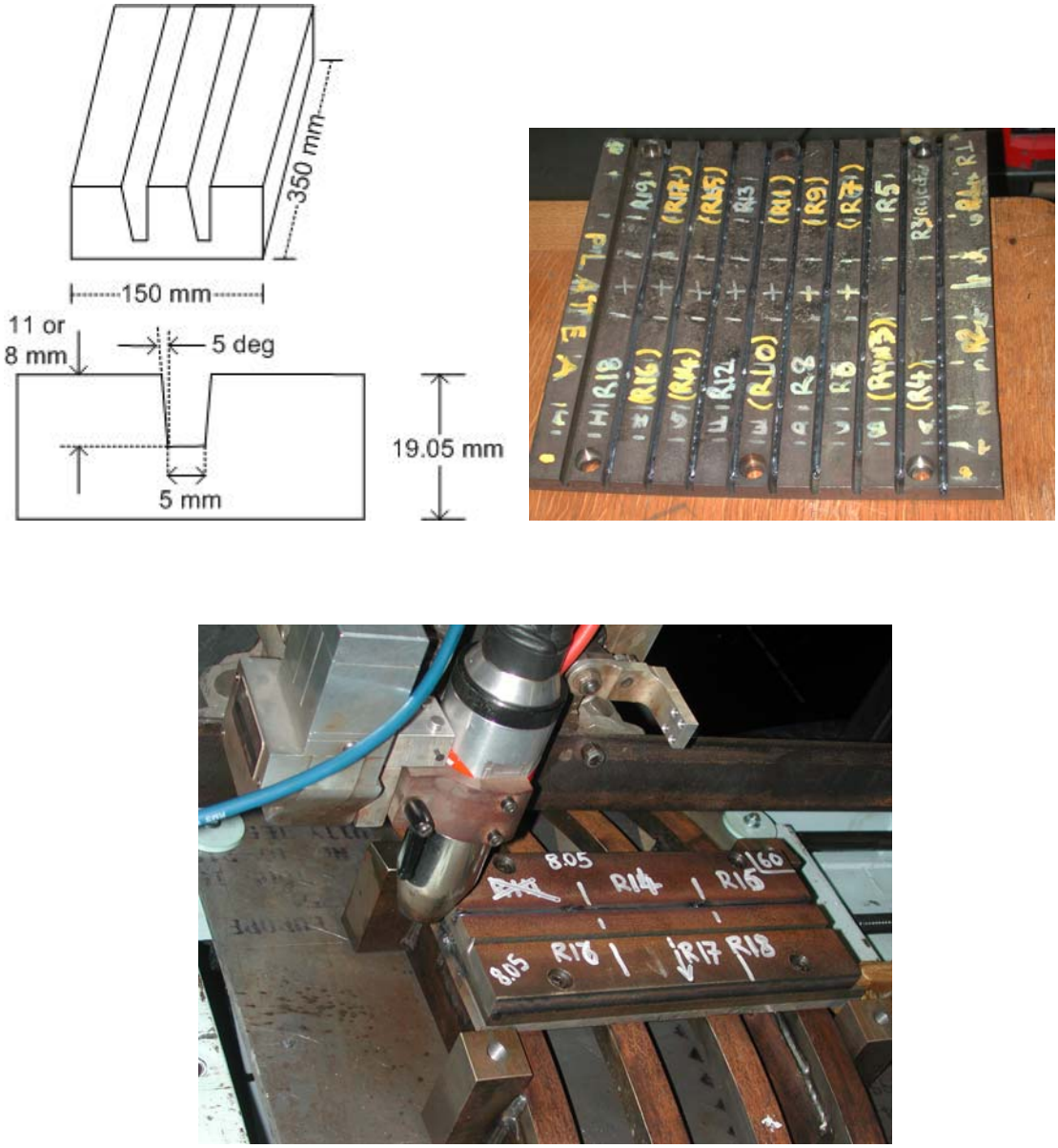

Fig. 5-9 Plate bevel preparation and experimental setup

5.2.4 Weld Bead Shape Measurements

The measured weld bead parameters are shown in Figure 5.10.

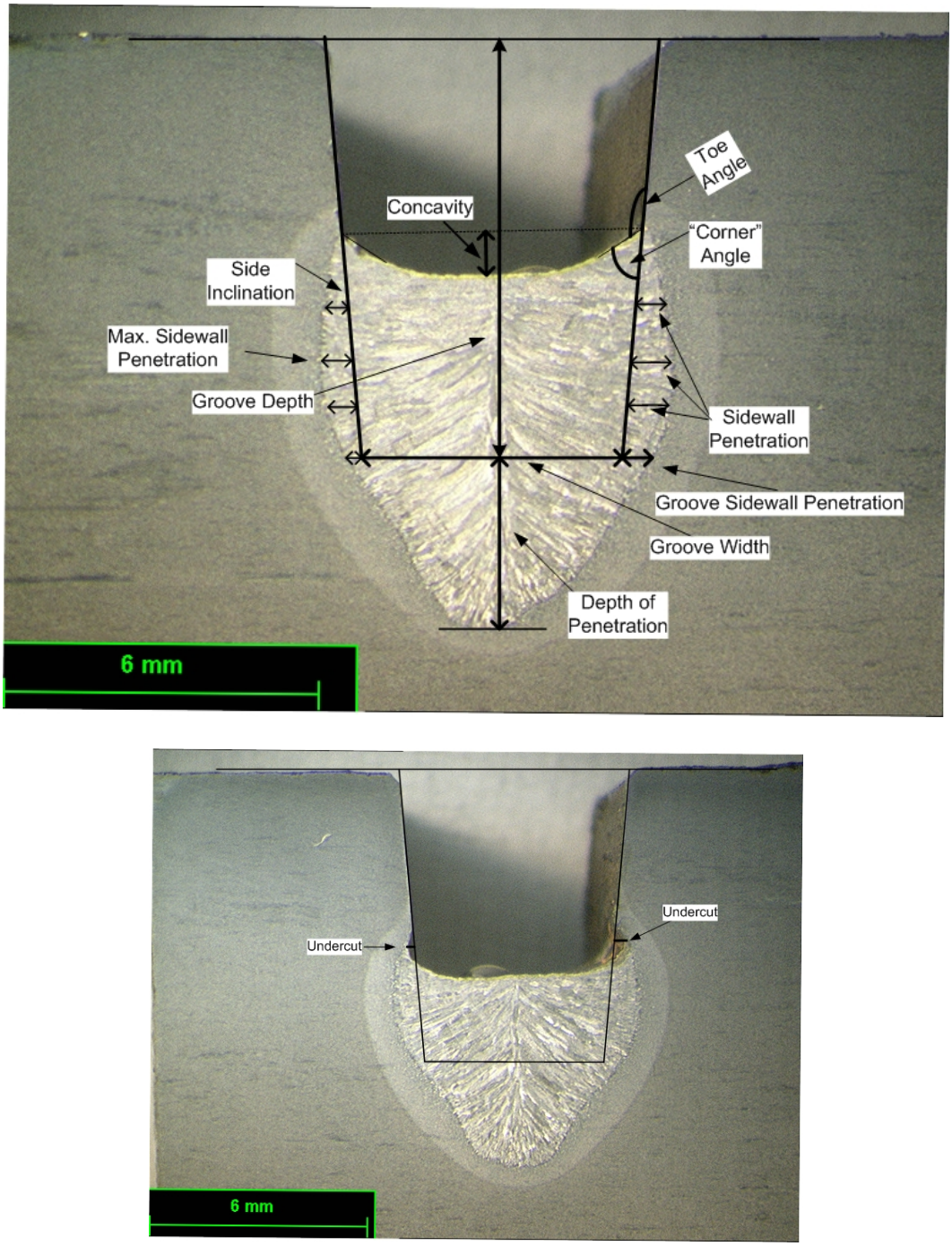

Fig. 5-10 Weld bead shape measurement definitions

For the shielding gas trials, measurements were made of:

- depth of penetration,
- concavity, and
- sidewall penetration

The sidewall penetration was considered as the average of six measurements (three each side). Two measurements were taken at approximately 0.5-0.7mm from both the bottom

of the groove and the surface of the weld profile. The third measurement was the maximum sidewall penetration.

For the welding parameter trials, measurements were made of:
- "corner" angle,
- depth of penetration, and
- groove sidewall penetration

Some welds had sidewall undercut defects which were included in the weld bead geometry analysis.
Initial welding parameter trials showed that penetration at the corners of the groove bottom (groove sidewall penetration) was more sensitive to the probability of lack-of-sidewall fusion defects than the average sidewall penetration measurement, and hence the groove sidewall penetration measurement was used for the welding parameter trial analyses. In some of these welds it was difficult to measure the concavity (considered in the shielding gases trials) due to the shape of the bead profile (Figure 5.11). Hence the corner angle was measured instead. Corner angle (180°-toe angle) has a strong influence on the probability of potential defects in the subsequent welding runs. Low corner angle increases the probability of better fusion.

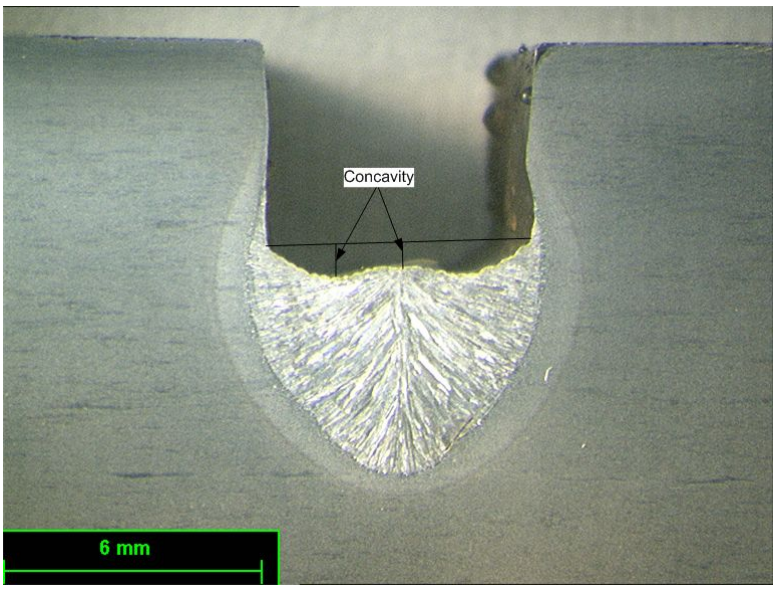

Fig. 5-11 Concavity discrepancies example (flat position)

5.2.5 High Speed Video Images

Bead on plate experiments were carried out and high speed video images were recorded. High quality images are important in measuring the exact arc length, in characterising the transfer mode, and in estimating droplet rates and size etc.
Early experiments used plain welding shield filters for the camera to prevent the arc glare but this did not result in good images. Improvement was achieved by replacing the filters with neutral density filters and by adding backlight behind the arc.
The camera (Phantom 4.1) was positioned at 0.7-1m distance from the arc and after several trials the best settings for groove welds were established, these are as follows:

shutter speed or exposure time 132μs, frame delay 1μs, resolution of the image 256 x 256 pixels, sampling rate 3500fps; (or some videos the sampling rate was increased up to 5000fps and resolution reduced to 256x128pixels).
The lens was a Sigma 50-500mm zoom and operated at f16 aperture (although f11 and f22 also produced acceptable results).
Between camera and lens a x2 teleconverter that doubles the focal length was inserted.
A combination of neutral density filters (ND4 +ND8; or ND2+ND4+ND8) was used. An ultraviolet filter was placed in front of the last (ND8) filter.
A 2000W halogen lamp was placed behind the arc at 1m distance. This backlight significantly improved the quality of the images.
The camera, the back light and the relevant settings are shown in Figure 5.12

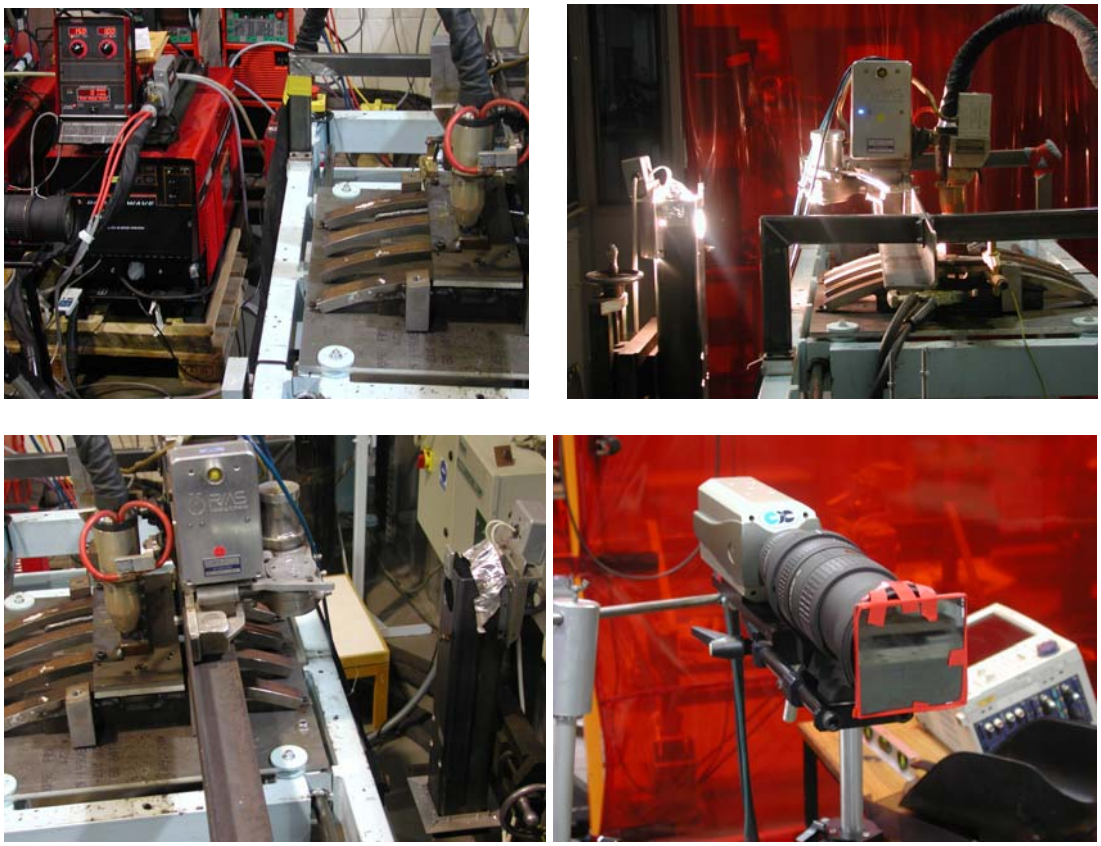

Fig. 5-12 High speed video camera, neutral density filters and backlight technique

Videos were recorded and arc images were saved as bitmap (bmp) files.

Additional trials were carried out using two different band pass filters: 950+/-10nm and 635+/-10nm inserted between the camera and the lens, but both failed to provide adequate images.
For the narrow groove welds, no backlight was used as only one arc was recorded (lead arc) and the trail arc had a similar effect as the backlight. Additionally, positioning the backlight effectively inside the groove was difficult and no evident improvement was reported. In this case, good images were obtained without the backlight.

A schematic diagram of the welding rig is shown in Figure 5.13

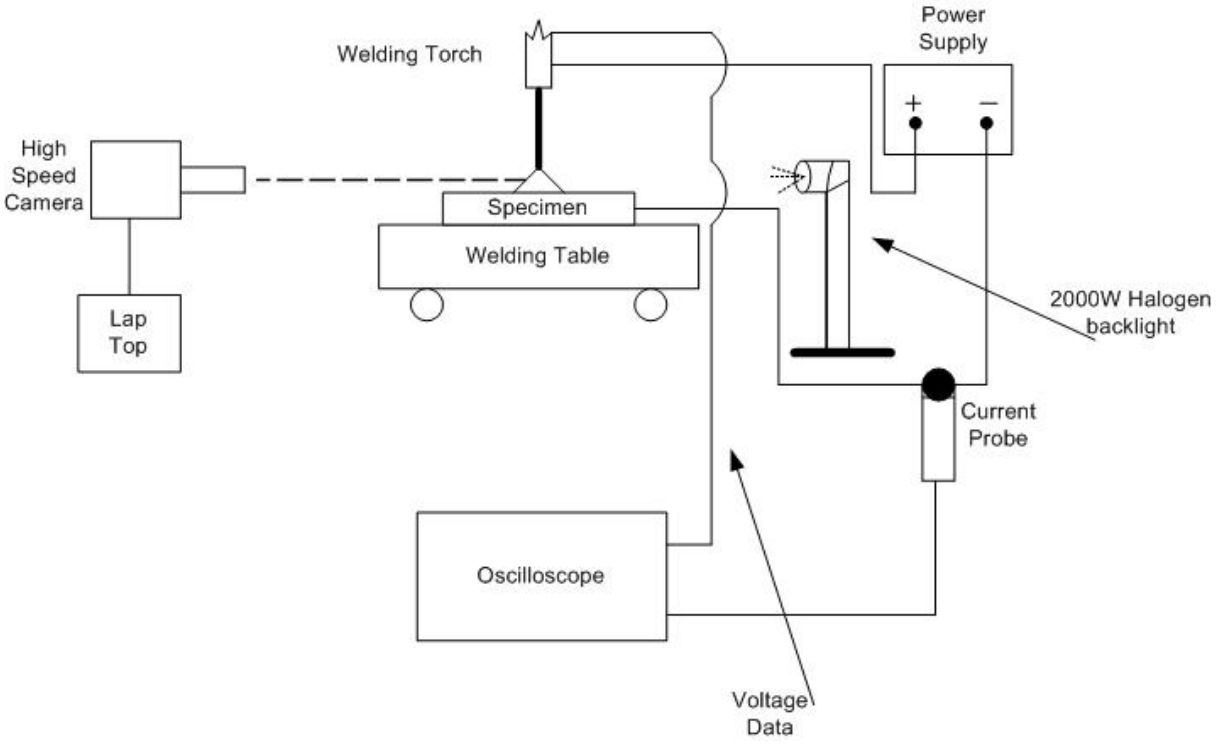

Fig. 5-13 Schematic diagram of the high speed video welding rig.

5.2.6 Validation of Mixer Panel Calibration

The calibration charts reported in section 4.3.1(page 52) refer to gas flow rates obtained from the flow meter readings.
The validity of the calibration charts was confirmed by the use of a mass spectrometer analyser. The mass spectrometer analysis was carried out at BOC premises in Wolverhampton
The gas composition at the outlet of the mixer panel was directed to the mass spectrometer and the gas percentages were displayed. Several readings were recorded and the average values calculated.

The results of the analysis are shown in Table 5.1

Prior to the analysis the accuracy of the mass spectrometer was tested by analysing gas mixtures contained in certified gas bottles and some of the verification tests are shown in Table 5.2.

		Mass Spec. Readings (%)	
Test No.	Mixer Composition (%)	Average	Standard deviation
7	Ar = 73.37	73.55	0.10
	CO_2 = 19.38	20.22	0.05
	He = 5	4.27	0.03
	O_2 = 2.25	1.98	0.02
8	Ar = 76	76.18	0.07
	CO_2 = 11	12.72	0.05
	He = 10	9.01	0.06
	O_2 = 3	2.13	0.01
17	Ar = 84.38	83.82	0.05
	CO_2 = 8.38	9.75	0.03
	He = 5	4.57	0.04
	O_2 = 2.25	1.91	0.01
18	Ar = 70	69.06	0.25
	CO_2 = 20	21.85	0.10
	He = 10	9.24	0.08
16	Ar = 85	83.28	0.08
	CO_2 = 5	6.56	0.03
	He = 10	10.17	0.06
6	Ar = 80	78.41	0.08
	CO_2 = 13.33	15.48	0.05
	He = 6.67	6.10	0.07
22	Ar = 82.5	80.94	0.15
	CO_2 = 12.5	14.41	0.05
	He = 5	4.76	1.16
4	Ar = 72.5	69.89	0.21
	CO_2 = 7.5	8.7	0.10
	He = 20	21.35	0.13
14	Ar = 85	83.25	0.08
	CO_2 = 5	6.59	0.04
	He = 10	10.18	0.07
10	Ar = 92	92.27	0.02
	CO_2 = 5	5.58	0.02
	O_2 = 3	2.17	0.01
5	Ar = 81	82.67	0.05
	CO_2 = 16	15.14	0.04
	O_2 = 3	2.15	0.01
9	Ar = 70	73.88	0.15
	CO_2 = 27	24.13	0.06
	O_2 = 3	2.06	0.01
24	Ar = 92	92.16	0.02
	CO_2 = 5	5.66	0.02
	O_2 = 3	2.19	0.02

Test No.	Mixer Composition (%)	Mass Spec. Readings (%)	
		Average	Standard deviation
11	Ar = 82	82.27	0.06
	CO_2 = 5	6.13	0.02
	He = 10	8.69	0.03
	O_2 = 3	2.95	0.01
21	Ar = 71.75	72.03	0.12
	CO_2 = 6.75	7.54	0.03
	He = 20	18.93	0.13
	O_2 = 1.5	1.46	0.01
3	Ar = 73.37	74.14	0.14
	CO_2 = 10.88	12.05	0.06
	He = 15	13.04	0.01
	O_2 = 0.75	0.75	0.02
13	Ar = 70	71.47	0.12
	CO_2 = 17	17.55	0.05
	He = 10	8.14	0.07
	O_2 = 3	2.86	0.02
20	Ar = 70	69.96	0.12
	CO_2 = 7	7.97	0.02
	He = 20	19.24	0.10
	O_2 = 3	2.84	0.01
25 & 26	Ar = 95	93.57	0.04
	CO_2 = 5	6.43	0.04
2	Ar = 82.5	80.84	0.06
	CO_2 = 17.5	19.14	0.08
1 & 12	Ar = 70	69.57	0.07
	CO_2 = 30	30.43	0.06

Table 5-1 Validation of mixer panel calibration

Certified Gas Bottle Mixture (%)	Mass Spectrometer Reading (%)
CO_2 = 31.15	31.308
Ar = 68.85	68.692
O_2 = 3.39	3.252
Ar = 90.53	90.495
CO_2 = 6.08	6.292
Ar = 54.72	55.588
CO_2 = 15.08	14.890
He = 30.2	29.522

Table 5-2 Mass spectrometer analysis and certified gas bottle mixture comparison

As a further check on accuracy the flow rate at the outlet of the tandem torch was performed. It was found to be only 22 L/min at the torch outlet instead of the "theoretical" 30 L/min according to the valve setting at the mixer panel. The difference of pressure between the inlet and the outlet of the hose assembly was considered to be the cause.

5.2.7 Temperature Measurement Equipment

Thermocouple trials were carried out to examine the effect of shielding gases on the thermal cycle within the weld metal. The welds tested were the same as those used during the shielding gas trials.
A small extension (3-4mm) of the wires from the ceramic tube was plunged into the molten welding pool behind the arc, far enough to avoid the arc itself. As the molten steel solidified the cooling cycle was recorded. The limbs had been joined together by TIG welding before they were harpooned into the pool.
One channel of the National Instruments module was used to record the thermoelectric voltage from the R-type thermocouples. The sampling rate used was 400Hz. The recorded data was transferred to an Excel program to present the data in a graphical format.

5.3 Process Modelling

5.3.1 Modelling of the Experimental Procedure

The main objective of this modelling process was to identify the influence of the separate input parameters (variables or factors) and their interactions on the weld bead geometry expressed in terms of mathematical equations.

5.3.1.1 Design of Experiments

Design of Experiments is a systematic approach to planning the experiments. Statistical analysis (modelling) relies on data contained in the experiments, therefore properly designed and conducted experiments are essential for successful models.

The flowchart presented in Figure 3.2 (page 44) can be coded as follows:

- Process definition
- Selection of factors and levels
- Selection of responses
- Selection of the experimental design
- Performance of experiments
- Data selection and analysis
- Model development
- Mathematical equation development
- Model adequacy checking and validation
- Conclusions

The modelling process (model development, analysis of variance, model diagnostics etc) followed the procedure referred to the in the Design Expert Software Manual [95]. Some definitions are included in section 6.3.1.1 (page 123).

5.3.2 Choice of Experimental Design

The aim of selecting the appropriate experimental design was to develop a model that could successfully represent the system.

5.3.2.1 Shielding gas trials

The gases (factors) selected and their ranges were:

Ar = 70%-95%
CO_2 = 5%-30%
He = 0%-20%
O_2 = 0%-3%

This selection was based on a review of the literature and on the assumption that a shielding gas combining the components within the above ranges would be expected to establish a stable and smooth transfer mode.
A D-Optimal design was selected resulting in 24 experiments, including 5 replicates.
The reasons for using D-Optimal designs instead of classical designs (e.g. factorials) are as follows:

- require a relative small number of trials compared i.e. to factorials to estimate model coefficients
- estimate the presence of curvature in the system.

The experimental design is shown in Table 5.3 including the flow rates and the mixer panel valve settings. The table includes two additional runs (welds) added to the original design: Run 23 used the commercial (BOC) Ar82.5%$CO_2$12.5%He5% gas mixture and Run 22 used this composition but generated using the mixer panel. This resulted in a total of 26 experiments.

The following welding parameters were held constant throughout these trials:
- wire feed speed: 10m/min,
- welding speed: 1220mm/min(48 in/min),
- wire distance from sidewall: 1.35mm,
- torch travel angle: 90°,
- filler wire: Oerlikon NiMo-1, 1.0mm diameter(lead and trail),
- preheating temperature: 100°C,
- arc length: 1.2-1.8mm,
- CTWD: 13.5mm

	Gas											
	Argon			CO_2			He			O_2		
Weld	%	L/ min	Valve Reading	%	L/ min	Valve Reading	%	L/ min	Valve Reading	%	L/ min	Valve Reading
1	70.00	21.00	677	30.00	9.00	295						
2	82.50	24.75	800	17.50	5.25	122						
3	73.37	22.00	710	10.88	3.30	20	15.00	4.50	460	0.75	0.22	-797
4	72.50	21.75	702	7.50	2.25	-955	20.00	6.00	605			
5	81.00	24.30	785	16.00	4.80	98				3.00	0.90	-933
6	80.00	24.00	775	13.33	4.00	60	6.67	2.00	240			
7	73.37	22.00	710	19.38	5.81	150	5.00	1.50	200	2.25	0.67	-896
8	76.00	22.80	737	11.00	3.30	20	10.00	3.00	333	3.00	0.90	-933
9	70.00	21.00	677	27.00	8.10	250				3.00	0.90	-933
10	92.00	27.60	892	5.00	1.50	-907				3.00	0.90	-933
11	82.00	24.60	795	5.00	1.50	-907	10.00	3.00	333	3.00	0.90	-933
12	70.00	21.00	677	30.00	9.00	295						
13	70.00	21.00	677	17.00	5.10	115	10.00	3.00	333	3.00	0.90	-933
14	85.00	25.50	825	5.00	1.50	-907	10.00	3.00	333			
15	77.33	23.20	750	20.67	6.20	170				2.00	0.60	-885
16	85.00	25.50	825	5.00	1.50	-907	10.00	3.00	333			
17	84.38	25.31	818	8.38	2.51	-968	5.00	1.50	200	2.25	0.67	-896
18	70.00	21.00	677	20.00	6.00	160	10.00	3.00	333			
19	70.00	21.00	677	27.00	8.10	250				3.00	0.90	-933
20	70.00	21.00	677	7.00	2.10	-946	20.00	6.00	605	3.00	0.90	-933
21	71.75	21.50	693	6.75	2.02	-940	20.00	6.00	605	1.50	0.45	-855
22	82.5	24.75	800	12.5	3.75	41	5	1.50	200			
23	82.5			12.5			5					
24	92.00	27.60	892	5.00	1.50	-907				3.00	0.90	-933
25	95.00	28.50	920	5.00	1.50	-907						
26	95.00	28.50	920	5.00	1.50	-907						

Table 5-3 Experimental design; shielding gas flow rates and mixer panel valve settings

5.3.2.2 Welding parameter trials

5.3.2.2.1 Initial Welding Trials

Considering the large number of welding parameters that may affect the weld bead shape, a detailed study was carried out to select those to be considered in the experimental design.
A list of welding parameters is shown below:

- Wire feed speed (mean welding current)
- Welding speed (travel speed)
- Pulsed parameters:
  - Pulsed current (I_p)
  - Peak time (T_p)
  - Background current (I_b)
  - Background time (T_b)
  - Frequency (F)
- Arc voltage
- Arc length (l_a)
- Power supply characteristics
- Filler wire diameter
- Filler wire chemical composition
- Contact tip to work distance (CTWD)
- Wire extension (l)
- Gap width / joint details
- Shielding gas composition
- Shielding gas flow rate
- Welding position
- Torch angle
- Oscillation width
- Oscillation frequency
- Preheating temperature
- Contact tip configuration (angle and separation)

It was immediately obvious that a simultaneous study of such an extensive number of welding parameters would require a very large number of experiments. It was therefore decided to reduce the number of welding variables (predictors or factors) to a more reasonable number.
The parameters selected and their range were limited to the following because they were believed to be the most important in affecting the weld bead geometry:

- wire feed speed : 8.2 – 13.2 m/min
- welding speed : 900 – 1400 mm/min
- wire distance from the sidewall : 0.3 – 1.2 mm
- arc length correction (arc length) : -25% - +25%

Although arc length correction is not a totally independent parameter (e.g. from voltage and/or current) and is likely to be different using different power supplies, it was

considered of fundamental importance to keep the arc length constant due to its considerable effect on weld bead profile. The remaining parameters not listed above were held constant throughout the experimentation:

- oscillation frequency: 450beats/min (7.5Hz)
- preheating temperature: 100°C,
- torch travel angle: 90°
- filler wire: Oerlikon NiMo-1 (lead and trail)
- CTWD: 13.5mm

Despite the significant advantages of DOE (section 2.4.3.4, page 34) their application can be constricted by certain assumptions and limitations:
-variables are assumed to be independent
-the presence of noise in the system can obscure the effect when the range of the parameters level selected is narrow but necessary in order to obtain "sound" welds. A wider range may provide much clearer information regarding the effect, but may not always reasonable weld bead profile
-adopting a design system (e.g. factorial, central composite, etc) for the analysis assumes a certain profile for the response (linear, quadratic, etc) and therefore different profiles in the response may not always be detected.
Nevertheless, in this work variables were selected to be as independent as possible, and at levels where we expect effects to be seen.

The wire distance from the wall was the distance between the outer wire surface and the edge of the groove after the wire was extended to 13.5mm (Figure 5.14).

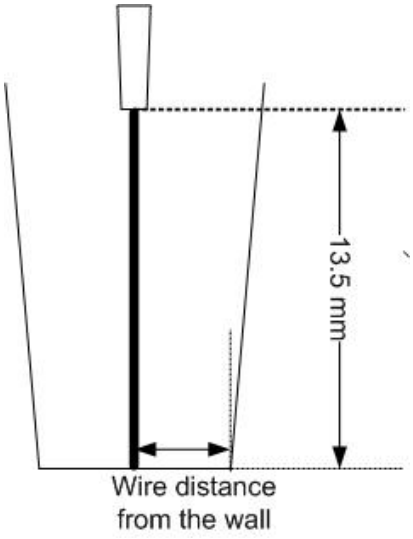

Fig. 5-14 Wire distance from the wall definition

With the number of factors established at four and considering five levels for the factors (coded values are: -2, -1, 0, +1, +2) the minimum number of runs necessary to perform the experiment would be 30. This includes four replicates.
The experimental design is shown in Table 5.4. This was applied in: flat (0°), vertical (90°) and overhead (180°) positions.

	Factors			
Weld	Wire Feed Speed (m/min)	Welding Speed (mm/min)	Wire Distance from Wall (mm)	Arc length Correction (%)
1	10.70	900	0.90	0.00
2	11.95	1025	0.60	-12.50
3	10.70	1150	0.90	0.00
4	10.70	1150	0.30	0.00
5	10.70	1150	0.90	0.00
6	10.70	1150	0.90	0.00
7	11.95	1275	0.60	-12.50
8	10.70	1150	0.90	0.00
9	11.95	1275	1.20	-12.50
10	11.95	1025	1.20	-12.50
11	9.45	1275	1.20	12.50
12	10.70	1400	0.90	0.00
13	9.45	1275	0.60	12.50
14	10.70	1150	0.90	0.00
15	11.95	1025	1.20	12.50
16	13.20	1150	0.90	0.00
17	9.45	1275	1.20	-12.50
18	9.45	1025	1.20	-12.50
19	9.45	1275	0.60	-12.50
20	11.95	1275	0.60	12.50
21	9.45	1025	1.20	12.50
22	9.45	1025	0.60	12.50
23	11.95	1275	1.20	12.50
24	8.20	1150	0.90	0.00
25	10.70	1150	0.90	-25.00
26	9.45	1025	0.60	-12.50
27	11.95	1025	0.60	12.50
28	10.70	1150	0.90	25.00
29	10.70	1150	1.50	0.00
30	10.70	1150	0.90	0.00

Table 5-4 Experimental design for the initial welding trials

The selected design consists of 16 factorial points (welds 2,7,9,10,11,13,15,17, 18,19, 20,21,22,23,26,27) plus 6 centre points (welds 3,5,6,8,14,30) and 8 axial (star) points (welds 1,4,12,16,24,25,28,29) and allows the estimation of linear, quadratic and interaction effects of the welding variables on the weld bead profile. The factorial points estimate the coefficients of the main factor and their interaction effects. The axial and centre points estimate the coefficients of the quadratic terms.

The factor levels in relation to the coded values are as shown in Table 5.5.

	Coded Values				
	-2	-1	0	+1	+2
Factor					
Wire Feed Speed (m/min)	8.20	9.45	10.70	11.95	13.20
Welding Speed (mm/min)	900	1025	1150	1275	1400
Wire Distance from Wall (mm)	0.30	0.60	0.90	1.20	1.50
Arc Length Correction (%)	-25.00	-12.50	0.00	+12.50	+25.00

Table 5-5 Coded values and factor levels

The ranges of the welding parameters were selected based on the experience acquired during the procedures development work and were expected to produce sound welds.
At the time of the experimental work, access to the waveform was not possible and modifications to the arc length were obtained through the arc length correction (A.L.C) control available on the front panel of the Fronius power sources. Arc length correction varies between -30% and +30% where the minus (-) determines a shorter arc and the plus (+) a longer arc. All welding trials were recorded using a high speed camera. The arc length was then determined by replaying the recorded section and freezing the image. The average arc length after 10 to 15 measurements was calculated. The video recordings showed significant changes in the arc length during the process, so measurement of the average arc length represents a more realistic approach. Measurements were carried out as close as possible to the centre of the groove.
The design selected for the purposes of this experimental work was the central composite design (CCD). This is a class of designs suitable for fitting second order models. The CCD is part of the RSM techniques (response surface methodology), a collection of mathematical and statistical techniques where the aim is the optimisation of the response.
Initially, welds in the flat position were carried out and factor effects were analysed. Mathematical relationships to bead profile were established and then the study was expanded to the vertical and overhead positions. The results from the three positions suggested that “angular position” has a very strong effect on weld bead shape.

5.3.2.2.2 Complementary Welding Trials

A factorial D-Optimal design was adopted in order to determine correlations between the angular positions and the weld bead profile. In this design, the angular position was considered as a factor or variable. The factors and their ranges are shown below:

- Wire feed speed: 10.4 – 12.6 m/min
- Welding speed: 1025 – 1275 mm/min
- Wire distance from the wall: 0.6 – 1.2mm
- Arc length correction (Arc length): -13 - +13%
- Angular Position (angular): 30°, 60°, 120°and 150°.

The total number of experiments was 36; this included five replicates.

The experimental design is shown in Table 5.6.

	Factors				
Weld	Wire Feed Speed (m/min)	Welding Speed (mm/min)	Wire Distance from Wall (mm)	Arc length Correction (%)	Angular Position (°)
1	12.60	1275	1.20	-13.00	30
2	12.60	1025	0.60	-13.00	30
3	10.40	1025	1.20	+13.00	30
4	12.60	1275	0.60	-13.00	30
5	12.60	1275	1.20	-13.00	30
6	10.40	1275	0.60	-13.00	30
7	10.40	1025	0.60	-13.00	30
8	12.60	1025	0.60	+13.00	30
9	10.40	1275	1.20	+13.00	30
10	10.40	1025	1.20	+13.00	60
11	12.60	1025	1.20	-13.00	60
12	10.40	1025	1.20	-13.00	60
13	10.40	1275	1.20	-13.00	60
14	12.60	1025	0.60	+13.00	60
15	10.40	1025	1.20	-13.00	60
16	12.60	1025	0.60	-13.00	60
17	10.40	1275	0.60	-13.00	60
18	12.60	1275	1.20	+13.00	60
19	10.40	1275	1.20	-13.00	120
20	12.60	1275	0.60	-13.00	120
21	10.40	1275	1.20	+13.00	120
22	12.60	1275	1.20	+13.00	120
23	12.60	1025	0.60	+13.00	120
24	10.40	1275	0.60	+13.00	120
25	10.40	1025	0.60	-13.00	120
26	10.40	1025	1.20	+13.00	120
27	10.40	1275	0.60	+13.00	120
28	12.60	1275	0.60	-13.00	150
29	12.60	1025	1.20	+13.00	150
30	12.60	1025	1.20	-13.00	150
31	12.60	1275	1.20	+13.00	150
32	10.40	1275	0.60	-13.00	150
33	10.40	1025	0.60	+13.00	150
34	12.60	1275	1.20	+13.00	150
35	12.60	1275	0.60	+13.00	150
36	10.40	1025	0.60	+13.00	150

Table 5-6 Experimental design for the angular position welding trials

6. Results

The results of the experiments described in chapter 5 (page 66) will be presented in three areas:

a) Tandem pulsed GMAW, dual tandem pulsed GMAW, double jointing dual tandem pulsed GMAW and tie-in pulsed FCAW procedure development for X100 girth welds.
Feasibility of the process, filler wire selection, development of the procedures and weld metal mechanical properties will be reported. Complete welding procedures for 5G girth X100 welds will be reported.

b) Effect of welding parameters on weld bead geometry.
This consisted of the investigation of the effects of the welding parameters on weld bead geometry of X100 tandem pulsed narrow gap welds. Welds were carried out in all positions (flat, vertical down, overhead and intermediate or angular) simulating the pipe circumference. Mathematical relationships between weld bead profile and welding parameters, and process optimisation will be described.

c) Effect of shielding gas composition on weld bead geometry.
The results of varying gas mixtures composition on weld bead geometry will be reported.

6.1 Procedure Development for X100 Girth Welds

Three pipes were supplied by two manufacturers and tested during the procedure development research work. An alphanumeric code was used for pipe identification:

-pipe B19 (36 in OD x 19.05mm),
-pipe D1 (52 in OD x 22.9mm) medium carbon content, and
-pipe D2 (52 in OD x 22.9mm) low carbon content.

Pipes coded as D1 and D2 were supplied by the same manufacturer.
The chemical compositions and mechanical properties of the pipes were provided by the manufacturers but some additional tests were carried out by an independent accredited test house (Bodycote).
The chemical compositions of the three pipes are reported in Table 4.4 (page 49). Elements such carbon, manganese, molybdenum, silicon are the principal constituents of strengthening while vanadium, aluminium, niobium contribute to grain refinement and increase toughness properties.
Three carbon equivalent formulations were used in order to investigate the weldability of the pipes used in this work: The CE_{IIW} [112], P_{CM} [113] and CET [114].
Two pipe spools of the same diameter were initially assembled and internally welded (root pass in dip GMAW) to form a pipe joint. Hot and fill runs were externally deposited. Welding was started at the 12 o'clock position and was completed at the 6 o'clock position on the pipe. The welding torch was fixed on a welding carriage which was travelling on a steel band installed around the pipe circumference. On completion of a welding pass (half pipe), the welding carriage was positioned on the other half and the same pass was deposited. This technique was used for the remaining passes until

joint completion. The technique adopted for the double jointing procedure work will be explained in section 6.1.5.

6.1.1 X100 Seam Weld Hardness Survey

The mechanical properties and chemical compositions of the pipes used for the procedure development work are reported in Tables 4.2, 4.3 and 4.4 (pages 47-49).
Macrographs of the submerged arc welds are shown in Figure 6.1.
Hardness survey (HV10) of the submerged arc weld seams was carried out. The results are reported in Tables 6.3 and 6.4 (page 113). An average value around 300HV10 was reported for the three seam welds. The hardness level of the seam weld of pipe marked as B19 was in agreement with Hudson's survey [1]. Microhardness survey results of the parent metal are reported in Table 6.5 (page 114).

a) pipe B19

b) pipe D1

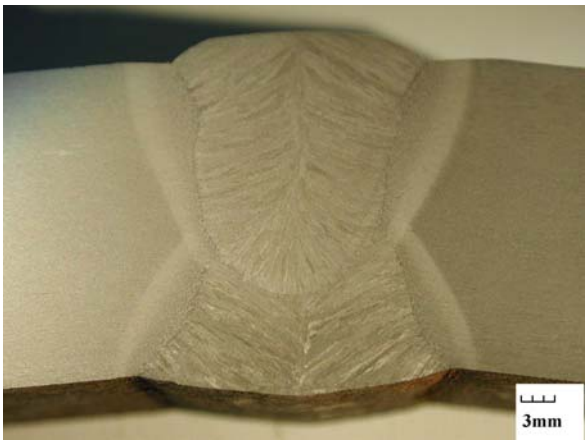

c) pipe D2

Fig. 6-1 Macrographs of the submerged arc welds

The base material microstructures are shown in Figure 6.2.

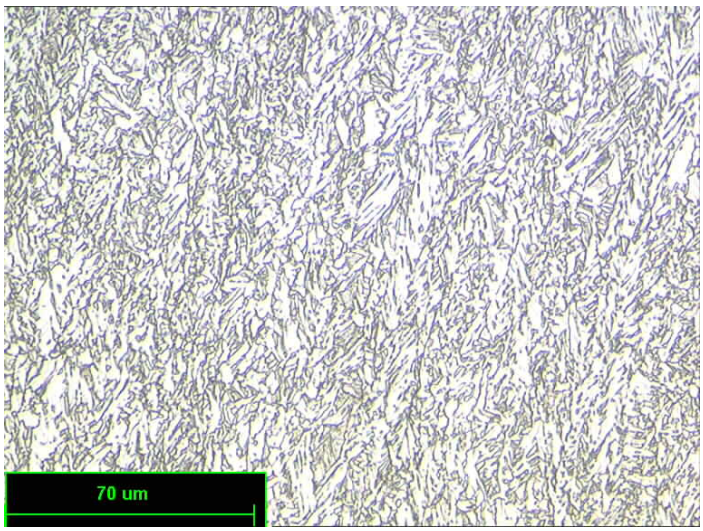

a) pipe B19

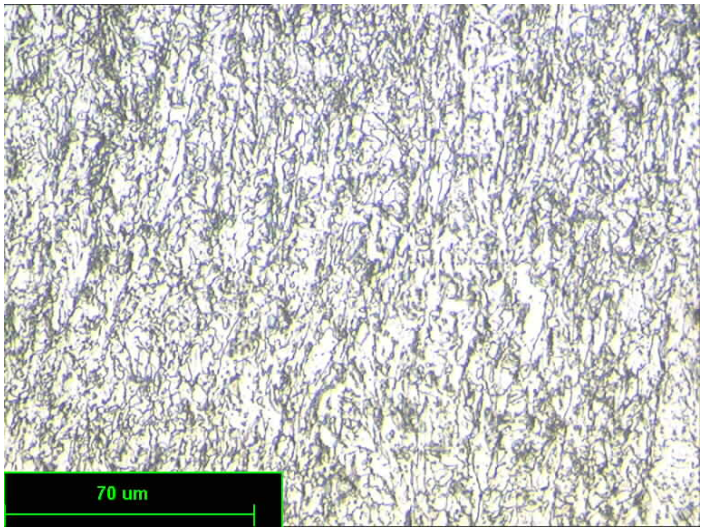

b) pipe D1

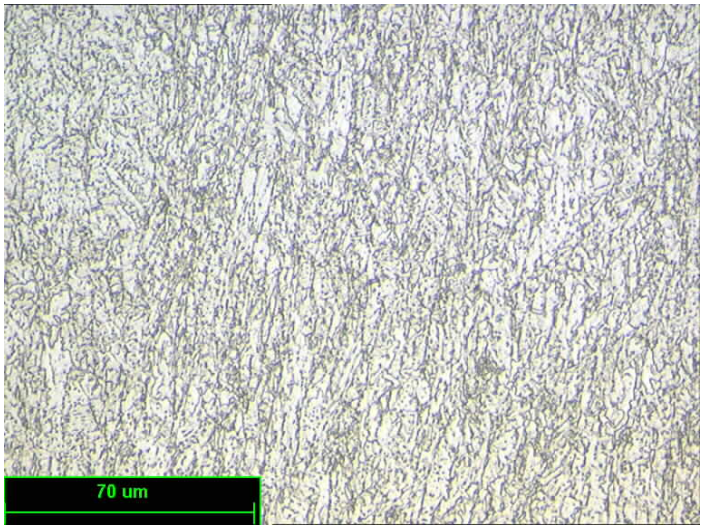

c) pipe D2

Fig. 6-2 Base material microstructure (approx. 1/3 thickness from outer surface transverse to the pipe axis

6.1.2 Single Tandem Procedure Welds (36 in OD x 19.05mm)

Welding trials were carried out on full pipe length and thickness. Process and equipment consistencies were tested. Sections of the weld were polished and etched. Fusion characteristics and defective sections (if any) were investigated.
The single tandem procedure weld (identified as ML-ST-S006) used the Oerlikon NiMo-1(1%Ni 0.3%Mo) filler wire. This selection was based on results reported from previous work at Cranfield [1].
Tensile results (strip all weld metal) and hardness results (cross weld traverse) are shown in Table 6.6 (page 114).
Detailed hardness and microhardness survey values are shown in Tables 6.7 and 6.8 (pages 115 and 116).
Table 6.10 (page 118) shows the Charpy impact results; tests were made at -20°, -40°C, -60°C and -80°C, while CTOD testing (Table 6.11, page 120) was performed at -10°C.
Cross weld tensile, side bend and nick break test results are listed in Table 6.9 (page 117).
A typical weld macrograph section and microstructures are shown in Figures 6.3 & 6.4 accordingly.
Impact transition curves were plotted and are shown in Figure 6.5.
The locations of the specimens on the pipe circumference are shown in Figure 5.4 (page 71).

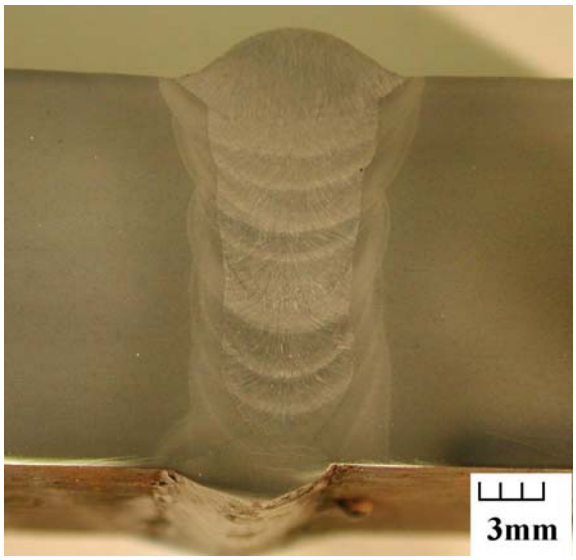

Fig. 6-3 Typical single tandem (ML-ST-S006) procedure macro section

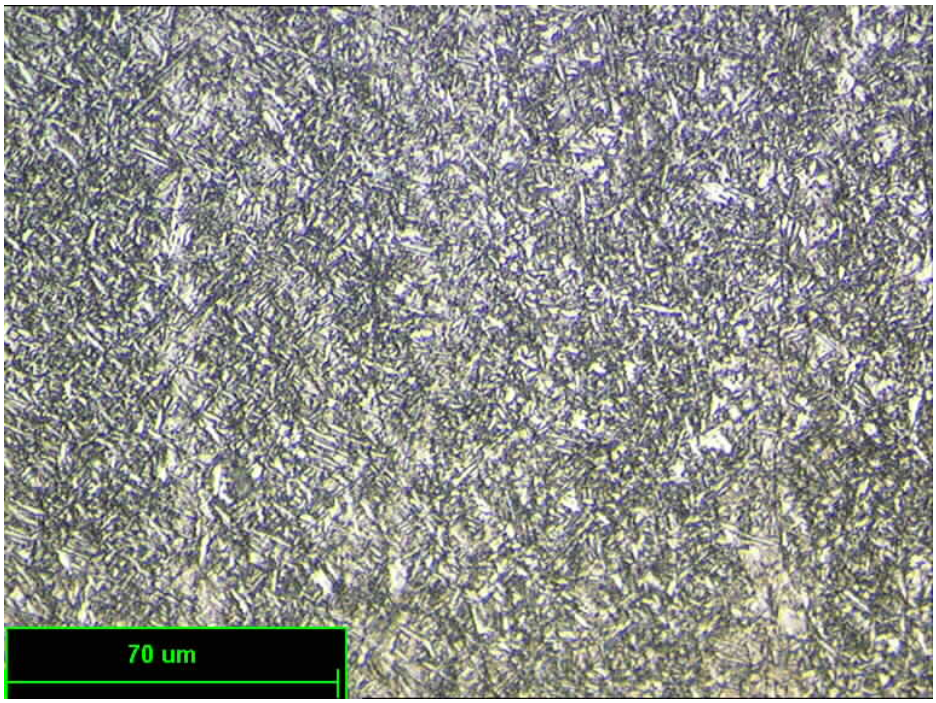

a) weld metal

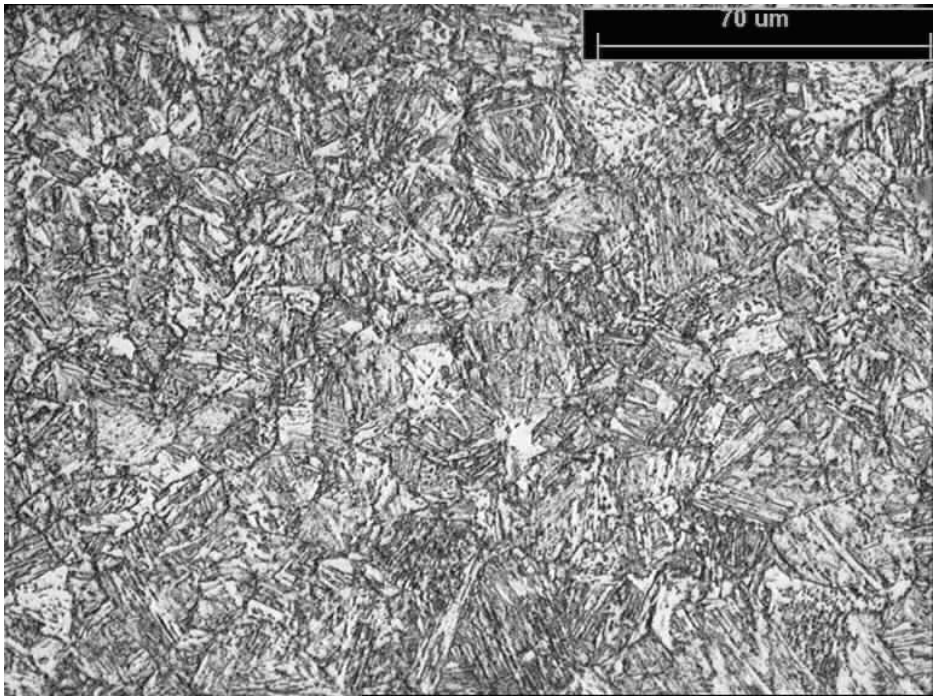

b) HAZ (next to fusion line)

Fig. 6-4 Single tandem procedure cap weld metal microstructures (ML-ST-S006; NiMo-1)

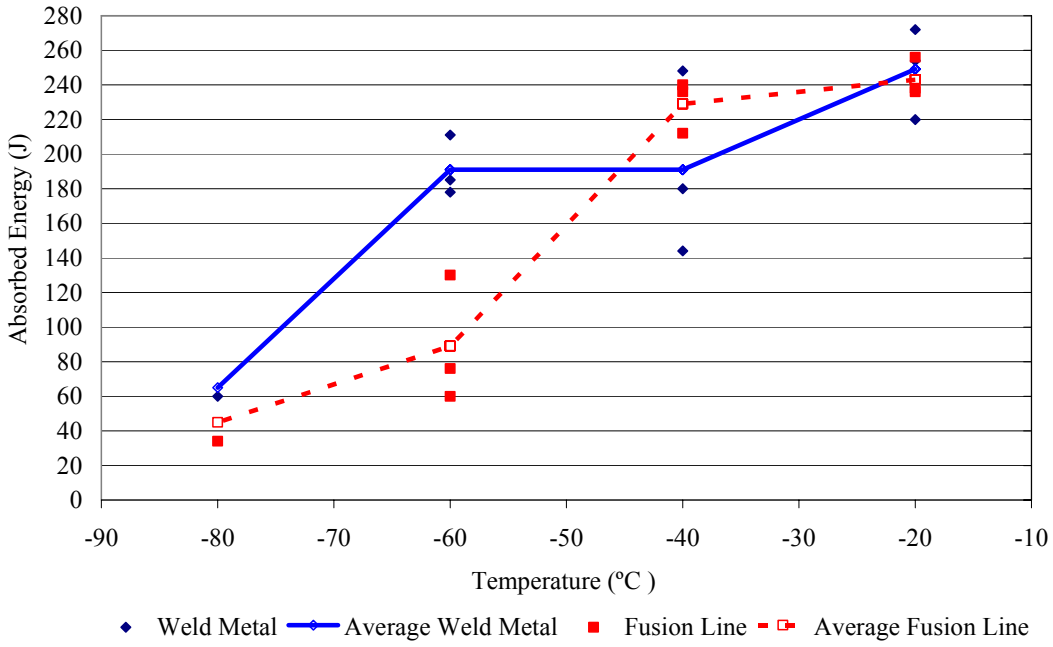

Fig. 6-5 Single tandem procedure impact (root) transition curves (ML-ST-S006; NiMo-1)

6.1.3 Dual Tandem Procedure Welds (36 in OD x 19.05mm)

Initially, dual tandem welding trials (200-300mm length) with the Oerlikon NiMo-1 (1%Ni 0.3%Mo) and the Bohler X70-IG (1.3%Ni 0.25%Mo 0.25%Cr) failed to achieve the overmatching criterion, with the weld metal proof strength ($Rp_{0.2}$) of 728MPa and 803MPa respectively (Table 6.1, page 112). Tests were expanded to complete 5G girth welds and further consumables were tested (Table 6.2, page 112). Hardness survey was also performed. Since some consumables provided weld metal yield strength just below the optimum range and others considerably above the optimum range, it was thought that a mixture of a low and a high strength wire could be the solution to obtaining welds in the desired weld metal strength range.

The dual tandem procedure weld identified as ML-DT-S016 was carried out and the wires tested were Oerlikon NiMo-1 (1.0%Ni 0.3%Mo) as lead and Thyssen Union X-85 (1.8%Ni 0.5%Mo 0.3%Cr) as trail.

Tensile results (strip all weld metal) and hardness results (cross weld traverse) are shown in Table 6.6 (page 114).

Detailed hardness and microhardness survey values are shown in Tables 6.7 and 6.8 (pages 115 and 116).

Table 6.10 (page 118) shows the Charpy impact results; tests covered the temperature range -20°C to -80°C, while CTOD testing (Table 6.11, page 120) was performed at -10°C.

Cross weld tensile, side bend and nick break test results are listed in Table 6.9 (page 117).

A typical weld macrograph section and microstructures are shown in Figures 6.6 and 6.7.
Impact Transition curves were plotted and are shown in Figure 6.8.

Fig. 6-6 Typical dual tandem procedure (ML-DT-S016) macro section

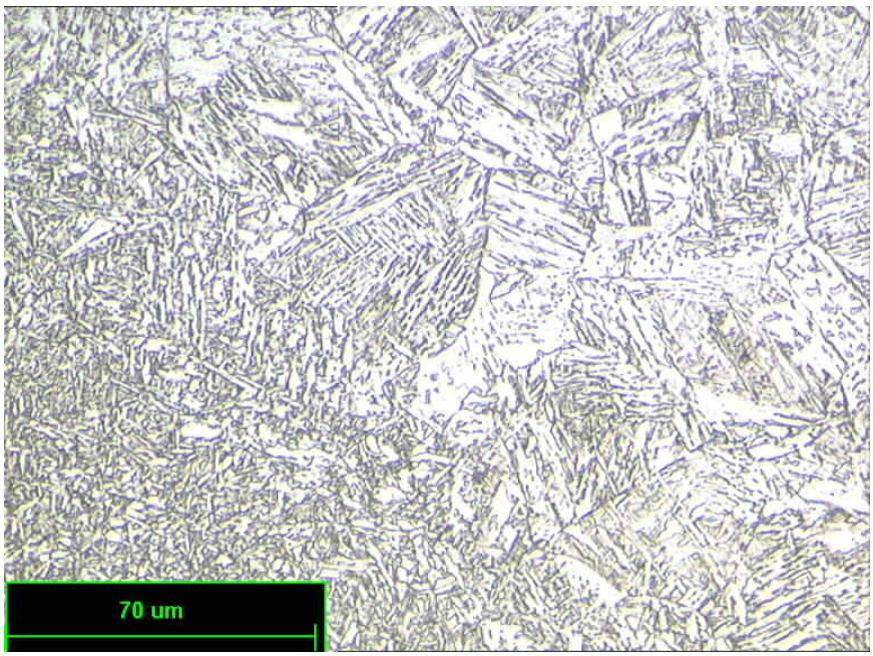

Fig. 6-7 Dual tandem procedure cap weld metal and heat affected zone adjacent to fusion line microstructures (ML-DT-S016; NiMo-1/ X-85)

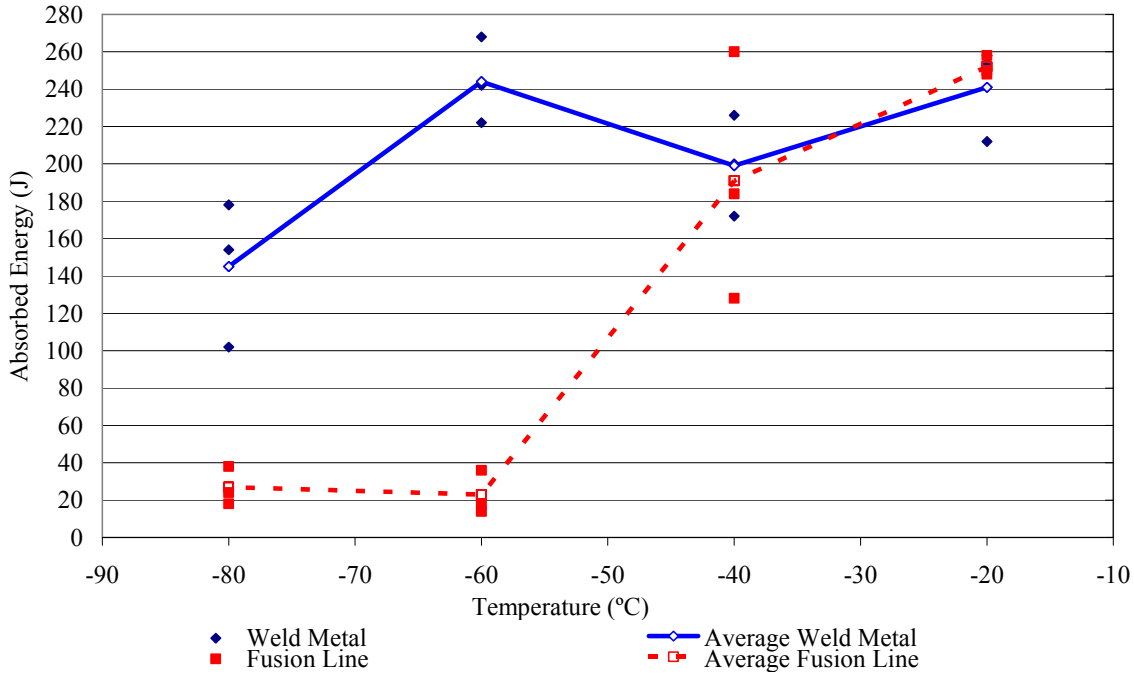

Fig. 6-8 Dual tandem procedure impact (root) transition curves (ML-DT-S016; NiMo-1 / X85-IG)

6.1.4 Dual Tandem Procedure Welds (pipe D2, low carbon=0.043%, 52 in OD x22.9mm)

The "combined" filler wire technique described in section 6.1.3 was adopted for further implementation. The procedure weld was marked as ML-DT-N009.
Tensile results (strip all weld metal) and hardness results (cross weld traverse) are shown in Table 6.6 (page 114).
Detailed hardness and microhardness survey values are shown in Tables 6.7 and 6.8 (pages 115 and 116).
Table 6.10 (pages 118 and 119) shows the Charpy impact results; tests covered the temperature range -20°C to -80°C, while CTOD testing (Table 6.11, page 120) was performed at -10°C.
Cross weld tensile, side bend and nick break test results are listed in Table 6.9 9 (page 117).
A typical weld macrograph section and microstructures are shown in Figures 6.9, 6.10 and 6.11.
Impact transition curves (root and cap) are shown in Figures 6.12 and 6.13.

Fig. 6-9 Typical dual tandem low carbon procedure (ML-DT-N009) macro section

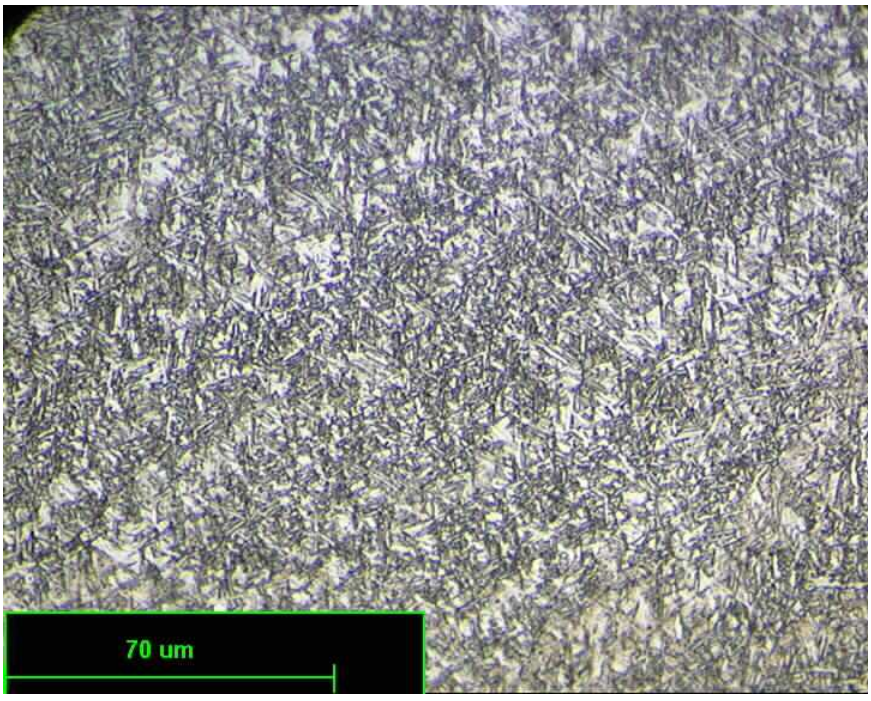

Fig. 6-10 Dual tandem low carbon procedure cap weld metal microstructures (ML-DT-N009; NiMo-1/X-85)

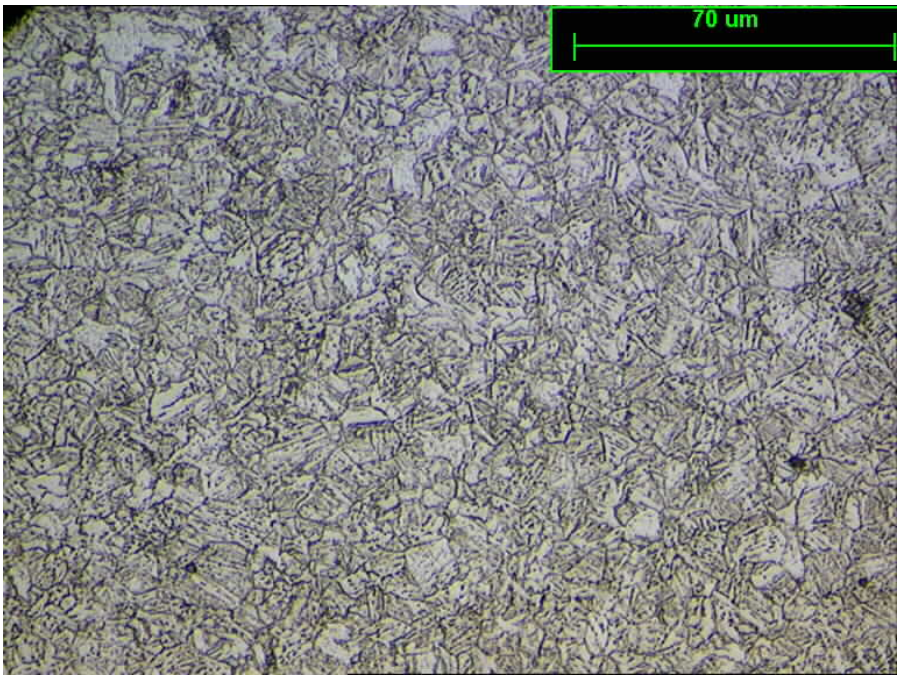

Fig. 6-11 Dual tandem low carbon procedure cap heat affected zone adjacent to fusion line microstructures (ML-DT-N009; NiMo-1/X-85)

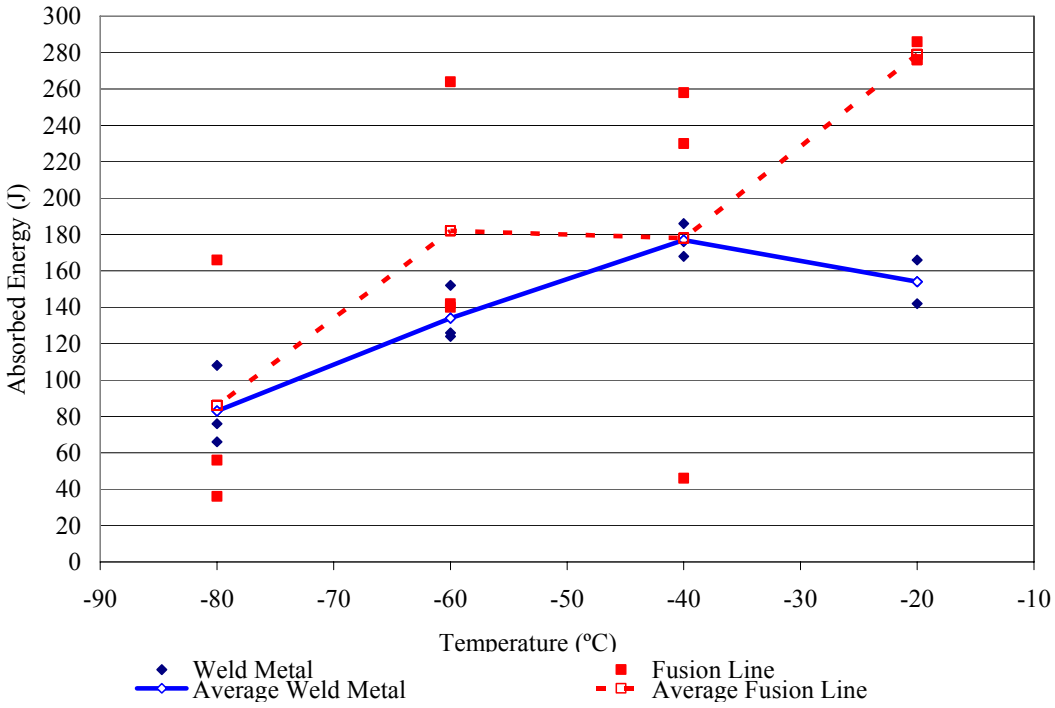

Fig. 6-12 Dual tandem low carbon procedure impact (root) transition curves (ML-DT-N009; X85-IG; NiMo-1)

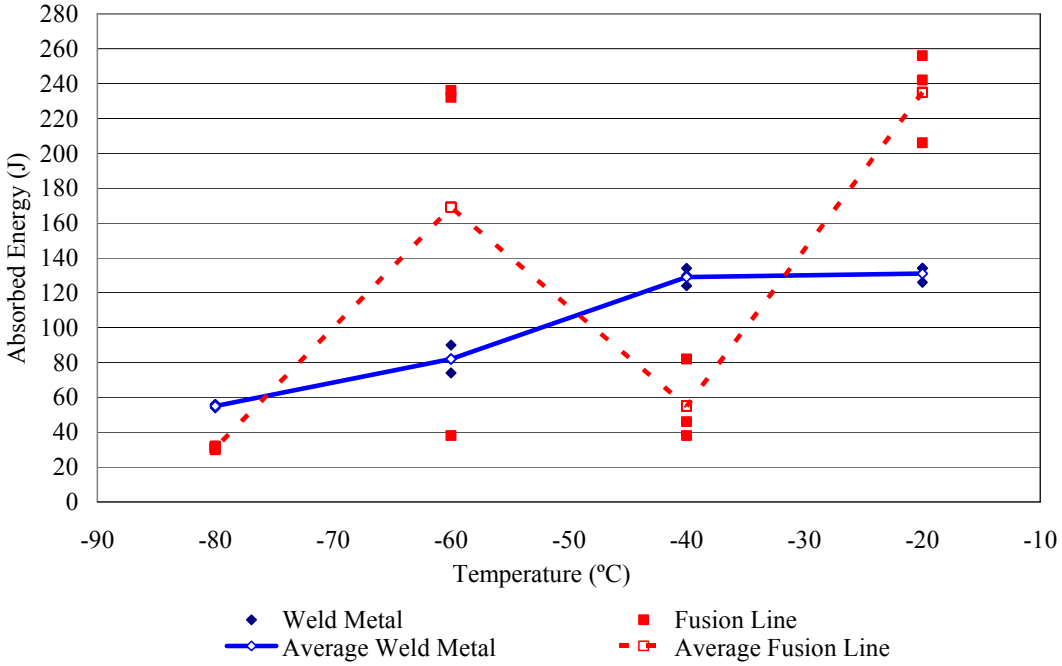

Fig. 6-13 Dual tandem low carbon procedure impact (cap) transition curves (ML-DT-N009; X85-IG; NiMo-1)

6.1.5 Dual Tandem Procedure Weld (pipe D1, medium carbon=0.057%, 52 in OD x 22.9mm)

The present procedure (ML-DT-N013) development work was attempted to compare the mechanical properties of medium carbon and low carbon pipe girth welds (section 6.1.4).
Tensile results and hardness results are shown in Table 6.6 (page 114).
Detailed hardness and microhardness survey values are shown in Tables 6.7 and 6.8 (pages 115 and 116).
Table 6.10 (pages 118 and 119) shows the Charpy impact results; tests covered the temperature range -20°C to -80°C, while CTOD testing (Table 6.11, page 120) was performed at -10°C.
Weld metal chemical analysis is shown in Table 6.12 (page 121).
Cross weld tensile, side bend and nick break test results are listed in Table 6.9 (page 117).
A typical weld macrograph section and microstructures are shown in Figures 6.14, 6.15 and 6.16.
Impact transition curves (root and cap) were plotted and are shown in Figures 6.17 and 6.18.
Full scale welds sometimes presented areas with defects. The defect map shown in Figure 6.19 ensured that weld specimens for mechanical properties tests were only taken from sound areas.

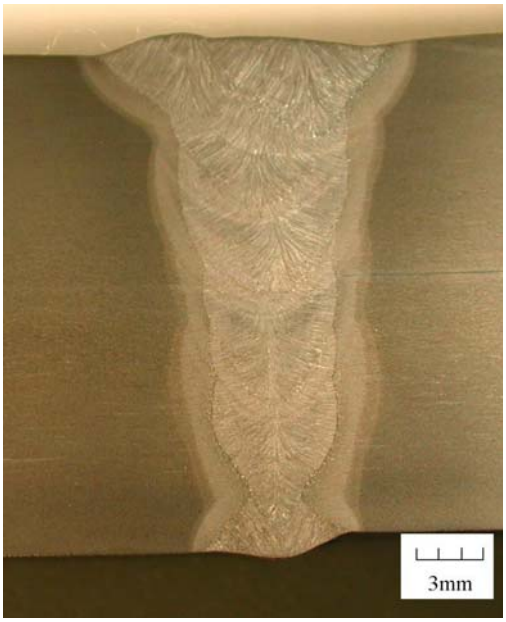

Fig. 6-14 Typical dual tandem medium carbon procedure (ML-DT-N013) macro section

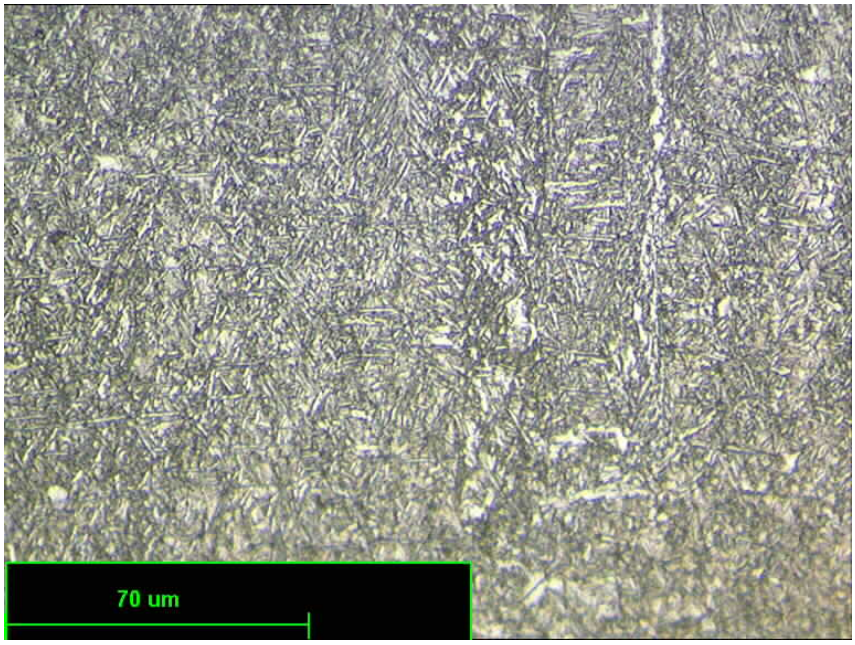

Fig. 6-15 Dual tandem medium carbon procedure cap weld metal microstructures (ML-DT-N013; NiMo-1/ X-85)

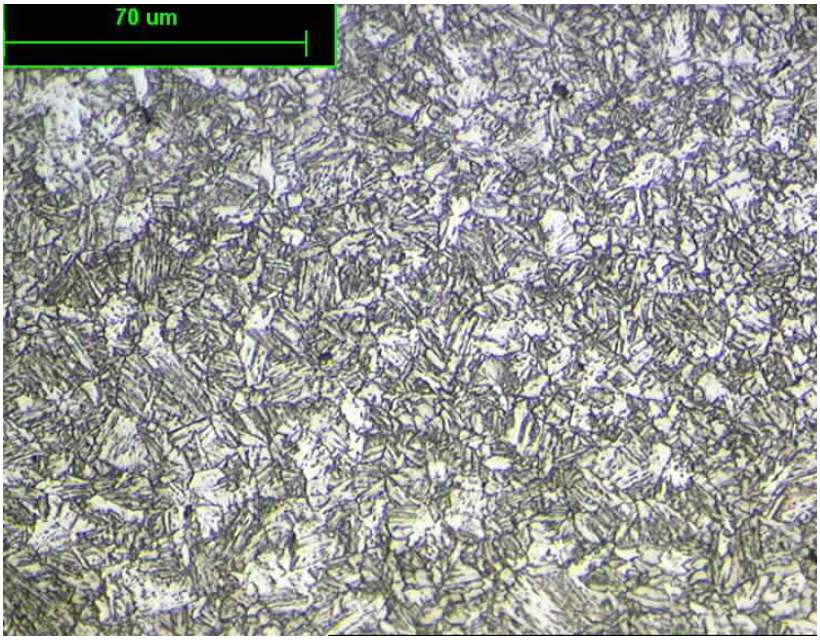

Fig. 6-16 Dual tandem medium carbon procedure cap heat affected zone adjacent to fusion line microstructures (ML-DT-N013; NiMo-1/X-85)

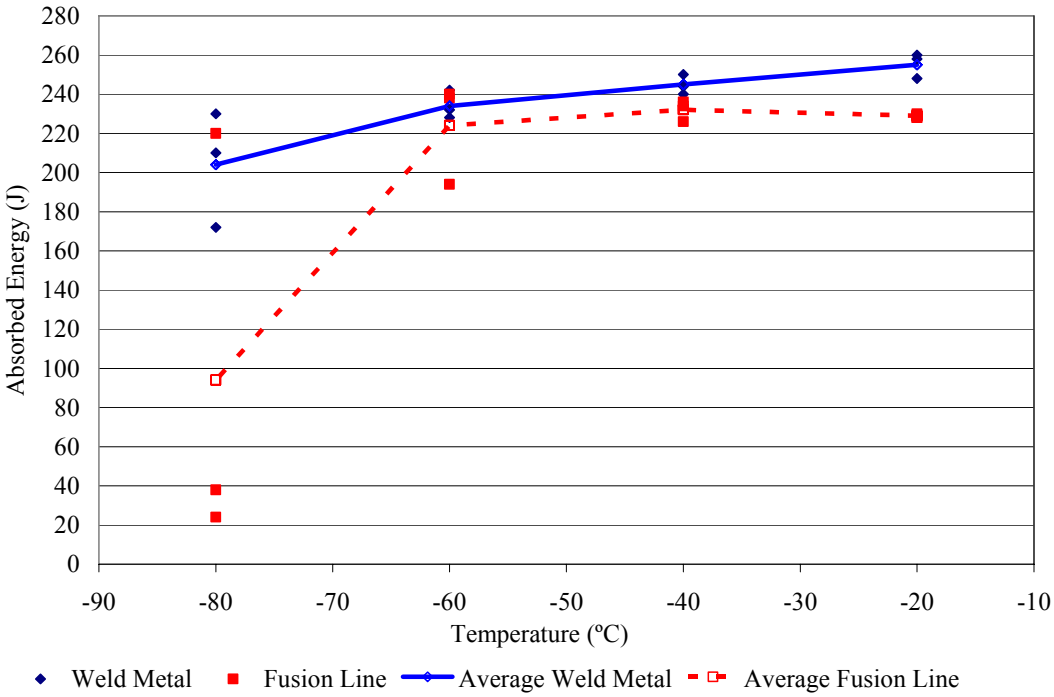

Fig. 6-17 Dual tandem medium carbon procedure impact (root) transition curves (ML-DT-N013;NiMo-1/ X85-IG)

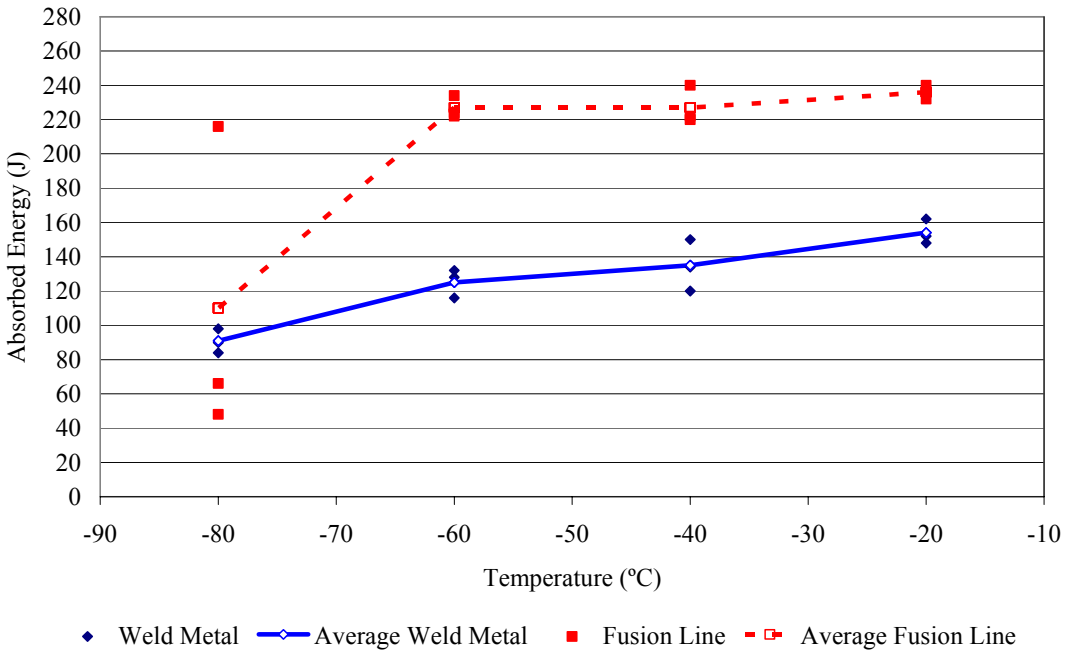

Fig. 6-18 Dual tandem medium carbon procedure impact (cap) transition curves (ML-DT-N013;NiMo-1/X-85)

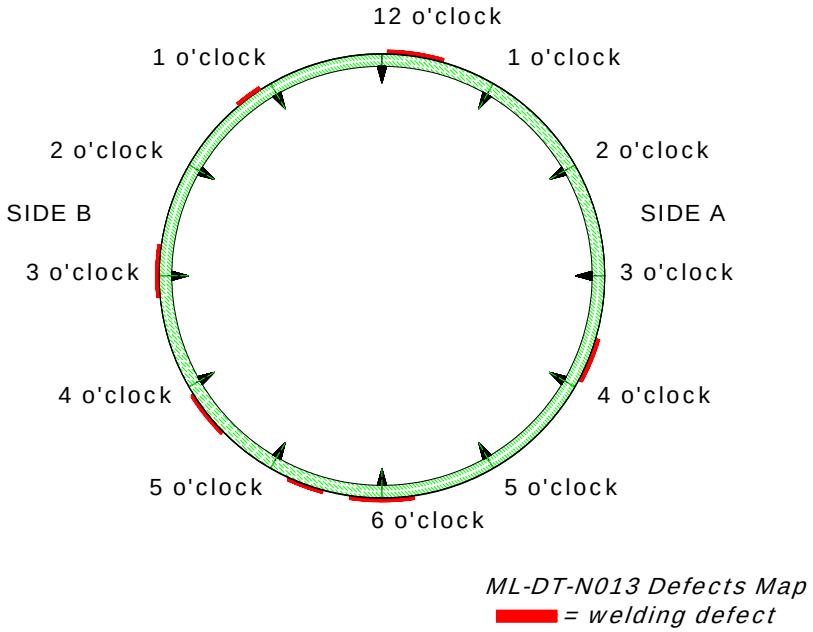

Fig. 6-19 Defect map for the dual tandem procedure weld (ML-DT-N013)

6.1.6 Dual Tandem Double Joint Procedure Welds (pipe D1, medium carbon=0.057%, 52 in OD x 22.9mm)

Traditionally, submerged arc welding has been used for double jointing procedures in onshore pipeline applications. The high levels of heat input and dilution associated with the process, can compromise its ability in the case of high strength steels (X100).
The potential application of the dual tandem process was investigated in order:
-to confirm that acceptable mechanical properties of the weld metal can be achieved, and
-to establish the high productivity capabilities of the process.
Bevel dimensions were similar to 5G girth welds, described in Figure 5.1 (page 66). However, accidentally during the machining process a 3mm offset was used. This resulted in a 6mm gap at the base of the groove and therefore the overall weld cross section was considerably increased.
The double joint procedure was identified as DJ-DT-N012.
Tensile results (strip all weld metal) and hardness results (cross weld traverse) are shown in Table 6.6 (page 114).
Detailed hardness and microhardness survey values are shown in Tables 6.7 and 6.8 (pages 115 and 116).
Table 6.10 (pages 118 and 119) shows the Charpy impact results; tests covered the temperature range -20°C to-80°C, while CTOD testing (Table 6.11, page 120) was performed at -10°C. Impact transition curves (root and cap) were plotted and are shown in Figure 6.22.
Cross weld tensile, side bend and nick break test results are listed in Table 6.9 (page 117).
A typical weld macrograph section and microstructures are shown in Figures 6.20 and 6.21.

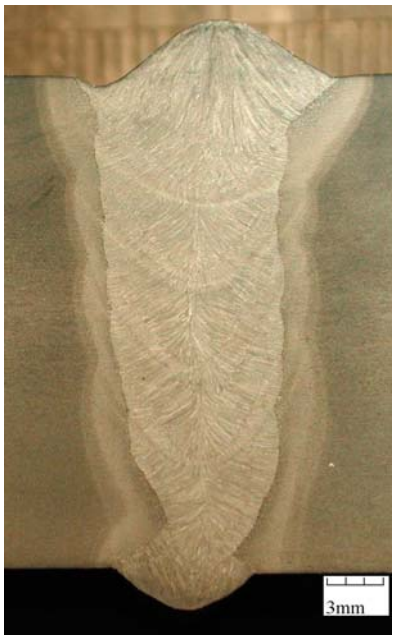

Fig. 6-20 Typical dual tandem double joint procedure (DJ-DT-N012) macro section

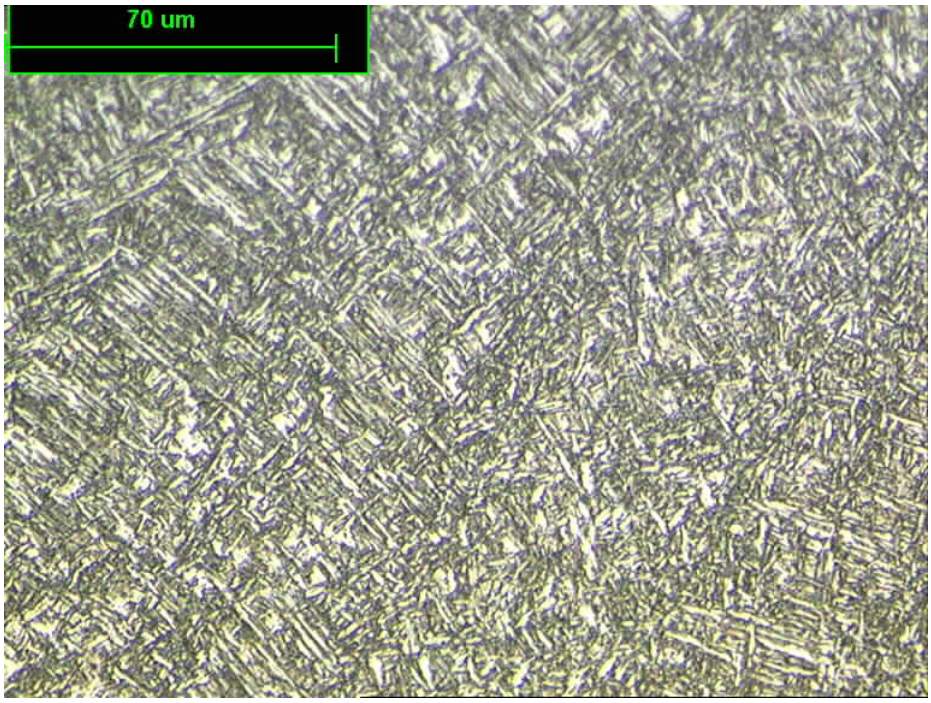

a) weld metal

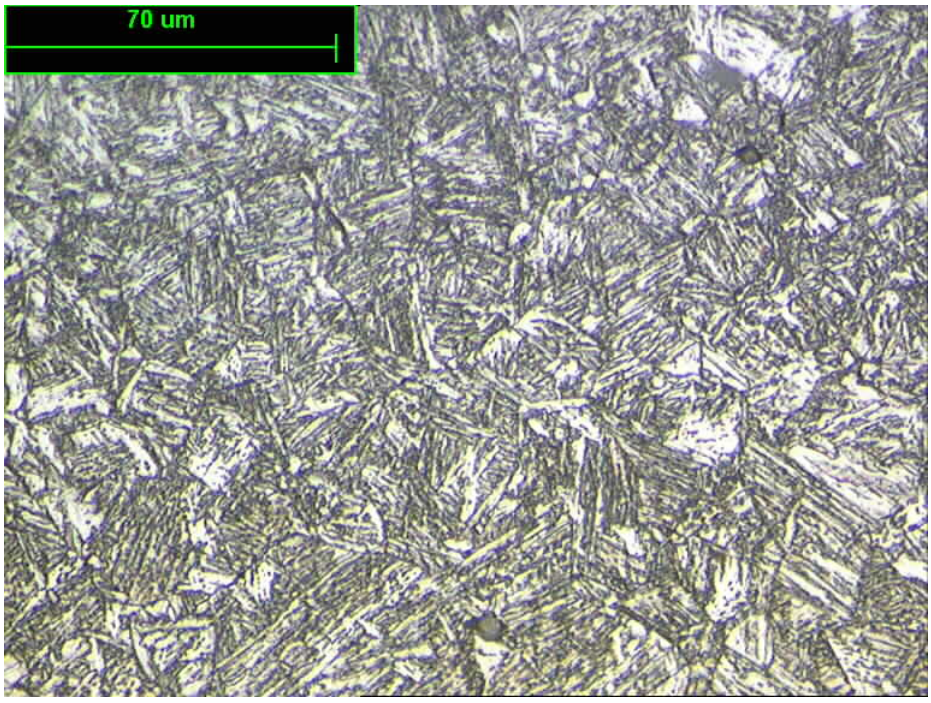

b) HAZ (adjacent to fusion line)

Fig. 6-21 Dual tandem double joint procedure cap weld metal and heat affected zone adjacent to fusion line microstructures (DJ-DT-N012;NiMo-1/ X-85)

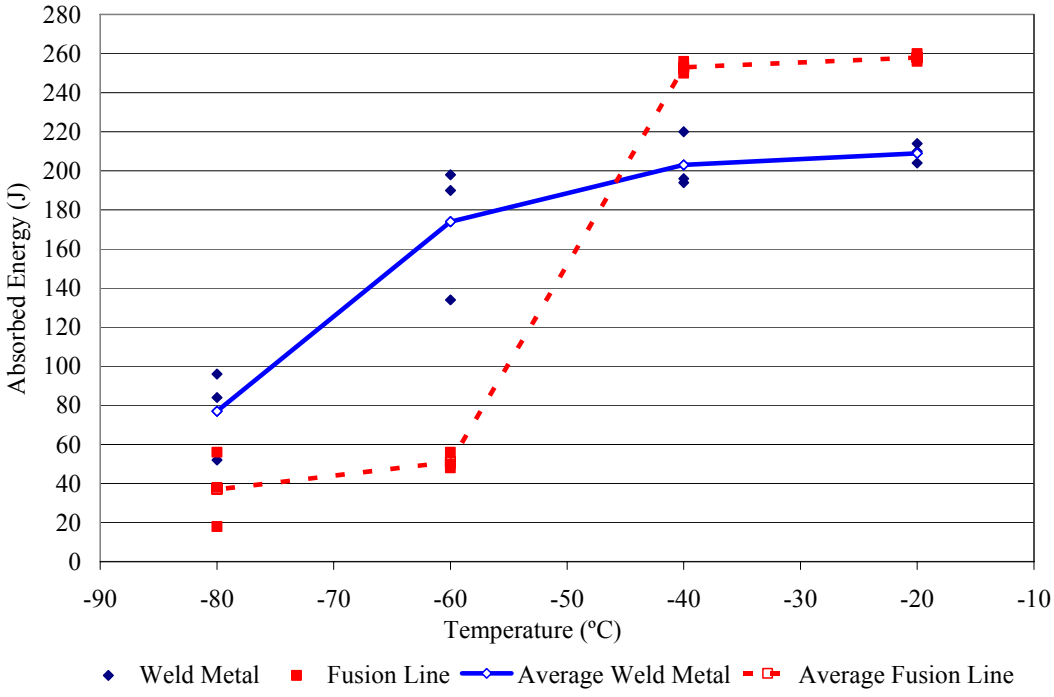

a) Root impact transition curves (DJ-DT-N012;NiMo-1/ X85-IG)

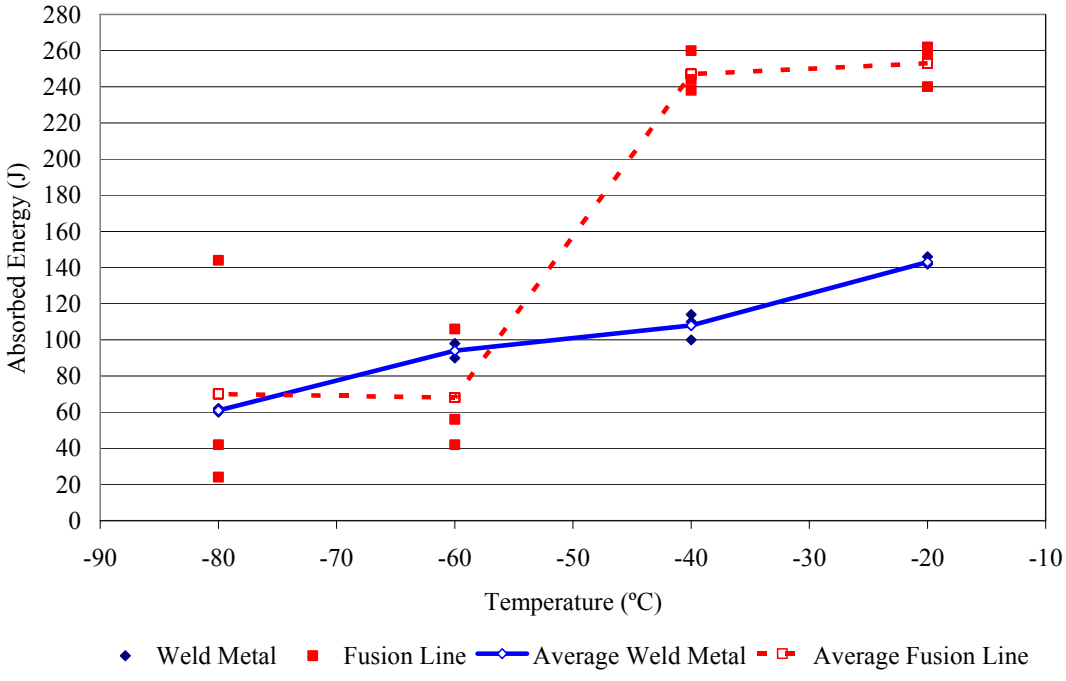

b) Cap impact transition curves (DJ-DT-N012; NiMo-1/X-85)

Fig. 6-22 Dual tandem double joint procedure impact transition curves (DJ-DT-N012; NiMo-1/X85-IG)

Comparison between impact transition curves including single tandem (ML-DT-S016) and dual tandem (ML-DT-N009, DJ-DT-N012, and ML-DT-N013) welding procedures as described above are shown in Figures 6.23, 6.24, 6.25 and 6.26.

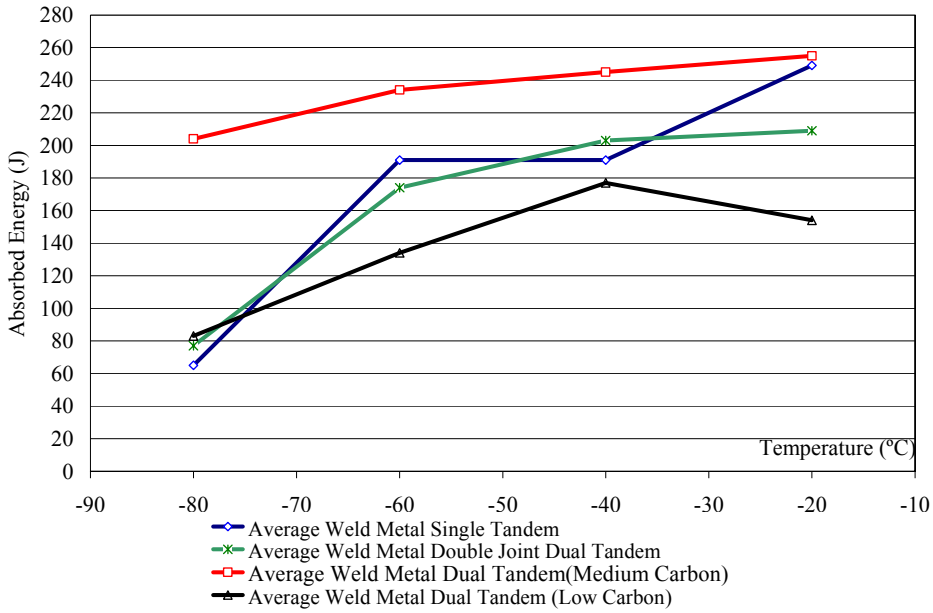

Fig. 6-23 Tandem and dual tandem comparison root (weld metal) impact (average) transition curves (ML-DT-S006, ML-DT-N009, ML-DT-N013, and DJ-DT-N012)

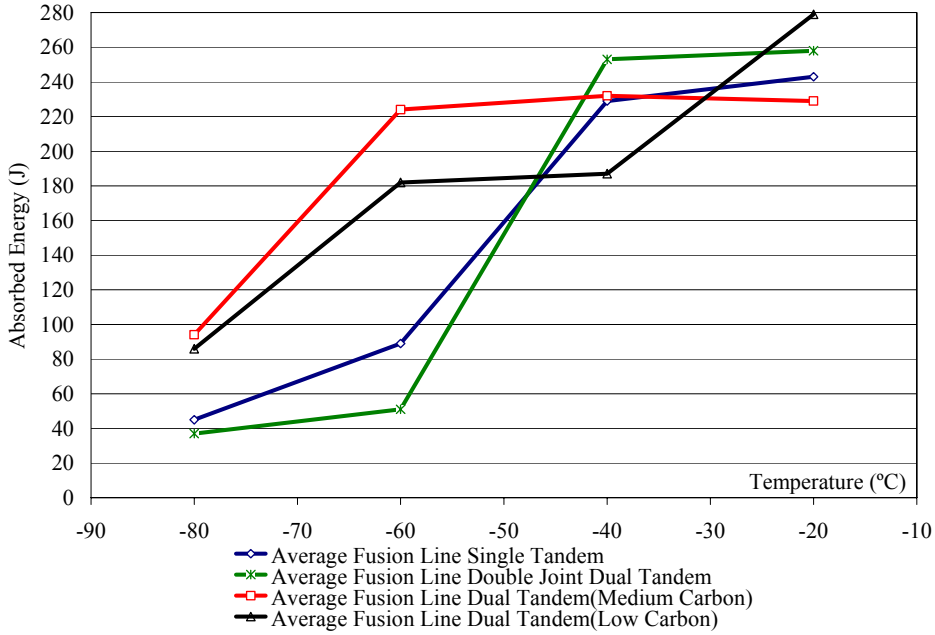

Fig. 6-24 Tandem and dual tandem comparison root (fusion line) impact (average) transition curves (ML-DT-S006, ML-DT-N009, ML-DT-N013, and DJ-DT-N012)

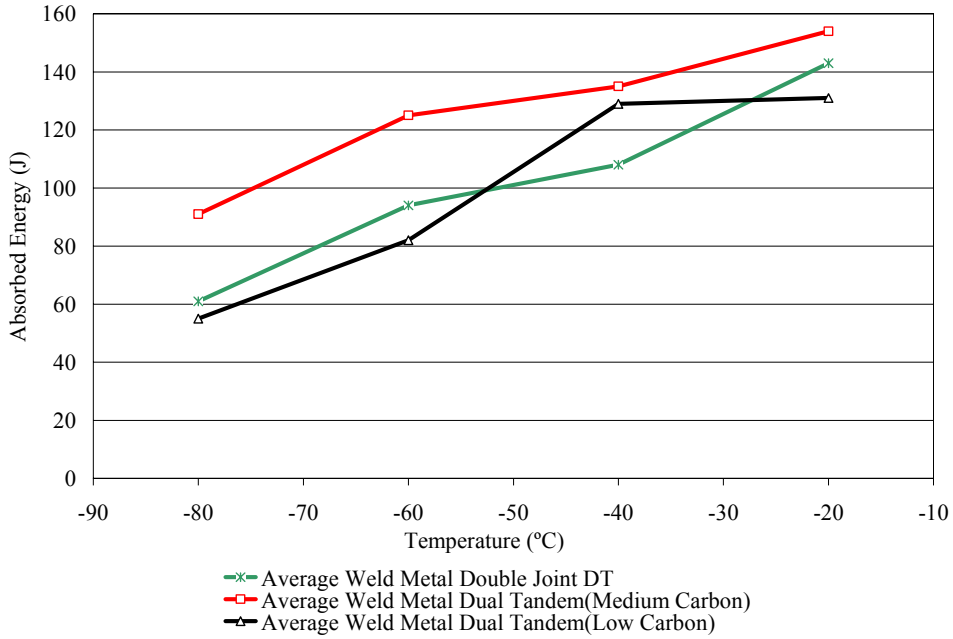

Fig. 6-25 Tandem and dual tandem comparison cap (weld metal) impact (average) transition curves (ML-DT-N009, ML-DT-N013, and DJ-DT-N012)

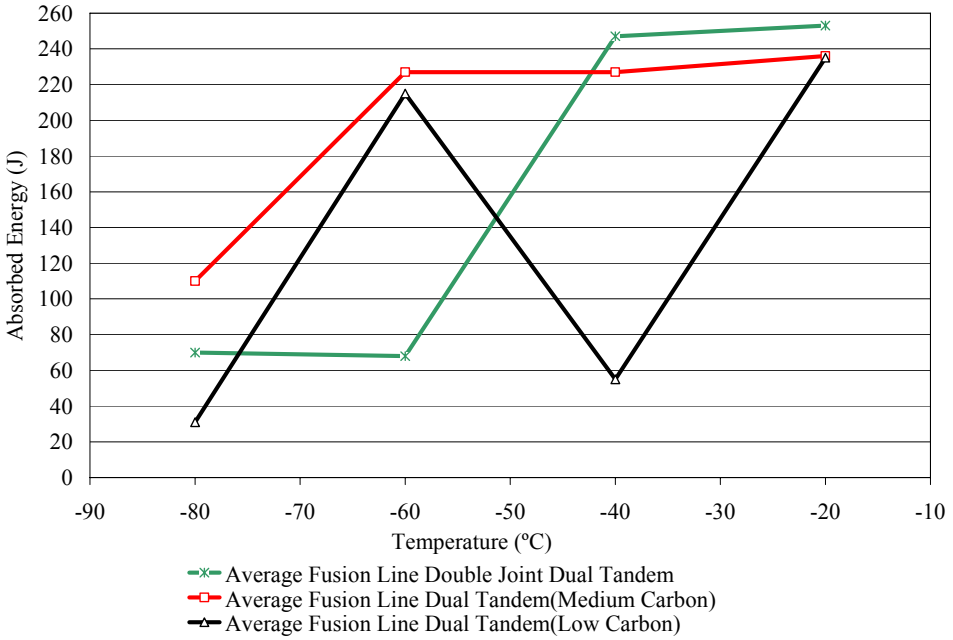

Fig. 6-26 Tandem and dual tandem comparison cap (fusion line) impact (average) transition curves (ML-DT-N009, ML-DT-N013, and DJ-DT-N012)

The high scatter in the absorbed energy observed in the above Figure 6.26 is difficult to be explained with the available data. Note however that Charpy impact tests were considered in the present work in order to evaluate the toughness properties of the procedure welds compared to the required toughness levels (e.g. minimum 60J at -40°C).

6.1.7 Single Wire Tie-in Procedure Welds (36 in OD x 19.05mm)

Previous work at Cranfield [1] failed to meet the overmatching criterion when rutile flux-cored wires were used in the qualification of X100 pipeline steel.
The present work tested basic flux wires together with a reduced bevel angle (15°).
Two basic flux-cored wires, Philarc PZ 6148 (AWS A5.29:E111T5-K4) and Philarc PZ 6149 (AWS A5.29:E121T5-G) were selected, short length pipe welds (300-350mm) were performed and all weld metal tensile tests were carried out (Table 6.1).
The Philarc PZ 6149 showed very promising results and was selected for the procedure development work.
The tie-in procedure weld was marked as Tie-In S01.
Tensile results (strip all weld metal) and hardness results (simple cross weld traverse) are shown in Table 6.6 (page 114).
Detailed hardness and microhardness survey values are shown in Tables 6.7 and 6.8 (pages 115 and 116).
Table 6.10 (page 118) shows the Charpy impact results; tests covered the temperature range -20°C to -80°C, while CTOD testing (Table 6.11, page 120) was performed at -10°C. Impact transition curves (root and cap) were plotted and are shown in Figure 6.29.
Cross weld tensile, side bend and nick break test results are listed in Table 6.9 (page 117).
The weld metal chemical analysis is shown in Table 6.12 (page 121).
A typical weld macrograph section and microstructures are shown in Figures 6.27 and 6.28.

Fig. 6-27 Typical Tie-In procedure (Tie-In S01) macro section

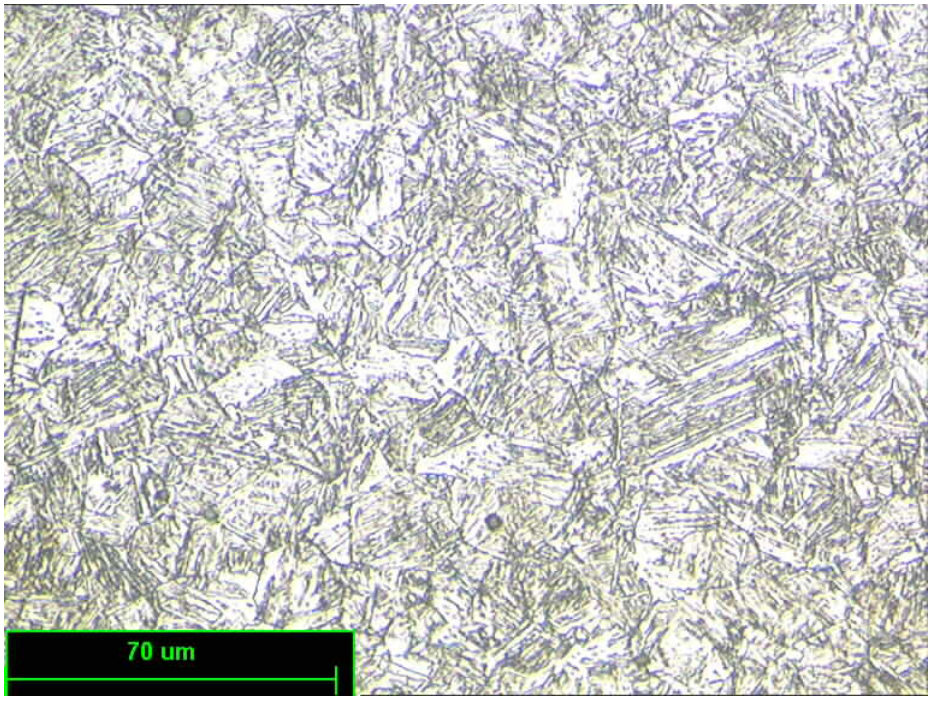

Fig. 6-28 Tie-In procedure cap weld metal and heat affected zone adjacent to fusion line microstructures (Tie-In S01; PZ6149)

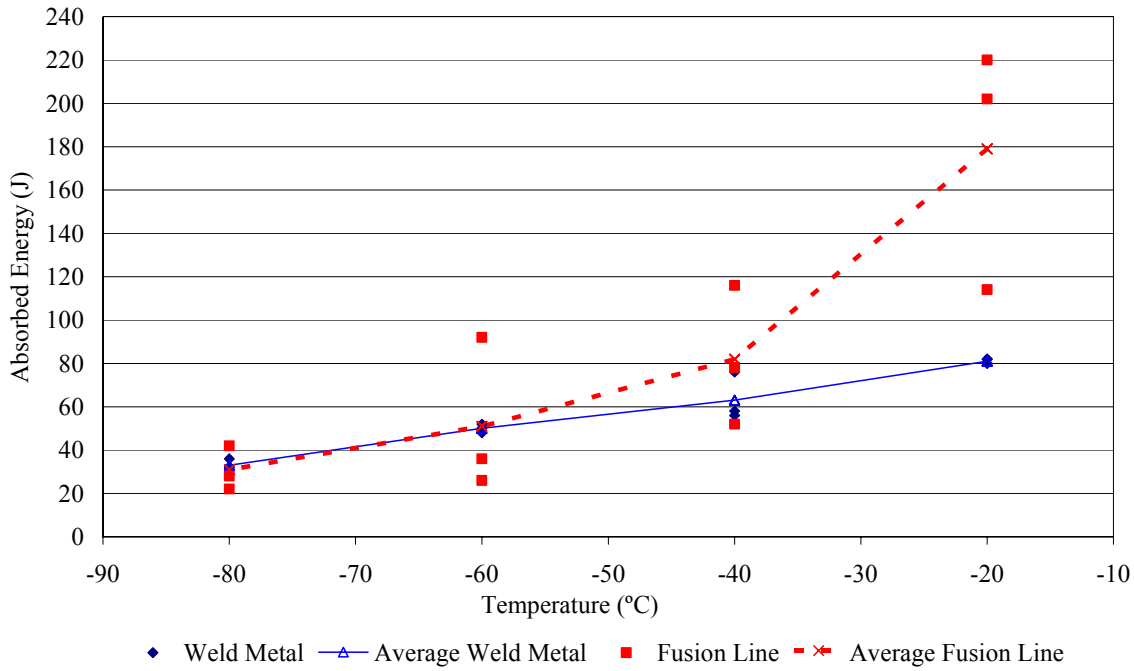

Fig. 6-29 Tie-In procedure impact (root) transition curves (Tie-In S01; PZ6149)

GMAW Solid wires used for the preliminary dual tandem trials

a)

Manufacturer	Wire Name	Strip Dim. (mm)	$Rp_{0.2}$ (MPa)	Rm (MPa)	A (%)
Oerlikon	NiMo-1	4.03 x 8.13	728	807	19.5
Bohler	X70-IG	4.00 x 8.24	803	864	18

FCAW Wires used for the preliminary Tie-In trials

Manufacturer	Wire Name	Round Bar (mm)	$Rp_{0.2}$ (MPa)	Rm (MPa)	A (%)
Filarc	PZ 6148	5.5	758	847	19.5
Filarc	PZ 6149	5.5	844	966	20

b)

Table 6-1 All weld metal strip tensile preliminary trials for (a) dual tandem and (b) Tie-In welds

Weld Reference	Welding Process	Filler Wire	Mechanical Test Results			
			$Rp_{0.2}$ (MPa)	Rm (MPa)	A (%)	Max Hardness(HV10)
ML-DT-S002	Dual Tandem	Bohler X70-IG-	784	860	19.5	354 (Parent Material)
ML-DT-S003	Dual Tandem	Oerlikon NiMo-1	771	834	21.5	
ML-DT-S010	Dual Tandem	Thyssen X85-IG				387 (Weld Cap)
ML-DT-S011	Dual Tandem	Thyssen X85-IG	912	980	19.0	
N.A	Dual Tandem	Oerlikon Carbofil 120	889	993	7.5	
N.A	Dual Tandem	Bohler X90-IG	1006	1029	6.5	
ML-DT-S016	Dual Tandem	Thyssen X85-IG / Oerlikon NiMo-1	842	944	18.0	363(Weld Cap)

Table 6-2 Preliminary dual tandem welding procedures all weld tensile results and hardness survey

Pipe	Location	Base Material	Base Material	Base Material	HAZ	HAZ	HAZ	Seam Weld	Seam Weld	Seam Weld	HAZ	HAZ	HAZ	Base Material	Base Material	Base Material
		HV10	HV10	HV10	HV10	HV10	HV10	HV10	HV10	HV10	HV10	HV10	HV10	HV10	HV10	HV10
19.05 mm WT,	2mm Sub OD	268	264	260	238	233	245	299	304	299	243	233	236	262	270	262
Pipe B19	Pipe Mid Thickness	258	260	260	256	243	293	302	306	306	242	238	264	254	253	251
	2mm Sub ID	285	287	287	264	268	264	294	292	292	245	262	264	274	262	270
22.9 mm WT,	2mm Sub OD	279	272	281	270	270	262	297	287	287	272	281	270	274	276	268
Pipe D2	Pipe Mid Thickness	272	264	268	281	268	270	302	292	289	289	270	268	266	268	268
Low C	2mm Sub ID	276	268	266	274	287	285	319	319	319	289	281	292	285	287	274
22.9mm WT,	2mm Sub OD	249	242	240	245	242	240	312	312	312	242	236	238	242	245	249
Pipe D1	Pipe Mid Thickness	249	242	239	249	254	247	276	287	283	242	240	255	252	250	251
Medium C	2mm Sub ID	249	249	251	246	251	253	285	283	292	247	252	250	246	252	251

Table 6-3 Pipe seam weld hardness (HV10) traverses

Manufacturer	BM Av.	BM Max.	HAZ Av.	HAZ Max.	WM Av.	WM Max.
B19	266	287	252	293	299	306
D2	273	287	277	292	301	319
D1	247	252	246	255	293	312

Table 6-4 Summary of pipe seam weld survey

	Survey Points (from OD to ID)																							
Pipe	1	2	3	4	5	6	7	8	9	10	11	12	13	14	15	16	17	18	19	20	21	22	23	24
B19	262	252	253	249	245	245	252	252	258	253	249	249	N.A	240	249	N.A	241	253	248	241	249	253	245	252
D1	241	238	238	234	234	234	234	241	238	226	N.A	244	240	241	238	240	245	245	245	249	248	244	244	245
D2	280	266	274	258	269	262	262	262	258	253	253	258	265	260	253	262	260	260	262	258	265	265	265	262

	Survey Points (from OD to ID)																				
Pipe	25	26	27	28	29	30	31	32	33	34	35	36	37	38	39	40	41	42	43	44	**Average**
B19	249	258	253	262	252	258	266	260	260	258	262	271	N.A	N.A	N.A	N.A	N.A	N.A	N.A	N.A	253
D1	249	252	244	245	241	249	249	245	245	241	244	241	241	238	244	238	252	249	245	238	242
D2	253	258	262	276	262	269	276	266	274	262	279	266	280	275	266	279	274	274	N.A	N.A	265

Point 1 = OD, Point 44 = ID

Table 6-5 Parent material microhardness (HV0.5) survey

		All Weld Metal Strip Tensile (1:00 to 2:30 o'clock position)					**Hardness Survey (2mm sub Root)**						**Hardness Survey (2mm sub Cap)**					
Weld Procedure	X100 Pipe OD x WT	$Rp_{0.2}$ (MPa)	Rm (MPa)	Yield / Tensile Ratio $Rp_{0.2}$/Rm	A (%)	Hv Survey location	Weld Metal Average HV10	Weld Metal Max HV10	HAZ Average HV10	HAZ Max HV10	Parent Mat. Average HV10	Parent Mat. Max HV10	Weld Metal Average HV10	Weld Metal Max HV10	HAZ Average HV10	HAZ Max HV10	Parent Matt. Average HV10	Parent Mat. Max HV10
ML-ST-S006	36" x 19.05 Pipe B19	910	934	0.97	19.5	3:00 o'cl. Seam	235 257	240 264	269 302	292 345	275 278	279 285	311 335	322 342	286 342	317 **370**	269 281	274 287
ML-DT-S016	36" x 19.05 Pipe B19	842	944	0.89	18	3:00 o'cl. Seam	239 260	247 270	275 341	297 **357**	306 295	322 302	**354** **380**	**363** **383**	284 **365**	311 **390**	284 290	292 297
TIE-IN S01	36" x 19.05 Pipe B19	966	1035	0.93	13.5	3:00 o'cl. Seam 4 to 5 o'cl.	254 284 243	256 299 247	296 343 279	309 **360** 290	337 286 281	**360** 294 287	**359** **409** **382**	**383** **413** **390**	295 303 294	319 311 **351**	277 291 273	294 302 279
ML-DT-N009	52" x 22.9 Pipe D2	877	951	0.92	19	3:00 o'cl. Seam	297 312	317 322	297 **361**	311 **366**	296 325	302 336	337 344	348 **351**	316 343	342 **390**	291 270	299 279
DJ-DT-N012 double joint	52 x 22.9 Pipe D1	766	945	0.81	19	3:00 o'cl. Seam	304 298	306 302	276 **358**	297 **373**	270 304	274 317	329 315	333 317	277 343	302 **357**	267 270	276 279
ML-DT-N013	52" x 22.9 Pipe D1	838	965	0.87	25.5	3:00 o'cl. Seam	241 309	243 339	268 333	294 **373**	277 315	281 322	335 344	342 **351**	293 **353**	327 **370**	272 262	281 274

Bold Indicates HV10 > 350

Table 6-6 X100 Pipe 5G procedure tests single tandem, dual tandem and Tie In tensile and hardness results

Weld Procedure	Location	Parent Material HV10	Parent Material HV10	Parent Material HV10	HAZ HV10	HAZ HV10	HAZ HV10	Weld Metal HV10	Weld Metal HV10	Weld Metal HV10	HAZ HV10	HAZ HV10	HAZ HV10	Parent Material HV10	Parent Material HV10	Parent Material HV10
ML-ST-S006	2mm sub root (3 o'clock)	279	268	276	270	252	258	235	240	230	292	285	260	279	274	274
	2mm sub cap (3 o'clock)	270	266	268	256	266	317	309	322	302	319	297	262	268	274	270
	Girth / Seam Root	283	276	281	345	327	314	264	256	252	304	272	258	281	285	262
	Girth / Seam Cap	281	283	287	**370**	**370**	**370**	342	327	336	336	322	285	283	272	281
ML-DT-S016	2mm sub root (3 o'clock)	304	294	290	260	285	262	247	227	242	297	285	262	322	319	309
	2mm sub cap (3 o'clock)	292	281	279	262	285	290	339	**363**	**360**	311	285	274	283	283	285
	Girth / Seam Root	297	302	302	345	**351**	**357**	270	251	260	**351**	339	302	292	290	290
	Girth / Seam Cap	285	287	290	**387**	**390**	**376**	**376**	**383**	**380**	**366**	345	325	292	287	297
TIE IN S01	2mm sub root (3 o'clock)	309	325	333	292	304	302	251	256	256	309	294	276	348	**360**	345
	2mm sub cap (3 o'clock)	264	264	264	276	281	274	**383**	317	**376**	304	319	317	290	287	294
	2mm sub root (4-5 o'clock)	283	285	283	268	283	290	247	240	242	290	274	272	274	287	276
	2mm sub cap (4-5 o'clock)	270	276	279	304	314	**351**	**370**	**387**	**390**	287	262	249	270	274	268
	Girth / Seam Root	283	279	283	325	336	327	276	276	299	**360**	**354**	**354**	294	292	287
	Girth / Seam Cap	287	302	290	304	297	297	**405**	**413**	**409**	311	306	306	290	292	283
ML-DT-N009	2mm sub root (3 o'clock)	292	299	292	311	309	281	260	314	317	279	297	304	292	302	297
	2mm sub cap (3 o'clock)	292	299	290	302	297	309	339	325	348	342	314	330	290	285	292
	Girth / Seam Root	322	319	325	**357**	**366**	**363**	322	317	297	**351**	**363**	**366**	336	327	319
	Girth / Seam Cap	290	287	287	339	333	325	330	**351**	**351**	**363**	**390**	306	283	281	279
DJ-DT-N012	2mm sub root (3 o'clock)	270	264	268	262	287	285	306	304	302	297	270	254	270	272	274
	2mm sub cap (3 o'clock)	260	270	272	260	272	302	327	327	333	302	268	258	262	264	276
	Girth / Seam Root	299	294	299	**370**	**357**	348	299	292	302	342	**373**	**357**	317	311	306
	Girth / Seam Cap	262	266	270	**357**	**351**	339	311	317	317	333	345	336	276	270	279
ML-DT-N013	2mm sub root (3 o'clock)	279	279	279	252	274	294	238	243	242	272	256	262	274	281	272
	2mm sub cap (3 o'clock)	263	274	281	281	297	327	333	330	342	266	297	292	276	274	266
	Girth / Seam Root	322	317	311	325	**354**	**373**	325	339	262	270	**357**	319	317	306	317
	Girth / Seam Cap	274	274	272	336	325	**357**	345	336	**351**	**366**	**366**	**370**	270	268	216

Bold indicates hardness HV10 >350

Table 6-7 X100 Pipe 5G procedure tests single tandem, dual tandem and Tie In hardness results

Welding Procedure	Location	Weld Metal HV0.5	Weld Metal HV0.5	Weld Metal HV0.5	Weld Metal HV0.5	Weld Metal HV0.5	HAZ HV0.5	HAZ HV0.5	HAZ HV0.5	HAZ HV0.5	HAZ HV0.5	Parent Material 0.5HV	Parent Material 0.5HV	Parent Material 0.5HV	Parent Material 0.5HV	Parent Material 0.5HV
ML-ST-S006	2mm sub OD	312	322	316			310	304	252			253	291	288	307	
	Pipe mid Thk.	294	304	301			249	258	256			258	280	258	252	
	2mm sub ID	258	238	226			276	301	280			279	299	309	326	
ML-DT-S016	2mm sub OD	334	336	324	336	**371**	350	312	307	279	253	241	238	258	262	291
	Pipe mid Thk.	312	293	299			258	244				249	241	252	245	
	2mm sub ID	230	236	230			285	243				259	265	278	285	280
TIE IN S01	2mm sub OD	**411**	**411**	**420**			336	328	318			296	291	299	285	
	Pipe mid Thk.	**383**	**391**	**386**			296	238				266	271	271	252	
	2mm sub ID	248	256	266			316	271	238			291	330	330	296	
ML-DT-N009	2mm sub OD	312	324	336	340	336	312	312	271	280	287	265	266	276	280	
	Pipe mid Thk.	310	340	310			322	291				279	262	269	274	271
	2mm sub ID	301	291	294			291	274				276	271	285	288	
DJ-DT-N012	2mm sub OD	299	318	312			288	271	249			231	253	265	266	
	Pipe mid Thk.	301	312	310			285	245	242			245	244	249	266	
	2mm sub ID	263	276	283			271	258	240			231	230	230	239	
ML-DT-N013	2mm sub OD	336	324	324	330		318	307	271			245	259	269	279	276
	Pipe mid Thk.	322	324	318			266	248	231			249	249	260	260	
	2mm sub ID	225	220	218			285	249	239			248	258	271	274	

Welding Procedure	PM Av.	PM Max.	HAZ Av.	HAZ Max.	WM Av.	WM Max.
ML-ST-S006	283	326	276	310	286	301
ML-DT-S016	260	291	281	350	300	**371**
TIE IN S01	290	330	293	318	**352**	**420**
ML-DT-N009	274	288	293	322	317	340
DJ-DT-N012	246	266	261	288	297	318
ML-DT-N013	261	279	268	318	294	336

Bold indicates HV0.5 >350

Av=average, **Max**=maximum

Table 6-8 X100 Pipe 5G procedure tests single tandem, dual tandem and Tie In tensile microhardness results

	Cross Weld Tensile (API 1104)									Nick Break (API 1104)				Side Bend (API 1104)			
Welding Procedure	X100 Pipe ODxWT(mm)	Rm(MPa) 45^0	Fracture Locatin	Rm(MPa) 135^0	Fracture Location	Rm(MPa) 225^0	Fracture Location	Rm(MPa) 315^0	Fracture Location	45^0	135^0	225^0	315^0	45^0	135^0	225^0	315^0
ML-ST-S006 Oerlikon NiMo-1 Thyssen K-Nova,Root	36” x 19.05 Pipe B19	809	PM Fracture	821	PM Fracture	820	PM Fracture	818	PM Fracture	Acc.	Acc.	Acc.	Acc.	Acc.	Acc.	Acc.	Acc.
ML-DT-S016 Oerlikon NiMo-1/ Thyssen X-85 Thyssen K-Nova,Root	36” x 19.05 Pipe B19	799	PM Fracture	825	PM Fracture	791	PM Fracture	787	PM Fracture	Acc.	Acc.	Acc.	Acc.	Acc.	Acc.	Acc.	Acc.
TIE IN S01 Filarc PZ6149 Fluxofil M10S, Root	36” x 19.05 Pipe B19	802	PM Fracture	826	PM Fracture	760	PM Fracture	765	PM Fracture	Unacc. 3:o’cl.	Acc. 4 o’cl.	Acc. 4 o’cl.	Acc. 2 o’cl.	Acc 3 o’cl..	Acc. 4 o’cl.	Acc. 4 o’cl.	Unacc. 2 o’cl.
ML-DT-N009 Oerlikon NiMo-1/ Thyssen X-85 Thyssen K-Nova,Root	52” x 22.9 Pipe D2	812	PM Fracture	796	PM Fracture	803	PM Fracture	814	PM Fracture	Acc.	Acc.	Acc.	Acc.	Acc.	Acc.	Acc.	Acc.
DJ-DT-N012 Oerlikon NiMo-1/ Thyssen X-85 Thyssen K-Nova,Root	52” x 22.9 Pipe D1	765	PM Fracture	755	PM Fracture	770	PM Fracture	771	PM Fracture	Acc.	Acc.	Acc.	Acc.	Acc.	Acc.	Acc.	Acc.
ML-DT-N013 Oerlikon NiMo-1/ Thyssen X-85 Thyssen K-Nova,Root	52” x 22.9 Pipe D1	767	PM Fracture	748	PM Fracture	749	PM Fracture	762	PM Fracture	Acc.	Acc.	Acc.	Acc.	Acc.	Acc.	Acc.	Acc.

Acc. =Acceptable
Unacc. =Unacceptable Nick Break due to gas pore and lack of fusion (root); Side Bend due to tearing of side wall >3mm
PM= Parent Material

Table 6-9 X100 Pipe 5G procedure tests single tandem, dual tandem and Tie In cross tensile/nick breaks and side bend results

	Cv Root Impact Toughness (EN 288-9 : 1999)								
Welding Procedure	X100 Pipe OD x WT(mm)	Cv -20^{0}C (J) Weld Metal	Cv -20^0 C (J) Fusion Line	Cv -40^0 C (J) Weld Metal	Cv -40^0 C (J) Fusion Line	Cv -60^0 C (J) Weld Metal	Cv -60^0 C (J) Fusion Line	Cv -80^0 C (J) Weld Metal	Cv -80^0 C (J) Fusion Line
ML-ST-S006 Oerlikon NiMo-1, Fill Thyssen K-Nova, Root	36" x 19.05 Pipe B19	272 220 254 **Av.** **249**	236 256 238 **Av.** **243**	144 248 180 **Av.** **191**	212 236 240 **Av.** **229**	211 178 185 **Av.** **191**	76 130 60 **Av.** **89**	60 58 76 **Av.** **65**	34 34 66 **Av.** **45**
ML-DT-S016 Oerlikon NiMo-1 / Thyssen X-85, Fill Thyssen K-Nova, Root	36" x 19.05 Pipe B19	212 254 258 **Av.** **241**	258 248 250 **Av.** **252**	226 200 172 **Av.** **199**	184 128 260 **Av.** **191**	222 242 268 **Av.** **244**	36 18 14 **Av.** **23**	102 178 154 **Av.** **145**	24 38 18 **Av.** **27**
TIE-IN S01 Filarc PZ6149, Fill Fluofil M10S, Root	36" x 19.05 Pipe B19 Specimen extraction from different positions around the pipe	82 80 82 **Av.** **81**	114 202 220 **Av.** **179**	76 56 58 **Av.** **63**	78 116 52 **Av.** **82**	50 52 48 **Av.** **50**	36 26 92 **Av.** **51**	32 32 36 **Av.** **33**	42 28 22 **Av.** **31**
ML-DT-N009 Oerlikon NiMo-1 / Thyssen X-85, Fill Thyssen K-Nova, Root	52" x 22.9 Pipe D2	166 154 142 **Av.** **154**	276 286 276 **Av.** **279**	168 176 186 **Av.** **177**	258 46 230 **Av.** **178**	124 152 126 **Av.** **134**	140 142 264 **Av.** **182**	76 66 108 **Av.** **83**	166 36 56 **Av.** **86**
	2nd Test				242 272 76 **Av.** **197**				
DJ-DT-N012 Oerlikon NiMo-1 / Thyssen X-85, Fill Thyssen K-Nova, Root	52" x 22.9 Pipe D1	204 214 210 **Av.** **209**	258 260 256 **Av.** **258**	220 194 196 **Av.** **203**	256 250 252 **Av.** **253**	134 198 190 **Av.** **174**	48 56 50 **Av.** **51**	96 84 52 **Av.** **77**	56 18 38 **Av.** **37**
ML-.DT-N013 Oerlikon NiMo-1 / Thyssen X-85, Fill Thyssen K-Nova, Root	52" x 22.9 Pipe D1	258 260 248 **Av.** **255**	230 228 228 **Av.** **229**	250 240 244 **Av.** **245**	234 236 226 **Av.** **232**	228 232 242 **Av.** **234**	240 194 238 **Av.** **224**	210 172 230 **Av.** **204**	38 24 220 **Av.** **94**

Table 6-10 X100 Pipe 5G procedure tests single tandem, dual tandem and Tie In Charpy impact results for the weld root

Welding Procedure	X100 Pipe OD x WT(mm)	Cv -20^{0}C (J) Weld Metal	Cv -20^0 C (J) Fusion Line	Cv -40^0 C (J) Weld Metal	Cv -40^0 C (J) Fusion Line	Cv -60^0 C (J) Weld Metal	Cv -60^0 C (J) Fusion Line	Cv -80^0 C (J) Weld Metal	Cv -80^0 C (J) Fusion Line
		Cv Cap Impact Toughness (EN 288-9 : 1999)							
ML-DT-N009 Oerlikon NiMo-1 / Thyssen X-85, Fill Thyssen K-Nova, Root	52" x 22.9 Pipe D2	126 134 134 **Av. 131**	206 242 256 **Av. 235**	134 130 124 **Av. 129**	38 46 82 **Av. 55**	90 82 74 **Av. 82**	236 232 38 **Av. 169**	54 56 56 **Av. 55**	30 32 32 **Av. 31**
	2nd Test						260 262 264 **Av. 262**		
DJ-DT-N012 Oerlikon NiMo-1 / Thyssen X-85, Fill Thyssen K-Nova, Root	52" x 22.9 Pipe D1	142 146 142 **Av. 143**	240 258 262 **Av. 253**	110 114 100 **Av. 108**	238 244 260 **Av. 247**	98 94 90 **Av. 94**	42 106 56 **Av. 68**	60 62 62 **Av. 61**	42 144 24 **Av. 70**
ML-DT-N013 Oerlikon NiMo-1 / Thyssen X-85, Fill Thyssen K-Nova, Root	52" x 22.9 Pipe D1	148 162 152 **Av. 154**	240 232 236 **Av. 236**	120 150 134 **Av. 135**	220 240 222 **Av. 227**	116 128 132 **Av. 125**	224 234 222 **Av. 227**	90 84 98 **Av. 91**	66 216 48 **Av. 110**

Table 6-10 (cont.) X100 Pipe 5G procedure tests single tandem, dual tandem and Tie In Charpy impact results for the weld cap

CTOD Results							
Weld Procedures	OD x WT	CTOD (mm) at -10^{0}C ; Weld Metal			CTOD (mm) at -10^{0}C ; Heat Affected Zone		
ML-ST-S006	36" x 19.05 mm	M	M	M	C	M	M
Oerlikon NiMo-1, Fill	Pipe D2	0.14	0.23	0.17	0.13	0.45	0.36
Thyssen K-Nova, Root	Specimens extracted from	**Valid**	**Valid**	**Valid**	**Valid**	**Valid**	**Valid**
	4 to 5 o'clock position						
ML-DT-S016		M	M	M	C	M	M
Thyssen X-85 / Oerlikon NiMo-1, Fill	36" x 19.05 mm	0.21	0.18	0.15	0.08	0.53	0.50
Thyssen K-Nova, Root	Specimens extracted from	**Valid**	**Valid**	**Valid**	**Valid**	**Valid**	**Valid**
	3 to 4 o'clock position						
TIE-IN S01	36" x 19.05 mm	M	M	M	NOT TESTED		
Filarc PZ6149, Fill	Pipe D2	0.10	0.10	0.09			
Fluxofil M10S, Root	Specimens extracted from	**Valid**	**Valid**	**Valid**			
	4 to 5 o'clock position						
ML-DT-N009	52" x 22.9 mm	M(1,2)	M(1,2)	M(1,2)	U(1,2)	U(1,2)	U(1,2)
Thyssen X-85 / Oerlikon NiMo-1, Fill	Pipe D2	0.21	0.22	0.21	0.58	0.29	0.41
Thyssen K-Nova, Root	Specimens extracted from	**Invalid**	**Invalid**	**Invalid**	**Invalid**	**Invalid**	**Invalid**
	4 to 5 o'clock position						
DJ-DT-N012	52" x 22.9 mm	M	M	M(3)	M	C	C
Thyssen X-85 / Oerlikon NiMo-1, Fill	Pipe D1	0.36	0.30	0.42	0.67	0.23	0.38
Thyssen K-Nova, Root	Specimens extracted from	**Valid**	**Valid**	**Invalid**	**Valid**	**Valid**	**Valid**
	4 to 5 o'clock position						
ML-DT-N013	52" x 22.9 mm	M	M	M	M	C	C
Thyssen X-85 / Oerlikon NiMo-1, Fill	Pipe D2	0.35	0.36	0.38	0.54	0.23	0.04
Thyssen K-Nova, Root	Specimens extracted from	**Valid**	**Valid**	**Valid**	**Valid**	**Valid**	**Valid**
	4 to 5 o'clock position						

CTOD Classification :

C= Critical CTOD at the onset of brittle crack extension or pop-in when Δa is less than 0.2mm

M= Value of CTOD at the first attainment of a maximum force plateau for fully plastic behaviour

U= Critical CTOD at the onset of brittle crack extension or pop-in when the event is preceded by Δa equal to or greater than 0.2mm.

(1,2) CTOD Invalidity according to BS7448-1:1991. 1=section **10.2.2.b**(before the fracture test): both ends of the fatigue crack have extended for at least 1.3mm or 2.5% of the specimen width from the root of the machined notch, whichever is the greater. 2=section **10.2.3.d**(after carrying out the fracture test) :no part of the fatigue pre crack front is closer to the crack starter notch than 1.3mm or 2.5% of the specimen width whichever is the larger.

In both cases slightly below the standard requirements. Comment on the certificates of the testing company: Crack front shape technically invalid to BS 7448 but is unlikely to have had a significant effect on the result obtained.

(3) CTOD Invalidity according to BS 7448-2:1997. Section **12.4.1** (after carrying the test): no two of the inner seven crack length measurements shall differ by more than 20%a_0. The tested specimen crack at the centre-line was 20.3% greater than the crack length at the surface.

Table 6-11 X100 Pipe 5G procedure tests single tandem, dual tandem and Tie In toughness (CTOD) results

Chemical Composition (wt %)																			
	C	Mn	P	S	Si	Cr	Ni	Mo	Cu	Al	V	Nb	Ti	B ppm	O_2 ppm	N_2 ppm	CE_{IIW}	CET	P_{cm}
Dual Tandem Weld Procedure																			
ML-DT-N013 (Pipe D1);weld metal	**0.09**	**1.68**	**0.015**	**0.011**	**0.58**	**0.17**	**1.11**	**0.40**	**0.17**	**-**	**<0.01**	**0.04**	**<0.01**	**-**	**250**	**60**	**0.57**	**0.34**	**0.26**
52 in x 22.9mm;pipe	0.057	1.90	0.008	0.0012	0.28	0.02	0.41	0.26	0.40	0.004	0.002	0.049	0.015	<5	20	31	0.484	0.301	0.208
Oerlikon Carbofil NiMo1;filler wire	0.09	1.62	0.009	0.008	0.63	0.03	0.91	0.31	0.1	<0.005	<0.005	0.006	0.07		79	68	0.5	0.31	0.23
Thyssen Union X85-IG;filler wire	0.08	1.68	0.012	0.012	0.68	0.32	1.77	0.54									0.65	0.36	0.27
Preliminary Dual Tandem Weld Procedures																			
ML-DT-S003 (pipe B19);weld metal	**0.08**	**1.64**	**0.009**	**0.009**	**0.55**	**0.03**	**0.86**	**0.29**	**0.11**	**<0.01**	**<0.01**	**<0.01**	**0.05**	**<10**	**370**	**70**	**0.48**	**0.30**	**0.23**
36 in x 19.05mm;pipe	0.06	1.88	0.007	<0.005	0.18	0.022	0.50	0.26	0.30	0.04	0.005	0.06	0.018	<5			0.20	0.30	0.48
Oerlikon Carbofil NiMo1;filler wire	0.087	1.62	0.009	0.008	0.63	0.03	0.91	0.31	0.1	<0.005	<0.005	0.006	0.07		79	68	0.5	0.31	0.23
ML-DT-S002 (pipe B19);weld metal	**0.08**	**1.48**	**0.009**	**0.012**	**0.51**	**0.22**	**1.22**	**0.23**	**0.10**	**<0.01**	**<0.01**	**<0.01**	**<0.04**	**<10**	**350**	**60**	**0.50**	**0.30**	**0.23**
36 in x 19.05mm;pipe	0.06	1.88	0.007	<0.005	0.18	0.022	0.50	0.26	0.30	0.04	0.005	0.06	0.018	<5			0.20	0.30	0.48
Bohler X70-IG;filler wire	0.081	1.45	0.008	0.016	0.59	0.26	1.32	0.25	0.08	0.005	0.1	0.005	0.05		37	56	0.54	0.30	0.24
ML-DT-S011 (pipe B19);weld metal	**0.08**	**1.61**	**0.011**	**0.009**	**0.55**	**0.23**	**1.42**	**0.45**	**0.17**	**<0.01**	**<0.01**	**0.01**	**0.04**	**<10**	**390**	**60**	**0.59**	**0.34**	**0.26**
36 in x 19.05mm;pipe	0.06	1.88	0.007	<0.005	0.18	0.022	0.50	0.26	0.30	0.04	0.005	0.06	0.018	<5			0.20	0.30	0.48
Thyssen Union X85-IG;filler wire	0.08	1.68	0.012	0.012	0.68	0.32	1.77	0.54									0.65	0.36	0.27
Pipe B19 girth weld metal	**0.10**	**1.65**	**0.013**	**0.003**	**0.72**	**0.25**	**1.77**	**0.46**	**0.16**	**0.01**	**<0.01**	**<0.01**	**0.07**	**<10**	**250**	**180**	**0.65**	**0.37**	**0.29**
36 in x 19.05mm;pipe	0.06	1.88	0.007	<0.005	0.18	0.022	0.50	0.26	0.30	0.04	0.005	0.06	0.018	<5			0.20	0.30	0.48
Oerlikon Carbofil 120;filler wire	0.11	1.66	0.006	<0.005	0.9	0.32	2.24	0.56	0.16	0.014	0.007	0.006	0.1	8	41	83	0.72	0.41	0.33
Tie In Weld Procedure																			
TIE IN S01 (Pipe B19);weld metal	**0.09**	**1.90**	**0.012**	**0.011**	**0.55**	**0.91**	**2.01**	**0.47**	**0.04**	**-**	**<0.01**	**<0.01**	**<0.01**	**-**	**490**	**30**	**0.82**	**0.42**	**0.32**
36 in x 19.05mm;pipe	0.06	1.88	0.007	<0.005	0.18	0.022	0.50	0.26	0.30	0.04	0.005	0.06	0.018	<5			0.20	0.30	0.48
Filarc PZ6149;filler wire	0.079	1.73	0.011	0.017	0.44	0.9	2.25	0.51									0.80	0.40	0.30

CEIIW= C+Mn/6+(Cr+Mo+V)/5+(Ni+Cu)/15
CET(BS EN 1011-2) = C+(Mn+Mo)/10+(Cr+Cu)/20+Ni/40
PCM = C+Si/30+(Mn+Cu+Cr)/20+Ni/60+Mo/15+V/10+5B

Balance Fe
When elements are stated as < the given amount calculations for carbon equivalents are based on the following assumptions: B = 0.0004, V=0.01 and Nb=0.01
N.B Al and B were not detected

Table 6-12 Chemical analysis of procedure qualification welds, pipe material and filler wire

6.2 High Speed Video Technique

The experimental work on the effect of shielding gas composition on the weld bead geometry was carried out testing several gas mixtures at the same arc length.
Correct arc length measurement is critical in determining the effect on the weld bead geometry as well as in establishing the correlation between the arc length correction factor, determined by the power source, and the actual arc length. A detailed description of the technique used to measure the arc length using a high speed video camera is presented in section 5.2.5 (page 78). Some examples of images taken during pulsed tandem wire are shown in Figure 6.30.
Although the technique was not extensively tested during this experimental work, it showed very encouraging results and potential applications could include the investigation of the pulse parameters on droplet, weld pool, arc characteristics and transfer mode.

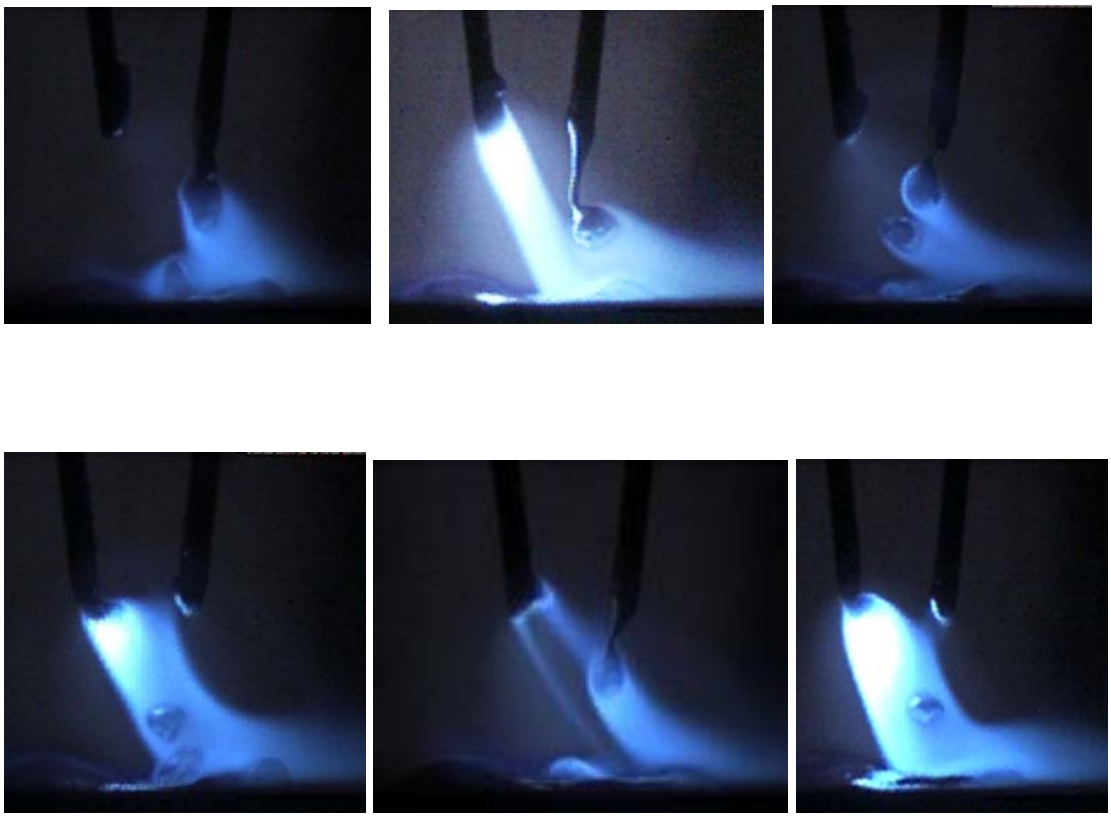

Fig. 6-30 Sequence of high speed video images in tandem PGMAW obtained with a 2000W halogen lamp as backlight

6.3 Welding Parameter Trials Modelling Results

The objective of this experimental work was to generate an adequate source of information in order to formulate valid relationships between the welding parameters (named factors or variables) and the weld bead geometry (responses). The welding parameters selected for this purposes were:

a)wire feed speed (abbreviated to wfs),
b)travel or welding speed (abbreviated to ts),
c)wire distance from the wall (abbreviated to wd), and
d)arc length correction (abbreviated to alc)
(Their ranges are shown in section 5.3.2.2.1; page 86)

Again, as explained in section 5.3.2.2.1 (page 89) the arc length was controlled by varying the arc length correction parameter. Due to considerable arc length variations that occur during PGMA narrow groove welding (Figure 6.121) only an "approximate" estimation of the real arc length could be obtained. Although extensive measurements of the arc length were carried out using high speed video images, it was decided to include the arc length correction parameter in the analysis. For each welding condition the relationship between the actual arc length and arc length correction setting was established (Table 6.13). Arc length measurements were taken when the arc was positioned in the centre of the groove.
For the design of the experiments and their analysis the Design Expert Software [95] was used. Thirty experiments with different welding conditions (Table 5.4, page 88) were developed and carried out in random sequence.
Two specimens were extracted from each welded section, polished and etched. Macrograph photos were taken, weld bead dimensions were measured and their average values were reported.

6.3.1 Flat Position

6.3.1.1 Modelling Results

The measured weld bead dimensions for the thirty experiments listed in Table 5.4 are shown in Table 6.14. The weld bead dimensions selected for the analysis were depth of penetration, groove side wall penetration, max sidewall penetration, undercut and corner angle. The definitions are shown in Figure 5.10 (page 77).
Originally, the weld bead concavity was also considered but due to some weld profile discrepancies (Figure 5.11, page 78) concavity was excluded and the corner angle was included in the analysis instead.

Weld No	Wire Feed Speed (m/min)	Travel Speed (mm/min)	Wire Distance from Sidewall(mm)	Arc Length Correction (%)	Arc Length (mm)
1	10.7	900	0.9	0.00	1.8
2	11.95	1025	0.6	-12.50	0.8
3	10.7	1150	0.9	0.00	1.4
4	10.7	1150	0.3	0.00	1.65
5	10.7	1150	0.9	0.00	1.65
6	10.7	1150	0.9	0.00	1.65
7	11.95	1275	0.6	-12.50	0.86
8	10.7	1150	0.9	0.00	1.7
9	11.95	1275	1.2	-12.50	0.84
10	11.95	1025	1.2	-12.50	0.75
11	9.45	1275	1.2	12.50	1.7
12	10.7	1400	0.9	0.00	1.5
13	9.45	1275	0.6	12.50	2.44
14	10.7	1150	0.9	0.00	1.26
15	11.95	1025	1.2	12.50	1.72
16	13.2	1150	0.9	0.00	1.35
17	9.45	1275	1.2	-12.50	0.95
18	9.45	1025	1.2	-12.50	0.86
19	9.45	1275	0.6	-12.50	0.88
20	11.95	1275	0.6	12.50	1.63
21	9.45	1025	1.2	12.50	1.8
22	9.45	1025	0.6	12.50	2.54
23	11.95	1275	1.2	12.50	2.0
24	8.20	1150	0.9	0.00	1.5
25	10.70	1150	0.9	-25.00	0.67
26	9.45	1025	0.6	-12.50	0.9
27	11.95	1025	0.6	12.50	2.3
28	10.70	1150	0.9	25.00	3.1
29	10.70	1150	1.5	0.00	1.4
30	10.70	1150	0.9	0.00	1.5

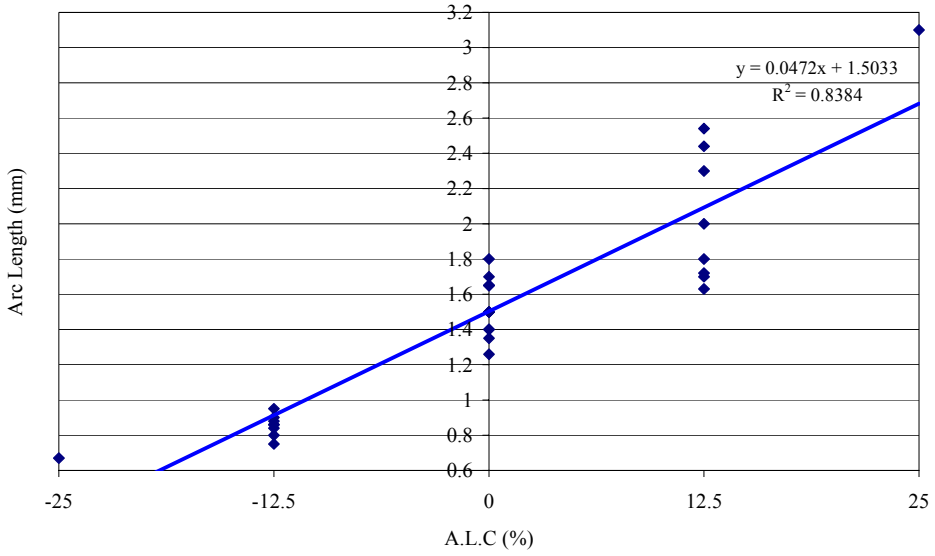

Table 6-13 Measured arc length associated with the welding conditions of the welding parameter trials

	Responses				
Weld No (Run No)	Depth of Penetration (mm)	Groove Sidewall Penetration (mm)	Max Sidewall Penetration (mm)	Undercut (mm)	Corner Angle (°)
1	3.08	0.34	0.78	0	46.5
2	2.34	0.25	0.53	0	50
3	2.43	0.18	0.58	0	56
4	1.95	0.12	0.75	0.26	~~46~~
5	2.83	0.31	0.57	0	51
6	2.88	0.28	0.59	0	50.5
7	2.40	0.36	0.48	0	59
8	2.75	0.26	0.62	0.03	54.5
9	2.60	0.21	0.38	0	55
10	2.51	0.26	0.39	0	54
11	1.91	0.02	0.49	0.15	~~33~~
12	1.88	0.06	0.32	0.09	42
13	1.2	0	0.50	0.14	~~25~~
14	2.76	0.19	0.59	0	54
15	3.7	0.50	0.71	0	49.5
16	3.24	0.36	0.65	0	44
17	2.15	0.111	0.31	0	53
18	2.36	0.18	0.39	0	43.5
19	2.15	0.20	0.41	0	55
20	2.79	0.34	0.77	0.09	47.5
21	2.73	0.31	0.75	0.23	~~32.5~~
22	2.45	0.26	0.85	0.13	38
23	2.6	0.13	0.51	0	~~47~~
24	1.73	0.06	0.43	0	47.5
25	1.91	0.14	0.39	0	52.5
26	1.62	0.05	0.53	0.10	44
27	3.10	0.58	0.93	0	45
28	2.85	0.29	0.94	0.34	30
29	3.17	0.15	0.39	0	53.5
30	2.6	0.26	0.66	0.07	56

Table 6-14 Measured weld bead geometric responses (flat position, 0°)

Some of the welds (4, 11, 13, 21 & 23) presented irregular beads and the corner angle values were difficult to measure. These welds were excluded from the analysis. It is very unlikely that the overall analysis is affected by this decision (quite common in statistical analysis), since the remaining twenty-five welds are considered sufficient for a reliable analysis. In any case, the model validation tests will confirm this decision.
Figure 6.31 shows the as welded bead profile for some of the experiments. Generally, all runs presented adequate bead morphology despite some isolated sidewall defects (Figures 6.31c and 6.32d) associated with arc instabilities. Some typical macrographs are shown in Figure 6.33.
Macrographs of the welds of Table 6.14 are shown in Appendix C.

Stable welding conditions for almost all the experiments were reported.

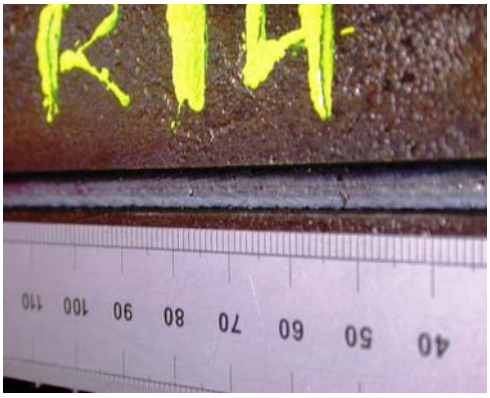

a) weld(run) No. 14

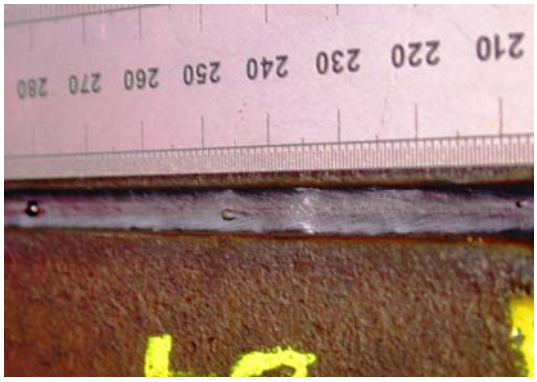

b) weld(run) No. 21

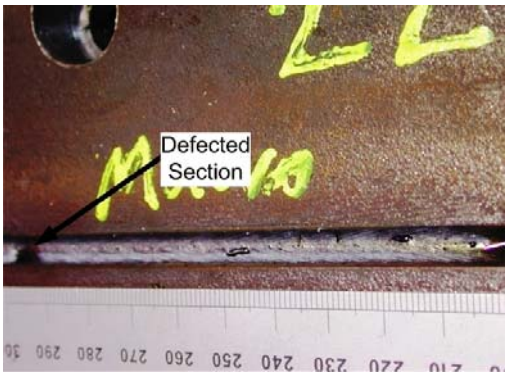

c) weld(run) No. 22

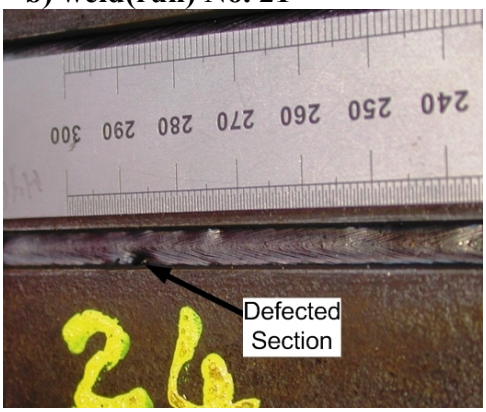

d) weld(run) No. 24

Fig. 6-31 As welded bead profiles in flat position including some sidewall defects (c and d)

The welds Nos.13 and 11 presented bead profile irregularities attributed to the welding conditions.
The Figure 6.32 shows two sections of the weld No. 13. The weld bead dimensions were the average of the two.

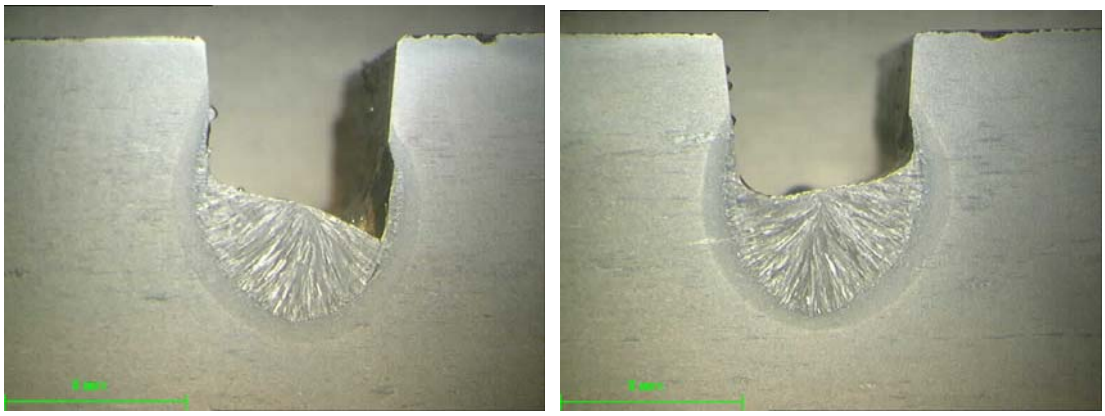

Fig. 6-32 Macrographs of two sections for the same weld No. 13

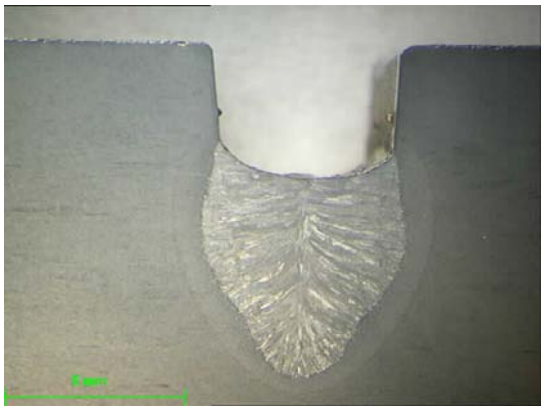

a) weld (run) No. 1

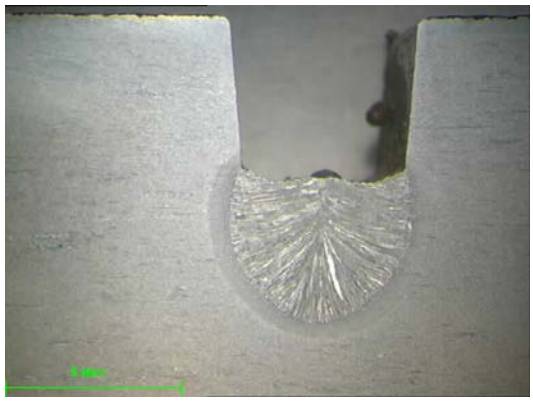

b) weld (run) No. 7

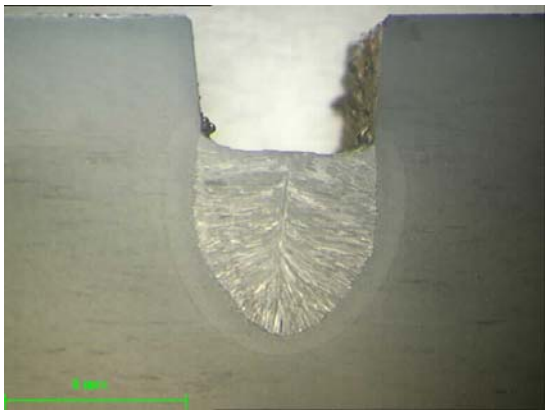

c) weld (run) No. 10

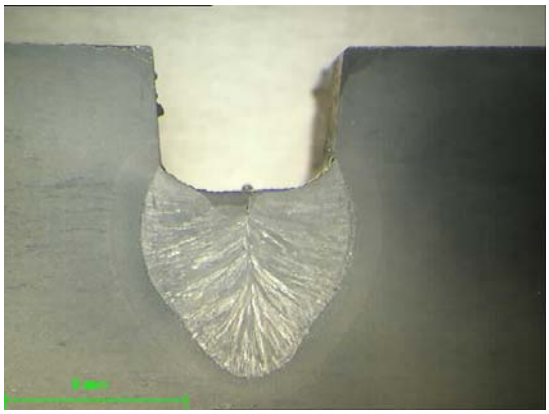

d) weld (run) No. 27

Fig. 6-33 Macrographs showing the difference in the weld profiles obtained from different welding conditions

Table 6.15 shows the variables (factors) selected after the backward elimination method. Backward elimination is a technique, often applied in statistics, where the least significant terms (factors, interactions etc) are removed from the model. A term is defined as significant in a model when the probability value (Prob>F) is less than 0.05. Additional statistical parameters used to evaluate the performance of a model are included in Table 6.15. A brief description [95] of these parameters is given below:

a)Prob>F*(p-value)* should be small (less than 0.05) for the terms of the model to have a significant effect on the model. If Prob >F is > 0.10 then the term is not significant
b)Model F-value is a test that compares the model variance with the residual (error) variance. If the two variances (mean squares) are similar the ratio will be close to one and this means that it is less likely for any of the factors to have a significant effect on the response.
c)Lack of Fit, F-value is the value for the lack of fit of the model. The higher the number, the more likely the model does not adequately fit the data.

d)Lack of Fit, Prob>F(p-value)measures how well the model fits the data. Strong lack of fit (p-value <0.05) is undesirable because it indicates that the model does not fit the data well. Insignificant lack of fit (p-value >0.1) is desirable.
e)Adeq. Precision is the signal to noise ratio and is preferred to be greater than 4 (Adeq. Precision>4).
f)Adj. R-squared is a measure of the amount of variation around the mean explained by the model, adjusted for the number of terms in the model. The Adj. R-squared decreases as insignificant terms are added to the model.
g)Pred. R-squared is a measure of the variation in new data explained by the model.
Generally adjusted R-squared and Pred.R-squared values should fall within 0.2 of each other.
In addition, if the objective is to create a model that can accurately represent a process and optimum parameters settings are to be determined it is desirable to have high values of both adjusted and predicted R-squared (70+).
The prediction equations for the responses that describe the weld bead geometry, depth of penetration, groove sidewall penetration, max sidewall penetration, undercut and corner angle obtained from the ANOVA (analysis of variance) are reported below in both coded and actual factors.
In statistics, design, description and analyses are often performed in coded factors. Using the coding form, the range of all the factors included in the model is reduced to a common scale -2 to +2 or -1 to +1 regardless of its relative magnitude. Besides it is easier to think in terms of low to high, rather than considering their actual values, especially in cases where one factor may vary from 150 to 550 while another varies from 0.5 to 0.9.
The mathematical equations derived from the model represent all the significant factors and interactions that are relevant for the range of the welding parameters selected. The units for the responses and the actual factors are as follows:
P_d, Depth of penetration: mm
$P_{GS,}$ Groove sidewall penetration: mm
$P_{S,}$ Sidewall penetration: mm
Θ, Corner angle: (°)
U, Undercut: mm
W, Wire feed speed (WFS): m/min
T, Travel speed (TS): mm/min
D, Wire distance from sidewall (WD): mm
A_C, Arc length correction (ALC): %

1.-Depth of Penetration (P_d)

a) coded factors:

$$P_d = 2.55 + 0.35 \cdot W - 0.23 \cdot T + 0.21 \cdot D + 0.18 \cdot A_c + 0.14 \cdot W \cdot A_c - 0.25 \cdot T \cdot A_c - 0.073 \cdot A_c^2 \qquad \textbf{Eqn. 6. 1}$$

b) actual factors:

$$P_d = 0.9786 + 0.2828 \cdot W - 1.806 \cdot 10^{-3} \cdot T + 0.6890 \cdot D + 0.0974 \cdot A_c + 9.26 \cdot 10^{-3} \cdot W \cdot A_c - 1.586 \cdot 10^{-4} \cdot T \cdot A_c - 4.671 \cdot 10^{-4} \cdot A_c^2 \quad \textbf{Eqn. 6. 2}$$

2.-Groove Sidewall Penetration (P_{GS})

a) coded factors:

$$P_{GS} = 0.24 + 0.087 \cdot W - 0.066 \cdot T - 0.011 \cdot D + 0.034 \cdot A_c - 0.034 \cdot W \cdot D + 0.026 \cdot W \cdot A_c - 0.034 \cdot T \cdot D - 0.080 \cdot T \cdot A_c - 0.021 \cdot D^2 \quad \textbf{Eqn. 6. 3}$$

b) actual factors:

$$P_{GS} = -1.843 + 0.1504 \cdot W + 2.792 \cdot 10^{-4} \cdot T + 2.369 \cdot D + 0.0435 \cdot A_c - 0.0895 \cdot W \cdot D + 1.692 \cdot 10^{-3} \cdot W \cdot A_C - 8.95 \cdot 10^{-4} \cdot T \cdot D - 5.124 \cdot 10^{-5} \cdot T \cdot A_c - 0.2328 \cdot D^2 \quad \textbf{Eqn. 6. 4}$$

3.-Sidewall Penetration (P_S)

a) coded factors:

$$P_S = 0.60 + 0.038 \cdot W - 0.086 \cdot T - 0.074 \cdot D + 0.13 \cdot A_c + 0.025 \cdot W \cdot T - 0.024 \cdot B \cdot D - 0.043 \cdot T \cdot D - 0.018 \cdot W^2 - 0.022 \cdot T^2 \quad \textbf{Eqn. 6. 5}$$

b) actual factors:

$$P_S = -0.6115 + 0.1579 \cdot W + 8.967 \cdot 10^{-4} \cdot T + 0.442 \cdot D + 0.0426 \cdot A_c + 1.568 \cdot 10^4 \cdot W \cdot T - 0.0643 \cdot W \cdot D - 2.784 \cdot 10^{-5} \cdot T \cdot A_c - 0.0117 \cdot W^2 - 1.417 \cdot 10^{-6} \cdot T^2 \quad \textbf{Eqn. 6. 6}$$

4.-Corner Angle (Θ)

a) coded factors:

$$\Theta = 53.20 + 3.07 \cdot W + 0.34 \cdot T - 0.098 \cdot D - 4.98 \cdot A_c - 1.86 \cdot T \cdot D - 2.73 \cdot T \cdot A_c - 2.47 \cdot T^2 - 3.22 \cdot D^2 \quad \textbf{Eqn. 6. 7}$$

a) actual factors:

$$\Theta = -236.6 + 2.456 \cdot W + 0.4113 \cdot T + 56.75 \cdot D + 1.613 \cdot A_c - 0.0496 \cdot T \cdot D - 1.75 \cdot 10^{-3} \cdot T \cdot A_c - 1.582 \cdot 10^{-4} \cdot T^2 - 0.0206 \cdot A_c^2$$ **Eqn. 6. 8**

5.-Undercut (U)

a) coded factors:

$$\sqrt{U} = 0.14 - 0.067 \cdot W + 0.022 \cdot T - 0.064 \cdot D + 0.11 \cdot A_c$$ **Eqn. 6. 9**

b) actual factors:

$$\sqrt{U} = 0.7021 - 0.0537 \cdot W + 1.7373 \cdot 10^{-4} \cdot T - 0.213 \cdot D + 9.19 \cdot 10^{-3} \cdot A_c$$ **Eqn. 6. 10**

The response undercut is expressed in terms of square root, because a transformation is applied to the mathematical equation. Transformation is a mathematical conversion of the response values and is used to satisfy the assumptions required for the analysis of variance (lack of fit tests etc) and aims to improve model's prediction capabilities. However, considering the strong patterns presented in the diagnostic plots (Figures 6.40 and 6.41), it is likely that due to relatively few welds with undercut, the proposed model will probably be poor at predicting the response undercut and should be used with caution.

Response	Type of Model	Chosen Variables	Pred.R-squared	Adj.R-squared.	F-value	P-value (Prob.>F)	Std. dev.	Adeq. Precision	Lack of Fit	
									F-value	P-value
Depth of Penetration (mm)	Quadratic	wfs /ts /wd/ a.l.c / $a.lc^2$/ wfs*a.l.c/ ts*a.l.c	0.75	0.83	21.5	<0.0001 (significant)	0.22	20.50	2.04	0.2216 (not significant)
Groove Sidewall Penetration (mm)	Quadratic	wfs /ts /wd/ a.l.c / wd^2/ wfs*a.l.c/ ts*wd /wfs*wd	0.82	0.89	27.18	<0.0001 (significant)	0.04	21.17	0.67	0.7483 (not significant)
Max Sidewall Penetration (mm)	Quadratic	wfs /ts /wd/ a.l.c / wd^2/ wfs*ts/ ts*a.l.c/ wfs*wd/ wfs^2/ts^2	0.89	0.93	47.48	<0.0001 (significant)	0.04	25.90	2.02	0.2246 (not significant)
Corner Angle (°)	Quadratic	wfs /ts /wd/ a.l.c/ $a.lc^2$/ ts*a.l.c /ts^2	0.66	0.85	17.17	<0.0001 (significant)	2.58	19.14	1.23	0.4331 (not significant)
Undercut (mm)	Linear	wfs /ts /wd /a.l.c	0.24	0.41	5.98	0.0016 (significant)	0.15	8.78	1.68	0.2971 (not significant)

Table 6-15 Selected variables, model order after backward elimination and statistical parameters (flat (0°) position)

6.3.1.2 Model Adequacy Checking

Model adequacy checking consists of analysis of the residuals in order to confirm that the assumptions of the analysis of variance are met. This adequacy control was carried out using the model diagnostic plots and the influence plots.

a) Model Diagnostic Plots [95]
This is a series of plots of residuals and includes:

-Normal Probability Plot (Figure 6.34). The normal probability plot indicates if the residuals (error) follow a normal distribution. In that case the points will follow a straight line (some scatter is always expected). Attention needs to be paid in the case of patterns, where transformation of the response may provide a better analysis.

-Residuals vs Predicted (Figure 6.35). This is a plot of the residuals versus the ascending predicted response values and tests the assumption of constant variance. This plot should present a random scatter and if expanded variance occurs then the plot indicates the need for a transformation. The two lines (+3.00/-3.00) are the limits for the 99.7% confidence interval. Points outside this confidence limit indicate that the model does not fit well.

-Residuals vs Run (Figure 6.36). This is the plot of the residuals versus the experimental run order. The plot should show a random scatter.

-Predicted vs Actual (Figure 6.37). This graph helps to detect a value or group of values that are not easily predicted by the model.

b) Influence Plots [95]
These test the influence of the individual runs on the response as follows:

-Externally Studentised Residuals (Outlier t-values), (Figure 6.38)
This is a plot obtained by removing each run, one after another and seeing how this affects the model fit. Runs outside the lines do not fit as well as the others and high values indicate problems with the model or the need for transformation ("problematic" runs can be ignored).

-Leverage vs Run (Figure 6.39). This is a measure of how each point influences the model fit. The black line plotted above the value 0.25 indicates the average leverage of all the design points and the red line is the double of the average leverage. It is recommended that the design points fall within the two lines. However if a point has a leverage of 1, the model must go through that point and the point controls the model. High leverages near to one (1) must be reduced by adding or replicating points.

Model diagnostic and influence plots (Figures 6.34 to 6.39) represent the response depth of penetration. The equivalent plots of the other responses were examined but are not included in this thesis, except in the case of an indication of deviation when the plot will be shown and discussed.

1. Depth of Penetration

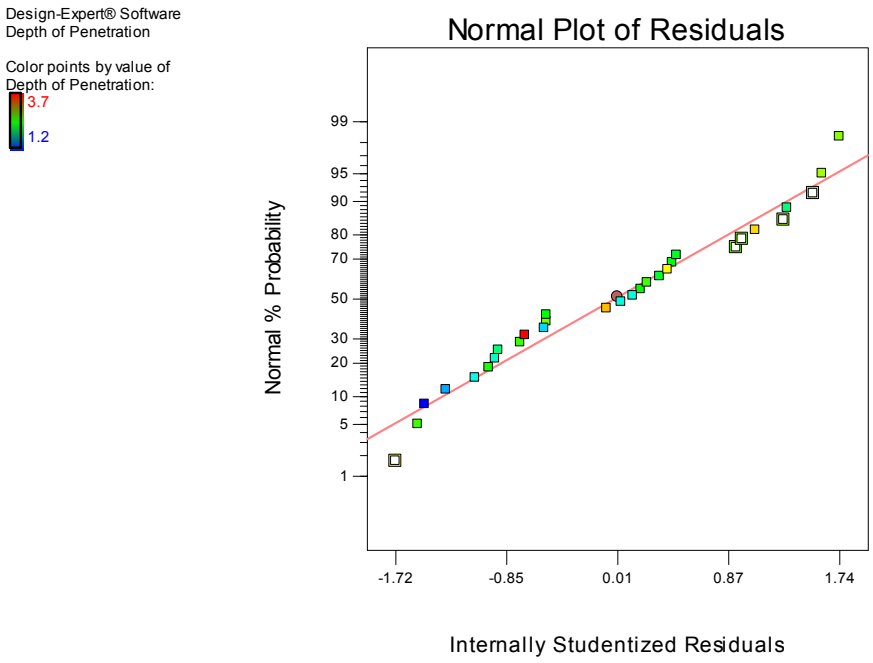

Fig. 6-34 Normal plot of residuals for the response depth of penetration

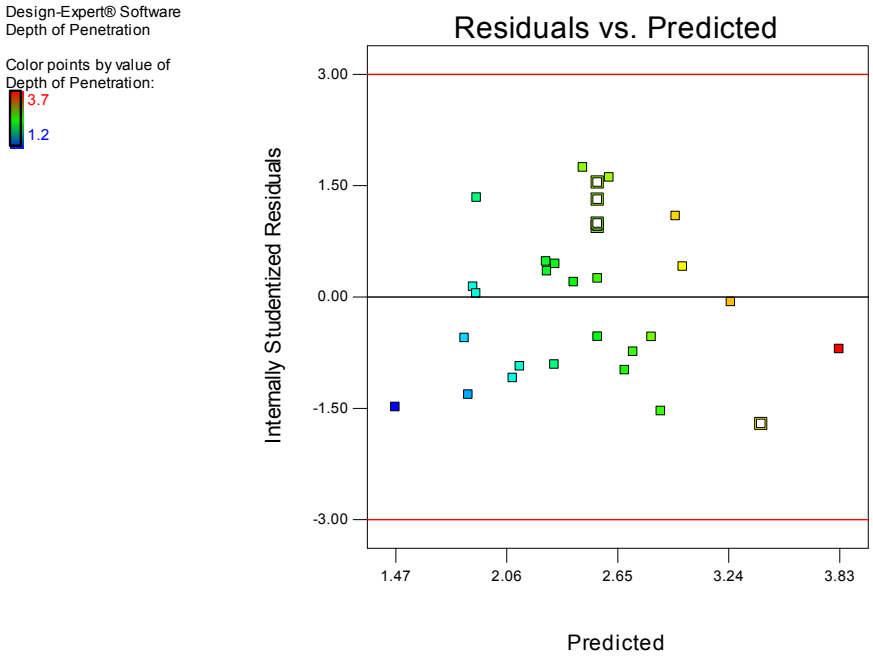

Fig. 6-35 Plot of residuals vs predicted for the response depth of penetration

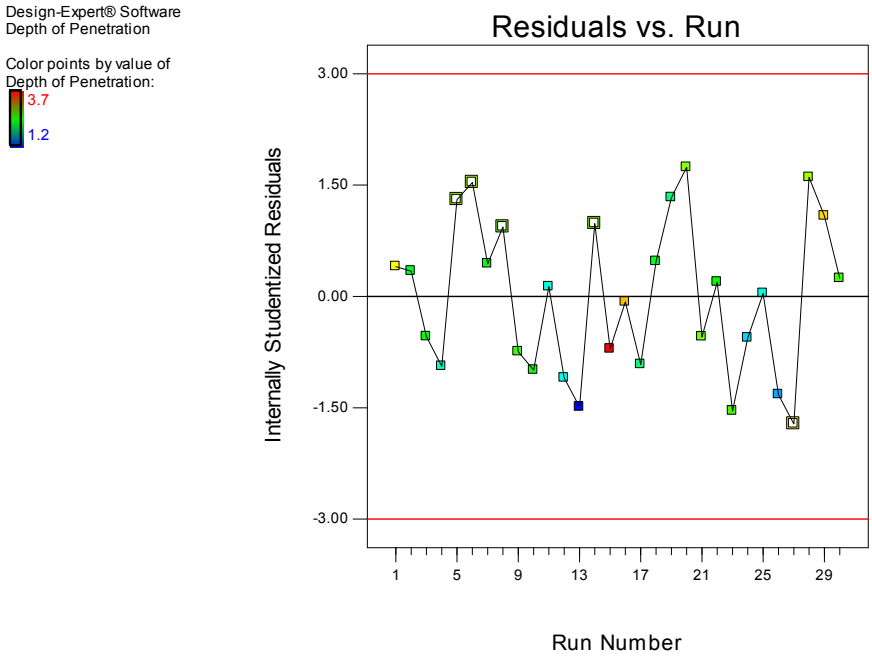

Fig. 6-36 Plot of residuals vs run No. for the response depth of penetration

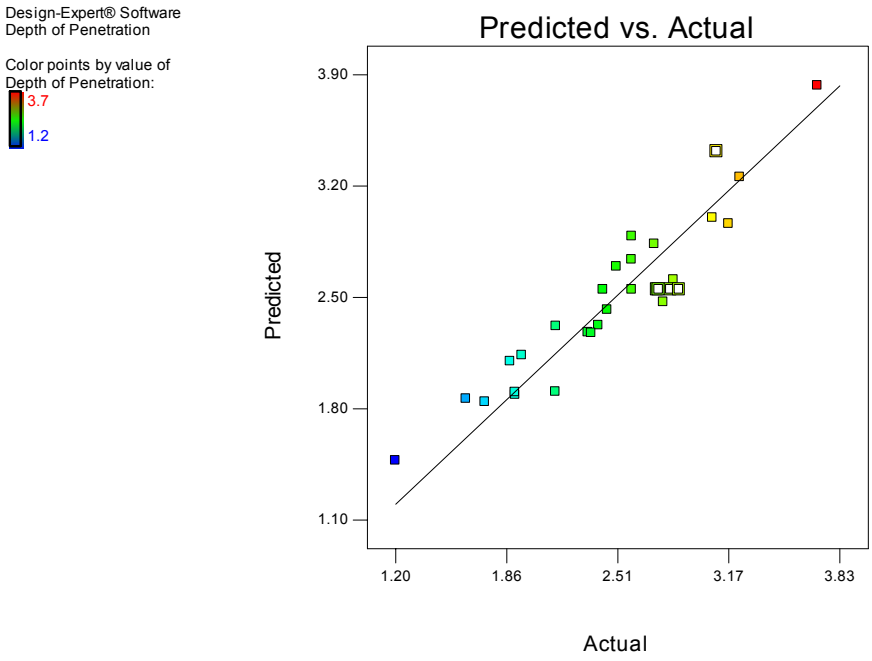

Fig. 6-37 Plot of predicted vs actual for the response depth of penetration

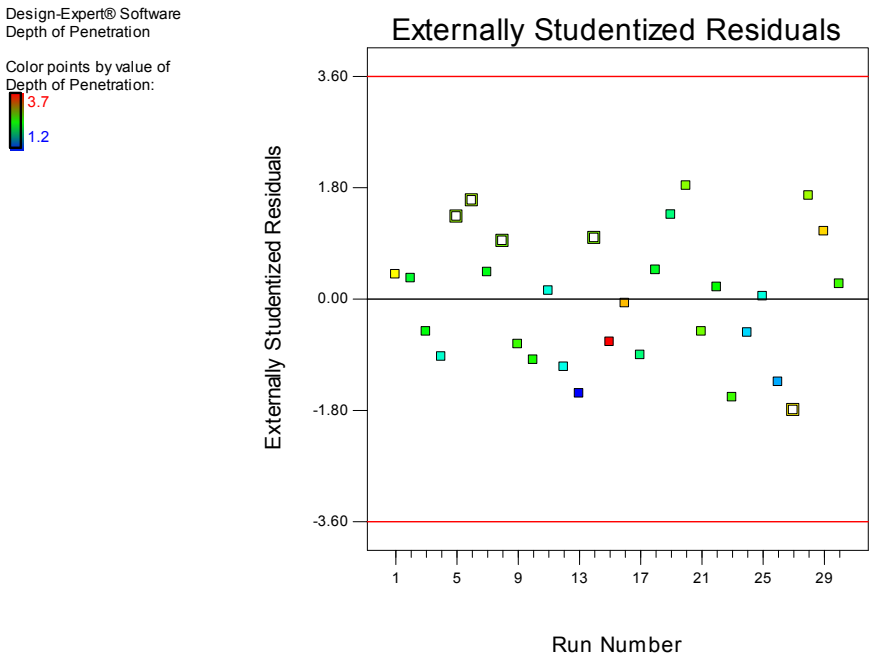

Fig. 6-38 Plot of externally studentized residuals (outlier t-values) vs run No. for the response depth of penetration

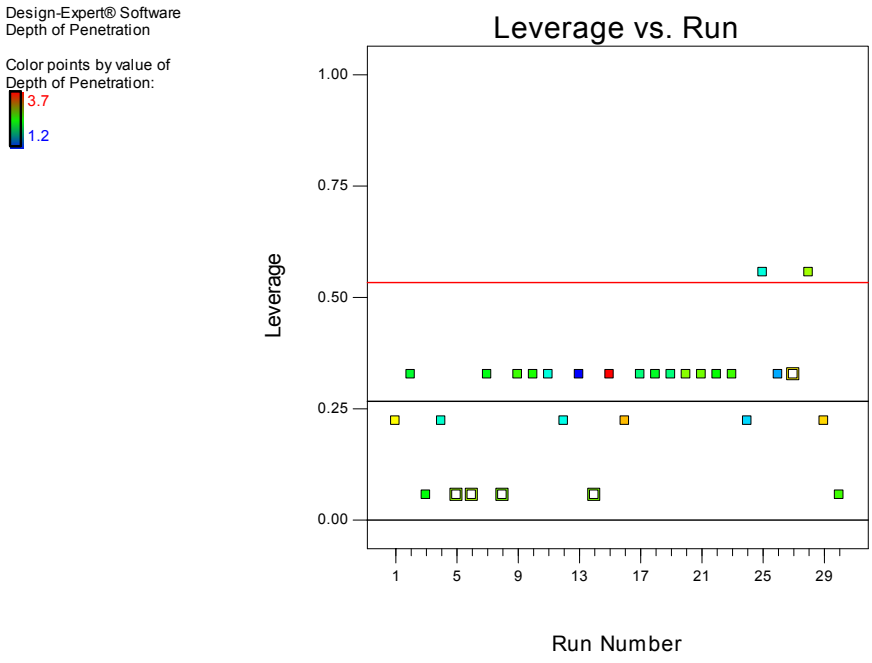

Fig. 6-39 Plot of leverage vs run No. for the response depth of penetration

The above graphs show that no anomalies occur with this model, although two points (welds Nos. 25 and 28) in the leverage vs run plot were located just above the double average leverage. Despite this, the very good values of the statistical parameters shown in Table 6.15 (Pred. R-squared, Adj. R-squared, Adeq. Precision, Lack of Fit tests, etc), indicate that it is very unlikely that the model overall prediction is affected. Again, the "actual" model performance was tested by the validation trials, this will be discussed later.

2. Groove Sidewall Penetration, Sidewall Penetration, Corner Angle

All the model diagnostics and influence plots show no relevant anomalies, and together with the acceptable values shown in Table 6.15 (page 131), confirm that the models are good predictors.

3. Undercut

The diagnostic plots for the response undercut showed some anomalies. In particular the predicted vs. actual and the residuals vs. predicted showed strong patterns (Figures 6.40, 6.41):

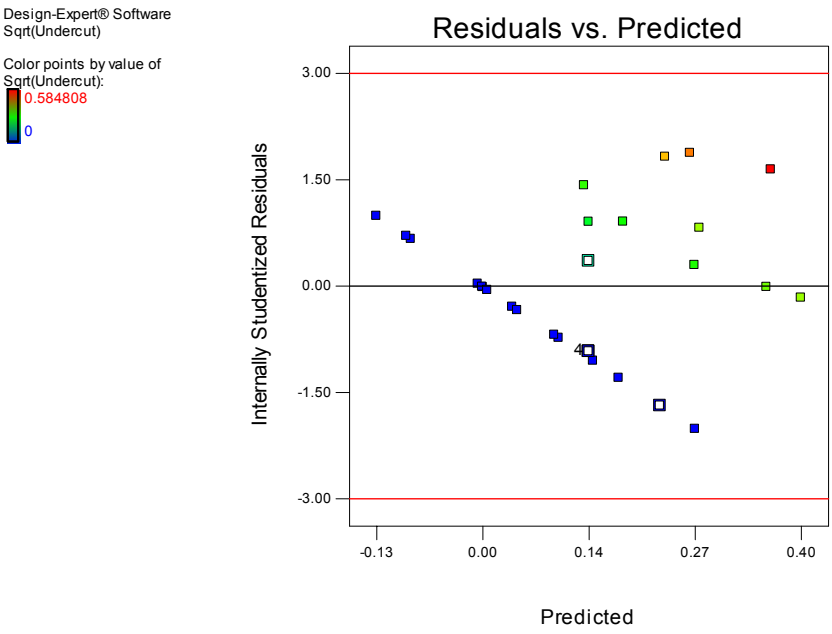

Fig. 6-40 Diagnostic plot (residual vs. predicted) for the response undercut showing pattern

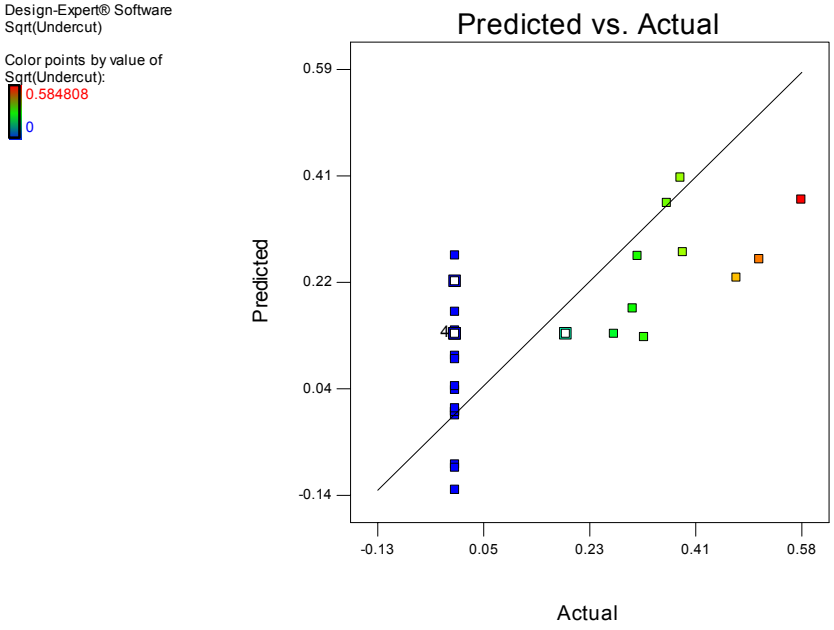

Fig. 6-41 Diagnostic plot (predicted vs actual) for the response undercut showing patterns

The patterns detected on the plots, and the low values of the Pred. R-squared and Adj. R-squared indicate that the model cannot be used for reliable predictions and the results need to be treated with caution. Nevertheless, it was decided to include this model in our analysis as a good example of patterns in the model diagnostic plots (the anomalies may be because only a few welds presented undercut defects). The data can be used as an indication of the best direction to follow for the determination of the most significant terms of the models and generally to determine if the high or low factor levels perform better.

6.3.1.3 Effects of the Welding Parameters on Weld Bead Profile

In the coded factors regression equation, the coefficients represent the change in the response when a factor changes by one coded unit whereas in the equation of actual factors, the coefficients cannot be intuitively interpreted because they depend on the scaling of the factor levels. The influence of the response is qualitative (positive or negative) and quantitative but does not provide detailed information about the trend of the response as a function of the factor levels.
The analysis of the results is fundamental to understand the effect of the factors and their interaction on the response. Therefore, considering the appropriate factor effect graphs can be very effective in utilising the results.
Contour plots provide very detailed information on the responses sensitivity to very small modifications of factor levels within the design space. The drawback of this approach is the risk of producing a large number of graphs thus complicating the conclusion process.
In the present work targets for the responses were established and the influence of the factor levels was investigated.

The graphs considered here are either single factor plots, where the factor is not involved in an interaction or interaction plots, where the effect of one factor depends on the level of another. Graphically this is indicated by two non parallel lines. In the discussion section further plots (e.g. 3D or contour plots) will be considered when necessary.

1. Depth of Penetration

The target was to maximise the depth of penetration.
The following series of Figures 6.42, 6.43 and 6.44 show the effects of the factors and their interactions on the response depth of penetration.

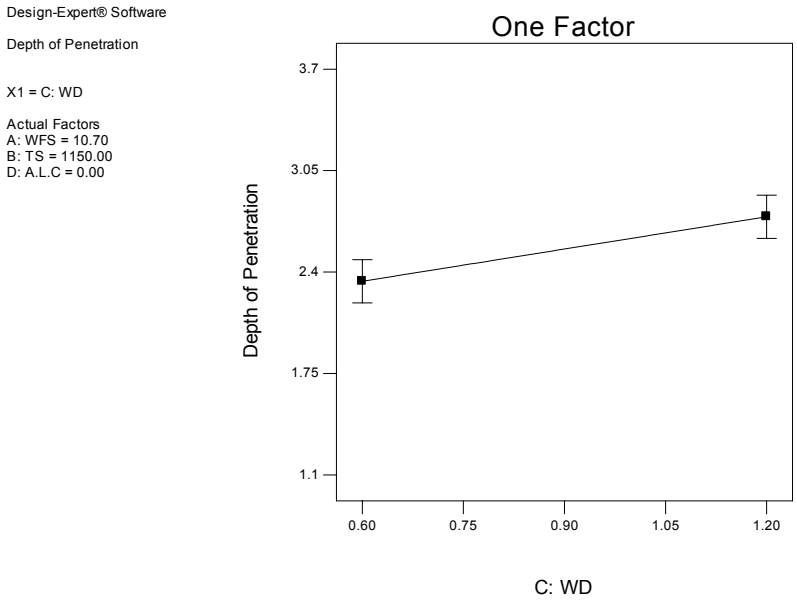

Fig. 6-42 Effect of wire distance from the wall (mm) on depth of penetration (mm)

The plot in Figure 6.42 shows that an increase of 0.6mm in wire distance from the sidewall will always produce an increase of approximately 0.3 to 0.4mm in depth of penetration irrespective of the values of wire feed speed, travel speed and arc length correction (arc length). In this case there is no interaction with other factors and the slope of the graph remains invariable. Note however, that the absolute magnitude of depth of penetration will be affected by the other factors.
The plot in Figure 6.43 was obtained for the high value of the wire distance from the sidewall parameter in Figure 6.42. The graph (Figure 6.43) shows two lines; the upper one representing the variation of depth of penetration with wfs for a constant level of 12.5% for alc and the lower one is for the low value -12.5% for alc (other plots are shown in similar ways). The plot shows that the depth of penetration significantly increases when the wire feed speed increases from the low level (9.45m/min) to the high level (11.95m/min), and that the slope strongly depends on the level of the arc length. At the low level of wire feed speed, the arc length correction provides the same depth of

penetration whether its low (-12.5%) or high level (+12.5%) is considered. However, at the high level of wire feed speed, changing the arc length correction from the low to high level increases the depth of penetration by almost by 1mm.

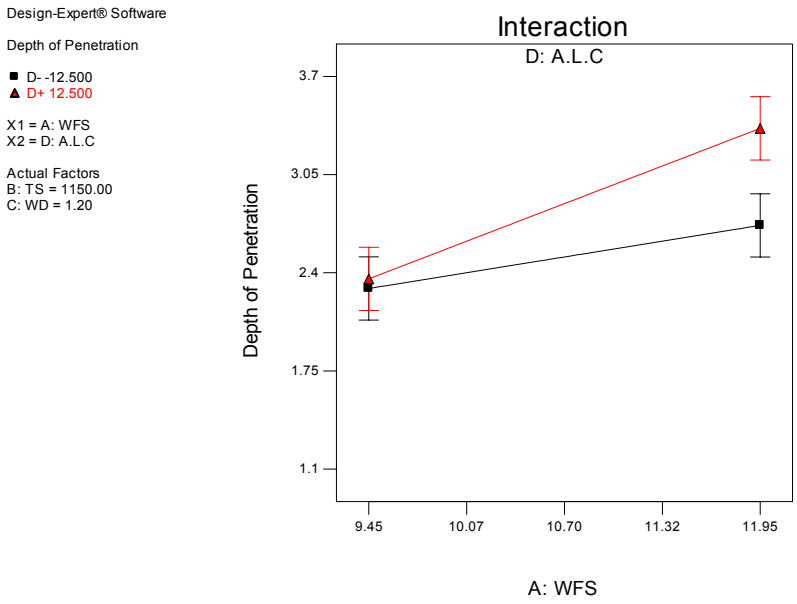

Fig. 6-43 Interaction plot for the effects of wire feed speed (m/min) and arc length correction (%) on depth of penetration (mm)

The plot in Figure 6.44 was obtained when wire distance from sidewall, wire feed speed and arc length correction were selected at their high levels. This plot shows, that when travel speed decreases from the 1275mm/min (high level) to 1025mm/min (low level) and the arc length correction (arc length) is considered at the high level (12.5%), depth of penetration increases by 1.2mm more than in the case when the low level of the arc length correction is considered.
In conclusion, depth of penetration increases when the welding parameters are selected at the following levels:
Wire feed speed: high ; Travel speed : low ; Wire distance from the wall : high and
Arc length correction (arc length) : high.

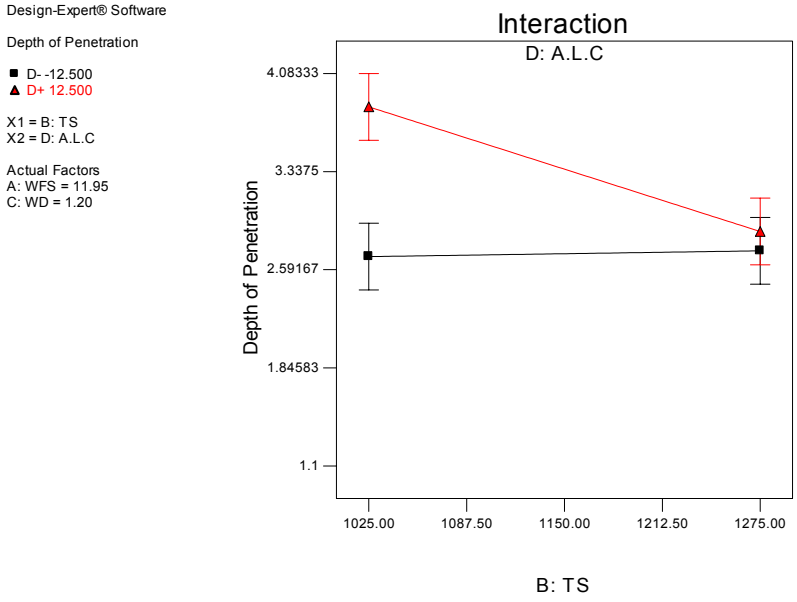

Fig. 6-44 Interaction plot for the effects of travel speed (mm/min) and arc length correction (%) on depth of penetration (mm)

2 Groove Sidewall Penetration

The target for the groove sidewall penetration was to maximise it. The procedure followed for the analysis was identical to the one applied to the depth of penetration response.

Figure 6.45 shows the interaction between wire feed speed and wire distance from the sidewall. This indicates that higher groove sidewall penetration is obtained when wire feed speed is set at high level and wire distance from sidewall at low (black line) level. This combination of the welding parameters produces an increase in groove sidewall penetration of almost 0.12mm compared to the combination of high wire feed speed and high wire distance from the sidewall.

At the low levels of wire feed speed, the effects of the wire distance from the sidewall on groove sidewall penetration are almost identical.

Figure 6.46 is the result of the above conclusions: wfs high and wd low. This plot shows that higher groove penetration is obtained when a.l.c(arc length) is at its high level. This combination of the welding parameters produces an increase in groove sidewall penetration of almost 0.25mm compared to wfs high and a.l.c low.

At low wfs levels, arc length level (low or high) produces identical results (same groove sidewall penetration).

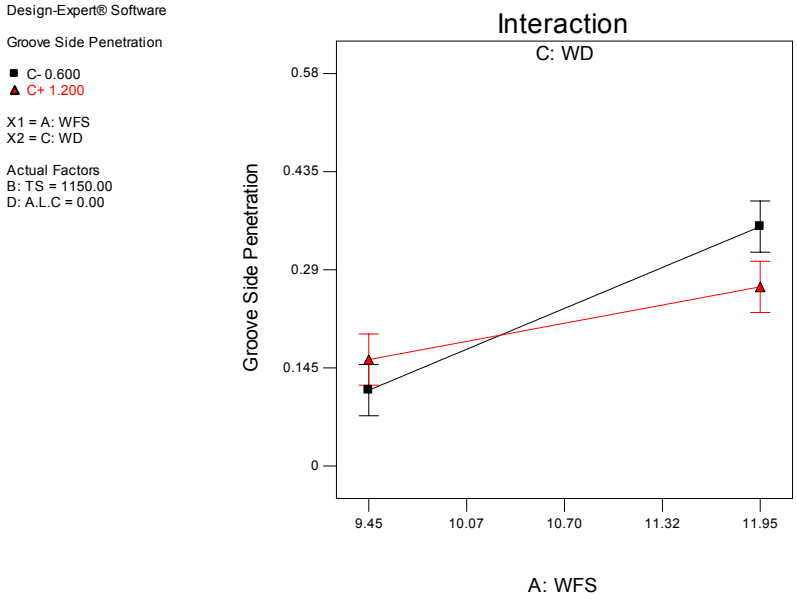

Fig. 6-45 Interaction plot for the effects of wire feed speed (m/min) and wire distance from the sidewall (mm) on the groove sidewall penetration (mm)

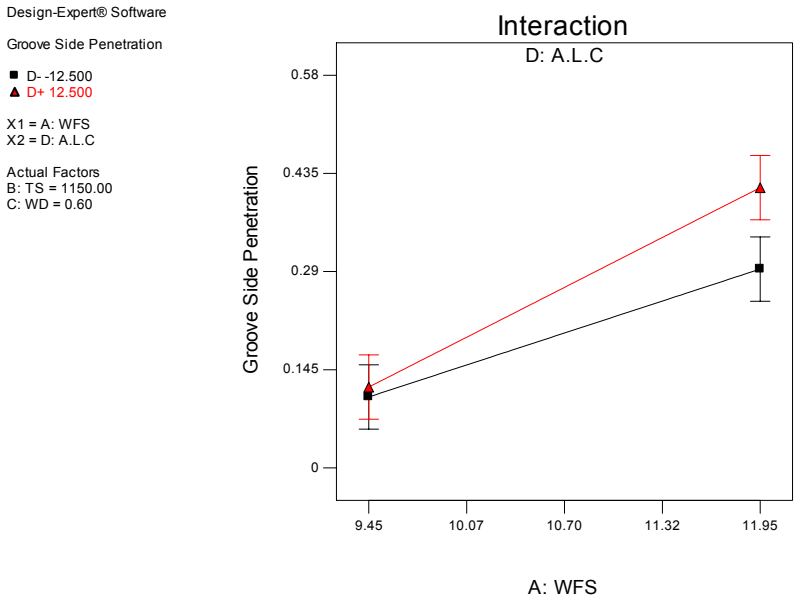

Fig. 6-46 Interaction plot for the effects of wire feed speed (m/min) and arc length correction (%) on the groove sidewall penetration (mm)

Figures 6.47 and 6.48 were obtained by for wfs high, wd low and a.l.c high. Figure 6.47 shows that the groove sidewall penetration significantly increases at low level travel speed as compared to high level, and that the effect of wire distance level is almost negligible. The Figure 6.48 confirms this conclusion.

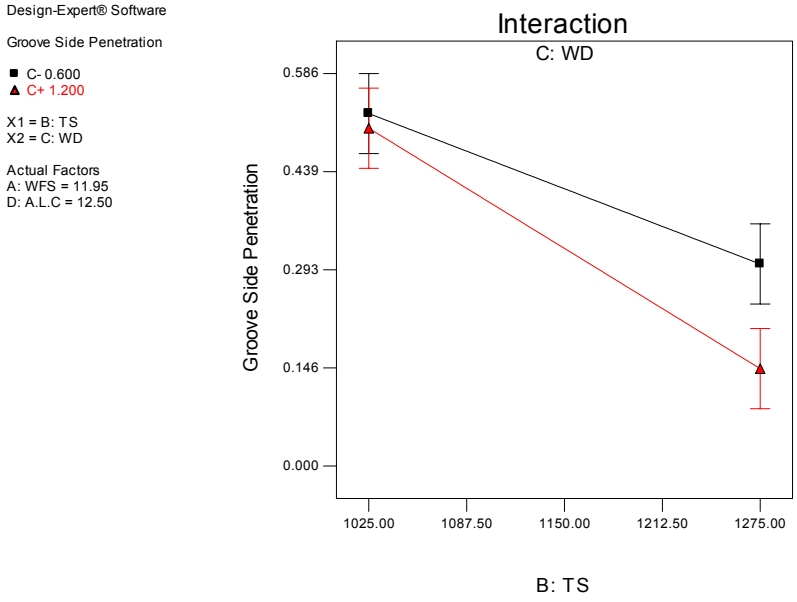

Fig. 6-47 Interaction plot for the effects of travel speed (mm/min) and wire distance from the sidewall (mm) on the groove sidewall penetration (mm)

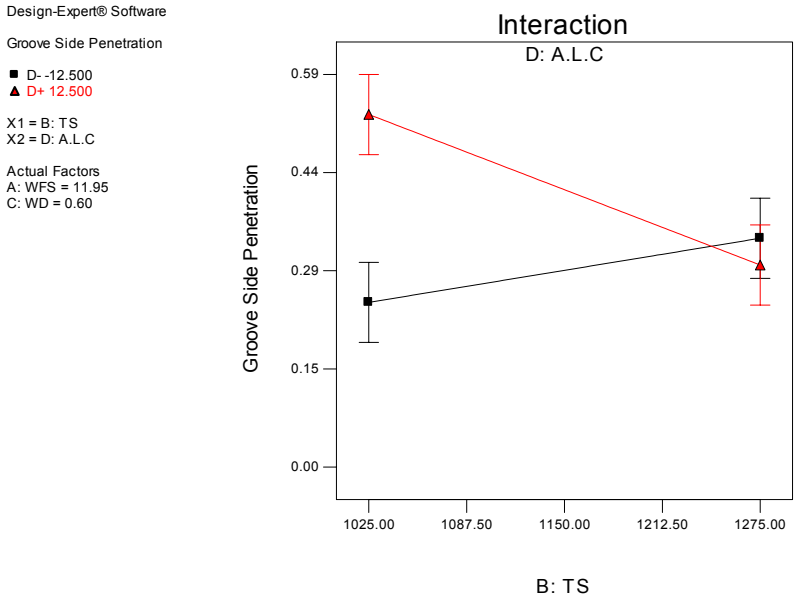

Fig. 6-48 Interaction plots for the effects of travel speed (mm/min) and arc length correction (%) on the groove sidewall penetration (mm)

The fact that effect of travel speed on groove sidewall penetration changes slope, depending on the level of the arc length is difficult to explain based on the available data.

Analysis of the above four graphs shows that groove sidewall penetration can be maximised with the following combination of welding parameters:

Wire feed speed : high ; Travel speed : low ; Arc length correction (arc length) ; high, and Wire distance from the sidewall : low (although values of wire distance from sidewall at high level provide similar results according to Figure 6.47)

3 Sidewall Penetration

The target was to maximise sidewall penetration. Figure 6.49 clearly shows that sidewall penetration always increases when wfs increases but that overall, sidewall penetration depends on the level of wd involved in the interaction. The combination of levels, wfs high and wd low, produces an increase of almost 0.2mm in sidewall penetration compared to the combination, wfs high and wd high.

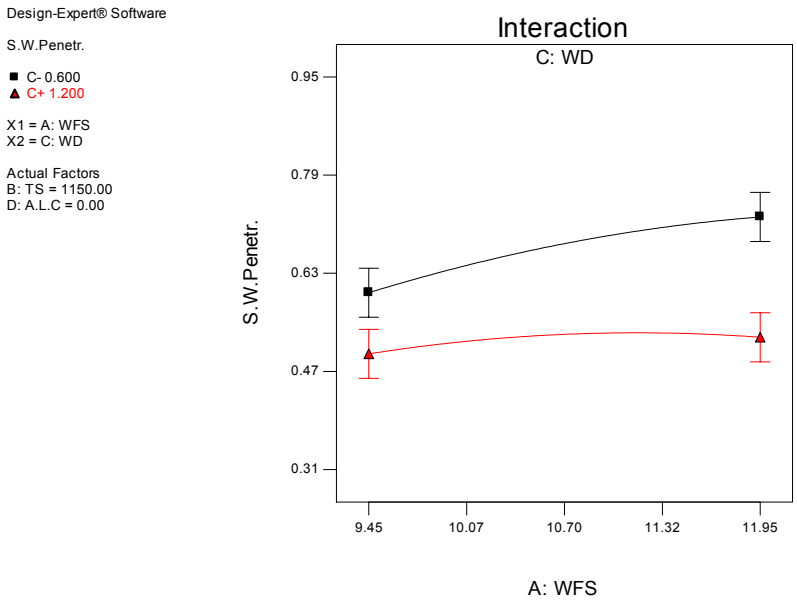

Fig. 6-49 Interaction plot for the effects of the wire feed speed (m/min) and wire distance from the sidewall (mm) on the sidewall penetration (mm)

Selecting the wfs at high level and the wd at low level Figure 6.50 clearly shows that sidewall penetration increases when travel speed is at low level. In particular, wfs high and ts low produce an increase in sidewall penetration of almost 0.12mm compared to wfs high and ts high.
Figure 6.51 shows the effect of the arc length correction (arc length) on sidewall penetration obtained after selecting wfs at high level and wd at low level. Sidewall penetration considerably increases when arc length correction increases. The combination low level ts and high level a.l.c produces an increase in sidewall penetration of almost 0.3mm more than the combination ts low and a.l.c low.
The analysis of the above three graphs shows that groove sidewall penetration can be maximised with the following combination of the welding parameters:
Wire feed speed : high ; Travel speed : low ; Arc length correction (arc length) ; high, and Wire distance from the sidewall : low.

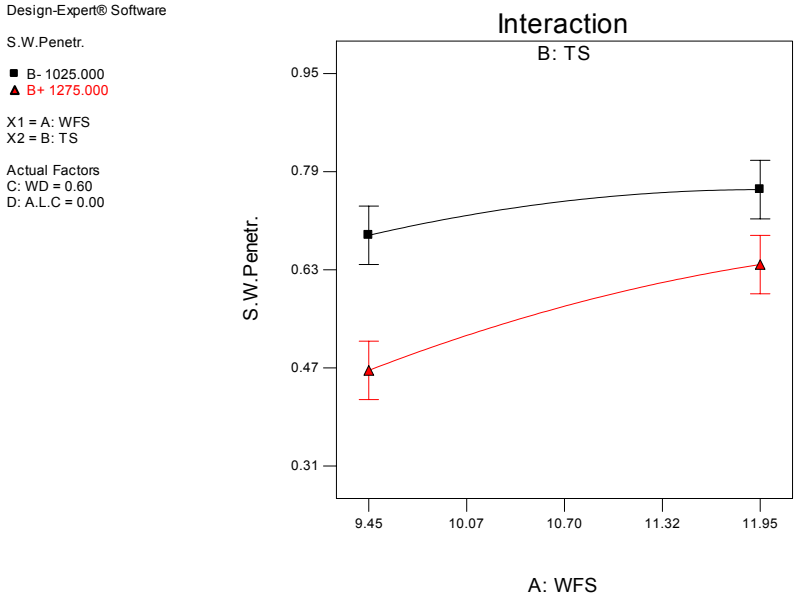

Fig. 6-50 Interaction plot for the effect of the wire feed speed (m/min) and travel speed (mm/min) on the sidewall penetration (mm)

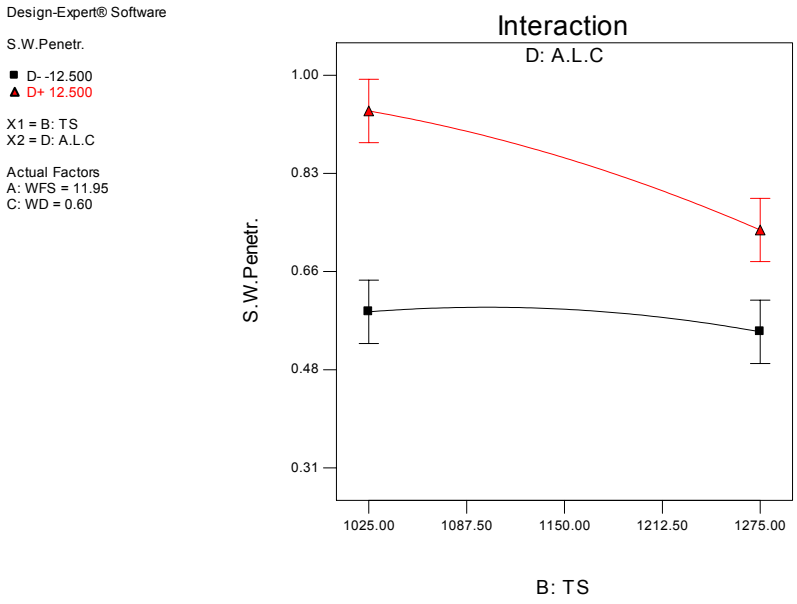

Fig. 6-51 Interaction plot for the effect of the travel speed (mm/min) and arc length correction (%) on the sidewall penetration (mm)

4. Corner Angle

The corner angle was defined as the angle between the projected preparation sidewall and a line joining the intersection of the weld bead surface and a point on the weld bead

surface 1mm away from the intersection point. The corner angle determines the toe angle (Figure 5.10, page 77) where a high toe angle is preferred because it provides better sidewall fusion and a smoother weld bead profile at the sidewall. By minimising the corner angle, toe angle increases. Therefore, the effect of the welding parameters on minimising corner angle was investigated.
Figure 6.52 is a one factor plot. A decrease of 2.5m/min in the wire feed speed always produces a decrease of 7.0° in the corner angle irrespective of travel speed, arc length correction and wire distance from the sidewall. In this case, the "slope of the graph" does not interact with other factors. However the absolute magnitude of the corner angle will be affected by the other factors.

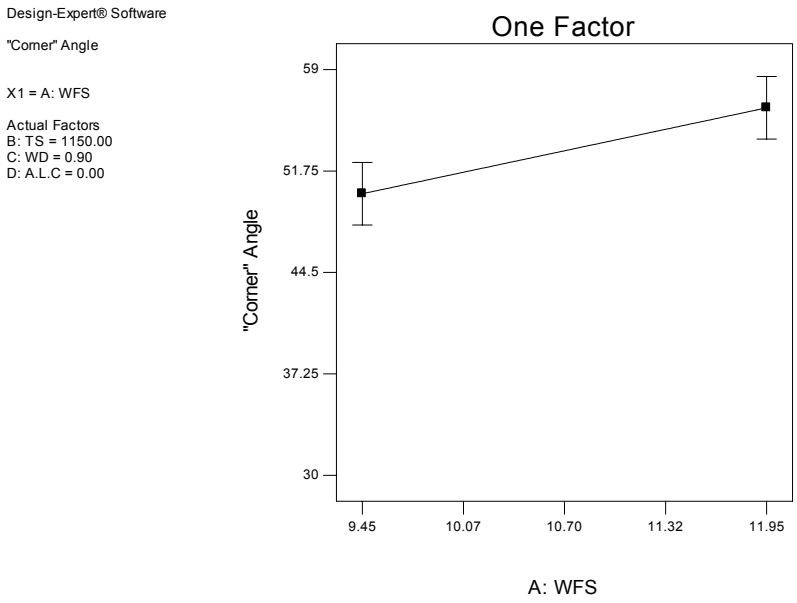

Fig. 6-52 Effect of wire feed speed (m/min) on corner angle (°)

Figure 6.53 shows that after selecting low level wfs, corner angle decreases in association with high levels of both ts and a.l.c. With high ts and high a.l.c corner angle is reduced by 4° compared to low ts and high a.l.c.
Another interesting conclusion is that while ts high and a.l.c high produce a corner angle of 15° less than ts high and a.l.c low, this difference drops to almost 5° when ts is low and a.l.c is high or low. A very important "property" of the interaction plots is that optimum conditions for the process can be defined within the design space. In similar manner as discussed for the Figure 6.48, the difference in the direction of the effect of travel speed on the corner angle when the low or the high level of the arc length correction parameter is considered can not be easily explained with the present data.

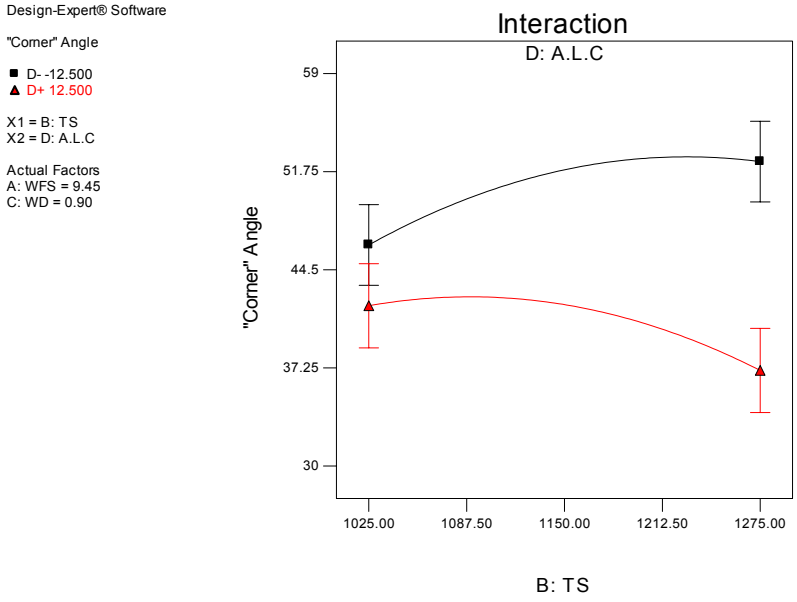

Fig. 6-53 Interaction plot for the effect of the travel speed (mm/min) and arc length correction (%) on the corner angle (°)

Figure 6.54 obtained after selecting wfs low, ts high and a.l.c high shows that the corner angle decreases if both ts and wd increase and furthermore this combination produces a smaller angle of 3.5° compared to the combination ts high and wd low.

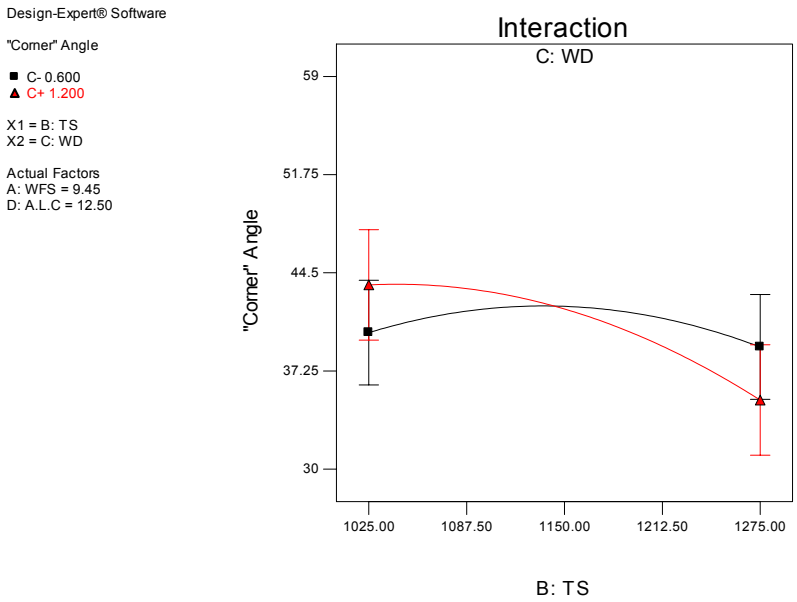

Fig. 6-54 Interaction plot for the effect of the travel speed (mm/min) and wire distance from the sidewall (mm) on the corner angle (°)

The analysis of the above three graphs shows that corner angle can be minimised if:

Wire feed speed : low ; Travel speed : high ; Arc length correction (arc length) ; high, and Wire distance from the sidewall : high.

5 Undercut

The target was to minimise the undercut.
Conclusions in this section need to be treated with caution for the reasons discussed in the model adequacy checking plots (Figures 6.40 and 6.41; pages 136 and 137).
No interactions between the welding parameters were detected. This means that the slopes in the graphs will be unaffected by factors not included in the graphs.
Figure 6.55 shows that undercut decreases when wfs increases and becomes almost zero when wfs reaches its high level.

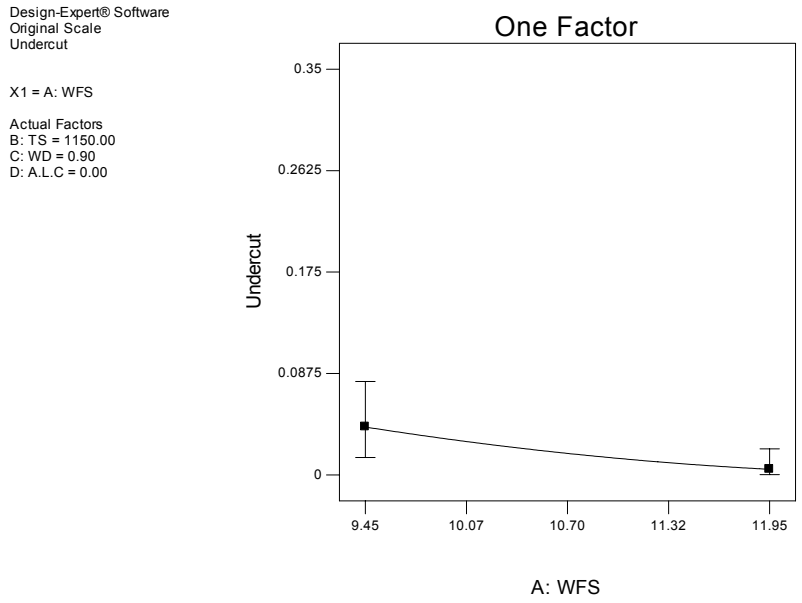

Fig. 6-55 Effect of wire feed speed (m/min) on undercut (mm)

The effect of travel speed on undercut is almost negligible as Figure 6.56 shows, although a very small increase in undercut is produced when travel speed is at high level.
Figure 6.57 shows that undercut decreases when wire distance from the sidewall increases, and
Figure 6.58 shows that undercut decreases when arc length correction (arc length) decreases.
Analysis of the four plots leads to the conclusion that undercut can be minimised if the welding parameters are selected at the following levels:
Wire feed speed: high ; Travel speed : low ; Wire distance from the sidewall : high, and Arc length correction (arc length) : low.

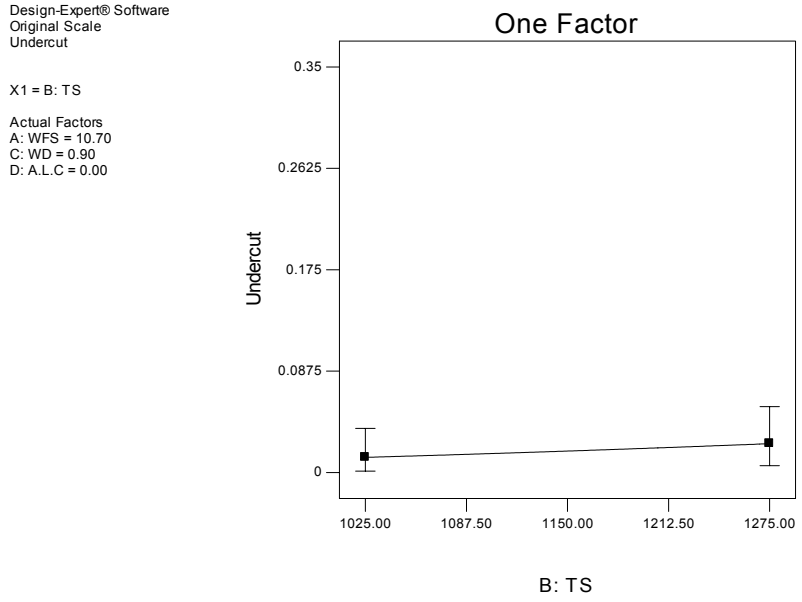

Fig. 6-56 Effect of travel speed (mm/min) on undercut (mm)

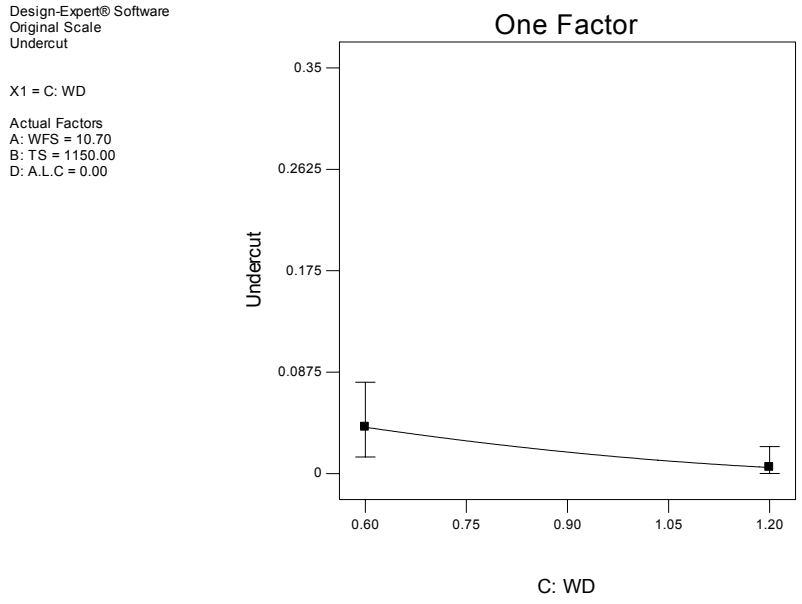

Fig. 6-57 Effect of wire distance from the sidewall (mm) on undercut (mm)

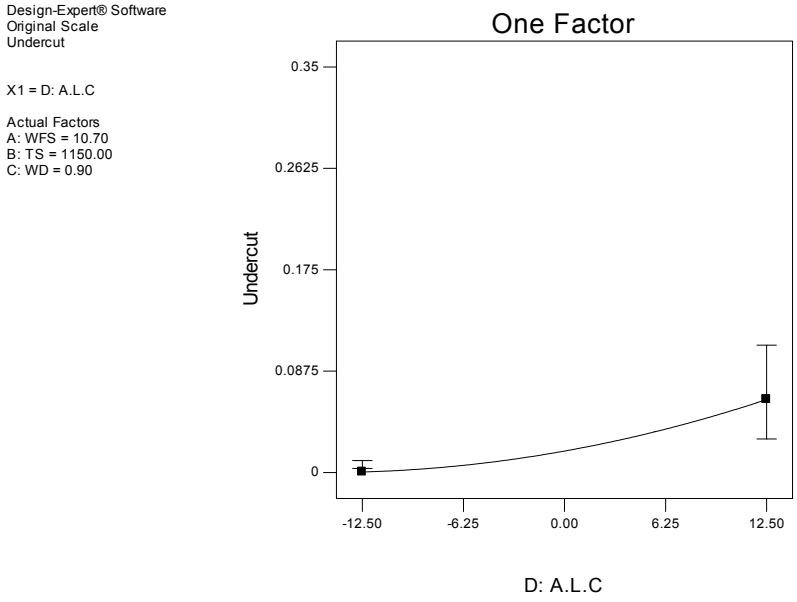

Fig. 6-58 Effect of arc length correction (%) on undercut (mm)

6.3.2 Vertical (down) Position (90°)

6.3.2.1 Modelling Results

The measured weld bead dimensions resulting from the experiments (Table 5.4, page 88) are included in Table 6.16.
The weld bead dimensions selected for the analysis were depth of penetration, groove sidewall penetration and corner angle.

	Responses		
Weld No (Run No)	Depth of Penetration (mm)	Groove Sidewall Penetration (mm)	Corner Angle (°)
1	1.9	0.21	28.8
2	1.45	0.10	26
3	1.68	0.10	26.5
4	1.10	0.05	17.75
5	1.67	0.10	25
6	1.75	0.14	24
7	1.35	0	27.5
8	1.67	0.13	26.3
9	1.80	0.08	34
10	1.70	0.11	43
11	2.06	0.09	29
12	1.56	0.05	22.5
13	1.35	0.04	21.5
14	1.59	0	27
15	2.33	0.29	37
16	2.31	0.30	38.5
17	1.62	0.08	29.2
18	1.68	0.07	29.3
19	1.09	0	27.4
20	1.71	0.09	18.8
21	1.97	0.05	21.3
22	1.54	0.16	20
23	2.68	0.14	30.8
24	1.31	0	30
25	1.47	0	34
26	1.05	0	23
27	1.97	0.05	23.5
28	1.71	0	19
29	2.10	0.06	31.9
30	1.65	0.11	27

Table 6-16 Measured weld bead geometric responses (vertical position, 90°)

Figure 6.59 shows the as welded bead profile for some of the experiments carried out at different welding conditions. Generally, all presented adequate bead morphology.

a) weld (run) No. 22

b) weld (run) No. 11

c) weld (run) No. 3

d) weld (run) No. 6

Fig. 6-59 Weld bead profiles in vertical down (90°) position

Some typical macrographs are included in Figure 6.60, showing the effects of the welding parameters and in particular the strong effect of the position (90°) in the morphology of the weld bead geometry. The macrographs of the welds reported in Figure 6.33 (flat position, page 127) were carried out with the same welding conditions to the ones in Figure 6.60 and hence show that position has a significant effect on the weld bead geometry.
Macrographs of the welds of Table 6.16 are shown in Appendix C.
Stable welding conditions for all the experiments were reported.

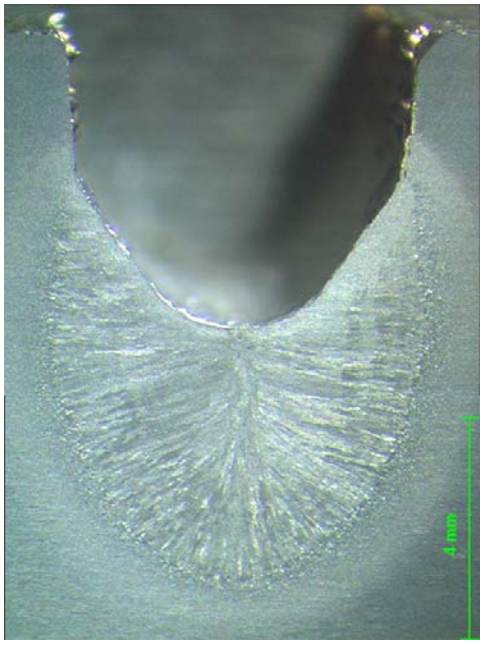

a) weld (run) No. 1

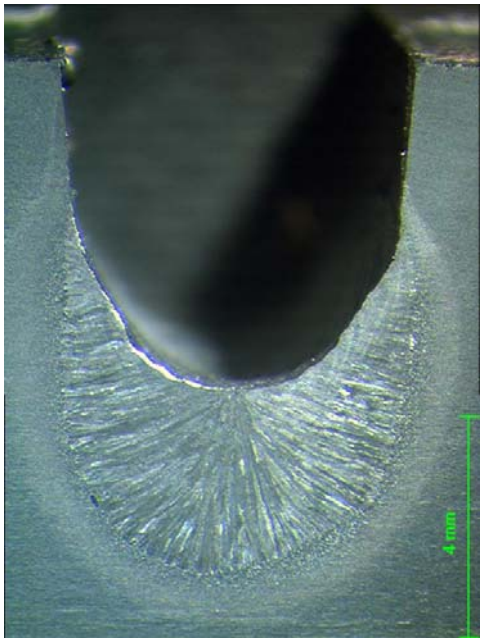

b) weld (run) No. 7

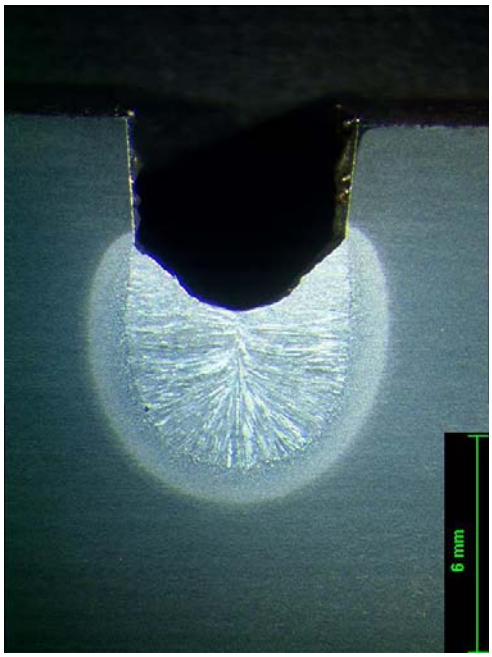

c) weld (run) No. 10

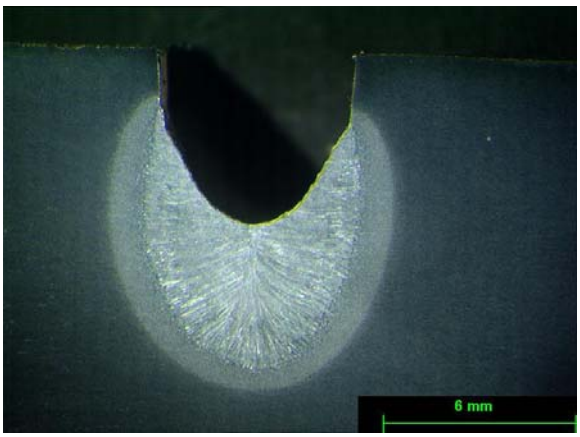

d) weld (run) No. 27

Fig. 6-60 Macrograph sections of welds in vertical (90°) position

Table 6.17 shows the variables (factors) selected after backward elimination, and type of model, F-value, P-value, the Adj.R-squared, Pred.R-squared, adequate precision, standard deviation, and the lack of fit tests (F-value and P-value).
The prediction equations for the responses describing the weld bead geometry, e.g. depth of penetration, groove sidewall penetration and corner angle, determined from the ANOVA (analysis of variance), in coded and actual factors together with the units of the responses and actual factors are reported below:

Response	Type of Model	Chosen Variables	Pred.R-squared	Adj.R-squared.	F-value	P-value (Prob.>F)	Std. dev.	Adeq. Precision	Lack of Fit	
									F-value	P-value
Depth of Penetration (mm)	Linear	wfs /ts / wd /a.l.c / ts * wd	0.78	0.84	32.03	<0.001 (significant)	0.15	21.41	10.20	0.0087 (significant)
Groove Sidewall Penetration (mm)	Quadratic	wfs /ts / wd /a.l.c/ $a.l.c^2$	0.2579	0.4545	5.83	<0.0012 (significant)	0.12	9.467	0.65	0.7765 (not significant)
Corner Angle (°)	Quadratic	wfs /ts / wd /a.l.c / wfs*ts /wfs*wd / wfs^2	0.84	0.890	37.02	<0.0001 (significant)	1.92	23.92	2.97	0.1163 (not significant)

Table 6-17 Selected variables, model order after backward elimination and statistical parameters (vertical (90°) position)

$P_{d;}$ Depth of penetration: mm
P_{GS}; Groove sidewall penetration: mm
Θ; Corner angle: (°)
W; Wire feed speed (WFS): m/min
T; Travel speed (TS): mm/min
D; Wire distance from sidewall (WD): mm
A_C; Arc length correction (ALC): %

1. Depth of Penetration ($P_{d)}$

a) coded factors:

$$P_d = 1.69 + 0.19 \cdot W - 0.03 \cdot T + 0.26 \cdot D + 0.063 \cdot A_c \quad \textbf{Eqn. 6. 11}$$

b) actual factors:

$$P_d = 1.269 + 0.1545 \cdot W - 1.757 \cdot 10^{-3} \cdot T - 1.063 \cdot D + 0.0145 \cdot A_c + 1.69 \cdot 10^{-3} \cdot T \cdot D \quad \textbf{Eqn. 6. 12}$$

2. Groove Sidewall Penetration (P_{GS})

a) coded factors:

$$\sqrt{P_{GS}} = 0.30 + 0.075 \cdot W - 0.042 \cdot T + 0.051 \cdot D + 0.045 \cdot A_c - 0.066 \cdot A_c^2 \quad \textbf{Eqn. 6. 13}$$

b) actual factors:

$$\sqrt{P_{GS}} = -0.1074 + 0.0603 \cdot W - 3.384 \cdot 10^{-4} \cdot T + 0.1684 \cdot D + 3.595 \cdot 10^{-3} \cdot A_c - 4.227 \cdot 10^{-4} \cdot A_c^2 \quad \textbf{Eqn. 6. 14}$$

3. Corner Angle (Θ)

a) coded factors:

$$\Theta = 25.66 + 2.37 \cdot W - 0.73 \cdot T + 3.92 \cdot D - 2.81 \cdot A_c - 1.99 \cdot W \cdot T + 2.01 \cdot W \cdot D + 2.07 \cdot W^2 \quad \textbf{Eqn. 6. 15}$$

b) actual factors:

$$\Theta = 46.60 - 16.61 \cdot W + 0.1307 \cdot T - 44.16 \cdot D - 0.225 \cdot A_c - 0.0128 \cdot W \cdot T + 5.35 \cdot W \cdot D + 1.3258 \cdot W^2 \quad \textbf{Eqn. 6. 16}$$

6.3.2.2 Model Adequacy Checking

The model adequacy control was carried out using the model diagnostic plots and the influence plots (section 6.3.1.2, page 132).
All plots were acceptable and no anomalies with the model fitting the data were determined.
Significant lack of fit tests were reported for the response depth of penetration (Table 6.17) F-value=10.2 and p-value=0.0087, meaning that the model maybe does not fit all the design points well. Although additional replicates (welds) were carried out, the model did not improve much. Nevertheless, since the other parameters of Table 6.17 showed very good values (Pred. R-squared, Adj. R-squared, Adeq. Precision etc), and the model diagnostic plots have not presented any significant anomalies, it was decided to accept the model and rely on the confirmation runs to validate the experimental results.

6.3.2.3 Effects of the Welding Parameters on Weld Bead Profile

For the analysis of the effects of the welding parameters on weld bead geometry the same procedure as described in section 6.3.1.3 (flat position, page 137) was used.
Figure 6.61 shows the effect of wire feed speed on depth of penetration. An increase of wire feed speed of 2.5m/min produces an increase in depth of penetration of 0.4mm irrespective of the values of the other factors (travel speed, wire distance from the sidewall and arc length correction (arc length). In this case the response (slope of the graph) does not interact with the other factors. However the absolute magnitude of depth of penetration will be affected by the other factors.

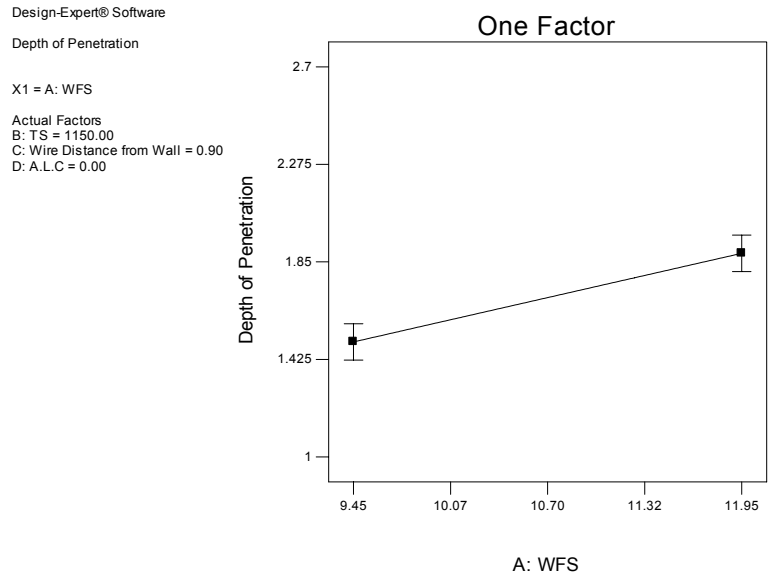

1 Depth of Penetration

Fig. 6-61 One factor plot for the effect of the wire feed speed (m/min) on depth of penetration (mm)

Figure 6.62 shows the effect of the arc length correction (arc length) on depth of penetration. An increase of 25% in arc length correction produces an increase in depth of penetration of 0.4mm irrespective of the values of the other factors.
Figure 6.63 represents the effect of the interaction between the travel speed and the wire distance from the sidewall on depth of penetration, obtained after selecting high levels of wfs and a.l.c. Depth of penetration is considerably increased with high travel speed and high wire distance. However, the effect of high wire distance on depth of penetration is independent of the travel speed value.

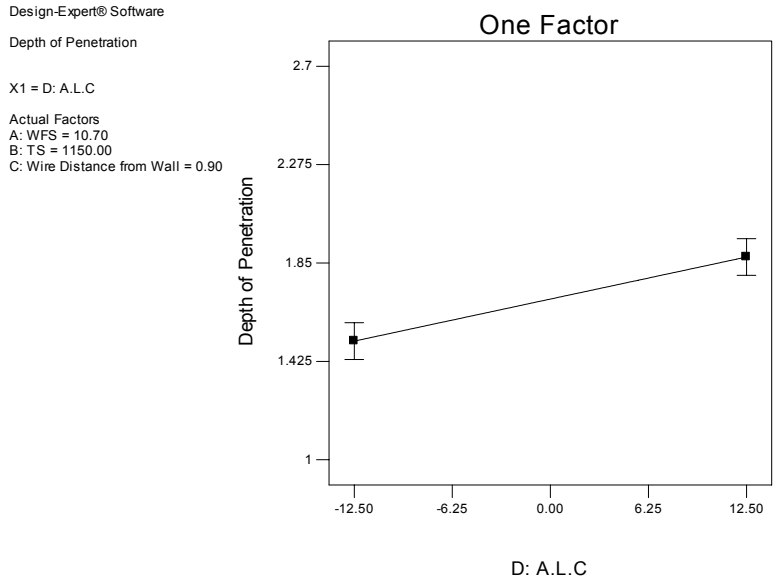

Fig. 6-62 One factor plot for the effect of the arc length correction (%) on depth of penetration (mm)

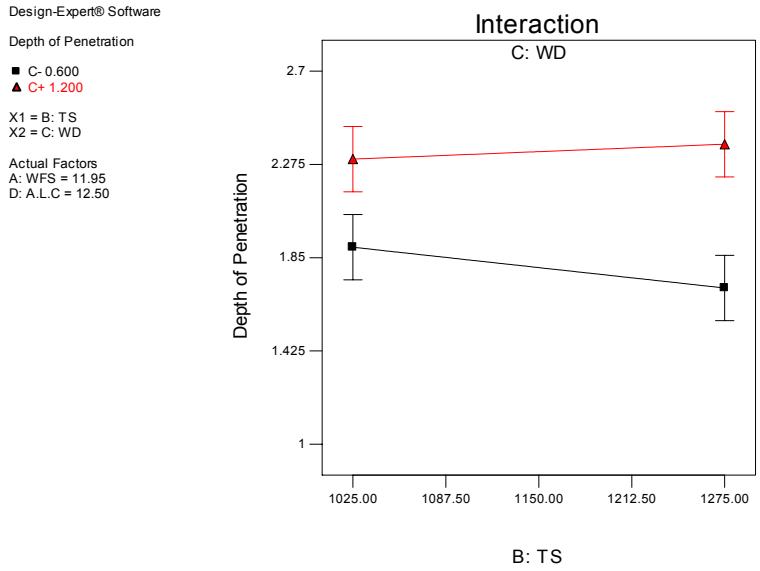

Fig. 6-63 Interaction plots for the effects of travel speed (mm/min) and wire distance from the sidewall (mm) on depth of penetration (mm)

Analysis of the above shows that depth of penetration is maximised when the welding parameters are selected as follows:
Wire feed speed : high ; Travel speed : low(or high) ; Wire distance from the sidewall : high, and Arc length correction (arc length) : high

2 Groove Sidewall Penetration

Figure 6.64 shows that an increase of 2.5m/min in wire feed speed produces an increase of approximately 0.075mm in groove sidewall penetration irrespective of the values of travel speed, wire distance from the sidewall and arc length correction (arc length). In this case there is no interaction with the other factors and the slope of the graph remains invariable. As in all the previous one factor plots, the absolute magnitude of groove sidewall penetration will be affected by the other factors.

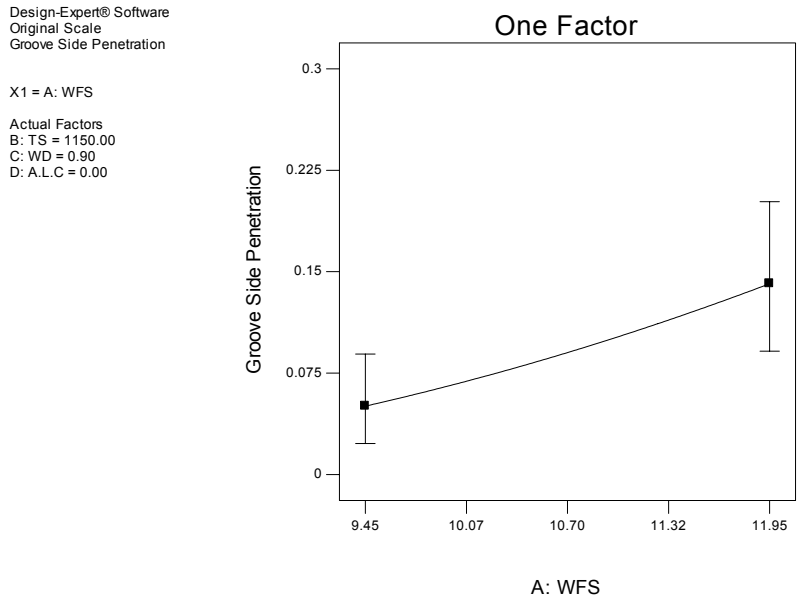

Fig. 6-64 Effect of the wire feed speed (m/min) on groove sidewall penetration (mm)

Figure 6.65 shows that a decrease in travel speed produces an increase of approximately 0.04mm in groove sidewall penetration, irrespective of the values of the other welding parameters.
Similarly, Figure 6.66 shows that an increase of 0.6mm in wire distance from the sidewall produces an increase of approximately 0.05mm in groove sidewall penetration.
Figure 6.67 shows that an increase of 19% in arc length correction produces an increase of approximately 0.04mm in groove sidewall penetration.
Groove sidewall penetration is maximised when the welding parameters are selected as follows:
Wire feed speed: high ; Travel speed : low; Wire distance from the sidewall : high,
and Arc length correction (arc length) : high (more precisely at the +5% value).

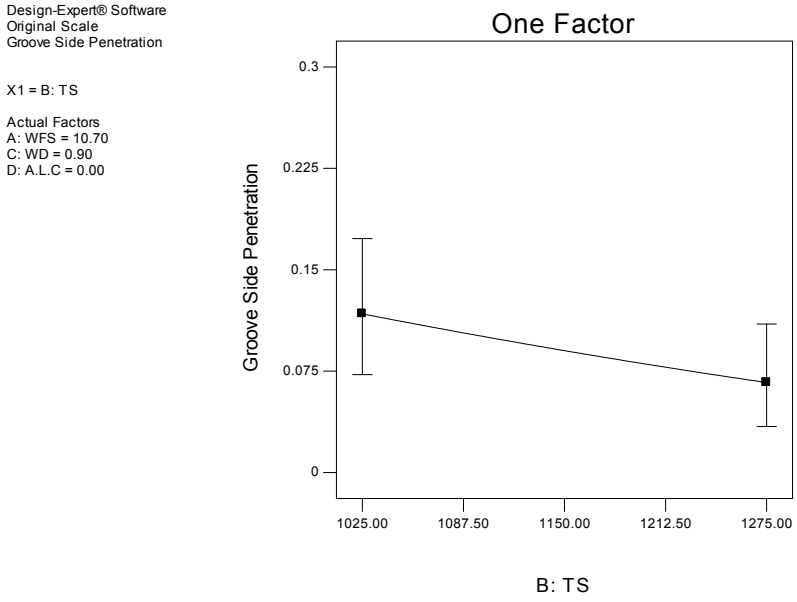

Fig. 6-65 Effect of the travel speed (m/min) on groove sidewall penetration (mm)

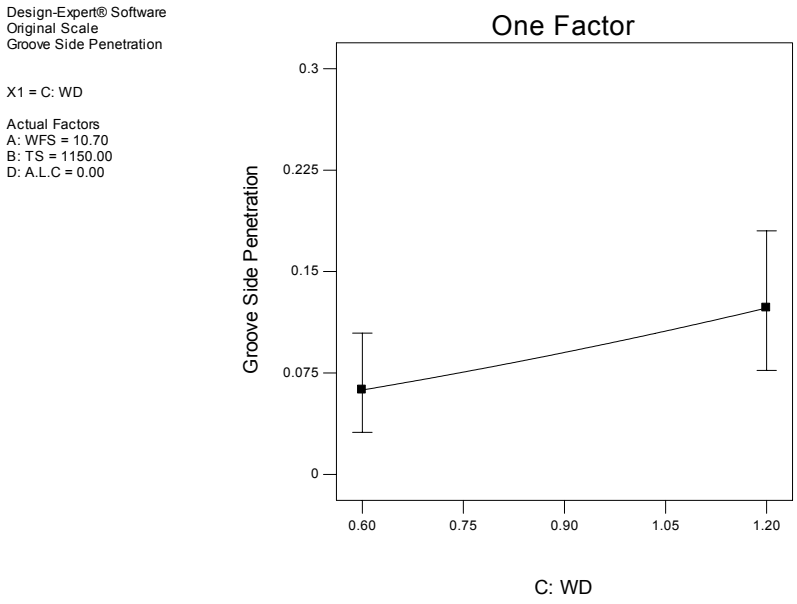

Fig. 6-66 Effect of the wire distance from the sidewall (mm) on groove sidewall penetration (mm)

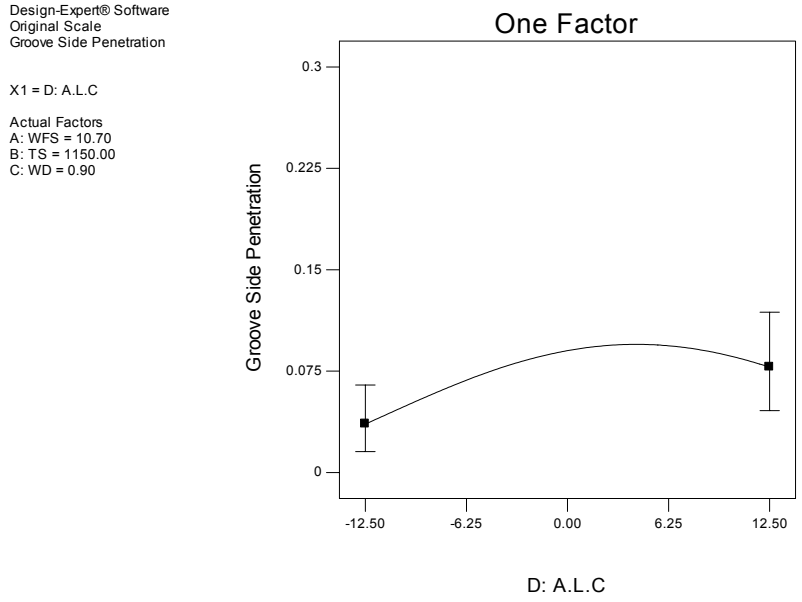

Fig. 6-67 Effect of the arc length correction (%) on groove sidewall penetration (mm)

3 Corner Angle

Figure 6.68 shows that, a decrease in arc length correction (arc length) of 25% produces a decrease in corner angle of 6.4° irrespective of the values of the other factors. As in all one factor plots, the slope of the graph remains invariable but the absolute magnitude of the corner angle will be affected by the other factors.

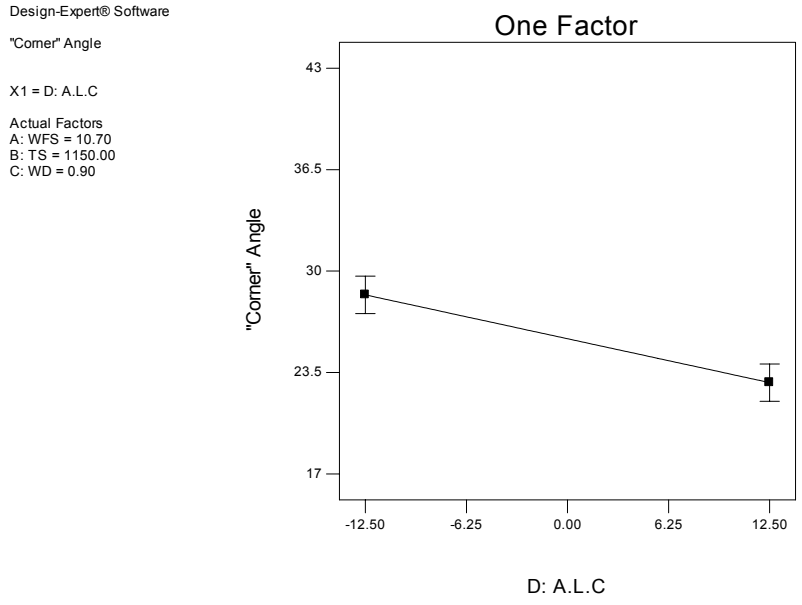

Fig. 6-68 Effect of arc length correction (%) on corner angle (°)

The plot in Figure 6.69 was obtained after the arc length correction was set at high level (+12.5%). The graph shows that corner angle decreases when wire feed speed decreases and wire distance is at low value. More precisely, the minimum corner angle is obtained when the value of the wire feed speed is approximately 10.7m/min.

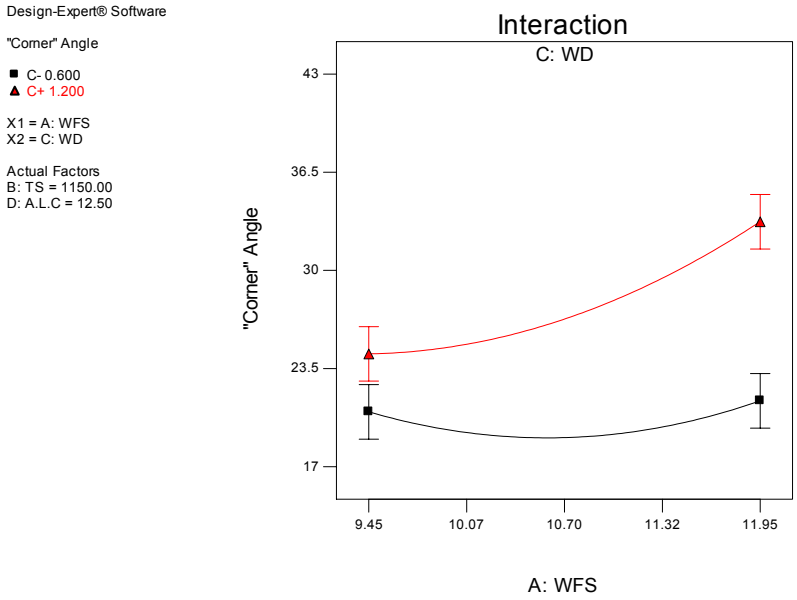

Fig. 6-69 Interaction plot for the effects of the wire feed speed (m/min) and wire distance from the sidewall (mm) on the corner angle (°)

The plot in Figure 6.70 was obtained after the arc length correction was set at high value and the wire distance from sidewall at low. The graph shows that the combination wfs and ts both at low values and the combination wfs and ts both at high values produce almost the same corner angle. At the intersection point of the two curves (10.3m/min) the value of the corner angle is the same for either low or high values of the travel speed.
Corner angle is minimised under the following conditions:
Wire feed speed : high ; Travel Speed : high ; Arc length correction(arc length) : high, and Wire distance from the wall : low (an almost equivalent result is obtained for WFS_{low}, TS_{low}, WD_{low}, ALC_{high}.

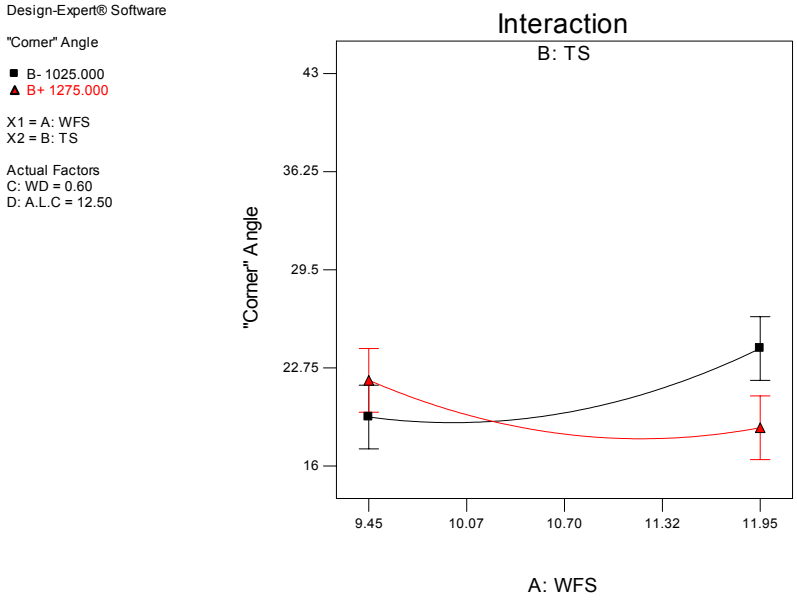

Fig. 6-70 Interaction plot for the effects of the wire feed speed (m/min) and travel speed (mm/min) on corner angle (°)

6.3.3 Overhead Position (180°)

6.3.3.1 Modelling Results

The measured weld bead dimensions resulting from the experiments (Table 5.4, page 88) are recorded in Table 6.18. The weld bead dimensions selected for the analysis were depth of penetration, groove sidewall penetration, and corner angle.

	Responses		
Weld No (Run No)	Depth of Penetration (mm)	Groove Sidewall Penetration (mm)	Corner Angle (°)
1	3.61	0.42	85
2	2.78	0.40	71.5
3	2.55	0.33	79
4	2.05	0.40	68
5	2.53	0.37	75
6	2.61	0.32	80
7	2.13	0.09	79.5
8	2.56	0.31	83
9	2.88	0.24	85
10	3.09	0.26	96
11	~~0~~	~~0~~	~~0~~
12	2.26	0.27	89
13	~~0~~	~~0~~	~~0~~
14	2.83	0.40	78
15	3.84	0.54	80.5
16	3.17	0.46	85
17	2.12	0.18	76.5
18	2.53	0.27	73
19	1.65	0.17	60
20	2.61	0.39	87
21	2.92	0.32	85
22	2.35	0.33	85
23	3.36	0.40	79.5
24	1.67	0.07	70.5
25	1.96	0.22	70
26	2.12	0.37	62
27	3.09	0.55	93.5
28	~~0~~	~~0~~	~~0~~
29	3.49	0.29	85
30	2.84	0.40	75.5

Table 6-18 Measured weld bead geometric responses (overhead position, 180°)

Figures 6.71 and 6.73 show the as welded bead profiles and the macrographs for some of the experiments and emphasize the effects of the welding conditions on the weld bead geometry. Welds Nos. 11, 13 and 28 reported droplet transfer instabilities and irregular bead profile (associated with the welding conditions) and are excluded from the analysis (Figure 6.72).
Macrographs of the welds of Table 6.18 are shown in Appendix C.

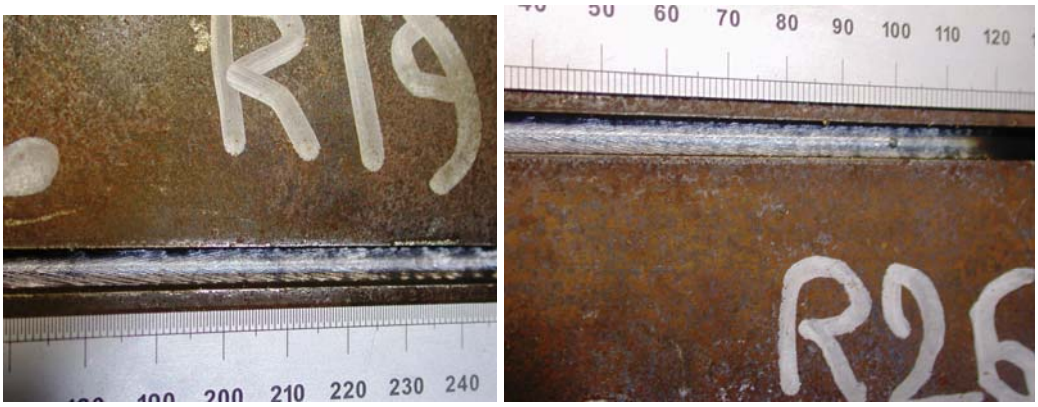

a) weld (run) No. 19 b) weld (run) No. 26

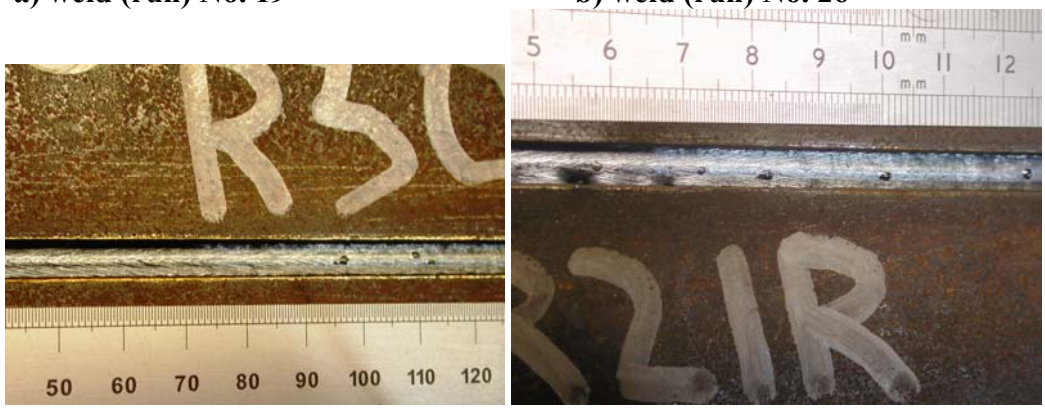

c) weld (run) No. 30 d) weld (run) No. 21

Fig. 6-71 Weld bead profiles in overhead (180°) position

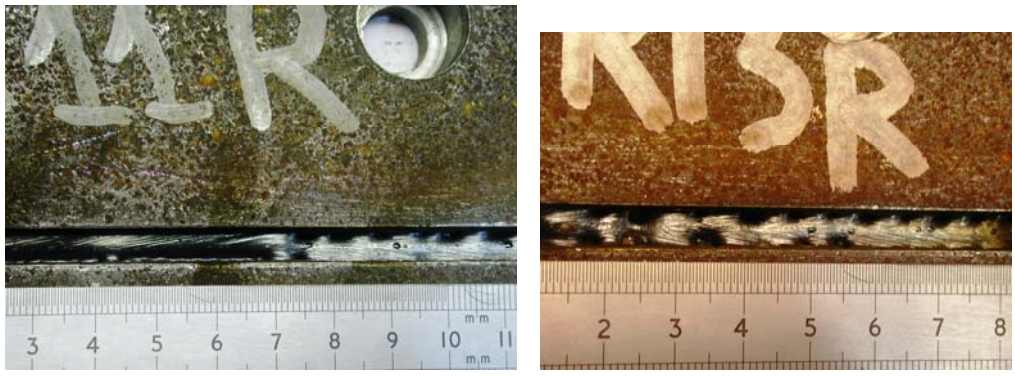

a) weld (run) No. 11 b) weld (run) No. 13

c) weld (run) No. 28

Fig. 6-72 Typical rejected welded profiles in the overhead (180°) position

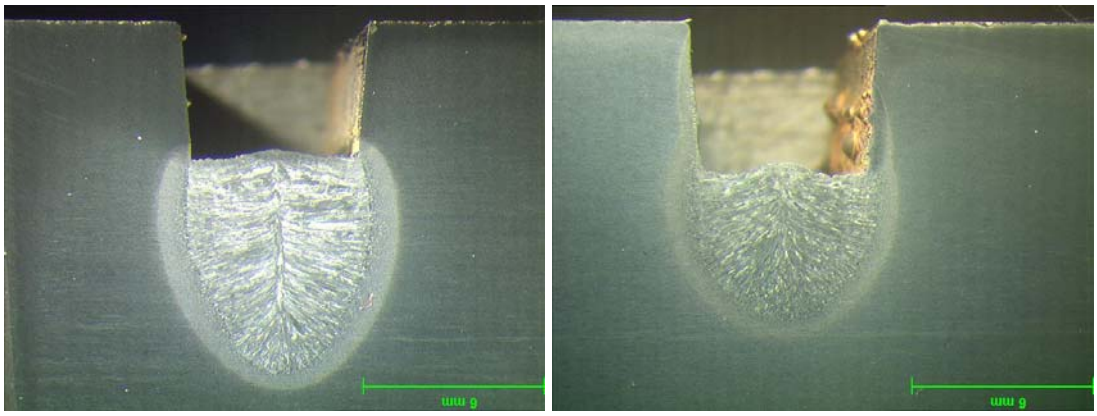

a) weld (run) No. 1 **weld (run) No. 7**

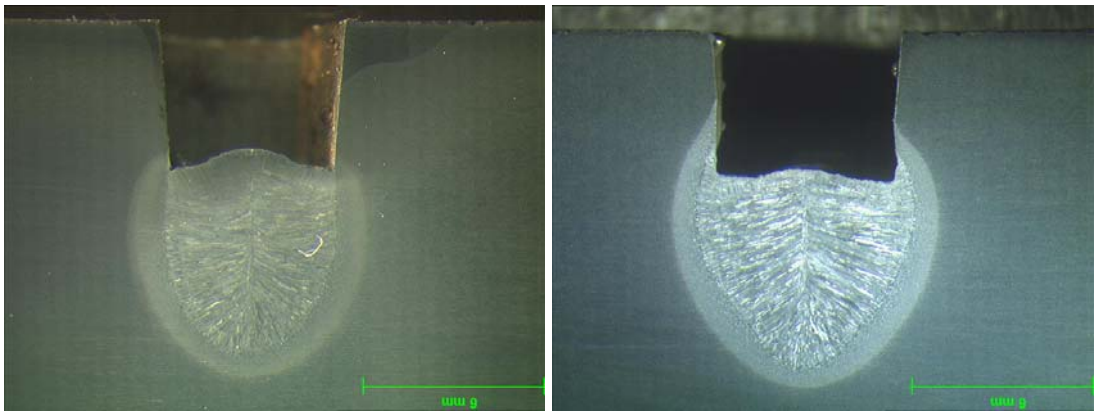

c) weld (run) No. 10 **d) weld (run) No. 28**

Fig. 6-73 Macrograph sections of welds in overhead (180°) position

Table 6.19 shows the significant variables (factors) included in the model after the backward elimination, and the type of model, the F-value, the P-value (Prob>F), etc. The responses analysed, were depth of penetration, groove sidewall penetration and corner angle.

The prediction equations for the responses in both coded and actual factors alongside to the units of the responses and actual factors are shown below:
P_d; Depth of penetration: mm
P_{GS}; Groove sidewall penetration: mm
Θ; Corner angle: (°)
W; Wire feed speed (WFS): m/min
T; Travel speed (TS): mm/min
D; Wire distance from sidewall (WD): mm
A_C; Arc length correction (ALC): %

Response	Type of Model	Chosen Variables	Pred.R-squared	Adj.R-squared.	F-value	P-value (Prob.>F)	Std. dev.	Adeq. Precision	Lack of Fit	
									F-value	P-value
Depth of Penetration (mm)	Quadratic	wfs /ts/ wd /a.l.c. wfs^2 /ts^2 / $a.l.c^2$	0.90	0.94	59.30	<0.0001 (significant)	0.14	30.30	0.90	0.6022 (not significant)
Groove Sidewall Penetration (mm)	Quadratic	wfs /ts / wd /a.l.c/ ts*wd / wfs^2	0.82	0.65	18.06	<0.0001 (significant)	0.005	18.17	1.71	0.2895 (not significant)
Corner Angle (°)	Quadratic	wfs /ts /wd / a.l.c /ts^2 / wfs*a.l.c / wd* a.l.c	0.71	0.83	18.77	<0.0001 (significant)	3.60	15.80	1.63	0.3076 (not significant)

Table 6-19 Selected variables, model order after backward elimination and statistical parameters (overhead (180°) position)

1. Depth of Penetration (P_d)

a) coded factors:

$$P_d = 2.69 + 0.36 \cdot W - 0.26 \cdot T + 0.31 \cdot D + 0.21 \cdot A_c - 0.064 \cdot W^2 + 0.065 \cdot T^2 - 0.075 \cdot A_c^2 \quad \textbf{Eqn. 6. 17}$$

b) actual factors:

$$P_d = 1.887 + 1.164 \cdot W - 0.0117 \cdot T + 1.041 \cdot D + 0.0165 \cdot A_c - 0.0408 \cdot W^2 + 4.171 \cdot 10^{-6} \cdot T^2 - 4.774 \cdot 10^{-4} \cdot A_c^2 \quad \textbf{Eqn. 6. 18}$$

2. Groove Sidewall Penetration (P_{GS})

a) coded factors:

$$P_{GS} = 0.34 + 0.067 \cdot W - 0.061 \cdot B - 0.011 \cdot D + 0.059 \cdot A_c + 0.054 \cdot W \cdot A_c + 0.029 \cdot T \cdot D - 0.024 \cdot W^2 \quad \textbf{Eqn. 6. 19}$$

b) actual factors:

$$P_{GS} = -0.6190 + 0.3848 \cdot W - 1.179 \cdot 10^{-3} \cdot T - 0.9197 \cdot D - 0.0324 \cdot A_c + 3.465 \cdot 10^{-3} \cdot W \cdot A_c + 7.689 \cdot 10^{-4} \cdot T \cdot D - 0.0155 \cdot W^2 \quad \textbf{Eqn. 6. 20}$$

3. Corner Angle (Θ)

a) coded factors:

$$\Theta = 78.00 + 3.77 \cdot W - 0.062 \cdot T + 2.76 \cdot D + 4.63 \cdot A_c - 3.72 \cdot W \cdot A_c - 5.18 \cdot D \cdot A_c + 2.24 \cdot T^2 \quad \textbf{Eqn. 6. 21}$$

b) actual factors:

$$\Theta = 227.6 + 3.017 \cdot W - 0.3302 \cdot T + 9.19 \cdot D + 4.159 \cdot A_c - 0.238 \cdot W \cdot A_c - 1.381 \cdot D \cdot A_c + 1.44 \cdot 10^{-4} \cdot T^2 \quad \textbf{Eqn. 6. 22}$$

6.3.3.2 Model Adequacy Checking

The diagnostic plots show no significant anomalies. However, the plot leverage vs run for the response depth of penetration presents some of the design runs (1, 12, 16, 24, 25) with leverage at just above double the leverage average. Given that all the other diagnostic plots and the values of the parameters in Table 6.19 are very good it was

decided to accept the model and to rely on confirmation runs to validate the experimental results.

6.3.3.3 Effect of the Welding Parameters on Weld Bead Profile

1 Depth of Penetration

Figure 6.74 shows that an increase in wire feed speed produces an increase in depth of penetration irrespective of the values of the other factors.

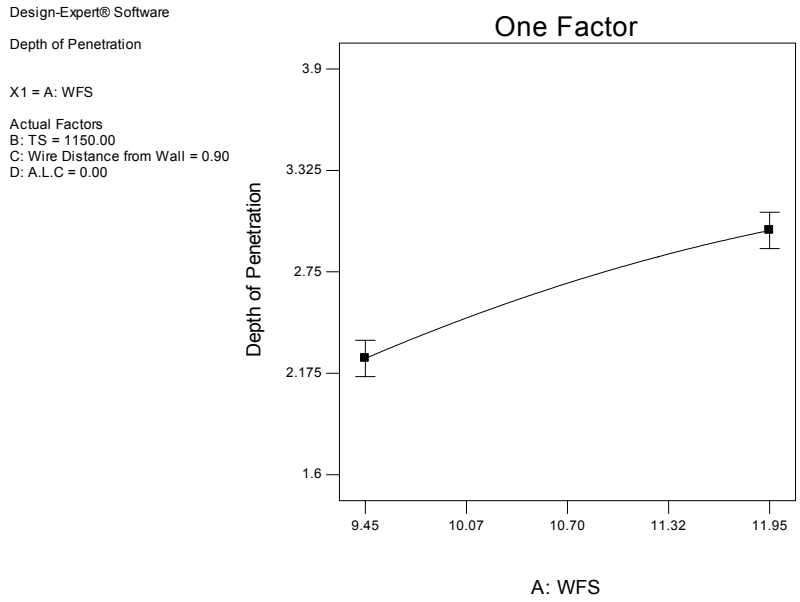

Fig. 6-74 One factor plot for the effect of the wire feed speed (m/min) on depth of penetration (mm)

Figure 6.75 shows that an increase in travel speed produces a decrease in depth of penetration. As for all one factor plots, the slope of the graph does not depend on the values (levels) of the other parameters, however the absolute magnitude of depth of penetration will be affected by other factors.

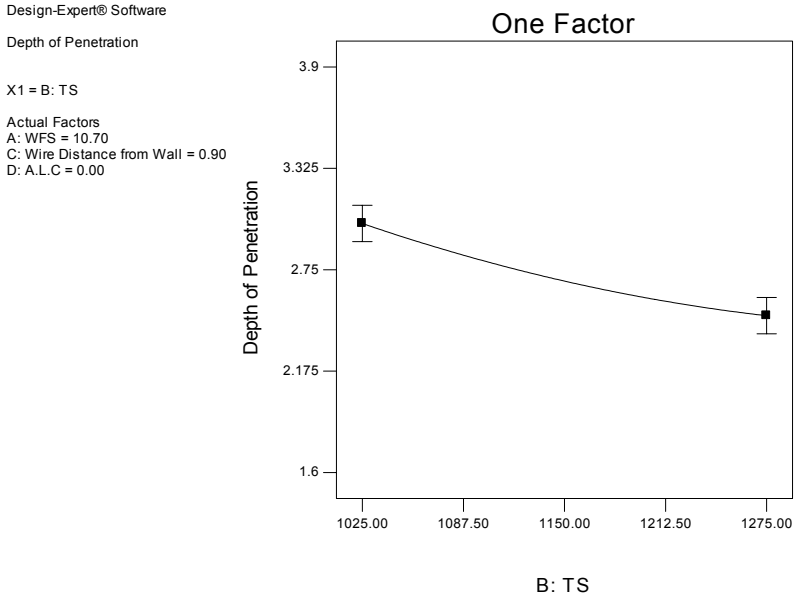

Fig. 6-75 One factor plot for the effect of the travel speed (mm/min) on depth of penetration (mm)

Figure 6.76 shows that an increase in wire distance from the sidewall produces an increase in depth of penetration.

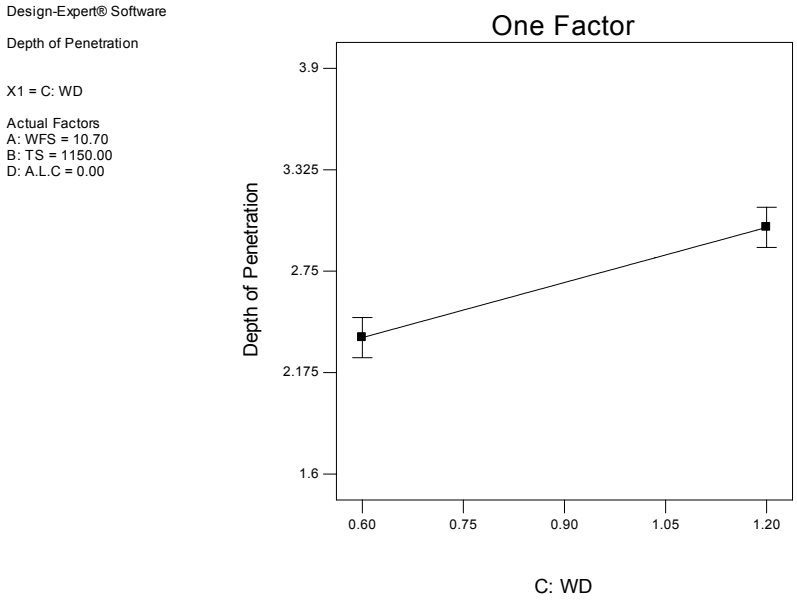

Fig. 6-76 One factor plot for the effect of the wire distance from the sidewall (mm) on depth of penetration (mm)

Figure 6.77 shows that an increase in arc length correction (arc length) produces an increase in depth of penetration.

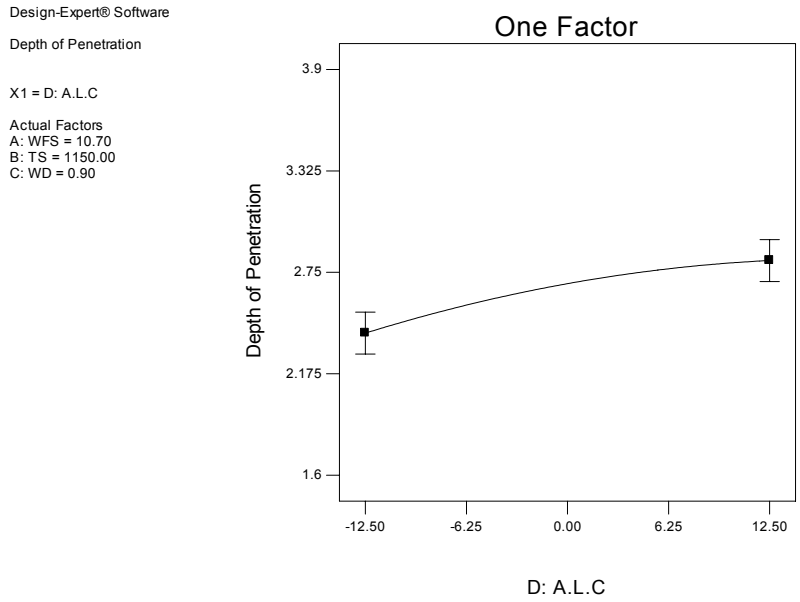

Fig. 6-77 One factor plot for the effect of the arc length correction (%) on depth of penetration (mm)

Analysis of the above plots shows that depth of penetration is maximised for the following values of the welding parameters: Wire feed speed : high ; Travel speed : low ; Wire distance from the sidewall : high, and Arc length correction (arc length) : high.

2 Groove Sidewall Penetration

The interaction plot Figure 6.78 shows that groove sidewall penetration increases when the low values (levels) of both travel speed and wire distance from the sidewall are selcted. This combination of the welding parameters (ts=low and wd=low) produces an increase of 0.11mm in groove sidewall penetration compared to the combination ts=low and wd=high.

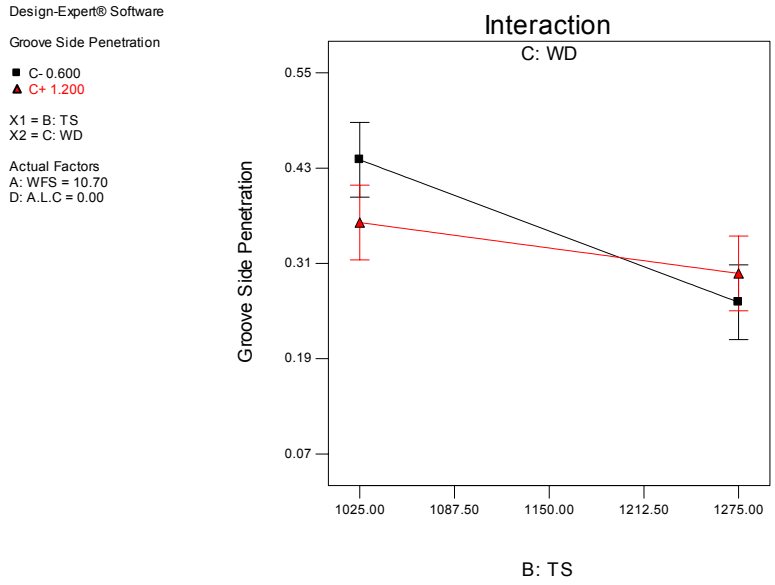

Fig. 6-78 Interaction plot for the effects of travel speed (mm/min) and wire distance from the sidewall (mm) on groove sidewall penetration (mm)

Figure 6.79 shows (for ts=low and wd=low) that groove sidewall penetration increases when both wire feed speed and arc length correction increase. This combination (wfs=high and a.l.c=high) produces an increase in groove sidewall penetration of 0.25mm more than the combination wfs=low and a.l.c.=low.
Analysis of the interaction plots shows that groove sidewall penetration is maximised for the combination of the levels (values) of the welding parameters:
Wire feed speed : high ; Travel speed : low ; Wire distance from sidewall : low, and Arc length correction (arc length) : high.

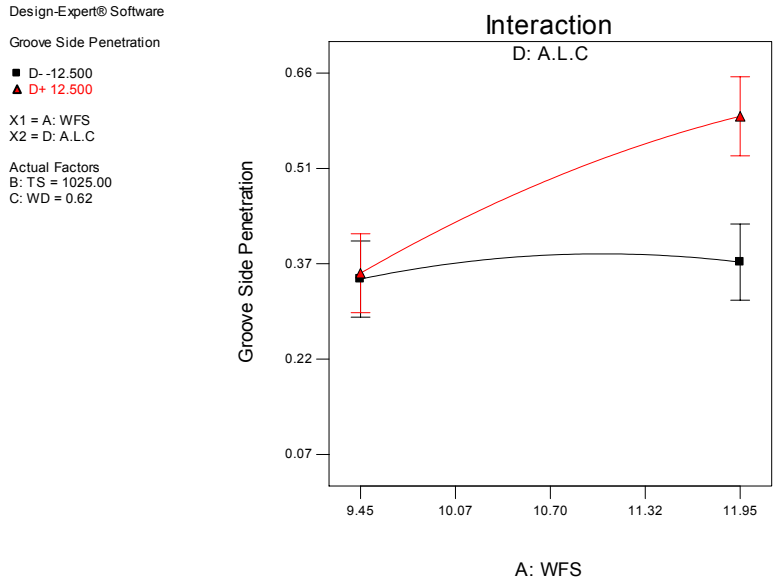

Fig. 6-79 Interaction plot for the effects of the wire feed speed (m/min) and arc length correction (%) on groove sidewall penetration (mm)

3 Corner Angle

The plot in Figure 6.80 shows an insignificant effect of travel speed on corner angle. Almost identical corner angle values are reported whether travel speed increases or decreases. However, the lowest corner angle corresponds to the travel speed at the centre point (1150mm/min).

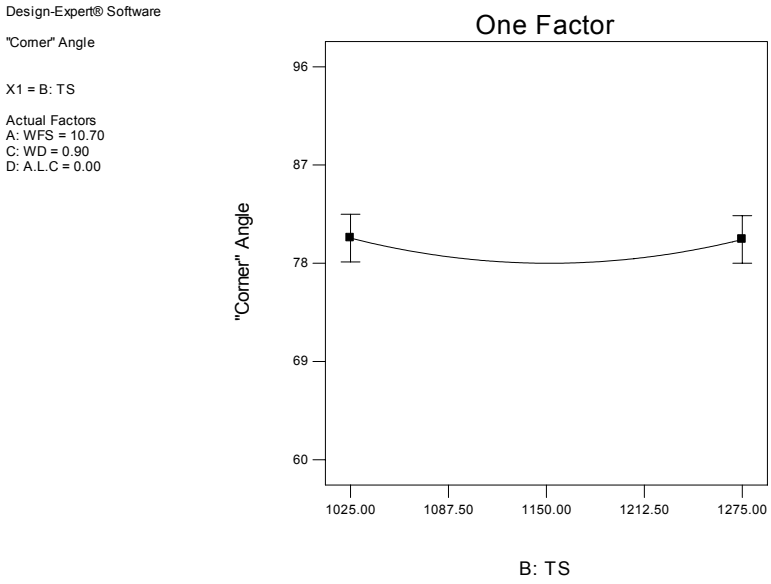

Fig. 6-80 Effect of the travel speed (mm/min) on corner angle (°)

The plot in Figure 6.81 shows that corner angle clearly decreases when both the wire feed speed and arc length correction (arc length) are at their low levels.

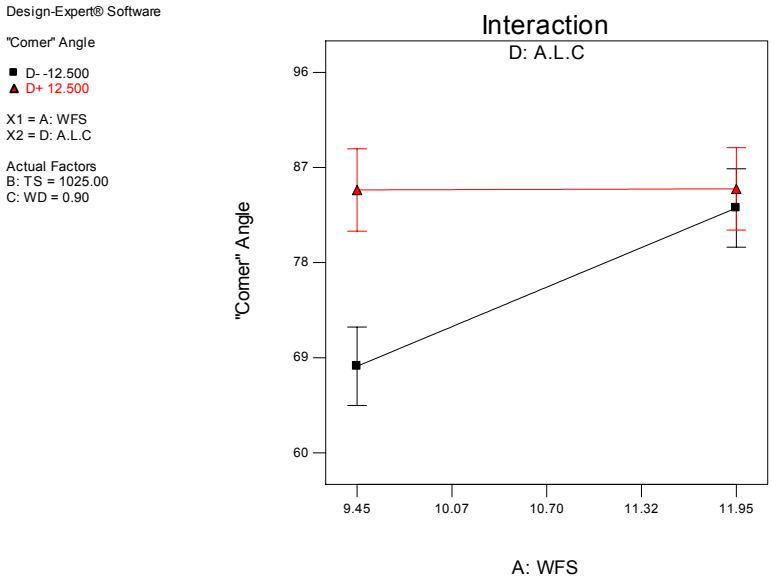

Fig. 6-81 Interaction plot for the effects of the wire feed speed (m/min) and arc length correction (%) on corner angle (°)

Figure 6.82 obtained after the low values of wire feed speed and travel speed were selected, shows that corner angle is decreased when both wire distance from the sidewall and arc length correction are at their low values.
Analysis of the interaction plots shows that corner angle is minimised for the combination of levels (values) of the welding parameters:
Wire feed speed : low ; Travel speed : low (or high) ; Wire distance from sidewall : low, and Arc length correction (arc length) : low

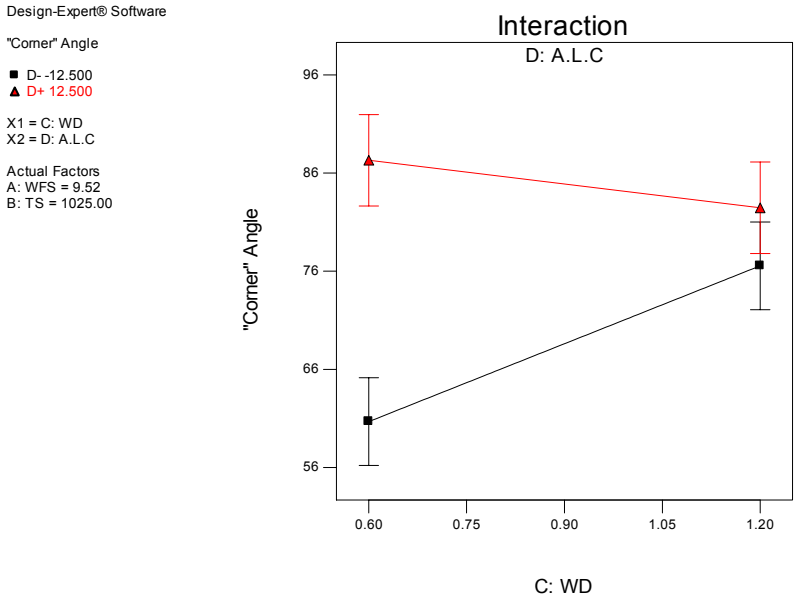

Fig. 6-82 Interaction plot for the effects of the wire distance from the sidewall (mm) and arc length correction (%) on corner angle (°)

6.3.4 Angular Position

The macrograph sections obtained from the welds in flat, vertical down and overhead position have shown the significant effect of the welding position on weld bead geometry. Additional experiments in the intermediate (angular) positions were carried out in an attempt to extend the study of the welding position.
If the original intention of the experiments had been to investigate the effect of the welding position, then the experimental design could have been different.
The factors and their levels are reported in section 5.3.2.2.2 (page 89) and the results (responses) of the experimental design are recorded in Table 6.20.

6.3.4.1 Modelling Results

		Responses		
Position (°)	Weld No (Run No)	Depth of Penetration (mm)	Groove Sidewall Penetration (mm)	Corner Angle (°)
30	1	2.03	0.12	47.7
30	2	1.93	0.15	21.9
30	3	2.80	0.14	18.25
30	4	2.17	0.40	35.5
30	5	2.32	0.16	34
30	6	1.40	0	28.8
30	7	1.67	0.08	32.3
30	8	2.81	0.37	24.5
30	9	2.46	0.06	35.3
60	10	1.86	0.01	19.2
60	11	2.25	0.20	33.9
60	12	1.67	0	26.6
60	13	1.18	0	23.8
60	14	1.97	0.18	29.1
60	15	1.84	0	25
60	16	1.85	0.09	29.55
60	17	1.27	0	26
60	18	3.17	0.37	25.45
120	19	1.93	0.16	36.3
120	20	2.28	0.17	30.6
120	21	2.81	0.19	37.85
120	22	3.29	0.38	34.3
120	23	2.89	0.44	25.8
120	24	1.75	0.19	26.3
120	25	1.58	0.09	26.3
120	26	3.02	0.2	38.5
120	27	1.84	0.13	22.5
150	28	2.32	0.17	57.2
150	29	4.00	0.55	67.2
150	30	2.98	0.40	84.0
150	31	3.42	0.49	56.5
150	32	1.75	0.19	42.3
150	33	2.36	0.32	48
150	34	3.09	0.28	53.5
150	35	2.67	0.42	45.2
150	36	2.37	0.26	50.3

Table 6-20 Measured weld bead geometric responses (angular position; 30°, 60°, 120° and 150°)

All welds show very good bead shape and the ranges of welding parameters selected have provided quite significant differences in the bead geometry.
Figure 6.83 shows typical macrographs obtained in different positions. Macrographs of the welds of Table 6.20 are shown in Appendix C.

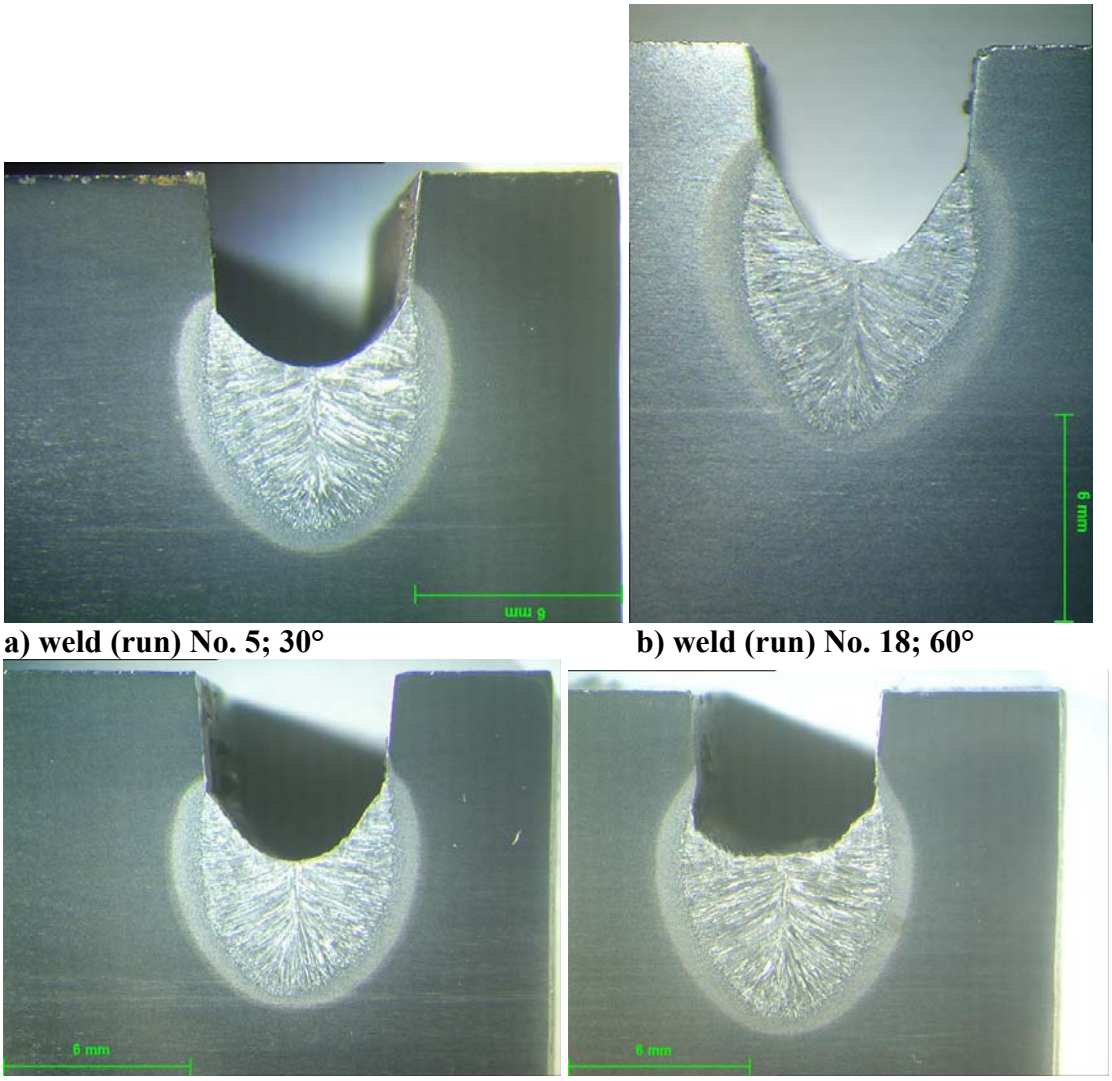

a) weld (run) No. 5; 30° **b) weld (run) No. 18; 60°**

c) weld (run) No. 20; 120° **d) weld (run) No. 35; 150°**

Fig. 6-83 Typical macrographs of welds in angular positions (30°, 60°, 120°, 150°)

The model prediction equations together with the units of the responses and actual factors are shown below:
P_d; Depth of penetration: mm
P_{GS}; Groove sidewall penetration: mm
Θ; Corner angle: (°)
W; Wire feed speed (WFS): m/min
T; Travel speed (TS): mm/min
D; Wire distance from sidewall (WD): mm

A_C; Arc length correction (ALC): %
Π; Position : (°)

1. Depth of Penetration (P_d)

a) coded factors:

$$P_d = 2.09 + 0.30 \cdot W - 0.098 \cdot T + 0.26 \cdot D + 0.30 \cdot A_c + 0.24 \cdot \Pi + 0.12 \cdot D \cdot A_c + 0.33 \cdot \Pi^2 \quad \textbf{Eqn. 6. 23}$$

b) actual factors:

$$P_d = -0.5543 + 0.2740 \cdot W - 7.836 \cdot 10^{-4} + 0.8536 \cdot D - 5.435 \cdot 10^{-3} \cdot A_c - 0.0123 \cdot \Pi + 0.0316 \cdot D \cdot A_c + 9.087 \cdot 10^{-5} \cdot \Pi \quad \textbf{Eqn. 6. 24}$$

2. Groove Sidewall Penetration (P_{GS})

a) coded factors:

$$\sqrt{P_{GS}} = 0.34 + 0.10 \cdot W + -8.833 \cdot 10^{-3} \cdot T + 7.239 \cdot 10^{-3} \cdot D + 0.069 \cdot A_c + 0.10 \cdot \Pi - 0.059 \cdot W \cdot \Pi + 0.12 \cdot \Pi^2 \quad \textbf{Eqn. 6. 25}$$

b) actual factors:

$$\sqrt{P_{GS}} = -1.484 + 0.1750 \cdot W - 7.066 \cdot 10^{-5} \cdot T + 0.0242 \cdot D + 5.270 \cdot 10^{-3} \cdot A_c + 5.692 \cdot 10^{-3} \cdot \Pi - 8.885 \cdot 10^{-4} \cdot W \cdot \Pi + 3.439 \cdot 10^{-5} \cdot \Pi^2 \quad \textbf{Eqn. 6. 26}$$

3. Corner Angle (Θ)

a) coded factors:

$$\Theta = 25.33 + 2.67 \cdot W - 1.09 \cdot T + 4.18 \cdot D - 3.05 \cdot A_c + 13.10 \cdot \Pi - 4.20 \cdot T \cdot \Pi + 2.75 \cdot A_c \cdot \Pi + 18.14 \cdot \Pi^2 \quad \textbf{Eqn. 6. 27}$$

b) actual factors:

$$\Theta = -29.56 + 2.428 \cdot W + 0.0412 \cdot T + 0.1896 \cdot D - 0.2342 \cdot A_c - 0.1820 \cdot \Pi - 5.5979 \cdot 10^{-4} \cdot T \cdot \Pi + 0.1526 \cdot D \cdot \Pi + 5.037 \cdot 10^{-3} \cdot \Pi^2 \quad \textbf{Eqn. 6. 28}$$

6.3.4.2 Model Adequacy Checking

All the diagnostic plots together with the parameters in Table 6.21 show no discrepancy and are considered acceptable.

6.3.4.3 Effects of the Welding Parameters on the Weld Bead Profile

One factor and interaction plots were used for the estimation of the effects of the welding parameters on the responses, depth of penetration, groove sidewall penetration and corner angle.

1. Depth of Penetration

The plot in Figure 6.84 shows that an increase of 2.2m/min in wire feed speed produces an increase of 0.57mm in depth of penetration and similarly in Figure 6.85, an increase of 250mm/min in travel speed produces a decrease of 0.4mm in depth of penetration irrespective of the values of the other welding parameters.

Response	Type of Model	Chosen Variables	Pred.R-squared	Adj.R-squared.	F-value	P-value (Prob.>F)	Std. dev.	Adeq. Precision	Lack of Fit	
									F-value	P-value
Depth of Penetration (mm)	Quadratic	wfs /ts /wd /a.l.c /position /wd*a.l.c /position^2	0.81	0.86	31.00	<0.0001 (significant)	0.25	21.51	3.05	0.1093 (not significant)
Groove Sidewall Penetration (mm)	Quadratic	wfs /ts /wd /a.l.c /position /wfs*position /position^2	0.71	0.78	18.85	<0.0001 (significant)	0.091	13.83	2.42	0.1652 (not significant)
Corner Angle (°)	Quadratic	wfs /ts /wd /a.l.c /position /ts*position /wd*position /position^2	0.78	0.85	25.67	<0.0001 (significant)	5.58	19.84	1.52	0.3414 (not significant)

Table 6-21 Selected variables, model order after backward elimination and statistical parameters (angular 30°, 60°, 120°, 150°) position)

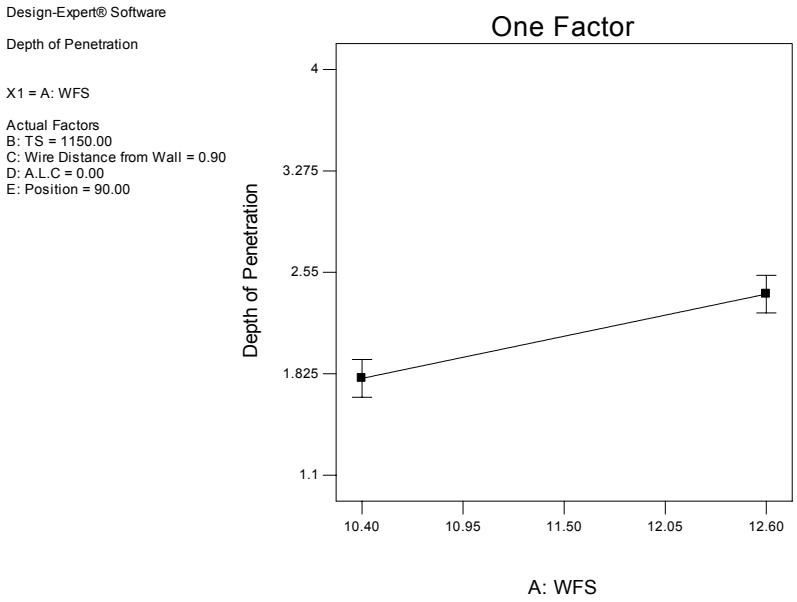

Fig. 6-84 One factor effect of the wire feed speed (m/min) on depth of penetration (mm)

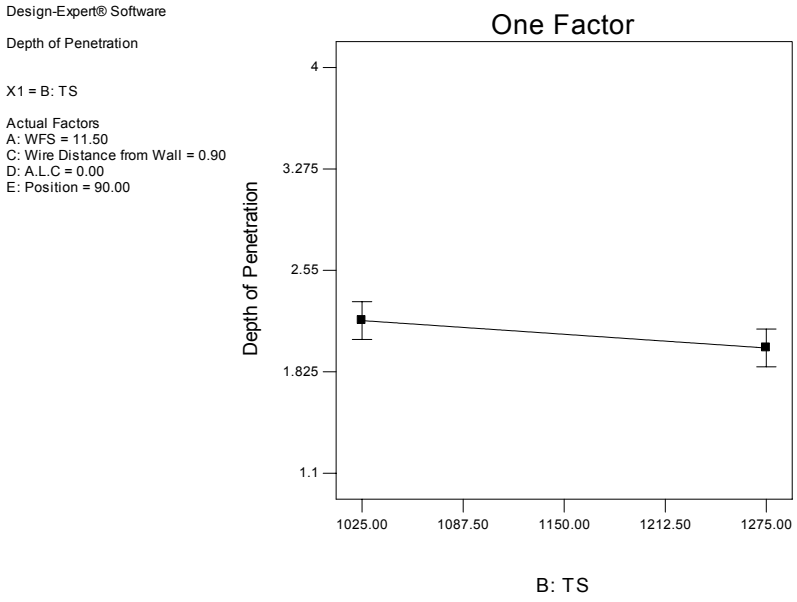

Fig. 6-85 One factor effect of the travel speed (mm/min) on depth of penetration (mm)

The plot in Figure 6.86 shows that depth of penetration initially decreases slightly with an increase in angular position up to 70° and then increases with a steeper slope.
The interaction plot in Figure 6.87, obtained after the high value for the wire feed speed, the position and the low value for the travel speed were selected, shows that an increase

in the wire distance from the sidewall and in the arc length correction produces an increase in depth of penetration.

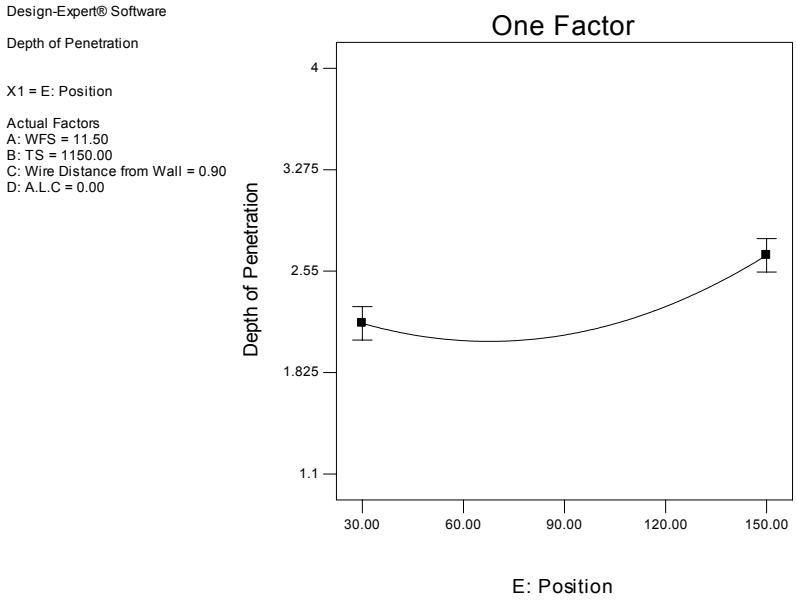

Fig. 6-86 One factor effect of the position (°) on depth of penetration (mm)

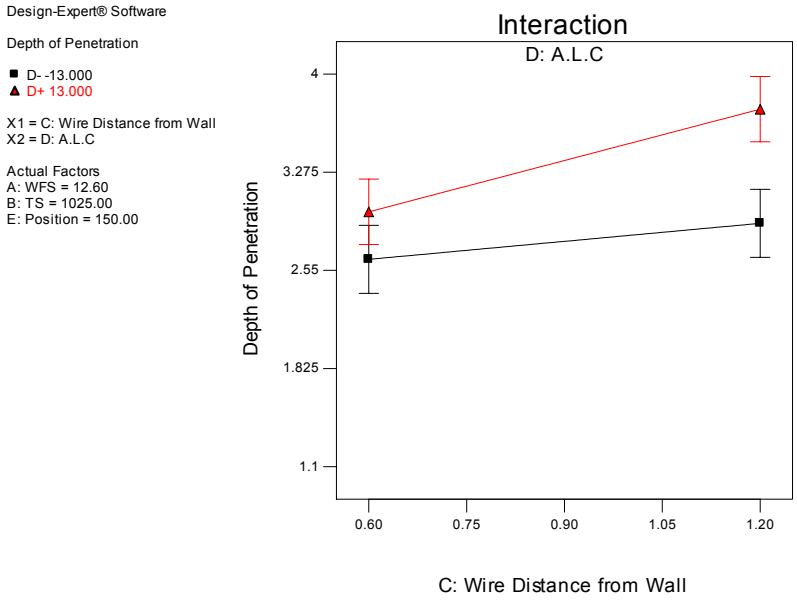

Fig. 6-87 Interaction plots for the effect of the wire distance from the sidewall (mm) and the arc length correction (%) on depth of penetration (mm)

Analysis of the above plots shows that depth of penetration is maximised for the following combination of levels (values) of the welding parameters:

Wire feed speed : high ; Travel speed : low ; Wire distance from sidewall : high, and Arc length correction (arc length) : high, Position: high

2. Groove Sidewall Penetration

In both the one factor plots (Figures 6.88 and 6.89) the effects of travel speed and wire distance from the sidewall on the groove sidewall penetration are almost negligible whether their low or high level values are considered.

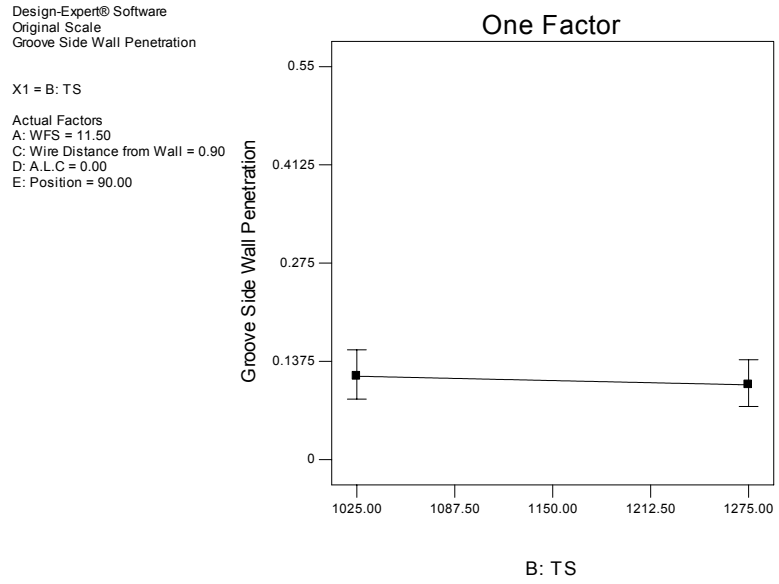

Fig. 6-88 One factor plot for the effect of the travel speed (mm/min) on groove sidewall penetration (mm)

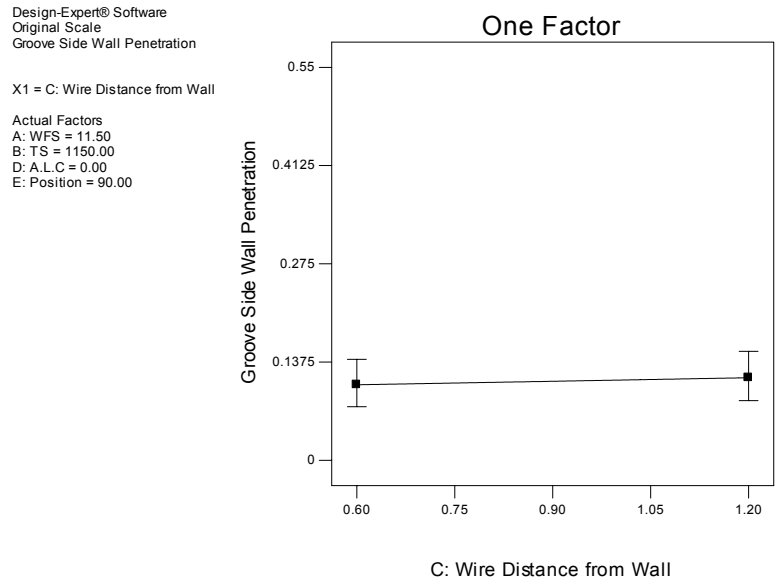

Fig. 6-89 One factor plot for the effect of the wire distance from the sidewall (mm) on groove sidewall penetration (mm)

The plot in Figure 6.90 shows that an increase in arc length correction produces an increase in groove sidewall penetration. An increase of 26% in arc length correction produces an increase in groove sidewall penetration of 0.08mm.
The interaction plot in Figure 6.91 shows that the groove sidewall penetration increases when both wire feed speed and welding position increase.

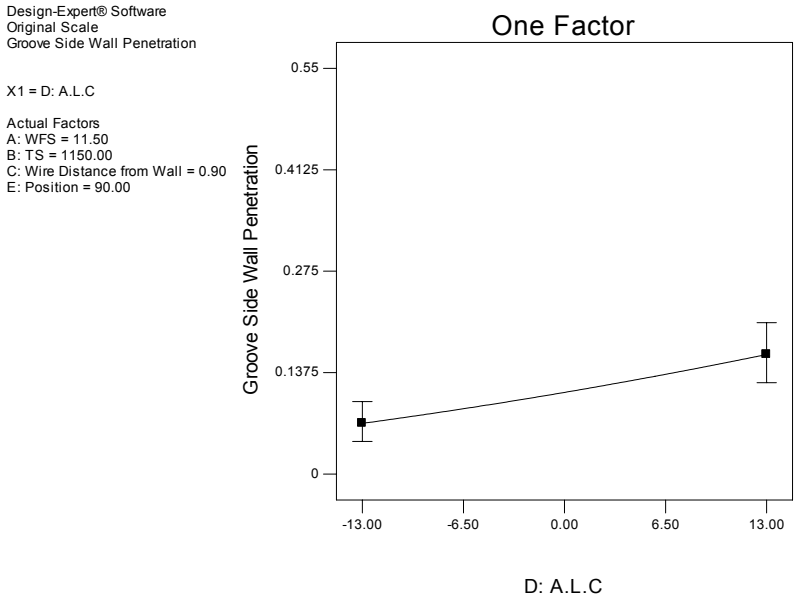

Fig. 6-90 One factor plot for the effect of the arc length correction (%) on groove sidewall penetration (mm)

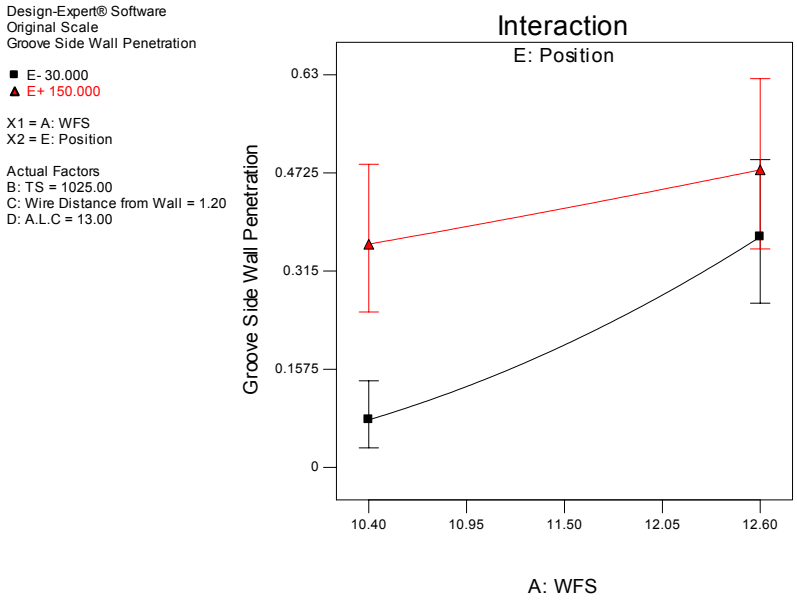

Fig. 6-91 Interaction plot for the effects of the wire feed speed (m/min) and position (°) on groove sidewall penetration (mm)

Groove sidewall penetration is maximised for the following set of the welding parameters: Wire feed speed: high; Travel speed: low; Wire Distance: low or high; Arc length correction: high; Position: high

3. Corner Angle

The plot in Figure 6.92 shows that a decrease of 2.2m/min in wire feed speed produces a decrease of 5° in corner angle, while the plot in Figure 6.93 shows that an increase of 26% in arc length correction produces a decrease of 6.5° in corner angle.

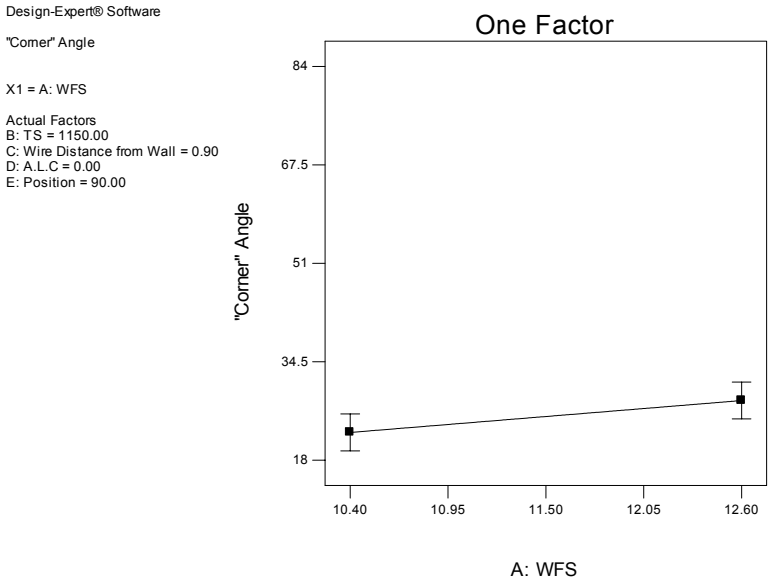

Fig. 6-92 One factor plot for the effect of the wire feed speed (m/min) on corner angle (°)

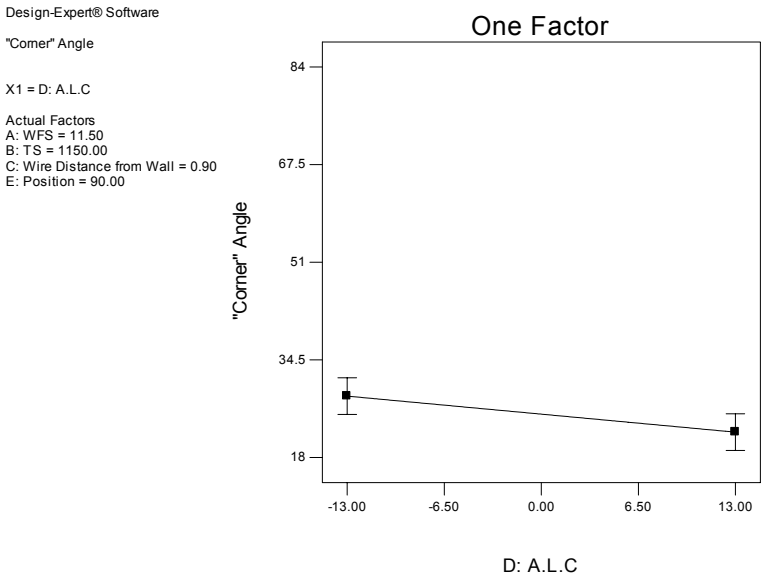

Fig. 6-93 One factor plot for the effect of the arc length correction (%) on corner angle (°)

Figure 6.94 shows that the corner angle decreases when travel speed decreases and welding position decreases (low level value).
Figure 6.95 shows that corner angle decreases slightly (almost negligible) when the wire distance from the sidewall decreases.

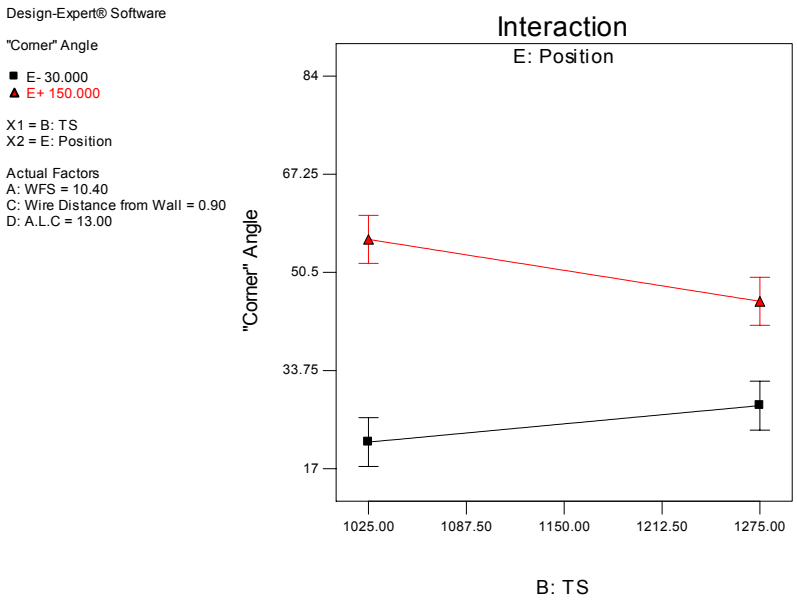

Fig. 6-94 Interaction plot for the effect of the travel speed (mm/min) and position on corner angle (°)

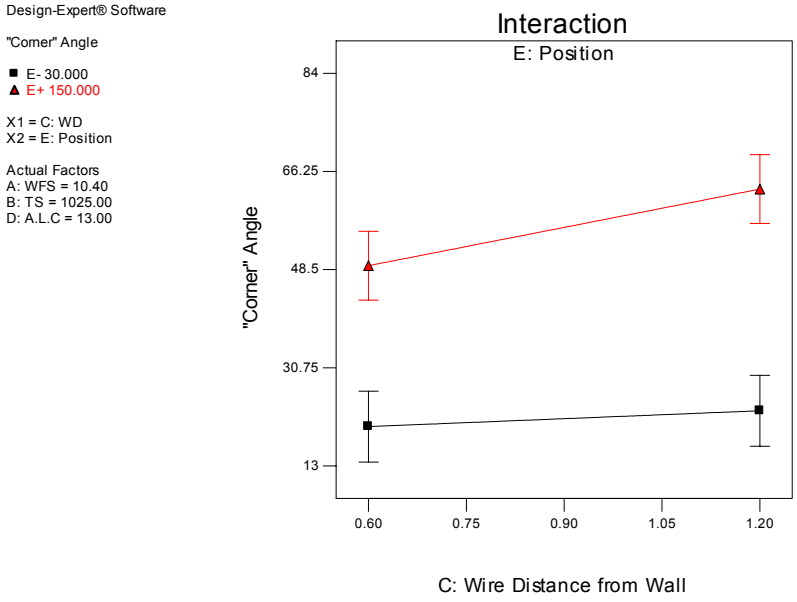

Fig. 6-95 Interaction plot for the effect of the wire distance from the sidewall (mm) and position on corner angle (°)

Analysis of the above plots shows that corner angle is minimised for the following combination of levels (values) of the welding parameters:
Wire feed speed : low ; Travel speed : low ; Wire distance from sidewall : low, Arc length correction (arc length) : high, and Position : low.

The noticeable effect of the position on the corner angle (and therefore on bead profile) is clearly shown in the modelling equation (section 6.3.4.1, page 173) where the value of the position coefficient is considerably higher (13.10) than that of the welding parameters.
The model predictions for the positions equivalent to 30°, 60°, 90°, 120° and 150° were plotted (Figures 6.96 and 6.97). The following values for the welding parameters were used: wfs=11.5m/min; ts=1150mm/min; wd=0.9mm and a.l.c=0%.

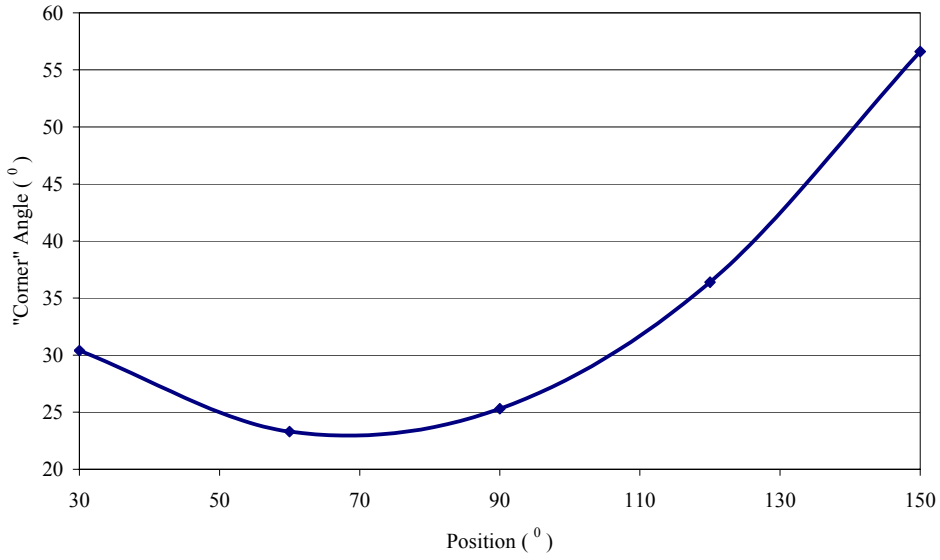

a

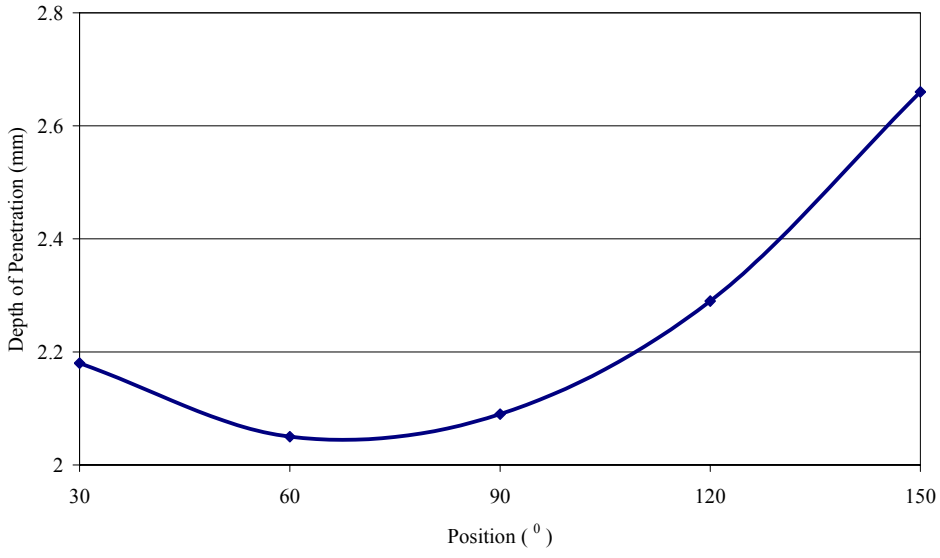

b

Fig. 6-96 Effect of the position on (a) corner angle and (b) depth of penetration

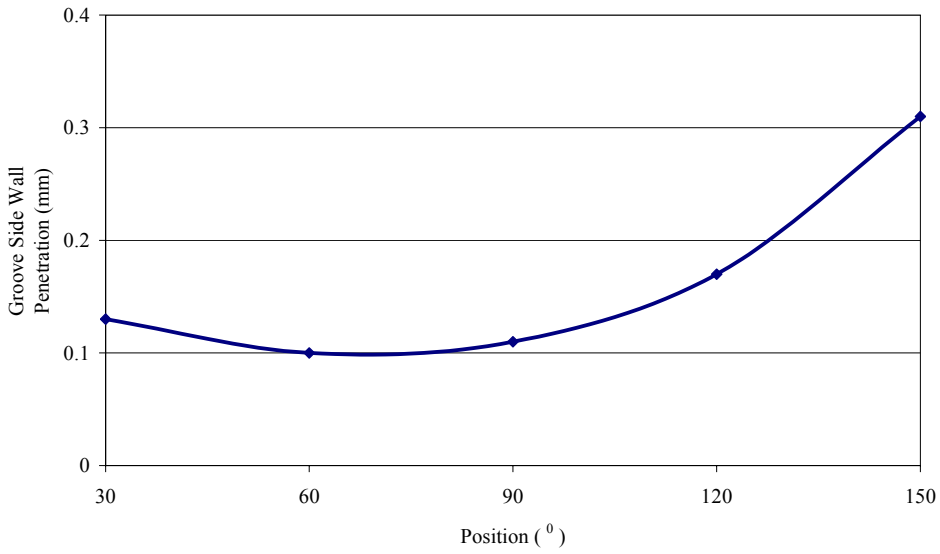

Fig. 6-97 Effect of the position on groove sidewall penetration

6.3.5 Combined Model

Considering the distinct effect of the welding position on the bead geometry, resulting from the previous analysis, it was decided to combine all the available data on flat, vertical and overhead positions to generate a global model for all positions. The combined model consisted of a statistical treatment of the three models developed in flat, vertical and overhead positions. The three designs and their responses (weld bead dimensions) were combined together and considered as a "single" design. This design has 90 runs (30 in each position) and five variables (wire feed speed, travel speed, wire distance from the sidewall, arc length correction and position). The design type was central composite D-optimal.

This is a "theoretical" global model and no additional runs (welds) were carried out. The aim of this attempt was to develop one model able to predict the weld bead geometry in all positions (from 0° to 180°)

The responses considered for analysis were depth of penetration, groove sidewall penetration and corner angle.

The model prediction equations together with the units of the responses and actual factors are reported below:

P_d; Depth of penetration: mm

P_{GS}; Groove sidewall penetration: mm

Θ; Corner angle: (°)

W; Wire feed speed (WFS): m/min

T; Travel speed (TS): mm/min

D; Wire distance from sidewall (WD): mm

A_C; Arc length correction (ALC): %

Π; Position : (°)

1. Depth of Penetration (P_d)

a) coded factors:

$$P_d = 1.74 + 0.30 \cdot W - 0.17 \cdot T + 0.26 \cdot D + 0.19 \cdot A_c + 0.068 \cdot \Pi + 0.085 \cdot W \cdot A_c - 0.086 \cdot T \cdot A_c - 0.055 \cdot A_c + 0.86 \cdot \Pi^2 \quad \textbf{Eqn. 6. 29}$$

b) actual factors:

$$P_d = 0.7448 + 0.2434 \cdot W - 1.387 \cdot 10^{-3} \cdot T + 0.8655 \cdot D + 0.0197 \cdot A_c - 0.0184 \cdot \Pi + 5.462 \cdot 10^{-3} \cdot W \cdot A_c - 5.488 \cdot 10^{-5} \cdot T \cdot A_c - 3.526 \cdot 10^{-4} \cdot A_c^2 + 1.065 \cdot 10^{-4} \cdot \Pi^2 \quad \textbf{Eqn. 6. 30}$$

2. Groove Sidewall Penetration (P_{GS})

a) coded factors:

$$P_{GS} = 0.086 + 0.065 \cdot W - 0.051 \cdot T - 8.286 \cdot 10^{-4} \cdot D + 0.035 \cdot A_c + 0.046 \cdot \Pi + 0.030 \cdot W \cdot A_c - 0.027 \cdot T \cdot A_c + 0.19 \cdot \Pi^2 \quad \textbf{Eqn. 6. 31}$$

b) actual factors:

$$P_{GS} = 0.1389 + 0.0524 \cdot W - 4.091 \cdot 10^{-4} \cdot T - 2.762 \cdot 10^{-3} \cdot D + 2.780 \cdot 10^{-3} \cdot A_c - 3.612 \cdot 10^{-3} \cdot \Pi + 1.891 \cdot 10^{-3} \cdot W \cdot A_c - 1.757 \cdot 10^{-5} \cdot T \cdot A_c + 2.289 \cdot 10^{-5} \cdot \Pi^2 \quad \textbf{Eqn. 6. 32}$$

3. Corner Angle (Θ)

a) coded factors:

$$\Theta = 27.33 + 3.13 \cdot W - 0.10 \cdot T + 2.87 \cdot D - 1.06 \cdot A_c + 15.39 \cdot \Pi + 4.23 \cdot A_c \cdot \Pi + 36.65 \cdot \Pi^2 \quad \textbf{Eqn. 6. 33}$$

b) actual factors:

$$\Theta = 14.09 + 2.504 \cdot W - 7.969 \cdot 10^{-4} \cdot T + 9.576 \cdot D - 0.4235 \cdot A_c - 0.6435 \cdot \Pi + 3.761 \cdot 10^{-3} \cdot A_c \cdot \Pi + 4.525 \cdot 10^{-3} \cdot \Pi^2 \quad \textbf{Eqn. 6. 34}$$

6.3.5.1 Modelling Results

For the "combined" model, the results reported in Tables 6.14 (flat position), 6.16 (vertical down position) and 6.18 (overhead position) were considered.

6.3.5.2 Model Adequacy Checking

The diagnostic plots presented some minor anomalies that do not affect the model predictions. Table 6.22 reports the variables included in the model and the statistical parameters of the combined model for the three responses. Both depth of penetration and corner angle reported significant lack of fit tests. However considering the very high values of the Pred. R-squared and Adj. R-squared it was decided to use the model for prediction.

Response	Type of Model	Chosen Variables	Pred.R-squared	Adj.R-squared.	F-value	P-value (Prob.>F)	Std. dev.	Adeq. Precision	Lack of Fit	
									F-value	P-value
Depth of Penetration (mm)	Quadratic	wfs /ts /wd /a.l.c /position /wfs*a.l.c /ts*a.l.c /a.l.c^2 /position^2	0.84	0.87	63.21	<0.0001 (significant)	0.24	34.65	3.86	0.0028 (significant)
Groove Sidewall Penetration (mm)	Quadratic	wfs /ts /wd /a.l.c /position /wfs*a.l.c /ts*a.l.c /position^2	0.70	0.75	32.72	<0.0001 (significant)	0.074	24.29	2.83	0.0144 (not significant)
Corner Angle (°)	Quadratic	wfs /ts /wd /a.l.c /position /a.l.c*position /position^2	0.93	0.94	193.45	<0.0001 (significant)	5.41	40.06	6.18	0.0003 (significant)

Table 6-22 Selected variables, model order after backward elimination and statistical parameters (combined model)

6.3.5.3 Effect of the Welding Parameters on Weld Bead Profile

1. Depth of Penetration

The plot in Figure 6.98 shows that an increase of 0.6mm in wire distance from the sidewall produces an increase of 0.4mm in depth of penetration irrespective of the values of the other factors. The plot in Figure 6.99 shows that depth of penetration remains the same (max) in flat and overhead positions but reaches its minimum in vertical (90°) position.

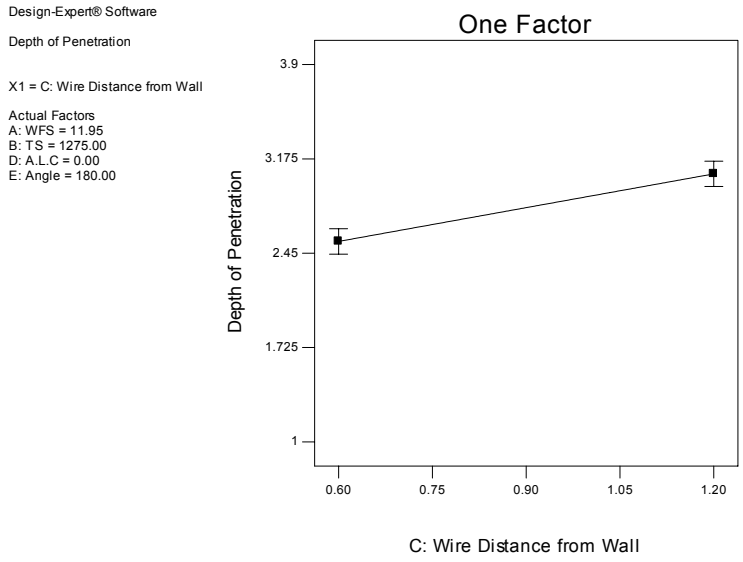

Fig. 6-98 One factor plot for the effect of the wire distance from the sidewall (mm) on depth of penetration (mm)

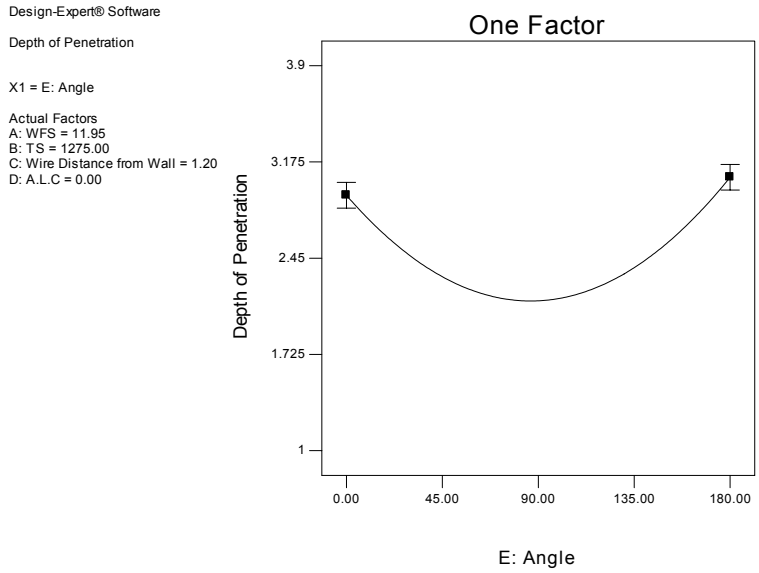

Fig. 6-99 One factor plot for the effect of the angle (°; angular position) on depth of penetration (mm)

Figure 6.100 shows that depth of penetration increases when both wire feed speed and arc length correction (arc length) increase. Figure 6.101 shows that depth of penetration increases when travel speed decreases.

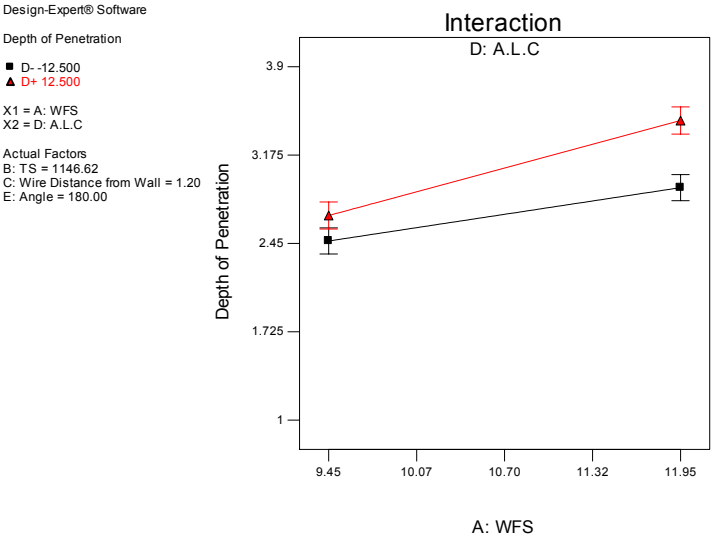

Fig. 6-100 Interaction plot for the effects of the wire feed speed (m/min) and arc length correction (%) on depth of penetration (mm)

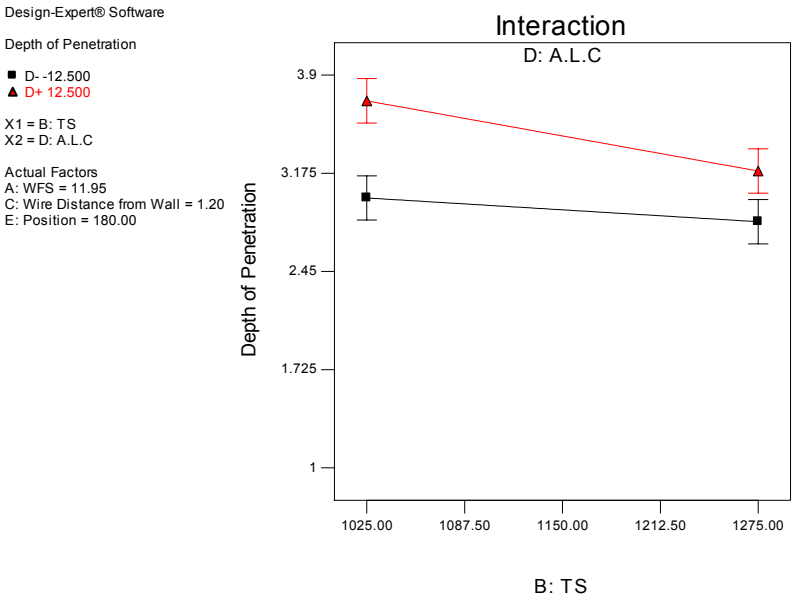

Fig. 6-101 Interaction plot for the effects of the travel speed (mm/min) and arc length correction (%) on depth of penetration (mm)

Analysis of the above one factor and interaction plots shows that depth of penetration is maximised for the following values of the welding parameters:

Wire feed speed: high ; Travel speed : low ; Wire distance from the sidewall : high ; Arc length correction : high, and Angle (angular position) : high

2. Groove Sidewall Penetration

Figure 6.102 shows that the effect of the wire distance from the sidewall wall is insignificant; while Figure 103 shows that the max. value in groove sidewall penetration is obtained in the overhead (180°) position and reaches its minimum in the vertical (90°) position.

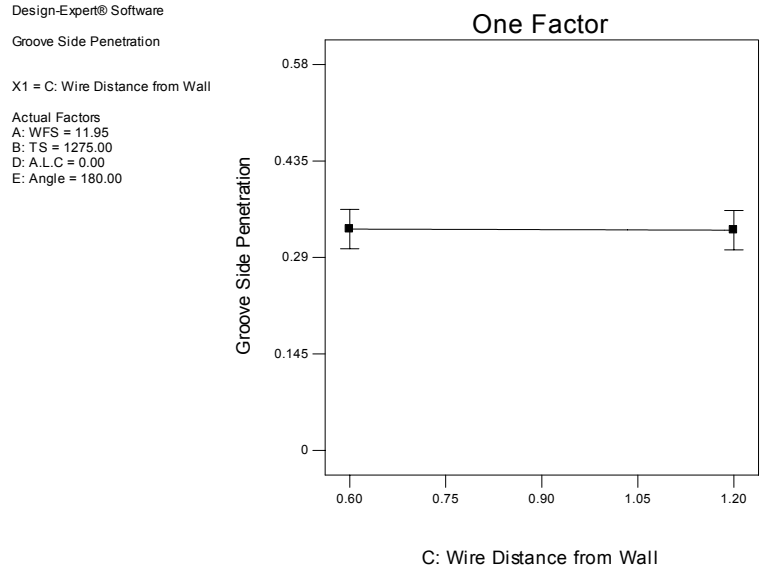

Fig. 6-102 One factor plot for the effect of the wire distance from the sidewall (mm) on groove sidewall penetration (mm)

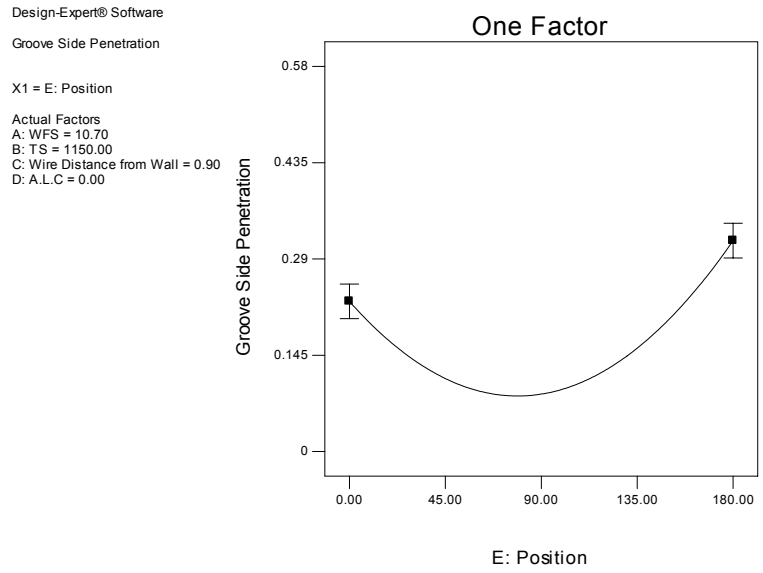

Fig. 6-103 One factor plot for the effect of the angle (°; angular position) on groove sidewall penetration (mm)

The plot in Figure 6.104 with wire distance at high level, shows that groove sidewall penetration increases when both wire feed speed and arc length correction increase (high level).

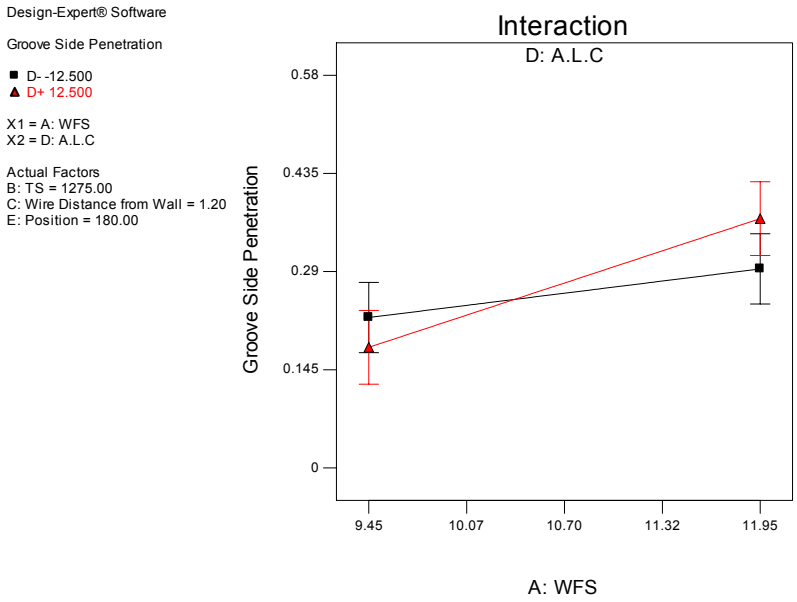

Fig. 6-104 Interaction plot for the effects of the wire feed speed (m/min) and arc length correction (%) on groove sidewall penetration (mm)

Figure 6.105 (with wire feed speed: high, arc length correction: high and position: high) shows that when travel speed decreases, groove sidewall penetration increases.

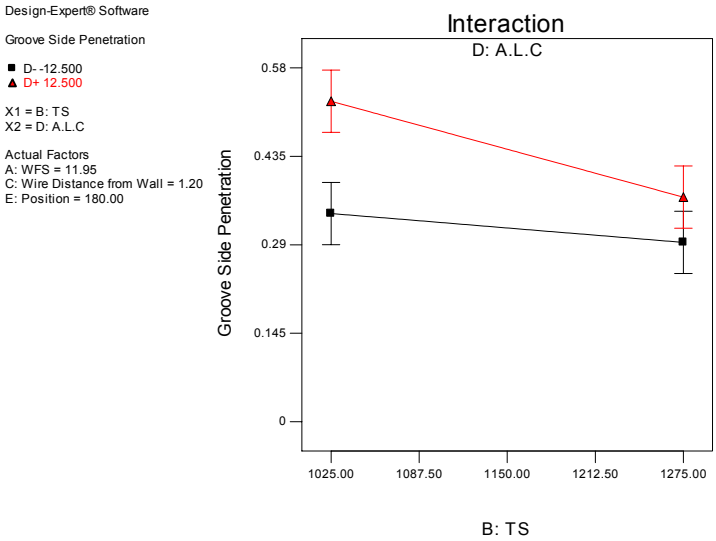

Fig. 6-105 Interaction plots for the effect of the travel speed (mm/min) and arc length correction (%) on groove sidewall penetration (mm)

The maximum in groove sidewall penetration is produced when: Wire feed speed: high ; Travel speed : low ; Arc length correction : high, Position : high, and Wire distance from the wall : low (or high)

3. Corner Angle

The plot in Figure 6.106 shows that a decrease in wire feed speed of 2.5m/min produces a decrease in corner angle of 6.1° while Figure 6.107 shows that the effect of travel speed on corner angle is insignificant.

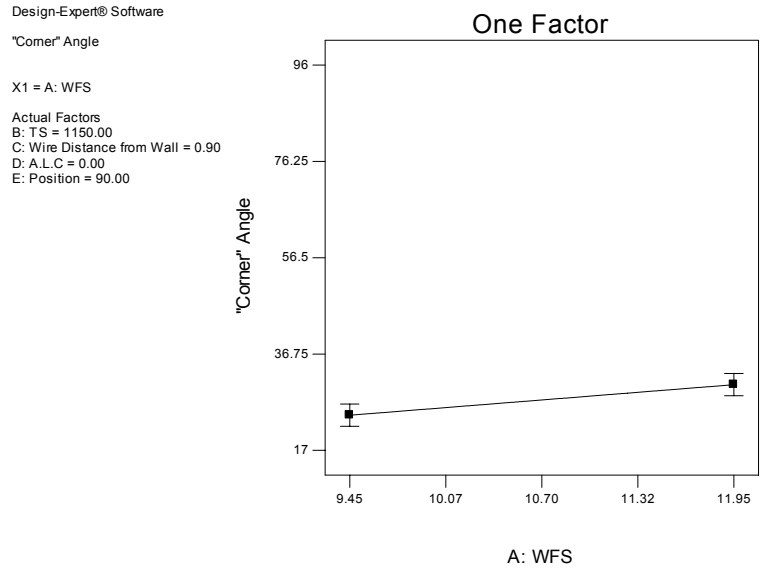

Fig. 6-106 One factor plot for the effect of the wire feed speed (m/min) on corner angle (°)

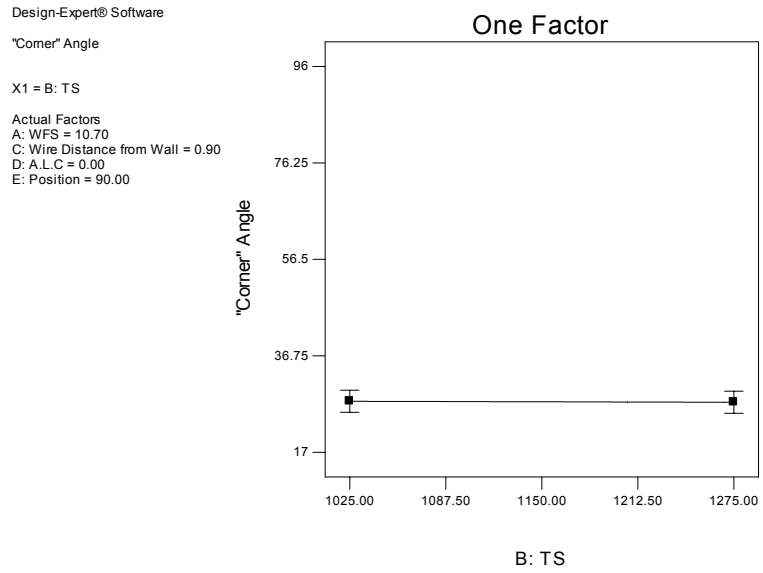

Fig. 6-107 One factor plot for the effect of the travel speed (mm/min) on corner angle (°)

The plot in Figure 6.108 shows that a decrease in wire distance from the sidewall of 0.6mm produces a decrease in corner angle of 4.6°.

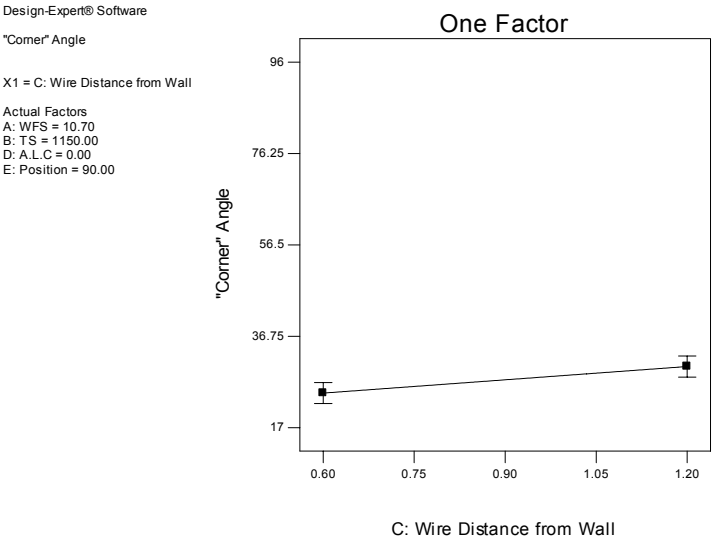

Fig. 6-108 One factor plot for the effect of the wire distance from the sidewall (mm) on corner angle (°)

The plot in Figure 6.109 shows that corner angle decreases when arc length correction increases in the flat position.

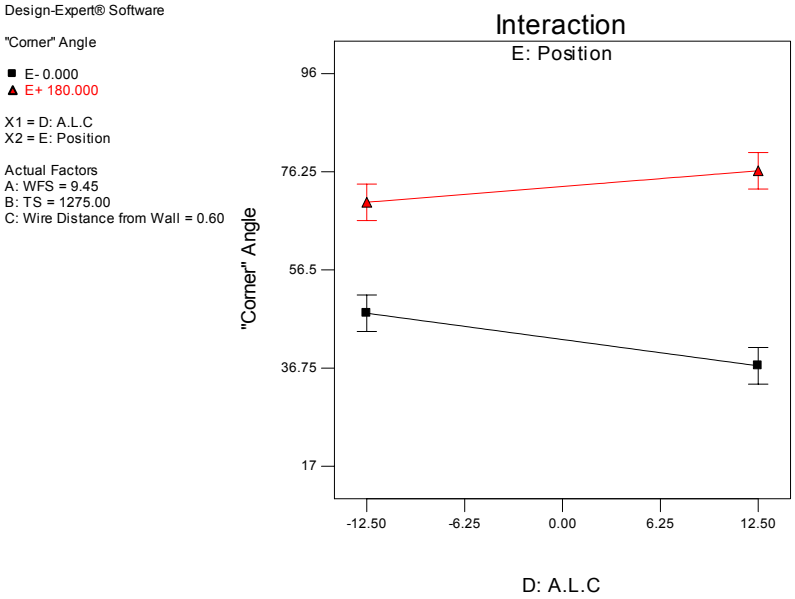

Fig. 6-109 Interaction plots for the effect of the arc length correction (%) on corner angle (°)

The corner angle is minimised for the following values of the parameters: Wire feed speed: low; Travel speed: low or high; Wire distance: low; Arc length correction: high; Position: low.

6.4 Model Validation

All models developed in the three positions (0°, 90° and 180°) are properly calibrated and shown to be acceptable by the statistical adequacy checking. To provide additional validation, a series of new tests (welds) were conducted to compare the model predictions with the actual values. The model generated the predicted responses, for a given set of the welding parameters. Actual welds were carried out using the parameters selected. This allowed a direct comparison between model predictions and actual welds. Table 6.23 shows the validation results.

The 90% to 99% low/(or high) prediction intervals of the models were used to evaluate the performance of the model predictions. For example the 95% PI high [95] is the high value of the prediction interval that will contain the true value of an individual observation 95% of the time.

The validation tests present encouraging results and the models predictions are considered very acceptable.

The prediction performance of the combined design was also estimated. The results of the angular design were considered the “fresh” data to compare with the combined predictions. The actual values, the predicted values and the 90% to 99% (low/high) model prediction intervals are reported in Tables 6.24, 6.25 and 6.26.

Again, model predictions are considered very encouraging.

Welding Parameters wfs/ts/wd/a.l.c	Position	Weld No	Response	Actual Value	Predicted Value	90% PI Low	90%PI High	95% PI Low	95% PI High	Percentage deviation=[(predicted-actual)/predicted]*100
11.9;1025;0.8 13%	**0°**	1	P_d	3.19	3.55	3.12	3.99	3.02	4.08	10.00
			P_{GS}	0.50	0.54	0.45	0.63	0.43	0.64	7.40
			Θ	47.5	46.9	41.77	52.06	40.66	53.17	-1.30
10;1025;1.2; 13%	**90°**	2	P_d	2.3	2.1	1.73	2.28	1.67	2.34	-9.50
			P_{GS}	0.18	0.12	0.008	0.36	0.0016	0.42	-50.00
			Θ	20.95	24.47	20.8	28.12	20.06	28.8	14.40
10;1366;0.6; 0%	**90°**	3	P_d	1.49	1.16	0.86	1.46	0.8	1.52	28.40
			P_{GS}	0	0.02	0.031	0.11	0.052	0.15	-
			Θ	23.4	22.85	19.09	26.62	18.3	27.4	-2.40
11.9;1025;1.2; 13%	**90°**	4	P_d	2.7	2.3	2.02	2.58	1.96	2.64	-17.40
			P_{GS}	0.31	0.17	0.041	0.51	0.023	0.59	-82.30
			Θ	40	35.41	31.63	39.2	30.84	39.99	-13.00
11.9;1025;0.9; 13%	**180°**	5	P_d	3.36	3.43	3.17	3.70	3.11	3.76	2.00
			P_{GS}	0.44	0.55	0.46	0.65	0.44	0.67	20.00
			Θ	79.8	85	78.06	91.98	76.6	93.44	6.10
9.4;1025;0.6; -13%	**180°**	6	P_d	2.10	1.96	1.69	2.22	1.64	2.28	-7.10
			P_{GS}	0.3	0.34	0.24	0.44	0.22	0.46	11.80
			Θ	66	59.41	52.09	66.72	50.55	68.26	-11.00
11.9;1275;1.2; 13%	**180°**	7	P_d	3.46	3.22	2.95	3.50	2.89	3.56	-7.40
			P_{GS}	0.46	0.45	0.35	0.55	0.33	0.57	-2.20
			Θ	85	82.27	74.95	89.58	73.41	91.12	-3.30

P_d= depth of penetration (mm) ; **P_{GS}**=groove sidewall penetration (mm) ; Θ=corner" angle (°)
90% PI High (Low) = This is the high (low) value of the prediction interval (PI) that will contain the true value of an individual observation 90% of the time.
wfs=wire feed speed(m/min); **ts**=travel speed(mm/min); **wd**=wire distance from sidewall (mm); **a.l.c**=arc length correction (%)

Table 6-23 Validation test results for the models in flat (0°), vertical (90°) and overhead (180°) positions

		Model Predictions											
		90% PI Low			90% PI High			Measured Values			Predicted Values		
Weld No	Position (°)	P_d (mm)	P_{GS} (mm)	Θ (°)	P_d (mm)	P_{GS} (mm)	Θ (°)	P_d (mm)	P_{GS} (mm)	Θ (°)	P_d (mm)	P_{GS} (mm)	Θ (°)
1	60	1.96	0.055	16.54	2.79	0.31	35.30	**1.86**	**0.01**	19.2	2.37	0.18	25.9
2	60	1.8	-0.004	27.02	2.66	0.20	46.12	2.25	0.198	33.9	2.22	0.13	36.57
3	60	1.44	-0.061	21.7	2.26	0.2	40.43	1.67	0	26.6	1.85	0.07	31.00
4	60	1.27	-0.11	21.51	2.09	0.15	40.21	**1.18**	0	23.8	1.68	0.02	30.86
5	60	2.12	0.22	16.17	2.98	0.49	35.20	**1.97**	**0.18**	29.1	2.55	0.35	25.6
6	60	1.44	-0.061	21.7	2.26	0.2	40.43	1.71	0	25	1.85	0.07	31
7	60	1.28	-0.003	21.26	2.14	0.27	40.39	1.85	0.09	29.55	1.71	0.13	30.82
8	60	0.75	-0.10	15.75	1.57	0.15	34.48	1.27	0	26	1.16	0.02	25.12
9	60	2.11	0.060	21.69	2.97	0.33	40.77	**3.17**	**0.368**	25.45	2.54	0.19	31.2
10	30	1.9	-0.002	35.41	2.75	0.27	54.44	2.03	0.125	47.7	2.32	0.13	44.9
11	30	1.55	0.044	29.82	2.40	0.31	48.94	1.93	0.149	**21.9**	1.97	0.18	39.4
12	30	2.23	0.10	22.13	3.05	0.36	40.95	2.25	0	**18.25**	2.64	0.23	31.5
13	30	1.38	-0.0008	29.65	2.23	0.27	48.71	1.71	**0.397**	35.5	1.80	0.13	39.1
14	30	1.90	-0.002	35.41	2.75	0.27	54.44	2.32	0.156	**34**	2.32	0.131	44.9
15	30	1.01	-0.057	24.31	1.84	0.20	43.04	1.29	0	28.8	1.43	0.07	33.7
16	30	1.18	-0.012	24.5	2.01	0.25	43.24	1.67	0.08	32.3	1.59	0.12	33.87
17	30	2.38	0.27	21.76	3.24	0.54	40.85	2.81	0.373	24.5	2.81	0.4	32.3
18	30	1.7	-0.058	21.89	2.53	0.20	40.79	2.46	0.06	35.3	2.11	0.07	31.3
19	120	1.31	-0.075	28.83	2.14	0.18	47.55	1.93	0.158	36.3	1.72	0.05	38.19
20	120	1.16	-0.017	28.43	2.01	0.25	47.48	**2.28**	0.173	30.6	1.58	0.12	37.95
21	120	1.48	-0.075	29.51	2.31	0.19	48.32	**2.81**	0.19	37.85	1.89	0.055	38.9
22	120	2.16	0.090	34.9	3.02	0.36	53.96	**3.29**	**0.376**	**34.3**	2.59	0.22	44.43
23	120	2.16	0.25	29.36	3.02	0.52	48.40	2.89	0.44	**25.8**	2.59	0.38	38.88
24	120	0.96	-0.073	23.77	1.79	0.23	42.03	1.75	0.188	26.3	1.37	0.06	33.17
25	120	0.96	-0.029	23.27	1.79	0.23	42.03	1.58	0.088	26.3	1.37	0.10	32.65
26	120	2.01	0.085	29.74	2.83	0.34	48.49	**3.02**	0.284	38.5	2.42	0.21	39.11
27	120	0.96	-0.073	23.77	1.79	0.19	42.57	1.84	0.131	**22.5**	1.37	0.06	33.17
28	150	1.47	0.060	44.32	2.32	0.33	63.38	2.32	0.166	57.2	1.90	0.19	53.84
29	150	2.99	0.33	53.9	3.85	0.6	72.99	**4**	0.55	67.2	3.42	0.46	63.4
30	150	2.16	0.10	50.24	3.01	0.44	72.8	2.98	0.399	**84**	2.58	0.24	59.79
31	150	2.47	0.17	53.68	3.32	0.44	72.8	**3.42**	**0.487**	56.5	2.9	0.30	63.24
32	150	1.11	0.004	38.97	1.93	0.26	57.69	1.75	0.192	42.3	1.52	0.13	48.33
33	150	1.80	0.16	42.78	2.62	0.42	61.60	2.36	0.322	48	2.21	0.29	52.19
34	150	2.47	0.17	53.68	3.32	0.44	72.80	3.09	0.279	53.5	2.90	0.30	63.2
35	150	1.95	0.17	47.94	2.81	0.44	67.06	2.67	0.419	**45.2**	2.38	0.30	57.50
36	150	1.80	0.16	42.78	2.62	0.42	61.60	2.37	0.262	50.3	2.21	0.29	52.19

90% PI High (Low)= This is the high (low) value of the prediction interval (PI) that will contain the true value of an individual observation 90% of the time.
P_d=depth of penetration; P_{GS}=groove sidewall penetration; Θ= Corner Angle
Bold values are outside the prediction interval

Table 6-24 Validation test results for the "combined" design for the 90% prediction intervals

		Model Predictions											
		95% PI Low			95% PI High			Measured Values			Predicted Values		
Weld Nr	Position (°)	P_d (mm)	P_{GS} (mm)	Θ (°)	P_d (mm)	P_{GS} (mm)	Θ (°)	P_d (mm)	P_{GS} (mm)	Θ (°)	P_d (mm)	P_{GS} (mm)	Θ (°)
1	60	1.88	0.029	14.7	2.87	0.34	37.14	**1.86**	**0.01**	19.2	2.37	0.18	25.9
4	60	1.19	-0.13	19.68	2.17	0.18	42.05	**1.18**	0	23.8	1.68	0.02	30.86
5	60	2.03	0.19	14.3	3.06	0.52	37.07	**1.97**	**0.18**	29.1	2.55	0.35	25.6
9	60	2.03	0.033	19.82	3.05	0.35	42.64	**3.17**	**0.368**	25.45	2.54	0.19	31.2
11	30	1.46	0.018	27.95	2.48	0.34	50.81	1.93	0.149	**21.9**	1.97	0.18	39.4
12	30	2.15	0.076	20.28	3.13	0.38	42.80	2.25	0	**18.25**	2.64	0.23	31.5
13	30	1.29	-0.027	27.78	2.32	0.29	50.58	1.71	**0.397**	35.5	1.80	0.13	39.1
20	120	1.07	-0.044	26.56	2.10	0.28	49.36	**2.28**	0.173	30.6	1.58	0.12	37.95
21	120	1.4	-0.10	27.67	2.39	0.21	50.17	**2.81**	0.19	37.85	1.89	0.055	38.9
22	120	2.07	0.064	33.03	3.10	0.38	55.83	**3.29**	0.376	34.3	2.59	0.22	44.43
23	120	2.08	0.22	27.49	3.11	0.55	50.27	2.89	0.44	**25.8**	2.59	0.38	38.88
26	120	1.93	0.06	27.9	2.91	0.37	50.34	**3.02**	0.284	38.5	2.42	0.21	39.11
29	150	2.91	0.3	52.03	3.93	0.62	74.86	**4**	0.55	67.2	3.42	0.46	63.4
30	150	2.07	0.077	48.36	3.09	0.40	71.21	2.98	0.399	**84**	2.58	0.24	59.79
31	150	2.39	0.14	51.81	3.42	0.46	74.68	3.42	**0.487**	56.5	2.9	0.30	63.24
35	150	1.87	0.14	46.06	2.89	0.46	68.94	2.67	0.419	**45.2**	2.38	0.30	57.50

95% PI High (Low)= This is the high (low) value of the prediction interval (PI) that will contain the true value of an individual observation 95% of the time.
P_d=depth of penetration; P_{GS}=groove sidewall penetration; Θ= Corner Angle
Bold values are outside the prediction interval

Table 6-25 Validation test results for the "combined" design for the 95% prediction intervals

		Model Predictions											
		99% PI Low			99% PI High			Measured Values			Predicted Values		
Weld Nr	Position (°)	P_d (mm)	P_{GS} (mm)	Θ (°)	P_d (mm)	P_{GS} (mm)	Θ (°)	P_d (mm)	P_{GS} (mm)	Θ (°)	P_d (mm)	P_{GS} (mm)	Θ (°)
11	30			24.2			54.56	1.93	0.149	**21.9**	1.97	0.18	39.4
13	30		0.079			0.35		1.71	**0.397**	35.5	1.80	0.13	39.1
21	120	1.24			2.55			**2.81**	0.19	37.85	1.89	0.055	38.9
30	150			44.63			74.94	2.98	0.399	**84**	2.58	0.24	59.79

99% PI High (Low)= This is the high (low) value of the prediction interval (PI) that will contain the true value of an individual observation 99% of the time.
P_d=depth of penetration; P_{GS}=groove sidewall penetration; Θ= Corner Angle
Bold values are outside the prediction interval

Table 6-26 Validation test results for the "combined" design for the 99% prediction intervals

6.5 Shielding Gas Trials

6.5.1 Shielding Gas Composition, Weld Profile and Arc Length

6.5.1.1 Weld Bead Profile and Arc Characteristics

Welding trials with shielding gases in different composition were carried out in narrow groove preparations (tandem PGMAW). High speed video images of the trials were recorded, weld sections were polished, etched and weld bead geometry was measured. Figure 6.110 shows the effect of carbon dioxide content in argon shielding gas on the weld geometry. It is clear that finger and round profiles occur at low and high carbon dioxide content respectively in the shielding gas. This is in accordance with other published data [44].
The shielding gas composition affects arc stability, transfer mode and arc length [44]. High speed images (Figure 6.111) show the differences in arc length measurements for different shielding gas compositions.
The criterion established prior to welding was that for a valid comparison of the effects of different shielding gas mixtures on the weld bead profile, welding trials should all be carried out at the same arc length.

a) 70%Ar30%CO_2 **b)95%Ar5%CO_2**

Fig. 6-110 Typical penetration profiles for (a) high carbon dioxide and (b) low carbon dioxide in argon shielding gas

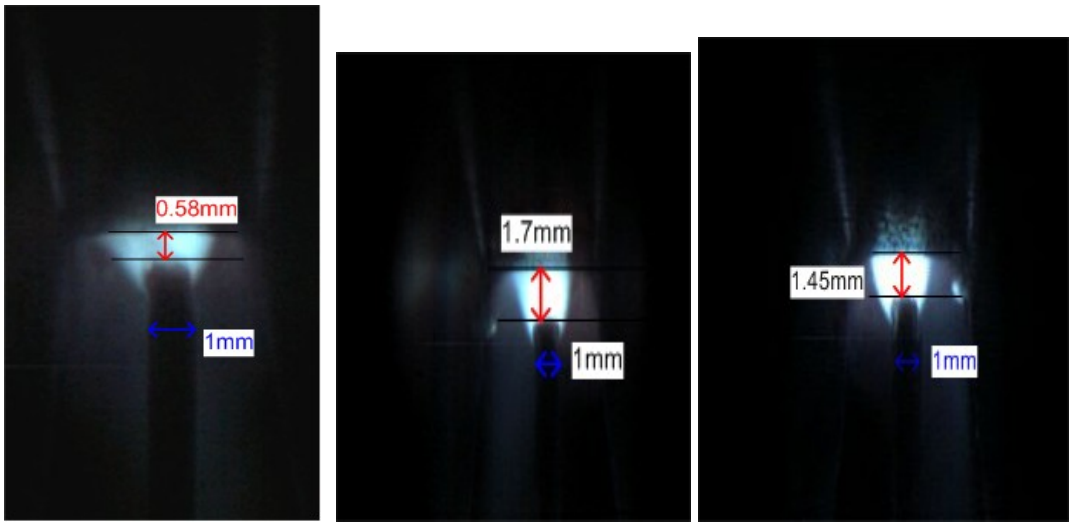

a **b** **c**

Fig. 6-111 (a) 70%Ar30%CO_2, (b)71.75%Ar6.75%$CO_2$20%He1.5%O_2 and (c) 82.5%Ar12.5%$CO_2$5%He shielding gas composition showing the different arc lengths (reference used :1.0mm wire diameter)

6.5.1.2 Arc Length and Arc Voltage Relationship

The conclusions of section 6.5.1.1 established the importance of arc length control. Several bead in groove welding trials were carried out and the relationship of arc length to arc voltage was determined.
Figure 6.112 shows arc voltage vs arc length plots for some of the shielding gases used in this experimental programme.
All welding trials were performed with the same welding conditions (section 5.3.2.1, page 84):

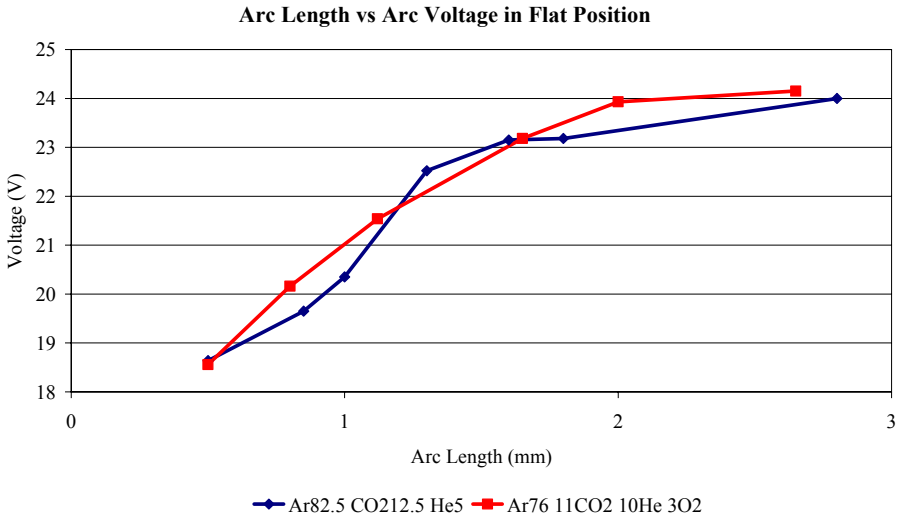

Fig. 6-112 Arc length vs arc voltage comparison plot for 82.5%Ar12.5%CO_2%5He and 76%Ar11%$CO_2$10%He3%O_2

As explained in section 5.3.2.2.1(page 89) the arc length was adjusted by the arc trim control available on the front panel of the power supply. This arc length correction mechanism allows the operator to select between a range of short to long arc lengths (-30% to +30%). Detailed information on this mechanism has not been supplied by the manufacturer (Fronius)
The high speed images revealed significant variations in the arc length during the process and the average of several arc length measurements is considered as the actual arc length. Arc length correction vs arc voltage plots are reported in Figure 6.113.
However, it is necessary to underline that the relationships described in the following graphs (Figure 6.113 to 6.119) are likely to be due to particular algorithms in the Fronius TPS 4000 power sources

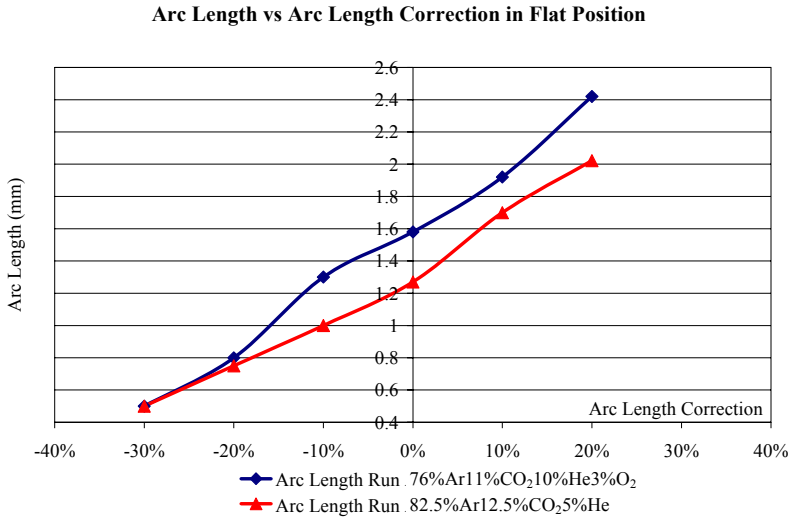

Fig. 6-113 Arc length correction vs arc voltage for 82.5%Ar12.5%$CO_2$5%He and 76%Ar11%$CO_2$10%He 3O_2 shielding gases

Arc voltage and arc length plots were developed in overhead position for some of the shielding gases and are reported in Figure 6.114.

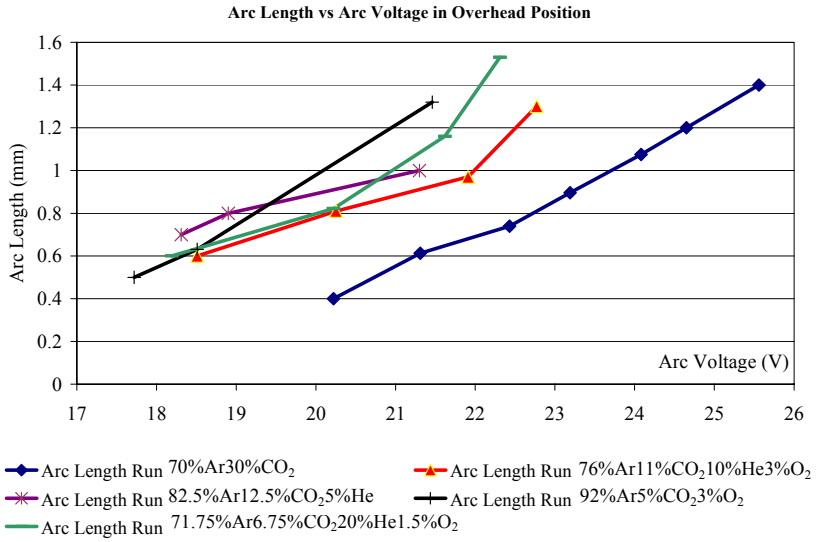

Fig. 6-114 Arc length vs arc voltage plots for some of the shielding gases in the overhead position

Arc length correction vs arc length plots are shown in Figure 6.115

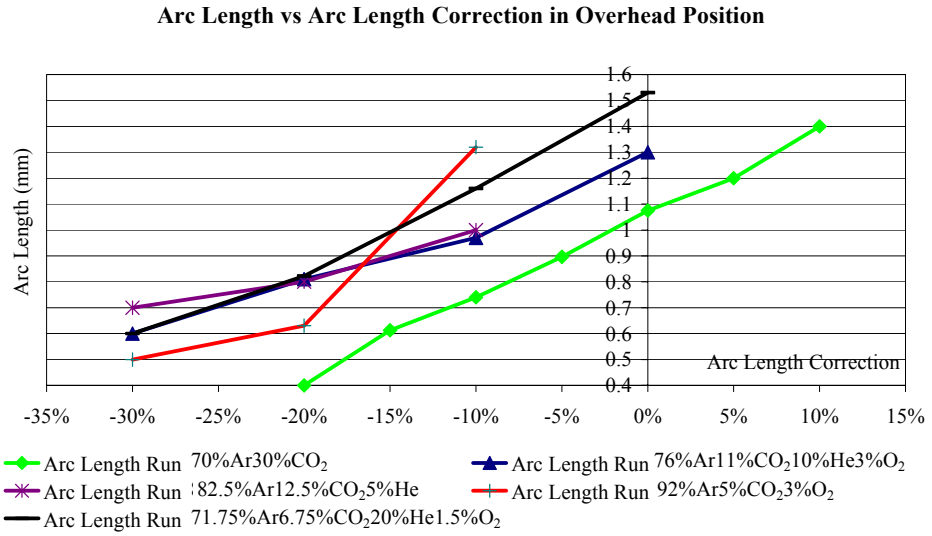

Fig. 6-115 Arc length vs arc length correction plots for some of the shielding gas compositions in the overhead position

6.5.1.3 Welding Current and Arc Length

In section 6.5.1.2 arc length and arc voltage relationships were established. Generally, in this experimental work with the Fronius power supplies an increase in arc length correction (arc length) produces an increase in the welding current (Figures 6.116, 6.117, 6.118 and 6.119). The mean current values refer to the lead and trail wires.

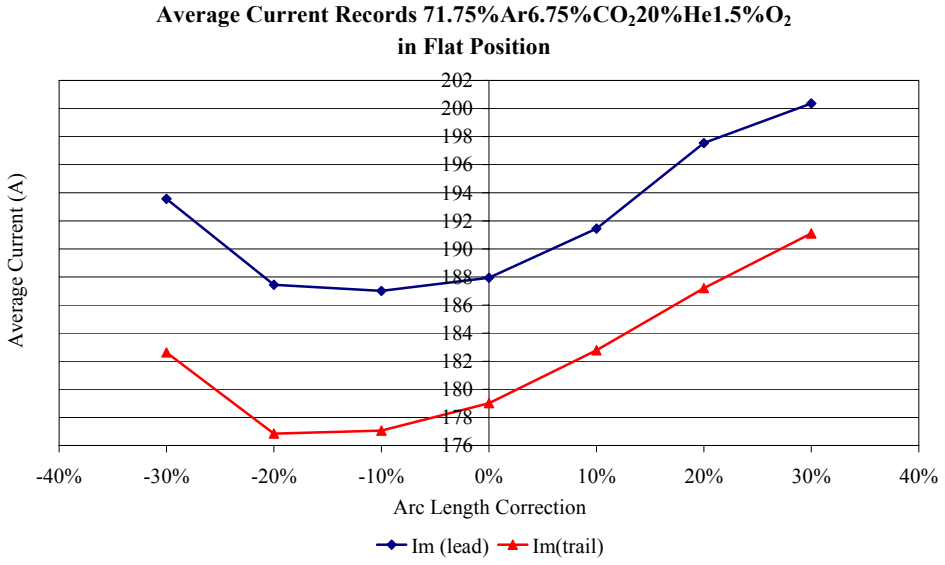

Fig. 6-116 Current traces vs arc length correction plots for the shielding gas 71.75%Ar6.75%$CO_2$20%He1.5%O_2

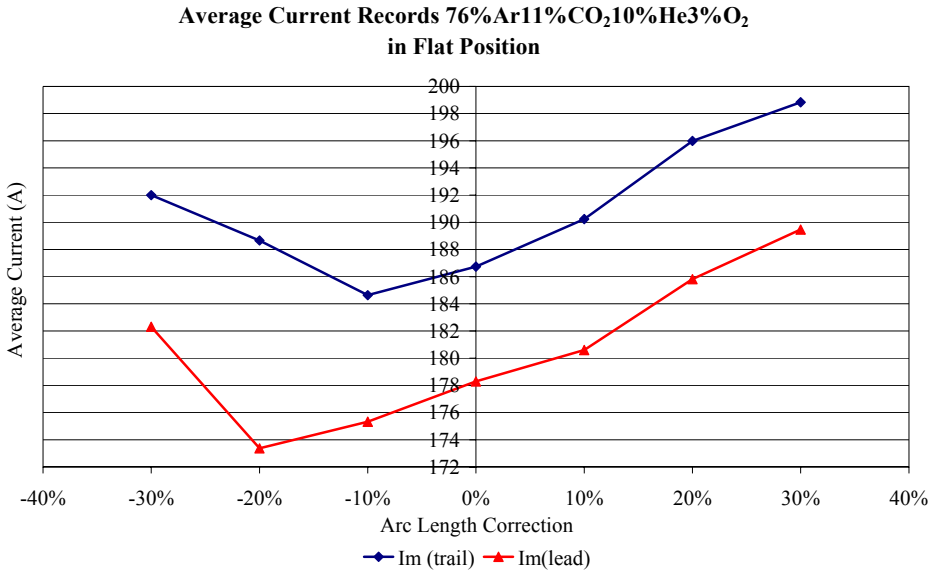

Fig. 6-117 Current traces vs arc length correction plots for the shielding gas 76%Ar11%$CO_2$10%He3%O_2

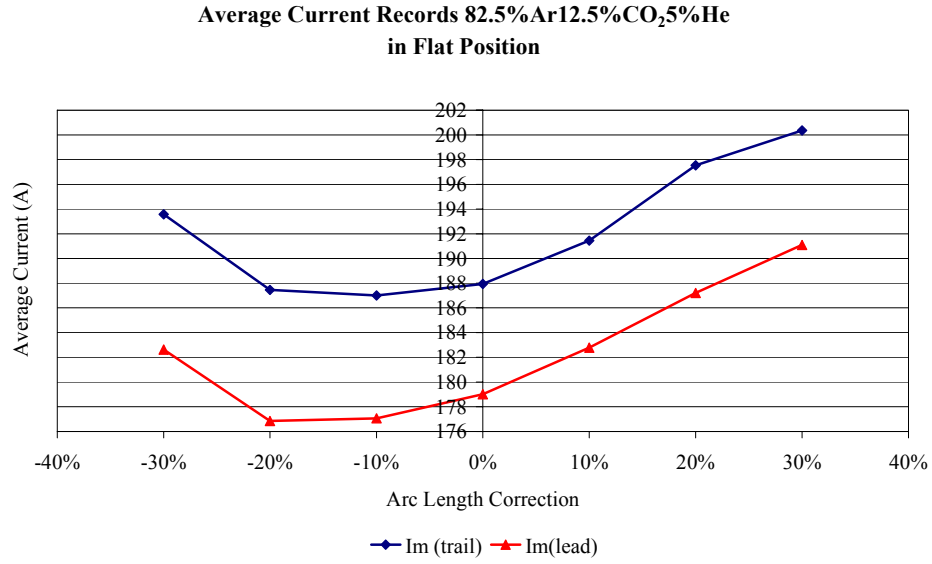

Fig. 6-118 Current traces vs arc length correction plots for the shielding gas 82.5%Ar12.5%$CO_2$5%He

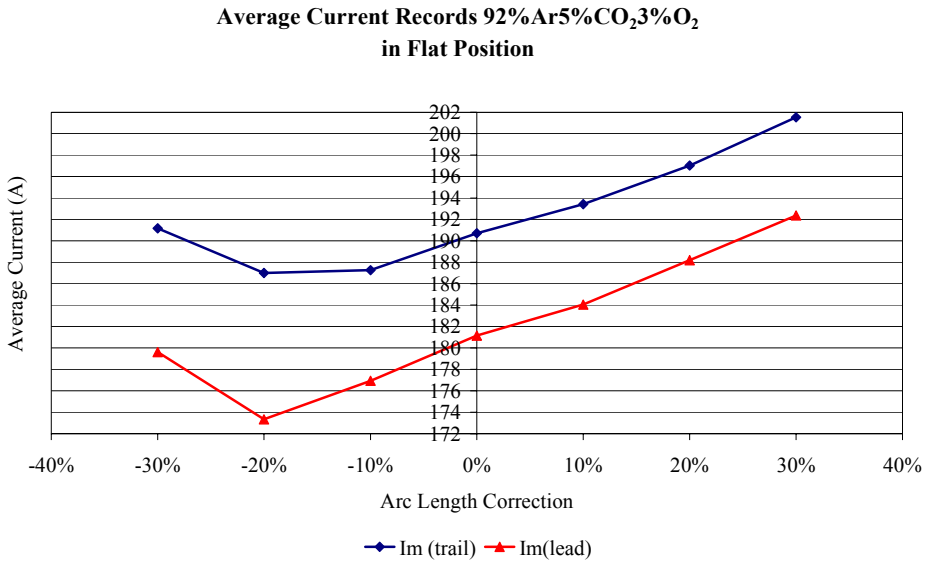

Fig. 6-119 Current traces vs arc length correction plots for the shielding gas 92%Ar5%$CO_2$3%O_2

6.5.1.4 Weld Bead Profiles for Different Arc Lengths

As-welded bead profiles and macrograph sections in both flat and overhead positions, representative of different arc lengths are shown in Figure 6.120. All welds were carried out with the same welding conditions.

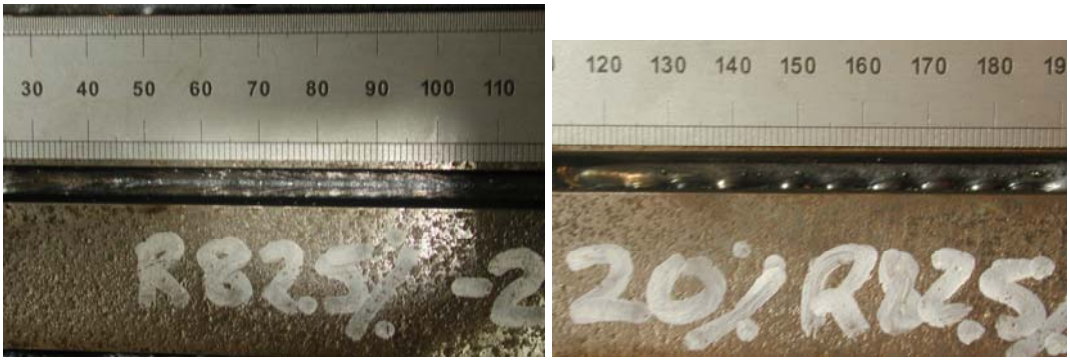

a)A.L.C=-20% **b) A.L.C=+20%**

Fig. 6-120 Weld bead profiles for different arc length correction values and for the shielding gas composition 82.5%Ar12.5%$CO_2$5%He in flat position

There are some uncertainties in determining a precise value for the arc length, which can be attributed to one or both of the following reasons:

- pulsed GMAW is generally a process where arc length varies considerably during the process. Figure 6.121 includes three different arc lengths measured for a weld lasting 1s .

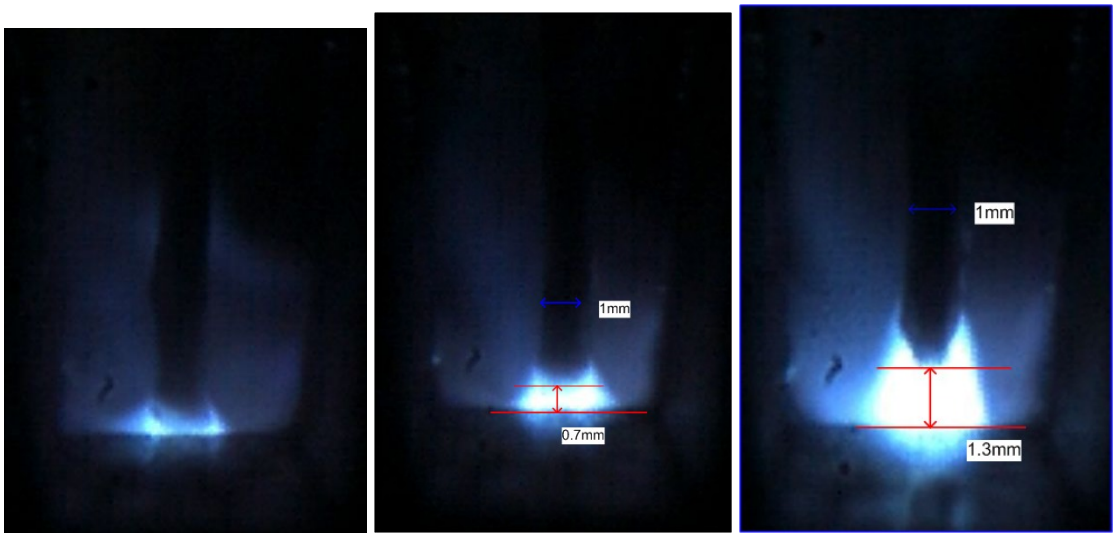

Fig. 6-121 Arc length variation during the PGMAW process

- errors in the measurements depending on individual evaluations, quality of images etc.

The following Figures 6.122 shows a series of welds performed in the range of the shortest (-30%) to the longest (+30%) arc lengths and emphasise the importance of the arc length on the weld bead profile. Generally, long arcs result in an erratic arc and significant sidewall defects.

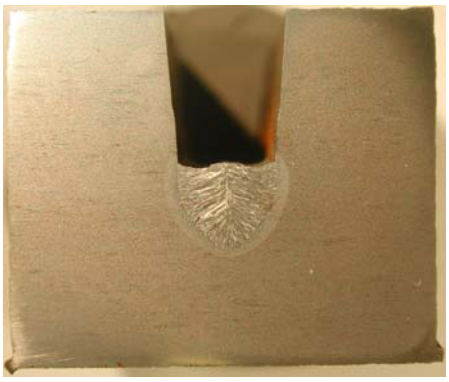

a) A.L.C=-30%

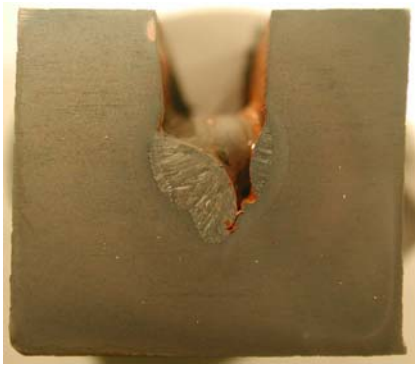

b) A.L.C=+30%

b) A.L.C=-20%

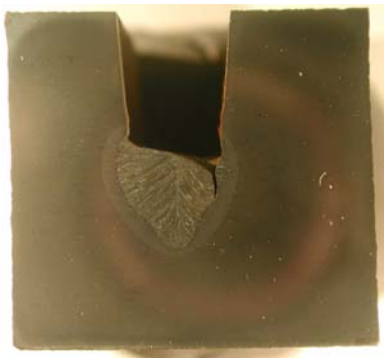

f) A.L.C=+20%

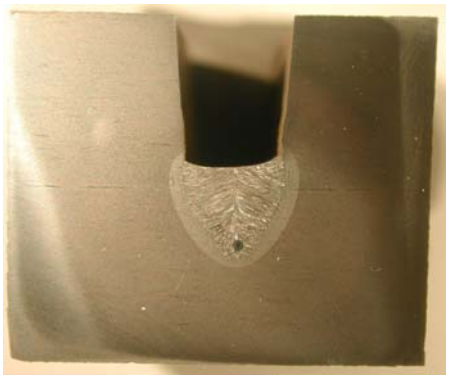

c) A.L.C=-10%

e) A.L.C=+10%

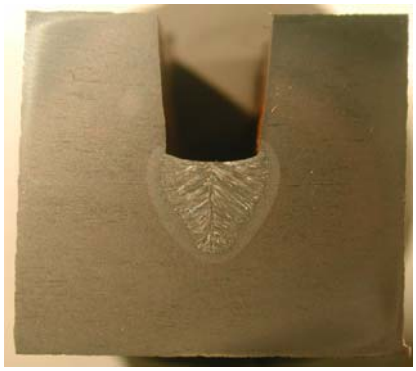

d) A.L.C=0%

Fig. 6-122 Macrographs of welds carried out at different arc length correction values and for the shielding gas composition 82.5%Ar 12.5%$CO_2$5%He in the flat position

Figures 6.123 and 6.124 show macrographs of welds performed at the same arc length in flat and overhead positions using 92%Ar5%$CO_2$3%O_2 as shielding gas. Different weld bead geometries were produced in the two positions.

A.L.C=-30% (flat)

A.L.C=-30% (overhead)

A.L.C=-20% (flat)

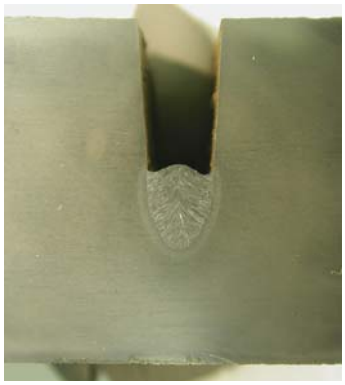

A.L.C=-20% (overhead)

A.L.C=-10% (flat)

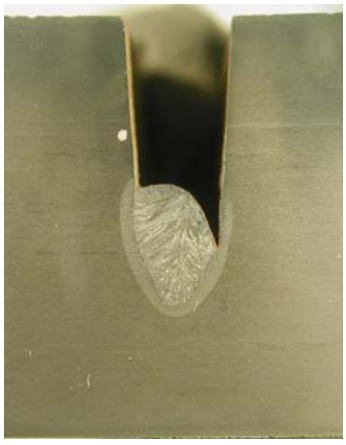

A.L.C=-10%(overhead)

Fig. 6-123 Macrographs of welds performed at different arc length correction values and positions (flat/overhead) for the shielding gas composition 92%Ar5%$CO_2$3%O_2

A.L.C=+30% (flat)

A.L.C=+20% (flat

A.L.C=+10% (flat)

A.L.C=0% (flat)

Fig. 6-124 Macrographs of welds performed at different arc length correction values and positions (flat/overhead) for the shielding gas composition 92%Ar5%$CO_2$3%O_2

6.5.1.5 Welding Current and Voltage Traces and Shielding Gas Composition

The "stability" of the arc was assessed using the current and voltage traces recorded during welding with the various shielding gas mixtures. Some typical voltage records are shown in Figures 6.125 and 6.126.

All records refer to the same recording time and were extracted from the middle part of the full waveform, avoiding the beginning and the end parts of the welds where instabilities most frequently occur.

Welds performed with shielding gas rich in carbon dioxide more frequently developed short circuit transfers indicated by low voltage spikes. However, when shielding gas compositions with low carbon dioxide content were used, fewer dip transfer signals were recorded.

In the graphs below both lead (V_l) and trail (V_t) wire voltage traces were recorded.

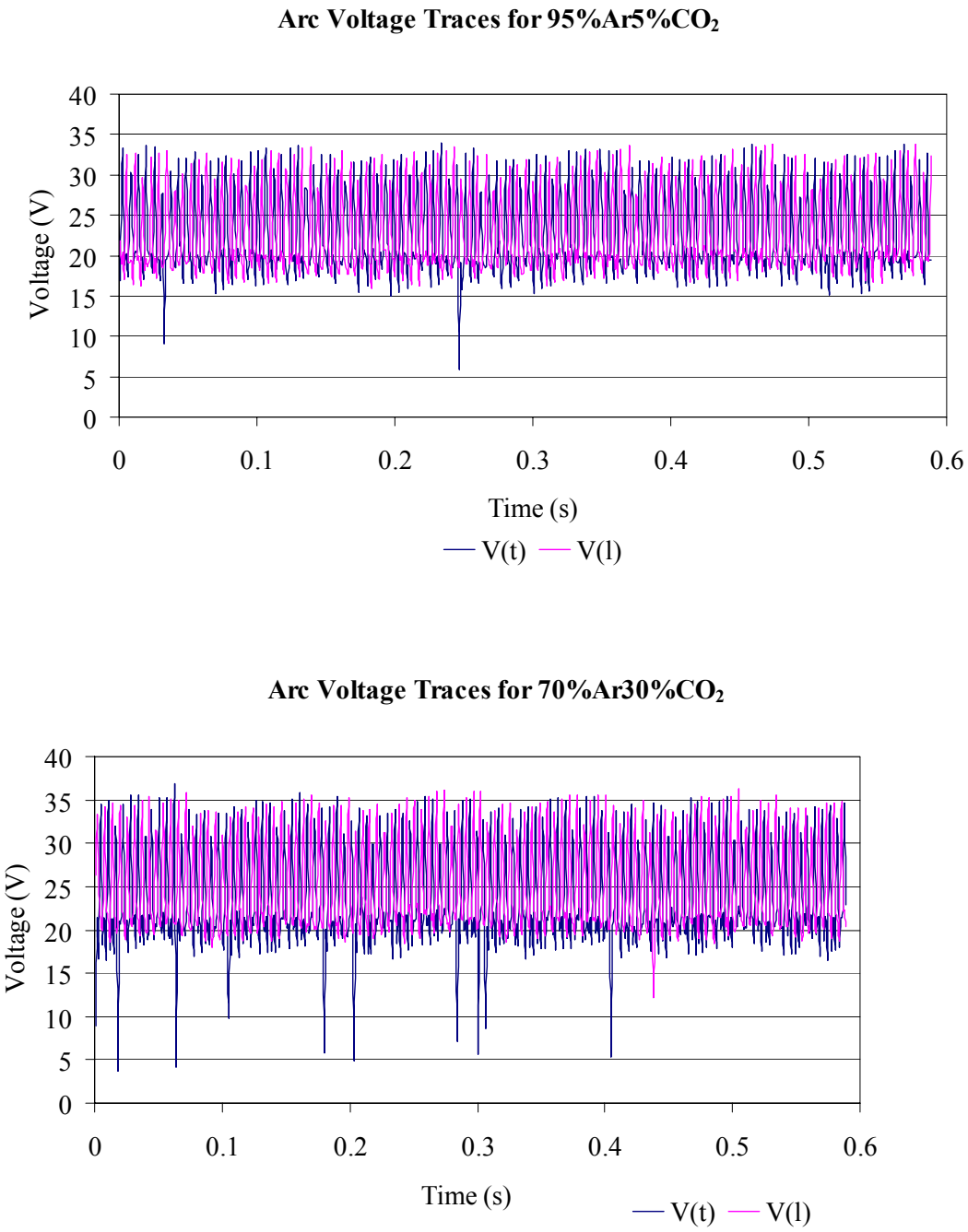

Fig. 6-125 Arc voltage traces for welds performed with different shielding gas compositions

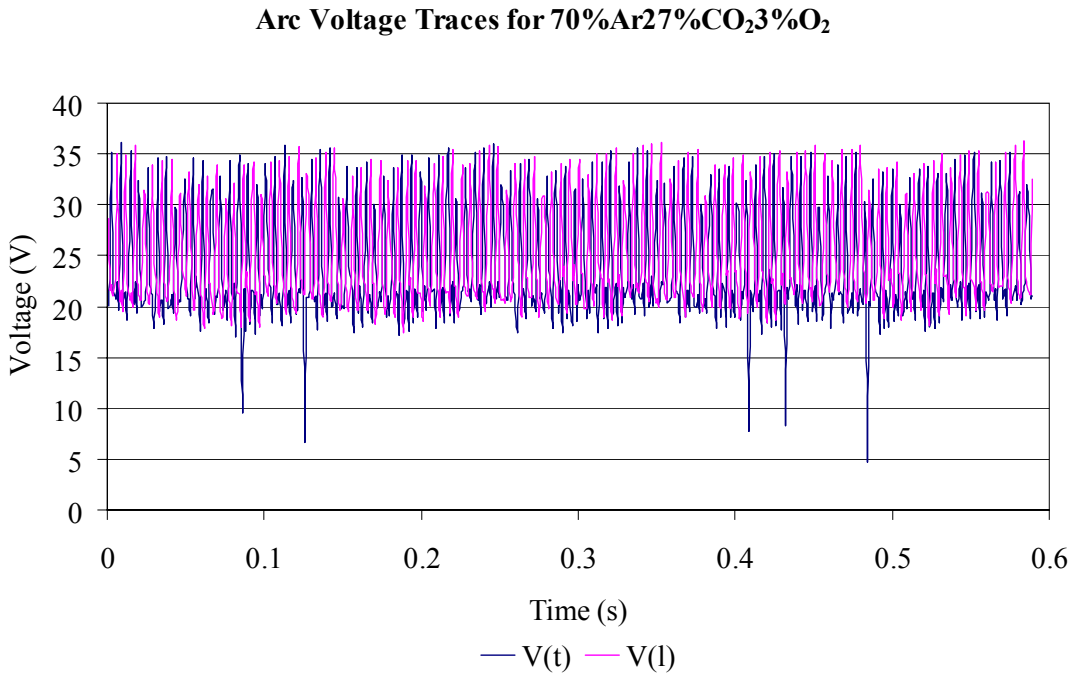

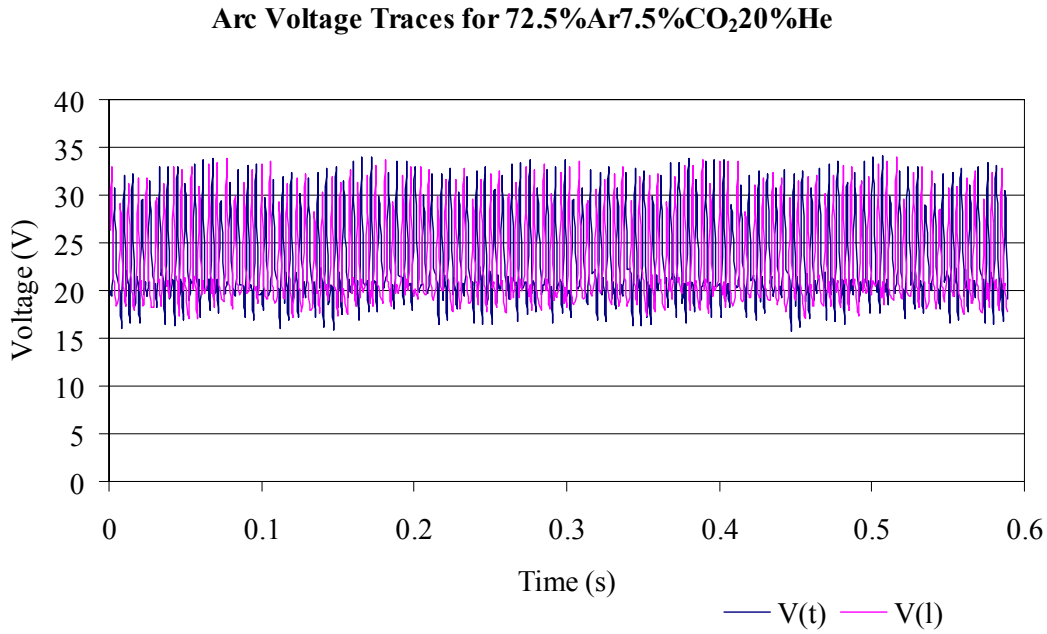

Fig. 6-126 Arc voltage traces for welds performed with different shielding gas compositions

6.5.2 Shielding Gas Thermal Cycle Trials

Thermocouple cycle measurements were carried out for the welds in Table 5.3 (page 85) to investigate if significant differences in the cooling times occur depending on the shielding gas composition. The thermocouple wires were harpooned in the weld pool.

All welds were tested at the same preheating temperature (100°C).
No significant trends in the cooling time in relation to the different shielding gas compositions were reported. Some examples are shown in Figures 6.127 and 6.128 below:

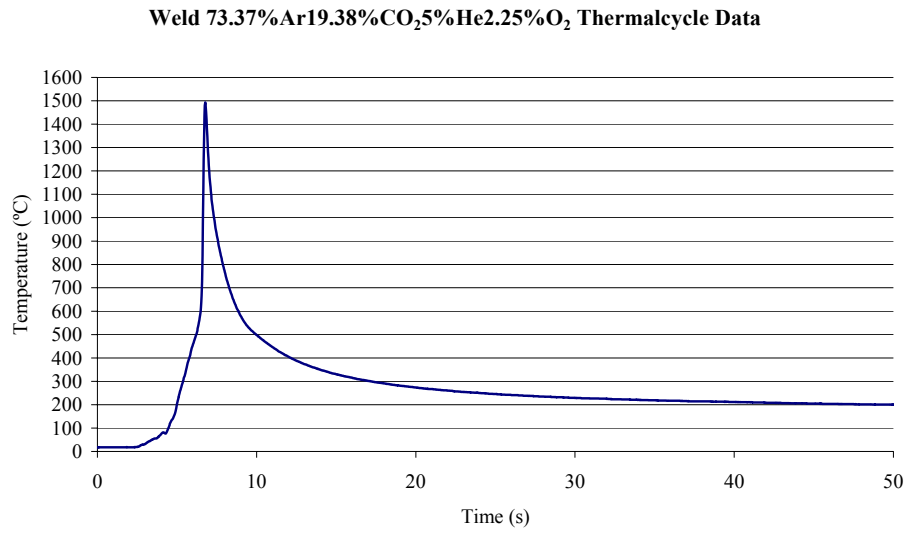

Fig. 6-127 Typical thermal cycle for narrow groove weld bead in tandem PGMAW

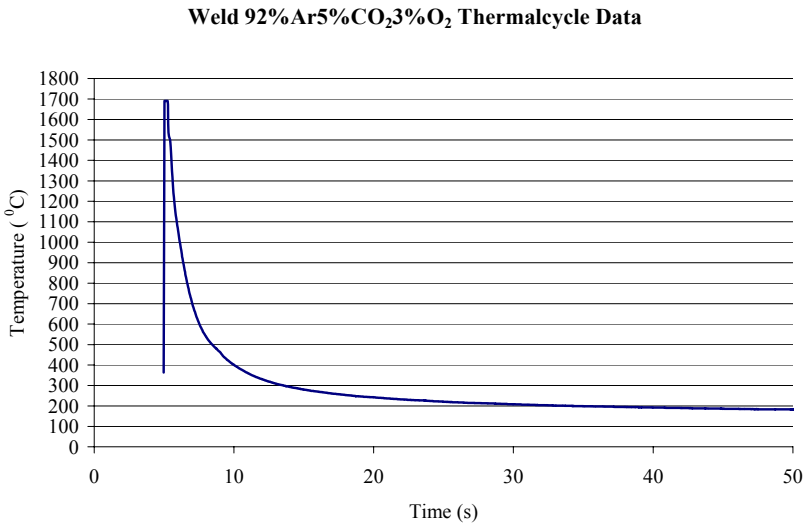

Fig. 6-128 Typical thermal cycle for narrow groove weld bead in tandem PGMAW

Examination of the cooling curves allowed the identification of the peak temperature of the weld pool and the estimation of the cooling times from 800°C to 500°C, 400°C and 300°C. The cooling times recorded for all gas compositions are reported in Table 6.27.

Shielding Gas Composition	t_{800} (s)	t_{500} (s)	t_{400} (s)	t_{300} (s)	t_{800}-t_{500} (s)	t_{800}-t_{400} (s)	t_{800}-t_{300} (s)
84.38%Ar8.38%$CO_2$5%He 2.25%O_2	4.99	7.12	9.4	15.72	2.13	4.41	10.73
95%Ar 5%CO_2(A.L.C= 0%) (A.L.C= -10%)	3.58 6.75	5.62 8.37	7.97 10.04	13.85 13.15	2.04 1.62	4.39 3.29	10.27 6.4
77.33%Ar20.67%$CO_2$2%O_2							
82.5%Ar17.5%CO_2	4.44	6.12	8.07	12.07	1.68	3.63	7.63
92%Ar5%$CO_2$3%O2 (A.L.C= -10%)	6.29	7.74	9.56	12.5	1.4	3.27	6.21
95%Ar5%CO_2	5.09	6.99	9.59	15.82	1.9	4.5	10.73
70%Ar30%CO_2	9.58	11.42	13.8	19.12	1.84	4.22	9.54
82%Ar5%$CO_2$10%He3%O_2(A.L.C= 0%) (A.L.C= -10%)	10.3 8.27	12.7 9.75	15.4 11.1	22.52 13.65	2.4 1.48	5.1 2.83	12.22 5.38
81%Ar16%$CO_2$3%O2	9.09	11.00	12.97	17.32	1.91	3.88	8.23
70%Ar27%$CO_2$3%O_2	7.44	9.47	11.24	16.12	2.03	3.8	8.68
70%Ar20%$CO_2$10%He	4.74	6.55	8.45	12.52	1.81	3.71	7.78
71.75%Ar6.75%$CO_2$20%He1.5%O_2 (A.L.C= 0%) (A.L.C= -10%)	7.65 6.13	9.67 7.51	11.5 9.01	15.57 11.47	2.02 1.38	3.85 2.88	7.92 5.35
85%Ar5$CO_2$10%He	8.34	9.96	11.86	15.25	1.62	3.52	6.91
80%Ar13.33%$CO_2$6.67%He	7.07	8.76	10.90	15.27	1.69	3.83	8.2
73.37%Ar19.38%$CO_2$5%He 2.25%O_2	7.88	9.97	12.16	17.15	2.09	4.28	9.27
73.37%Ar10.88%$CO_2$15%He 0.75%O_2	5.51	7.21	8.97	13.05	1.7	3.46	7.54
70%Ar27%$CO_2$3%O_2	7.45	9.37	11.12	15.50	1.92	3.67	8.05
72.5%Ar7.5%$CO_2$20%He	6.62	8.26	10.12	13.60	1.64	3.5	6.98
70%Ar30%CO_2	7.83	9.82	11.64	15.70	1.99	3.81	7.88
92%Ar5%$CO_2$3%O_2	6.66	8.45	10.02	13.50	1.79	3.36	6.84
85%Ar5%$CO_2$10%He	5.44	6.91	8.50	11.22	1.47	3.06	5.78
76%Ar11%$CO_2$10%He3%O_2 (A.L.C= 0%) (A.L.C= -10%)	3.23 4.82	5.15 6.32	6.69 7.71	10.15 10.30	1.92 1.51	3.46 2.89	6.92 5.48
70%Ar17%$CO_2$10%He3%O_2	6.7	8.55	10.09	13.55	1.85	3.39	6.85
70%Ar7%$CO_2$20%He3%O_2 (A.L.C= 0%) (A.L.C= -10%)	8.61 6.00	10.27 7.38	12.02 8.82	15.4 11.15	1.66 1.38	3.41 2.82	6.79 5.15
82.5%Ar12.5%$CO_2$5%He	12.39	14.77	16.42	18.36	2.38	4.03	5.97
82.5%Ar12.5%$CO_2$5%He (BOC)	7.83	9.37	11.30	14.50	1.54	3.47	6.67

Table 6-27 Thermal cycle data (cooling times) for the shielding gas trials

A few trials tested the significance of the arc length on the cooling rates for a given gas mixture (Table 6.27) and the corresponding thermal cycles are shown in Figures 6.129 and 6.130. For simplicity, the percentage of the A.L.C rather than the actual arc length is reported. An A.L.C of -10% compared to an A.L.C of 0% provides an approximately 0.5mm shorter arc length.

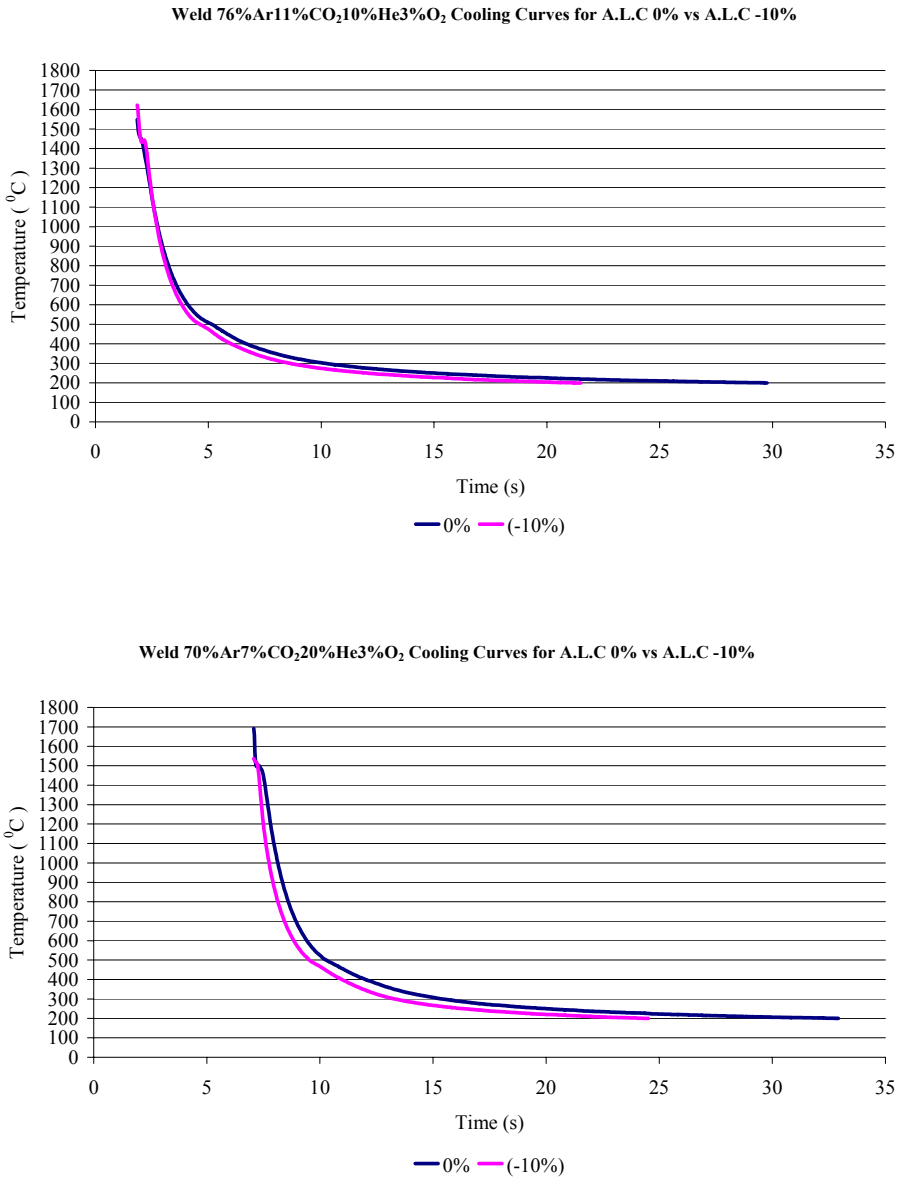

Fig. 6-129 Comparison cooling curves for welds performed at different arc lengths and shielding gas compositions

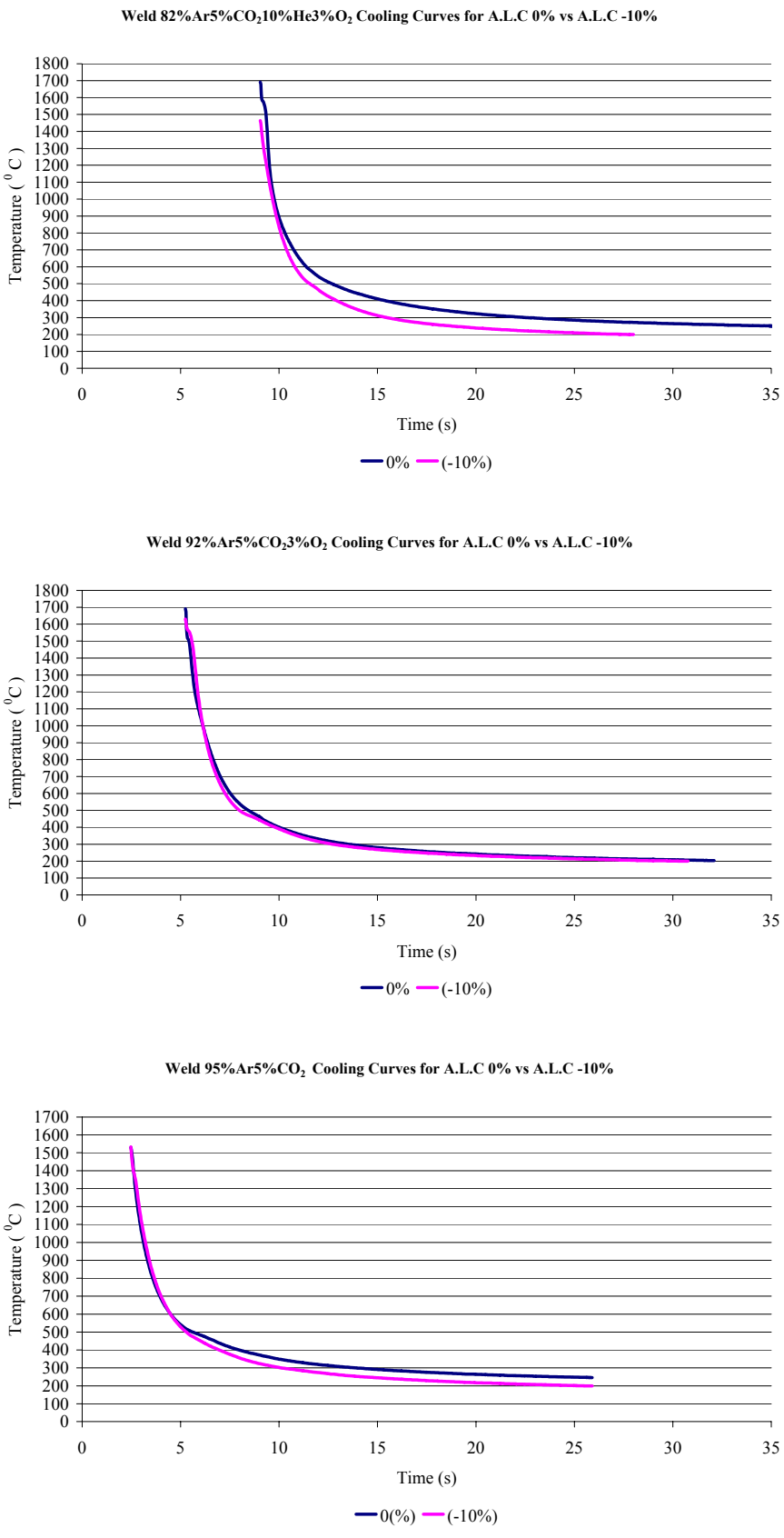

Fig. 6-130 Comparison cooling curves for welds performed at different arc lengths and shielding gas compositions

The above thermal cycle graphs show that welds at shorter arc lengths typically produce faster cooling rates than welds at longer arc lengths.

6.5.3 Shielding Gas Trials

The welds were carried out in the order shown in Table 5.3 (page 85), in the flat position and with the same welding conditions (section 5.3.2.1, page 84)).
The weld bead dimensions considered in the analysis are depth of penetration, sidewall penetration and concavity and the results are shown in Table 6.28. Two additional welds performed with the commercial gas BOC 82.5%Ar12.5%$CO_2$5%He and the same shielding gas composition the gas mixer, were included in the analysis.
The mathematical models developed for the three responses together with the units of the responses are shown below:
P_d; Depth of penetration: mm
P_α; Average sidewall penetration: mm
ζ; Concavity: mm
G_{Ar}=Argon
G_{CO2}=Carbon Dioxide
G_{He}=Helium
G_{O2}=Oxygen

1. Depth of Penetration (P_d)

a) actual components:

$$P_d = 0.0172 \cdot G_{Ar} - 0.125 \cdot G_{CO2} + 0.0551 \cdot G_{He} - 0.804 \cdot G_{O2} + 2.723 \cdot 10^{-3} \cdot G_{Ar} \cdot G_{CO2} + 0.0104 \cdot G_{Ar} \cdot G_{O2} + 0.0812 \cdot G_{CO2} \cdot G_{O2} - 1.067 \cdot 10^{-3} \cdot G_{Ar} \cdot G_{CO2} \cdot G_{O2} \quad \textbf{Eqn. 6. 35}$$

2. Sidewall Penetration (P_α)

b) actual components:

$$P_\alpha = 1.446 \cdot 10^{-3} \cdot G_{Ar} - 0.0363 \cdot G_{CO2} + 4.634 \cdot 10^{-3} \cdot G_{He} + 0.0198 \cdot G_{O2} + 6.552 \cdot 10^{-4} \cdot G_{Ar} \cdot G_{CO2} + 6.14 \cdot 10^{-4} \cdot G_{CO2} \cdot G_{He} - 3.054 \cdot 10^{-3} \cdot G_{He} \cdot G_{O2} \quad \textbf{Eqn. 6. 36}$$

3. Concavity (ζ)

c) actual components:

$$\zeta = 3.263 \cdot 10^{-3} \cdot G_{Ar} + 0.0139 \cdot G_{CO2} + 4.181 \cdot 10^{-3} \cdot G_{He} + 0.0283 \cdot G_{O2} \quad \textbf{Eqn. 6. 37}$$

The analysis of variance (Table 6.29) and the diagnostic plots did not present significant discrepancies except the predicted vs actual values (Figure 6.131) for the concavity response, where, some scatter was reported.

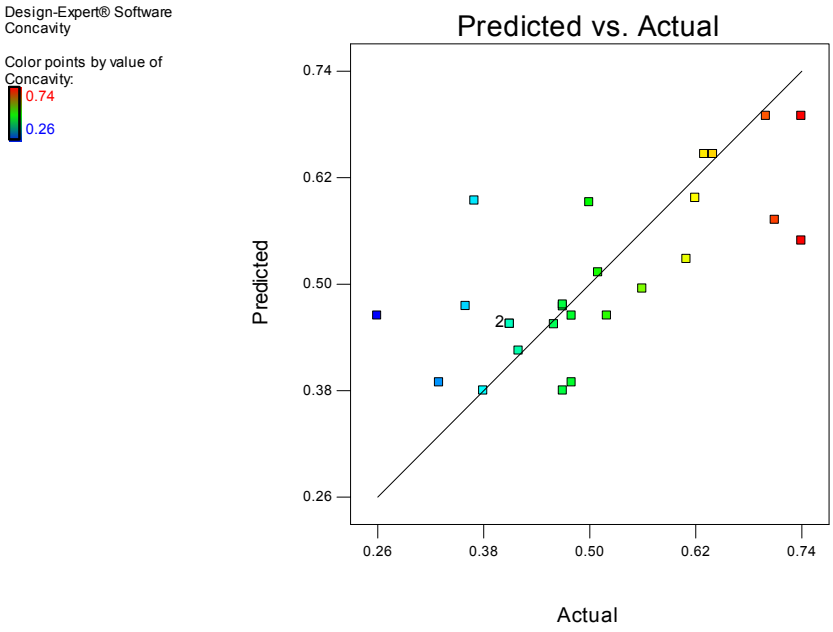

Fig. 6-131 Predicted vs actual plot for the response concavity

This scatter in the prediction plot together with the low values of the Pred.R-squared and Adj.R-squared (Table 6.29) indicate that model predictions for concavity should be treated with some caution. Nevertheless, the model was accepted for further analysis and conclusions will be reported accordingly.

6.5.4 Modelling Results

The gas mixture 82.5%Ar12.5%$CO_2$5%He was established as the reference blend and the model predictions for the reference blend were calculated. Each component (CO_2/He/O_2) was varied within its range while the other components remained constant. For each of the compositions the model predictions were estimated and the normalised change to the reference blend prediction was calculated. (Table 6.30).
The percentage of the normalised change was plotted at the different factor levels and the magnitude of the contribution to the response was established.

1. Depth of Penetration

The following plot (Figure 6.132) show the effect of carbon dioxide, helium and oxygen on depth of penetration. Carbon dioxide has the most significant effect on depth of penetration: an increase of 15% in carbon dioxide produces an increase of almost 24% in depth of penetration.

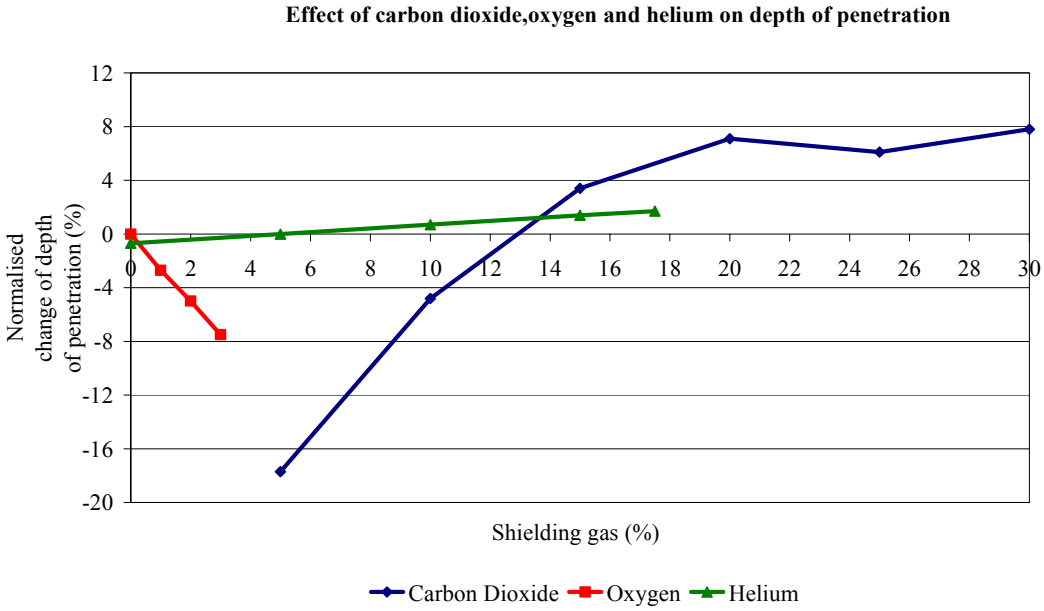

Fig. 6-132 Effects of carbon dioxide, oxygen and helium on depth of penetration

2 Sidewall Penetration

Figure 6.133 shows the effect of carbon dioxide, oxygen and helium on sidewall penetration. The major contribution to sidewall penetration is attributed to carbon dioxide with a smaller contribution attributed to helium.

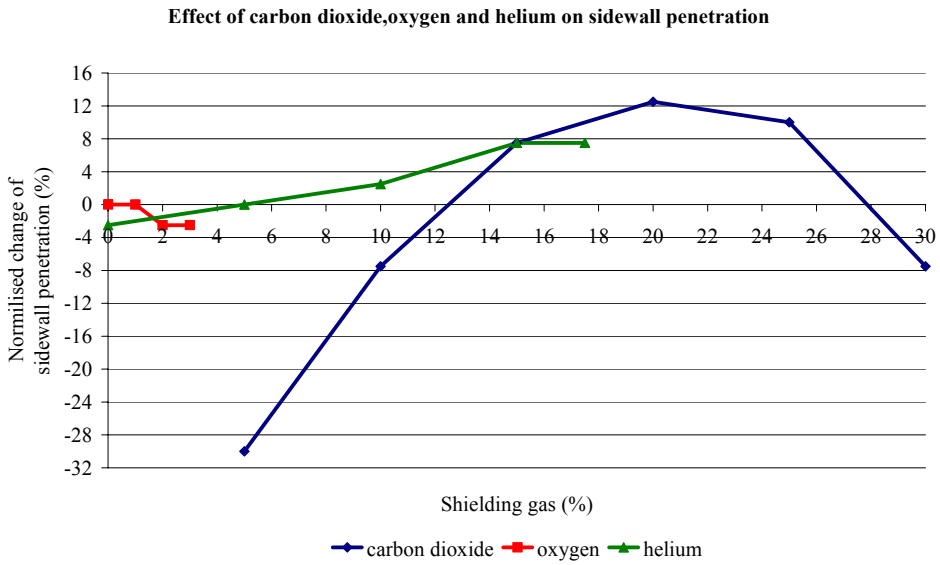

Fig. 6-133 Effects of carbon dioxide, oxygen and helium on sidewall penetration

3 Concavity

Figure 6.134 shows the effect of the three gas components on concavity.
The strong influence of the carbon dioxide is reported followed by the effect of oxygen.
The effect of helium is insignificant.

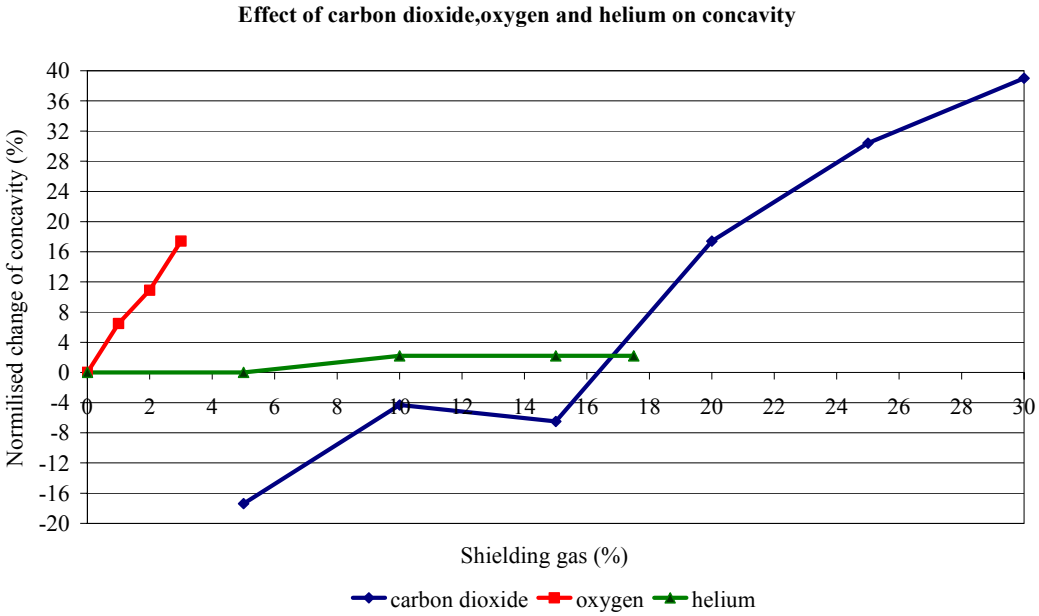

Fig. 6-134 Effects of carbon dioxide, oxygen and helium on concavity

The average current and voltage values for all the experiments and the calculated power (P=V x I) are reported in Table 6.31.

	Responses		
Weld No. (Run No.)	Depth of Penetration (mm)	Sidewall Penetration (mm)	Concavity (mm)
1	3.13	0.41	0.64
2	3.12	0.46	0.51
3	3.04	0.39	0.36
4	2.88	0.37	0.42
5	2.67	0.49	0.71
6	3.22	0.39	0.47
7	3.06	0.45	0.37
8	2.73	0.28	0.61
9	3.22	0.44	0.7
10	2.49	0.34	0.41
11	2.45	0.3	0.48
12	3.17	0.34	0.63
13	3.03	0.36	0.5
14	2.39	0.33	0.48
15	3.18	0.43	0.62
16	2.56	0.29	0.33
17	2.64	0.30	0.47
18	3.05	0.51	0.74
19	3.26	0.40	0.56
20	2.67	0.26	0.56
21	2.71	0.25	0.46
22	2.74	0.34	0.26
23	2.9	0.43	0.52
24	2.37	0.27	0.41
25	2.37	0.21	0.47
26	2.32	0.33	0.38

Weld No. 22=Cranfield 82.5%Ar12.5%$CO_2$5%He,
Weld No. 23=BOC Commercial 82.5%Ar12.5%$CO_2$5%He

Table 6-28 Measured weld bead geometry responses for the shielding gas trials

Response	Type of Model	Chosen Variables	Pred.R-squared	Adj.R-squared.	F-value	P-value (Prob.>F)	Std. dev.	Adeq. Precision	PRESS	Lack of Fit	
										F-value	P-value
Depth of Penetration (mm)	Cubic	Ar /CO_2 /He /O_2 /Ar*CO_2 /Ar*O_2 /CO_2*O_2 /Ar*CO_2*O_2	0.83	0.88	27.31	<0.0001 (significant)	0.11	16.34	0.41	2.29	0.16 (not significant)
Sidewall Penetration (mm)	Quadratic	Ar /CO_2 /He /O_2 /Ar*CO_2 / CO_2*He /He*O_2	0.50	0.68	9.95	<0.0001 (significant)	0.044	10.38	0.08	0.50	0.86 (not significant)
Concavity (mm)	Linear	Ar /CO_2 /He /O_2	0.37	0.44	7.58	0.0012 (significant)	0.1	8.06	0.27	1.21	0.43 (not significant)

Table 6-29 Selected variables, model order after backward elimination and statistical parameters of shielding gas trials

Shielding Gas Composition	Predicted Depth of Penetration (mm)	Normalised Change of Predicted Depth of Penetration (*) (%)	Predicted Sidewall Penetration, (mm)	Normalised Change of Predicted Sidewall Penetration (*) (%)	Predicted Concavity (mm)	Normalised Change of Predicted Concavity (*) (%)
Reference blend 82.5%Ar12.5%$CO_2$5%He	**2.94**		**0.4**		**0.46**	
90%Ar5%$CO_2$5%He	2.42	-17.69	0.28	-30	0.38	-17.39
85%Ar10%$CO_2$5%He	2.8	-4.76	0.37	-7.5	0.44	-4.35
80%Ar15%$CO_2$5%He	3.04	3.4	0.43	7.5	0.49	6.52
75%Ar20%$CO_2$5%He	3.15	7.14	0.45	12.5	0.54	17.39
70%Ar25%$CO_2$5%He	3.12	6.12	0.44	10	0.6	30.43
70%Ar30%CO_2	3.17	7.82	0.37	-7.5	0.64	29.13
82.5%Ar12.5%$CO_2$5%He0%O_2	2.94	0	0.4	0	00.4	0
81.5%Ar12.5%$CO_2$5%He1%O_2	2.86	-2.72	0.4	0	0.49	6.52
80.5%Ar12.5%$CO_2$5%He2%O_2	2.79	-5.1	0.39	-2.5	0.51	10.87
79.5%Ar12.5%$CO_2$5%He3%O_2	2.72	-7.48	0.39	-2.5	0.54	17.4
87.5%Ar12.5%$CO_2$0%He	2.92	0.7	0.39	-2.5	0.46	0
82.5%Ar12.5%$CO_2$5%He	2.94	0	0.4	0	0.46	0
77.5%Ar12.5%$CO_2$10%He	2.96	0.7	0.41	2.5	0.47	2.17
72.5%Ar12.5%$CO_2$15%He	2.98	1.36	0.43	7.5	0.47	2.17
70%Ar12.5%$CO_2$17.5%He	2.99	1.7	0.43	7.5	0.47	2.17

(*)Normalised Change=[(Predicted Value-Predicted Value of the Reference Blend)/ Predicted Value of the Reference Blend] 100

Table 6-30 Normalised change of depth of penetration, sidewall penetration and concavity for the effects of carbon dioxide, helium and oxygen

Shielding Gas Composition	Vm(l)	Vm(t)	Im(l)	Im(t)	A.L.C (%)	P=IxV
84.38%Ar 8.38%CO_2 5%He 2.25%O_2	22.307	22.914	184.83	172.41	0	8074
73.37%Ar 19.38%CO_2 5%He 2.25%O_2	23.115	24.223	183.38	168	0	8308
73.37%Ar 10.88%CO_2 15%He 0.75%O_2	22.864	23.0944	184.27	170.50	0	8151
76%Ar 11%CO_2 10%He 3%O_2	21.285	22.336	185.48	173.95	-10	7833
70%Ar 17%CO_2 10%He 3%O_2	22.775	23.44	183.95	169.61	0	8165
70%Ar 7%CO_2 20%He 3%O_2	21.072	21.999	186.24	174.77	-10	7769
70%Ar 7%CO_2 20%He 3%O_2	21.072	21.99	186.24	174.77	0	7768
82%Ar 5%CO_2 10%He 3%O_2	20.742	22.005	186.60	174.84	-10	7718
77.33%Ar 20.67%CO_2 2%O_2	23.912	24.230	182.32	169.46	0	8466
92%Ar 5%CO_2 3%O_2	21.215	22.013	186.09	174.73	-10	7794
81%Ar 16%CO_2 3%O_2	22.687	23.764	183.61	168.99	0	8182
70%Ar 27%CO_2 3%O_2	24.326	24.696	181.72	167.04	0	8546
70%Ar 27%CO_2 3%O_2	23.57	24.75	181.41	167.32	0	8417
					0	
95%Ar 5%CO_2	20.49	21.32	187.59	175.96	-10	7595
82.5%Ar 17.5%CO_2	23.673	23.991	182.44	170.09	0	8400
70%Ar 30%CO_2	23.19	24.675	182.21	170.00	0	8420
70%Ar 30%CO_2	23.808	24.519	181.99	171.00	0	8526
70%Ar 20%CO_2 10%He	23.713	24.419	181.75	167.71	0	8405
85%Ar 5%CO 10%He	21.653	22.395	186.75	172.04	0	7897
85%Ar 5%CO_2 10%He	21.323	22.392	191	178.79	0	8076
80%Ar 13.33%CO_2 6.67%He	22.965	23.421	184.38	169.82	0	8212
72.5%Ar 7.5%CO_2 20%He	22.79	23.017	184.54	170.42	0	8128
82.5%Ar 12.5%CO_2 5%He(Cranfield)	22.635	23.4389	184.91	169.59	0	8160
82.5%Ar 12.5%CO_2 5%He (BOC)	22.681	22.970	184.13	170.43	0	8091

Table 6-31 Average current, voltage and power for the shielding gas trials in flat position

7 Discussion

This chapter includes a discussion of the results generated during the present work and their comparison to other published data. It is consisted in three sections:

a) welding procedures development for 5G X100 girth welds.
The potential application of the process (e.g. dual tandem) in the pipeline industry is expected to contribute in significant economic savings. Comparison with other processes will be discussed and weld metal mechanical properties will be investigated and conclusions will be drawn.

b) welding parameter trials
The effect of the welding parameters on the weld bead geometry will be analysed and discussed. Understanding the relationship between welding variables and bead profile will allow a better control of the weld pool formation and consequentially minimisation of defects (e.g. side-lack-of-fusion).

c) shielding gas trials
The performance of several shielding gas mixtures on the weld bead geometry will be investigated and the effect of the individual components on the bead shape will be evaluated and discussed. Optimised mixtures will be proposed.

7.1 Girth Welding

The generation of a sound weld or the development of a successful girth weld combines a few essential steps that in sequence can be summarised as:

-evaluation of the pipe chemical composition and mechanical properties. The parent material tensile properties are very important in relation to the overmatching criterion for the yield strength of the weld metal.

-selection of suitable welding consumables based on their chemical composition, mechanical properties and the thermal cycle of the welding process.

-preliminary dual tandem girth welds aimed at determining the limits of the weld metal mechanical properties.

Full girth welds were qualified in accordance with international standards.
A detailed description follows.

7.1.1 X100 Pipe Properties

The parent metal main constituents are bainite and ferrite (Figure 6.2, page 93) and this is in agreement with other published data [9], [1].

Tables 4.2 and 4.3 (pages 47 and 48) report the longitudinal and the transverse tensile properties of the pipe material where some of the proof strength levels are below the

690MPa. The manufacturer of the pipes D1 and D2 reported tensile tests on both round bar and flattened strip specimens in longitudinal and transverse directions of the pipe. All flattened specimens presented clearly lower strength values due to the Bauschinger effect. This is in agreement with other published data [13],[115]. However, Gianetto [2] reported that measured yield strengths of a given pipe material (X70, X80 and X100) using round bar or prismatic strip tensile (not flattened) specimens were very similar, although round bar yield strength values of the narrow gap girth weld metal were higher than the prismatic strip tensile specimens.

In Table 4.2 (page 47) the yield strength value reported is the $R_{p0.2}$ (used in general engineering) and the $R_{t0.5}$ yield point specified by the API 5CT. These two proof stress values are generally very close to each other. Pipe B19 presented yield to tensile ratios (Y/T) typically between 0.80 and 0.90 when round bar transverse tensile specimens were used. The same range is reported for pipes D1 and D2 although with some higher Y/T values up to 0.96. Most of the flattened strip, Y/T results (pipes D1 and D2) were lower than the round bars, in agreement with similar published results [13]. High values (0.93) of the Y/T ratio for pipe round bar specimens have been reported in other published data [115] for X100 steels.

High values of the yield to tensile ratio are expected as the material yield strength increases. The Canadian standard CSA Z245.1 [116] requires a maximum Y/T of 0.93MPa for 690 MPa yield strength steel, while the maximum allowable according to API 5L [117] is 0.93 MPa for X80 pipe steel grade.

This yield to tensile ratio is of considerable importance since high levels of Y/T indicate reduced strain hardening capability of the materials and hence the safety factor.

Figure 7.1 emphasizes the differences in proof strength for the two different pipe compositions (low and high carbon content) and in Table 4.3 (page 48) the proof strength in different directions (longitudinal / transverse) is reported. Although pipe D2 has lower carbon content (0.043%) compared to pipe D1 (0.057%) yield strength is considerably higher. The higher strength levels can be attributed to the higher alloy content (e.g chromium (0.42%/0.02%) and molybdenum (0.41%/0.26%). All the three carbon equivalent formulations (CE_{IIW}, P_{CM}, CET) for pipe D2 are higher than D1.
Low, high and average strength measurements are plotted in Figure 7.1.

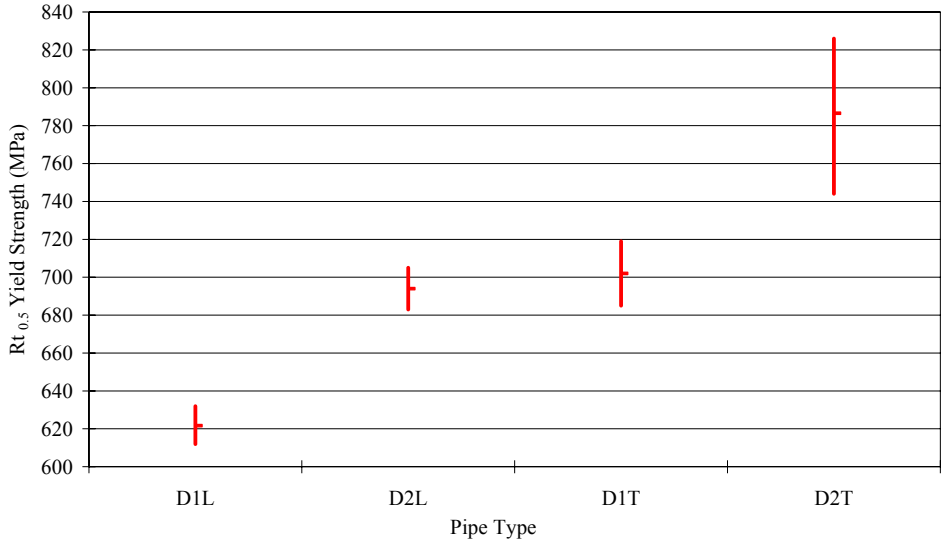

Fig. 7-1 Mean and range round bar longitudinal and transverse proof stress ($Rt_{0.5}$) for medium (D1) and low (D2) carbon content pipes (52 in OD x 22.9mm)

7.1.2 Tandem Wire Narrow Gap Welds (Single Tandem; ML-ST-S006)

The development of tandem welding procedures for high strength pipeline girth welds has been carried out at Cranfield University for several years [18],[5]. The present research work follows on from the development work carried out by Hudson [1]. Some of the power sources, consumables and parent materials used were similar for both research works and therefore direct comparisons can be made.

As described in Chapter 4 (page 45), the welding torch used was the Fronius water cooled torch (Figures 4.14, page 63 and 5.9, page 76) based on development work at Cranfield University. This torch has reduced overall weight which was beneficial since high torch weight makes significant demands on the mechanical oscillator in the welding bug. Also the cooling system was extended up to the shielding gas nozzle and this was considered a further advantage since overheating was reported during the preliminary trials with the original Cranfield air cooled torch, thus affecting process performance. In the early stages of the trials the contact tips melted due to overheating.
Some defects were reported in trial welds: Figure 6.19 (page 104) shows a map of the defective sections of a 52 in OD x 22.9mm pipe weld and similar locations for defects were found for the 36 in OD x 19.05mm pipe. The defects reported are mainly associated with sidewall-lack-of-fusion and scattered porosity. The latter could be associated with lack of adequate gas shielding.
This could be due to two reasons:
-the gas nozzle was not close enough to provide adequate weld pool protection from air draughts etc, and

-a relatively low flow rate of 22L/min of shielding gas was used. In retrospect a higher flow rate (e.g. 30L/min) might have been more appropriate.
The importance of arc length in influencing the chances in sidewall-lack-of-fusion defects was confirmed during the present work. Determination of the "optimum" arc length and achieving constant arc length throughout the pipe circumference is considered very important. Instabilities in the process due to arc length variations during welding can be caused by CTWD alterations or intermittent wire feed.
In addition to arc length and/or CTWD control, seam tracking, (control of the position of welding torch in respect to the joint) and adequate oscillation width are also considered of high importance. Access to the pulsed parameters was not available during this work and therefore the weld profile was determined by regulating travel speed, wire feed speed and oscillation width. Following Hudson's [1] conclusions, the present work confirmed that a concave bead profile is preferred in order to minimise undesired defects. Again, this and the subsequent procedure work revealed the importance of a better understanding of the welding variables or parameters on the weld bead profile, and the potential benefits of the generation of a mathematical relationship able to satisfactorily describe the weld bead geometry.
Initial trials repeated the work originally carried out by Hudson. Tandem welds were made with Oerlikon NiMo-1 filler wire which had previously given acceptable results [1]. The proof stress ($R_{P0.2}$) of 910MPa (Table 6.6, page 114) obtained was well above the "overmatching" requirement (section 2.2.1.1, page 5) but considerably below the 967MPa (for the 36 in OD x19.05mm) reported by Hudson [1]. Although no significant differences in the arc energy were reported between the two research works, in Hudson's work the arc energy was calculated in the range 0.35-0.43kJ/mm while the present work reported more consistent arc energy values for the fill passes of around 0.36kJ/mm.
It is likely that the difference in strength levels is due to the difference in weld bevel preparation. In the present work a gap width at the base of the groove of 5.0mm was used, compared to 3.8mm in Hudson's work. This narrower bevel increases the weld metal cooling rate. The strength level was further reduced (902MPa) when the groove width was increased to 5.6mm, although a different pipe was tested (36 in OD x 14.9mm).
Despite the high proof strength weld metal value (910MPa), the other mechanical tests were successfully completed and showed good properties. It was decided to accept that value and use the acquired experience in order to achieve the desired strength level in the dual tandem process.
The elongation (weld ML-ST-S006, Table 6.6, page 114) was considered quite high (19.5%), with the yield to tensile ratio also high (0.97) considering the high strength levels.
The toughness values (Table 6.10, page 118) were excellent, well above 50J at -60°C and also good at -80°C where the toughness average dropped to just below 50J on the fusion line. Generally, all the toughness levels were well above those reported by Hudson.
No codes or standards were applied regarding the toughness level of acceptability except for the client's recommendations. The range of interest for the temperatures was determined between -20°C to -40°C and the average toughness values was established at 60J with 50J minimum of the individual samples. The impact toughness transition curves (Figure 6.5, page 96) show toughness levels lower on the fusion line

(except at -40°C) than the weld metal. This is due to the presence of a transition region between the fine grain structure of the weld metal and the bigger grains reported in the HAZ next to the fusion line zone (Figure 6.7, page 97). In addition, the reduction of toughness properties with temperature (slope of the transition curves) on the fusion line is steeper than that for the weld metal toughness. The good toughness properties were confirmed by the CTOD test results, which were predominantly classified as δm (value of CTOD at the first attainment of a maximum force plateau for fully plastic behaviour). CTOD tests were carried out at -10°C as the client required.

Cross weld tensile results (Table 6.9, page 117) give values of the ultimate tensile strength between the 809 and 821MPa and all fractures were in the parent metal. Side bend and nick break tests (Table 6.9) are also acceptable.

At this point it is necessary to clarify that, although the welds were acceptable after the X-Ray examination, isolated defects, within the limits of acceptability, were almost always present. The philosophy of the present research work is to try to obtain the most reliable information from the mechanical tests, with no misleading conclusions because of the presence of defects in the test specimens. Hence all the defected areas reported in the X-Ray films were identified on the actual welds, and only specimens from the "clean" weld sections were extracted for mechanical tests.

The hardness and microhardness surveys (Tables 6.6, 6.7 and 6.8, pages 114-116) show higher values for the cap weld metal compared to the root. This is due to the "stronger" filler wire (Oerlikon Carbofil NiMo-1) used for the fill passes rather than the Thyssen K-Nova (ER 70S-G) used for the internal root pass and to the lack of any tempering effect on the cap weld metal. The weld metal hardness reported is always above 300HV10 but never exceeds 350HV10. The seam/girth interaction presented very consistent hardness values, mostly below 350HV10, except for some hardness traverses in the cap HAZ that exceed 350HV10. The 350HV10 was considered as the maximum hardness level, in consistency with Hudson's [1] work for X100 pipelines.

The microstructures shown in Figure 6.7 (page 97) refer to the "cap" weld metal. The small grain size may be explained by the low heat input and the high cooling rates associated with the process [1]. The HAZ microstructure next to the fusion line presented a larger grain size and martensitic microstructure although the hardness traverses do not necessarily lead to such conclusions suggesting that is likely that the martensite is tempered.

A typical macrograph of the single tandem weld is shown in Figure 6.6 (page 97).

It has been demonstrated here that tandem welding can be applied for X100 linepipes and the mechanical properties achieved showed very encouraging results. The presence of some isolated minor defects associated with side-lack-of-fusion indicated that further research needs to be carried out in order to establish the relationships between welding parameters and weld bead geometry.

Subsequently, the single tandem process has been successfully implemented on the construction of a 2km section of 36 in OD x 13.2mm X100 pipeline (Peerless Project). The project consisted of 174 welds and there were seven repairs for lack-of-fusion [118]. Another 5km X100 pipe length project (TransCanada Stittsville/Deux Rivieres) was completed using the tandem welding process developed at Cranfield [119].

7.1.3 Dual Tandem Narrow Gap Welds

7.1.3.1 36 in OD x 19.05mm Dual Tandem Welds (ML-DT-S016)

This research programme is the first reported work on dual tandem welding of pipelines. The challenge undertaken consisted in the process development and in the investigation of the mechanical properties for X100 pipeline steels.
Regarding the selection of the filler wires, preliminary trials of several consumables were carried out and the results are reported in Tables 6.1 and 6.2 (page 112) and are summarised graphically in the following Figures 7.2, 7.3 and 7.4.

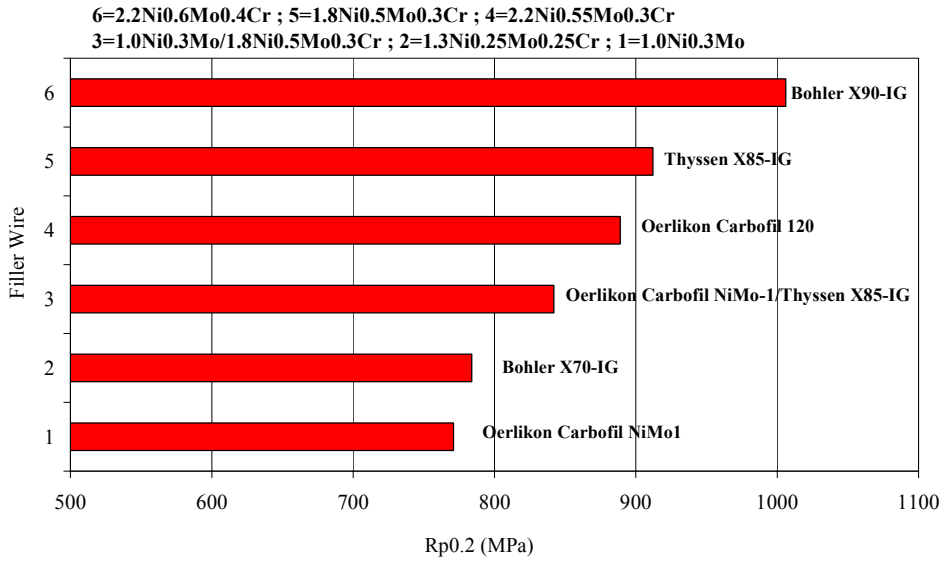

Fig. 7-2 Dual tandem (36 in OD x 19.05mm) weld metal proof stress ($Rp_{0.2}$) for different filler wires

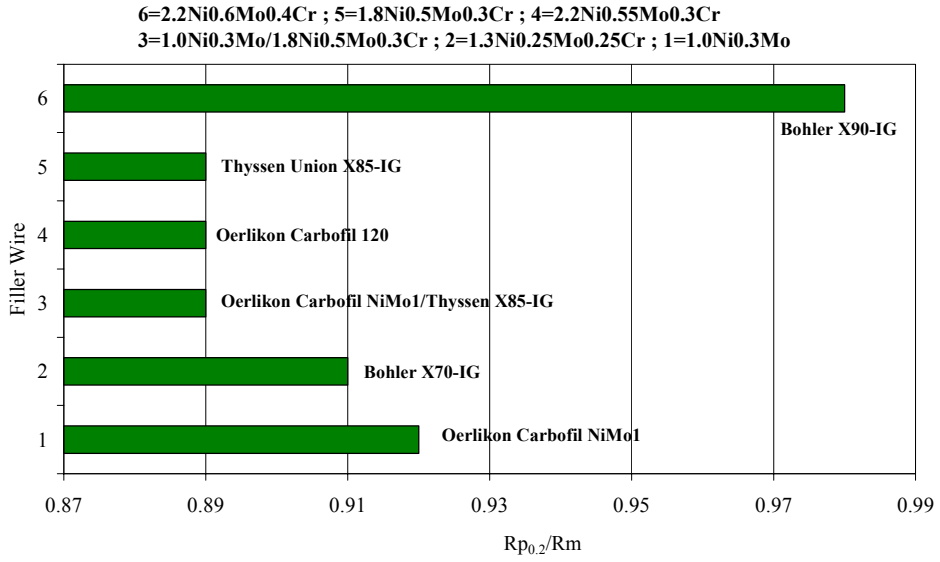

Fig. 7-3 Dual tandem (36 in OD x 19.05mm) weld metal yield to tensile ratio for different filler wires

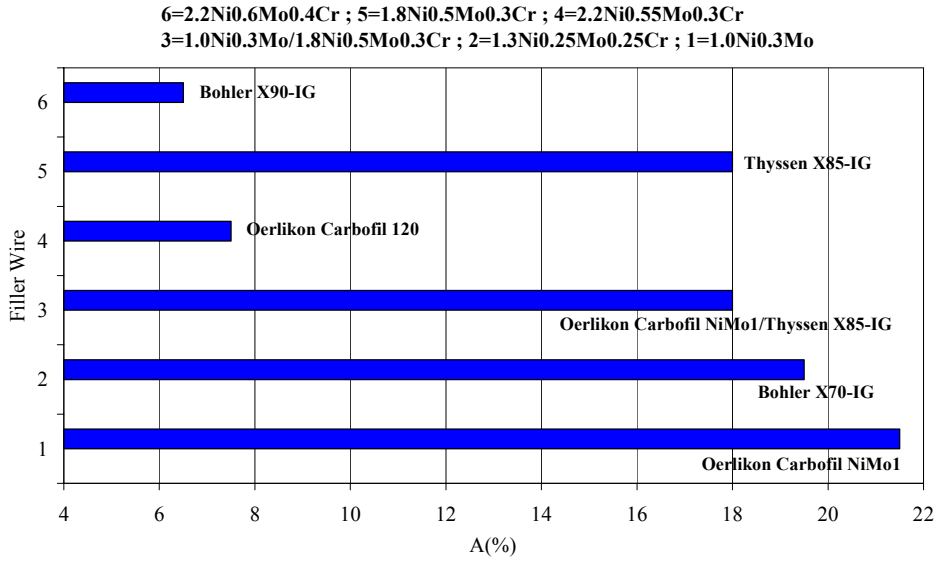

Fig. 7-4 Dual tandem (36 in OD x 19.05mm) weld metal elongation for different filler wires

The results in Figures 7.2 and 7.4 indicate a strong effect of filler wire composition on weld metal strength and tensile elongation. The weld metal strength of the welds obtained using the Bohler X90-IG and the Oerlikon Carbofil 120 were among the strongest while presented the lowest elongation. Conversely, the lower strength welds derived from Bohler X70-IG and Orlikon Carbofil NiMo-1 presented the highest elongation. Surprisingly the Thyssen X85-IG presented a high proof strength ($Rp_{0.2}$=912MPa) and combined very good elongation (18%). This important result cannot be easily explained based on the filler wire composition, and requires further investigation. Nevertheless, a quite clear trend in weld metal strength, yield to tensile ratio, elongation and filler wire composition has been established.

It is interesting that the "mixed" wires showed intermediate weld metal properties located in the middle regions of the graphs reported in Figures 7.2 and 7.4. Considerably improved yield to tensile ratios were achieved and orientated towards the low values (0.89, Figure 7.3) compared to the single tandem weld values (0.97; Table 6.6, page 114). Denys [14] states that high yield to tensile ratio is associated with lower weld metal toughness. Considering the strength levels of the parent material (X100) and for comparison with the previous work [1] an approximate maximum value of Y/T=0.95 was adopted for reference.

The weld metal analysis provides very useful information on the contribution of constituents to strength. The actual weld metal compositions for the above group of the preliminary dual tandem welds (36 in OD x 19.05mm) together with the qualified procedure (ML-DT-N013; 52 in OD x 22.9mm) are reported in Table 6.12 (page 121).

An analysis of this table shows the very strong contribution (>90%) of the filler wire alloy elements to the weld metal composition compared to the contribution of the pipe material. This is consistent with calculations of percentage dilution, which also

indicated that the pipe material forms less than 10% of the weld volume. The total weld fusion area was compared to the weld preparation joint area, in order to estimate the percentage dilution. It is concluded that the weld metal strength is mainly governed by the filler wire composition.

The P_{CM}, CET and CE_{IIW} formulations for the calculation of the weld metal carbon equivalent for the above five preliminary dual tandem welds were calculated and the corresponding $Rp_{0.2}$ proof stress graphs were plotted. The three plots are shown in the following Figures 7.5, 7.6 and 7.7. Development of a statistical model based on regression analysis of weld metal strength as a function of weld metal composition was attempted but did not succeed due to insufficient data.

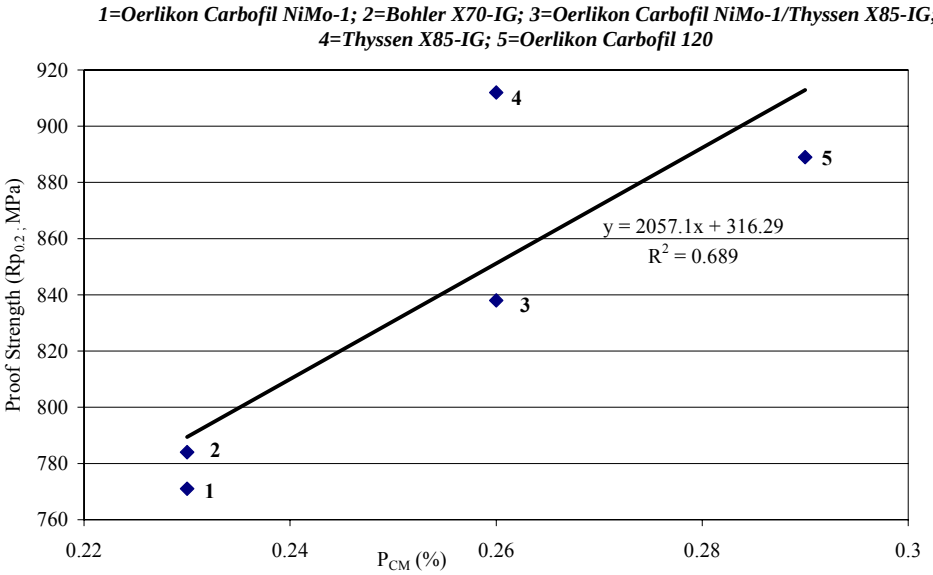

Fig. 7-5 Weld metal 0.2% Proof strength vs P_{CM} for different solid wires and dual tandem 5G welds

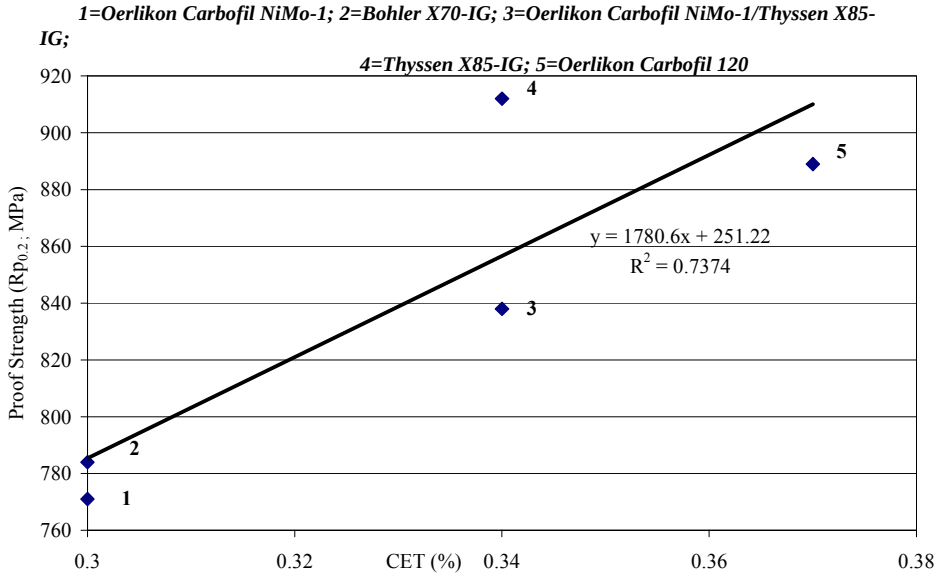

Fig. 7-6 Weld metal 0.2% Proof strength vs CET for different solid wires and dual tandem 5G welds

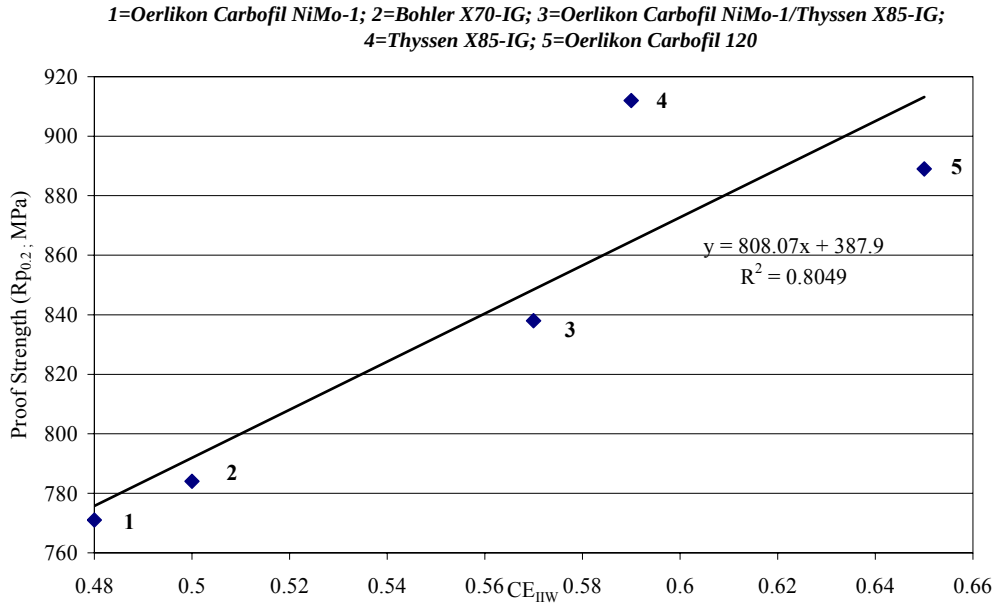

Fig. 7-7 Weld metal 0.2% Proof strength vs CE_{IIW} for different solid wires and dual tandem 5G welds

Figure 7.8 shows the plot of tensile elongation (%) versus the CE_{IIW}

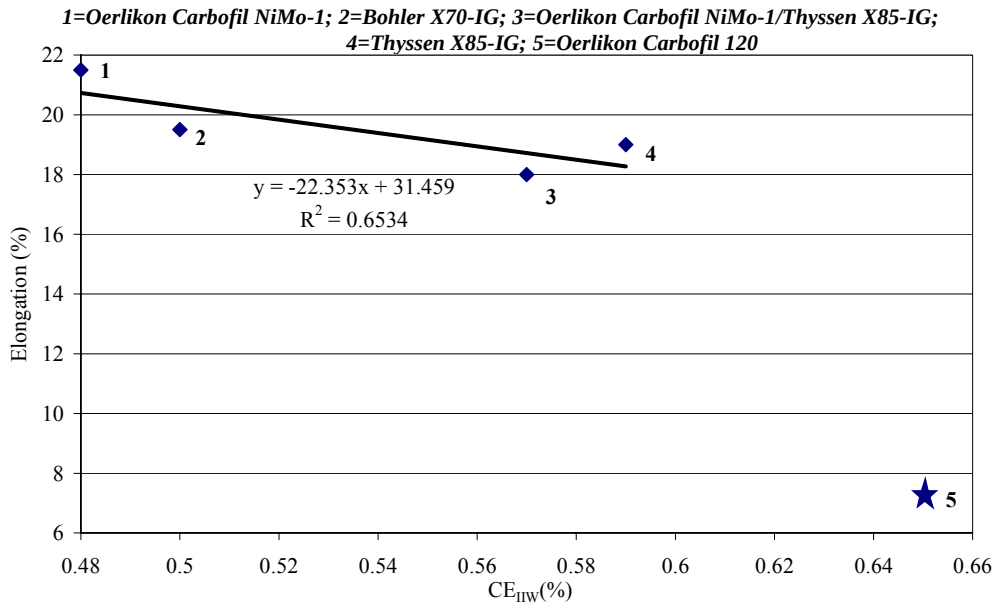

Fig. 7-8 Tensile elongation vs CE_{IIW} for different solid wires and dual tandem 5G weld trials

Although relatively few results were available, very clear relationships between weld metal carbon equivalent and weld strength and elongation were established (Figures 7.7

and 7.8) with acceptable distribution of scatter for the data. However, due to the limited data available for the low elongation level of point 5 (Figure 7.8) a detailed analysis is not possible and more tests are needed to confirm this value. The trend line plotted in the graph is based on the four remaining points.
Widgery [22] refers to two patents which address the issue of high strength weld metals and changes in welding procedures (change in cooling rate). These patents recommend filler wire compositions which lead to the formation of either very low carbon bainite microstructures or low carbon martensite microstructures. Figure 7.9 shows a plot of the predicted strength from the patents for GMAW following equation (462+3345C+70Mn+35Ni+68Cr+142Mo-59HEAT INPUT)
compared to the actual strength values (Table 6.2, page 112) achieved in the dual tandem trials with 82.5%Ar12.5%$CO_2$5%He shielding gas.

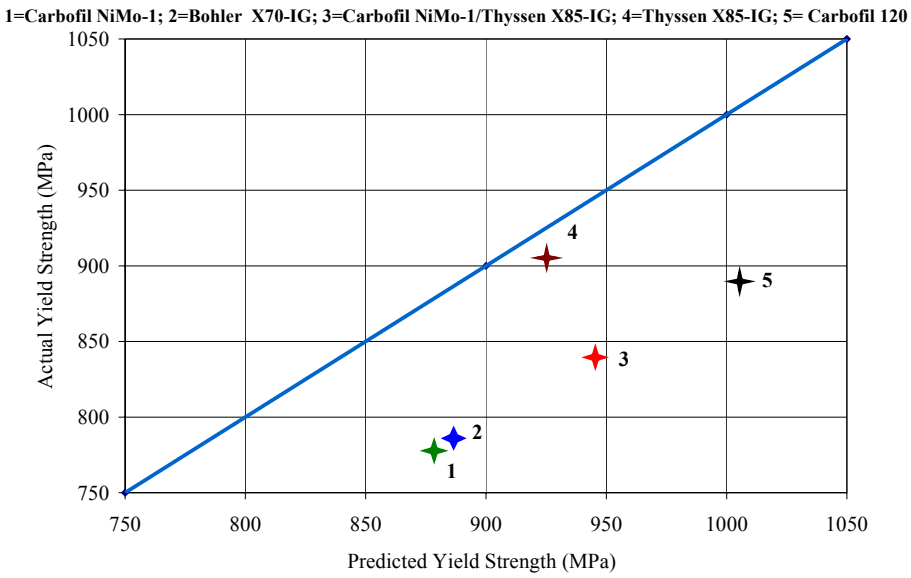

Fig. 7-9 Predicted vs actual weld metal strength

The predicted strength was calculated based on the chemical analysis of the welds (Table 6.12, page 121). The welds are marked as follows: 1=ML-DT-S003(NiMo-1); 2=ML-DT-S002(X70-IG); 3=ML-DT-N013(NiMo-1/X85-IG); 4=ML-DT-S011(X85-IG); 5=Pipe B19(Carbofil 120). 0.41kJ/mm heat input level for the lead torch and 0.31kJ/mm for the trail was considered.
Although a certain trend for the welds numbered 1, 2, 3 and 5 is shown, there is significant displacement between the predicted values and the dual tandem weld values. This is probably due to differences between the process characteristics (joint configuration, heat input etc) represented by the equation from the patents and the narrow groove dual tandem PGMAW considered in our study. This emphasises the importance of relying on regression equations generated only for a particular welding procedure.
The Oerlikon Carbofil NiMo-1 that was successfully tested during the qualification of the tandem weld trials failed (771MPa, Table 6.2; page 112) to meet the established overmatching criterion (section 2.2.1.1, page 5) for the weld metal yield point in dual tandem welding trials. Similarly the Bohler X70-IG produced a low yield point. This immediately made evident the effect of the second tandem torch bead being deposited

on the bead of the first tandem torch, resulting in a reduction of the weld metal strength, due to the changes in thermal cycles. This can be explained by the fact that the transformation of the first weld bead was not completed when the second torch reached the same position. This can be seen in Figure 7.10 which reports the cooling curves for the various mechanised GMAW pipeline welding systems [1].
The increased time spent for each layer at temperatures above the Ar1 leads to an increase in the grain size and therefore a decrease in the strength. Similar conclusions were made by Hudson [1]. For all processes (Figure 7.10) the same heat input was considered but, in the case of the dual tandem torch, the travel speed was doubled and therefore the second torch passed a given point quicker than in the case of the dual torch process. Although there is no available data regarding the transformation temperature for the "mixed" (Oerlikon NiMo-1 /Thyssen X85-IG) wires, this is likely to be in the region of 450°C to 550°C [1] and therefore it is probable that little or no transformation occurs. The typical transformation temperature for the NiMo-1 filler wire is between the 450°C to 550°C for the single tandem process and heat input of 0.36kJ/mm as shown in Figure 7.11.

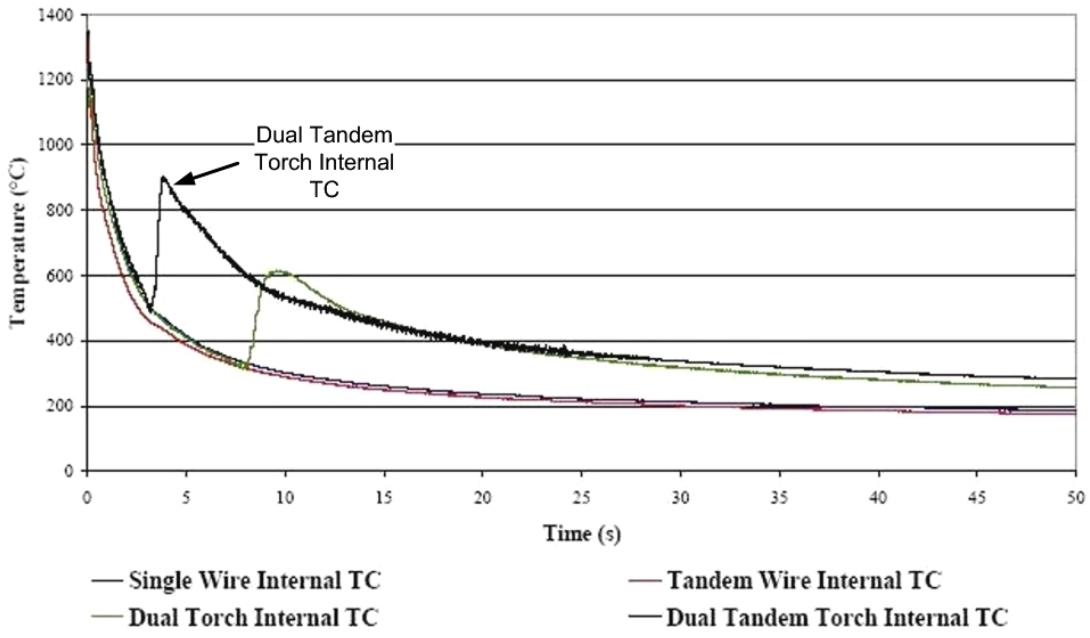

Fig. 7-10 Cooling curves for an internal thermocouple with various mechanised GMAW pipeline welding systems [1]

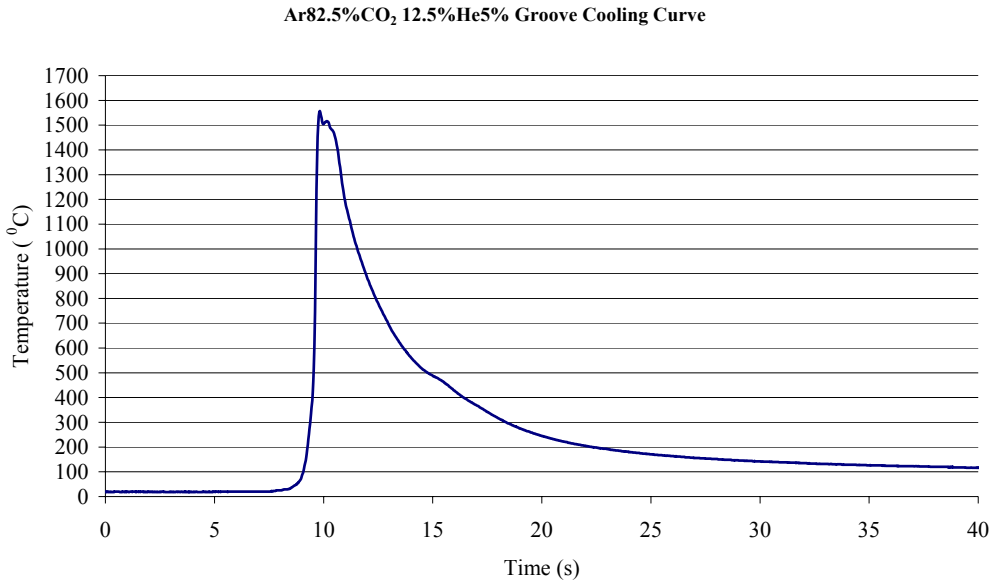

Fig. 7-11 Cooling curve for an external thermocouple with single tandem mechanised PGMAW obtained for a single weld bead.

When more highly alloyed filler wires (e.g. Thyssen Union X85-IG, Oerlikon Carbofil 120 and Bohler X90-IG) were adopted, yield strength levels were considerably increased. Note that the weld metal composition is mainly determined by the filler wire composition, with a secondary influence from the pipe (Table 6.12, page 121). The Bolher X90-IG and the Oerlikon Carbofil 120 presented weld metal proof strength well above the desired range (810-860MPa) but both exhibited very low elongations. The Thyssen X85-IG, also achieved high weld metal strength, with a good yield to tensile ratio. Considering the yield to tensile ratios and the elongation results (Figures 7.3 and 7.4) the Thyssen Union X85-IG was selected for further investigation. The overmatching challenge was accomplished by using the Oerlikon Carbofil NiMo-1 consumable as the first wire, in combination with the Thyssen Union X-85 as the second wire, in each tandem torch where both lead and trail wires work in the same weld pool. Torch separation is of a great importance in determining mechanical properties of the weld metal, but was not investigated in this work and the research programme was carried out at a torch separation of 60-70mm. This weld procedure (ML-DT-S016) gave very satisfactory tensile results ($R_{p0.2}$=842MPa), yield to tensile ratio (Y/T=0.89) and very good elongation (A=18%).
Toughness results were all good and well above 150J for the weld metal and for all testing temperatures including -80°C (Table 6.10, page 118 and Figure 6.8, page 98). The fusion line transition curves show a sharp drop at temperatures below -40°C. The scatter between the weld metal and the fusion line toughness results can be explained by the fact that the heat affected zone is quite narrow and not generally extended over the 2.0mm and this can lead to changes in the microstructure characteristics. The cap microstructures are shown in Figure 6.7 (page 97) and emphasize the change in the grain size and the microstructure of the weld metal and the heat affected zone adjacent to the fusion line. Coarse grains just next to the fusion line are also apparent.

Despite a greater time above the transformation temperature Ar1 for the dual tandem weld, toughness values were very similar to the single tandem weld even though the larger mean grain size might be expected to lead to lower toughness.
A typical macrograph of the dual tandem process is shown in Figure 6.6 (page 97).
CTOD results were between 0.15 and 0.21mm for the weld metal and between 0.08 and 0.50mm at the fusion line. Most of the results were classified as δm.
Cross weld tensile results (Table 6.9, page 117) were good, all greater than 787MPa and all four specimens failed in the parent metal. Side bend, and Nick break results were all acceptable.
Hardness and microhardness surveys are reported in Tables 6.6, 6.7 & 6.8 (pages 114-116). The cap weld metal levels were clearly higher than the single tandem results and some were above 350HV10. This can be explained by the different arc energies of the cap pass. The split cap technique applied in the dual tandem procedure weld used considerably lower arc energy (0.23kJ/mm) than the single tandem process (0.36kJ/mm). The same trend was apparent in the hardness survey of the heat affected zone. Some of the cap HAZ microhardness (HV0.5) levels were above 300HV0.5 with a maximum of 350HV0.5.
The pipe seam hardness traverses (Table 6.4, page 113) were acceptable with higher values in the seam weld metal (292-306HV10). The seam/girth weld metal interaction exhibited some hardness levels above 350HV10 and this can be attributed to the higher level of alloying elements in the consumables used in the girth weld. Some hardness traverses in the HAZ have shown similar patterns to the weld metal with values exceeding 350HV10.
When productivity is considered, the dual tandem process completed the joint in half the time for single tandem. The single tandem process completed the full pipe thickness in almost eight runs while the dual tandem required just four.

7.1.3.2 52 in OD x 22.9 mm Dual Tandem Welds (Low Carbon Content Pipe, Pipe D2; C=0.043; ML-DT-N009)

Transfer of the process to the 52 in OD x 22.9mm X100 pipes was based on the experience acquired during the work described above. Again, the aims remained the same and concentrated on the selection of an adequate consumable able to successfully satisfy the overmatching criterion (section 2.2.1.1, page 5) associated with the process development and performance.
The bulk of the procedure test work was performed using the “mixed” wire technique of Carbofil NiMo-1/ Thyssen X85-IG. This gave a reasonable proof stress of 877MPa (Table 6.6, page 114).
On completion of the pipe joint, the weld was X-Ray tested and showed plenty of “clean” sections available to conduct a full series of destructive tests.
Impact toughness tests were performed on specimens extracted from both root and cap sections [105] and the acceptance criteria are reported in section 7.1.2. Root impact toughness results are very acceptable giving well over 50J even at -80°C (Table 6.10; page 118). The fusion line results present some scatter mainly at -40°C and -60°C. The cap impact toughness results are still above 50J at -60°C (Table 6.10; page 119) and only the fusion line tests at -80°C drop below 50J (the values referred to are averages of three individual test specimen). The impact transition curves (Figures 6.12 and 6.13, pages 100 and 101) for both weld metal and fusion line show a trend to much lower

values compared to the root and this can be associated with higher hardness levels, as will be seen later.
A considerable scatter between the individual toughness values is reported for the fusion line results at -60°C due to either the very narrow transition region or difficulty in positioning the notch on the fusion line. CTOD weld metal results (Table 6.11, page 120) were all classified as δm and the heat affected zone as δu.
Cross weld tensile results (Table 6.9, page 117) are all good, in a range between 796 and 814MPa and all four specimens failed in the parent metal. Side bend, and nick break results are all acceptable.
Hardness and microhardness survey results (Tables 6.6, 6.7 and 6.8, pages 114-116) for the girth weld/base material show for both weld metal and HAZ, values lower than 350HV10. The seam/girth weld interaction produced high levels in the HAZ of the seam weld. High weld metal hardness levels are reported also.
Typical weld metal and heat affected zone microstructures (Figures 6.10 and 6.11, pages 99 and 100) show similarities to the 36 in OD x 19.05mm dual tandem welds.
A typical macrograph is shown in Figure 6.9 (page 99).

7.1.3.3 52 in OD x 22.9 mm Dual Tandem Welds (Medium Carbon Content Pipe, Pipe D1; C=0.057; ML-DT-N013)

The same "mixed" consumables technique was adopted for the development of the medium carbon pipe weld procedure. Plenty of defect free weld sections were obtained and the full series of specimens for mechanical tests were extracted.
The weld metal yield strength reached 838MPa with an excellent elongation of 25.5% and a very good ratio yield to tensile equal to 0.87, similar to other tests conducted for pipe welds at this strength level [6],[62],[120].
All toughness tests show good results, well above the 50J average for both weld metal and fusion line (Figures 6.17; page 103, 6.18; page 104 and Table 6.10; pages 118 and 119). In both root and cap transition curves a large scatter in the individual results is observed. Again, as stated earlier, this can be attributed to the very narrow regions (1.0 to 2.0mm) with significant changes in microstructural characteristics. This emphasises the importance of the positioning of the notch on the fusion line. CTOD results are good and most tests are classified as δm (Table 6.11, page 120).
Cross weld tensile tests (Table 6.9, page 117) all failed in the parent metal with UTS values falling within the range 749 to 762MPa. All nick break and side bend results (Table 6.9) are acceptable.
Weld metal chemical analysis (Table 6.12, page 121) highlights the good toughness and strength properties obtained. Relatively low levels of O_2 (approximately 250ppm) are associated with good toughness properties while the levels of the alloying elements determine the strength [121],[122],[123],[124].
The hardness and microhardness for the parent metal/girth weld traverses all present values below 350HV10 (Tables 6.6, 6.7 and 6.8, pages 114-116). The seam/girth interaction produced high hardness in the HAZ of the seam weld for both root and cap specimens tested.
Typical macrographs of the dual tandem weld are shown in Figure 6.14 (page 102). The cap weld microstructure and heat affected zone show results similar to the typical dual tandem welds reported earlier and are shown in Figures 6.15 (page 102) and 6.16 (page 103).

The dual tandem process was field tested in March 2004 in Canada. The field tests were completed successfully and the potential of the system demonstrated in arctic conditions [118].
The new process is intended to be suitable for use on the long distance (5700km) gas pipeline known as the Alaskan Gas Pipeline. It is estimated that there will be $150m in welding cost savings arising from the application of the dual tandem process [125].

7.1.3.4 Review of Tandem and Dual Tandem Weld Results and Comparison to other Processes

All dual tandem 5G girth welds showed very good mechanical properties, including toughness. No significant problems were found, and the process is expected to be implemented by the pipeline industry relatively easily. Very high rates of productivity were recorded. The presence of four simultaneous arcs doubled the deposition rates leading to considerably fewer (half) required passes for the joint completion compared to e.g. single tandem. In addition, less welding equipment and personnel are associated with the process allowing the pipeline contractors to gain significant overall cost savings.
The regression equation (Figure 7.7) of proof strength vs CE_{IIW} shows very reasonable prediction capabilities and it appears that weld metal proof strength can be initially estimated on the basis of the CE_{IIW} weld metal value.
Figures 7.12, 7.13 and 7.14 show the mechanical properties results for different processes, filler wires and pipe composition. Although these results cannot be compared directly, considering the different heat inputs involved, they clearly show that targets in mechanical properties can successfully be met with the dual tandem process, together with considerable advantages in productivity. The results for the single wire and dual torch welds were extracted from the work reported by Hudson [1].
It is clear that if the effect of the process on the mechanical properties of the welds is to be compared, then welds would have been performed at the same heat input, with the same filler wire, and at the same pipe material. However, the objective in each case was to emphasise that the required mechanical properties can be met in association with different welding parameters, and that acceptable mechanical properties can be obtained with the dual tandem process.

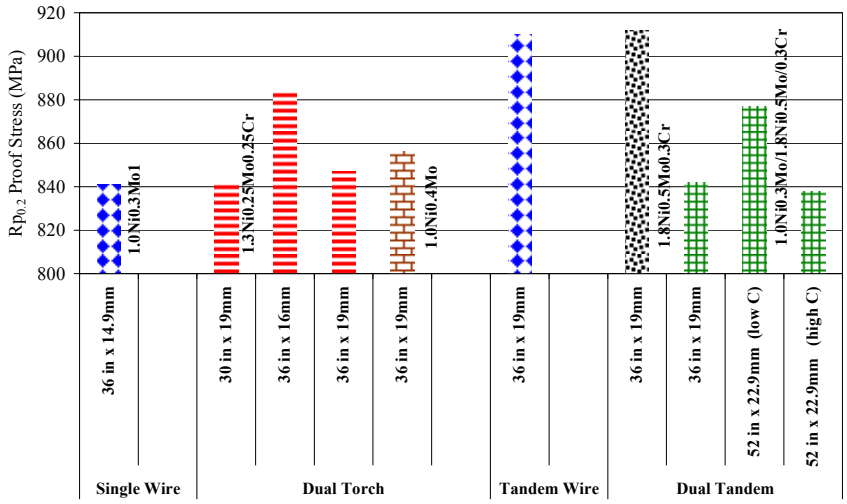

Fig. 7-12 Weld metal 0.2% Proof strength for different processes in 5G girth X100 pipe steel welds (single and dual tandem results : this thesis; other results Hudson [1])

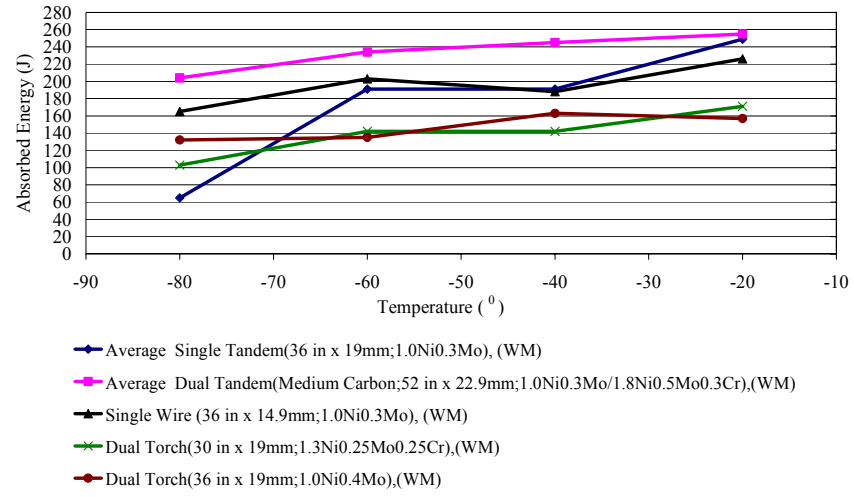

a

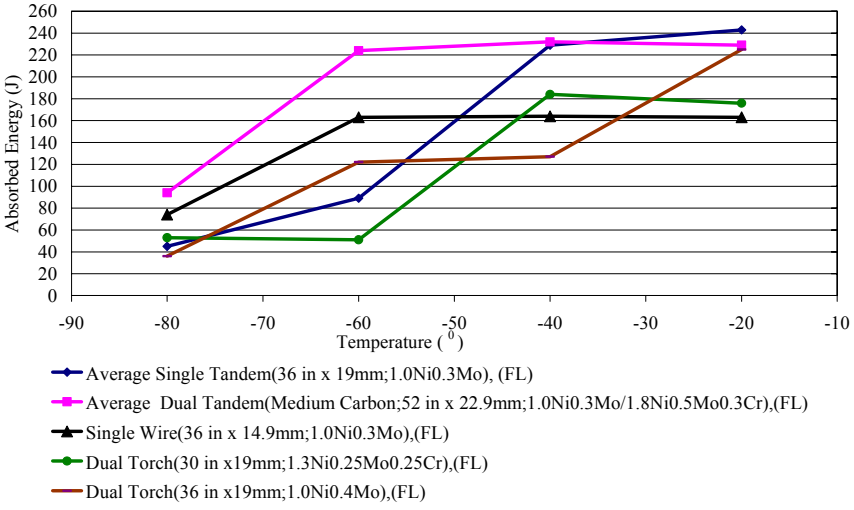

b

Fig. 7-13 Charpy toughness results for different processes in 5G girth X100 pipe steel welds for the (a) weld metal and (b) fusion line (single and dual tandem results: this thesis; other results Hudson [1])

The reheating effect of the second torch on the weld bead deposited from the first, and the consequently longer time spent above the transformation temperature is likely to cause an increase in the grain size, but it could be compensated for by the lower heat input and faster cooling rates. Toughness properties in both weld metal and fusion line tests show the highest values for dual tandem welding, followed by the single tandem process in comparison with other processes.
The higher cap dual tandem hardness survey values (Figure 7.14) can be explained again on the basis of the faster cooling rates (low heat input), in addition to the fact that fill passes are tempered by the subsequent passes that are deposited on top of them.

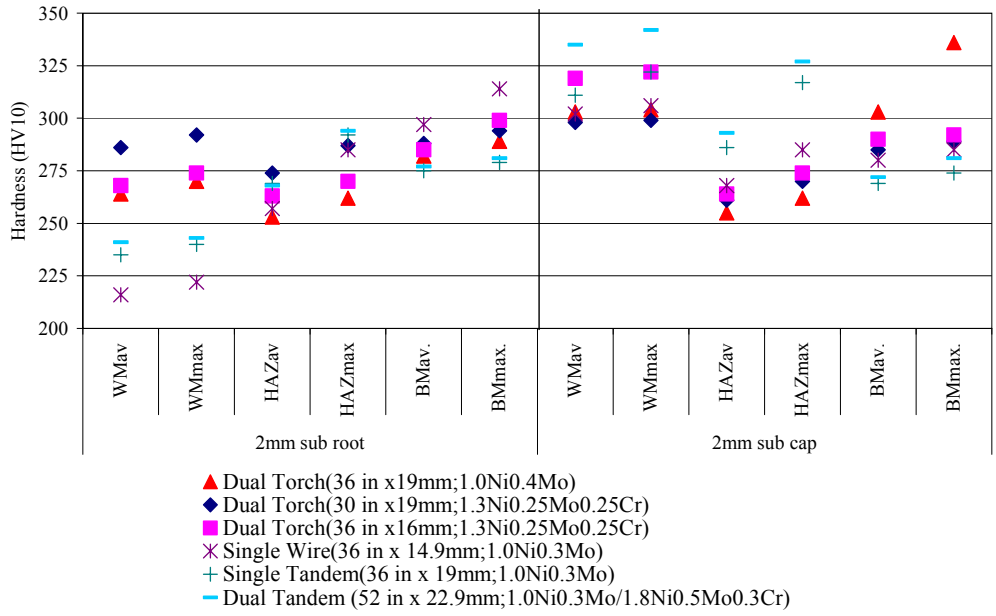

Fig. 7-14 Hardness (HV10) survey for different processes in 5G girth X100 pipe steel welds (single and dual tandem results: this thesis; other results Hudson [1])

7.1.4 Double Jointing Dual Tandem Narrow Gap Welds (DJ-DT-N012)

Traditionally for steel grades up to X70, submerged arc welding can be considered as the normal practice for the application of double jointing procedures. For higher alloy steels the high heat inputs and the high dilution levels associated with the SAW process can compromise the success of the procedure. Indeed, attempts to evaluate potential welding procedures for modern onshore X80 pipe materials and girth welds failed to achieve overmatching strength [23]. The reasons for this lack of success were concentrated on the high levels of dilution that reduced the levels of the alloying elements in the weld metal and the high heat input that reduced the weld metal strength because of the slower cooling rates.
When this work was undertaken, dual tandem GMAW appeared the only competitive process for the development of double jointing procedures.
Pipe D1 (medium carbon content) was used for the double jointing procedure development and the completed weld was X-Ray tested and accepted. Only minor

defects within the limits of acceptability were reported. This gave plenty of clean sections for full mechanical tests as the applicable standards require.
The "mixed" consumables technique described in the previous sections was used. The all weld tensile gave an $R_{p0.2}$ of 766MPa, 19% elongation and YS/UTS=0.87(Table 6.6, page 114) and clearly failed to meet the overmatching criterion (desired range 810-860MPa; section 2.2.1.1, page 5). This may be explained by the higher arc energies (0.35-0.59kJ/mm) used compared with the girth weld procedures (0.3-0.45kJ/mm), and the wider bevel (gap width at the groove base=6.0mm), that may have caused a reduction in the cooling rates. A solution to that would be the use of high alloying elements in both torches and both wires (e.g. Thyssen X85-IG; 1.8Ni0.5Mo0.3Cr) and/or a reduced bevel width.
An estimate of the 0.2% proof strength of the weld metal using the Thyssen X85-IG in both lead and trail wires can be determined as follows:
The "mixed" wires used with the 5G narrow gap girth welds provided an $Rp_{0.2}$=838MPa (Table 6.6), while in the double jointing welds the strength reduced to 91% of this value (766MPa). When the Thyssen Union X85-IG was used in both wires in the case of the 5G girth welds, it gave an $Rp_{0.2}$=912MPa. By using the same wire in the double jointing welds, it is estimated that weld strength will be reduced by 9% of the original value. This leads to an estimate of the $Rp_{0.2}$ proof strength at 830MPa, clearly within the required range.
All hardness and microhardness (Tables 6.6, 6.7 and 6.8, pages 114-116) levels for the parent metal/ girth weld were below 350HV10. The seam/girth weld interaction hardness traverses showed levels above 350HV10 located in the HAZ of the cap.
The cross weld tensile results (Table 6.9, page 117) gave UTS values between 755 and 771MPa and all failures were in the parent metal. The nick break and side bend results were all acceptable.
The toughness values (Table 6.10, pages 118 and 119) were all good and the transition curves (Figure 6.22, page 107) show a "smooth" drop in the toughness levels with the weld metal and a "sharp" drop in the toughness levels associated with the fusion line, in the temperatures between -40 to -60°C, for both root and cap. This and the scatter in the values observed in the fusion line can be associated with the very narrow widths of the heat affected zone, where significant changes in the microstructure characteristics may occur. CTOD weld metal results were always higher than in the heat affected zone and most of the tests were classified as δm.
Figures 6.23 and 6.24 (page 108) show the root impact toughness transition curves for both weld metal and fusion line of all the procedure welds (single tandem, dual tandem and double joint). All toughness levels at -40°C are very good and the average values are quite close. Larger differences were observed in the values at -60°C and -80°C. These results are shown in Table 7.1 together with the carbon, carbon equivalent, oxygen, nitrogen contents and heat input levels for all procedure welds.

Weld No.	Cv Root Impact Toughness		C (%)	CE_{IIW}	O_2 (ppm)	N_2 (ppm)	Heat Input kJ/mm
	-80°C	-60°C					
ML-ST-S006 (Single Tandem)	65	191	0.08	0.48	370	70	0.37
ML-DT-N009 (Dual Tandem)	83	134	-	-	-	-	0.36/0.29
ML-DT-N013 (Dual Tandem)	204	234	0.09	0.57	250	60	0.41/0.31
DJ-DT-N012 (Dual Tandem)	77	174	-	-	-	-	0.54/0.4

Table 7-1 Toughness properties comparison for different processes and pipe chemical composition

No clear conclusions can be drawn from the comparison of the toughness levels against the variables plotted in the Table 7.1.
Generally all welds presented fine bainitic/martensitic microstructures revealed in conformity with other research [2] although acicular ferrite in addition to bainite is reported by Hudson [1]. It is necessary to underline that with the limited available data in the present work and in the literature, further detailed work needs to be carried out in order to determine the boundaries of the factors affecting toughness properties.
Figures 6.25 and 6.26 (page 109) show the cap impact toughness transition curves (dual tandem and double jointing). Generally similar patterns were revealed, as explained above, although with some scatter.
Reviewing the toughness properties of the four welds, results in the fusion line are sometimes higher than in the weld metal for both impact and CTOD results. This can be explained by the presence of mixed microstructures in both the weld and the heat affected zone, in the location of the notch (impact) and in the different principles of the two tests. The wider notch in the Cv test and the higher speed of the test compared to the sharp notch and lower speed test of the CTOD increase the probabilities of detecting brittle structures and increases the rate of the crack propagation [1].
Weld microstructure (Figure 6.21, page 106) has shown similar patterns to the other dual tandem welds. A dual tandem double jointing macrosection photograph is shown in Figure 6.20 (page 105).
This new dual tandem process for double jointing welding procedure was successfully developed and qualified for first time for X100 pipe steel.
Only a few minor defects were reported (well within the limits of acceptability). It appears from some of the development trials that transfer instabilities were reduced, wire feeding was more consistent and better sidewall fusion was obtained at the 11:00 to 11:30 o'clock welding position rather than at the 12:00 o'clock position. However, the process has provided very good tolerance to the variations in welding parameters, with some potential further improvement.
The productivity comparison between the submerged arc welding and the dual tandem for double jointing procedures is reported below:

A low heat input (double butt 60° vee) and a typical submerged arc welding double jointing procedure were analysed for comparison with the dual tandem PGMAW process. The SAW joint preparation and the dual tandem joint preparation are shown in Figure 7.15.

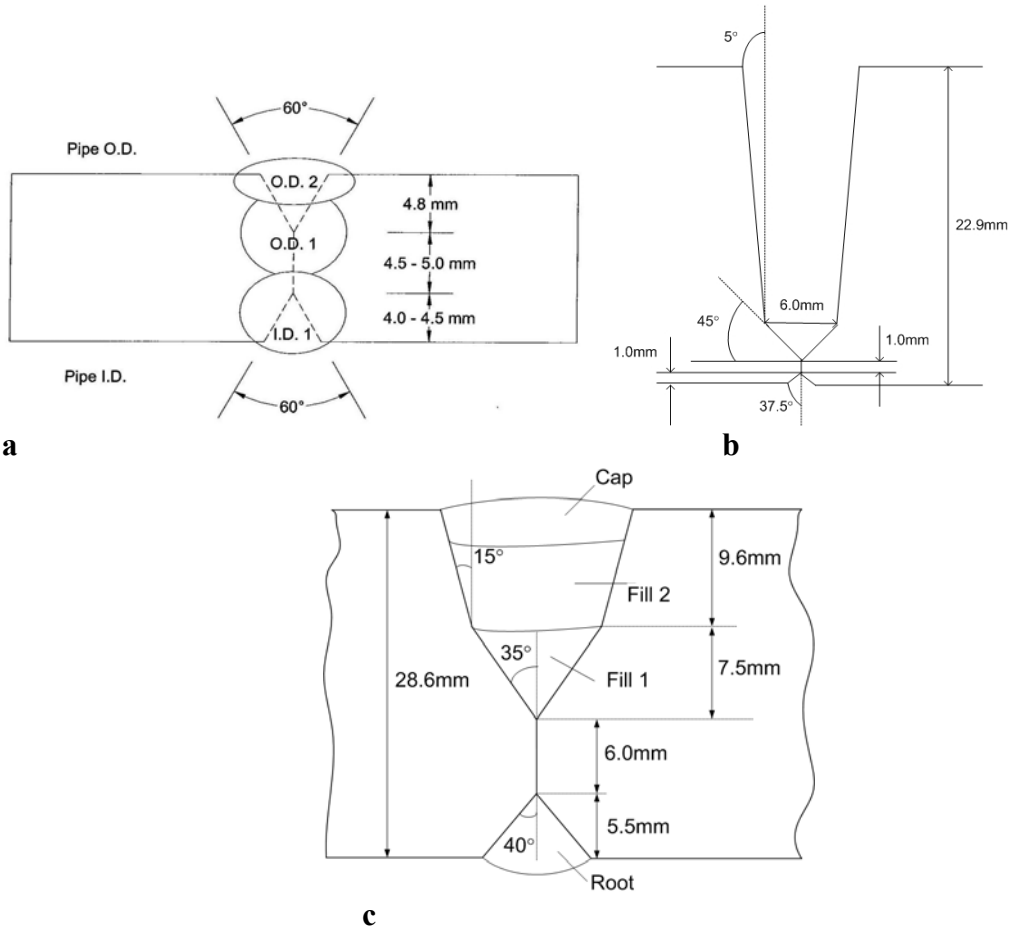

Fig. 7-15 Joint preparation for (a) low heat input submerged arc welding (42 in OD x 13.8mm WT), (b) Cranfield dual tandem PGMAW (52 in OD x 22.9mm WT) and (c) typical submerged arc welding (40 in OD x 28.6mm WT) for pipe double jointing procedures

The low heat input [24] submerged arc welding procedure(Figure 7.15a) was developed on a 42 in OD x 13.8mm WT pipe (CSA Z245.1 Grade 483) in downhand position (1G). The joint was completed in three runs; two deposited externally and one internally. The process parameters were as follows: Travel speed: O.D.1=1158mm/min; O.D.2=1248mm/min; I.D.1=1050mm/min.
Wire feed speed: O.D.1=1.6m/min; O.D.2=1.45m/min; I.D.1=1.45mm/min.
Filler wire: 4.0mm diameter.
Heat input: 0.9-1.4kJ/mm.
The overall deposition rate was 8.9kg/hr.
A typical [126] submerged arc welding procedure (Figure 7.15c) on a 40 in OD x 28.6mm WT pipe (X65 grade) in downhand position (1G) was completed in four runs

(root run, two fill runs and one cap), at four welding speeds (600 mm/min(cap), 750mm/min(root), 750mm/min(fill2) and 900mm/min(fill1)), with1.6mm diameter tandem filler wire (except for the root run where a 4.0mm single wire was used). High heat input levels of 2.1kJ/mm to 3.1kJ/mm were reported. The deposition rate was estimated as 17.15kg/hr based on the volume of the joint preparation and the travel speed for each pass.
The ranges of the dual tandem welding parameters were:
Travel speed:1295 to 1422mm/min; wire feed speed:15.2 to 16.0m/min for the lead torch and 11.5 to 12.00m/min for the trail torch, 1.0mm filler wire and arc energy levels:0.5 to 0.59kJ/mm for the lead torch and 0.35 to 0.43kJ/mm for the trail torch.
The estimated deposition rate was 20.5kg/hr, well above the 8.9kg/hr of the low heat input submerged arc and slightly higher than the typical tandem (17.15kg/hr) submerged arc. Despite the good deposition rates provided by the tandem SAW process, it must be emphasised that the high heat inputs and high dilution make it difficult or impossible to achieve the overmatching criterion for the weld metal yield strength for high strength steels.
A direct comparison of the tandem SAW performance to dual tandem PGMAW is shown in Table 7.2. The weld metal weight and the total time required for the completion of a 40 in OD x 28.6mm joint was calculated for both processes. The two joint volumes were almost identical.
The completion times are almost identical despite the inclusion of a considerable root completion time (4.6min) for dual tandem GMAW.
Considering the very good deposition rates and the low heat input levels reported for the dual tandem PGMAW this appears to be the only process that can be successfully qualified for overmatching double jointing procedures on high strength pipeline steels.

Tandem SAW		Dual Tandem PGMAW	
Weld Metal Deposited (kg)	Joint Completion Time (min)	Weld Metal Deposited (kg)	Joint Completion Time (min)
5	17	5	19 **(*)**

(*): refers to 3.0mm bevel offset (gap width 6.0mm at the base of the groove)
Time for completion of the root run (4.6 min) using dip GMAW is included in the dual tandem PGMAW completion time

Table 7-2 Productivity performance for tandem SAW and dual tandem PGMAW (40 in OD x 28.6mm pipe)

The dual tandem PGMAW for double jointing procedures may become a potential alternative to the submerged arc process considering the excellent productivity performance reported above. No submerged arc welding tests for X100 pipe steels have been reported yet in the literature. The lack of success of the submerged arc welding is mainly due to high heat inputs and high dilution levels from the parent metal. Nevertheless, some recent tests with tubular wires have shown quite promising results [127].

For lower grades of pipe steels submerged arc welding with high heat inputs (higher productivity) is commonly used. Some companies (Saipem) enhance productivity by using a twin SAW system (two torches) for X65 pipeline steels [25].
Practical adoption of the dual tandem process must take into consideration the following factors:
-risks and uncertainties associated with the new process,
-investment in new equipment (power sources etc.),
-investment in training for the new process and equipment, and initial loss of productivity due to lack of experience,
-welding equipment maintenance (power sources, welding carriage) and repair.
Despite these limitations, the dual tandem process at the moment represents the most likely process for successful X100 double jointing welding procedures.

7.1.5 Tie-In Procedure Welds

Tie-in welds are typical parts of pipeline construction and are required for the connection of the pipe to a facility, or for bridges/road crossings, or for connection to different pipe sections, for example special fittings.
Flux-cored wires have been developed [23] and found to provide a minimum yield strength of 620MPa when they were used in X-80 pipes tie-in welds. Widgery [26] reports that rutile wires are used for their smooth transfer attributed to the low surface tension due to high oxygen content. However, high oxygen content may reduce weld toughness.
Previous work at Cranfield [1] failed to meet the overmatching criteria ($R_{P0.2}$=730-740MPa) when rutile flux-cored wire was used in X-100 for a strain-based pipe design.
This possibility of using basic flux-cored wires in order to meet the yield strength criteria was investigated in this project.
Due to the benefits of good mechanical properties associated with the pulsed transfer mode, it was decided to test the basic flux-cored wire in pulsed mode and in downhill direction (root pass was deposited in conventional uphill GMAW with a 1.2mm metal cored wire according to AWS A5.20 E71T1MJH4).
Two basic flux-cored wires were selected for the preliminary tests:
a) the Philarc PZ6148 (AWS A5.29:E111T5-K4), and
b) the Philarc PZ6149 (AWS A.529:E121T5-G)
Initial tests were carried out using the waveform preinstalled in the Lincoln PowerWave450 source, developed for 1.0mm section solid wires. However, several modifications were made to the waveform pulsed parameters in an attempt to satisfactorily operate with a 1.2mm basic-flux cored wire. Due to limitations of time, only one synergic point was developed and all the procedure development work was carried out at that point. The preliminary tests resulted in 300mm length of full thickness welds. Originally, the BOC Argoshield Heavy (78%Ar20%$CO_2$2%O_2) was used as shielding gas, but spatter was generated. Spatter was reduced when the standard BOC Argoshield Light (91.9%Ar5%$CO_2$3.1%O_2) was used. Welds with Argoshield Light were mechanically tested and tensile strength levels are reported in Table 6.1 (page 112). Both wires provided excellent elongation values but only the Philarc PZ6149 met the overmatching criterion ($R_{P0.2}$=844MPa).
A complete pipe girth weld joint was completed afterwards. Generally a smooth weld profile was obtained, but large droplets were formed at the end of the melted wire and

expelled from the arc, indicating that further optimisation of the waveform is required. The globular transfer characteristics can be partially explained by the high surface tension due to the relatively low oxygen content (490ppm) in the weld metal offered by the basic wires (Table 6.12, page 121). Typically rutile wires are formulated to give weld metal oxygen between 500-750ppm [128]. In fact while the upper limit enhances droplet transfer the lower limit reduces transferability while generating better toughness properties. Hot and first fill passes were deposited as "single" pass while for the rest of the passes the single wire split technique was found to produce considerable improvement of the weld profile. This split technique had the risk of slag inclusions remaining trapped in the overlapping region of the two passes. Generally, the slag was removed quite easily but a grinding wheel was used for better cleaning of the deposited weld bead. Issues with high fluidity of the weld pool (due to the basic constituents of the flux) at 3:00 o'clock position were controlled by increasing the welding speed.

The basic flux wire performed badly (non uniform weld profile, unstable transfer) in vertical-up welding direction contrary to the good performance in vertical-down. This can be explained by the fact that basic constituents have lower melting points than the steel and form slag not stiff enough to support the weld pool in the vertical-up direction. The weld pool may be successfully supported in the vertical-up if lower current levels (and reduced welding speed) are used [129], but this will considerably reduce productivity.

However, rutile flux wires succeeded in terms of welding direction (vertical-up) and productivity due to the melting point of their constituent elements. Their melting point (approx. 1800°C) is very similar to the steel and this provides a very stiff slag that adequately controls the weld pool, allowing the use of higher currents and contributing to an increase of productivity in both terms of deposition and welding speed (increase). In fact the arc energy levels used in the tie-in welds using rutile flux cored wires (vertical-up) were in the range (0.82-1.82kJ/mm),[1] considerably higher than the arc energies used in the present work(0.82-0.96kJ/mm).

The PZ6149 wire tested gave proof stress $P_{P0.2}$=966MPa (Table 6.6, page 114) clearly overmatching and the ratio Y/T=0.93 but the elongation was limited at 13.5%. The equivalent weld metal strength provided by the rutile wire (ESAB 15.09) used in Hudson's work as reported earlier was considerably lower (746MPa) and small differences in both Y/T (0.90) and elongation (16%) were reported.

The high weld metal strength for the basic wire (composition as Table 6.12, page 121) and the low weld metal strength (composition (wt%): C=0.054, Mn=1.24, Cr=0.03, Mo=0.31, Si=0.36, Ni=2.56, V=0.02, Cu=0.02; CE_{IIW}=0.505, CET=0.276, P_{cm}=0.221; [1]) strength level for the rutile can be explained by the "narrow" bevel preparation of 30° and low arc energies that were used in the present work instead of the 60° bevel preparation and high arc energy levels used in Hudson's work [1]. These increased the weld metal cooling rates increasing the strength level accordingly. In addition, the basic wire used in this work had a higher carbon equivalent than the rutile wire used by Hudson [1].

The hardness traverses HV10 (Tables 6.6, 6.7 and 6.8, pages 114-116) are relatively high between 350 to 420HV10. The high hardness levels were associated with the high weld metal strength level, and the high levels of the alloying elements in the weld metal (Table 6.12, page 121). As expected, all hardness survey levels of the present work were higher than the rutile flux wire procedure (exhibiting a max. of 304HV10 in the weld metal) for the same reasons.

Impact toughness results (Table 6.10, page 118) were similar (slightly lower at 63J) to the rutile flux wire weld (typically 70J at -40°), even though the weld metal oxygen level of the basic wire in the present work (490ppm) was significantly lower than the one obtained with the rutile filler wire (620ppm).
The toughness impact levels are shown in the following comparison toughness transition curves (Figures 7.16 and 7.17).

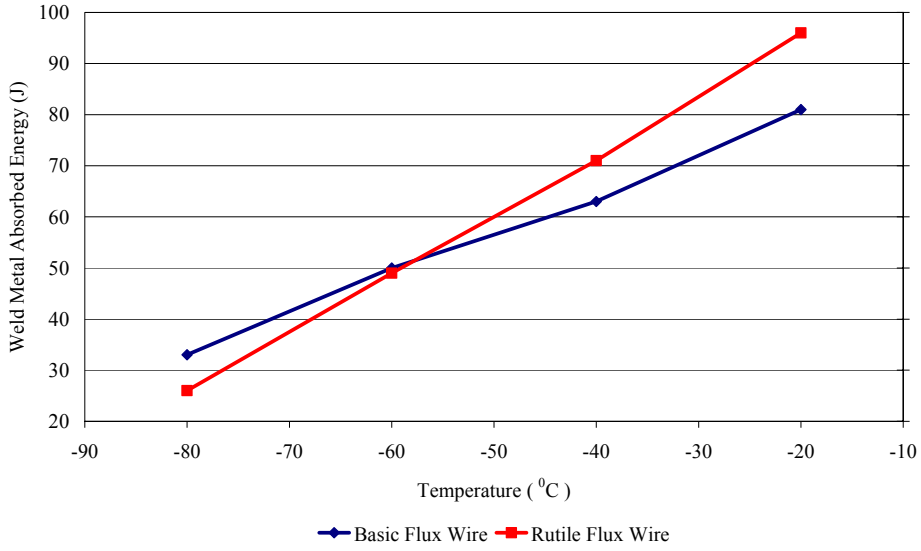

Fig. 7-16 Comparison impact toughness transition curves (weld metal) for tie-in welds carried out with rutile and basic flux cored wires

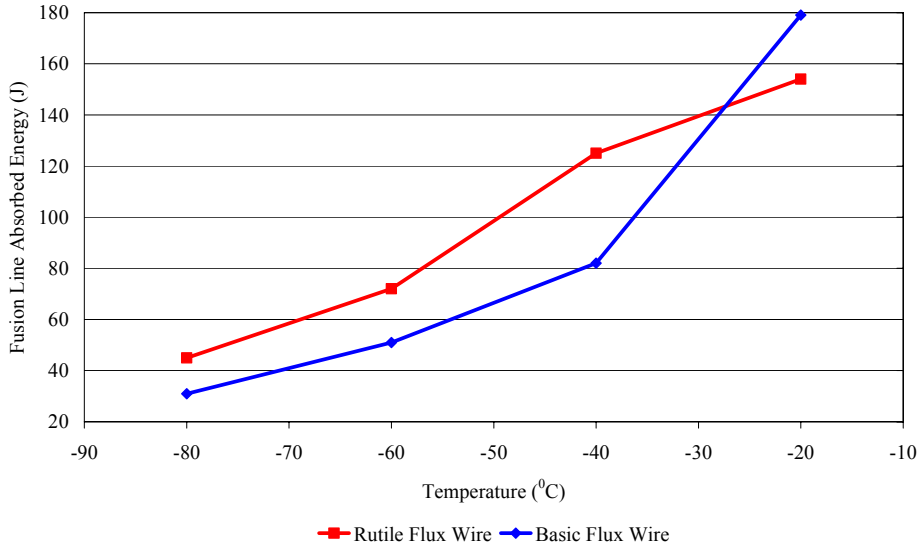

Fig. 7-17 Comparison impact toughness transition curves (fusion line) for tie-in welds carried out with rutile and basic flux cored wires

Compared to mechanised narrow gap welds (oxygen level 250ppm), toughness levels may be lower as a consequence of the higher oxygen levels in the tie-in welds.
The transition curves (Figure 6.29, page 111) exhibited a smooth drop in the toughness properties with decreasing test temperature for both weld metal and fusion line. CTOD weld metal values (page 120) were typically 0.10mm and all classified as δm.
The cross weld tensile results (Table 6.9, page 117) all failed in the parent metal at UTS levels greater than 760MPa. Nick break and side bend tests were mostly acceptable; two specimens failed due to side lack of fusion (nick break) and side wall tearing (side bend).
A macrograph of typical tie-in weld section is shown in Figure 6.27 (page 110). Microstructures of the cap weld metal and the heat affected zone adjacent to the fusion line have revealed the presence of martensitic islands which may be associated with the high hardness levels measured (Figure 6.28, page 111).
Despite the limited time dedicated to the development of the process and the low number of welding consumables tested, the present work is of significant importance since this is the first time (as far as is known) that mechanised basic flux cored wire for 5G X100 girth welds has successfully developed.
Although the weld metal strength is outside the desired range (810-860MPa), the results are very promising and further research work will contribute to process and weld metal property optimisation.

7.2 Welding Parameter Trials

7.2.1 Experimental Design

In an experimental design, the value of a response depends on the process variables selected and their number. The process variables are deliberately varied and the effect of these changes on the response is observed and described by mathematical equations, which for a linear model and two factors can be:

$y=\boldsymbol{\alpha_0}+\boldsymbol{\alpha_1}X_1+\boldsymbol{\alpha_2}X_2+\boldsymbol{\alpha_{12}}X_1X_2+$experimental error;
X_1, X2 are the variables, $\boldsymbol{\alpha}$ the coefficients of the variables and α_0 is the response when the variables are zero. These equations contain data generated from the actual experimental procedures (welding trials).Welding is a complex process because:

-it is not a linear process

-it has high variability

-there are a large number of variables and interactions

The philosophy of the present research programme was to define the relationships that occur between welding parameters and their responses, and to optimise the process. As far as is known no attempts have been made in modelling the weld bead geometry in pulsed tandem welding for application to 5G pipe welding. The procedure development work has defined a quite narrow range of stable welding conditions for the welding parameters values. In a narrow range of the factor levels, no significant difference among the responses may occur. This increases the influence of experimental error in the data and the risk of misleading conclusions regarding the importance of the factors on the responses. In a wider range between the "high" and "low" levels of the factors, more statistically significant responses are obtained but process stability and sound welds may be compromised.

The 2 factor levels statistical designs have successfully been used in welding, but assume that responses are linear between the 2 factor levels.

Since it is necessary to produce "sound" welds in order to carry out the necessary measurements of the weld bead profile, this means that the welding parameters cannot always be chosen very far apart, however if the parameters are too close effects may be obscured by variability and/or experimental error.

The Central Composite Design was selected for the following reasons:

-reasonably efficient i.e. small number of trials to estimate model coefficients

-estimates the presence of curvature in the responses

-determines regions of the design space where the process performs better.

The large number of welding variables (section 5.3.2.2.1, page 86) affecting weld profile was reduced to four for a more viable design that included significant "controlled" welding parameters: wire feed speed, welding speed, wire distance from the wall and arc length. The procedure development work indicated that parameters have a strong influence on process performance and weld profile.

The modelling technique adopted in this research work is described graphically in Figure 3.2 (page 44).

7.2.2 Modelling Results

In gas metal arc welding (GMAW) the weld bead profile is determined by two components:
a) the filler wire which is deposited on the parent metal in the form of droplets and
b) the melted parent metal.

The mechanisms relating to the weld pool geometry and penetration characteristics have been studied and modelling techniques have been developed for fluid flow [78], [80] for droplet impact on the liquid metal weld pool [77], [81], and for convection in the weld pool [75].These models were limited to welding trials carried out as bead on plate. The phenomena are more complex when narrow groove welding is considered. For example, while depth of penetration for bead on plate welds is considered in one direction (under the weld pool), for groove welds, penetration of the sidewalls of the groove must be considered.

The modelling techniques described above are characterised by their complexity, their limited versatility, their development based on trials limited to one position, and weld beads deposited on plate rather in groove. In comparison, statistical models are characterised by their relative ease of use, their application in determining the effects of main factors and their interactions with a relatively small number of experiments, and can be orientated to industrial applications where time and cost are very important parameters.

7.2.2.1 Effect of the Welding Parameters on Depth of Penetration

Figure 7.18 is intended to give only a simplified graphical view of the effect of the factors in different welding positions. A detailed and appropriate analysis will follow in the next sections where interactions are included. It is important to understand that effects are not absolute; in other words the size of the effect depends, at least in part, on the values of the factor levels chosen. However, Figure 7.18 gives some indication of effects, since the factor levels were chosen to generate welds which were still of reasonable quality.

The graphs were obtained from the modelling mathematical equations (actual factors: Eqn. 6.2; page 129/ Eqn. 6.12; page 154/ Eqn. 6.18; page 166) considering the low and high levels of the factors each time while all others were held constant (centre point of the design). It is obvious that conclusions refer only to this particular condition.

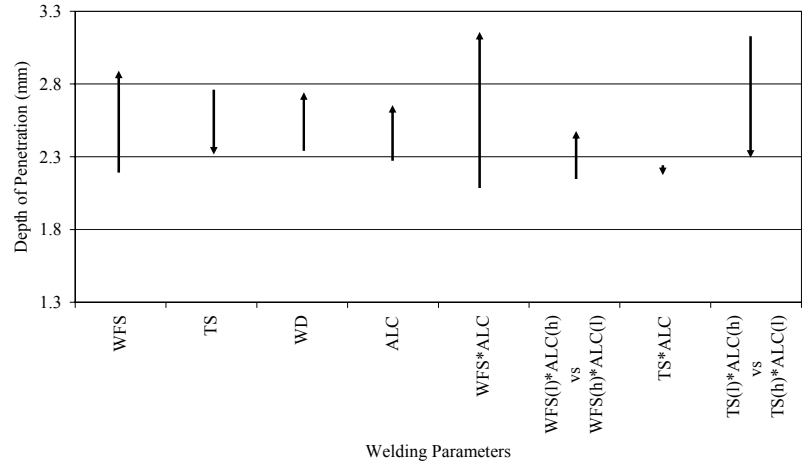

a

b

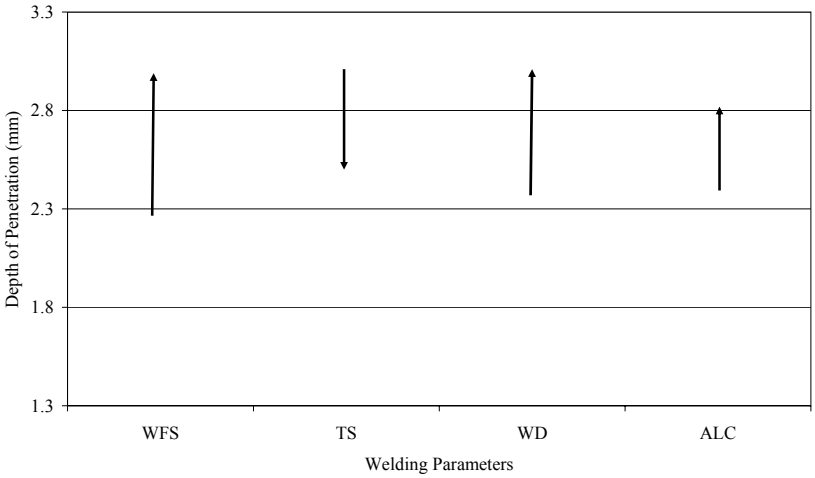

c

Fig. 7-18 Effect of the welding parameters on depth of penetration in (a) flat, (b) vertical down and (c) overhead position

WFS: m/min; TS: mm/min; WD: mm; ALC: %

The upwards direction of the arrows shows an increase in the response when the high level value of the factors is considered, while the downwards direction indicates the contrary effect. The arrow length indicates the magnitude of effect on the response. The arrows relative to (e.g TS(l)*ALC(h) vs TS(h)*ALC(l)) indicate that the second factor combinations produce a decrease in the response depth of penetration, otherwise shown as upwards arrow (where h and l stand for high and low value). As can immediately be seen the main factor effects (wire feed speed, travel speed, wire distance from the sidewall and arc length correction) are always consistent in the direction of the response that is produced, although the magnitudes vary.

In general terms:

- an increase in wire feed speed produces an increase in depth of penetration.
- an increase in travel speed produces a decrease in depth of penetration.
- an increase in wire distance from the sidewall produces an increase in depth of penetration.
- an increase in arc length (arc length correction) produces an increase in depth of penetration

A brief explanation of the above statements is given below:

By increasing the wire feed speed, mean current increases hence, arc energy (heat input) increases accordingly with immediate effect on depth of penetration.

By increasing the travel speed, arc energy (heat input) decreases per unit length and consequently depth of penetration decreases.

When the wire distance from the sidewall increases, the arc is located closer to the groove centreline (where depth of penetration is measured) and produces an increase in depth of penetration.

When arc length increases, mean current and voltage generally increase (this is a power source characteristic) hence also arc energy (heat input) and depth of penetration.

The travel speed effect on depth of penetration in the vertical down position is almost negligible as shown in Figure 7.18b. This may be due to the fact that at low travel speeds (welding speeds) the volume of the welding pool can be high (depending on the quantity of the melted wire and wire feed speed) and due to gravity effect flows below the arc acting as a cushioning effect in melting the base metal and reducing depth of penetration. The cushioning effect of the weld pool on the arc in narrow groove welds (V and I type) due to low welding speeds was reported by Matsunawa and Nishiguchi [130] for welds carried out in 95%Ar5%CO_2 shielding gas environment and MIG welding. Depth of penetration significantly decreased in vertical down compared to flat and overhead positions.

However, other authors have established critical travel speeds (0.06-0.18m/min) for pulsed GMAW [84] below which depth of penetration considerably decreases.

In Figure 7.18a (flat position) the interaction WFS and arc length produces an increase in depth of penetration when both WFS and arc length increase, in agreement with the conclusions discussed above. In the same graph, the travel speed and arc length interaction shows that the effect of travel speed is stronger than arc length alone, and consequently depth of penetration reduces.

Similarly, in Figure 7.18b (vertical down) the interaction travel speed and wire distance from sidewall shows that the depth of penetration is mostly affected by the wire distance from the sidewall, rather than travel speed which has negligible effect. As was discussed above, for an increase in the wire distance, the arc column is concentrated in the centre of the groove, and depth of penetration increases.

Detailed analysis of the phenomena is given below:

Flat Position (0°)

The macrographs in Figure 6.32 (page 126) are of weld No. 13 and represent some of the typical "problems" associated with a given combination of welding parameters. Similar weld profiles were reported for the weld Nos. 12, 11 and 28 where intermittent deflection to the sidewall was observed. These "one sidewall" welds can be explained by two reasons:

a)low wire feed speeds in association with high travel speeds produce a low amount of energy input per unit length of weld with limited capability to melt both filler and parent metal, and
b) long arc lengths (Table 6.13, page 124) produce erratic and preferential droplet detachment to the side of the weld preparation as revealed by high speed video images (Figure 7.19).

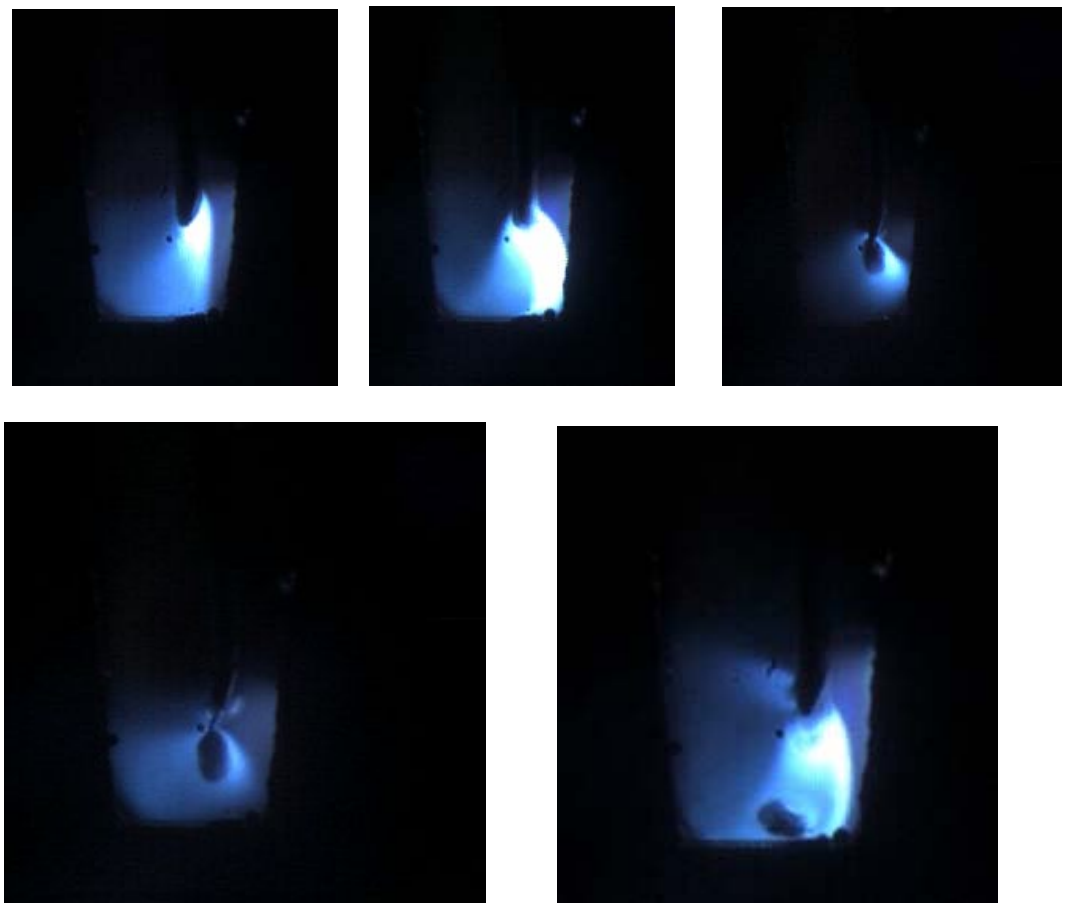

Fig. 7-19 Effect of long arc length on arc and droplet direction

The modelling equations for depth of penetration are described in the equations of Section 6.3.1.1 (Eqns. 6.1-6.2, pages 128-129) and expressed in both coded and actual factors. The coefficients in the coded factors equation show the factor effect and their

magnitude on the response over the range tested. This is representative of the single factor effect but when one or more factors are involved in an interaction the single factor effect has to be correlated to the interaction. The main effects are the slope of a flat plane.
The two-factor interactions are the amount of twist in the plane (if no interaction occurs the two lines in an interaction plot would be exactly parallel). It can be considered that the interaction coefficient is a correction to the main effect coefficients, an adjustment because the response depends on the settings of two factors at the same time. The magnitude of the interaction coefficient indicates how non parallel the lines are, or how much the plane is twisted. A larger coefficient means more twist in the plane [131].

The Figures 6.43 and 6.44 (pages 139 and 140) illustrate the interaction effect of the factors together with the one factor plot in Figure 6.42 (page 138) used in the analysis. Considering that optimisation is included in the scope of this work, the effect of the welding parameters that contribute to an increase in depth of penetration will be considered.
The Figure 6.42 shows that depth of penetration increases when the wire distance from the wall increases. This implies that, in order to maximise depth of penetration the high level of the factor wire distance from the wall has to be selected. The plot is related to a determined set of welding parameters. By varying the other welding parameters (welding speed, wire feed speed and arc length) the graph may change position but importantly, the slope will remain invariable. Depth of penetration was measured along the vertical axis to the weld centreline; when the arc is positioned closer to the groove centreline depth of penetration increases. The following Figure 7.20 shows the arc at the minimum wire distance (0.3mm) from the sidewall defined by the experimental design while Figure 7.21 shows the arc behaviour at the maximum wire distance (1.5mm) from the sidewall.

Fig. 7-20 Arc and droplet transfer at the minimum (0.3mm) wire distance from the sidewall (run No. 4 of the experimental design)

Correlating the results associated with the one factor plot in Figure 6.42 (page 138) and the group of pictures in Figures 7.20 and 7.21 it can be seen that at the minimum distance of the wire from the sidewall the arc was distributed on the sidewall rather than in the weld pool and the sidewall was melted, as undercut defects were reported. When the wire was positioned at the maximum distance from the sidewall, a conical arc profile of the arc core was observed and the energy (including the energy associated with the droplets and their momentum) was concentrated and located on the centre of the weld pool, with a direct effect on depth of penetration.

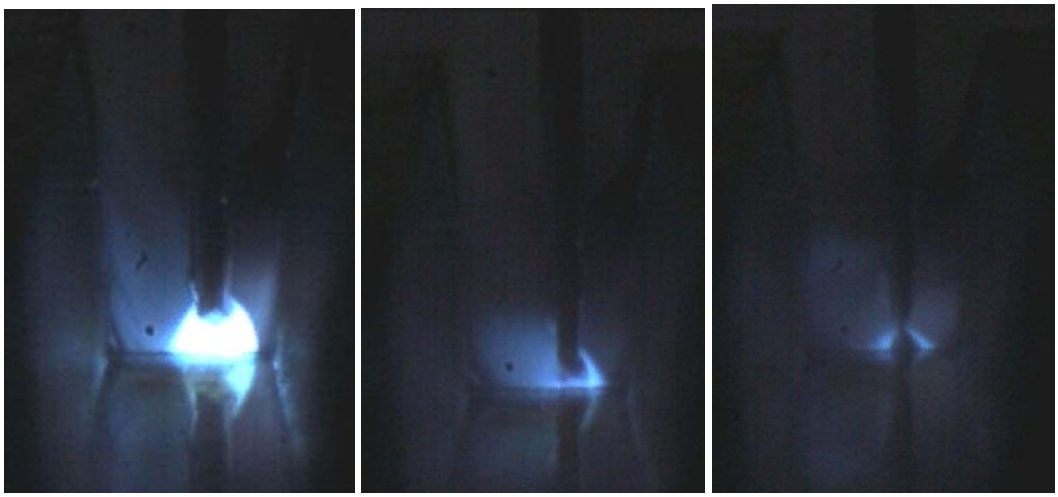

Fig. 7-21 Arc and droplet transfer at the maximum (1.5mm) wire distance from the sidewall (run No 29 of the experimental design)

The interaction plot wire feed speed*arc length correction (arc length) in Figure 6.43 (page 139) was obtained after the parameter wire distance from the sidewall was set at the high level (as established earlier) and the travel speed at the level corresponding to the default centre point of the design space. The interaction plots (Figure 6.43 and 6.44) will be further explained by introducing 3D representations (Figure 7.22).

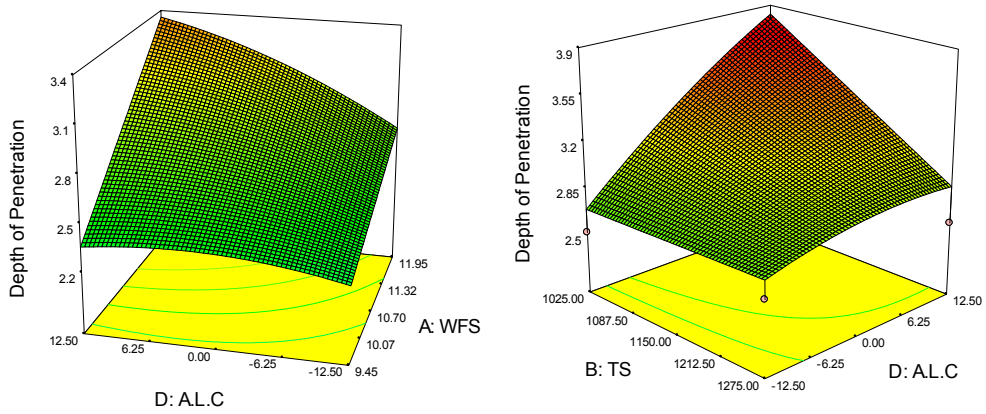

a (wd=1.2mm ; ts=1150mm/min) **b (wfs=11.9m/min ; wd=1.2mm)**

Fig. 7-22 3D Plots for the interaction (a) wire feed speed (m/min)*arc length correction (%) and (b) travel speed (mm/min)*arc length correction (%) on depth of penetration (mm

Depth of penetration increases when wire feed speed and arc length correction (arc length) are at high levels. This can be explained by the fact that, by increasing the wire feed speed, mean current and heat input are increased accordingly with significant effect on depth of penetration. The level of arc length tested in this experimental work was in the range 0.6mm to 3mm (Table 6.13, page 124) and generally it was observed that with longer arc lengths, arc voltage increases and usually current increases as well. Allen [132] described similar findings in his work (bead on plates deposited in pulsed MIG) . Generally, he found that arc voltage increases as a function of the welding current but again no details on arc length values are reported.
Modenesi [4] carried out narrow groove welds in downhand position and concluded that current (and groove gap) are the main variables controlling the axial penetration area. The axial area is the area located below the weld pool.
The influence of the welding current on depth of penetration was confirmed by Essers and Walter [133]. In their investigation of the physical basis of the current influence, they concluded that heat content in the droplets determines the cross-sectional area of penetration and their impact on the molten pool governs the depth of penetration. Furthermore, they reported, that for tests performed with long arcs (8-10mm) the effect of the arc was negligible due to very low current density. When the arc length was reduced to 2-3mm a considerable influence of the arc pressure was noticed. Again, bead on plate trials were carried out.
Kaligerakis [134] found that depth of penetration increases as mean current increases. This is attributed to both higher heat input and droplet momentum. Here, beads were deposited on stainless steel plates using pulsed MIG.
Kim et al [135] carried out their experimental work on mild steel plates and bead on plates in GMAW process was deposited. They reported that, depth of penetration increased as welding current and voltage increased.
Similar conclusions are reported by Gupta [136]. He carried out bead on plate welds in GMAW in flat and vertical positions. Almost all welds presented lower depth of penetration in vertical down position and increasing welding current strongly influenced (increased) depth of penetration. The voltage effect on depth of penetration was related to the fact that, for low voltages and high currents, the weld metal may be larger and acts as a barrier to arc penetration leading to a reduction in depth of penetration. When voltage increases, the weld width increases and deposited metal spreads over a larger area leading in a thin layer of molten metal allowing arc penetration to increase.
Conversely, Minehisa [137], in experimental work performed in narrow groove mild steel plates (MIG; 500A D.C and 300A pulsed, in reverse polarity), found that welding current has a small effect on depth of penetration. This is because depth of penetration is affected by heat conduction of the molten metal and not by heat radiation.
In an attempt to correlate the results of the present work to other published data, it is necessary to emphasise that there is no directly comparable (pulsed tandem, narrow groove, all positions, level of welding parameters including defined arc length values etc) research work similar to the work described here.
The plot in Figure 7.22b indicates that depth of penetration increases at low levels of travel speed and high levels of arc length.
Summarising, depth of penetration is maximised under the following combination of welding parameters: $\mathbf{WFS_{high}}$, $\mathbf{TS_{low}}$, $\mathbf{WD_{high}}$, $\mathbf{ALC_{high}}$. The terminology adopted, “low”

and “high”, does not necessarily refer to maximum or minimum values level values but indicates the direction for the level of the factor in order to optimise the response.

Vertical Down Position (90°)

Typical macrographs of welds in the vertical position are shown in Figure 6.60 (page 152) where there is a significant transition in the weld bead profile compared to the flat position profile (Fig. 6.33, page 127). This confirms the significant effect of position on weld bead geometry for the same set of welding parameters.

The optimisation procedure established above indicates that in order to maximise depth of penetration, the following level values (Figures 6.61, 6.62 and 6.63, pages 155-156) of the welding parameters need to be considered:
WFS_{high}, $TS_{low(or\ high)}$, WD_{high}, ALC_{high}

The travel speed effect is irrelevant since the high or low values produce the same effect. In vertical down position more weld metal is spread to the sidewall than in flat and overhead positions and this reduces depth of penetration.

Overhead Position (180°)

A different weld profile in the overhead position was obtained, for the same welding conditions, as the macrographs in Figure 6.73 (page 164) show.

The one factor plots (Figures 6.74, 6.75, 6.76, 6.77; pages 167-169) reported in section 6.3.3.3 (page 167) established that depth of penetration is maximised by the following set of levels for the welding parameters:
WFS_{high}, TS_{low}, WD_{high}, ALC_{high}

Generally, the effect of the main welding parameters on the depth of penetration is similar for all positions. Therefore, the possible explanations presented for flat position also apply to the overhead position.

7.2.2.2 Effect of the Welding Parameters on Groove Sidewall Penetration

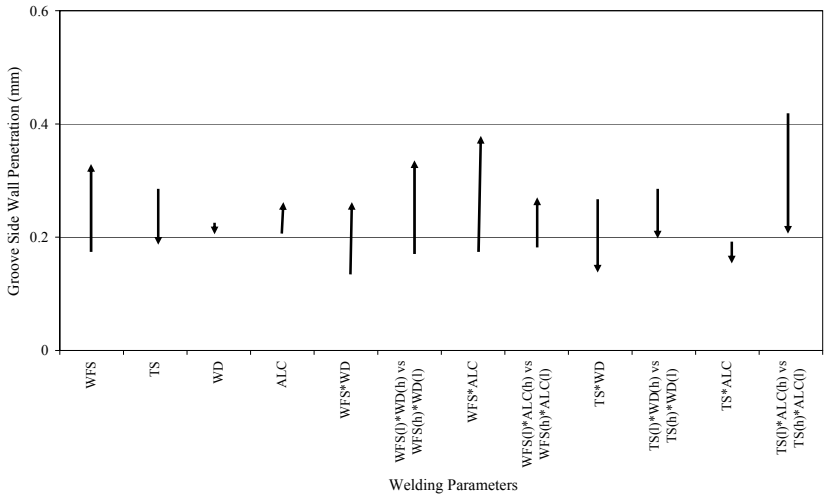

a

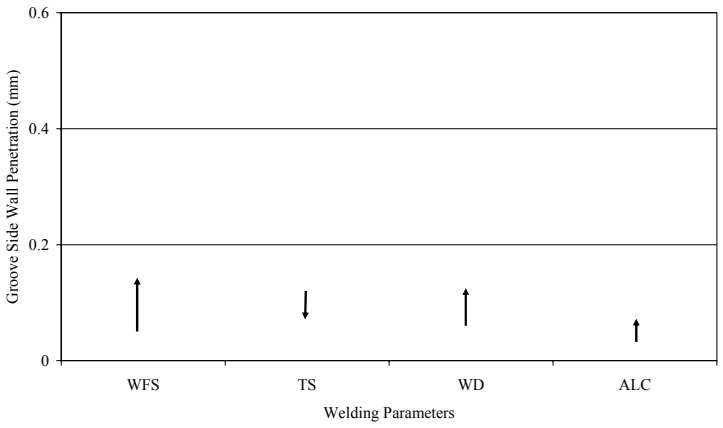

b

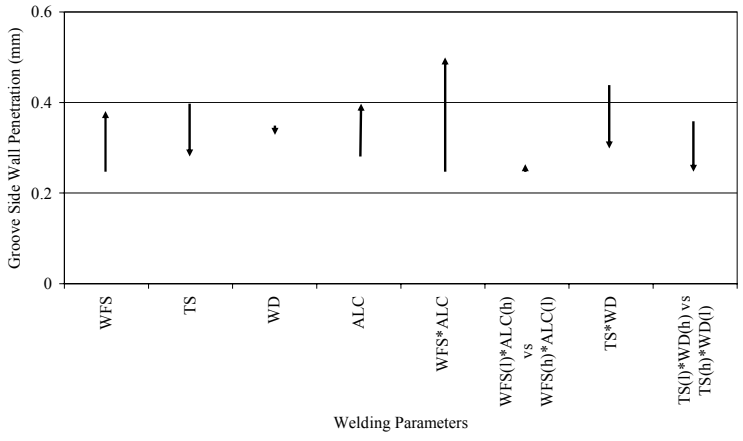

c

Fig. 7-23 Effect of the welding parameters on groove sidewall penetration in (a) flat, (b) vertical down and (c) overhead position

WFS: m/min; TS: mm/min; WD: mm; ALC: %

As in section 7.2.2.1 simplified graphical views for immediate comparison purposes of the effects of the welding parameters on groove sidewall penetration were plotted (Figure 7.23).
The graphs were obtained from the modelling equations (Eqn. 6.4; page 129/ Eqn. 6.14; page 154/ Eqn. 6.20; page 166). Again, the low and high level value for each factor was considered, while the centre point of the design value was considered for the remaining factors. The centre points of the design for the welding parameters are:
WFS=10.7m/min; TS=1150mm/min; WD=0.9mm and ALC=0%.
Regarding the effects of the main factors on groove sidewall penetration the following conclusions can be drawn:

- in all three welding positions, when wire feed speed increases, groove sidewall penetration increases
- in all three welding positions, when travel speed increases, groove sidewall penetration decreases
- in all three welding positions, when arc length increases, groove sidewall penetration increases (with different magnitude).
- in both flat and overhead positions, when wire distance from the sidewall increases, groove sidewall penetration decreases by a very small amount. The opposite effect is reported in the vertical position.

The effect of the welding parameters on groove sidewall penetration is very similar to the analysis relating to depth of penetration (with a minor difference relating to wire distance) establishing a significant correlation between groove sidewall penetration and depth of penetration. It is expected therefore, that for a determined set of welding parameters, when depth of penetration increases, groove sidewall penetration will increase accordingly.
When wire feed speed increases, more filler metal is melted, mean current and therefore arc energy (heat input) increase with a significant benefit to groove sidewall penetration.
As discussed in depth of penetration, when travel speed increases, heat input per unit length decreases and consequently groove sidewall penetration decreases.
The high speed images have revealed that in “sound” welds obtained by different arc lengths, the longer arc presented a better spread of the arc cone in the narrow groove. This led to a better distribution of the arc radial heat to the sidewall. Considering that sidewall fusion is probably more affected by the radial heat diffusion from the arc column, this may be correlated to the arc length [130]. Longer arcs, within the limits used in this experimental work, increased groove sidewall fusion. In all the experiments here when arc length increased, arc voltage increased and this may cause higher radial heat flow to the sidewall due to arc radiation thus enhancing groove sidewall penetration.
The importance of the arc length in sidewall fusion is mentioned by Modenesi [4], despite the fact that no conclusions were drawn. The same author [4] has concluded that in downhand position the lateral penetration area in narrow groove MIG welding increases with current.
When wire distance from the sidewall increased, it produced a marginal decrease in groove sidewall penetration in flat and overhead position (Figure 7.23) leading to a negligible effect. In flat and overhead positions, the arc is more associated with side defects and welds carried out with the wire close to the sidewall produced undercuts. Conversely, in vertical down position, groove sidewall penetration increased as the wire

distance from the sidewall increased. The longer the distance of the wire from the sidewall, the better the spread of the arc and higher radial arc heat to the groove sidewall is obtained. This can be seen in both Figures 7.20 and 7.21 (pages 253 and 254).
In both flat and overhead positions an increase in the level of the combination wire feed speed*arc length produced the highest effect on groove sidewall penetration.

Flat Position (0°)

The modelling equations for groove sidewall penetration are described in the equations 6.3 and 6.4 (page 129) and expressed in terms of coded and actual factors (Eqns. 6.3 and 6.4; page 129).
The meaning of the coloured bars in Figure 7.23a has been discussed already (section 7.2.2.1). The plots reveal the considerable reduction in groove sidewall penetration in the vertical down position compared to the flat and overhead positions.
All factors (welding parameters) are involved in interactions meaning that the effect of a single factor depends on the level of the associated factor in the interaction. This means that reliable conclusions can only be obtained from interaction plots rather than one factor plots.
Optimisation of a response consists of selecting the appropriate levels of the welding parameters to maximise the response.
Figure 6.45 (page 141) shows the interaction between the wire feed speed and the wire distance from the sidewall. This is a characteristic example of the importance of interaction plots in the optimisation process. For wire feed speeds below 10.5m/min, groove sidewall penetration increases in relation to the high value of the wire distance from the sidewall. Conversely, for greater wire feed rates, groove sidewall penetration increases with a decrease in the wire distance from sidewall. Therefore, depending on the point selected within the design space, there is an optimum set of factors (welding parameters) that provides the optimum for the response.
Figure 7.23a implies that when wire feed increases (high level) and wire distance from sidewall decreases (low level) groove sidewall penetration increases. Also to be considered is the fact that at the same time, wire feed speed and travel speed are also involved in interactions with the factor arc length. Selecting the wire feed speed at high level and the wire distance from the sidewall at low level, the interaction plot between the wire feed speed and the arc length (Figure 6.46, page 141) implies that higher penetration is obtained when the high level of the arc length is considered. Adopting this last conclusion, the interaction plot travel speed*arc length (Figure 6.48, page 142) shows that higher groove sidewall penetration is expected at low levels of the travel speed and that, at the low welding speed, wire distance from the sidewall shows quite small effects (Figure 6.47, page 142).
The following 3D plots (Figure 7.24) emphasise the above conclusions and together with the 2D interaction plots can be used to optimize the process within any section of the design space.

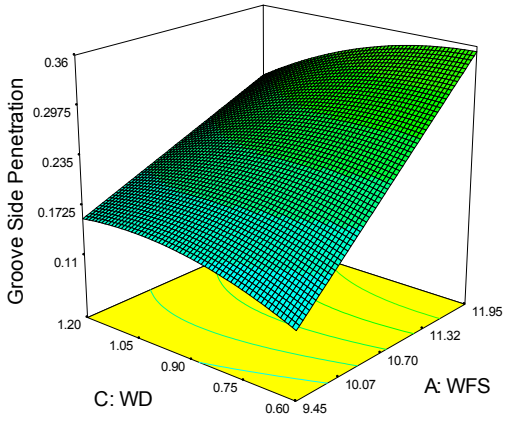

a) (ts=1150 ; a.l.c=0%)

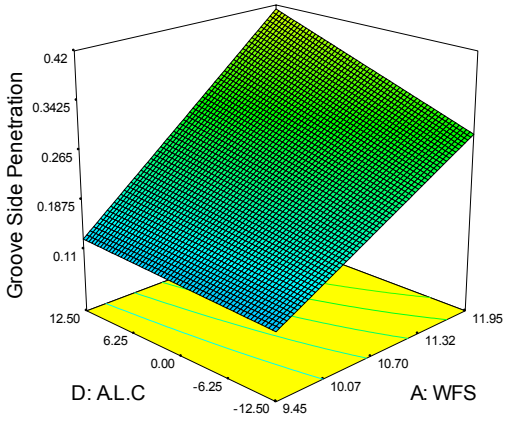

b) (ts=1150; wd=0.6)

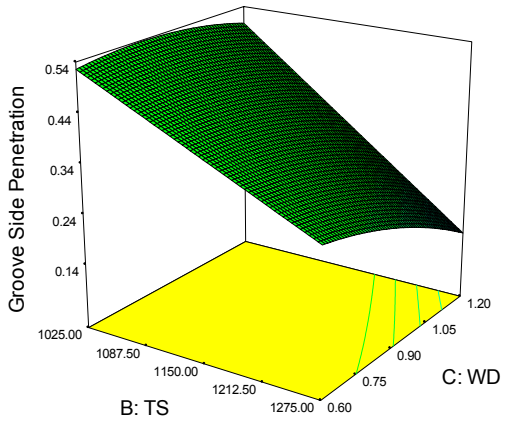

c) (wfs=11.9; alc=12.5%)

Fig. 7-24 3D Plots for the interaction (a)wire feed speed (m/min) *wire distance from sidewall (mm), (b) wire feed speed (m/min)* arc length correction (%) and(c) travel speed (mm/min)*wire distance from sidewall (mm) on groove sidewall penetration (mm)

In conclusion groove sidewall penetration is maximised with the following combination of the welding parameters: **WFS_{high}, TS_{low}, $WD_{low\ or\ high}$, A.L.C $_{high}$.**
The wire distance effect on groove sidewall penetration is almost identical whether its low or high value is selected when the low level of the travel speed is considered.

Vertical Down Position (90°)

The optimisation process based on the one factor plots (Figures 6.64, 6.65, 6.66 and 6.67; pages 157-159) leads to the following set of the welding parameters:

WFS_{high},TS_{low} WD_{high} $ALC_{5\%}$.
The effect of the welding parameters on the response groove sidewall penetration has been discussed in the introduction of the present section.

Overhead Position (180°)

The main welding parameters and their interaction effects are quite similar to those discussed in the flat position, although with different magnitudes.
The 2D interaction plots (Figures 6.78 and 6.79;page 170) together with the 3D plots (Figure 7.25) provide the following set of the levels for the welding parameters in order to maximise groove sidewall penetration: **WFS_{high},TS_{low} WD_{low} ALC_{high}.**

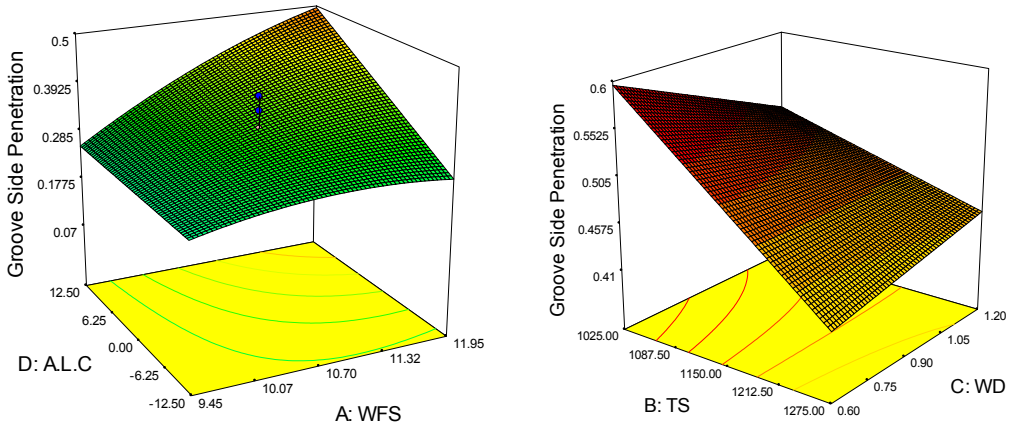

a) (ts=1150mm/min; wd=0.9mm) **b) (wfs=11.95m/min ; alc=12.5%)**

Fig. 7-25 3D Plots for the interaction (a) wire feed speed (m/min) *arc length correction (%) and (b) travel speed (mm/min)*wire distance from sidewall (mm) on groove sidewall penetration (mm)

7.2.2.3 Effect of the Welding Parameters on Corner Angle

As in sections 7.2.2.1 and 7.2.2.2 a simplified graphical view (Figure 7.26) for an assessment of the effect of the welding parameters on corner angle was used.
The graphs refer to a given set of values of the welding parameters (Eqn. 6.8; page 130/ Eqn. 6.16; page 154/Eqn. 6.22; page 166). This means one factor was tested at low/high values, while the others were held constant (centre point of the design) and the response was estimated. The Figure 7.26a (flat position) shows that an increase of the travel speed produces an increase in the value of the corner angle. This may not always be the case due to the fact that travel speed is involved in an interaction with two other parameters (wire distance from the sidewall and arc length), meaning that the effect of the factor travel speed depends on the level of these other factors in the interaction.

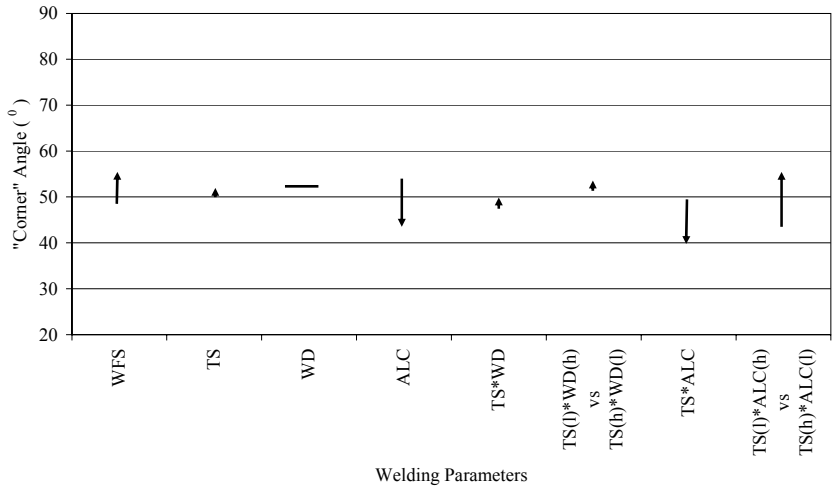

a

b

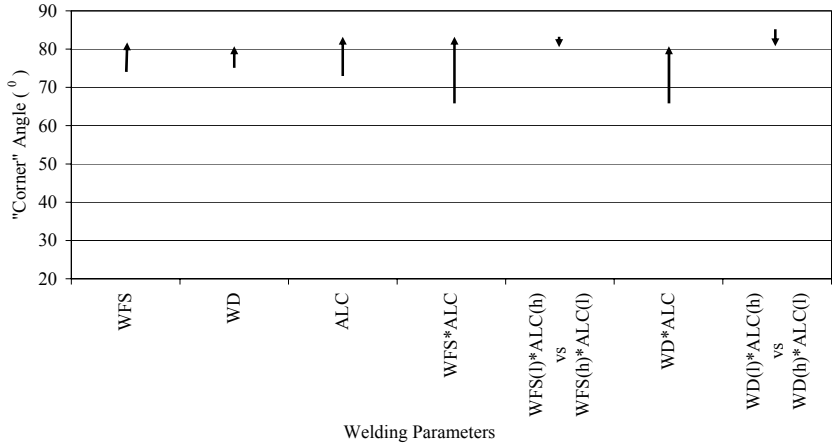

c

Fig. 7-26 Effect of the welding parameters on corner angle in (a) flat, (b) vertical down and (c) overhead position

WFS: m/min; TS: mm/min; WD: mm; ALC: %

It is apparent from Figure 7.26 that the welding parameters have different effects depending on welding position. In fact, the welding procedure could be optimised for each welding position, and these changes are possible with the latest pipe welding systems.
The Figure 7.27 (interaction plot travel speed * arc length) shows that corner angle decreases with increasing travel speed at high values of arc length, but increases with increasing travel speed at low values of arc length.

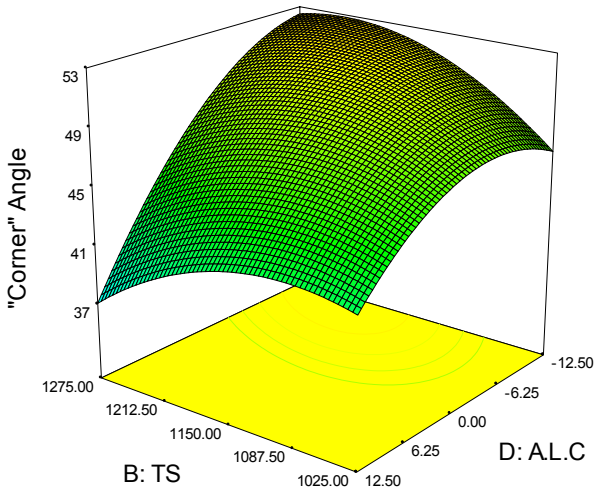

Fig. 7-27 3D Plot for the interaction travel speed (mm/min)*arc length correction %) for the effect on corner angle (°)

This example demonstrates the importance of taking full account of interactions (as in this case) using a DOE (Design of Experiments) approach which can account for interactions and illustrates that simple experiments, varying one factor at a time, may lead to erroneous conclusions.
Nevertheless, it is noted that the different corner angle levels are strongly dependent on the three different positions. In flat position corner angle range is 40° to 55°, in vertical down 20° to 35° and in overhead 65° to 85°.
This emphasises that the welding position is probably the most important parameter in 5G girth welds.
This result is highly significant, since corner angle can play a major role in determining whether defects are formed in this area during the next welding pass.
The corner angle was analysed throughout this work. However, the wetting angle can be estimated (Fig. 5.10, page 77) after corner angle is calculated. The goal set was to minimise the corner angle and therefore maximise the wetting angle.

Flat Position (0°)

The 2D plots (Figures 6.52, 6.53, and 6.54; pages 145-146) together with the following 3D plots (Figure 7.28) emphasise the effect of the welding parameters and their range on corner angle.

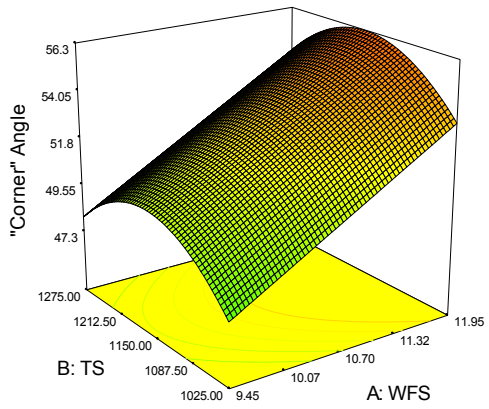

a) ts=1150m/min; wd=0.9mm; alc=0%

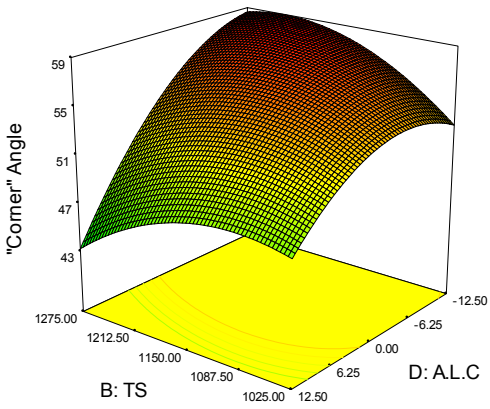

b) wfs=9.45m/min; wd=0.90mm

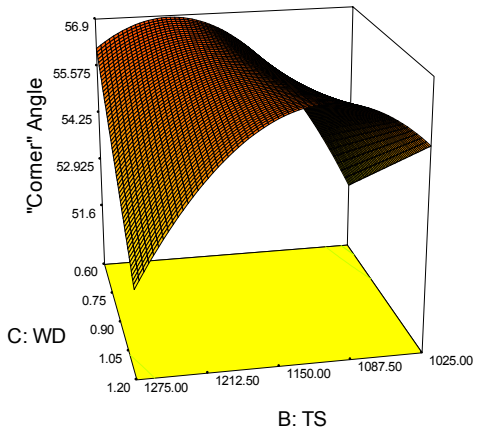

c) wfs=9.45m/min; alc=12.5%

Fig. 7-28 3D Plots for the (a) wfs (m/min) effect and the interactions (b) travel speed (mm/min) *arc length correction (%) and (c) travel speed (mm/min)*wire distance from sidewall (mm) on corner angle (°)

Analysis of the plots, show that corner angle can be minimised for the following set of the welding parameters: **WFS_{low}, TS_{high}, WD_{high}, ALC_{high}.**

Vertical Down Position (90°)

The effect of the welding parameters on the weld geometry can be estimated using the following 3D plots (Figure 7.29) in association with the 2D plots (Figures 6.68, 6.69 and 6.70; pages 159-161).

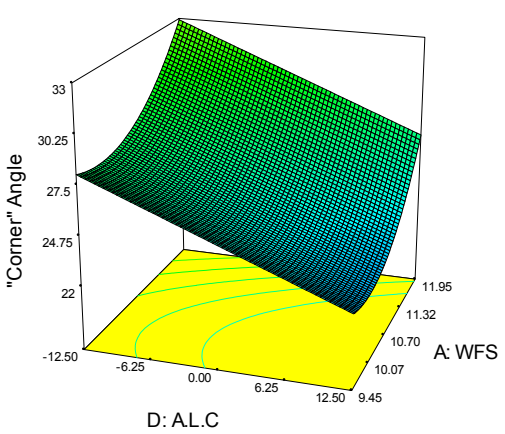

a) ts=1150mm/min, wd=0.9mm

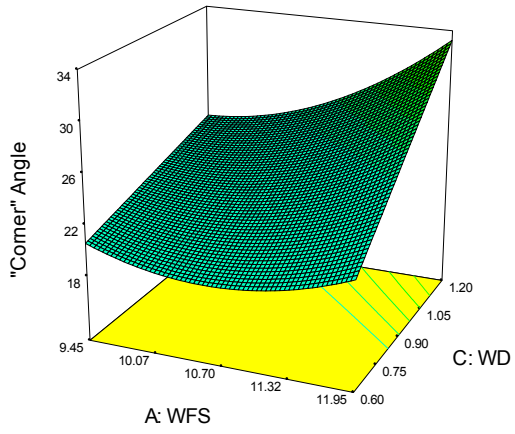

b) ts=1150mm/min, alc=12.5%

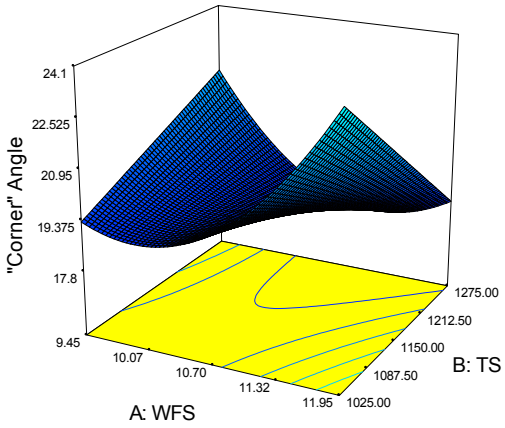

c) wd=0.6mm; alc=12.5%

Fig. 7-29 3D Plots for the (a) alc(%) effect and the interactions (b) travel speed (mm/min) *arc length correction (%) and (c) travel speed (mm/min)*wire feed speed (m/min) on corner angle (°)

Analysis of the graphs shows that minimum corner angle can be obtained:
WFS_{high}, TS_{high}, WD_{low}, ALC_{high}.

However, it should be noted that in both plots (Figures 7.29c and 6.70) corner angle can be minimised for some low values of the wire feed rate (below 10.3m/min; WFS_{low}) and

the low value of the travel speed (1025mm/min; TS_{low}). This is another important example, showing that an investigation of the effect of a factor on a response may generate multiple solutions. Therefore, the effect can vary (e.g. depending on interactions) in relation to the different levels of the factors within the design space.

Overhead Position (180°)

As with flat and vertical down positions, the effects of the welding parameters on the corner angle can be obtained from the 2D plots (Figures 6.80, 6.81 and 6.82; pages 171-172) together with the 3D plots (Figure 7.30).

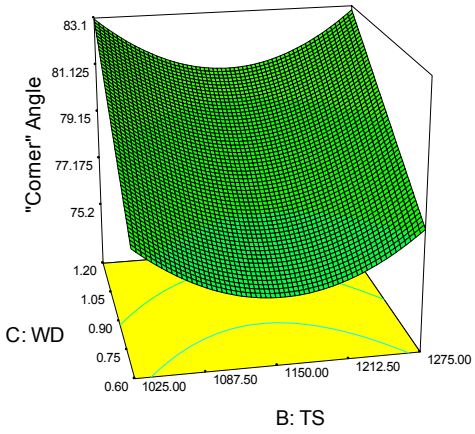

a) wfs=10.7m/min; alc=0%

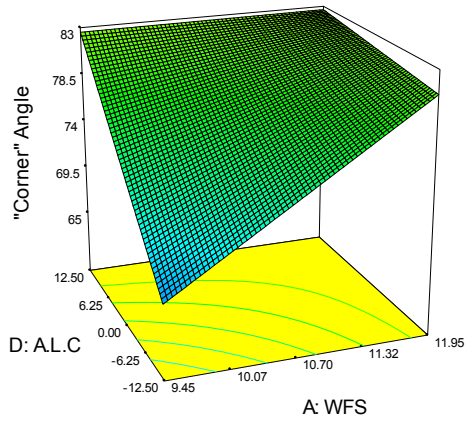

b) ts=1150mm/min; wd=0.9mm

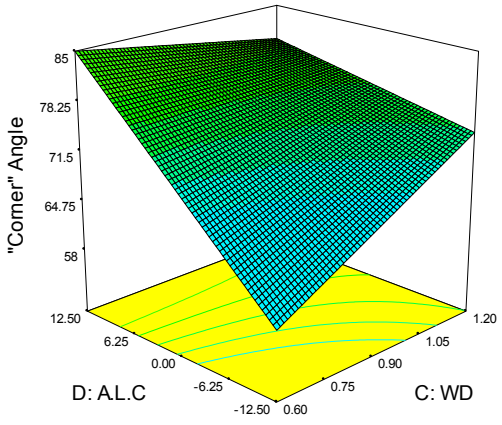

c) wfs=9.45m/min; ts=1150mm/min

Fig. 7-30 3D Plots for the (a) ts (mm/min) effect and the interactions (b) wire feed speed (m/min) *arc length correction (%) and (c) wire distance from the sidewall (mm)*arc length correction (%) on corner angle (°)

The above graphs show that, corner angle can be minimised for the following set of the welding parameters.
WFS_{low}, TS_{centre}, WD_{low}, ALC_{low}.
However, it should be noted that any setting for the travel speed between low to high produces similar results for the corner angle.

Both 2D and 3D graphs underline the variation of the factor effects on corner angle depending upon the welding position and emphasise the strong effect of the welding position on the weld pool behaviour and spread within the groove. It is likely that gravity forces become the predominant factor in controlling the weld pool although surface tension forces effect depending on the position may not be necessarily ignored.
Attempts to explain the effect of the remaining factors are presented below.

If the wire feed rate decreases, corner angle decreases and therefore wetting angle (toe angle) increases. This may be due to less material being deposited.
Similarly, when travel speed increases, it is expected to produce less material to build up, and therefore corner angle decreases (wetting angle increases). Stepanov [138] who carried out narrow gap welds in flat position confirmed that an increase in the travel speed produced an increase in the wetting angle.
However, although not directly comparable, Quintino [84] in bead on plates welds (PGMAW, flat position) reported slightly different results: when heat input increased, wetting angle increased and fusion angle remained constant. Fusion angle in Quintino's experiments is the equivalent to toe angle defined in the present work. When travel speed increased up to 0.12m/min fusion angle increased. Above the 0.12m/min fusion angle remained constant. Wetting angle decreased as travel speed increased.
She defined wetting angle (α) and fusion angle (β) as shown in Figure 7.31.

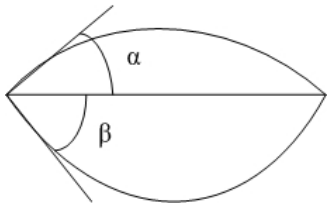

Fig. 7-31 Wetting and fusion angles for bead on plate welds

In the present experimental work an increase in arc length generally produced an increase in arc voltage and mean current. This generated an increase in the wetting angle as a result of more efficient spread and fusion of the sidewalls. Similar conclusions were reported by Stepanov [138] although in his trials an arc length of 5-6mm was used well above the maximum 3mm arc length measured during the present experimental trials.

7.2.2.4 Effect of the Welding Parameters on Sidewall Penetration

All welding conditions in the three positions presented acceptable sidewall penetration and no defects (e.g. side-lack-of-fusion) were reported. Analysis of the maximum sidewall penetration was limited to the flat position.

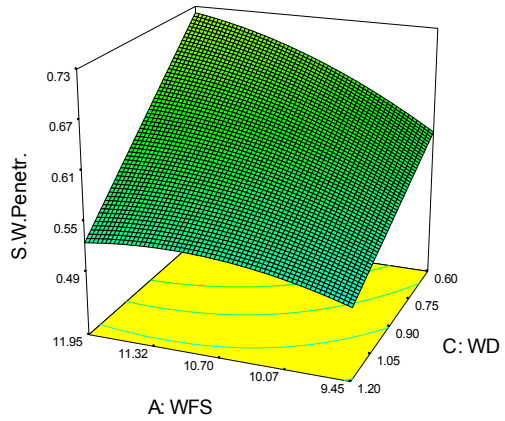

a) ts=1150mm/nin; alc=0%

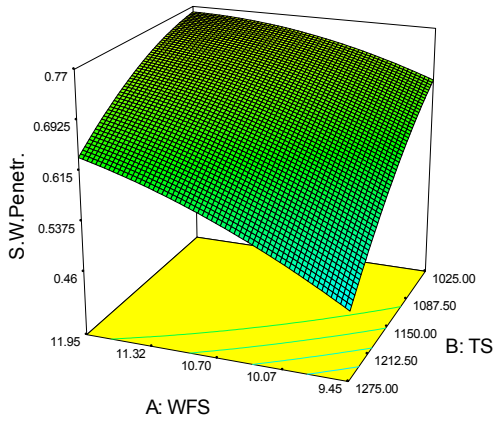

b) wd=0.60mm; alc=0%

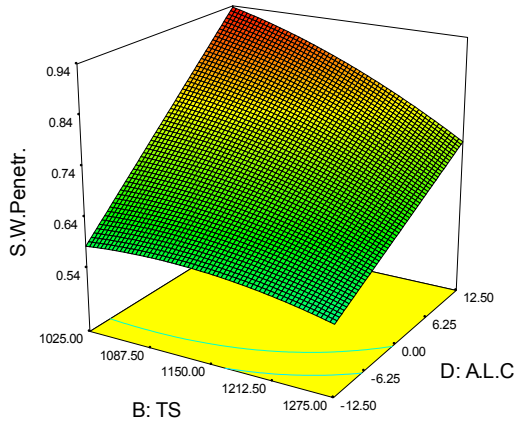

c) wfs=11.95m/min; wd=0.60mm

Fig. 7-32 3D Plots for the main and interaction effects of (a) wire feed speed (m/min)* wire distance from the sidewall (mm), (b) wire feed speed (m/min) * travel speed (mm/min) and (c) travel speed (mm/min)*arc length correction (%) on sidewall penetration (mm)

The above 3D plots (Figure 7.32) together with the 2D plots (Figures 6.49, 6.50 and 6.51; pages 143-144) show that side wall penetration can be maximised for the following set of the welding parameters:
WFS_{high} TS_{low} WD_{low} ALC_{high}

The effects of the welding parameters are similar to those for groove sidewall penetration (explained in section 7.2.2.2) and that indicates a relationship between the two responses. In order to investigate the potential correlation between sidewall and

groove sidewall penetration the following Figure 7.33 was obtained after the actual values of both responses were considered:

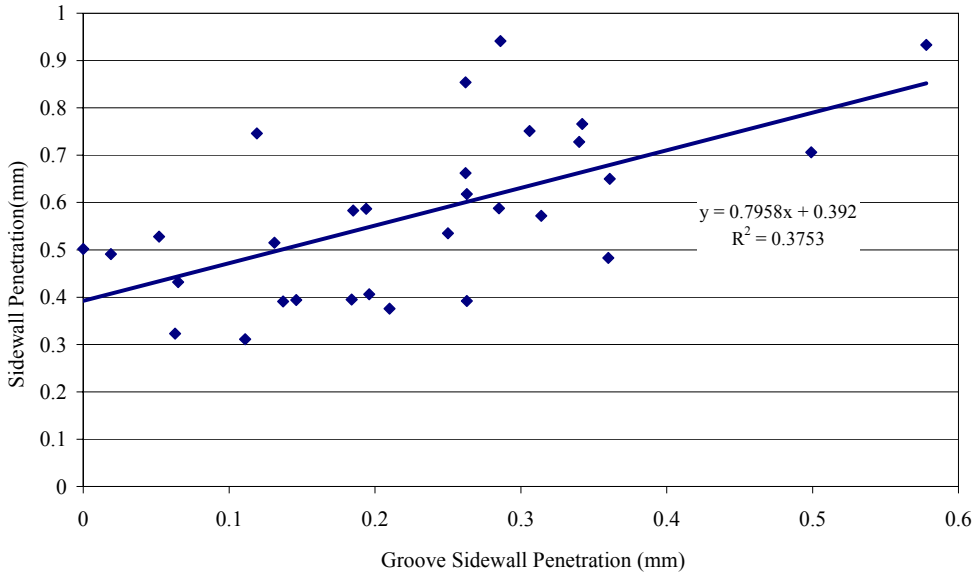

Fig. 7-33 Correlation plot between sidewall and groove sidewall penetration

Despite the scatter revealed it is evident some correlation exists between the two dimensions of the weld bead geometry. Therefore, for a selected set of the welding parameters if sidewall penetration increases it is likely that groove sidewall penetration will increase accordingly. However, sidewall penetration is not a very good predictor for groove sidewall penetration indicating that it is better if groove sidewall penetration is treated separately.

7.2.2.5 Effect of the Welding Parameters on Undercut

The welding conditions used throughout this experimental work produced relatively few welds with undercut. This reduces the ability of developing a useful model, meaning that the model will probably be poor at predicting the response undercut. The diagnostic plots (Figures 6.40, 6.41; pages 136-137) present strong patterns which indicate that the model should be used with caution. Despite this, the results obtained are discussed and probable causes analysed.

Figure 6.58 (page 149) shows that when arc length increases, undercut increases. This may be due to the higher voltage values associated with longer arc lengths where the arc core is more likely to climb to the sidewalls.
Figure 6.57 (page 148) shows that when wire distance from the sidewall decreases, undercut increases. This may due to the fact that the arc is then more likely to jump to the sidewall. Generally, visual inspection of the welded specimens confirmed this to be the case.
Figure 6.56 (page 148) shows a minimal effect of travel speed on undercut. The fact that undercut increases when travel speed increases may be associated with insufficient flow of weld metal, due to rapid solidification, to replace the base material melted.

Figure 6.55 (page 147) shows that undercut decreases when wire feed speed increases. This may be due to the high welding speeds used in the process where more welded material is needed to fill the regions of the base metal melted.
However, higher wire feed speeds are associated with higher currents and higher currents determine higher arc forces causing welding defects such as undercut associated with surface tension forces [139].
Undercut can be minimised if the welding parameter levels are selected as follows:
WFS_{high}, TS_{low}, WD_{high}, ALC_{low}

7.2.2.6 Validation of the Models

In order to provide a clear validation of the models developed in this project, new welds were carried out, and compared to the model predictions. The results are reported in Table 6.23 (page 196) and reproduced as graphical views in Figure 7.34.
The models showed reasonable agreement between predicted and measured values and successfully validated the weld bead profile predictions for the three positions. However, the discrepancies (welds Nos. 2, 3 and 4; Table 6.23 and Figure 7.34) outlined in the vertical down position (mainly associated with the groove sidewall penetration) emphasise that the model predictions need to be considered with caution. Potential reasons for this limited model performance is likely to be the significant lack of fit tests (depth of penetration) and the low levels for Adj. R-Squared and Pred. R-Squared (groove sidewall penetration).
Nevertheless this is the first development (as far as is known) of weld bead shape mathematical models for 5G girth welds, supported by very good prediction properties as the validation process has confirmed.
Furthermore, this will allow the design of the weld geometry using the model to determine appropriate levels for the welding parameters and hence to achieve the required weld profile.

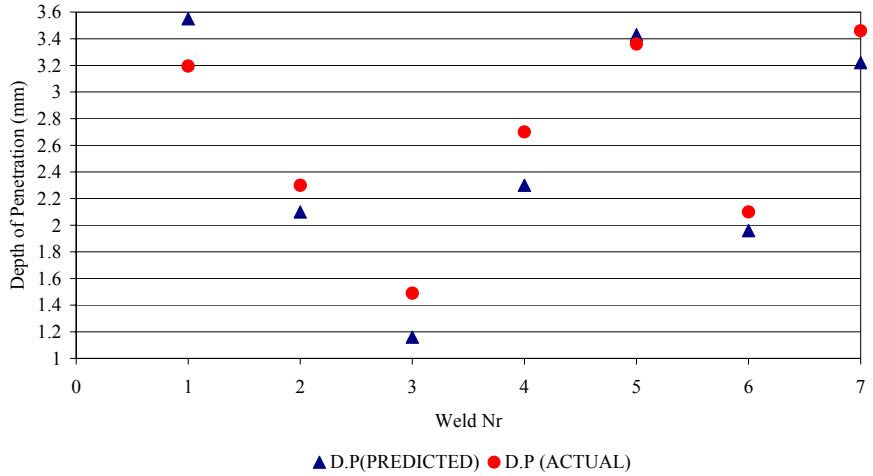

a

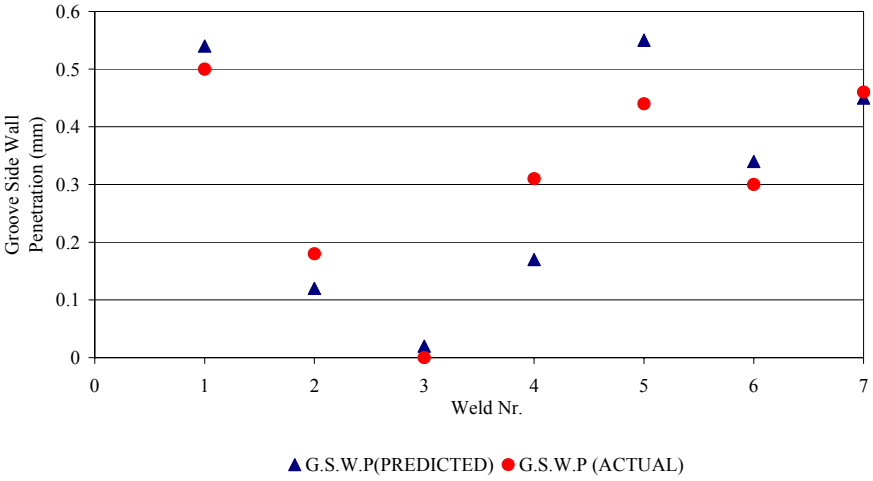

b

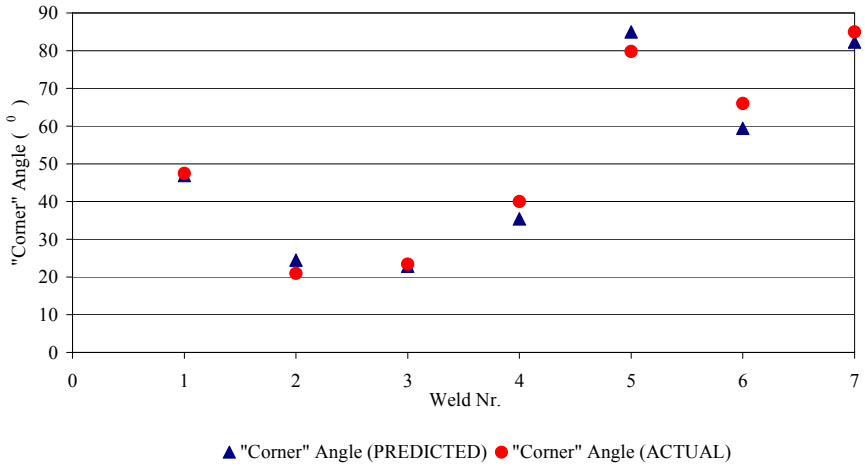

c

Fig. 7-34 Models validation tests in (a) flat, (b) vertical down, and (c) overhead position

7.2.2.7 Angular Position Model

In view of the major changes in bead shape between 0°, 90° and 180°, it was decided that a more detailed series of experiments should be performed at 30°, 60°, 120° and 150°.
The three responses, depth of penetration, groove sidewall penetration and corner angle presented almost similar trends to the ones developed for the individual positions. Detailed information regarding the model equation and factor effect on response plots are presented in section 6.3.4 (page 172).
In order to represent in a single plot the predictions of the angular model together with the points predicted from the individual models for 0°, 90° and 180°, predicted points were obtained (Figures 7.35 and 7.36) for the following welding conditions:
WFS=11.0m/min; TS=1100mm/min; WD=1.0mm; ALC=5.0%

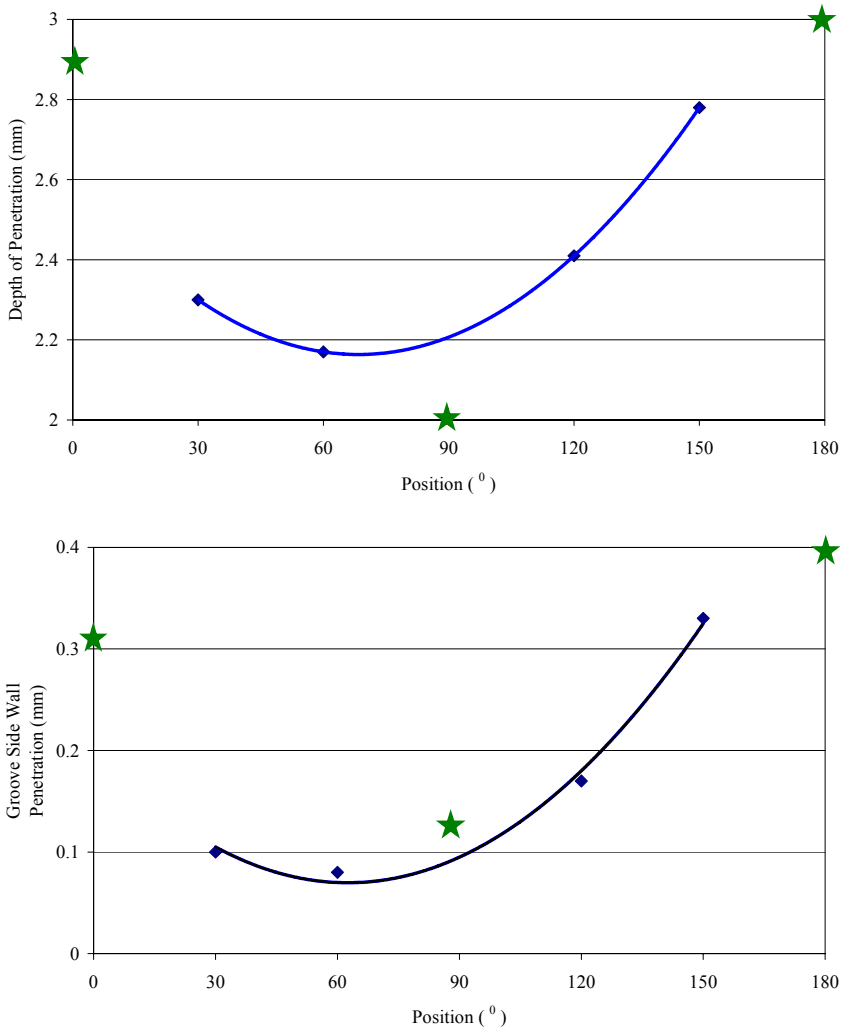

star points corresponded to model predictions in 0°,90° and 180° positions

Fig. 7-35 Model predictions for the responses depth of penetration, groove sidewall penetration in angular, flat, vertical down and overhead position

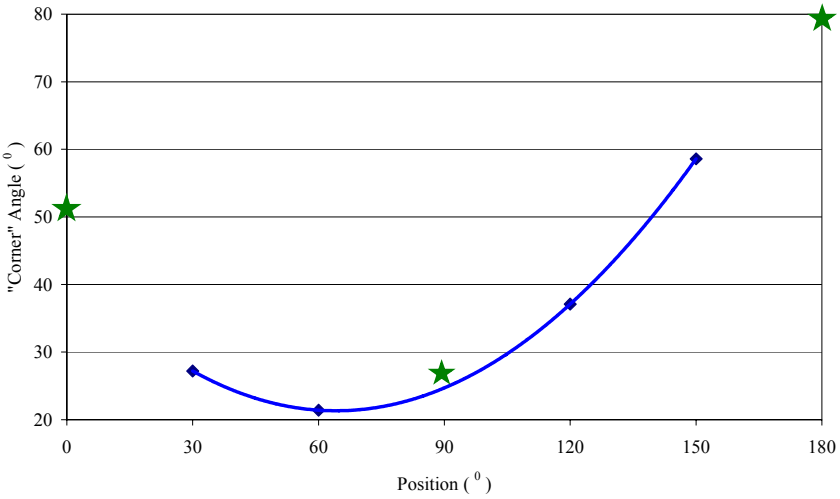

Fig. 7-36 Model predictions for the response corner angle in angular, flat, vertical down and overhead position

The above plots refer to four models and represent a very successful correlation of the three individual and the angular position predictions, meaning that for the major welding positions of a girth weld, adequate models for the weld bead shape are now available. Furthermore, the appropriate level for the factors can be selected in order to maximise the responses.

7.2.2.8 Combined Model

The combined model was generated after a statistical treatment (section 6.3.5; page 185) of the three individual models (flat, vertical down and overhead) aiming to provide one mathematical equation for every response capable of predicting the weld geometry in all positions.
The models are presented in section 6.3.5 and the effects of the factors on the responses are shown in detail in section 6.3.5.3 (Figures 6.98-6.109; pages 189-194) exhibiting similar trend as discussed in the previous sections.
The welding parameters used for the welds carried out in the angular design were used in the combined model equations and the predicted values of the weld geometry were compared to the ones of the actual angular welds. The validation results are summarised in Tables 6.24, 6.25 and 6.26 (pages 197-198) and again predictions are generally quite acceptable.

7.2.2.9 Summary

From all models developed and discussed above (0°,90°,180°,angular and the combined model), it can be concluded that welding position is the major factor controlling the weld shape. To emphasise this, a “map” of the minimum and the maximum actual values for each response in 0°, 90° and 180° was created and the equivalent macrograph sections associated with these positions were obtained (Figures 7.37, 7.38, 7.39). These

graphs emphasise the transition of the weld geometry with weld position, and show the range of weld geometry at a given welding position.

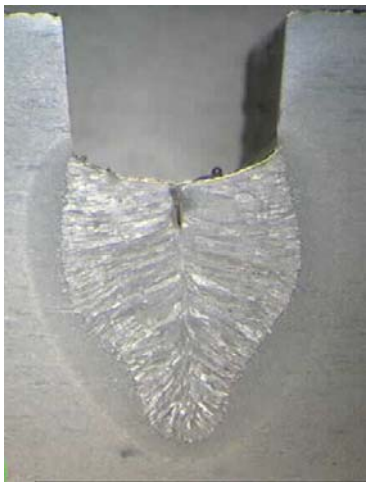

No. 15:11.95/1025/1.2/12.5

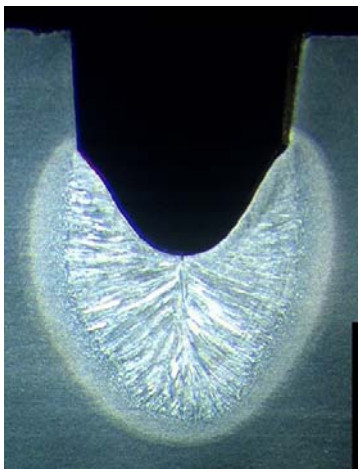

No. 23:11.95/1275/1.2/12.5

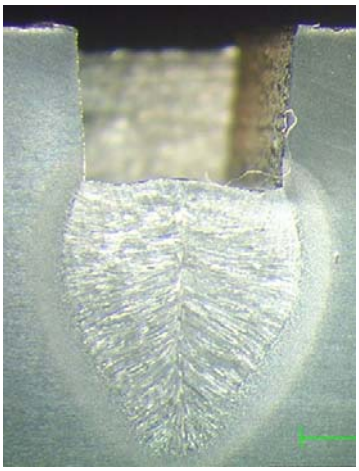

No. 15:11.95/1075/1.2/12.5

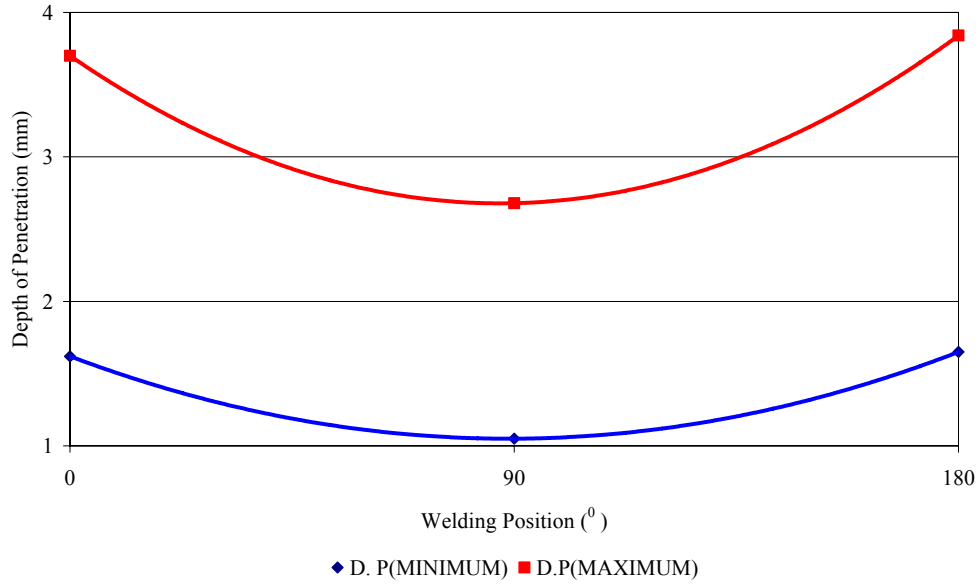

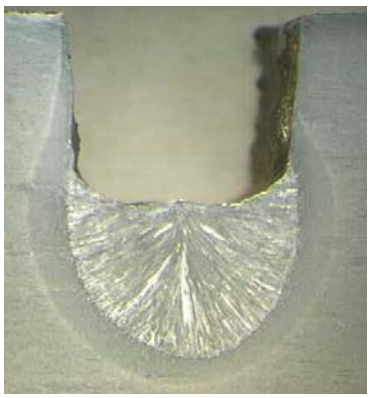

No. 26:9.45/1025/0.6/-12.5

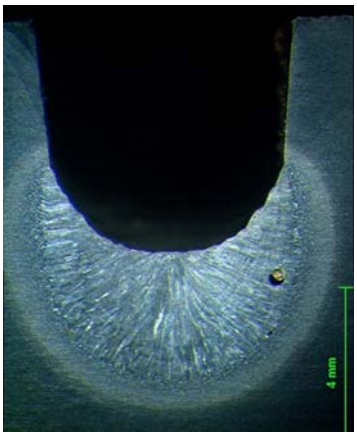

No. 26:9.45/1025/0.6/-12.5

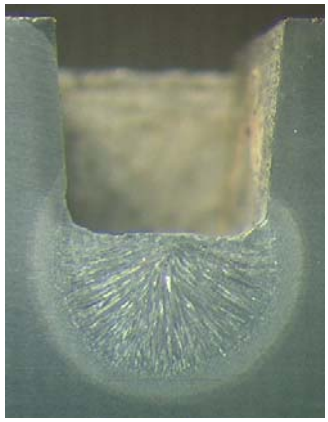

No. 19: 9.45/1275/0.6/-12.5

Key: *weld No.; wire feed speed (m/min); travel speed (mm/min); wire distance from sidewall (mm); arc length correction (%)*

Fig. 7-37 Macrographs for the minimum and maximum depth of penetration in relation to the welding position

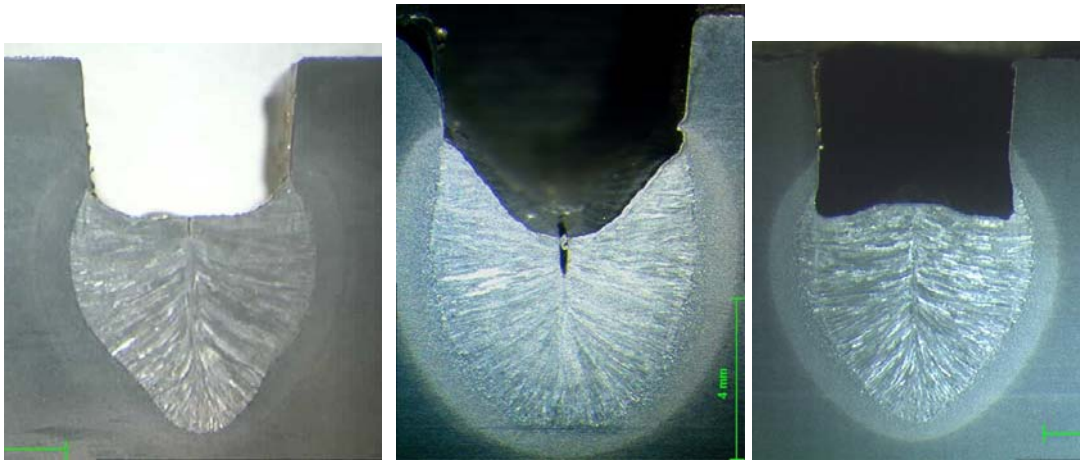

No. 27:11.95/1025/1.2/12.5 No. 16:13.2/1150/0.9/0.0 No. 27: 11.95/1025/0.6/12.5

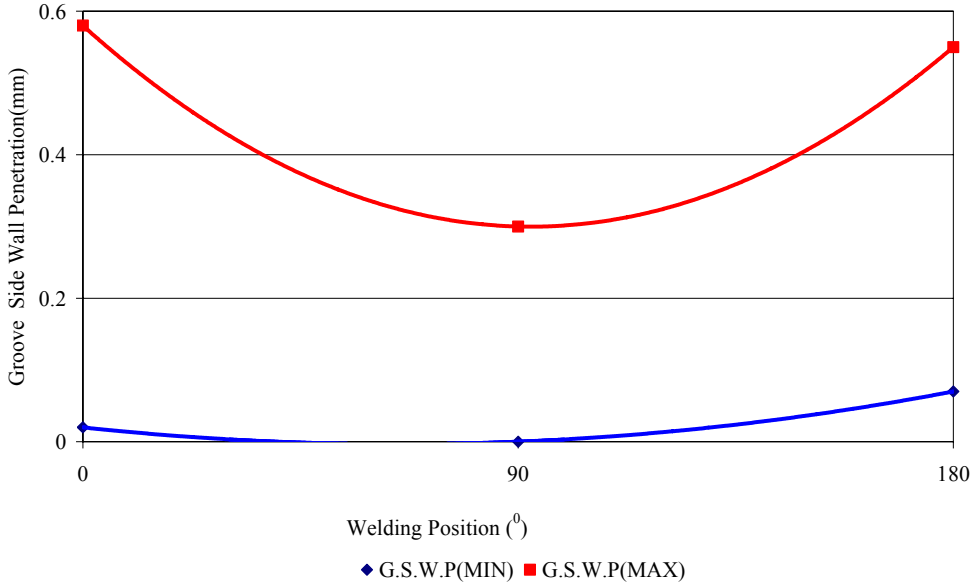

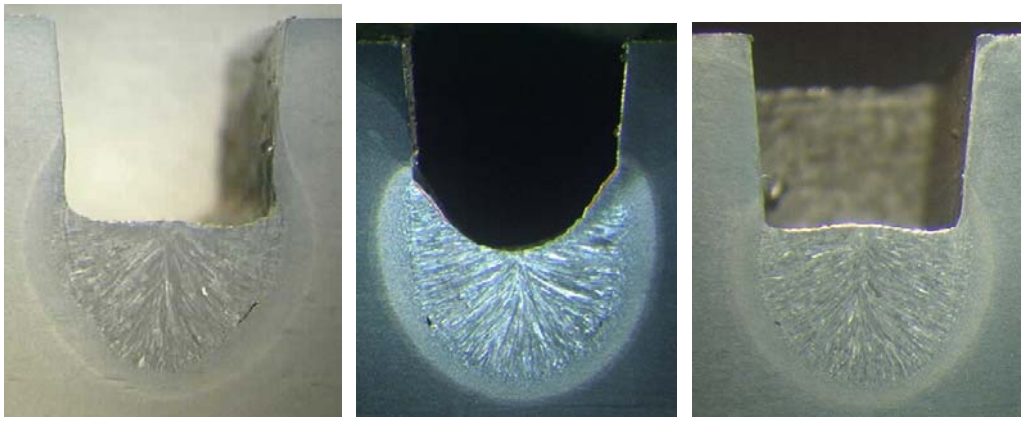

No. 11:9.45/1275/1.2/12.5 No. 7:11.95/1275/0.6/-12.5 No. 24:8.2/1150/0.9/0.0

Key: weld No.; wire feed speed (m/min); travel speed (mm/min); wire distance from sidewall (mm); arc length correction (%)

Fig. 7-38 Macrographs for the minimum and maximum groove sidewall penetration in relation to the welding position

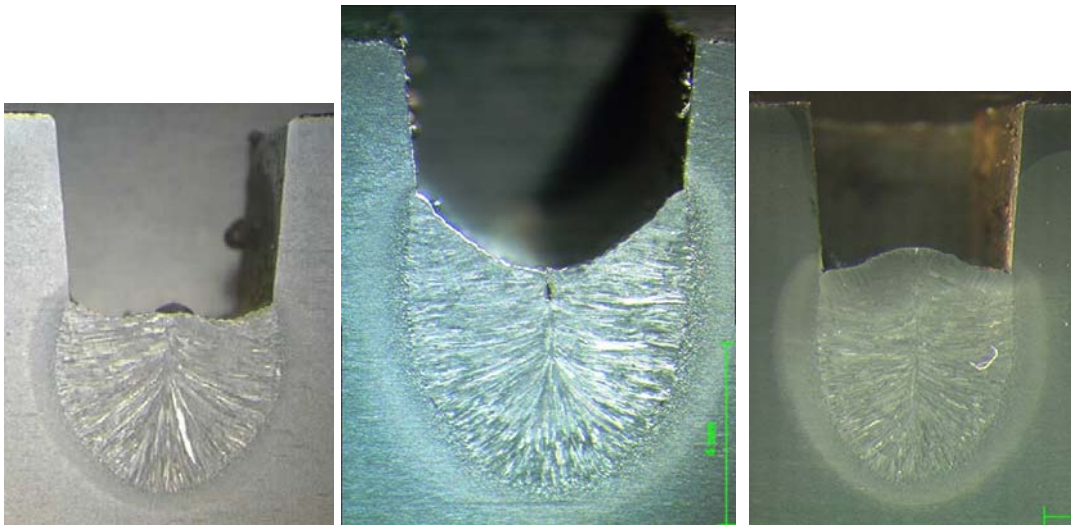

No. 7:11.95/1275/0.6/-12.5 No. 10:11.95/1025/1.2/-12.5 No .10:11.95/1025/1.2/-12.5

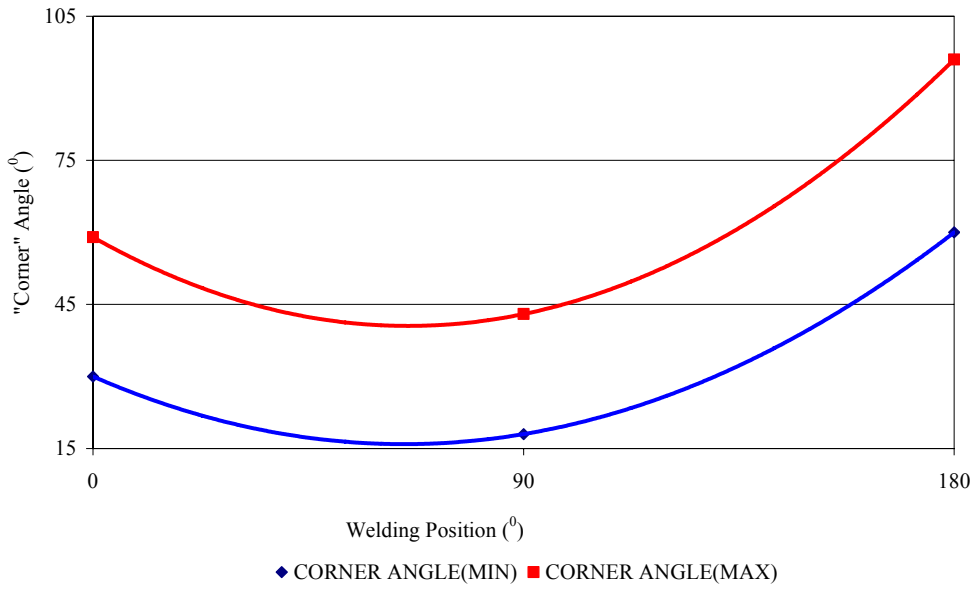

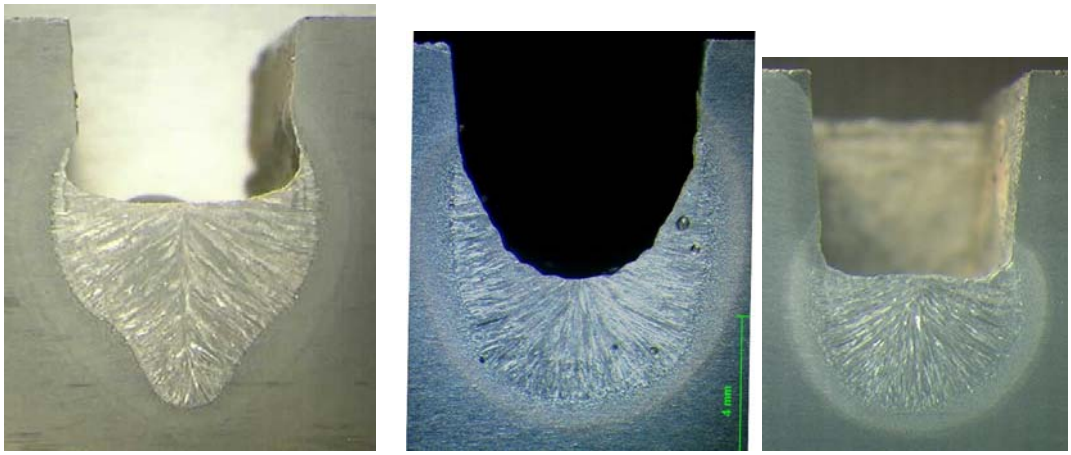

No. 28:10.7/1150/0.9/25.0 No. 4:10.7/1150/0.3/0.0 No. 19:9.45/1275/0.6/-12.5

Key: weld No.; wire feed speed (m/min); travel speed (mm/min); wire distance from sidewall (mm); arc length correction (%)

Fig. 7-39 Macrographs for the minimum and maximum corner angle in relation to the welding position

Some welds in vertical down position show solidification cracking defects. Although solidification cracking is not included in this study it is likely to be associated with the welding variables because of the significance of the weld bead height to width ratio [87].

7.2.2.10 Optimisation

The effect of the welding parameters on the weld bead geometry is based on the analyses of one-factor and interaction plots. These plots are useful in determining the value for a single response, but cannot be satisfactorily used when more than one response is required to be optimised. Instead, the numerical optimisation feature provided by the Design Expert Software allows the optimisation of more than one response at the same time. Groove sidewall penetration and corner angle are the most important dimensions of the weld profile. (Depth of penetration has not been a significant issue in tandem welding).
For the software optimisation, each response was assigned with an importance relative to the other responses. The least important was assigned a value of 1 and the most important a value of 5. Depth of penetration was assigned a value of 3 and groove sidewall penetration and corner angle 5.
The conclusions from the interaction plots are compared with the software optimisation as shown in Figures 7.40, 7.41 and 7.42.
The arrows indicate the level (high/low) of the welding parameters resulting from the interaction plots, while the horizontal line shows the centre point. The numbers are the results of the software optimisation. Arrows in both directions for the same parameter indicate that the same level of response is obtained whether the low or the high level of the parameter is considered. Numbers in bold indicate "discrepancies" between numerical and interaction plots predictions.

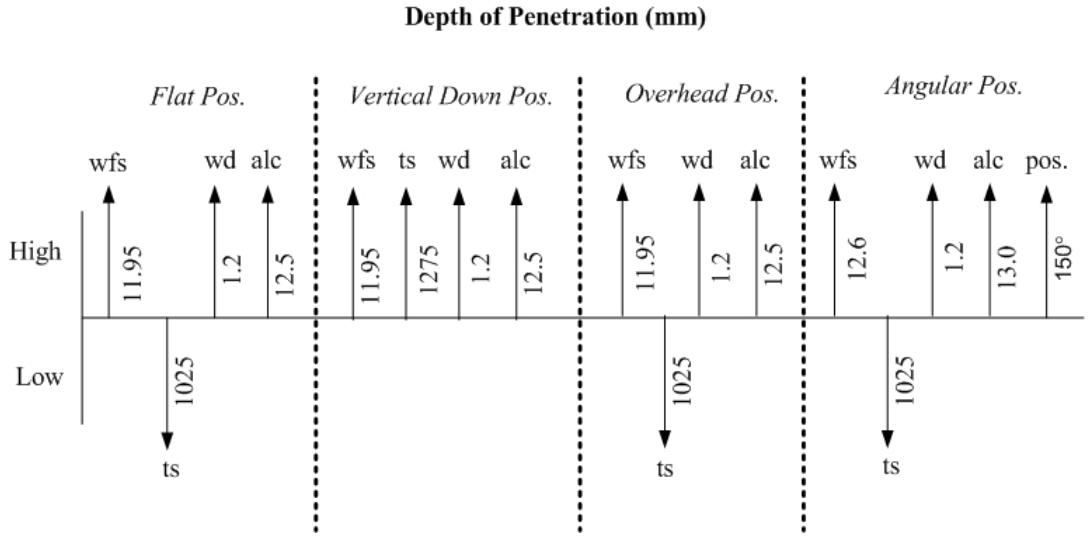

Fig. 7-40 Numerical (software) optimisation vs interaction plots optimisation

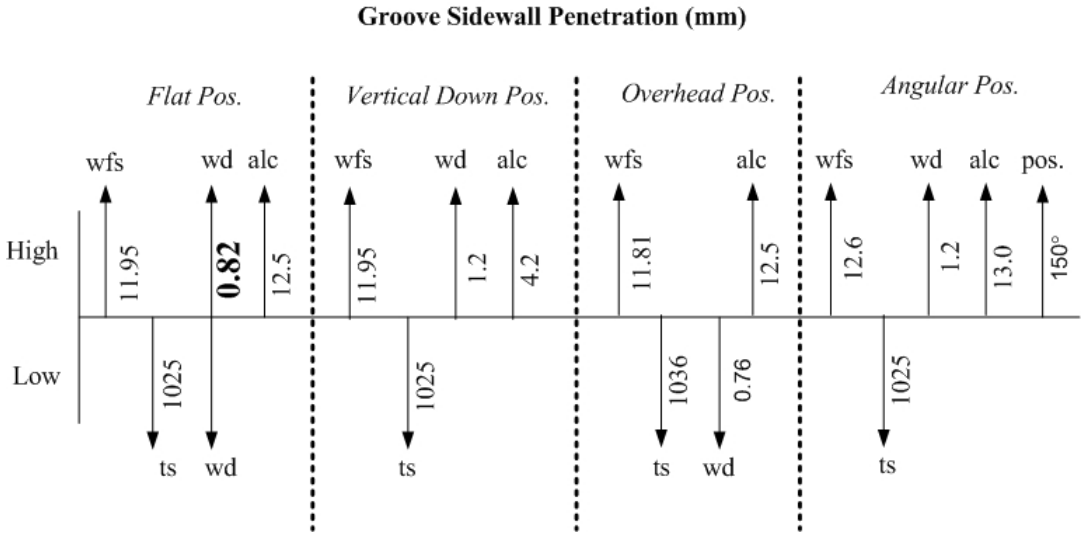

Fig. 7-41 Numerical (software) optimisation vs interaction plots optimisation

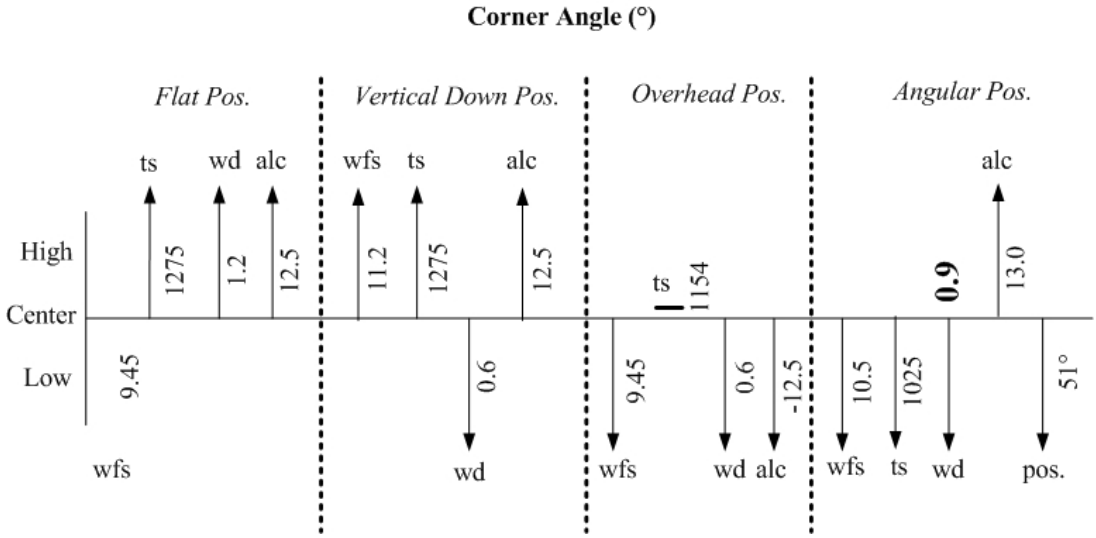

Fig. 7-42 Numerical (software) optimisation vs interaction plots optimisation

The software numerical predictions and the interaction plots conclusions of the optimisation procedure were in a very good agreement and only two minor discrepancies were reported:
In the response groove sidewall penetration (flat position) the same effect was obtained whether the low or high level of the wire distance is considered while the level of the centre point (0.82) is the optimum for the numerical optimisation.
Similarly, the optimum for the corner angle in the angular position corresponded with the low level of the wire distance parameter while the numerical optimisation was defined as the centre point (0.9).
Contrarily, Table 7.3 reports the numerical optimum parameter settings for the optimisation of both groove sidewall penetration and corner angle. It can be seen that some optimum parameter settings are different than those proposed from the individual

numerical optimisation (Figures 7.40, 7.41, 7.42). This is to be expected since the model algorithm searches for adequate settings for the factors in order to optimise two or more responses simultaneously. A typical example is shown in the angular model (Table 7.3) where parameter levels were modified compared to the ones used in the individual interaction plots.
The predicted responses for the angular and combined model are less sensitive to the wire distance from sidewall values and an optimum level of 0.6mm can be applied for all the positions of Table 7.3.
Generally, a trend in the welding parameter settings can be established for all positions despite some variations towards the low levels for the wire feed rate and arc length in the overhead position where a smaller and a faster cooling weld pool is required. Modern power supplies offer the possibility of changing the welding parameters throughout the pipe circumference.

Position	WFS (m/min)	TS (mm/min)	WD (mm)	A.L.C (%)	Groove Sidewall Penetration (mm)	Corner Angle (°)
Flat	11.95 11.10	1025 1025	0.6 1.02	12.5 12.5	0.53 0.41	46.2 46.6
Vertical Down	11.39	1025	0.6	8.6	0.11	22.4
Overhead	9.52	1025	0.6	-12.5	0.35	60.6
Angular 30° 34.24°	 12.6 12.57	 1025 1025	 0.6 1.17	 13.0 12.12	 0.35 0.35	 25.4 27.3
Combined 17.34° 14.17°	 11.95 11.95	 1025 1025	 0.6 0.97	 12.49 12.5	 0.38 0.39	 34.7 39.6

Table 7-3 Welding parameters settings and optimised groove sidewall penetration and corner angle model predictions

7.3 Shielding Gas Trials

7.3.1 Shielding Gas Composition, Weld Profile and Arc Length

Most of the previous [5],[18],[1] and present work on tandem welding at Cranfield, was based on 82.5%Ar12.5%$CO_2$5%He gas mixture. The use of the three gas composition was the result of the experimental work performed by Thompson [6] and subsequently by other researchers [62],[120],[103].
However, no statistically valid study had been performed on shielding gas composition for narrow groove pipe welding. Hence it was decided to carry out a systematic and statistically controlled investigation for this study. The D-Optimal design was selected as the most appropriate for mixtures.
In the first part of the discussion the effect of the arc length is considered. Although it is considered critical to obtain a sound weld bead many of the previous studies have ignored this fact. Relationships between arc length and arc voltage and the weld bead geometry are correlated to the shielding gas compositions.

7.3.1.1 Weld Bead Profile and Arc Characteristics

High speed video images (Figures 6.111, page 200) of different shielding gas mixtures show different arc lengths and arc profiles. Compositions rich in either argon or helium generally present longer arc length compared to compositions rich in carbon dioxide.
Quintino [140] reported similar conclusions in experiments conducted with Ar/CO_2 mixtures and she attributed the arc shape, to higher thermal conductivity with mixtures rich in CO_2 which leads to a more uniform arc distribution of the arc temperature and to shorter arc length. Conversely, mixtures with less carbon dioxide give a hotter inner zone as compared with the peripheral zone and longer arc length characteristics.
The weld bead profiles in Figure 6.110 (page 199) are associated with different shielding gas compositions. The “finger” profile obtained with low carbon dioxide content (95%Ar 5%CO_2) in the shielding gas is in agreement with other published data [44],[32] and can be attributed to the high-energy inner core of the argon plasma [32]. Furthermore, the low thermal conductivity in an argon rich environment leads to a narrow hot arc column (and a considerably cooler outer zone) contributing to the development of the finger shaped penetration profile. Conversely, in high thermal conductivity, carbon dioxide rich gas the arc core is wider which provides more heat spread on the parent metal surface leading to the bowl penetration profile [40],[35].
Generally, the droplet size increased with an increase of carbon dioxide in the gas mixtures. This means that the large droplets formed impinged a wider area of the parent metal. This is likely to explain the “bowl” shape of the weld profile associated with gas mixtures rich in carbon dioxide content.

7.3.1.2 Arc Length and Arc Voltage Relationship

The relationship between arc length and arc voltage has been discussed by few authors. With simplifying assumptions, some mathematical equations have been developed to describe that relationship [141], [142].

No reports were found in the literature of the relationship between arc length and arc voltage for different shielding gas mixtures. However, the present experimental work has investigated the link between arc length and arc voltage for different gas mixtures. Experiments included both flat and overhead positions and are reported in Figures 6.112 and 6.114 (pages 200 and 201).
The numbers representing the arc length values need to be treated with caution considering the error in the arc length measurements. The different arc length and arc voltage results recorded for the different gases may be attributed to the gas properties (e.g. thermal conductivity or ionisation potential).
In Figure 6.114 (page 201) for example, the gas composition 70%Ar30%CO_2 required higher voltage for the same arc length compared with the other gas mixtures. Generally, the current intensity levels monitored for all the gas mixtures were very similar, and due to high thermal conductivity of the carbon dioxide, heat losses by conduction increased and therefore higher voltage (for the same current) levels were required to stabilise the arc [140].
The higher voltage levels associated with higher percentages of carbon dioxide content in the shielding gas are confirmed in the voltage traces (Figures 6.125 and 6.126; pages 209-210). Furthermore, the number of short circuits (represented by the number of voltage drop spikes) increased with higher carbon dioxide content in the gas mixture (e.g. 70%Ar30%CO_2, 70%Ar27%$CO_2$3%O_2).
Arc length was controlled by the arc length correction controller (-30% to +30%) installed on the front panel of the power supplies and this relationship is reported in Figures 6.113 and 6.115 (pages 201 and 202). The availability of the relationship between arc voltage and arc length and the type of bead profile produced during this work is clearly important in the development and implementation of procedures for pipe welding.

7.3.1.3 Arc Length and Weld Bead Profile

Considering that arc length is dependent on shielding gas composition (section 7.3.1.2) the same arc length, for all the gas mixtures tested, was considered essential for a fair and direct comparison of their effects on weld bead profile. Little published data were found for the "same arc length "criterion. Most reports were limited to the weld metal geometry obtained from different gas mixtures, with no reference to arc length.
Figure 6.120 (page 204) shows the as welded profiles obtained from different arc lengths for the gas composition 82.5%Ar12.5%$CO_2$5%He. The macrographs in Figures 6.122, 6.123 and 6.124 (pages 206, 207 and 208) underline the significant effect of arc length on the weld bead profile. As the macrograph photographs show and as discussed in section 7.2.2.1, long arc lengths produce erratic and preferential droplet detachment to the side of the weld preparation or cause the arc to jump on the side wall. An arc length of 1.0mm to 2.0mm can be considered as a safe range of operation for "sound" welds. However arc lengths close to the low level of the range (or even lower) produce considerable spatter (dip transfer). All arc length values were maintained within the above range in order for the results to be directly comparable.
Different arc length values obtained by the arc length correction parameter (-30% to +30%) were tested and the weld profiles were analysed. Long arcs produced "finger" like penetration profiles while shorter arc produced more rounded profiles. Typical weld profiles are shown in Figure 7.43.

76%Ar11%$CO_2$10%He3%O_2

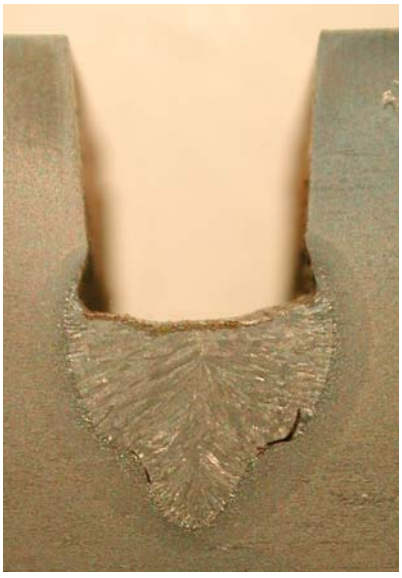

a) ALC=+30% (arc length 2.0mm)

b) ALC=-30% (arc length 0.4mm)

82.5%Ar12.5%$CO_2$5%He

a) ALC=+10% (arc length 1.3mm)

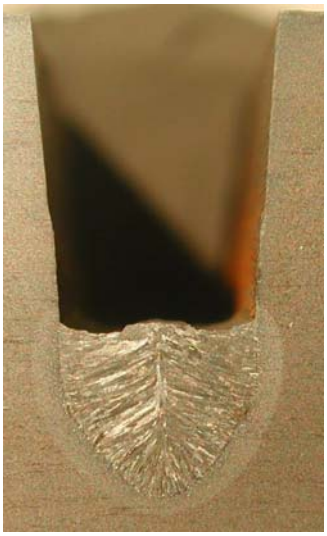

b) ALC=-30% (arc length 0.4mm)

Fig. 7-43 Typical penetration weld profiles for (a) long arc length and (b) short arc length

Similar results were reported by Yapp [143] who carried out bead on plate welds with 0mm and 6mm apparent arc length.
It is necessary to emphasise that very low values for the arc length related to the tandem narrow groove process, while much longer arc lengths (5mm) are reported by other authors [63].

7.3.1.4 Shielding Gas Thermal Cycles

The thermal cycle experimental results are presented in Table 6.27 (page 212) and include all the gas mixtures tested in the present work. Examples are shown in Figures 6.127 and 6.128 (page 211).
No clear trend or relationship between gas composition and weld cooling rates can be formulated. However, the three argon/carbon dioxide mixtures (95%Ar5%CO_2, $t_{8/5}$=1.62s; 82.5%Ar17.5%CO_2, $t_{8/5}$=1.7s; 70%Ar30%CO_2, $t_{8/5}$=1.9s) presented a certain trend. As the carbon dioxide content increases the corresponding cooling times (800°C to 500°C) increase accordingly. This may be due to the fact that heat input increases (Table 6.31; page 222) as carbon dioxide increases (Figures 7.44 and 7.45).

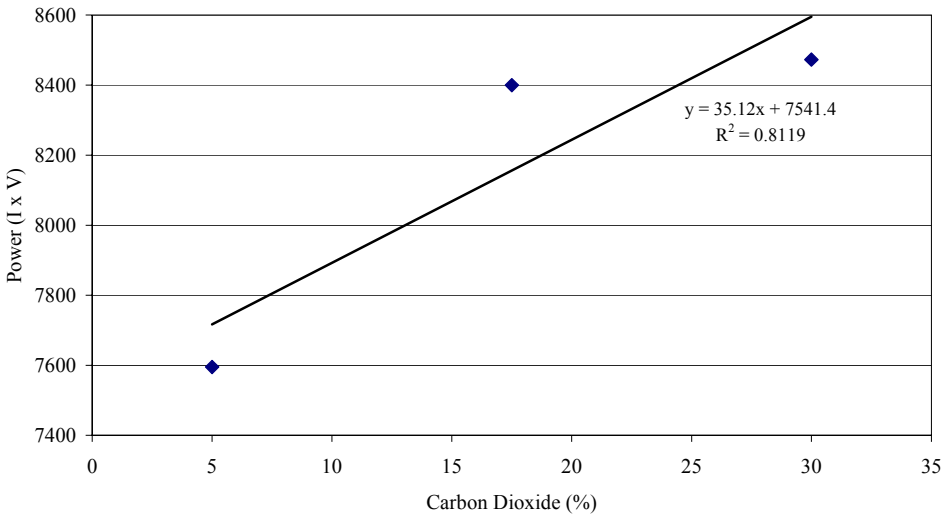

Fig. 7-44 Effect of shielding gas carbon dioxide content on power (V x I)

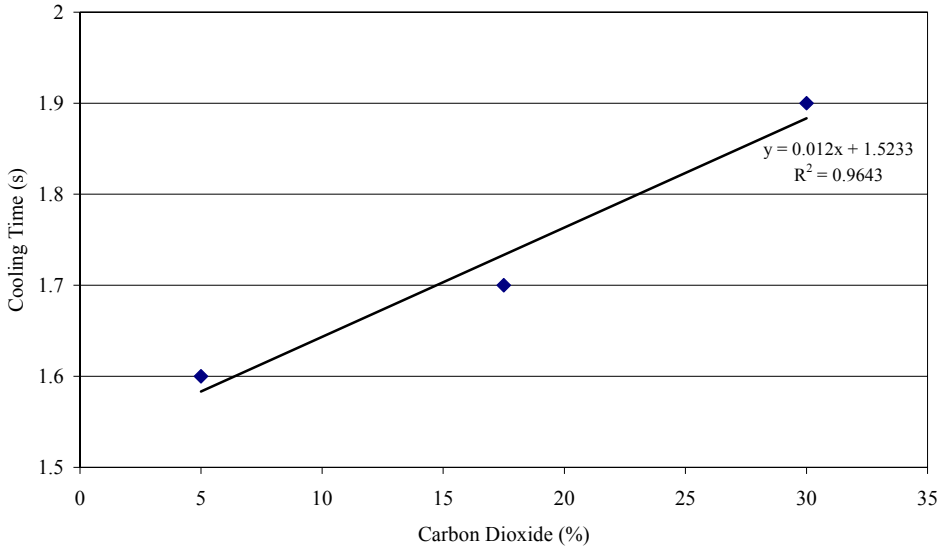

Fig. 7-45 Effect of shielding gas carbon dioxide content on weld cooling rate

Similar results are reported by Gouda [37], [45].
The effect of the arc length on the cooling times for several gas mixtures was investigated and the time vs temperature plots are reported in Figures 6.129 and 6.130 (pages 213 and 214). The welds obtained with longer arc lengths were marked as A.L.C=0% and with shorter arc as A.L.C=-10%. All test results have converged to the same conclusion: the welds performed with short arcs have faster cooling rates. Furthermore, in the present experimental design, welds with short arcs produced lower arc energy and therefore faster cooling times.

7.3.2 Shielding Gas Trials

Three models (mathematical equations; Eqns. 6.35, 6.36 and 6.37) for depth of penetration, sidewall penetration and concavity were developed (section 6.5.3, page 215) and the normalised change of the responses compared to the reference blend predictions (Table 6.30; page 221). These are shown graphically in Figures 6.132, 6.133 and 6.134 (pages 217 and 218).

7.3.2.1 Depth of Penetration

The normalised change of depth of penetration for the effect of carbon dioxide, helium and oxygen is shown in Figure 6.132 (page 217).
The effect of carbon dioxide is predominant compared to the effects of oxygen and helium. When carbon dioxide increases from 5% to 20% content in the shielding gas composition, depth of penetration increases by 24%. Changes to carbon dioxide content in the range 20% to 30% did not produce significant changes in depth of penetration.
The above result is in agreement with other published data [63],[39],[36],[40].. Generally, the addition of carbon dioxide in the shielding gas increases the arc energy (Table 6.31; page 222) and thus depth of penetration is enhanced. Furthermore, mixtures of CO_2 with O_2 additions are thought to develop more heat due to exothermic

reactions [39]. The arc energy levels calculated in the experiments for the ternary mixtures $Ar/CO_2/O_2$ were orientated towards the high arc energy range. Oxygen levels were very limited (max 3%) and therefore arc energy changes are likely to be due to carbon dioxide.
The effects of the other components (oxygen, helium) were found to be relatively insignificant. However, Modenesi [4] reported an increase in the penetration area with increasing helium, but he carried out the experiments in Ar/He mixtures only.

7.3.2.2 Sidewall Penetration

Lateral penetration (Figure 6.133, page 217) increased when carbon dioxide and helium content in the shielding gas composition increased. However, the effect of carbon dioxide is greater. If sidewall penetration is determined by the radial heat of the arc, then arc voltage, arc length and consequently arc energy are expected to contribute also. Church [144] reported that by adding helium to a shielding gas arc energy increases. The results (Table 6.31; page 222) have not confirmed this statement, which may be due to the stronger influence of carbon dioxide. However, additions of helium to Ar/CO_2 lead to an increase in the arc length and a smoother arc.
Modenesi [4] reported that the lateral penetration area in his narrow groove trials increased with %He in the shielding gas. Again he tested only Ar/He mixtures
Similarly, Thompson [6] in his experimental work concluded that fusion characteristics were affected by the addition of helium. Sidewall fusion was considerably increased when welding under 82.5%Ar12.5%$CO_2$5%He for the vertical down welding of pipelines steels. In the same work he reported that additions of oxygen greater than 1% to the above composition resulted in sidewall undercutting. This was not verified in the experiments here.
Sidewall penetration is considered the most important of the responses since side lack of fusion is the predominant defect in pipeline welding. 3D graphs for the sidewall penetration response were plotted (Figures 7.46, 7.47) in addition to the graph in Figure 6.133 (page 217).
Figure 7.46 shows that at 0% oxygen content in the gas mixture the maximum sidewall penetration is obtained for approximately 20% carbon dioxide content (80%Ar20%CO_2) while the effect of helium is negligible. When the oxygen increases to 2.96% the sidewall penetration remains at the same level as for 0% oxygen.
At 5% helium content (Figure 7.47) and 0% oxygen in the shielding gas the sidewall penetration obtained is similar to that for 80%Ar20%CO_2 (Figure 7.46). At 20% helium and 10% carbon dioxide the sidewall penetration is lower than that for 80%Ar20%CO_2.
Again, the carbon dioxide effect is likely to be the prevalent effect among the gas component effects.

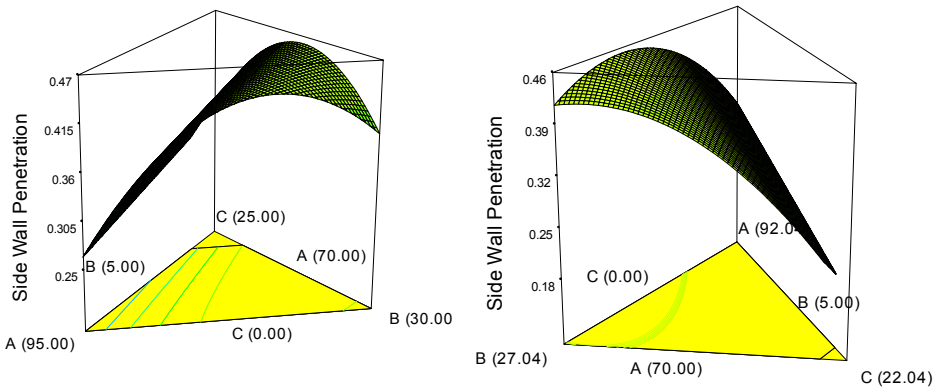

(a) A=Ar;B=CO_2; C=He; D=O_2:0.0% (b) A=Ar; B=CO_2; C=He; D=O_2:2.96%

Fig. 7-46 3D plots for the effect of (a) low oxygen and (b) high oxygen content in the shielding gas on sidewall penetration (mm)

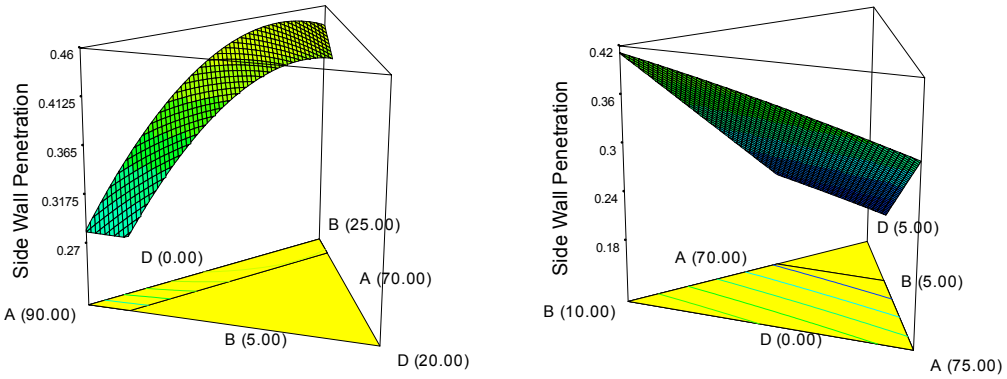

(a) A=Ar;B=CO_2; D=O_2; C=He:5% (b) A=Ar; B=CO_2; D=O_2:C=He20%

Fig. 7-47 3D plots for the effect of (a) low helium and (b) high helium content in the shielding gas on sidewall penetration (mm)

7.3.2.3 Concavity

The effects of carbon dioxide, helium and oxygen on concavity are presented in Figure 6.134 (page 218). While helium had an insignificant effect, carbon dioxide and oxygen both considerably influenced the weld bead concavity. The fact that the effect of on concavity is stronger than that of oxygen may be due to the higher percentages of

carbon dioxide in the gas mixture. Increased concavity leads to increased wetting of the weld bead to the sidewalls.
Concavity is improved when surface tension is decreased. It was found that oxygen reduces the surface tension [67],[46]. This confirms the conclusions of the present work. However, carbon dioxide dissociates in the arc to carbon monoxide and oxygen. This resulted in an increase of the oxygen level and therefore to a noticeable increase of concavity.

7.3.2.4 Factors Affecting the Selection of Shielding Gas Composition

Among the three gas components used in the experimental trials, carbon dioxide has the strongest effect on all the three responses: depth of penetration, sidewall penetration and concavity. Nevertheless, helium contributes to the sidewall penetration and oxygen to concavity but the carbon dioxide contribution is dominant. Although the shielding gas composition (82.5%Ar12.5%$CO_2$5%He) has been widely used for pulsed welding of high strength pipeline steels, the above results show that the 80%Ar20%CO_2 gas mixture can be successfully used to achieve acceptable weld bead geometry. However, it is necessary to also consider the effect on the weld metal properties when changing from the 12.5%CO_2 (82.5%Ar12.5%$CO_2$5%He) to 20%CO_2 (80%Ar20%CO_2).
All the weld metal analyses had oxygen content within the range 250ppm to 390ppm (Table 6.12, page 121).
Figure 7.48 shows the influence of the shielding gas oxygen and carbon dioxide concentration on weld metal oxygen content is taken from the work performed by Onsoien [51] (GMAW welding, ASTM A737 Grade B steel plate, 60° V-groove joint configuration, AWS 5.18 ER70S-3 filler wire, heat input 1.8kJ/mm).

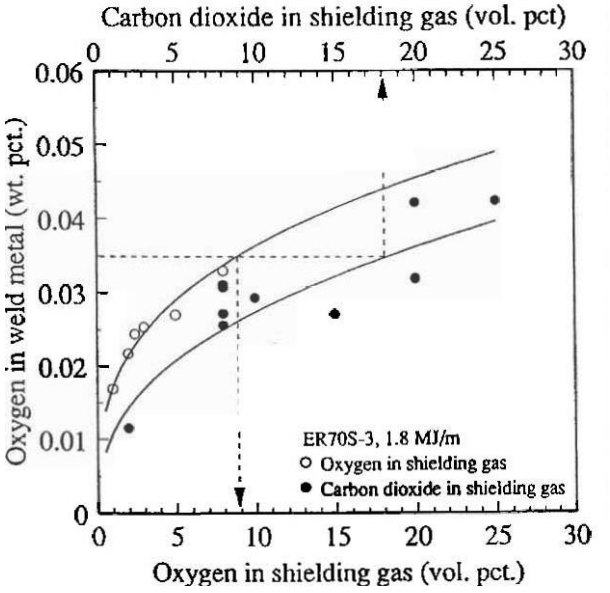

Fig. 7-48 Weld metal oxygen content as a function of oxygen and carbon dioxide in the shielding gas [51]**.**

Although Figure 7.48 is not directly equivalent to the present experimental work (tandem pulsed GMAW, X100 pipeline steel, AWS 5.28ER 100S-G/110S-G/120S-G filler wires etc), an attempt was made to predict the weld metal oxygen content when a gas mixture of 80%Ar20%CO_2 is used.
The 12.5%CO_2 content in the shielding gas is predicted to produce 290ppm of oxygen (Figure 7.48) in the weld metal while the 20%CO_2 is predicted to produce 350ppm of oxygen. This implies that changing from the 12.5%CO_2 to 20%CO_2 could lead to an increase of the oxygen content in the weld metal by a factor of 350/290=1.2.
Taking 390ppm of oxygen content in the weld metal as measured (Table 6.12, page 121) with 82.5%Ar12.5%$CO_2$5%He, then an approximate estimate of oxygen content with the gas mixture 80%Ar20%CO_2 is 470ppm of oxygen content in the weld metal. This may not be the optimum oxygen content for the best toughness properties. Ito [50] correlated the weld metal toughness properties with the oxygen content and the formation of acicular ferrite. Good toughness properties were associated with acicular ferrite. He defined 270ppm as the optimum level of the oxygen content in the weld metal. However, this is for pipeline steels where acicular ferrite is a significant constituent in the weld metal. Toughness properties in X100 steels are controlled by the fine martensitic/ bainitic weld metal structures [2] and to a smaller extent by acicular ferrite [1]. This last conclusion emphasises the importance of further investigations on the effect of the weld metal oxygen content in the case of tandem pulsed GMAW of X100 pipeline steels.

7.3.2.5 Optimisation

Analysis of the relationship between shielding gas composition and weld bead profile has established that a two gas composition (80%Ar20%CO_2) can be considered as an alternative to the three component mixture used for most of the work in this study. This conclusion will now be compared to the model optimised predictions. Depth of penetration is excluded from the optimisation process, since depth of penetration has never been a problem in tandem welding.
Two approaches are followed
a) The model is used to predict the “optimum” gas mixture that maximises sidewall penetration with no requirement to maximise concavity
b) The model is used to predict the “optimum” gas mixture that maximises both sidewall penetration and concavity
The optimised solutions for the sidewall penetration generated using the Design Expert software to optimise only on sidewall penetration is shown in Table 7.4. The highest importance level (5) was considered for the response.

Number	Ar(%)	CO_2(%)	He(%)	O_2(%)	Sidewall Penetration(mm)
1	70.00	18.99	11.01	0.00	0.46
2	70.00	19.41	10.59	0.00	0.46
3	70.01	20.48	9.52	0.00	0.46
4	77.33	19.67	0.00	3.00	0.45
5	77.79	19.21	0.00	3.00	0.45
6	71.29	20.53	7.81	0.37	0.45
7	79.21	17.64	0.97	2.18	0.44
8	78.82	21.18	0.00	0.00	0.44
9	72.75	22.12	2.50	2.63	0.43
10	73.30	24.32	1.12	1.26	0.43
11	81.94	16.82	0.5	0.74	0.43

Table 7-4 Model optimised predictions for sidewall penetration

Although the mixture 78.82%Ar21.18%CO_2 is proposed as choice No. 8, the predicted sidewall penetration is only 0.02mm lower than the prediction of the "best" (70%Ar18.99%$CO_2$11.01%He) among the optimum mixtures. However, the composition proposed (78.82%Ar21.18%CO_2) is almost identical to the "best" gas mixture (Ar80%20%CO_2) considered in the present study.

Table 7.5 was obtained optimising on both sidewall penetration and concavity. The highest importance level 5 was allocated to sidewall penetration and a value of 3 was allocated to concavity.

Number	Ar(%)	CO_2(%)	He(%)	O_2(%)	Sidewall Penetration(mm)	Concavity (mm)
1	74.32	22.68	0.00	3.00	0.45	0.64
2	73.03	23.97	0.00	3.00	0.44	0.66
3	70.00	27.00	0.00	3.00	0.42	0.69
4	73.33	21.56	2.18	2.93	0.43	0.63
5	70.00	22.67	7.33	0.00	0.45	0.57
6	70.00	23.32	6.68	0.00	0.45	0.58
7	72.45	24.20	3.32	0.03	0.44	0.59
8	75.53	24.47	0.00	0.00	0.43	0.59

Table 7-5 Model optimised predictions for sidewall penetration and concavity

It is clear that in optimising two responses the proposed gas mixtures are different from those proposed in Table 7.4. The best mixture in two components is No. 8 (75.53%Ar24.47%CO_2). Considering that (a) at the proposed carbon dioxide levels significant spatter will be produced, (b) the oxygen concentration in the weld metal will be increasingly reducing the toughness properties and (c) concavity optimisation is less significant than sidewall penetration, the carbon dioxide level can be reduced to 20% without significant reduction in the bead geometry dimensions.

7.3.2.6 Conclusions on Shielding Gas Trials

The above results have confirmed the predominant effect of carbon dioxide over the effects of helium and oxygen on the formation of the weld bead geometry. However, helium contributed to an increase in sidewall penetration, and oxygen to an increase in concavity but the carbon dioxide effect was significantly stronger. This indicates that argon and carbon dioxide gas composition can be considered as an alternative to the three gas mixture ($Ar/CO_2/He$). Mechanical tests of the weld metal (especially toughness) are required to confirm its potential application.
The three plots (Figures 6.132, 6.133, 6.134; pages 217 and 218) show that the $80\%Ar/20\%CO_2$ mixture can be selected as the best compromise for the three weld bead dimensions. The model predictions for depth of penetration, sidewall penetration and concavity for several gas mixtures are shown in Table 7.6.

Gas Mixture	Value	Depth of Penetration (mm)	Sidewall Penetration (mm)	Concavity (mm)
$82.5\%Ar12.5\%CO_25\%He$	Predicted	2.94	0.40	0.46
$78.82\%Ar21.18\%CO_2$	Predicted	3.25	0.44	0.55
$80\%Ar20\%CO_2$	Predicted	3.23	0.44	0.54
$85\%Ar15\%CO_2$	Predicted	3.05	0.41	0.49

Table 7-6 Predicted and actual values of the weld bead profile for different gas mixtures

No significant differences in the weld bead geometry are apparent between the $82.55\%Ar12.5\%CO_25\%He$ composition and $80\%Ar20\%CO_2$, implying that a two gas composition equivalent can produce acceptable and sound weld profiles. The "optimum" gas compositions may be slightly different from $80\%Ar20\%CO_2$, when considering the effect of weld metal oxygen content on mechanical properties.
The conclusions of the present work do not agree with the work carried out by Thompson [6] who concluded that sidewall fusion was considerably improved (60%) when welding with $82.5\%Ar12.5\%CO_25\%He$ compared to 0% helium content in the gas mixture. His results (marked as single wire) and the model predictions of the present work (tandem wire) are represented in the following Figure 7.49.

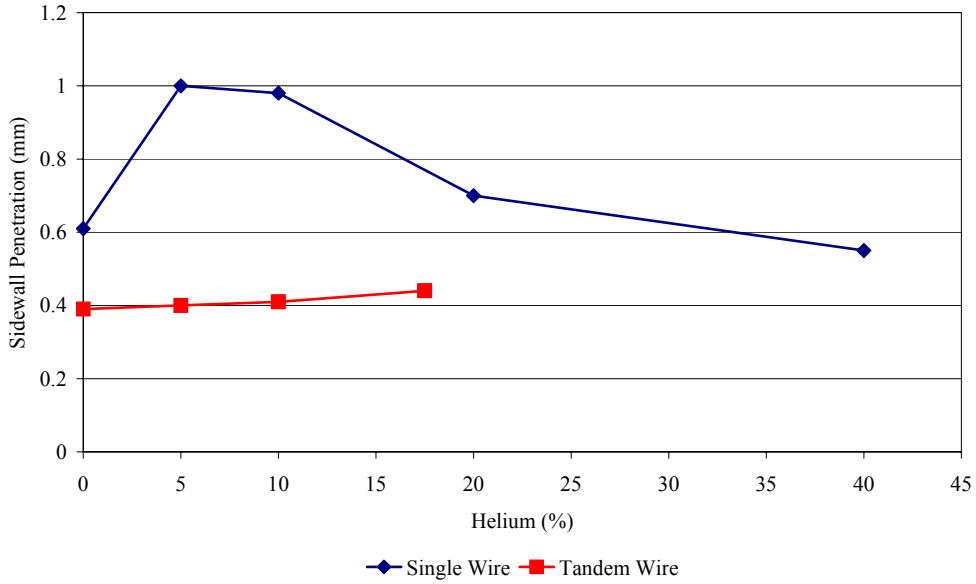

Fig. 7-49 Model predictions for sidewall penetration for single wire [6] and tandem wire welds (this project)

While a clear trend between sidewall penetration and helium content cannot be established in Thompson's results, helium was found to have a minor effect in the tandem wire trials in this project.
This could be due to one or more of the following reasons:

a. Thompson's conclusions on the effect of helium seem to be actually based on a single experimental point results at 0% helium.
b. Different measurement procedure. He measured the maximum sidewall penetration while in the present work the average of six measurements (three each side) was considered.
c. In his experimental work welds were carried out at significantly longer arc length (4mm) compared to the lower (max. 2mm) arc length used in the present work. Adopting 4mm arc length is very unlikely to produce satisfactory weld profile in the tandem PGMAW process used in the present experimentation.
d. For the single wire application in Thompson's work, significantly higher heat input level was used compared to the present work.

It appears quite clearly from this study that a simple binary gas mixture based on Argon and 18 to 22% CO_2 is quite adequate for narrow groove tandem PGMAW pipe welding. This conclusion is based on tandem welding with X100 steel, but it seems likely that it will apply more generally to narrow groove pipe welding. In any case, the importance of using a carefully controlled statistical method is evident.

8 Conclusions

- A new and innovative dual tandem welding process has been developed for pipeline welding in the 5G position. The dual tandem welding process offers the potential for a considerable increase in pipe welding productivity. Compared with conventional single wire mechanized welding, the number of welding stations on a pipeline spread can be reduced by a factor of 3 to 4, with a similar reduction in the number of operators. It has also been demonstrated that weld metal deposition rates twice that of the single tandem welding can be achieved. It has been shown that high quality welds, free from defects, can be made using the dual tandem process. For the Trans-Alaska pipeline project the cost saving resulting from the adoption of the dual tandem process has been estimated at $150m.

- Extensive welding trials have validated the tandem and dual tandem welding processes for application to high strength (X100) pipeline steels. The effect of consumable composition and thermal cycle on weld metal strength and toughness has been evaluated, and it was demonstrated that consumables could be chosen which produced overmatching of pipe yield strength, necessary for strain based design. The thermal cycle data was used to provide an explanation of the effect of the second torch on weld metal strength of the dual tandem welds. Single tandem welding of X100 pipeline steels has now been successfully implemented and used on commercial pipeline installations.

- For the first time, dual tandem double jointing procedures have been developed and qualified for X100 pipeline girth welds. Welds were made with a low heat input 0.54kJ/mm for the lead and 0.4kJ/min for the trail torch, compared with typical values of 2.5kJ/mm for conventional submerged arc double jointing. The faster thermal cycle associated with the dual tandem welding resulted in adequate hardness in both weld metal and heat affected zone. High deposition rates of 20.5 kg/hr were achieved. This project has clearly demonstrated the potential of dual tandem double jointing for industrial applications and confirmed that dual tandem may be the only viable alternative for the weld metal strength to meet the overmatching criterion in the case of X100 steels.

- Previous work using rutile flux cored wires for tie-in welds was not able to meet the overmatching criteria for X100 steels. In the current work, preliminary trials showed that it is possible to use basic wire in vertical down welding, and by application of pulsed welding to achieve acceptable metal transfer conditions and to achieve the desired overmatching for the weld metal yield strength.

- A comprehensive study of the effect of the welding parameters on weld geometry was performed. It was demonstrated that a statistically based design of experiments approach is essential in understanding the interaction between variables (welding parameters). Mathematical models describing the effect of welding parameters on weld profile were developed and validated for all welding conditions.
The central composite design of experiments was selected since it offers the possibility of optimizing parameter combinations to achieve a specific weld geometry target. These

models can now be used to predict optimum parameter combinations to minimize the possibility of defects in pipeline girth welding.

- The significant effect of welding position on weld bead geometry was outlined. This new understanding of weld geometry change with position has important implications for the achievement of sound welds.

- The effect of shielding gas composition on weld bead geometry in single tandem pulsed-GMAW was investigated using a statistical design (D-Optimal) intended for analysis of mixtures. It was shown that an argon-carbon dioxide (Ar/CO_2) gas mixture is capable of producing equivalent weld geometry to that produced using the Ar/CO_2/He mixture implemented during the procedure trials.

9 Recommendations for Further Work

- Although dual tandem procedures have been developed, further work on optimisation direction is suggested to ensure a successful transference to the field welding environment.

- The preliminary PGMAW basic flux cored wire procedures for tie-in welds have confirmed the potential application of the process. During the present research work only one synergic point of the process waveform was developed and only two basic flux cored wires from the same manufacture were tested.
The process requires further development and a wider selection of filler wires to be tested in order to ensure successful qualification and implementation.
It is proposed that statistical analysis should be used in the development of the pulse parameters.

- The main challenge for the tandem and dual tandem process was to produce high strength and toughness properties for the X100 pipeline steels. It is recommended that models of the weld metal yield strength and toughness as a function of composition should be developed, so that it may be possible to determine relationships between weld metal elements and mechanical properties.

- The importance of the oxygen content in weld metal is well established in the literature. A systematic investigation of the effect of the oxygen content on the weld metal in the tandem and dual tandem processes of X100 welds is recommended to establish whether existing guidelines need to be modified for application to X100 tandem and dual tandem process.

- The shielding gas trials carried out with argon and carbon dioxide composition provided “sound” welds. Since shielding gas composition affects process stability, transfer mode and weld metal properties the pulsed parameters have to be optimised and weld metal mechanical properties have to be investigated considering the carbon dioxide content.

- It is recommended a systematic study is made of the effect of the pulse parameters on the weld bead geometry (statistical design and analysis) and the arc characteristics. This will enable us to a better understanding and control the weld profile formation and optimisation.

- The procedure development work indicates a strong influence of the joint width on the weld bead characteristics and process behaviour. It is recommended a systematic study be carried out of the effect of the joint width on the weld bead fusion geometry together with the welding position.

- The welding parameters work indicated the very strong effect of welding position on the weld bead geometry. Attempts should be made to analyse the effect of the position (gravitational forces) and surface tension forces on the weld pool

characteristics. This should enable better weld pool control and minimise the probability of defect formation.

References

1. Hudson, M. (2004), *Welding of X100 pipeline* (unpublished PhD thesis), Cranfield University, Cranfield.

2. Gianetto, J. A., Bowker, J. T., Bouchard, R., Dorling, D. V. and Horsley, D. J. (2006), "Tensile and toughness properties of pipeline girth welds", *International Pipeline Conference (IPC 2006),* 25th-29th September 2006, Calgary, Alberta, Canada, International Institute of Welding, Lausanne, Switzerland.

3. Hudson, M. (2007), *Tie-in mechanised FCAW,* (personal communication).

4. Modenesi, P. J. (1990), *Statistical modelling of the narrow gap gas metal arc welding process* (unpublished PhD thesis), Cranfield University, Cranfield.

5. Michie, K. (1998), *Twin-wire GMAW of pipeline girth welds* (unpublished MSc thesis), Cranfield University, Cranfield.

6. Thompson, T. S., Rothwell, A. B. and Dorling, D. V. (1988), *The influence of shielding gas composition on pulsed gas metal arc welding of arctic and offshore structures and pipelines*, Report no. 13090, Nova Corporation of Alberta and the Metals Technology Labroatoris, Canada Centre for Mineral and Energy Technology, Energy Mines and Resources, Canada.

7. British Petroleum (2006), *Statistical review of world energy*, available at: http://www.bp.com/centres/energy/index.asp (accessed 1st February 2007).

8. Hillenbrand, H. G. and Kalwa, C. (2002), "High strength line pipe for project cost reduction", *World Pipelines,* vol. 2, no. 1.

9. Hillenbrand, H. G. (1995), "Manufacturability of linepipe in grades up to X100 from TM processed plate", *Proceedings of the Conference of Pipeline Technology,* Vol. 2, 11th-14th September 1995, Ostend, Belgium, pp. 273-286.

10. Terada, Y. (2003), "X100 Linepipe with excellent HAZ toughness and deformability", *Proceedings of the 22nd International Conference on Offshore Mechanics and Arctic Engineering (OMAE03),* 8th-13th June 2003, Cancun, Mexico.

11. Okatsu, M., Kawabata, F. and Amano, K. (1997), "Metallurgical and mechanical features of X100 linepipe steel", *Proceedings of the 16th International Conference on Offshore Mechanics and Arctic Engineering (OMAE97), III - Materials Engineering,* 13th-17th April 1997, Yokohama, pp. 119-124.

12. Glover, G., Horsley, D. J. and Dorling, D. (1999), "High-strength steel becomes standard on Alberta gas system", *Oil and Gas Journal,* vol. 97, no. 1, pp. 44-50.

13. Glover, A. G., Horsley, D. J. and Dorling, D. (2003), "Application and installation of grade 690 (X100) linepipe", *14th Biennal Joint Technical Meeting on Pipeline Research,* Berlin, pp. 7.1-7.14.

14. Denys, R., Leferve, A. and Beats, P. D. (2002), "A rational approach to weld and pipe material requirements for a strain based pipeline design", *Proceedings of Applications and Evaluation of High-Grade Linepipes in Hostile Enviroments,* 7th-8th November 2002, Pacifico Yokohama, Japan, pp. 121-157.

15. Wang, Y. H. and Horsley, D. J. (2003), "Tensile strain limits of pipelines", *14th Biennial Joint Technical Meeting on Pipeline Research,* pp. 35.1-35.13.

16. Blackman, S. and Dorling, D. V. (1999), "Mechanised GMAW for transmission pipelines", *Pipeline Welding and Technology Conference, The International Conference on Advances in Welding Technology,* 26th-28th October 1999, Galveston USA, paper 1.

17. Lassaline, E., Zajaczkoski, Z. and North, T. H. (1989), "Narrow groove twin-wire GMAW of high-strength steel", *Welding Journal,* vol. 68, no. 9, pp. 53-58.

18. Walker, A. P. (2000), *Twin-wire GMAW of X80 linepipe* (unpublished MSc thesis), Cranfield University, Cranfield.

19. Blackman, S. (2001), "Developments forecast to reduce pipeline construction costs", *Welding and Metal Fabrication,* vol. 69, no. 8, pp. 7-10.

20. Kostrivas, A. (1995), *Orbital welding of mild steel pipelines with twin wire GMAW process* (unpublished MSc thesis), Cranfield University, Cranfield.

21. Blackman, S. and Dorling, D. V. (2002), "High-speed tandem GMAW for pipeline welding", *Proceedings of IPC 2002: International Pipeline Conference,* Vol. IPC02-27295, 29th September 3rd October 2002, Calgary, Alberta Canada.

22. Widgery, D. J. (2002), "Welding high strength pipelines: theory, practice and learning", *Pipeline Construction Technology, Proceedings, International Conference,* 4th-5th March 2002, Wollongong, Australia, pp. paper 11.

23. Widgery, D. J. (2006), *Consumables for X100 girth welding*, Doc. XI-E-1004-06, International Institute of Welding, Lausanne, Switzerland.

24. Ostrom, R. (2006), *Submerged arc welding for double jointing procedures,* (personal communication).

25. Mariani, F. and Vago, F. (2003), "Saipem's blue stream project", *Svetsaren,* vol. 58, no. 2, pp. 9-11.

26. Widgery, D. J. (2002), "Welding high strength pipelines: beyond X80", *4th International Pipeline Conference,* 20th September-3rd October 2002, Calgary, Canada, pp. IPC01-27156.

27. Cording, W. (2002), "Go with the flow", *Practical Welding Today,* pp. 26-28.

28. Irving, B. (1994), "Trying to make some sense out of shielding gases", *Welding Journal,* vol. 73, no. 5, pp. 65-70.

29. Hunt, C., Bols, I. and Ortega, P. (1997), "Helium - a lightweight gas but a heavyweight performer", *Welding and Metal Fabrication,* vol. 65, no. 6, pp. 10,12,14.

30. Dixon, K. (1999), "Shielding gas selection for GMAW of steels", *Welding and Metal Fabrication,* vol. 67, no. 4, pp. 8-14.

31. Menzel, M. (2003), "The influence of individual components of an industrial gas mixture on the welding process and the properties of welded joints", *Welding International,* vol. 17, no. 4, pp. 262-264.

32. American Welding Society (1991), *Welding Processes,* 8th ed, American Welding Society, Miami, Florida.

33. Hilton, D. E. and Norrish, J. (1988), "Shielding gases for arc welding", *Welding and Metal Fabrication,* vol. 56, no. 4, pp. 189-196.

34. Dillenbeck, V. R. and Castagno, L. (1987), "The effect of various shielding gases and associated mixtures in GMAW welding of mild steel", *Welding Journal,* vol. 66, no. 9, pp. 45-49.

35. Cresswell, R. A. (1972), "Gases and gas mixtures in MIG and TIG welding", *Welding and Metal Fabrication,* vol. 40, no. 4, pp. 114-119.

36. Salesse, P. (1988), "Shielding gases for pulsed MIG", *IIW Asian Pacific Regional Welding Congress and 36th annual AWI,* Vol. 1, 14th-18th November 1988, Hobart, pp. 264.

37. Gouda, M. A., Takahashi, M., Kuroda, T. and Ikeuchi, K. (2002), "Influence of heat input and shielding-gas composition on microstructures and properties of weld metal of HSLA-100 class steel", *6th International Trends in Welding Research Conference Proceedings,* 15th-19th April 2002, Pine Mountain, ASM International, pp. 701.

38. Ramanathan, B., Harish Reddy, B. S., Raman, K. S., Murthy, K. S. S., Raia, A., Raghupathy, P. and Babu, R. S. (1995), "Effect of shielding gas on fusion characteristics and weld metal properties in flux cored arc welding", *Trends in Welding Research, 4th International Conference,* 5th-8th June 1995, Gatlinburg, TN, pp. 441-447.

39. Canto, M. A. A. and Macado, I. G. (1992), "MIG/MAG welding: shielding gas effects on weld metal mechanical properties and bead geometry", *IIW Latin American Regional Welding Congress,* Vol. 2, 4th-10th April 1992, Rio de Janeiro, Brazil, Associacao Brasileira de Soldagem, Sao Paulo, pp. 895-908.

40. Grubic, K. and Panic, V. (2001), "Influence of the type of shielding gas on the weld geometry", *4th European Conference on Welding Joining and Cutting (Eurojoin 4),* 24th-25th May 2001, Dubrovnik, pp. 685.

41. The Shielding Gas Handbook, AGA AB, Sweden, www.aga.se.

42. Meyendorf, N. (1988), "Metal gas reactions in gas-shielded arc welding", *WeldingInternational,* vol. 2, no. 7, pp. 653-657.

43. Uygur, B. and Gulenc, B. (2004), "The effect of shielding gas compositions for MIG welding process on mechanical behavior of low carbon steel", *Metalurgija,* vol. 43, no. 1, pp. 35-40.

44. Norrish, J. (1992), *Advanced Welding Processess,* Institute of Physics, Bristol.

45. Francis, R. E., Jones, J. E. and Olson, D. L. (1990), "Effect of shielding gas oxygen activity on weld metal microstructure of GMA melded microalloyed HSLA steel", *Welding journal,* vol. 69, no. 11, pp. 408-415.

46. Jonsson, P. G., Murphy, A. B. and Szekely, J. (1995), "The influence of oxygen additions on argon-shielded gas metal arc welding processes", *Welding Journal,* vol. 74, no. 2, pp. 49-57.

47. Walsh, D. W. and Savage, W. F. "The mechanism of minor element interaction in autogenous weld pools", *Advances in Welding Science and Technology,* Gaitlinburg, TN, pp. 59-63.

48. Stenbacka, N. and Persson, K. (1989), "Shielding gases for gas metal arc welding", *Welding Journal,* vol. 68, no. 11, pp. 41-47.

49. Doan, G. E. and Myer, J. L. (1932), "Arc discharge not obtained in pure argon gas", *Physics Review,* vol. 40, no. 3, pp. 36-40.

50. Ito, Y., Nakanishi, M. and Komizo, Y. (1982), "Effects of oxygen on low carbon steel weld metal", *Metal Construction,* vol. 14, no. 9, pp. 472-478.

51. Onsoien, M. I., Liu, S. and Olson, D. L. (1996), "Shielding gas oxygen equivalent in weld metal microstructure optimization", *Welding Journal,* vol. 75, no. 7, pp. 216-224.

52. Potapov, N. N. (Aug. 1993), "Oxygen effect on low alloy steel weld metal", *Welding Journal,* vol. 72, no. 8, pp. 367-370.

53. Schumann, O., Powell, G. and French, I. (1994), "Control of microstructure in gas metal arc (GMA) and flux cored arc (FCA) welding processes", *Australian welding research,* vol. CRC No.1.

54. Lucas, W. (1992), "Choosing a shielding gas, part 2", *Welding and Metal Fabrication,* vol. 60, no. 7, pp. 269-276.

55. Melmoth-Bennett, B. J. (1983), *Special shielding gas mixtures: exploiting MIG welding developments,* The Welding Institute.

56. Foote, W. (1985), *Pulsed gas metal arc welding*, PR-171-419, Welding Supervisory Committee and the Pipeline Research Committee.

57. Allum, C. J. and Quintino, L. (1984), "Pulsed GMAW: interactions between process parameters, part 2", *Welding and Metal Fabrication,* vol. 52, no. 3, pp. 126-129.

58. Urmston, S. A. (1985), *Effect of shielding gas composition on transfer and fusion characteristics in P-GMAW of carbon steels* (unpublished MSc thesis), Cranfield University, Cranfield.

59. Dorling, D. V., Huntley, R. M., Gerlings, J. and Rothwell, A. B. (1986), *Pulsed gas metal arc welding of thick-section steels for low temperature applications*, Contract serial number 0SQ84-00042, Nova Corporation of Alberta and the Metals Technolgy Laboratories and the Physical Metallurgy Research Laboratories, Canada Centre for Mineral and Energy Technology, Energy Mines and Resources, Canada.

60. Bicknell and Patchett, B. M. (1986), *Pulsed GMA welding: shielding gas effects on fusion characteristics* (unpublished document), University of Alberta, Department of Mineral Engineering.

61. Laing, B. S. (1990), "PGMAW welding of X80 pipe", *Offshore Pipeline Technology Conference,* Paris.

62. Brun, G. (1996), *Welding of X80 and X100 high strength pipeline steels* (unpublished MSc thesis), Cranfield University, Cranfield.

63. Norrish, J., Hilton, D. E. and Mistry, H. R. (1986), "The effect of shielding gas composition in the MAG welding of line pipe", *3rd International Conference: Welding and Performance of Pipelines,* Vol. 2, 18th-21st November 1986, London, pp. 211-219.

64. Green, J. and Stares, J. (1992), *Optimisation of Ar-CO2-O2 shielding gas mixtures for gas metal arc welding of carbon and low alloy steels*, COE/LIS/007, B.O.C., London.

65. Ostrom, R. (2007), *Shielding gas mixtures for pipeline welding,* (personal communication).

66. Dorling, D. (2006), *Tandem pulsed gas metal arc welding for X100 pipelines,* (personal communication).

67. Matsunawa, A. and Ohji, T. (1982), "Role of surface tension in fusion welding. Part 1: Hydrostatic effect", *Transactions of the JWRI,* vol. 11, no. 2, pp. 145-154.

68. Michie, K., Blackman, S. and Ogunbiyi, T. E. B. (1999), "Twin-wire GMAW : process characteristics and applications", *Welding Journal,* vol. 78, no. 5, pp. 31-34.

69. Cross, M. and Moscardini, A. O. (1985), *Learning the art of mathematical modelling,* Halstead Press, Chichester.

70. McGlone, J. C. (1982), "Weld bead geometry prediction: a review", *Metal Construction,* vol. 14, no. 7, pp. 378-384.

71. Rosenthal, D. (1941), "Mathematical theory of heat distribution during welding and cutting", *Welding Journal,* vol. 20, no. 5, pp. 220-234.

72. Christensen, N., Davies, V. and Gjermundsen, K. (1965), "The distribution of temperature in arc welding", *British Welding Journal,* vol. 12, no. 2, pp. 54-75.

73. Eagar, T. W. and Tsai, N. S. (1983), "Temperature fields produced by travelling distributed heat source", *Welding Journal,* vol. 62, no. 12, pp. 346-355.

74. Heiple, C. R. and Roper, J. R. (1982), "Mechanism for minor element effect on GTA fusion zone geometry", *Welding Journal,* vol. 61, no. 4, pp. 97-102.

75. Oreper, G. M., Eagar, T. W. and Szekely, J. (1983), "Convection in arc weld pools", *Welding Journal,* vol. 62, no. 11, pp. 307-312.

76. Nunes, J. R. A. C. (1983), "An extended Rosenthal weld model", *Welding Journal,* vol. 62, no. 6, pp. 165-170.

77. Essers, W. G. and Walter, R. (1981), "Heat transfer and penetration mechanisms with GMA and plasma-GMA welding", *Welding Journal,* vol. 60, no. 2, pp. 37-42.

78. Tsao, K. C. and Wu, C. S. (1988), "Fluid flow and heat transfer in GMA weld pools", *Welding Journal,* vol. 67, no. 3, pp. 70-75.

79. Kim, W. J. and Na, J. (1995), "A study on the effect of contact tube-to-workpiece distance on weld pool shape in gas metal arc welding", *Welding Journal,* vol. 74, no. 5, pp. 141-152.

80. Cao, Z., Yang, Z. and Chen, X. L. (2004), "Three-dimensional simulation of transient GMA weld pool with free surface", *Welding Journal,* vol. 83, no. 6, pp. 169-176.

81. Cao, Z. and Dong, P. (1998), "Modeling of GMA weld pools with consideration of droplet impact", *Engineering Materials and Technology,* vol. 120, no. 4, pp. 313-320.

82. McGlone, J. C. (1980), *The submerged arc butt welding of mild steel: a decade of procedure optimisation*, Report 133, The Welding Institute.

83. Lutsenko, V. T. (1973), "Method of approximate calculation of the parameters of the weld in CO_2 welding", *Welding Production,* vol. 20, no. 1, pp. 35-38.

84. Quintino, L. (1986), *Fusion characteristics in pulsed-GMAW of mild steel* (unpublished PhD thesis), Cranfield Institute of Technology, Cranfield.

85. Raveendra, J. and Parmar, R. S. (1987), "Mathematical models to predict weld bead geometry for flux cored arc welding", *Metal Construction,* vol. 19, no. 1, pp. 31-35.

86. Harris, P. and Smith, B. L. (1993), "Factorial techniques for weld quality prediction", *Metal Construction,* vol. 15, no. 11, pp. 661-665.

87. Absi Alfaro, S. C. (1989), *Mathematical modelling of narrow gap submerged arc welding* (unpublished PhD thesis), Cranfield Institute of Technology, Cranfield.

88. Paranhos, R. P. R. (1990), *A numerical method for the prediction and optimisation of welding procedures* (unpublished PhD thesis), Cranfield Institute of Technology, Cranfield.

89. Chatfield, C. (1983), *Statistics for Technology,* 3rd ed, Chapman and Hall, London.

90. Jones, S. B., Doherty, J. and Salter, G. R. (1977), "An approach to procedure selection in arc welding", *Welding Journal,* vol. 56, no. 7, pp. 19-31.

91. Harwig, D. (2000), "A wise method for assessing arc welding performance and quality", *Welding Journal,* vol. 79, no. 12, pp. 35-39.

92. Box, G. E. P., Hunter, S. J. and Hunter, G. W. (2005), *Statistics for Experimenters,* 2nd ed, Wiley, Hoboken, NJ.

93. Jiju, A. (2003), *Design of Experiments,* Butterworth Heinemann, Amsterdam.

94. Montgomery, D. C. (2001), *Design and Analysis of Experiments,* Wiley, New York.

95. Design Expert Software (2006), *Version 7 user's guide,* Stat-Ease Inc., Minneapolis, MI.

96. Tsygan, B. G. and Lebedev, B. D. (1975), "Determination of parameters ofthe submerged-arc welding of butt joints using granular metallic filler", *Welding Production,* vol. 22, no. 12, pp. 19-21.

97. Konkol, P. J. and Koons, G. F. (1978), "Optimisation of parameters for two-wire AC-AC submerged arc welding", *Welding Journal,* vol. 57, no. 12, pp. 367-374.

98. Palani, P. K. and Murugan, N. (2006), "Development of mathematical models for prediction of weld bead geometry in cladding by flux cored arc welding", *International Journal of Advanced Manufacturing,* vol. 30, no. 7-8, pp. 669-676.

99. Murugan, N. and Parmar, R. S. (1995), "Mathematical models for bead geometry prediction in automatic stainless steel surfacing by MIG welding", *International Journal for the Joining of Materials,* vol. 7, no. 2/3, pp. 71-80.

100. Pandey, S. and Parmar, R. S. (1989), "Mathematical models for predicting bead geometry and shape relationships or MIG welding of alumimum alloy 5083", *Recent Trends in Welding Science and Technology,* 14th-18th May 1989, Gatlinburg, TN.

101. Feldthusen, H. (1991), *Mathematical modelling of thin sheet steel GMA welding* (unpublished MSc thesis), Cranfield University, Cranfield.

102. Montgomery, D. C., Peck, E. and Vining, G. G. (2001), *Introduction to linear regression analysis,* 3rd ed, Wiley, New York.

103. Caizley, D. L. (1999), *The welding of high strength steel for transmission pipelines* (unpublished MSc thesis), Cranfield University, Cranfield.

104. BS EN 60584 Part 1 and 2 (1996), *Thermocouples. Reference tables and thermocouple tolerances,* British Standards Institution, London.

105. BS EN 288-9 (1999), *Specification and approval of welding procedures for metallic materials. Welding procedure test for pipeline welding on land and offshore site butt welding of transmission pipelines,* British Standards Institution, London.

106. BS 4515-1 (2000), *Specification for welding of steel pipelines on land and offshore. Part 1: Carbon and carbon manganese steel pipelines,* British Standards Institution, London.

107. API STD 1104 (1999), *Welding of pipelines and related facilities,* 19th ed, American Petroleum Institute, Ann Arbor, MI.

108. BS 7448 (1991), *Fracture mechanics toughness tests. Part 1 (1991): Method for determination of KIc, critical CTOD and critical J values of materials, and Part 2 (1997): Method for determination of KIc, critical CTOD and critical J values of welds in metallic materials,* British Standards Institution, London.

109. BS EN 10002-1 (2001), *Tensile testing of metallic materials. Part 1: Test method (V- and U- notches),* British Standards Institution, London.

110. BS EN 10045-1 (1990), *Charpy impact test on metallic materials. Part 1: Test method (V-and U-notches),* British Standards Institution, London.

111. BS EN 1043 (1996), *Destructive tests on welds in metallic materials: Hardness test. Part 1 (1996): Hardness test on arc welded joints and Part 2 (1997): Micro hardness testing on welded joints,* British Standards Institution, London.

112. Dearden, J. and O'Neil, H. (1940), "A guide to the selection and welding of low alloy structural steels", *Institute of Welding Transactions,* pp. 203-214.

113. Ito, Y. and Bessyo, K. (1968), *Weldability formula of high strength steels*, Doc. IX-576-68, International Institute of Welding, Lausanne, Switzerland.

114. BS EN 1011 *Welding - Recommendations for welding of metallic materials. Part 1 (1998): General guidance for arc welding and Part 2 (2001): Arc welding of ferritic steels,* British Standards Institition, London.

115. Barsanti, L., Pozzoli, G. and Hillenbrand, H. G., *Production and field weldability evaluation of X100 line pipe*, available at: http://www.europipe.de/www/download/EP-TP_38-01_en.pdf (accessed 14th February 2007).

116. CSA Z245.1-02 (2002), *Steel pipe,* Canadian Standards Association, Ontario.

117. API Specification 5L (2000), *Specification for line Pppe,* 42nd ed, American Petroleum Institute.

118. Blackman, S., Liratzis, T., Howard, R. D., Hudson, M. and Dorling, D. V. (2004), "Recent tandem welding developments for pipeline girth welds", *Pipeline Technology Proceedings, 4th International Conference,* Vol. 1, 9th-13th May 2004, Ostend, Belgium, pp. 335-355.

119. Yapp, D. (2006), *Application of tandem welding in commercial projects,* (personal communication).

120. Miranda Junior, A. B. (1997), *The effects of shielding gas and transfer mode on the weldability of X100 pipeline steels* (unpublished MPhil thesis), Cranfield University, Cranfield.

121. Farrar, R. A. and Harrison, P. L. (1987), "Acicular ferrite in carbon-maganese weld metals: an overview", *Jounals of Materials Science,* vol. 22, no. 11, pp. 3812-3820.

122. Bhadhesia, H. K. D. H. (2001), *Bainite in steels,* 2nd ed, IOM Communications Ltd, London.

123. Mills, A. R., Thewlis, G. and Whiteman, J. A. (1987), "Nature of inclusions in steel weld metals and their influence on formation of acicular ferrite", *Materials Science and Technology,* vol. 3, no. 12, pp. 1051-1055.

124. Zang, Z. and Farrar, R. A. (1996), "The role of inclusions in formation of acicular ferrite in low alloy weld metals", *Materials Science and Technology,* vol. 12, pp. 237-260.

125. Sanderson, N. (2005), *Alaska gas pipeline,* (personal communication).

126. Hudson, M. (2007), *Submerged arc welding for double jointing procedures,* (personal communication).

127. Widgery, D. J. (2006), *Submerged arc welding for X100 steel pipe using tubular wire,* (personal communication).

128. Widgery, D. J., Karlsson, L., Murugananth, M. and Keehan, E. (2002), "Approaches to the development of high strength weld metal", *High Strength Steel. 2nd International Symposium,* 23rd-24th April 2002, Stilkestad, Verdal, Norway, pp. Paper 1.1.

129. Widgery, D. J. (2006), *Welding with basic flux wires in vertical-up direction,* (personal communication).

130. Matsunawa, A. and Nishiguchi, K. (1979), "Arc behaviour, plate melting, and pressure balance of the molten pool in narrow grooves", *Arc Physics and Weld Pool Behaviour,* 8th-10th May 1979, London, pp. 301-310.

131. Kraber, S., (2006), *Coded factors equation*, Stat-Ease, Inc., Mineapolis.

132. Allen, D. J. and Degnan, G. "An investigation of fusion quality in conventional MIG, synergic pulsed MIG, flux cored arc and manual metal arc welding", *Second European Conference on Joining Technology (EUROJOIN 2),* 16th-18th May 1994, Florence, pp. 191-202.

133. Essers, W. G. and Walter, R. (1980), "Some aspects of the pentration mechanisms in metal-inert-gas (MIG) welding", *International Conference Proceedings: Arc Physics and Weld Pool Behaviour,* Vol. I & II, 8th-10th May 1979, London, pp. 289-295 and 447-454.

134. Kalligerakis, K. and Mellor, B. G. (1995), "Overlay welding using pulsed MIG welding: bead profile and dilution", *Journal for the Joining of Materials,* vol. 7, no. 1, pp. 16-22.

135. Kim, I. S., Basu, A. and Siores, E. (1994), "The effect of welding parameters on weld penetration in GMAW process", *Welding, Joining, Coating and Surface Modification of Advanced Materials. Pre-Assembly Symposium, 47th Annual Assembly of IIW,* Vol. 1, Dahian, China, pp. 238-243.

136. Gupta, S. R., Breazu, M. and Ashok, U. (1997), "Influence of welding parameters on bead geometry in GMAW vertical down position", *Indian Welding Journal,* vol. 30, no. 2, pp. 9-14.

137. Minehisa, S., Nagai, A., Ohtsuka, T., Sakabata, N. and Kunihito, T. (1980), "A study on narrow gap MIG welding", *Welding Research in the 1980's,* 27th-29th October 1980, Osaka, Japan, pp. 37-42.

138. Stepanov, V. V. and Yazovskikh, V. M. (1980), "The effect of welding conditions on the formation of the weld in automatic narrow-gap welding", *Welding Production,* vol. 27, no. 3, pp. 41-43.

139. Bradstreet, B. J. (1968), "Effect of surface tension and metal flow on weld bead formation", *Welding journal,* vol. 47, no. 7, pp. 314-322.

140. Quintino, L. and Pires, I. (1998), "Analysis of the influence of shielding gas mixture on features of MIG/MAG welding", *Eurojoin: Welding Technology at Work, 3rd European Conference on Joining Technology,* 30th March-1st April 1998, Bern, pp. 819-830.

141. Smati, Z. (1986), "Automatic pulsed MIG welding", *Metal Construction,* vol. 18, no. 1, pp. 38-44.

142. Ohsima, K., Morita, M., Fuzi, K., Yamamoto, M. and Kubota, T. (1988), "Observation and digital control of the molten pool in pulsed MIG welding", *Welding International,* vol. 2, no. 3, pp. 234-240.

143. Yapp, D. and Moran, S. P. (1998), "The effect of welding parameters on weld bead shape and size in GMAW", *AWS Convention,* St. Louis, Missouri.

144. Church, J. G. and Imaizumi, H. (1990), *T.IM.E process*, Doc. XII-1199-90, International Institute of Welding, Lausanne, Switzerland.

145 Joseph A.P. (2001), Assessing the effects of GMAW-Pulse parameters on arc power and weld heat input (unpublished MSc thesis), The Ohio State University, Ohio.

Appendix A - WERC Single Synergic Curve Waveform

Wire Feed Speed(m/min)	7.62
Rump Up Rate	260
Ramp Overshoot(%)	0
Peak Current(A)	410
Peak Time(ms)	2.4
Tailout Time(ms)	2
Tailout Speed	0.2
Step off Current(A)	100
Background Current(A)	70
Background Time(ms)	2.3
Frequency(Hz)	149.3
No Adaptive	
Open Circuit Voltage(V)	48
Strike Current(A)	450
Minimum Strike Time	2.5
Starting Voltage(V)	23
Starting Current(A)	180
Starting Time(ms)	0
End Time(ms)	550
Short Detect Volt(V)	2.5
Current Rise	5
Arc Re establish Volt	55
High Speed Mode	15
Amp. Sec	1.68
Set	off
Trim	0.95
Gas Preflow(s)	0.4
Run In	off
Arc Control	0.05
Burnback	0.05
Postflow(s)	2.0
Crater	off

Fig. A1 Electric Wave Designer 2000 Pro Template Pulse 1.2mm for use with Filarc PZ6149

Appendix B - Welding Procedure Record Sheets

Cranfield UNIVERSITY

Welding Procedure Specification

Weld No.: ML-ST-S006

Date: Root 07.08.03, Fill Runs :07.08.03

Description:

X100 Single Tandem Weld

Welders Name/Position:

Travis Klashinsky

Harry Liratzis

Material Grade:	X100
Heat Number:	KYYU1352, Pipe Nr. 2
Diameter:	36"
Thickness:	19.05mm
Welding Position:	ASME IX 5G(except root)
Preparation Method:	PFM
Alignment Method:	IWM
Alignment Removed:	After Root Run
Preheat Method:	Propane
Backing System	N/A
Cleaning Method:	Grind/ wire Brush

Joint Preparation:

Bevel offset=2.5mm

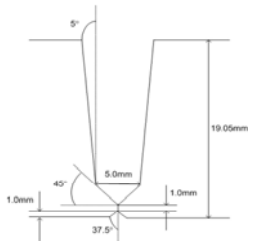

Run Sequence:

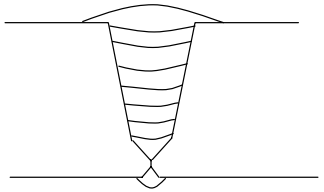

Pass	Process	Polarity	Electrode Brand	Batch	Size mm	Shielding Gas Type	Flow L/min	Temp @ Start °C	Lead Wire WFS m/min	Lead Wire Amps I	Lead Wire Volts V	Trail Wire WFS m/min	Trail Wire Amps I	Trail Wire Volts V	Osc. Freq beats per min.	Osc. Width mm	CTWD mm	Travel Speed mm/min	Arc Energy kJ/mm
Int. root	GMAW	DC+ve	Thyssen K-Nova	186096	0.9	78%Ar/20%CO_2/2%O_2	20	110-110	9.60	194	21.8				-		10.00-11.00	710	0.36
Hot(Run1)	PGMAW	DC+ve	NiMo-1	14233	1.0	82.5%Ar/12.5%CO_2/5%He	27-28	100-120	12.00	206.00	21.00	11.00	199.00	21.00	320	2.75	13.50	1270	0.44
Fill 1(Run 2)	PGMAW	DC+ve	NiMo-1	14233	1.0	82.5%Ar/12.5%CO_2/5%He	27-28	100-120	11.00	191.00	21.00	11.00	193.00	21.00	320	3.45	13.50	1270	0.39
Fill 2(Run 3)	PGMAW	DC+ve	NiMo-1	14233	1.0	82.5%Ar/12.5%CO_2/5%He	27-28	100-120	10.00	165.00	20.00	10.00	187.00	20.00	320	3.85	13.50	1270	0.34
Fill 3(Run 4)	PGMAW	DC+ve	NiMo-1	14233	1.0	82.5%Ar/12.5%CO_2/5%He	27-28	100-120	10.00	180.00	21.00	10.00	183.00	21.00	320	4.25	13.50	1270	0.36
Fill 4 (Run 5)	PGMAW	DC+ve	NiMo-1	14233	1.0	82.5%Ar/12.5%CO_2/5%He	27-28	100-120	10.00	182.00	20.50	10.00	185.00	20.50	320	4.65	13.50	1270	0.36
Fill 5 (Run 6)	PGMAW	DC+ve	NiMo-1	14233	1.0	82.5%Ar/12.5%CO_2/5%He	27-28	100-120	10.00	180.00	21.00	10.00	180.00	21.00	320	5.65	13.50	1270(+/-20%)	0.36
Fill 6 (Run 7)	PGMAW	DC+ve	NiMo-1	14233	1.0	82.5%Ar/12.5%CO_2/5%He	27-28	100-120	10.00	177.00	21.50	10.00	180.50	21.50	320	5.55	13.50	1270(+/-20%)	0.36
Cap	PGMAW	DC+ve	NiMo-1	14233	1.0	82.5%Ar/12.5%CO_2/5%He	27-28	100-120	8.00	140.00	21.00	8.00	146.00	21.00	280	7.00	15.00	889(+/-20%)	0.39

Additional Comments:

Internal weld:fixed head, rotated pipe. Torch at 7o'clock wire 90 deg to pipe surf., effectively vertical down welding, Esab Aristo 2000 power source.
External passes used Fronius TPS 4000 synchronised power sources.
Average I and V values include both sides A & B.
Hot Pass: Flat bead profile at 6 o'clock. Flappering trail wire at 6 o'clock. Repair both sides 60mm.
Arc Length Correction(A.L.C) for both wires set to 10.
Fill 1 : Good profile both sides. A.L.C. = 10
Fill 2 : Flat profile both sides. A. L. C. = 10
Fill 3 : Spatter on the contact tip caused instabilities. Two repairs.
200mm length(Side A). Side B: At 5:30 o'clock repair strip of 25mm. A. L. C = 8.
Fill 4 : Some irregularities for both sides at 6 o'clock. A short weld strip at the 12 o' cl. A. L. C =5
Fill 5 : Grinding at 6 o'clock for both sides. A. L. C = 0
Fill 6 : Some grinding at 6 o'clock. A. L. C = 0.
Cap : Good bead profile. A. L. C = 0
Other Settings (Fronius TPS 4000)
Gas Preflow : 0.3s.
Repair conditions : wfs=9.0m/min;travel speed=940mm/min(+/-10%); Osc. Frequency=320beats/min
SL=0.5(after fill 3, SL=0.7), t-E lead wire=0.1, t-E trail wire=0.1 one side and both 0 on the other side. (Settings are depended on weld pool characteristics)
Arc Force Correction=0 (for cap=0.5)
For both wires : I-S=135A, I-E=50A, t-S=off.
The +/- 20% travel speed was used as follows: We started "dead slow" at the top and gradually increased and regulated according to the weld pool fluidity.

Cap Gap Widths (mm)

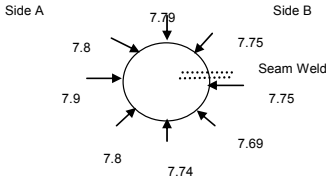

Depth Remaining to Cap (mm)

After Pass No.	12 o'c	3 o'c	6 o'c
0	18.5	18	17
Hot (Run 1)	14.5	14	14
Fill 1(Run 2)	10.5	12	11.5
Fill 2(Run 3)	8	10.5	9.5
Fill 3(Run 4)	7	8	6.7
Fill 4 (Run 5)	5	6	5
Fill 5 (Run 6)	3	4	3.2
Fill 6 (Run 7)	1	2	1

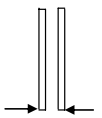

Oscillation Width Measurement

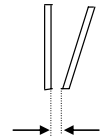

Wire Separation at 13.5mm extention : 3.5mm
Torch vertical to pipe axis

Fig. B1 Single Tandem PGMAW Narrow Gap Welding Procedure ML-ST-S006, Pipe B19

Cranfield UNIVERSITY

Welding Procedure Specification

Weld No.: ML-DT-S016

Date: Root 26.08.03, Fill Runs :28.08.03

Description:

X100 Dual Tandem Weld

Material Grade:	X100
Heat Number:	KYYU1352, Pipe Nr. 4
Diameter:	36"
Thickness:	19.05mm
Welding Position:	ASME IX 5G(except root)
Preparation Method:	PFM
Alignment Method:	IWM
Alignment Removed:	After Root Run
Preheat Method:	Propane
Backing System	N/A
Cleaning Method:	Grind/ wire Brush

Welders Name/Position:
Travis Klashinsky
Harry Liratzis

Joint Preparation:

Bevel offset=2.3mm

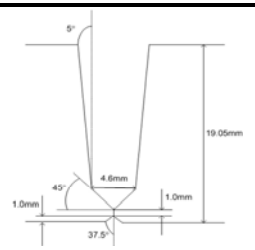

Run Sequence:

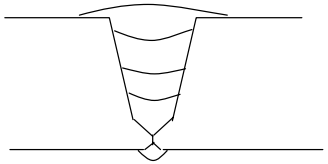

Pass	Process	Polarity	Electrode Brand	Electrode Batch	Electrode Size mm	Shielding Gas Type	Shielding Gas Flow L/min	Temp @ Start °C	Lead Torch WFS m/min	Lead Torch Amps I	Lead Torch Volts V	Trail Torch WFS m/min	Trail Torch Amps I	Trail Torch Volts V	Osc. Freq beats per min.	Osc. Width mm	CTWD mm	Travel Speed mm/min	Arc Energy kJ/mm
Int. root	GMAW	DC+ve	Thyssen K-Nova	186096	0.9	78%Ar/20%CO_2/2%O_2	20	110-110	10.00	205.05	20.78				-		10.0-11.0	710	0.36
Hot(Run1)	PGMAW	DC+ve	NiMo-1/ X-85	14233/496086	1.0	82.5%Ar/12.5%C02/5%He	27-28	100-120	12.20	214/218	22/22	9.20	166/139	19/20	350	1.45/2.65	13.5/16	1270	0.45/0.28
Fill 1(Run 2)	PGMAW	DC+ve	NiMo-1/ X-85	14233/496086	1.0	82.5%Ar/12.5%C02/5%He	27-28	100-120	11.50	202/200	20.5/20.5	8.50	147/149	20/20	350	2.7/2.95	13.5/16	1270	0.39/0.28
Fill 2(Run 3)	PGMAW	DC+ve	NiMo-1/ X-85	14233/496086	1.0	82.5%Ar/12.5%C02/5%He	27-28	100-120	11.00	195/141	20/20	8.00	143.5/142	19/19	350	3.35/3.85	13.5/16	1270(+/-20%)	0.32/0.26
Cap A Split	PGMAW	DC+ve	NiMo-1/ X-85	14233/496086	1.0	82.5%Ar/12.5%C02/5%He	27-28	100-120	7.00	133/117	19/19	7.00	133/128	18.5/19	350	1.75	15	1270(+/-20%)	0.22/0.23
Cap B Single	PGMAW	DC+ve	NiMo-1/ X-85	14233/496086	1.0	82.5%Ar/12.5%C02/5%He	27-28	100-120	8.00	141.5/127	20.5/20.5				350	7	15	889(+/-20%)	0.37
Single Strip B	PGMAW	DC+ve	NiMo-1/ X-85	14233/496086	1.0	82.5%Ar/12.5%C02/5%He	27-28	100-120	8.00	136/124	22/22				280	7.4	15	889(+/-20%)	0.38

Additional Comments:

Internal weld:fixed head, rotated pipe. Torch at 7 o'clock wire 90 deg to pipe surf., effectively vertical down welding, Esab Aristo 2000 power source.
External passes performed using Fronius TPS 4000 synchronised power sources.Lead wire Oerlikon NiMo-1, Trail wire Thyssen X-85.
Average I and V values include both sides A & B.
Hot Pass: Very Nice. Flat bottom. A. L. C. = 10 lead torch/10 trail torch.
Fill 1
Side A: Flat bottom A . L. C (both sides)= 8 lead torch/ 5 trail torch
Side B : A short repair (30mm) was performed at 6 o'clock using single torch.
Fill 2
Side A : Wrong alignement of trail torch caused a repair (40mm) at 6 o'clock using single torch.
Side B :Good Both sides, A. L. C =5 lead torch / 0 trail torch.
Cap A :
Split. Good. A. L. C. = 0 for both torches.
Cap B :
Single Torch up to 4 o'clock position and from 2 to 4 o'clock a strip with the same parameters. A. L. C. = 5
From 4 to 6 o'clock position split cap as side A. Arc Force Correction : 0.5.
Other Settings on the Fronius TPS 4000
Gas Preflow : 0.3s.
SL=0.7, t-E lead torch=off; t-E trail torch=0.1. For split cap both torches set to 0. For single cap t-E lead wire=0.1 & t-E trail wire=0.
Arc Force Correction=0 (for cap=0.5). For both wires : I-S=135A, I-E=50A, t-S=off.
Arc Energies for fill 2 and cap have been calculated using TS=1270mm/min & 889mm/min accordingly.
The +/- 20% of travel speed was used as follows: We started "dead slow" at the top and gradually increased and regulated according to the weld pool fluidity.
Repair conditions (single torch) : wfs=9.0m/min; TS=940mm/min(+/-10%); Osc. Frequency=350beats/min.
Longitudinal seam welds in line.

Cap Gap Widths (mm)

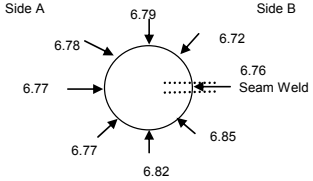

Depth Remaining to Cap(mm)

After Pass No.	12 o'c	3 o'c	6 o'c
0	17	17	16.5
Hot (Run 1)	10	11	10
Fill 1(Run 2)	5	7	7
Fill 2(Run 3)	1	2.2	2

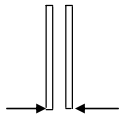

Oscillation Width Measurement

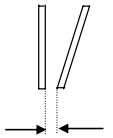

Wire Separation at 13.5mm extention:
Lead torch wire separation : 3.1mm
Trail torch wire separation :2.6mm
Torche Separation : 67mm
Lead Torch vertical to pipe axis
Trail Torch leading 2deg.

Fig. B2 Dual Tandem PGMAW Narrow Gap Welding Procedure ML-DT-S016, Pipe B19

Cranfield UNIVERSITY

Welding Procedure Specification

Weld No.: ML-DT-N009

Date:Root Pass:05.11.03,Fill Runs :18-20.11.03

Description:

X100 Dual Tandem Weld

Welders Name/Position:

John Savill

Material Grade:	X100
Heat Number:	G13768 Pipe No. 7
Diameter:	52"
Thickness:	22.9mm
Welding Position:	ASME IX 5G (except root)
Preparation Method:	PFM
Alignment Method:	IWM
Alignment Removed:	After Root Run
Preheat Method:	Propane
Backing System	N/A
Cleaning Method:	Grind/ wire Brush
Alignment Removed:	After Root Run
Preheat Method:	Propane
Backing System	N/A
Cleaning Method:	Grind/ wire Brush

Joint Preparation:

Bevel offset=2.5mm

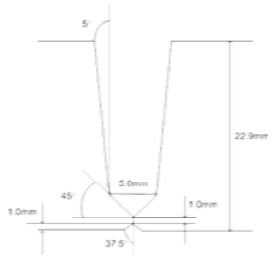

Run Sequence:

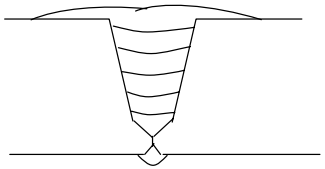

Pass	Process	Polarity	Electrode Brand	Batch	Size mm	Shielding Gas Type	Flow L/min	Temp @ Start °C	Lead Torch WFS m/min	Lead Torch Amps I	Lead Torch Volts V	Trail Torch WFS m/min	Trail Torch Amps I	Trail Torch Volts V	Osc. Freq beats per min.	Osc. Width mm	CTWD mm	Travel Speed mm/min	Arc Energy kJ/mm
Int. root	GMAW	DC+ve	Thyssen K-Nova	186096	0.9	78Ar/20%CO_2/2%O_2	20	100-110	9.70	196	20.8				-	-	10.0-11.0	710	0.34
Hot	PGMAW	DC+ve	NiMo-1 / X-85	14233/496086	1.0	82.5%Ar/12.5%CO_2/5%He	28-30	100-120	12.30	201/221	21.5/20	9.30	194/168	20/19	400	1.51/2.6	13.5/16.00	1295	0.40 / 0.33
FILL 1	PGMAW	DC+ve	NiMo-1 / X-85	14233/496086	1.0	82.5%Ar/12.5%CO_2/5%He	28-30	100-120	12.20	220/216	22/22	9.20	177/162	22/21	400	3.02/3.43	13.5/16.00	1270	0.44/0.34
FILL 2	PGMAW	DC+ve	NiMo-1 / X-85	14233/496086	1.0	82.5%Ar/12.5%CO_2/5%He	28-30	100-120	11.20	196/200	20/20	8.20	156/144	20/19	400	4.15/4.5	13.5/16.00	1295(+/-10%)	0.37/0.27
FILL 3	PGMAW	DC+ve	NiMo-1 / X-85	14233/496086	1.0	82.5%Ar/12.5%CO_2/5%He	28-30	100-120	11.20	196/194	21/21	9.20	153/142	20/19	400	4.67/5.22	13.5/16.00	1295(+/-15%)	0.38/0.27
FILL 4	PGMAW	DC+ve	NiMo-1 / X-85	14233/496086	1.0	82.5%Ar/12.5%CO_2/5%He	28-30	100-120	9.20	159/161	23/23	7.20	133/124	22/21	400	4.67/5.22	13.5/16.00	1295(+/-15%)	0.34/0.25
Cap Split	PGMAW	DC+ve	NiMo-1 / X-85	14233/496086	1.0	82.5%Ar/12.5%CO_2/5%He	28-30	100-120	7.00	120/122	22/22	7.00	129/120	23/22	300	2.5	15	1295(+/-20%)	0.25/0.26

Additional Comments:

Internal weld:fixed head,rotated pipe.Torch at ~7o'clock,wire 90 deg to pipe surf.,effectively vertical down welding ,Esab Aristo 2000 source.
External passes Fronius TPS 4000 Thermo synchronized power sources
Lead wire Oerlikon NiMo-1, Trial Wire Thyssen X-85 for each torch.
Hot Pass :Arc Length Correction :10 lead torch/10 trail torch.t-E=0.1trail torch;off lead torch.
Side A: Very smooth arc and flat 6 o'clock position.
Fill 1:Arc Length Corr.=10/10 Side B : Two pockets at the bottom. Oscillation width needs to be increased
Fill 2 : Arc Length Correction :8/5. Both sides not bad process/ bead profile. Some grinding at the bottom.
Fill 3: Side B: Too much material. Grinding and repair.
Side A**:** We decreased wfs=10/8m/min.
Fill 4 : Arc Length Correction :5/0. Side B: General ok. TS=1166mm/min at the bottom.
Side A: We started at the top at 1166mm/min(to fill some gaps) then speed up and decreased again at the bottom to 1166mm/min.
Cap(Split) : Arc Length Correction: 0/0.
Other settings on the Fronius TPS 4000:
Both Torches :I-S=135A, I-E=50A, t-S=off, S-L=0.7
Smooth grinding was performed between all passes.
After Hot Pass for both torches t-E=off was set.
Travel Speed Control: We started at 1143mm/min, then speed up and decreased to 1067mm/min at the bottom.

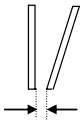

Wire Separation measurement at 13.5mm extension
Lead Torch Wire Separation : 2.2mm
Trail Torch Wire Separation : 2.0mm
Torche Separation : 78mm

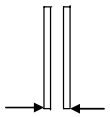

Oscillation Width Measurement

Depth Remaining to Cap (mm)

After Pass No.	12 o'c	3 o'c	6 o'c
0	19.75	19.8	19.7
Hot	13.7	14.5	13.3
Fill 1	9.22	9.8	-
Fill 2	5.8	7	-
Fill 3	2	3.2	-
Fill 4	Almost Flat	0.4	-

Cap Gap Widths(mm)

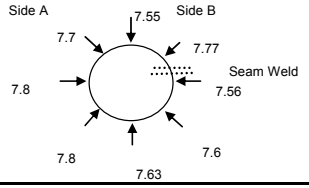

Fig. B3 Dual Tandem PGMAW Narrow Gap Welding Procedure ML-DT-N009, Pipe D2

Cranfield UNIVERSITY

Welding Procedure Specification

Weld No : ML-DT-N013

Date: Root 13.02.04 / Fill Runs 16-17.02.04

Description:

X100 Dual Tandem Weld

Material Grade:	X100
Heat Number:	G13416 , Pipe Nr. 3
Diameter:	52"
Thickness:	22.9mm
Welding Position:	ASME IX 5G (except root)
Preparation Method:	PFM
Alignment Method:	IWM
Alignment Removed:	After Root Run
Preheat Method:	Propane
Backing System	N/A
Cleaning Method:	Grind/ wire Brush

Welders Name/Position:
John Savill
Brian Brooks (Root)

Joint Preparation:

Bevel offset=2.3mm

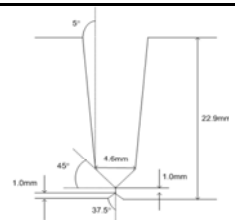

Run Sequence:

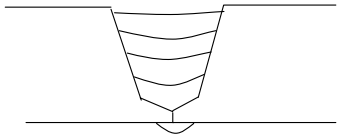

Pass	Process	Polarity	Electrode Brand	Batch	Size mm	Shielding Gas Type	Flow L/min	Temp @ Start °C	Lead Torch WFS m/min	Lead Torch Amps I	Lead Torch Volts V	Trail Torch WFS m/min	Trail Torch Amps I	Trail Torch Volts V	Osc. Freq beats per min.	Osc. Width mm	CTWD mm	Travel Speed mm/min	Arc Energy kJ/mm
Int. root	GMAW	DC+ve	Thyssen K-Nova	186096	0.9	78%Ar/20%CO_2/2%O_2	20	100-110	9.60	161	20.57				-		10.0-11.0	710	0.24
Hot(Run 1)	PGMAW	DC+ve	NiMo-1 / X-85	14233 / 496089	1.0	82.5%Ar/12.5%C02/5%He	25-30	100-110	12.30	214/205	23.5/23	9.30	173/167	20/20.5	430	1.55/2.55	13.5/16.0-16.5	1270	0.46/0.35
Fill 1(Run 2)	PGMAW	DC+ve	NiMo-1 / X-85	14233 / 496089	1.0	82.5%Ar/12.5%C02/5%He	25-30	100-110	12.30	211/207	23/23	9.20	166/163	21/21	430	2.6/2.85	13.5/16.0-16.5	1270(+/-10%)	0.45/0.33
Fill 2 (Run 3)	PGMAW	DC+ve	NiMo-1 / X-85	14233 / 496089	1.0	82.5%Ar/12.5%C02/5%He	25-30	100-110	11.20	195/186	23/22	8.30	149/145	20.5/20.5	430	3.15/3.75	13.5/16.0-16.5	1194(+/-10%)	0.43/0.30
Fill 3 (Run 4)	PGMAW	DC+ve	NiMo-1 / X-85	14233 / 496089	1.0	82.5%Ar/12.5%C02/5%He	25-30	100-110	10.40	187/180	23/22	8.10	153/148	19/20	430	3.95/4.15	13.5/16.0-16.5	1194(+/-10%)	0.41/0.30
Cap Split	PGMAW	DC+ve	NiMo-1 / X-85	14233 / 496089	1.0	82.5%Ar/12.5%C02/5%He	25-30	100-110	7.20	136/129	21/21	7.20	130/128	22/22	330	3.05/3.05	14.5/14.5	1168(+/-10%)	0.29/0.29

Additional Comments:

Internal weld:fixed head,rotated pipe.Torch at ~7o'clock,wire 90 deg to pipe surf.,effectively vertical down welding ,Esab Aristo 2000 source.
One stop at the root run after 540mm from starting point.
External passes Fronius TPS 4000 Thermo (lead set) and upgraded thermo (trail set) synchronized power sources.
Lead wire :Oerlikon NiMo-1 & Trail wire: Thyssen X-85
Gas Preflow : lead torch=0.0s & Trail Torch=0.4s.
Hot Pass (Run 1): Arc length correction:0 for lead set and 6 for trail set.
Side A:Good start and stop points.
Side B:Trail torch noisy. Spatter on the contact tips caused a stop at 4 o'clock position
Fill 1 (Run2): Arc length correction :0 for lead set and 4 for trail.
Side A: Width not bad. Few "explosions" at 3 to 4 o'clock. Some visual l.o.f at the bottom removed by grinding.
Side B:Generally good. Small "pocket" was generated at 6 o'clock position.
Fill 2 (Run 3)
Side A:Generally ok all around. Two small "pockets before 6 o'clock. Removed by grinding.We passed 6 o'clock by 100mm (ok). Oscillation width was increased at the bottom at 125/155mm.
Fill 3 (Run4)
Side A:Some spatter (trail torch) caused a stop at 5:30 oclock. Welding speed reduced to TS=44"/min
We restarted with the same conditions and finished the last 280mm with TS=41.4"/min.
Side B :Osc. Width=180/195. Some spatter but weld profile good.
Cap (Split)
Side A: Very good, although with some spatter
Side B:Some spatter but generally very good profile and stable process. End of weld at TS=41.4"/min.
Other Settings (Fronius TPS 4000):
Both Torches : I-S=135A, I-E=50A, t-S=off, S-L=0.7.
Lead Torch vertical to pipe axis; Trail Torch trailing 2deg.

Cap Widths(mm)

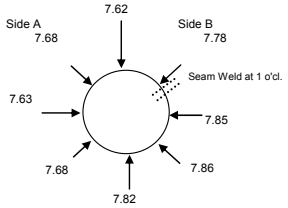

After Pass No.	Depth Remaining to Cap (mm) 12 o'c	3 o'c	6 o'c
0	19.2	19	19
Hot (Run 1)	13	13	12.6
Fill 1(Run 2)	8.6	9.4	7.6
Fill 2 (Run 3)	4.6	5	N.A
Fill 3(Run4)	0.78	1	N.A

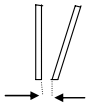

Wires Separation at 13.5mm extension
Lead torch wire separation :1.8mm
Trail torch wire separation :1.95mm
Torche Separation : 80mm

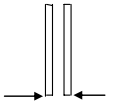

Oscillation Width Measurement

Fig. B4 Dual Tandem PGMAW Narrow Gap Welding Procedure, Pipe D1

Cranfield UNIVERSITY

Welding Procedure Specification

Weld No : DJ-DT-N012

Date: Root 07.11.03 / Fill Runs 07.01.04

Description:

X100 Dual Tandem Weld

Welders Name/Position:

John Savill

Brian Brooks (Root)

Material Grade:	X100
Heat Number:	G13416 , Pipe Nr. 2
Diameter:	52"
Thickness:	22.9mm
Welding Position:	ASME IX 5G (except root)
Preparation Method:	PFM
Alignment Method:	IWM
Alignment Removed:	After Root Run
Preheat Method:	Propane
Backing System	N/A
Cleaning Method:	Grind/ wire Brush

Joint Preparation:

Bevel offset=3.0mm

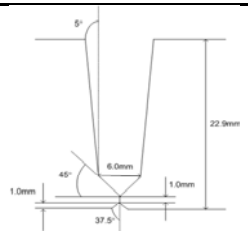

Run Sequence:

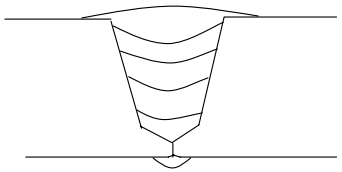

Pass	Process	Polarity	Electrode Brand	Batch	Size mm	Shielding Gas Type	Flow L/min	Temp @ Start °C	Lead Torch WFS m/min	Amps I	Volts V	Trail Torch WFS m/min	Amps I	Volts V	Osc. Freq beats per min.	Osc. Width mm	CTWD mm	Travel Speed mm/min	Arc Energy kJ/mm
Int. root	GMAW	DC+ve	Thyssen K-Nova	186096	0.9	78%Ar/20%CO_2/2%O_2	20	100-110	9.60	187	20.57				-		10,00-11,00	710	0.32
Hot(Run 1)	PGMAW	DC+ve	Ni Mo-1 / X-85	14233/ 496086	1.0	82.5%Ar/12.5%C02/5%He	25-30	100-120	15.20	236 / 246	25 / 24.5	11.50	201 / 190.5	21 / 22	450	2.35/3.35	14 / 17.5	1422	0.5 / 0.35
Fill 1(Run 2)	PGMAW	DC+ve	Ni Mo-1 / X-85	14233/ 496086	1.0	82.5%Ar/12.5%C02/5%He	25-30	100-120	15.50	235 / 244	26 / 26	12.00	195 / 190	25 / 25	450	3.35/3.95	14 / 17.5	1422	0.53 / 0.41
Fill 2 (Run 3)	PGMAW	DC+ve	Ni Mo-1 / X-85	14233/ 496086	1.0	82.5%Ar/12.5%C02/5%He	25-30	100-120	16.00	244 / 248	26 / 26	12.00	196 / 193	24 / 24	450	3.95/4.55	14 / 17.0-17.5	1422	0.54 / 0.40
Fill 3 (Run 4)	PGMAW	DC+ve	Ni Mo-1 / X-85	14233/ 496086	1.0	82.5%Ar/12.5%C02/5%He	25-30	100-120	16.00	241 / 247	26 / 27	12.00	195 / 192	24 / 24	450	4.55/5.05	14 / 17.0-17.5	1422	0.54 / 0.39
Cap	PGMAW	DC+ve	Ni Mo-1 / X-85	14233/ 496086	1.0	82.5%Ar/12.5%C02/5%He	25-30	100-120	16.00	244 / 246	25 / 27	12.00	194 / 192	24 / 24	450	5.15/5.95	14 / 16	1295	0.59 / 0.43

Additional Comments:

Internal weld:fixed head,rotated pipe.Torch at ~7o'clock,wire 90 deg to pipe surf.,effectively vertical down welding ,Esab Aristo 2000 source.
External passes Fronius TPS 4000 Thermo synchronized power sources
Lead wire :Oerlikon NiMo-1 & Trail wire: Thyssen X-85
Gas Preflow : lead torch=0.0s & Trail Torch=0.0s.
Welding Position : 11 o'clock. Arc Length Correction for both power sources :0%

Hot Pass (Run 1)
Very Good. Stable process. Nice bead profile.

Fill 1 (Run2)
Good . Stable process. Nice weld profile.

Fill 2 (Run 3)
Trail torch oscillation width to be reduced. Some spatter.

Fill 3 (Run4)
Nice weld profile. Stable process.

Other Settings on Fronius TPS 4000 :
Both Torches : I-S=135A, I-E=50A, t-S=off, S-L=0.7.
Grinding was carried out after completion of each run.
For monitoring purposes the Yokogawa Oscilloscope DL 750 was used.
Longitudinal seam welds in line.

Cap Gap Widths(mm)

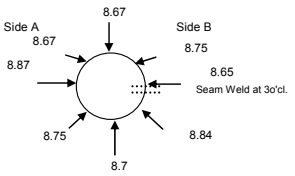

Depth Remaining to Cap (mm)

After Pass No.	12 o'c	3 o'c	6 o'c
0	19.89	19.65	19.9
Run 1	14.9	15	14.94
Run 2	10.5	10.5	10.5
Run 3	6	6.5	6.6
Run 4	2.3	2.5	2.4

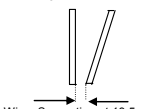

Wires Separation at 13.5mm extension
Lead torch wire separation :2.1mm
Trail torch wire separation :2.0mm
Torche separation : 68mm
Lead torch vertical to pipe axis.Trail torch trailing 2deg.

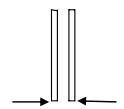

Oscillation Width Measurement

Fig. B5 Dual Tandem Double Jointing Narrow Gap Welding Procedure, Pipe D1

Cranfield UNIVERSITY

Welding Procedure Specification

Weld No.: TIE IN S01

Date: Root :Side A=14.10.03 / Side B=15.10.03
Hot to Cap Runs : 15.10.03-20.10.03

Description:

X100 Tie In Weld

Welders Name/Position:

Harry Liratzis

Brian Brooks

Material Grade:	X100
Heat Number:	KYYU1352(9B23017)/ Pipe No. 0002
Diameter:	36"
Thickness:	19.05mm
Welding Position:	ASME IX 5G(except root)
Preparation Method:	PFM
Alignment Method:	IWM
Alignment Removed:	After End of Fill Passes
Preheat Method:	Propane
Backing System	N/A
Cleaning Method:	Grind/ wire Brush

Joint Preparation:

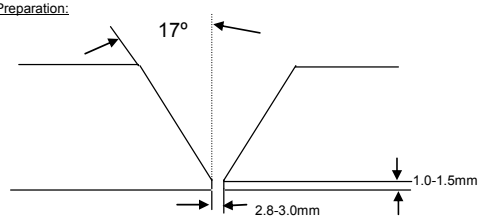

Run Sequence:

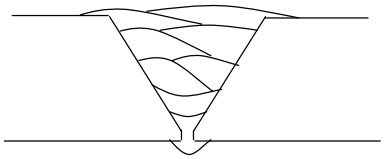

Pass	Process	Polarity	Electrode Brand	Batch	Size mm	Shielding Gas Type	Flow L/min	Temp @ Start °C	WFS m/min	Amps Iav	Volts Vav	Osc. Freq beats per min.	Osc. Width mm	CTWD mm	Travel Speed mm/min	Arc Energy kJ/mm	Remarks
Root	GMAW	DC+ve	Fluxofil M10S	2A6913	1.2	78Ar/20CO_2/2O_2	18-20	100-130	3.3-3.4	154	15	120	4.2	18.00	190	0.73	
Hot	PGMAW	DC-ve	Filarc PZ 6149	321029	1.2	92%Ar/5%CO_2/3%O_2	18-20	100-130	7.62	185	20	120	4.5	15.00	240	0.92	
Fill 1	PGMAW	DC-ve	Filarc PZ 6149	321029	1.2	92%Ar/5%CO_2/3%O_2	18-20	100-130	7.62	192	20	120	6.6	15.00	240	0.96	
Fill 2 Split1/2	PGMAW	DC-ve	Filarc PZ 6149	321029	1.2	92%Ar/5%CO_2/3%O_2	18-20	100-130	7.62	193	19	120	3.0/2.0	15.00	275	0.80	
Fill 3 Split1/2	PGMAW	DC-ve	Filarc PZ 6149	321029	1.2	92%Ar/5%CO_2/3%O_2	18-20	100-130	7.62	187	20/21	120	4.0	15.00	275	0.82/ 0.86	
Cap Split1//2	PGMAW	DC-ve	Filarc PZ 6149	321029	1.2	92%Ar/5%CO_2/3%O_2	18-20	100-130	7.62	190	21	120	4.0	15.00	290	0.82	

Additional Comments:

Root Pass:Esab Aristo 2000 Power Source was used.Program :Metal Core Fe. Torch vertical to pipe axis.
Side A: Run from 3o'clock to 12o'clock.
Run from 6 o'clock to 3 o'clock. For 50-80mm lack of root penetration.
Side B:Run from 6 o 'clock to 3 o'clock
Run from 3 o'clock to 12 o'clock. Lot of problems.
Hot / Fill Passes :Lincoln Power Wave 455 STT.
Hot Pass : Side A :Very good . Flat Bottom.Some undercuts at the top.Removed by grinding. Side B very good bead profile. Very smooth arc.
Fill 1 :
Side B : Weld pool too fluid at three o'clock position.Stop/ Restart with same conditions.At 4 o'clock welding speed decreased to 190mm/min. Smooth bead profile.
We may need to decrease TS further 160-180mm/min)
Fill 2 : Side B (Split 1) After 4 o'cl. TS decreased to 250mm/min.Very good bead profile and arc.Side A. Same technique.Nice Profile
Fill 2 : Side B (Split 2) : Oscill. width decreased to 2mm.Side A:. After 4 o'clock. Very long arc.Bad control of CTWD. 4 holes. Two repairs.
Fill 3 : Side A (Split 1):*Good* weld profile. Smooth Arc./ Split 2: Same conditions as above.Smooth Arc / Profile.
Fill 3 : Side B (Split 1): Same conditions as above.Smooth Arc / Profile. / Split2: Same conditions as above.Smooth Arc / Profile.
Cap Side A. Split 1**:** Repair at the bottom for 70mm length.TS=275mm/min at 12 o'clock and increaseed to 290 after 3 o'clock. Split 2 : Repair for 250mm at the bottom.Strip Cap: 330mm (position from 4 o'cl to 5:30 o'cl).
Cap Side B. Split 1**:** TS=275mm/min increased to 290mm/min after 3 o'cl. Oscill. width =5mm.Some side undercuts at the bottom. Split2: welding speed increased to TS=315mm/min.
REMARKS: No mechanicals from the bottom sections of the pipe. / Root repairs were performed (Manual TIG)
After each pass grinding and wire brushing were performed.
Longitudinal seam welds in line

Cap Gap Widths (mm)

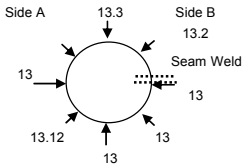

Depth Remaining to Cap (mm)

After Pass No.	12 o'c	3 o'c	6 o'c
Root	12.5	14	12.2
Hot	8.46	10.4	9.15
Fill 1	6.24	6.54	6.7
Fill 2	4.3	4.49	3.2
Fill 3	1.5	2	1.2

Fig. B6 Single Wire Pulsed FCAW Welding Procedure, Pipe B19

Appendix C - Welding Parameter and Shielding Gas Trials Macrographs

Fig. C1 Welding Parameter Trials / Flat Position (Table 5.4)

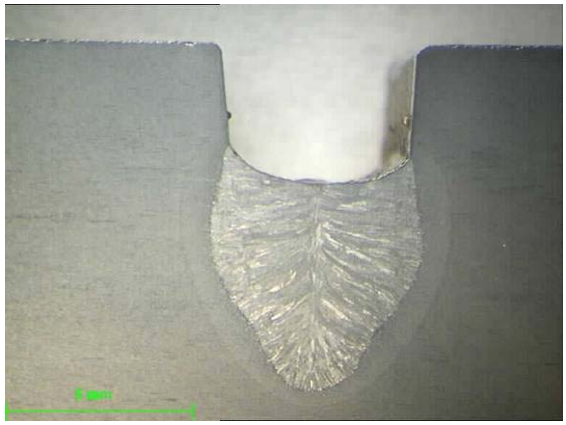

weld 1

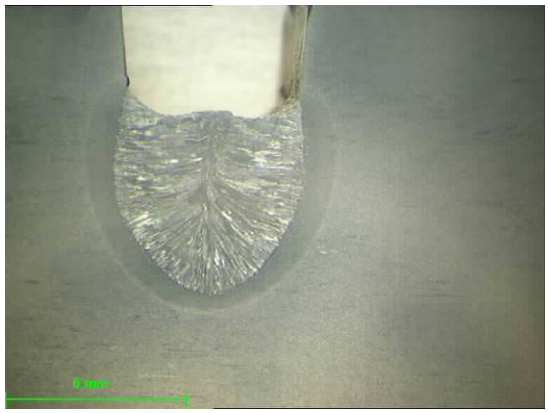

weld 2

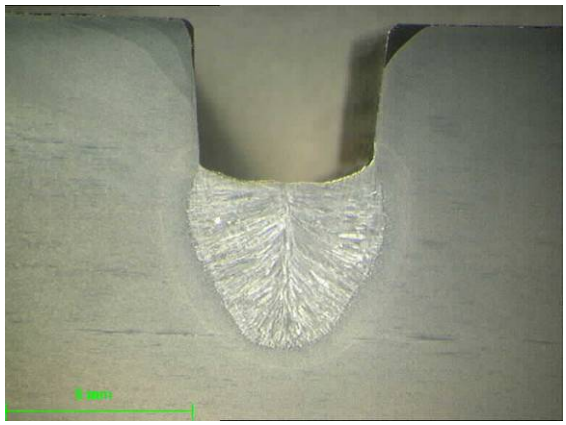

weld 3

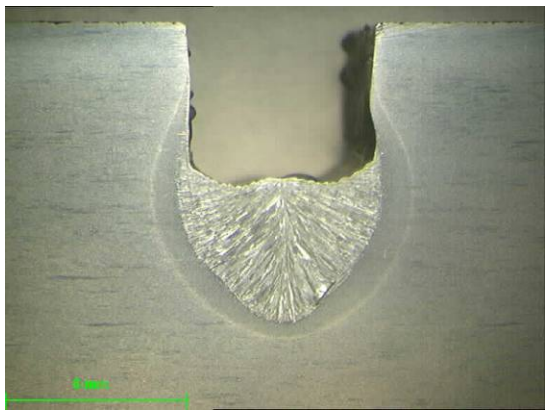

weld 4

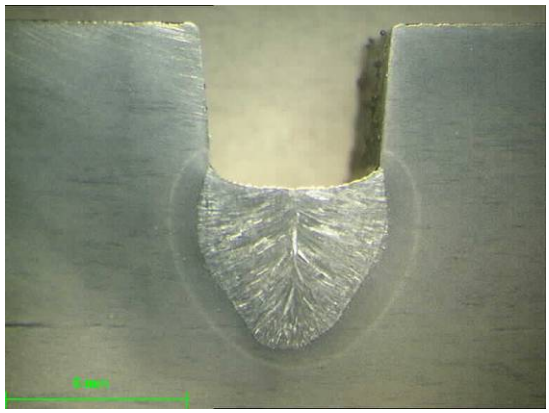

weld 5

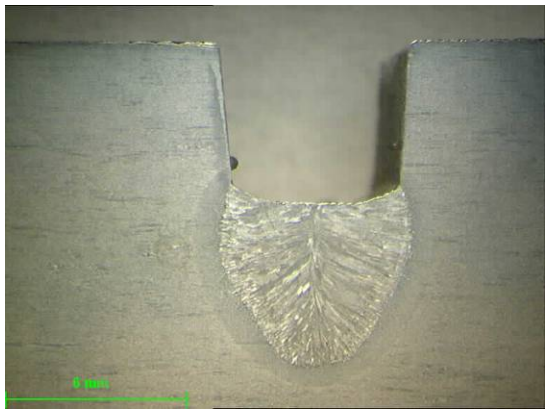

weld 6

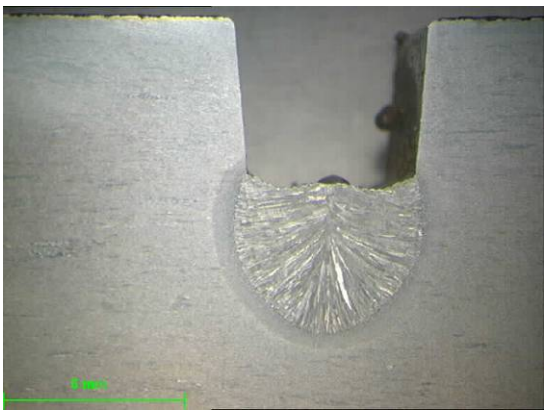

weld 7

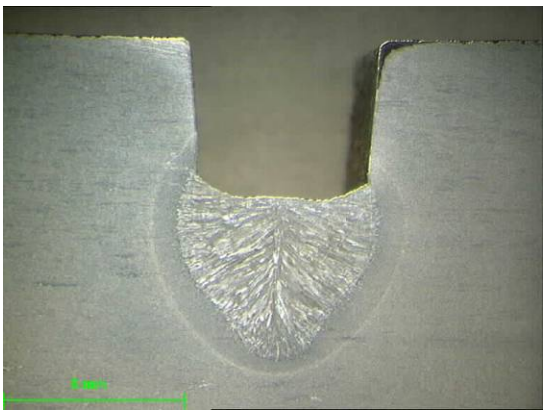

weld 8

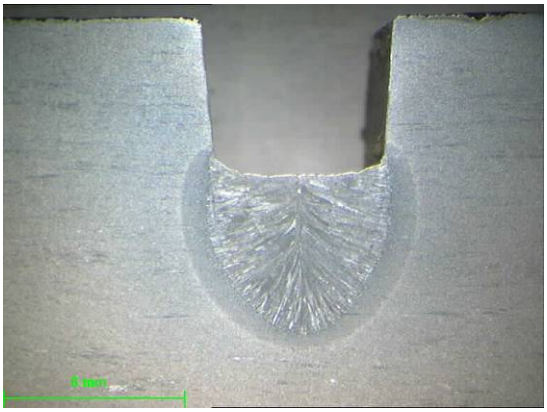

weld 9

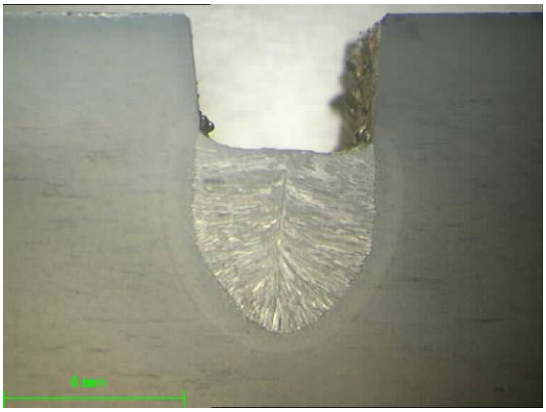

weld 10

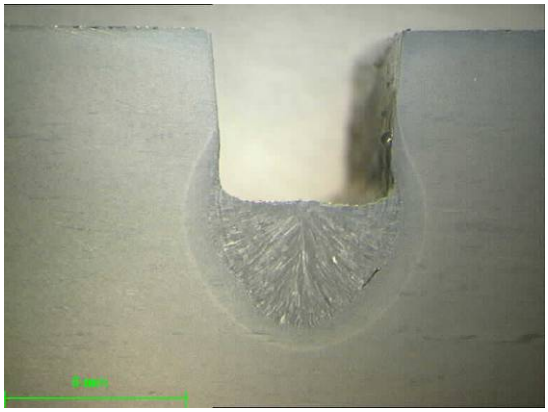

weld 11

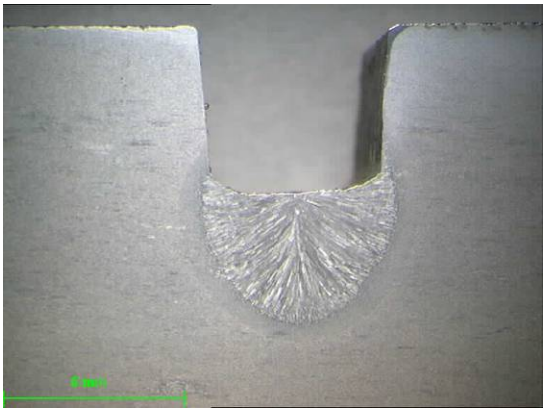

weld 12

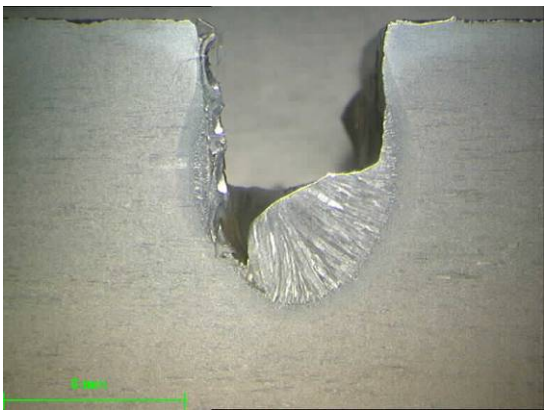

weld 13

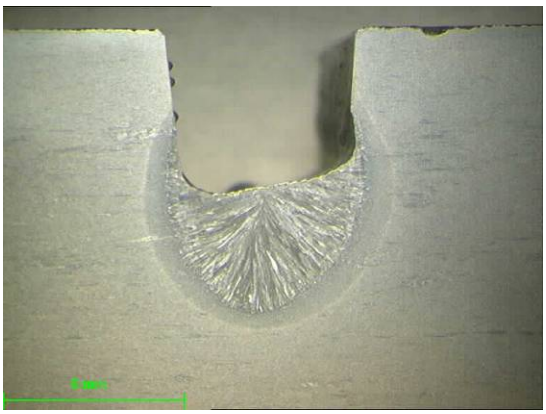

weld 13.1

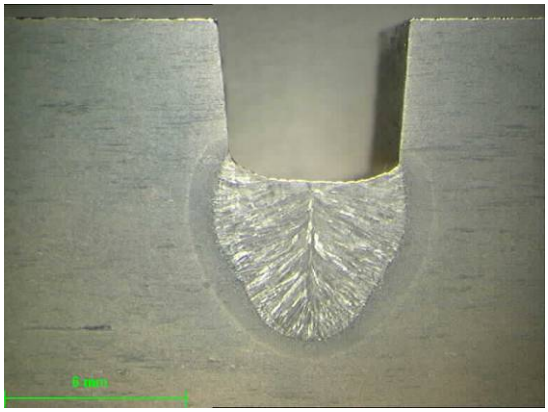

weld 14

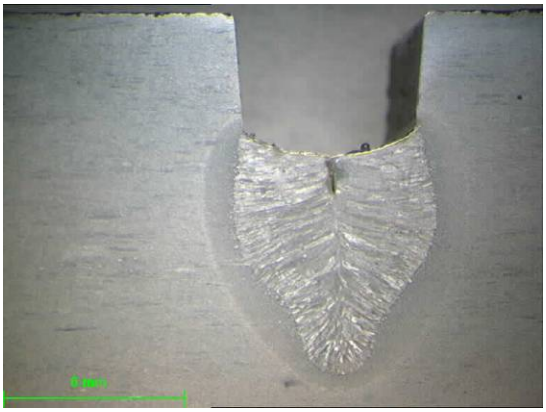

weld 15

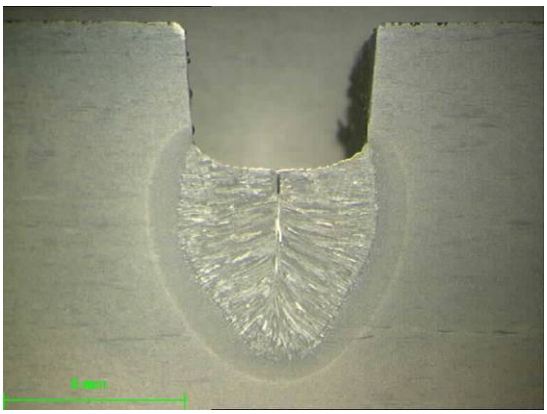

weld 16

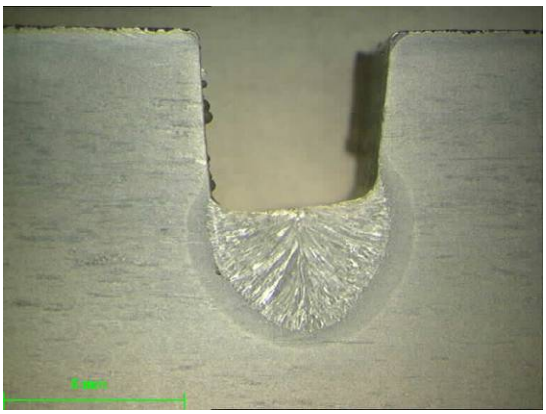

weld 17

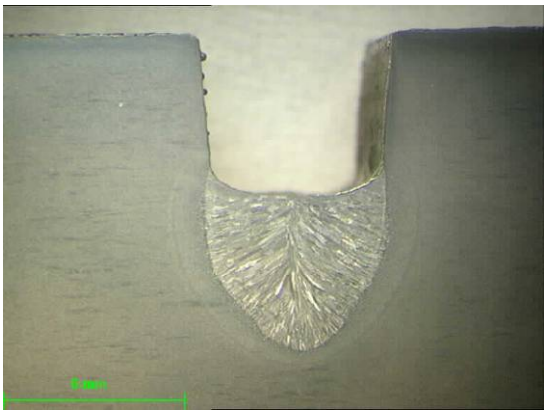

weld 18

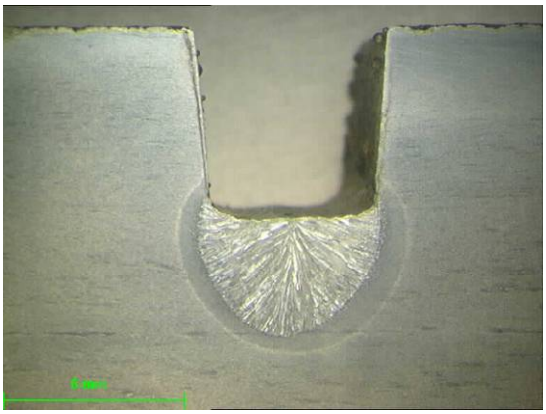

weld 19

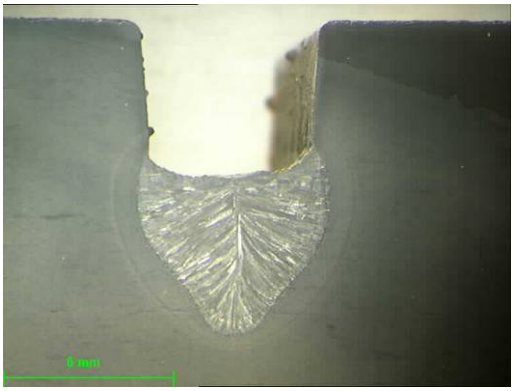

weld 20

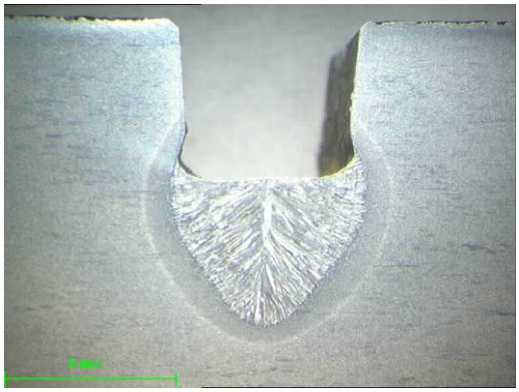

weld 21

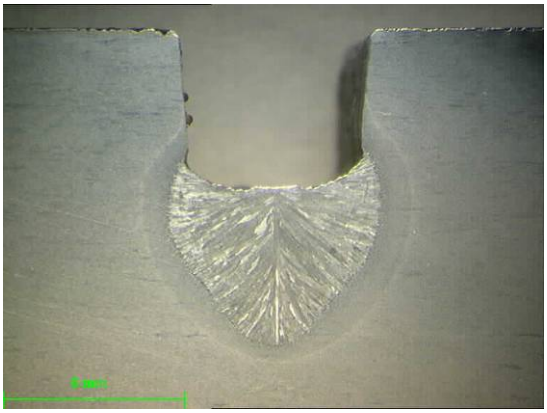

weld 22

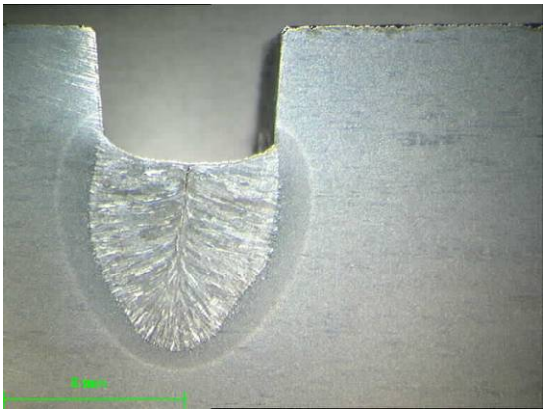

weld 23

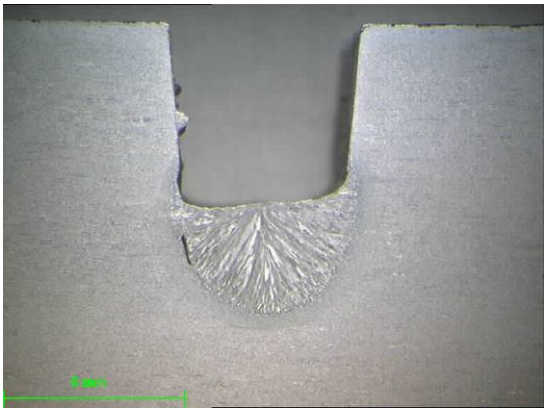

weld 24

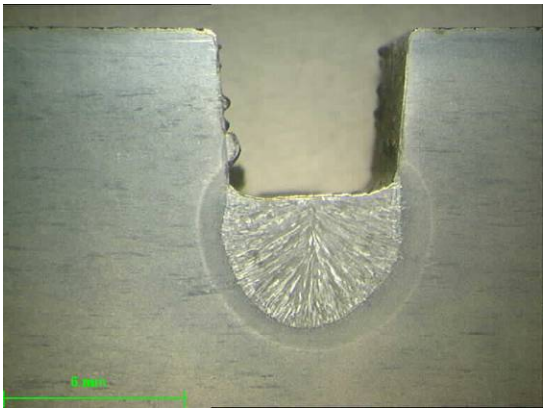

weld 25

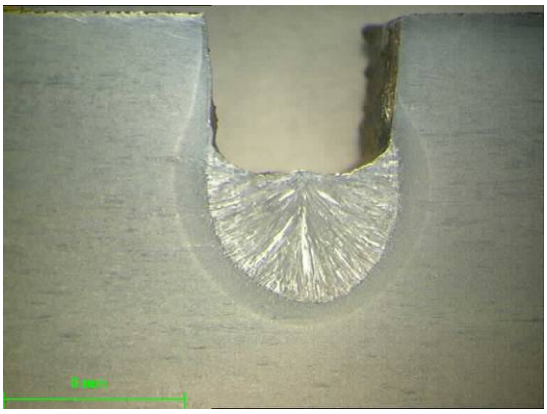

weld 26

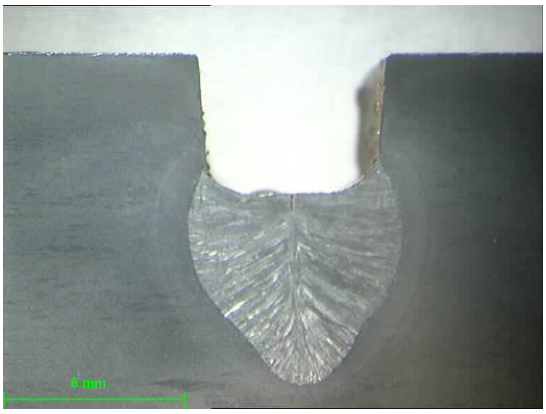

weld 27

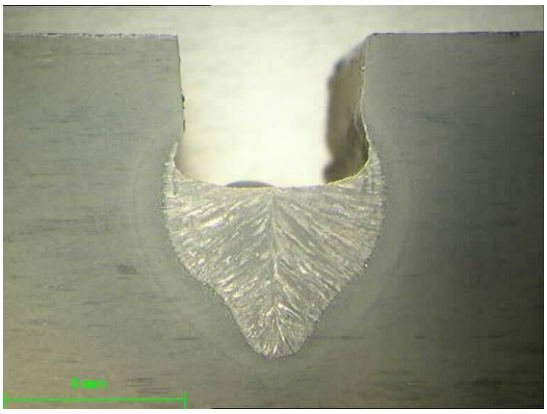

weld 28

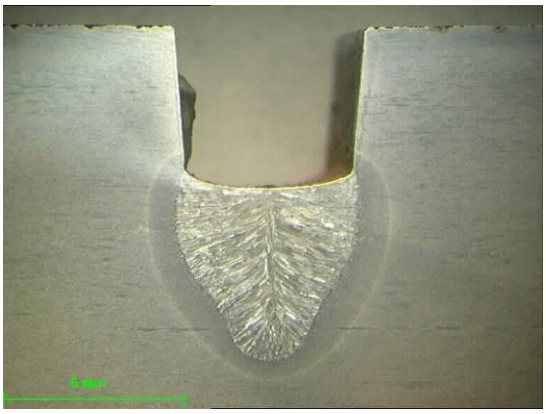

weld 29

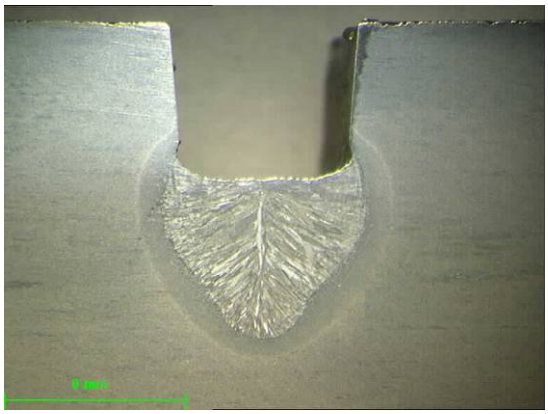

weld 30

Fig. C2 Welding Parameter Trials / Vertical Down Position (Table 5.4)

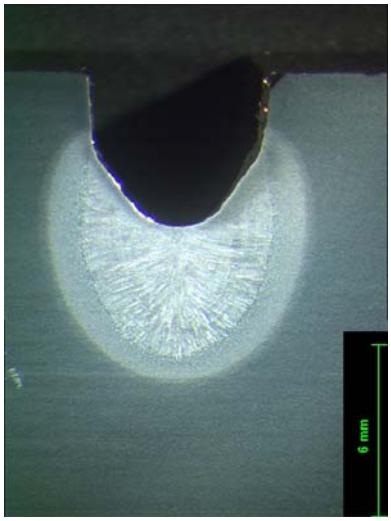

weld 1

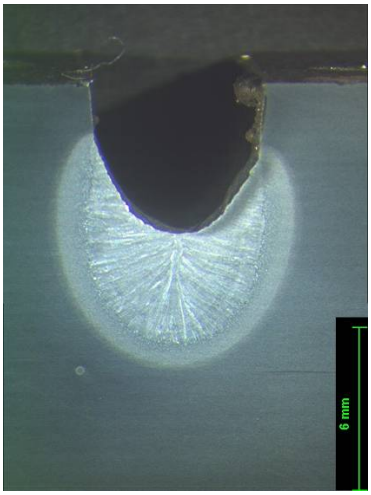

weld 2

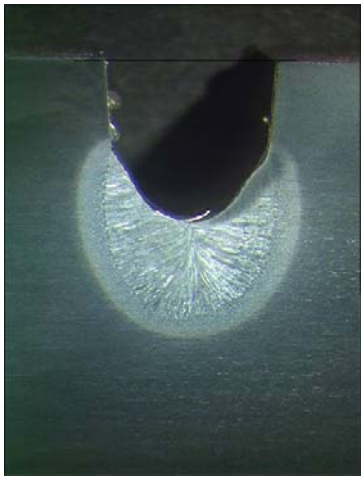

weld 3

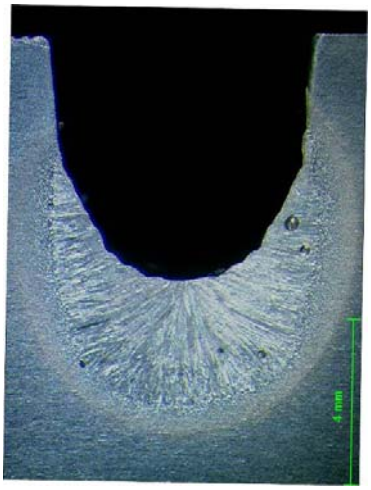

weld 4

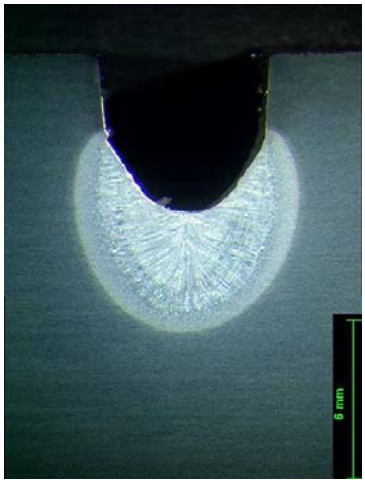

weld 5

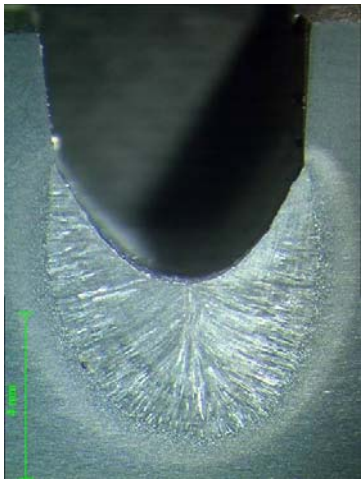

weld 6

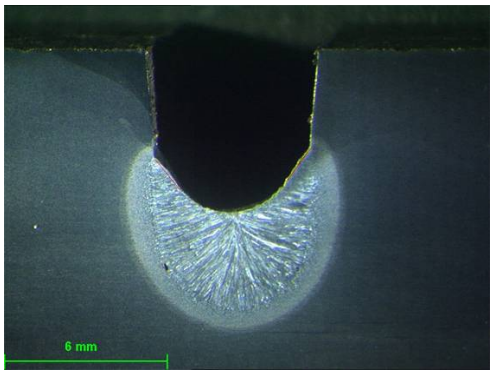

weld 7

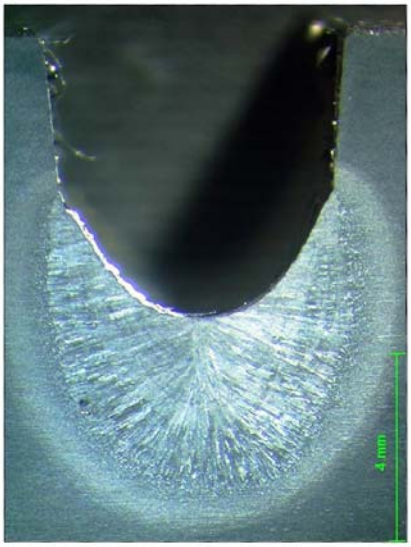

weld 8

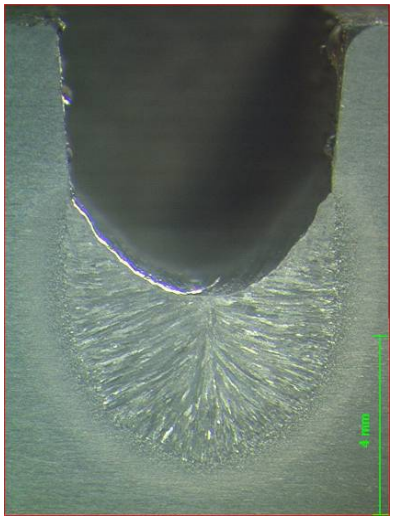

weld 9

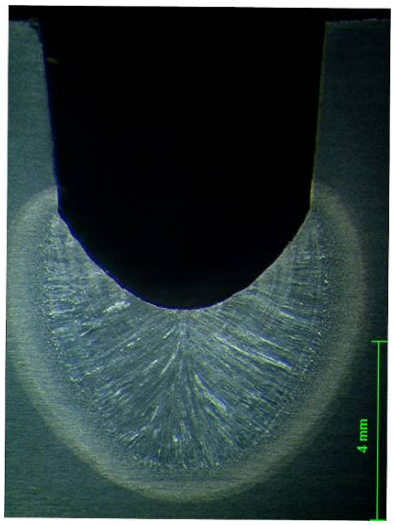

weld 10

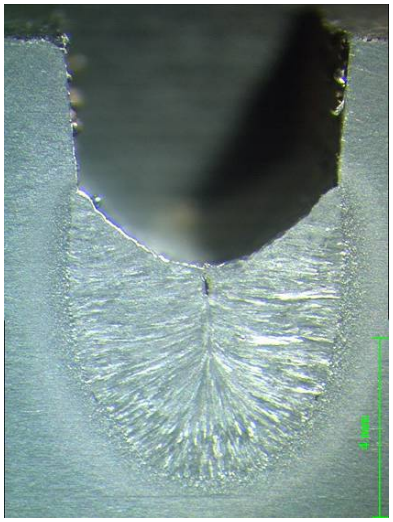

weld 11

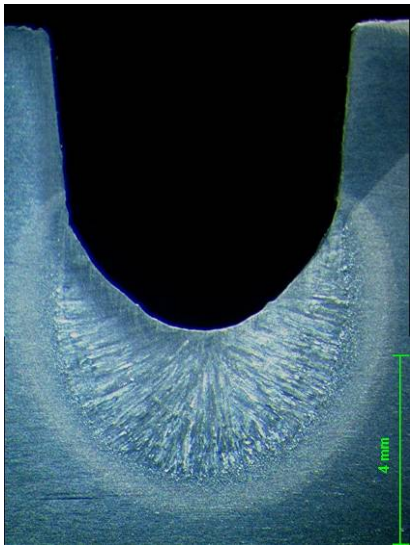

weld 12

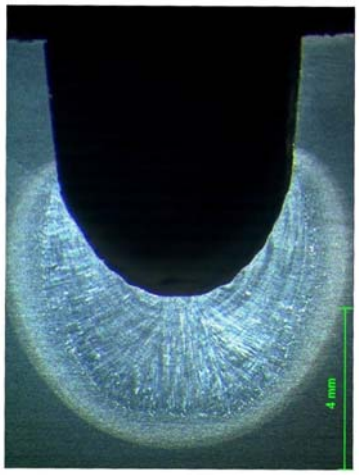

weld 13

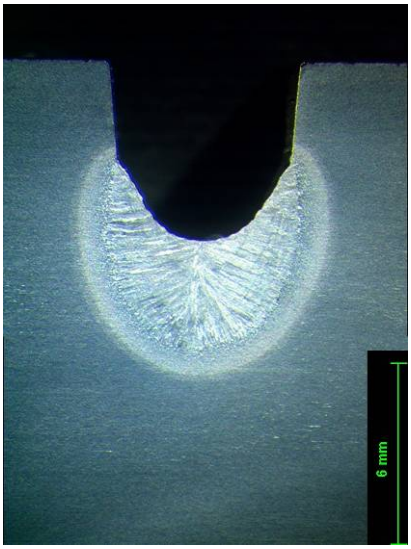

weld 14

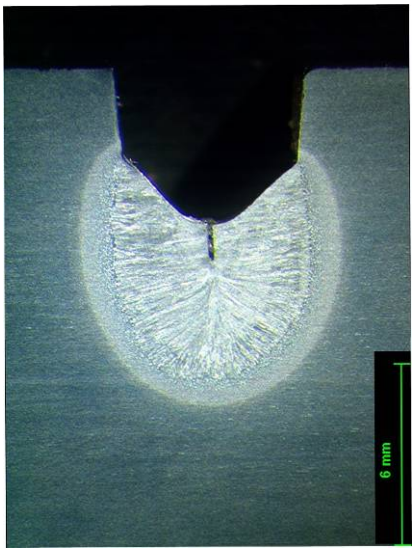

weld 15

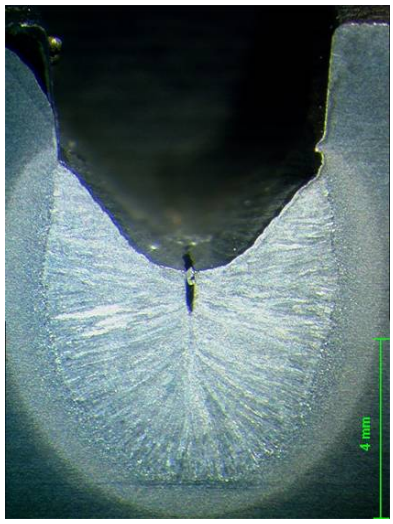

weld 16

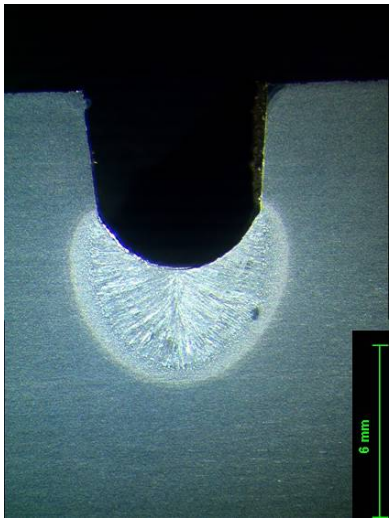

weld 17

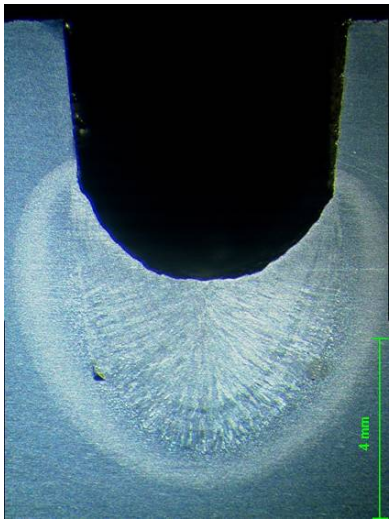

weld 18

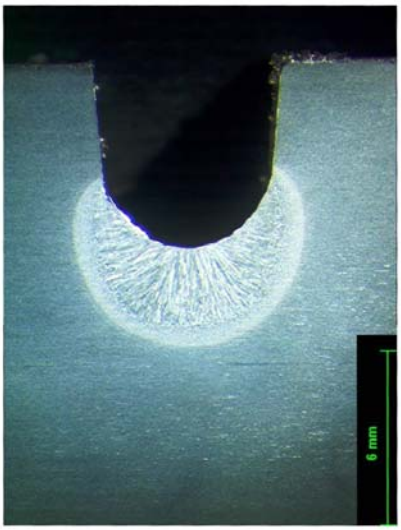

weld 19

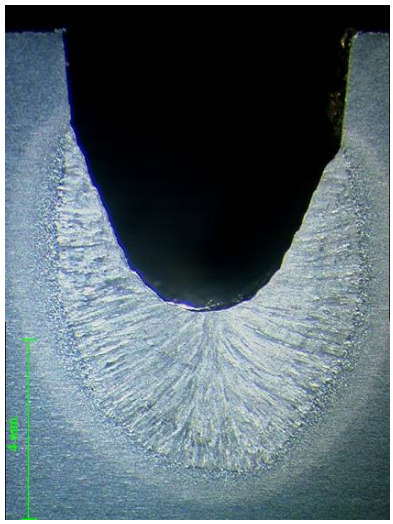

weld 20

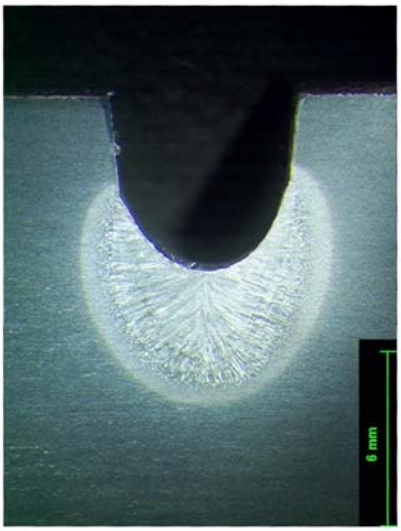

weld 21

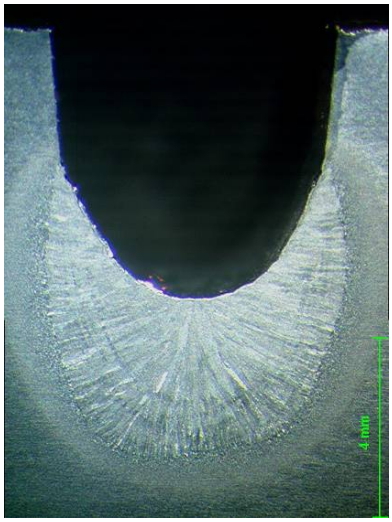

weld 22

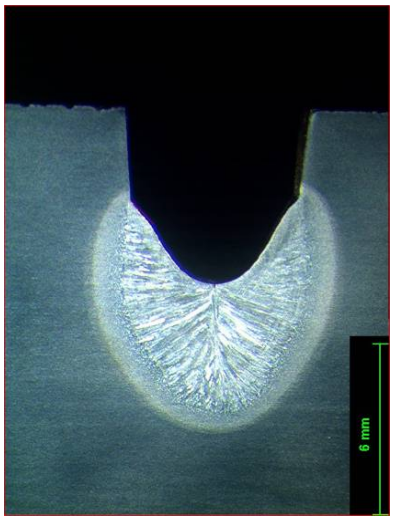

weld 23

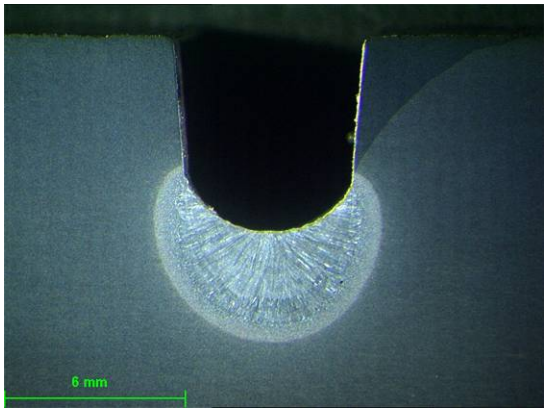

weld 24

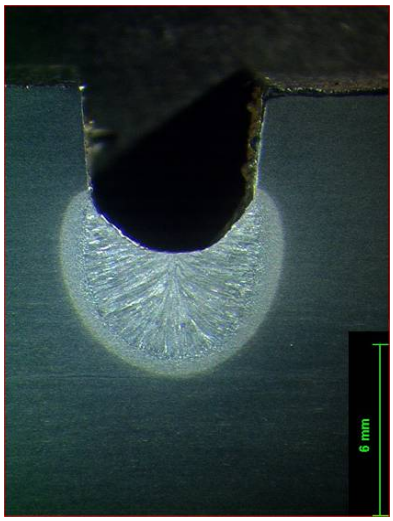

weld 25

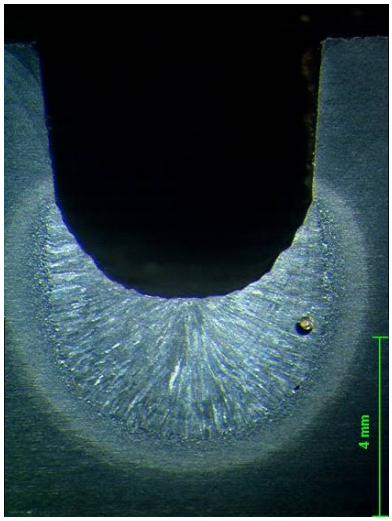

weld 26

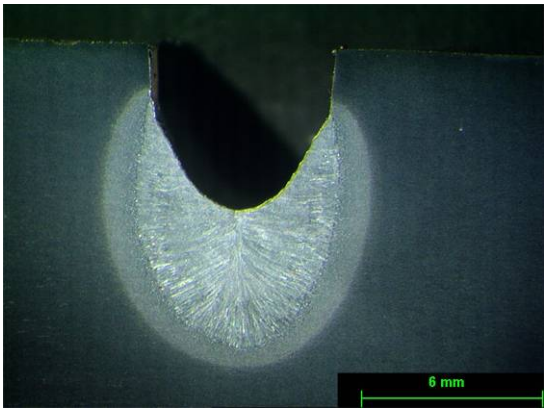

weld 27

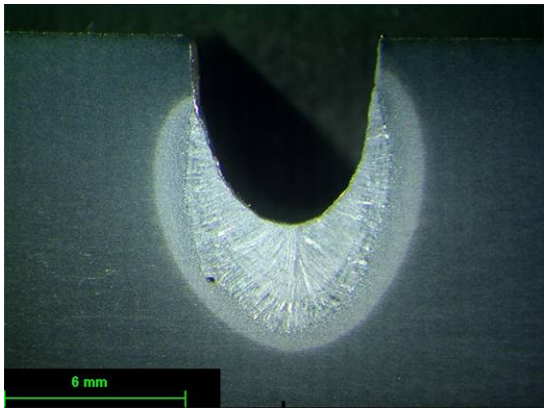

weld 28

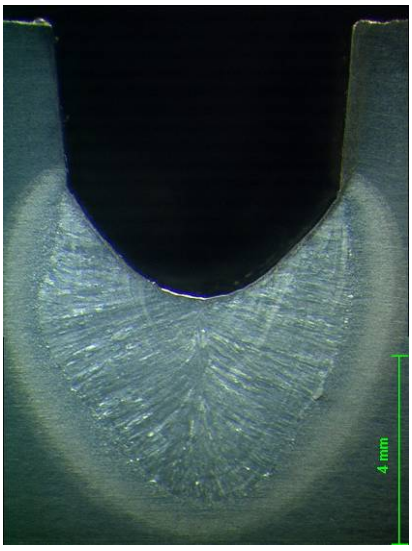

weld 29

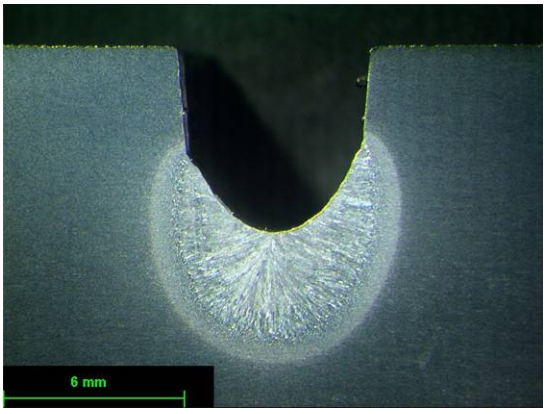

weld 30

Fig. C3 Welding Parameter Trials / Overhead Position (Table 5.4)

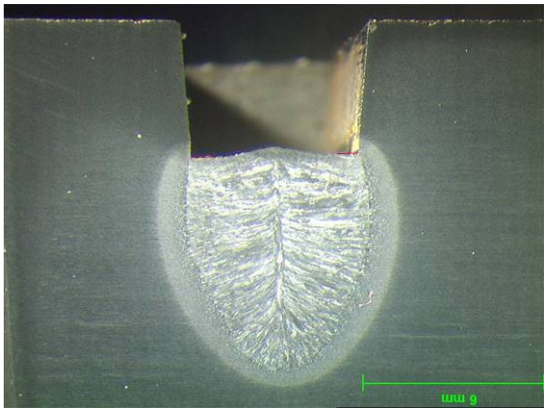

weld 1

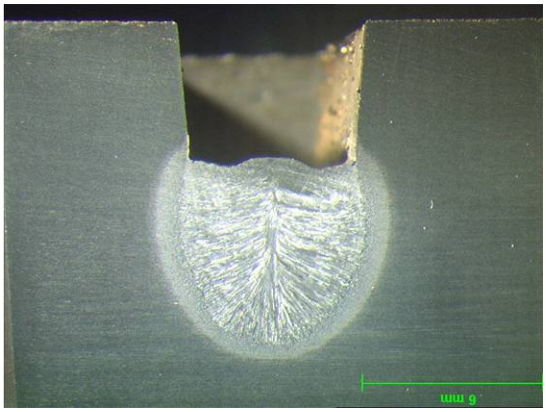

weld 2

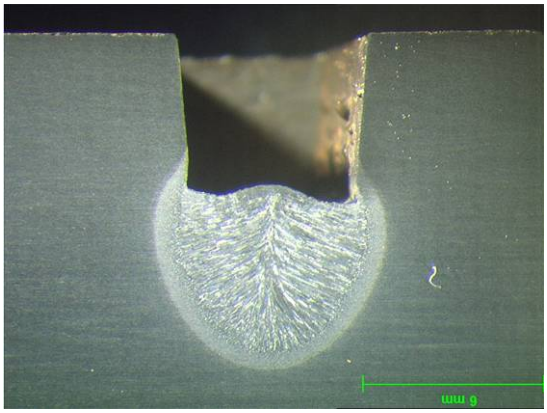

weld 3

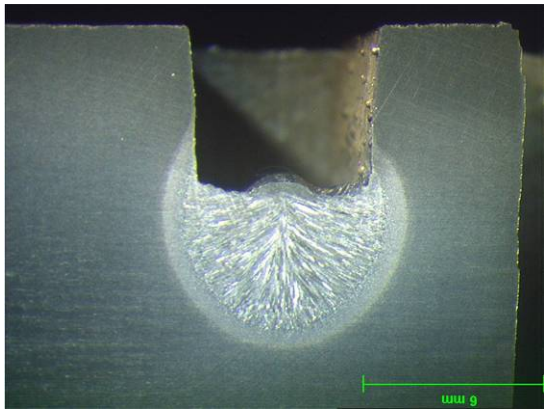

weld 4

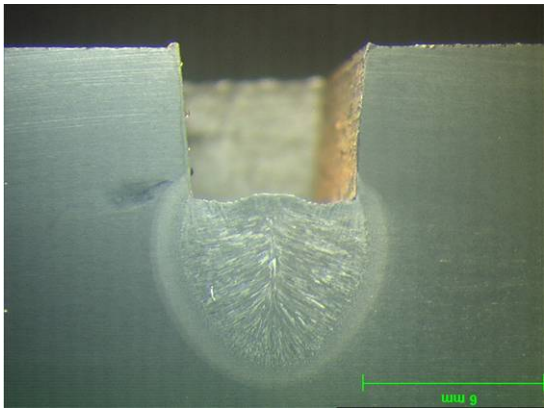

weld 5

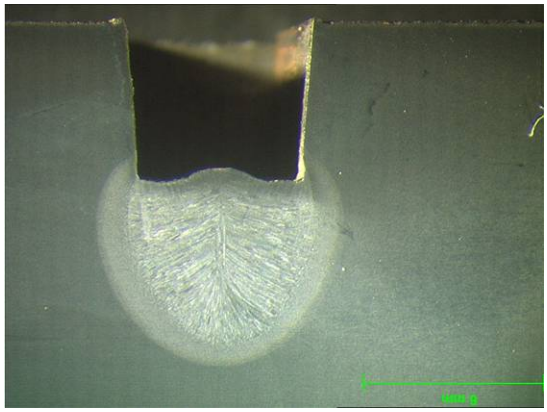

weld 6

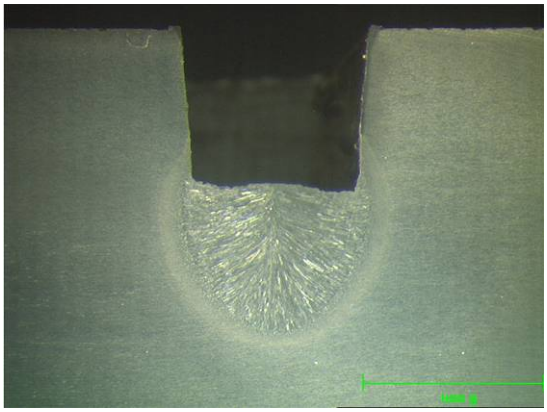

weld 7

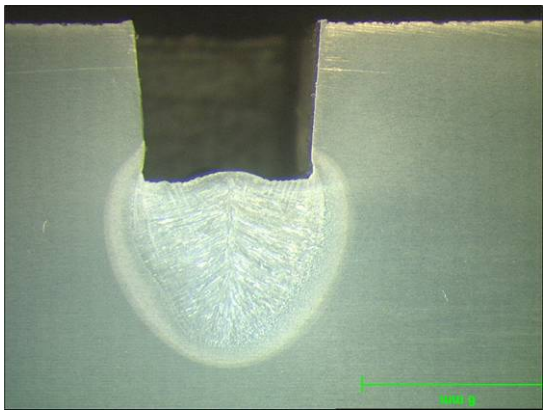

weld 8

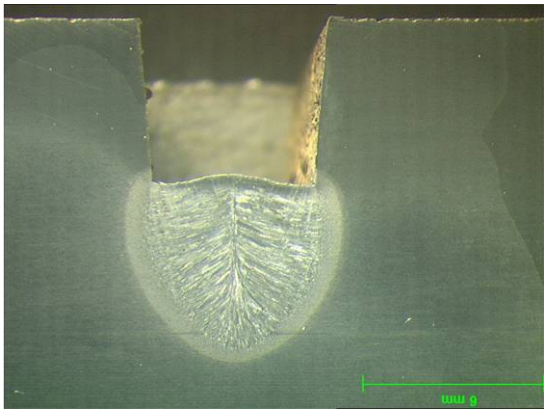

weld 9

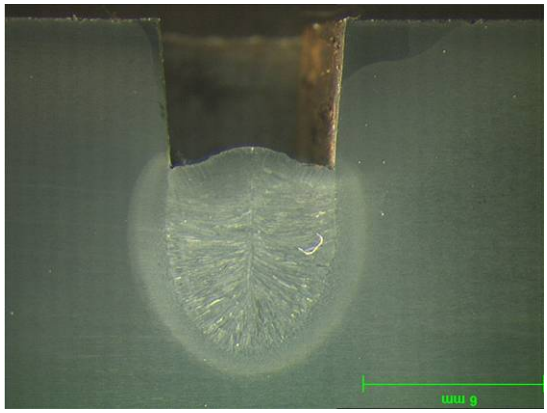

weld 10

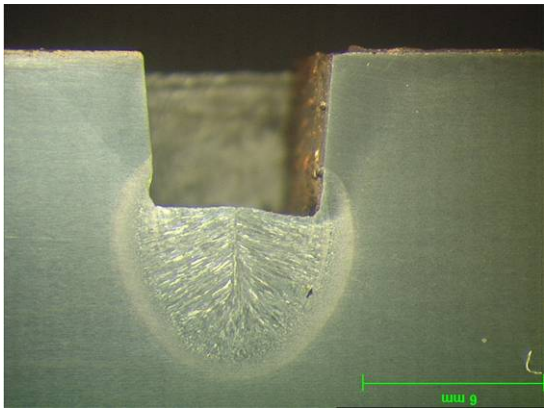

weld 11

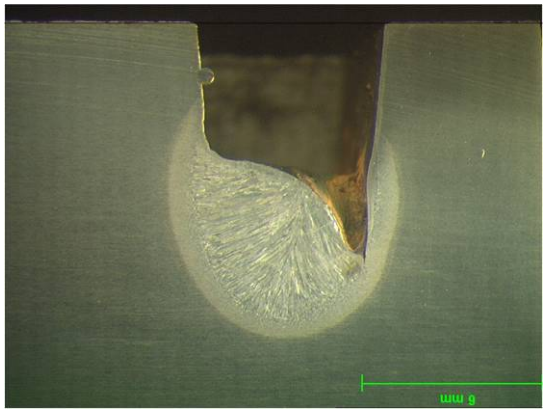

weld 11.1

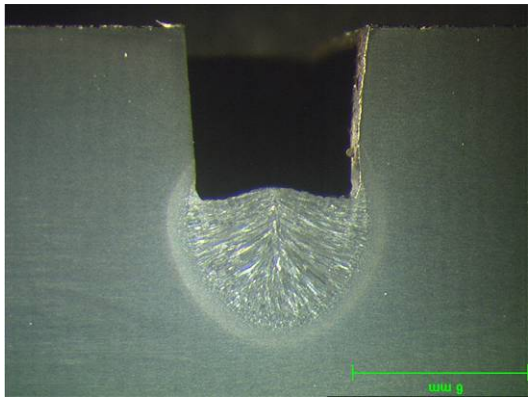

weld 12

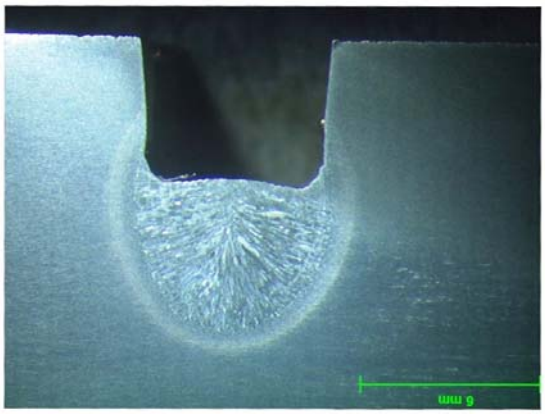

weld 13

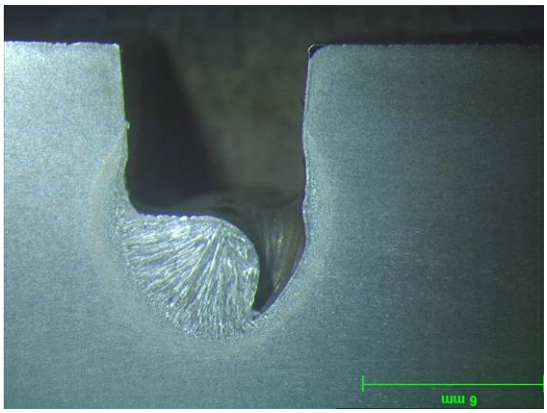

weld 13.1

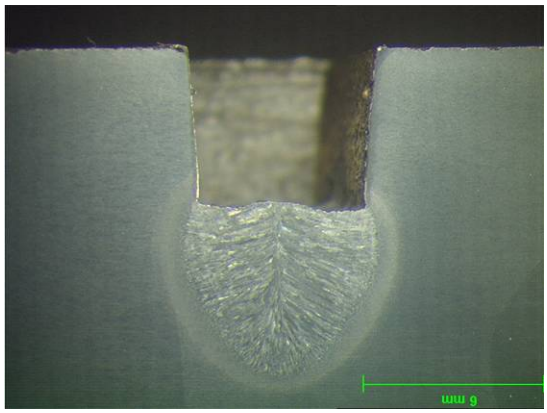

weld 14

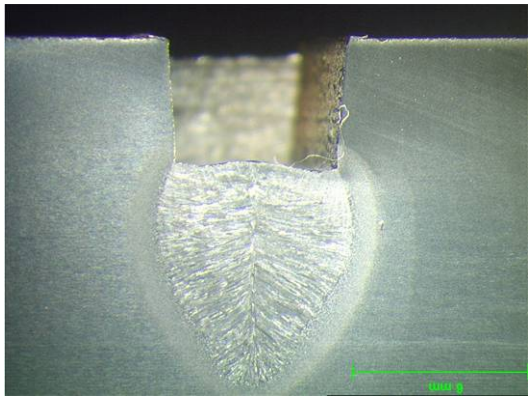

weld 15

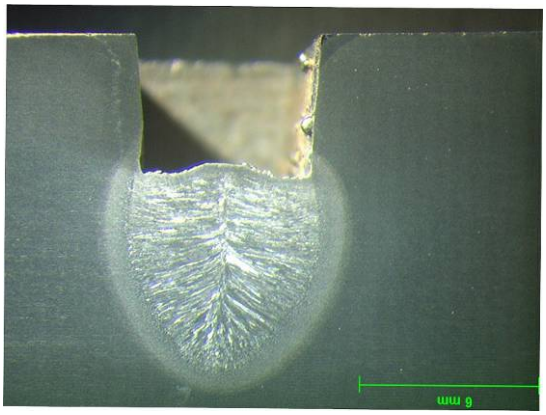

weld 16

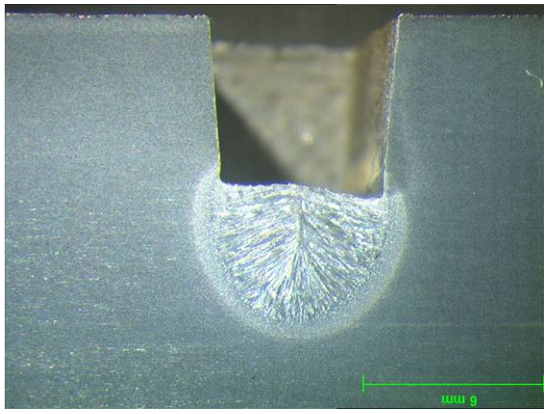

weld 17

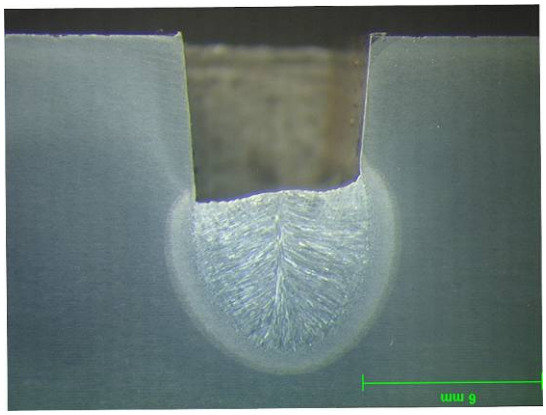

weld 18

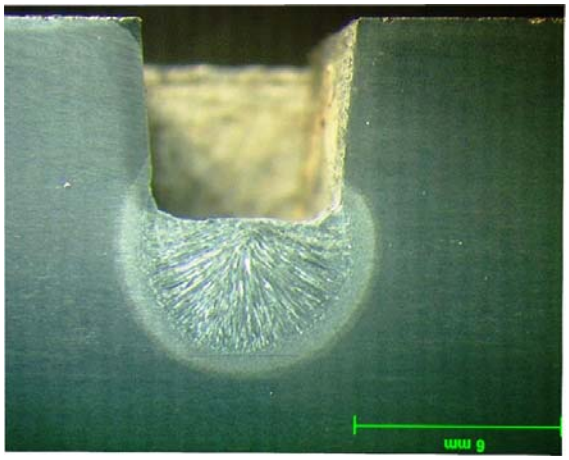

weld 19

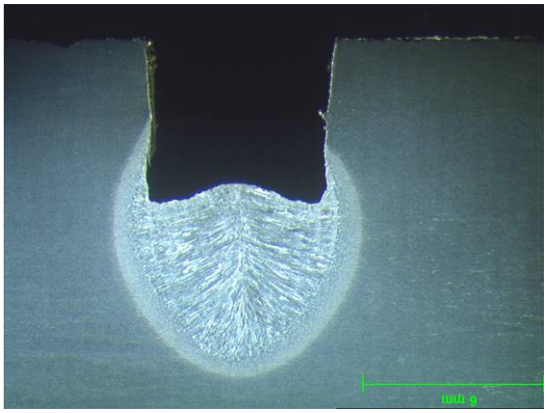

weld 20

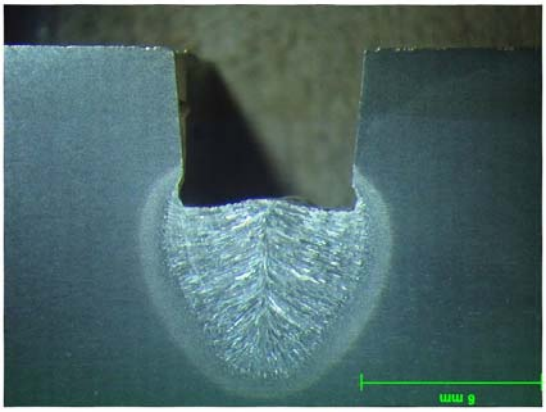

weld 21

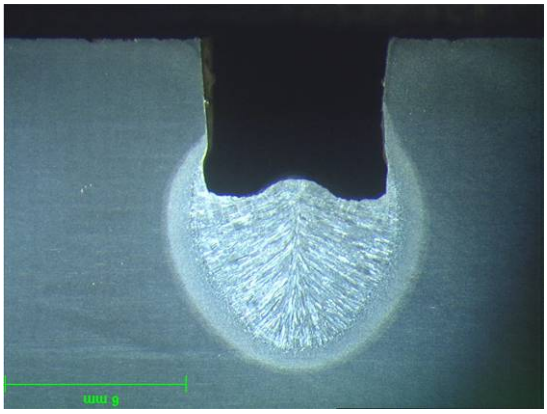

weld 22

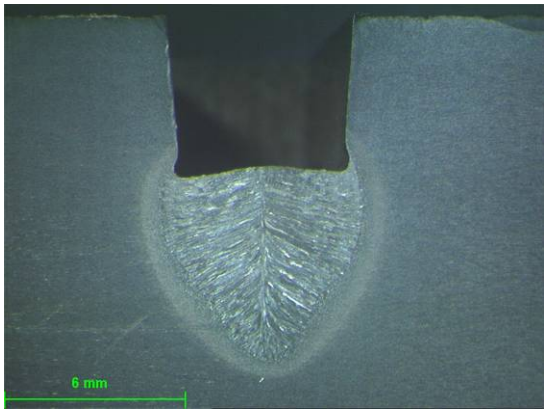

weld 23

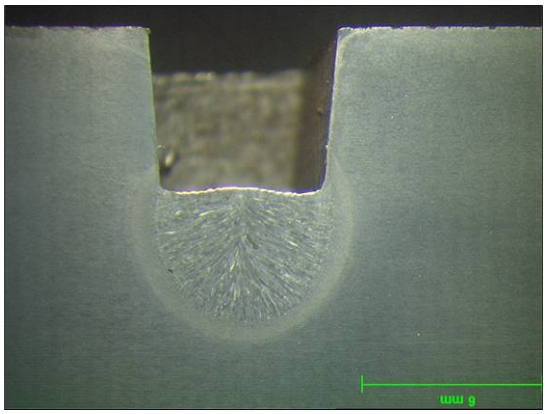

weld 24

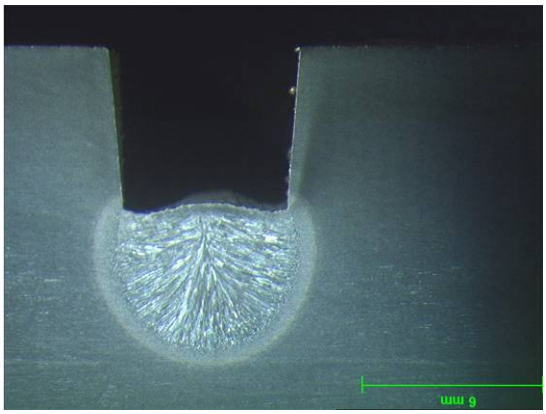

weld 25

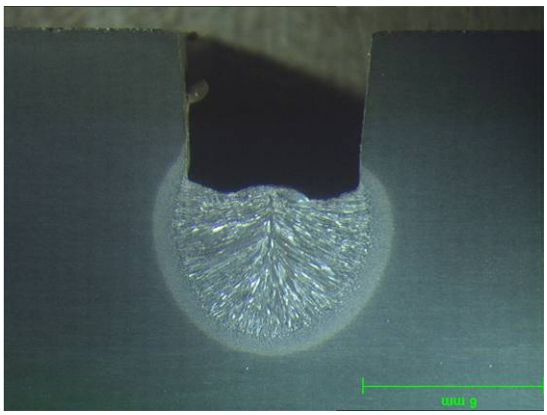

weld 26

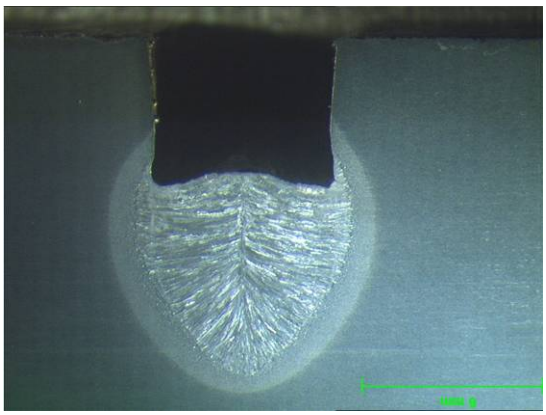

weld 27

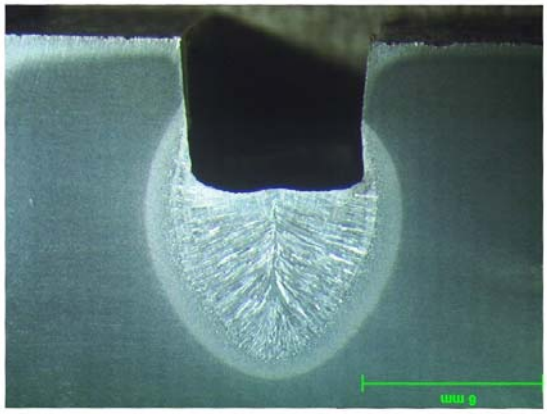

weld 28

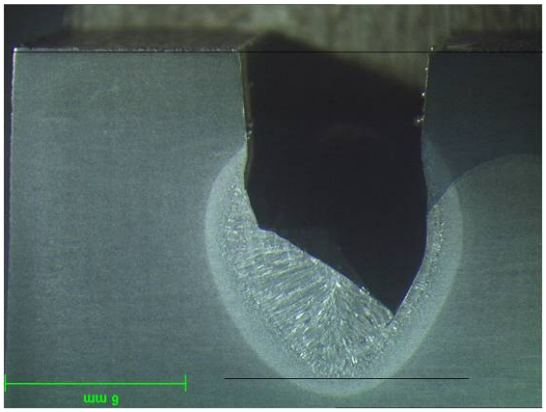

weld 28.1

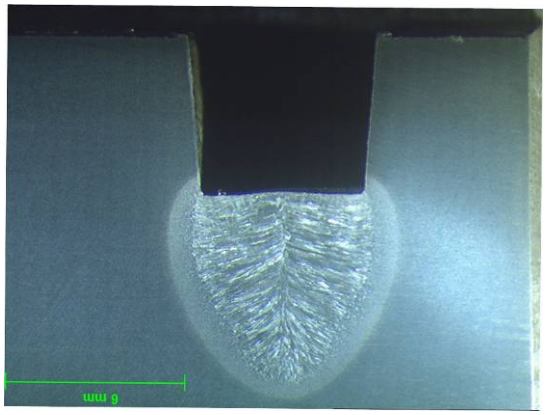

weld 29

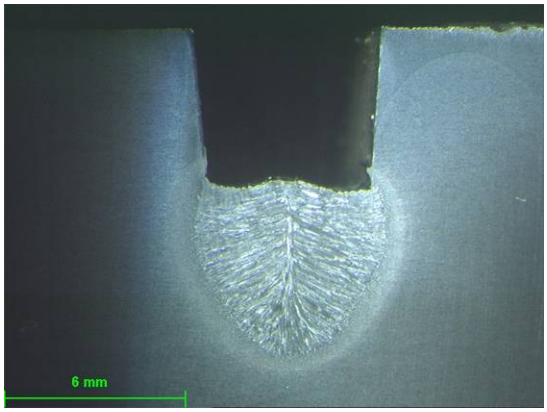

weld 30

Fig. C4 Welding Parameter Trials / Angular Position (Table 5.6)

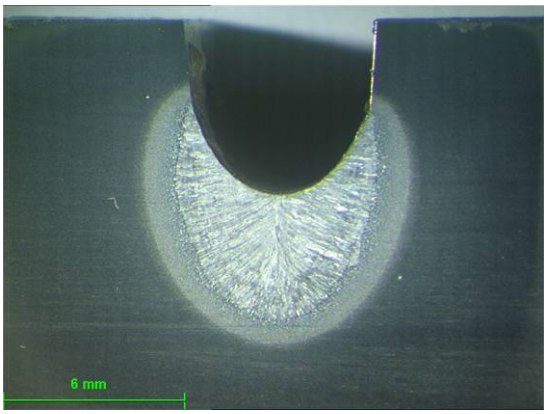

weld 1

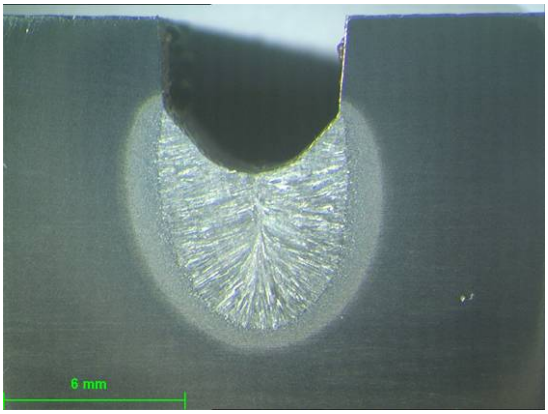

weld 2

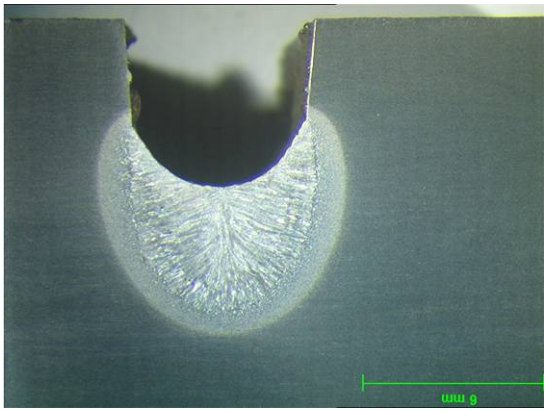

weld 3

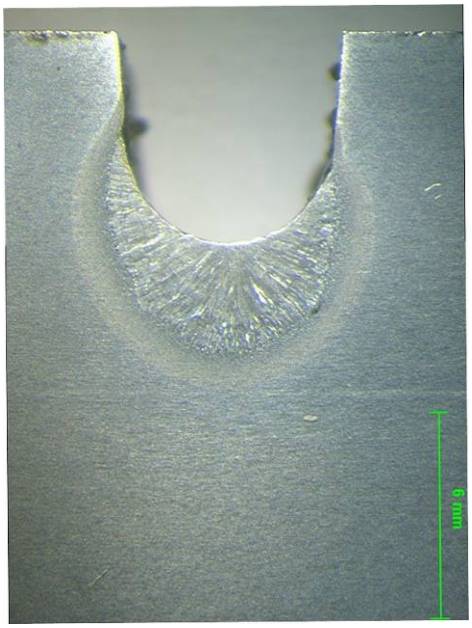

weld 4

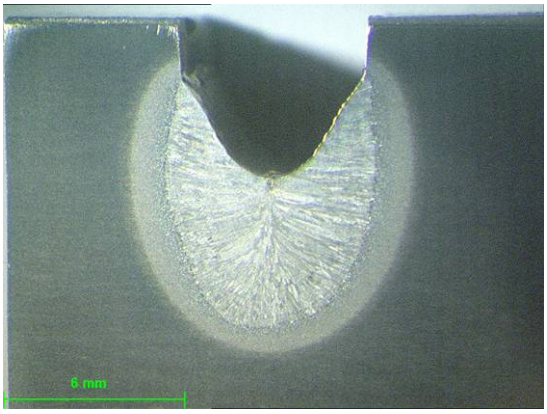

weld 5

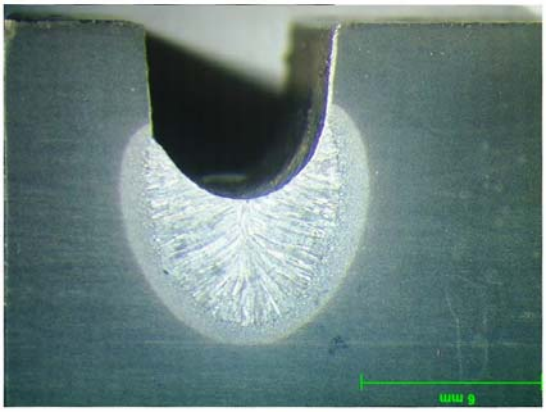

weld 6

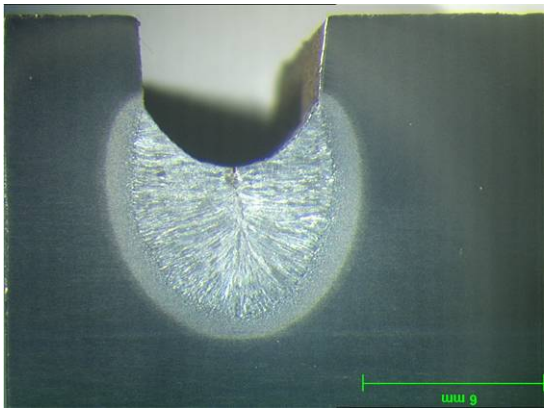

weld 7

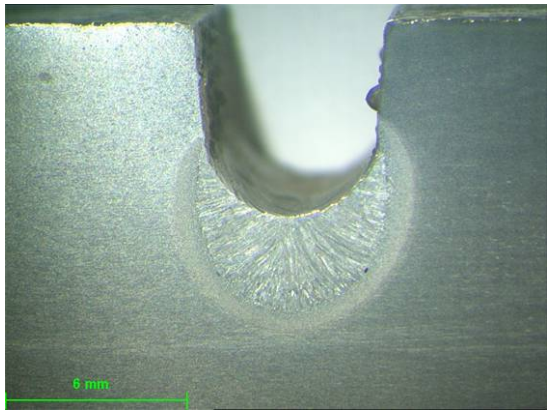

weld 8

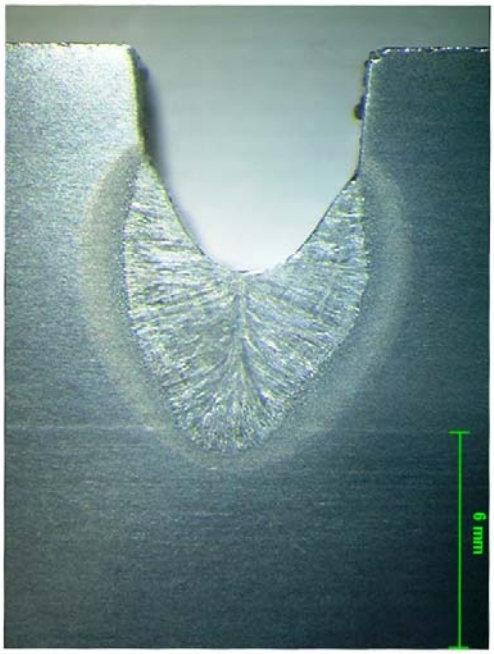

weld 9

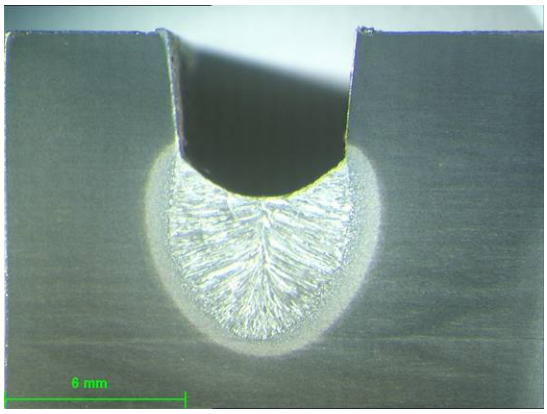

weld 10

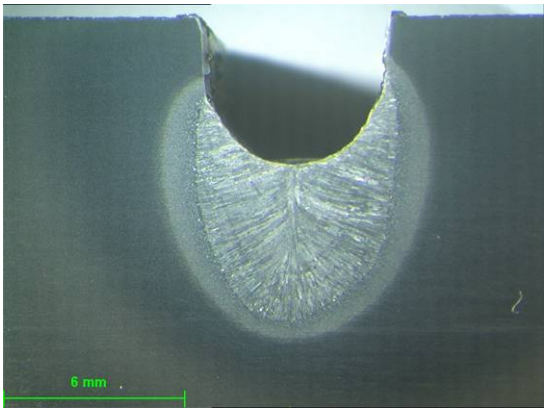

weld 11

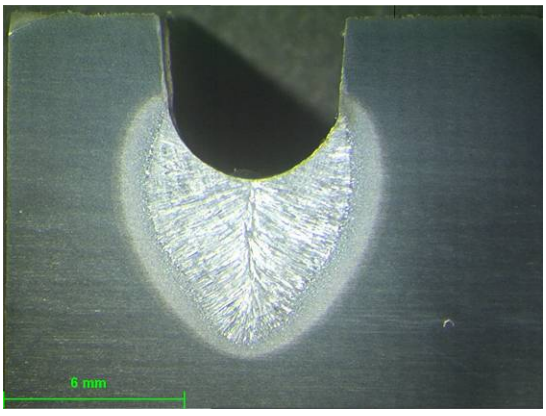

weld 12

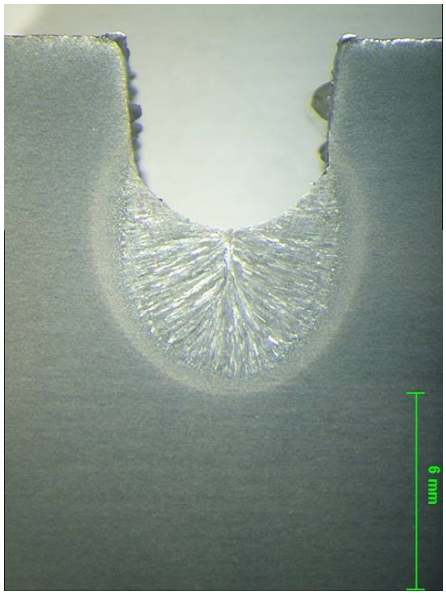

weld 13

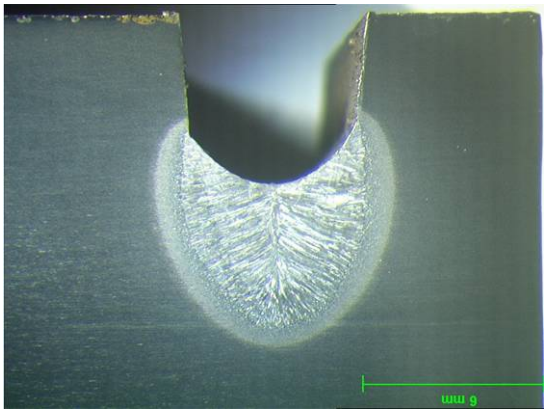

weld 14

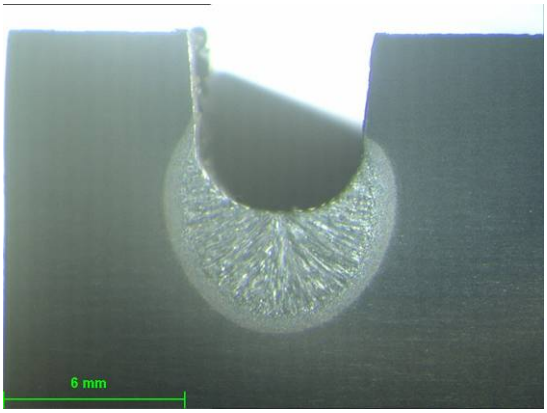

weld 15

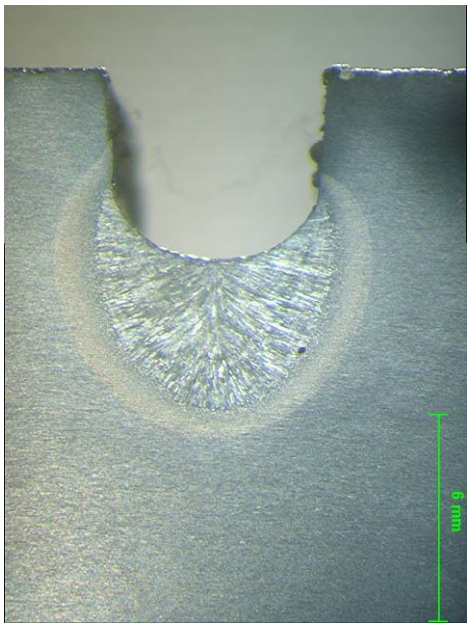

weld 16

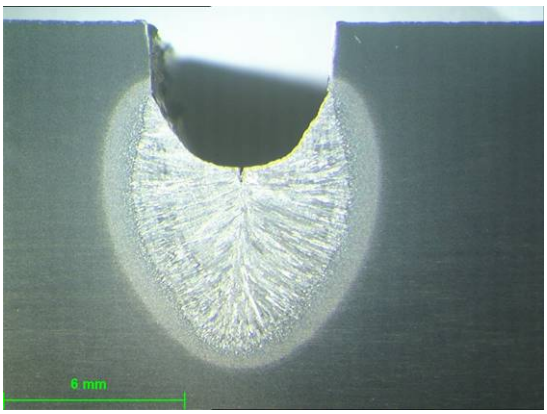

weld 17

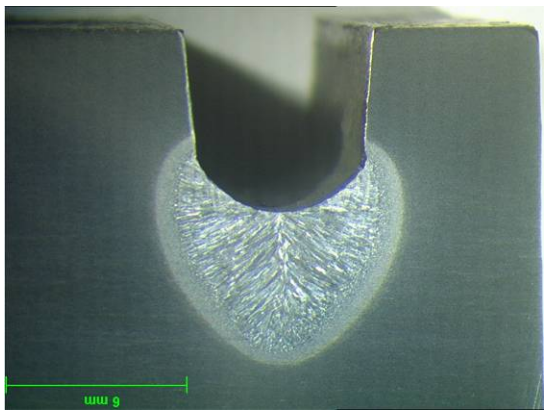

weld 18

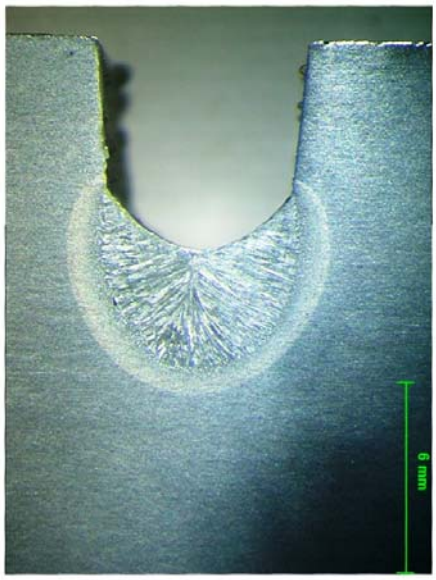

weld 19

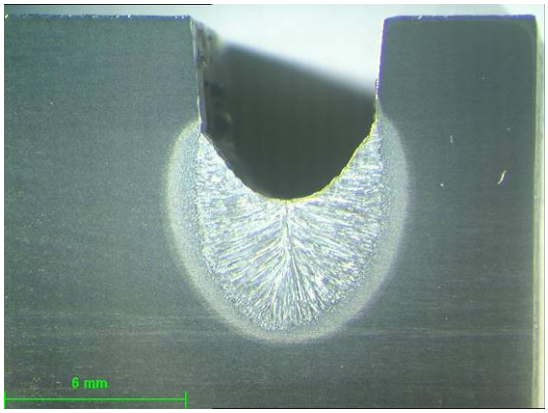

weld 20

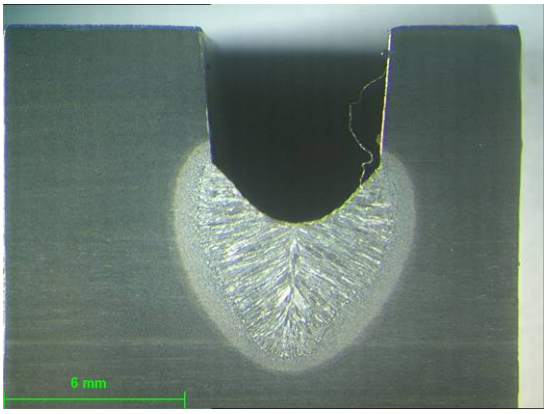

weld 21

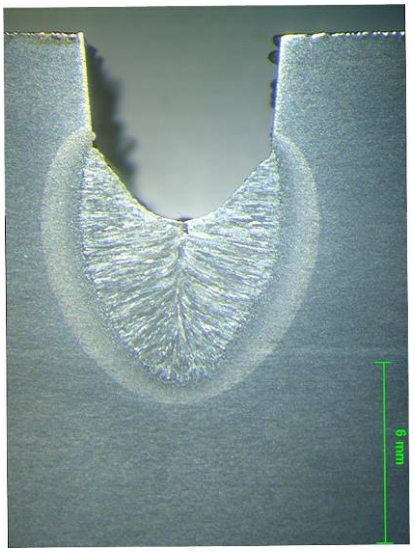

weld 22

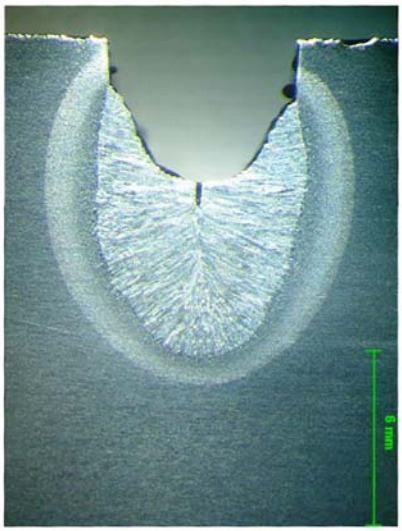

weld 23

weld 24

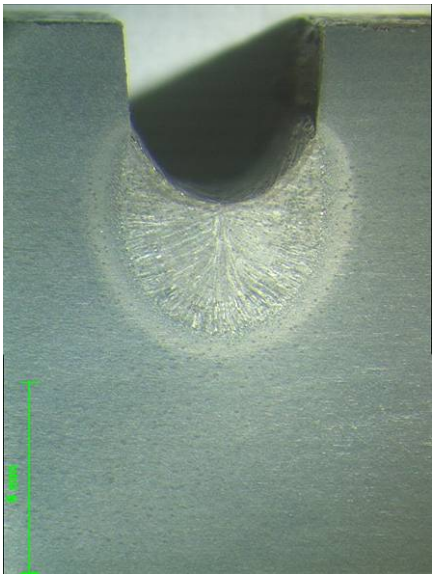

weld 25

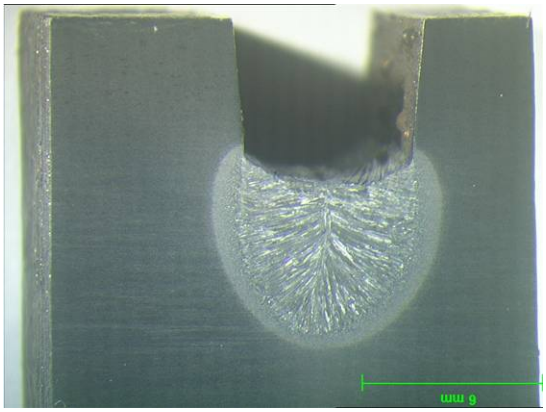

weld 26

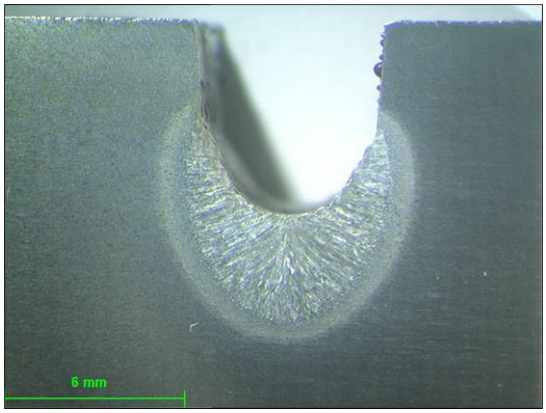

weld 27

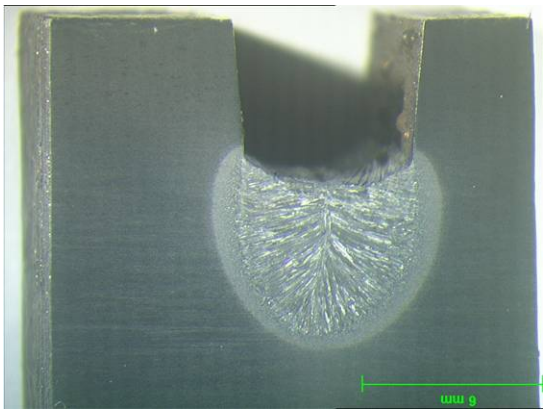

weld 28

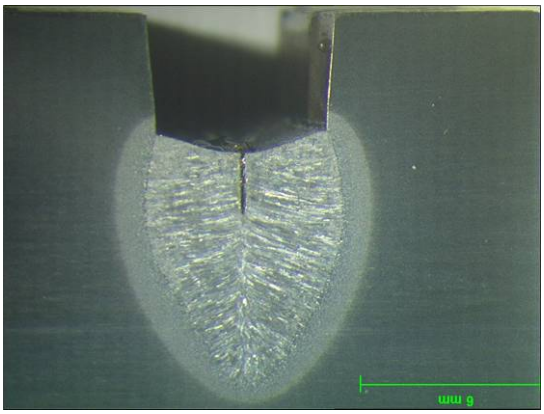

weld 29

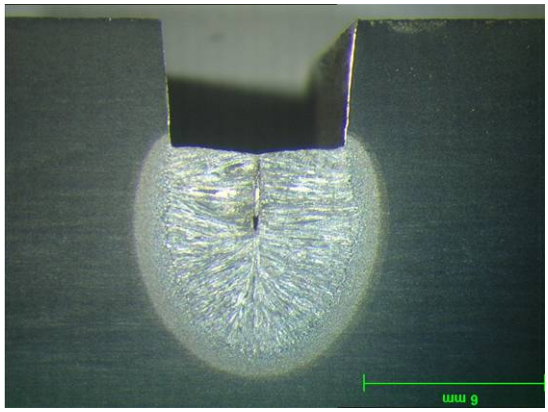

weld 30

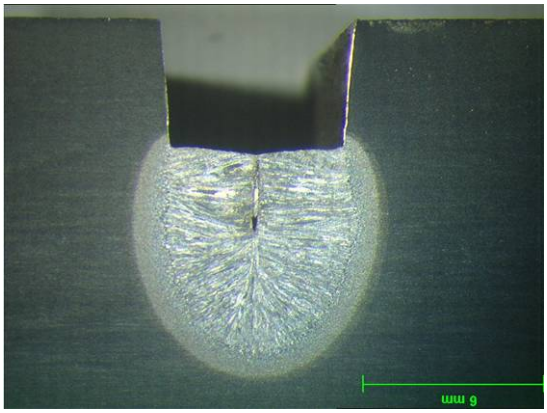

weld 31

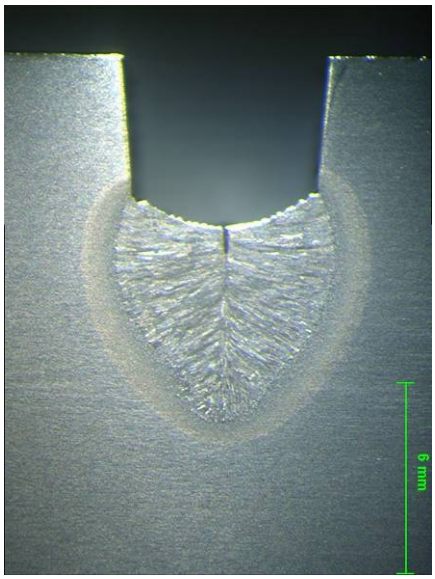

weld 32

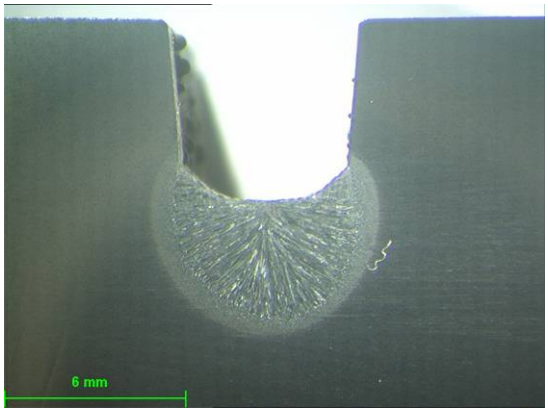

weld 33

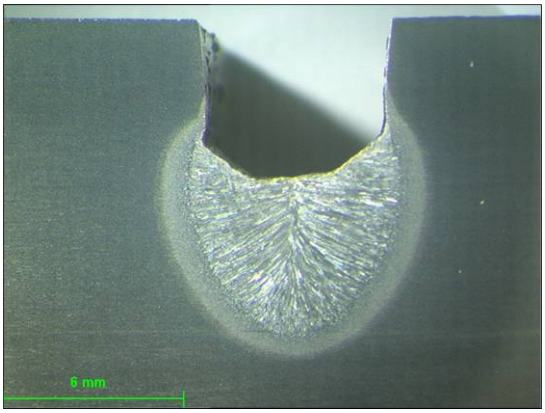

weld 34

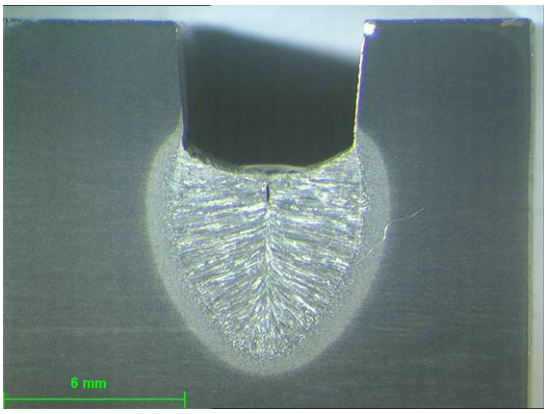

weld 35

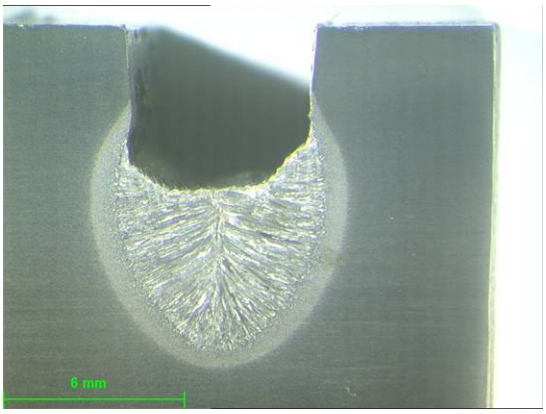

weld 36

Fig. C5 Shielding Gas Trials Macrographs (Table 5.3)

weld 1

weld 2

weld 3

weld 4

weld 5

weld 6

weld 7

weld 8

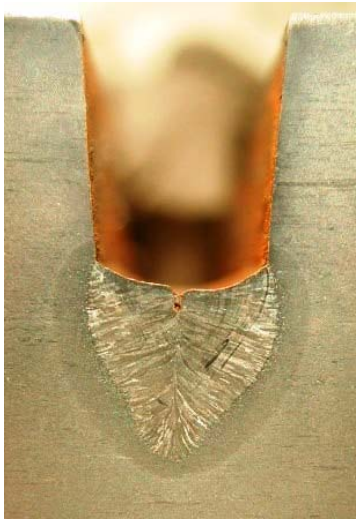

weld 9

weld 10

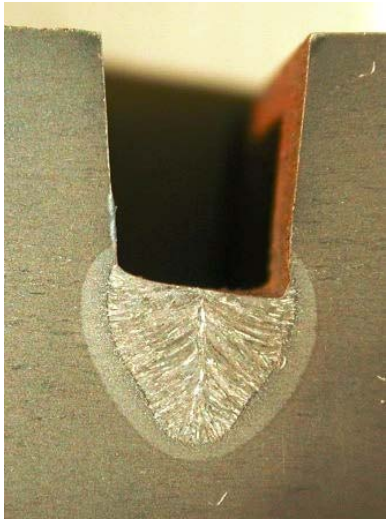

weld 11

weld 13

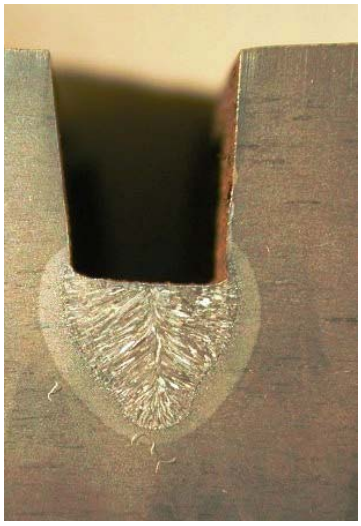

weld 14

weld 15

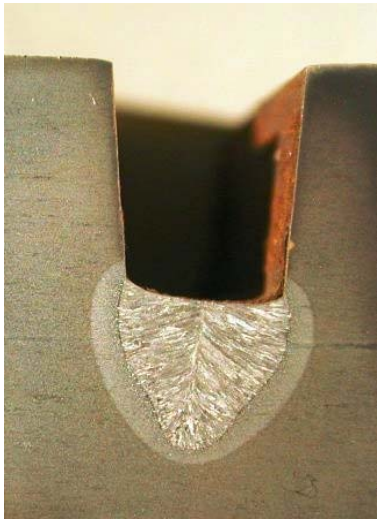

weld 17

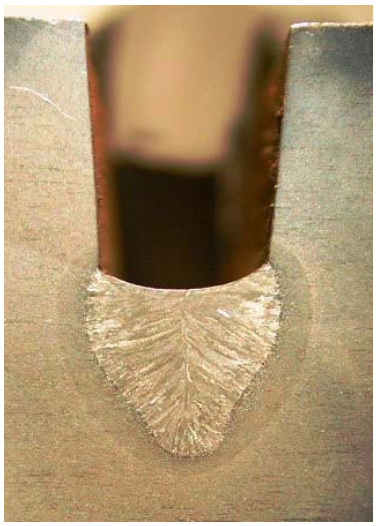

weld 18

weld 20

weld 21

weld 22

weld 23

weld 25